THE UNIVERSITY
of EDINBURGH

The role of WDR35 in the formation of functional cilia

Tooba Quidwai

s1478694

Thesis submitted for the degree of Doctor of Philosophy

The University of Edinburgh

2019

This thesis is composed of original research undertaken by myself, and have been duly acknowledged for any contribution made by others.

Tooba Quidwai

September 2019

Acknowledgements

There are many wonderful people I would like to thank for helping me in completing my Ph.D. Firstly, I am immensely thankful to my supervisor, Pleasantine Mill, for giving me an exciting project and always being open to new ideas. My work has highly benefited from her deep understanding and experience of cilia biology. I am also very thankful to her for helping me get on some excellent courses, and the right collaborations needed to complete the project. I can't thank her enough for not only making me a better scientist but also having by back whenever needed.

I want to thank my lab-mates starting with Emma Hall, the senior Post Doc in the lab for passing on her technical skills, scientific experience, and for being there during tough times. Next, I am very thankful to Margaret Keighren for very responsibly managing the mouse colonies. Many thanks to all my lab-mates Patricia Yayati, Daniel Dodd, Peter Tenant, Roly Megaw, Fraser Mcphie and some former lab members Girish R Mali, Peter Bud, Melissa Jungnickel and Robert Foster for their fantastic feedback in lab meetings. Thanks to Ian Jackson and his lab members Angus Ried, Amy Findlay, Sally Cross, Lisa McKie, Ivet Gazova, for inputs during a various presentation. Thanks to my thesis committee members Ian Adams, Toby Hurd and Colin Rickman for keeping me on track. Many thanks to Wendy Bickmore (Director MRC Human Genetics Unit IGMM) for her help whenever needed and Nick Gilbert for his contribution in co-ordinating IGMM Ph.D. graduate program.

I want to thank all the technical support team starting with Alex Von Kriegsheim for maintaining a world-class mass spec facility at IGMM and Jimi Bukowski-Wills for helping me with mass spec work. Thanks to Joe Marsh and Jonathan Wells for guidance in bioinformatics work. Thanks to Ann wheeler, Laura Murphy, Matt Pearson and Harris Morrison for maintaining excellent imaging facility at IGMM and Alison Dun for help with STED microscope at Heriot-Watt University. I am thankful to Elisabeth Freyer for helping me at FACs facility, Stefen Brown with sequencing and rest everyone maintaining the scientific infrastructure at HGU.

A significant part of acknowledging goes to my collaborator Gaia Pigino and MPI-CBG Dresden EM facility. I would not have concluded on some vital section of my thesis without using there EM-facility. Along with a big thank you to Gaia Pigino I

would also like to thank all fantastic people in her lab- Petra Kiesel, Gonzalo Alvarez Viar, Dennis Diener, Ludek Stepanek, Mareike Jordan, and Adam Schrofel for being amazing host. A big thank you to all MPI CBG EM facility members especially Tobias Fürstenhaupt for his hard work keeping facility in perfect shape, Weihua Leng and Daniela Vorkel for helping with experiments and Michaela Wilsch-Bräuniger for sharing her EM experience. I am also very thankful to Dimitrios Papadopoulos for his support and guiding me towards this collaboration and Kassiani Skouloudaki for helping while I stayed at Dresden.

I am also very thankful for the scientific skills I acquired at EMBL Heidelberg while working with Jonas Ries, which turned out very useful for my Ph.D. project. Thanks to some old friends for being outstanding support - Ulf Matti, Bettina Kaiser, Rahuman Sheriff, Deepak Kotiya, Vibhav Gautam, Markus Mund, Shveta Bisht, Aastha Mathur, Sarfarazhussain Farooqui, Muthumumaran Venkatachalapathy, Amit Mahamane, Anwesha Ghosh, Joran Deschamps, Konstanty Cieśliński, Li-Ling Yang, Rohit Prakash and Nagaraja Chandramohan.

Most important thanks to my very supportive family. Especially my Mom and Dad for accepting my life choices. Being an Indian woman, I understand how patient you have to be to justify your daughter's life choices to society. I love you from the bottom of my heart for that, and I am always proud of you. Thanks to my other family members, Zeenat, Adil, Sana, Shahid, Khalid, Ali and the two most adorable youngest members of family Gungun, and Amira. Thanks for all video chats even at odd times of the day and understanding my absence in important family functions. Love you all.

Lay summary

Cilia are small microtubule based filamentous projections from the surface of eukaryotic cells. Operating like tiny cellular antennae, cilia play critical signalling functions, as well as sometimes motile functions, necessary for our development and health during embryonic development and after birth. Defects in the structure or function of cilia can lead to a wide range of nearly 40 overlapping disorders, called the ciliopathies. As cilia are found on almost every tissue, when they don't form or function properly, ciliopathy patients may experience symptoms ranging from vision loss, chronic respiratory infections, obesity, infertility and cystic kidneys. At the most severe end of the spectrum, defects in cilia can also result in problems during embryonic development and in a range of debilitating birth defects. Identifying the genes involved in the human ciliopathies and understanding how they give rise to these disorders is of critical importance.

Our lab had previously found that lethal mutations in patients and mice in a gene *WDR35/IFT121* disrupts formation of functional cilia. In this thesis, I explore how loss of genes involved in trafficking within the cilia, like *WDR35*, disrupt the ability of cell to build a functional 'antenna'. How cells move things efficiently between their different compartments is not well understood. In the case of cilia, it has no way to make the structural or signalling proteins that it needs to function. These must be selectively shipped from the cellular compartments where they were made across the cilium's transition zone, which operates like a sorting gate. Using imaging techniques I looked in real-time how important cargos move within normal and mutant cells- where do they go if they can't get into cilia?. Using biochemistry techniques I examined what changes occur in how different trafficking 'machines' are assembled between control and mutant cells. Importantly, I found a novel role for the WDR35 protein in how the cell moves important building blocks needed to grow a cilium from where they are made in an organelle called the Golgi into newly assembling cilia membranes. My work adds novel insight into the complex process of ciliation, how a cell builds a functional cilia, as well a deeper understanding of the disease mechanisms resulting from when WDR35 is mutated.

Abstract

Cilia are microtubule-based organelles present on the surface of almost all mammalian cells that play key sensory and sometimes motile functions. Defects in cilia structure or function lead to a group of human diseases called the ciliopathies. In order to function, cilia must maintain a distinct protein and membrane composition from the surrounding plasma membrane and cytosol, highly enriched in signaling receptors and effectors. How this compartmentalization occurs remains unclear. There is no known protein synthesising machinery in cilia and the transition zone at the base of cilium forms the diffusion barrier, which does not allow free exchange between the cytoplasm to cilioplasm. Biogenesis of the cilium (ciliogenesis) requires many carriers and adaptors to facilitate passage of cargo across the transition zone. Once inside the cilia intraflagellar transport (IFT) proteins move the cargo along microtubules 'railways' of the axoneme. IFTs are known to assemble in two protein complexes, IFTA and IFTB protein complexes. IFT-B complex known to be made of 16 different proteins mediate anterograde transport with the help of kinesin motors, and IFT-A complex made of 6 different proteins help in retrograde transport powered by dynein motors. However, the exact mechanism of transport of cargo to cilia and entry across the diffusion barrier is not well understood, and the functions of each IFT protein remain unclear. In this thesis, I describe the critical role of one of the IFT-A complex protein WDR35/IFT121 in the formation of functional cilia by transporting structural elements of cilia via a vesicular mediated pathway.

Null mutations in the IFT-A component *WDR35/ IFT121* are embryonic lethal in both mouse models and human ciliopathies (Mill et al., 2011). Small, unstable *WDR35* mutant cilia are formed but fail to become enriched in diverse classes of integral and membrane-associated proteins (Caparrós-Martín JA et al., 2015; Fu W et al., 2016). To elucidate its role in the entry of membrane proteins to cilia, I present live and fixed cell imaging experiments to visualize the dynamics of membrane protein localization at the periciliary base. I also performed interaction studies by immunoprecipitation and mass spectrometry to define the molecular mechanism by which IFT proteins establish functional cilia.

There are few reports of some IFTs having similarity to COPI, II and clathrin vesicles (Jékely G and Arendt D, 2006; Taschner M et al., 2012; Dam TJPV et al., 2013). To

further explore its role, I performed deep sequence searches and homology modeling of the entire IFTA complex. I found that three of its core components and WDR35 have structural homology to COPI complex proteins α and ß'. To test whether WDR35 could function as a coatomer, I performed transmission electron microscopy tomography on cilia mutants. I found that in contrast to the electron-dense vesicles observed around WT cilia, *Wdr35*$^{-/-}$ cilia had a ten-fold increase in the number of vesicles all lacking this outer electron density. This suggests WDR35 may be involved in coating cilia-bound vesicles in order to transfer cargo into cilia, functioning similar to COPI complex proteins which selectively transports cargo between the endoplasmic reticulum and Golgi.

Abbreviations

aa	amino acids
%	Percent
5HT6	5-hydroxytryptamine receptor 6
ARF	ADP-ribosylation factor
ATCC	American type culture collection
BBS	Bardet-Biedl syndrome
BCA	Bicinchronic acid
BSA	Bovine serum albumin
ccdc	Coiled-coil domain containing protein
CCVs	Clathrin-coated vesicles
CLEM	Corelative light and electron microscopy
CME	Clathrin-mediated endocytosis
CTS	Ciliary targeting sequence
DAPI	4',6-diamidino-2-phenylindole
DAV	Distal appendage vesicles
DHH	Desert Hedgehog
DIC	Differential interference contrast microscopy
DMSO	Dimethyl sulfoxide
DNA	Deoxyribonucleic acid
dNTP	Deoxyribonucleotide triphosphate
DYNC2H1	Cytoplasmic dynein 2 heavy chain 1
E	Embryonic day
EDTA	Ethylene diamine tetra acetic acid
EHD1	EH domain-containing protein 1

EM	Electron microscopy
ENU	N-ethyl-N-nitrosourea
ER	Endoplasmic reticulum
FCS	Fetal calf serum
FGFR	Fibroblast growth factor receptor
g	Gravity
GPCR	G-protein coupled receptors
GAP	GTPase activating protein
GDI	GDP dissociation inhibitor
GEF	GDP exchange factor
GLI	Glioma-associated oncogene homologue
GUVs	Giant unilamellar vesicles
Hh	Hedgehog
hr	Hours
IFT	Intraflagellar transport
IHH	Indian hedgehog
INPP5E	Phosphatidylinositol polyphosphate 5-phosphatase
mTOR	Mammalian target of rapamycin
min	Minutes
MKS	Meckel Syndrome
NPHP	Nephronophthisis
ºC	Degrees Celsius
OCRL	Inositol phosphate-5-phosphatase
PCV	Primary ciliary vesicle
PIP	Phosphoinositide
PKD	Polycystic kidney disease

PCP	Planar cell polarity
PDGF	Platelet-derived growth factor
PLD	Phospholipase D
PCD	Primary ciliary dyskinesia
PKA	Protein kinase A
PTC-1	Patch-1
RP	Retinitis pigmentosa
RNAi	RNA interference
SDS-PAGE	Sodium dodecyl sulphate polyacrylamide gel electrophoresis
Sec	Seconds
SHH	Sonic hedgehog
SRP	Short rib polydactyly
SMO	Smoothened
SSTR3	Somatostatin receptor type 3
SuFu	Suppressor of fused
TCTN	Tectonic
TEM	Transmission electron microscopy
TPRs	Tetratricopeptide repeats
TGF-β	Transforming growth factor beta signaling
TMEM67	Transition zone proteins Meckelin
TUB	Tubby protein homolog
TULP-3	Tubby-related protein 3
TZ	Transition zone
VTC	Vesicular-tubular cluster
β-ME	β-mercaptoethanol

Contents

List of Figures

List of tables

List of movies

Chapter 1. Introduction

1.1 Structure of Cilia

1.1.1 Cilia: highly dynamic and biochemically complex organelle

Cilia and flagella are highly organized microtubule-based organelles present on eukaryotic cells that play crucial sensory and motile functions. They are membrane extensions from the plasma membrane, with a unique set of lipids and proteins. Broadly, the structure of cilia can be divided into three parts- the basal body, the transition zone, and the axoneme. The axoneme consists of 9 microtubule doublets extending from the basal body (a modified centriole) covered by a ciliary membrane kept separate from the plasma membrane by the transition zone, which acts as a ciliary gate (**Figure 1.1A**). Based on their structure and function, cilia are of two types: (1) **motile cilia** with (9+2) microtubule arrangement and (2) primary or **sensory cilia** with a (9+0) microtubule doublet arrangement (**Figure 1.1B**). Motile cilia or flagella function to propel the cell in the case of the sperm flagella or regulate the flow of fluids across the surface of various organs including the respiratory tract, the oviduct, and epididymis, as well as the ependymal surface lining the brain ventricles. Motile cilia are frequently present in large numbers on these cells, where they generate coordinated wave-like motions across the cell and eventually across the field. In contrast, sensory cilia mostly occur as a single extension from the cell's surface and were for long considered to be a vestigial organelle, a remnant from motile cilia. It was much later discovered to be essential for regulating various signaling pathways both during embryonic development and adult life (see **Section 1.2**). These are highly dynamic and biochemically complex structures, which require both active transport processes as well as passive structural components to form a distinct functional organelle.

1.1.2 Ciliary membranes have distinct protein compositions

During the course of evolution, cells were able to separate from their aqueous surroundings by developing cell membranes composed of lipid bilayers. Cilia are believed to have originated very early in eukaryotes, where the ciliary membrane evolved alongside the cell membrane. Moreover, both membranes are generated by similar trafficking mechanism of cargo proteins from the Golgi (see **Section 1.3**) and lipids from the endoplasmic reticulum (ER), as such could be assumed to have a

similar composition. Anatomically, the ciliary membrane appears to be a continuation of the cell membrane, which might also suggest that the cell membrane and ciliary membrane might have a similar composition. However, intriguingly cilia have evolved to maintain a distinct lipid and protein composition different to that of the cell membrane, which further varies between organisms. The ciliary membrane plays two essential functions: (1) it separates cilia from the extracellular environment; and (2) it is highly enriched in signaling receptors and downstream effectors for both extracellular and intracellular signaling (see **Section 1.2**). For example, in the unicellular green algae *Chlamydomonas reinhardtii,* sexual reproduction is initiated by adhesion of flagella of mates by agglutinin/adhesion molecules present in the flagellar membrane (*Ferris PJ et al., 2005; Mesland DAM et al., 1980; Pan J and Snell WJ, 2000*).

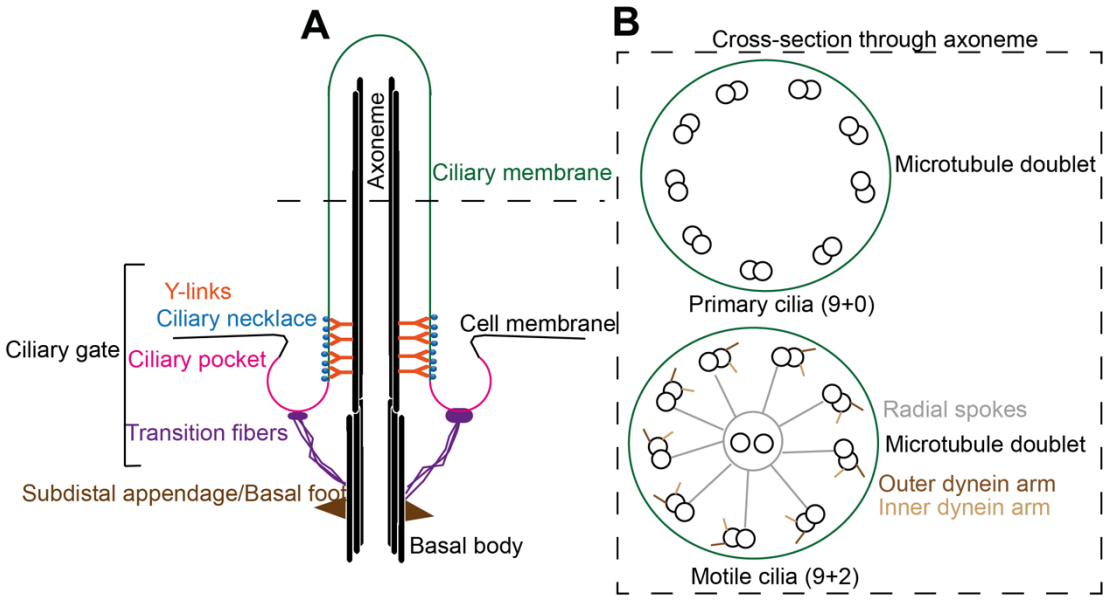

Figure 1.1. Schematic overview of cilia structure. (A) Ciliary gate. The ciliary pocket (magenta) encircles the base of cilia. Transition fibers (purple) fan out from each of nine microtubule triplets from the basal body and dock at the membrane of ciliary pocket. The transition zone is made of protein complexes (MKS, and NPHP see **Figure 1.2**), which appear to arrange in Y-shaped structures (orange) between the ciliary membrane and axoneme. Bead-like structures (blue) are found on the outer end of the Y-linkers are called the ciliary necklace. Together, the ciliary pocket, the transition fibers, and the transition zone make up the ciliary gate, which functions to keep the ciliary membrane (green) a distinct composition from the cell membrane (black). **(B) Schematic of a cross-section through axonemes** for sensory (top) and motile (bottom) cilia. In general, the axoneme has (9+0) arrangement of doublet microtubules in sensory cilia whereas the majority of motile cilia have (9+2)

arrangement (with two microtubule singlets as part of the central pair complex). Motile cilia axonemes have additional identifiable structures like the large outer (dark brown) and inner (light brown) dynein arms, as well as radial spokes (grey) used to power cilia beat.

Similarly, vertebrate cilia maintain ligand-dependent arrangement of receptors for the Hedgehog (Hh) signaling pathway, which regulates patterning of the limb bud and neural tube during embryonic development (*Corbit KC et al., 2005; Huangfu D et al., 2003; Huangfu D and Anderson KV, 2005; Rohatgi R et al., 2007*). In response to Hh ligand, stimulation of Smoothened (SMO), becomes enriched in cilia, whilst the inhibitory Patched (PTC1) co-receptor is shuttled out of cilia (**see Section 2.2**). This leads to the activation of the downstream pathway by activation of the GLI transcription factors at the ciliary tip (**Figure 1.4**) (*Corbit KC et al., 2005*). What is striking is that in the absence of cilia, although all the receptors and transcription factors are still expressed, but without localization to this specialized signaling organelle, cells can no longer adequately respond to the Hh ligand (*Corbit KC et al., 2005; Huangfu D and Anderson KV, 2005*). Although their mechanism of action is less clear, two other ciliary transmembrane proteins that also accumulate in the ciliary membrane and are essential for normal kidney function are PKD2 and PKD1 (*Yoder BK et al., 2002*). Finally, another example of a different organization of ciliary membrane is the presence of different agglutinins between the cell and ciliary membranes in *Chlamydomonas*, which even fail to mix under most conditions *in-vitro* (*Hunnicutt GR et al., 1990; Musgrave A et al., 1986*). See **Section 1.2** for more discussion on types of signaling proteins programmed to specifically localize to cilia. In summary, this organized and regulated localization of ciliary receptors distinct from the cell membrane is required for cilia signaling function.

1.1.3 The ciliary membrane has a distinct lipid composition

Although it appears to be continuous with the cell membrane, the ciliary membrane maintains a distinct lipid composition. Phosphoinositides (PI) are phosphorylated lipids, which provide a unique identity to different cellular membranes and hence regulate signaling between cellular organelles (*Balla T, 2013*). The plasma membrane is constituted of both PI(4)P and PI(4,5)P_2, whereas endosomes and Golgi membranes have PI(3)P and PI(4)P respectively (*Paolo GD and Camilli PD, 2006; Hammond*

GRV et al., 2014, 2012; Roth MG, 2008). Unlike either the Golgi and ER membranes which are physically separated from the plasma membrane, the ciliary membrane is continuous with cell membrane but still has comparatively high levels of PI(4)P and low levels of $PI(4,5)P_2$ (*Chávez M et al., 2015; Garcia-Gonzalo FR et al., 2015*). In order to selectively maintain these domains, cilia would need some type of localized phosphoinositide 5-phosphatases. There are three known phosphoinositide 5-phosphatases which can localize to cilia in mammals, with the main form being phosphatidylinositol polyphosphate 5-phosphatase (INPP5E). INPP5E is a cilia-specific peripheral membrane protein which converts $PI(4,5)P_2$ into PI(4)P, thus maintaining the high ciliary level of PI(4)P (*Chávez M et al., 2015; Garcia-Gonzalo FR et al., 2015*). For this, INPP5E is enriched explicitly in cilia by the coordinated function of the ARL13B-PDE6δ trafficking module (*Kösling SK et al., 2018; Thomas S et al., 2014*). Another phosphoinositide 5-phosphatase known to localize to cilia is inositol phosphate-5-phosphatase (OCRL) (*Attree O et al., 1992; Prosseda PP et al., 2017*). OCRL mutations result in Lowe syndrome, with symptoms including disorders of the eye, nervous system, and kidney (*De Matteis MA et al., 2017*). Patient-derived fibroblasts have a higher concentration of $PI(4,5)P_2$ and reduced levels of PI(4)P. These results suggest that more than one phosphoinositide 5-phosphatase enzyme may function in cilia to maintain its distinct lipid composition.

Once this distinct lipid composition is established, how does this difference of the ciliary membrane composition help in ciliary cargo transport? A specialized and highly conserved motor-driven trafficking system exists for carrying cargo into and out of cilia called intraflagellar transport (IFT) (see **Section 1.1.5**). Recent studies have shown that intraflagellar transport complex A (IFT-A) proteins are one of the key players for membrane protein transport into cilia (see **Section 1.1.6**). Tubby-related protein 3 (TULP3) has been described to function as an adaptor between IFT-A complex and membrane proteins to transport a broad range of ciliary membrane proteins into cilia (see **Figure 1.7**). TULP3, when attached to the (IFT-A complex), transports ciliary membrane proteins to cilia in a $PI(4,5)P_2$ dependent manner (*Badgandi HB et al., 2017; Mukhopadhyay S et al., 2010*) (See **Section 1.3.2**). Briefly, when TULP3 is bound to $PI(4,5)P_2$, it associates with the IFT-A complex to import membrane proteins into cilia. Once inside the ciliary compartment, $PI(4,5)P_2$ is

converted to PI(4)P by ciliary phosphoinositide 5-phosphatases, which weaken the bond between TULP-3 and the lipid, resulting in the release of membrane cargo inside cilia (*Badgandi HB et al., 2017; Ye F et al., 2018*). Since the loss of function mutations in any of these components including *TULP-3*, *IFT-A* subunits or *INPP5E*, disturbs Hh signaling (*Cameron DA et al., 2009; Liem KF et al., 2012; Mukhopadhyay S et al., 2013; Norman RX et al., 2009; Patterson VL et al., 2009; Qin J et al., 2011; Tran PV et al., 2008*), it is possible that INPP5E might be the candidate phosphatase controlling $PI(4,5)P_2$-TULP3-IFT-A mediated ciliary import of membrane proteins. Mutations in other TULP-3 related genes, like *TUBBY* or its paralog *TULP1*, are associated with other ciliopathy-like features including obesity and retinal degeneration (*Kleyn PW et al., 1996; Noben-Trauth K et al., 1996*). Tubby is predominantly expressed in brain and retina, where it is also involved in the import of GPCRs to cilia (*Badgandi HB et al., 2017; Norman RX et al., 2009*). It is likely that Tubby and TULP1 also use a similar mechanism to TULP3 in order to transport Rhodopsin to the outer segment of rod photoreceptors or MC4R into the paraventricular nucleus cilia (*Siljee JE et al., 2018*). Defects in this selective trafficking would lead to loss of vision and obesity, respectively. Moreover, like phosphoinositides, Tubby family proteins are also well conserved in ciliated organisms, which strongly suggests that they might have similar roles in other organisms, which have yet to be determined.

Other ciliary proteins have been shown to bind phosphoinositides, including the Bardet-Biedl syndrome complex proteins (BBSomes), although they were shown to have variable affinities to different phosphatidylinositol phosphatase (PIPs) in-vitro (*Jin H. et al., 2010*). The BBSome complex is made of eight BBS proteins BBS 1,2,4,5,7,8 9 and BBS18 (*Loktev et al., 2008; Nachury MV et al., 2007*), which unlike TULP-3, has been controversial adaptor for both import and export of ciliary membrane protein (see **Section 1.3.2**) This variable affinity of BBSomes to different PIPs might also explain its controversial role in the import of few and export of most ciliary membrane proteins (see **Section 1.3.2 and 4.2.1)**. In summary, the sharp distinction of phosphoinositides between the cell membrane and the ciliary membrane is thought to assist selective transport into cilia. Very little is known directly about the role of other types of lipids beyond phosphoinositides in this process. However, some cholesterols like oxysterols and ergosterol are known to bind to SMO in mammals and

C. reinhardtii respectively to regulate Hh signaling (*Byrne EFX et al., 2016; Myers BR et al., 2013; Nachtergaele S et al., 2013; Nedelcu D et al., 2013; Roux C et al., 2000; Sever N et al., 2016; Xu L et al., 2012*). Though few lipids have been established to provide ciliary membrane unique identity, there might be more of distinct ciliary lipids and their functions are yet to be explored.

There is emerging evidence that cilia might also have different lipid compositions in different parts of the cilia. For example, the base of cilia in many cells like fibroblasts form a curved structure surrounding the base, referred to as a ciliary pocket (**Figure 1.1A**) (*Sorokin S, 1962; Molla-Herman A et al., 2010; Rogowski M et al., 2013*). In contrast, the rest of the ciliary membrane is relatively straight. The lipid composition of membranes is known to determine their curvature (*McMahon HT and Boucrot E, 2015*). For example, lipids such as phosphatidylethanolamine and lysophosphatidylcholine, which are conical in shape, concentrate on more curved regions, whereas phosphatidylcholine, which is cylindrical in shape, concentrates to less curved regions (*McMahon HT and Boucrot E, 2015*). Moreover, ciliary lipid composition is also different in different organisms. For example, dehydroergosterol is highly enriched in the trypanosome flagellar membrane but is not found in vertebrates (*Tyler KM et al., 2009*). Similarly, unsaturated amino acids are enriched in the membrane of outer segments of the vertebrate photoreceptors but seem to be missing in *C. elegans* thermosensory AFD neurons. Cilia thus may have selective transport not only for proteins but also for lipids, which is maintained by the complex organization of diffusion barrier at cilia base.

1.1.4 A diffusion barrier maintains the distinct protein and lipid composition of the ciliary membrane

Once established the distinct composition and its importance for cilia function, the next question is, how is this distinct composition of cilia maintained? The junction of cilia and cytoplasm is a highly complex structure, necessary to provide this unique biochemical identity to the ciliary compartment. Electron microscopy images have shown this junction of cilia and cell to be made of three main structures (Figure **1.1A** and Figure **1.2**):

1. The ***ciliary pocket***: a bulged membrane curvature at the base of cilia, contiguous with the plasma membrane.
2. The ***transition fibers/distal appendages/alar sheets***: these structures help the basal body to dock on the periciliary vesicle (PCV) during the initial stages of ciliogenesis. As ciliogenesis proceeds, they become the attachment between the ciliary pocket and basal body, where they are likely required to maintain the curvature of the ciliary pocket. Transmission electron microscopy (TEM) images show transition fibers to fan-out one each from the nine microtubule triplets of the basal body, extending upwards towards ciliary pocket at an angle (*Pedersen LB et al., 2012; Rogowski M et al., 2013*).
3. The ***ciliary necklace***: an outer 'bead-like' decoration with an inner ring of Y-shaped forms in the cilia lumen, as visible by EM (*Reiter JF et al., 2012*).

Presumably together, the ciliary pocket, transition fibers, and ciliary necklace/transition zone, create the diffusion barrier which prevents free mixing of ciliary proteins and lipids, with those from those of cell membrane and cytoplasm (F**igure 1.1A** and Figure **1.2**). The curved membrane of ciliary pocket might be itself providing geometric constraint to stop plasma membrane lipids and proteins from diffusing into the ciliary compartment. Similarly, the fanned-out transition fibers from basal body to ciliary pocket might restrict both cytoplasmic and cell membrane material from diffusing into cilia. Finally, the circular ring of ciliary necklace and transition zone forms another barrier to 'gate' entry into cilia (*Garcia-Gonzalo FR and Reiter JF, 2017; Reiter JF et al., 2012*). Interestingly, the ciliary membrane in the necklace region itself has a distinct lipid composition from the rest of the ciliary membrane. Whilst the ciliary membrane in rest of shaft region is enriched in filipin-sterol complexes, these are absent in the ciliary necklace region (*Montesano R, 1979*).

Much progress has been made in the past 5 years defining the molecular identity of what makes up these structural components. Transition fibers are composed predominantly of 5 proteins: CEP83/CCDC41, CEP89/CCDC123/CEP123, SCLT1, FBF1 and CEP164 (*Graser et al., 2007; Joo et al., 2013; Schmidt et al., 2012; Tanos et al., 2013*). Defects in many of these block ciliogenesis at the very initial step, when the primary ciliary vesicles dock on the transition fibers extending from mother centriole (*Graser et al., 2007; Joo et al., 2013; Schmidt et al., 2012*) (see **Section**

1.3.4). The transition zone is made of several protein complexes including the nephronophthisis module (NPHP), and the Meckel Syndrome module (MKS) (**Figure 1.2**). Many other ciliary proteins complexes including IFTs and BBSomes, accumulate at the transition zone before entering inside cilia, as do several cargos including ciliary membrane proteins (*Milenkovic et al., 2015; Shi et al., 2017*). These studies demonstrate that the transition zone functions not only as a diffusion barrier, but also as 'transit' lounge for many cilia-destined cargos for selective entry. How exactly the transition zone proteins help these cargos proteins cross over into cilia remains unclear.

The MKS Module (Meckel Syndrome): One of the two transition zone complexes is the MKS complex, where mutations in components of this module result in a rare often lethal syndrome affecting multiple organs including cystic kidneys, polydactyly and occipital encephalocele. Intriguingly mouse mutations in these components suggest it is important for ciliogenesis in some tissues like neural tube and node, whilst not in others like limb bud (*Chih et al., 2011; Dowdle et al., 2011; Garcia-gonzalo FR et al., 2011; Roberson et al., 2015*). The origin of this tissue-specific sensitivity to loss is not well understood. Phenotypically, several ciliary membrane proteins like ARL13B, PKD2, GPR161, and SMO fail to accumulate in cilia in the absence of MKS components (*Chih et al., 2011; Dowdle et al., 2011; Garcia-gonzalo FR et al., 2011; Roberson et al., 2015; Sang et al., 2011; Yee et al., 2015*). Meanwhile non-ciliary fusion proteins GFP-CEACAM-1, which are normally excluded by the diffusion barrier, gain access to the ciliary membrane in MKS mutants (*Chih et al., 2011*). Similarly, *C. elegans* cilia fail to exclude non-ciliary proteins in the absence of MKS complex proteins like TCTN-1(*Williams et al., 2011; Yee et al., 2015*). Thus, the transition zone is required to both restrict non-ciliary proteins from cilia as well selectively facilitate ciliary cargo import into cilia; mutations in components of the transition zone disrupt this gating function.

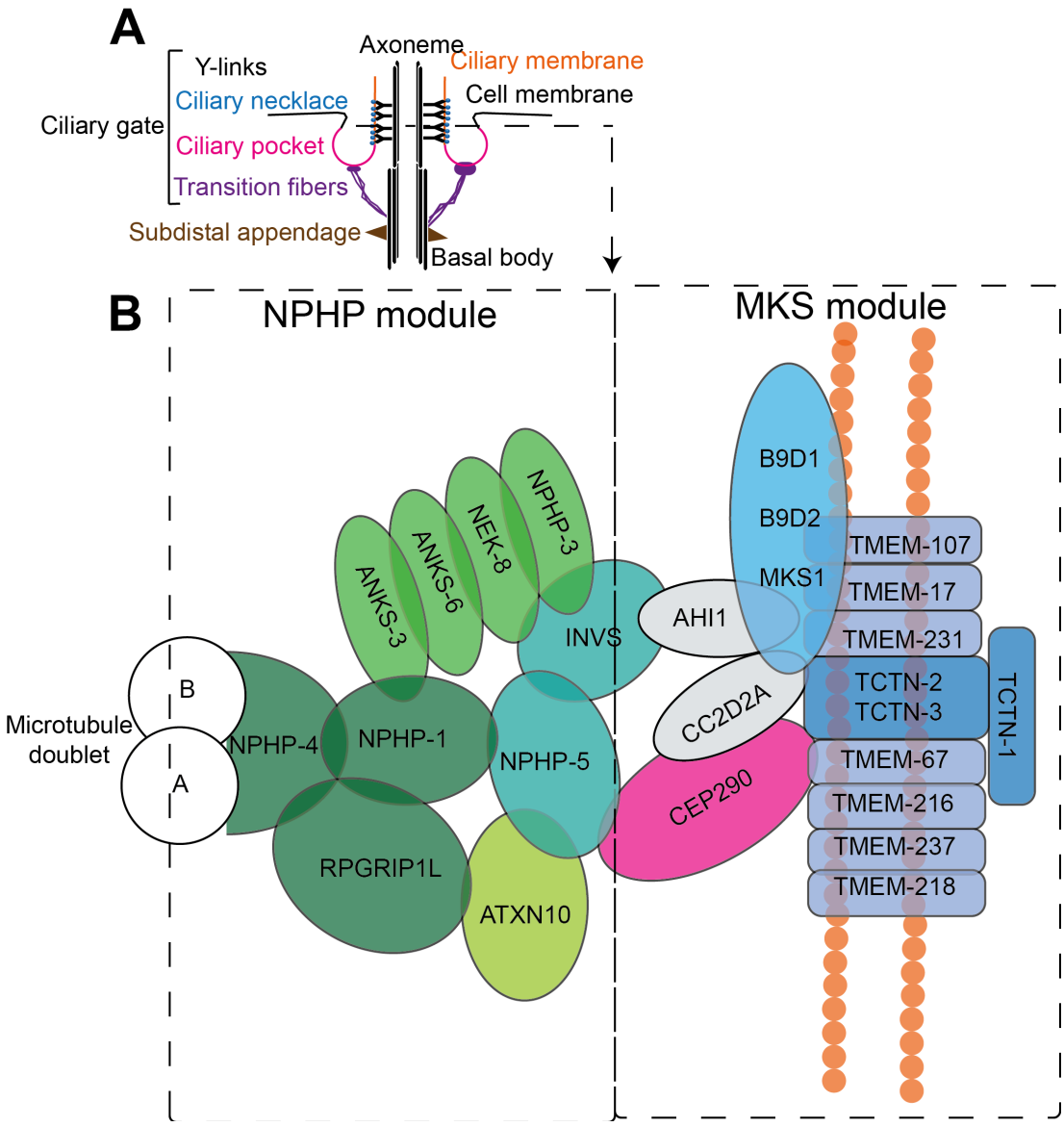

Figure 1.2. Schematic for higher magnification overview of the protein complex arrangement at the transition zone of cilia. (A) A cross-section through ciliary axoneme at the level of the ciliary gate. Here, the transition zone constitutes the ciliary necklace and Y-links between axoneme and ciliary membrane. **(B)** Zoomed in view of the schematic arrangement of protein complexes making transition zone including the MKS module (shades of blue) which is closest to the ciliary membrane and the NPHP module (shades of green), which lies closer to the microtubule doublets. These two modules are linked by NPHP-6/CEP290 (magenta) as well as the inversin complex (teal). (B) is adapted from (Garcia-Gonzalo FR and Reiter JF, 2017).

Mutations in MKS components also result in Joubert syndrome, a ciliopathy characterize by brainstem abnormalities and hypoplasia of cerebellar vermis (*Joubert et al., 1999*). Cells from some Joubert syndrome patients have defects in the transition

zone and ciliary membrane composition (*Shi et al., 2017*), which may suggest that defects in transition zone structure/function might underlie cilia defects in a subset of Joubert's patients. To date, many proteins have been identified as belonging to the MKS module; these include the three Tectonic proteins (TCTN-1, TCTN-2, TCTN-3), the three B9 domain proteins (MKS1, B9D1, B9D2), several coiled-coil proteins CC2D2A, and AHI1, as well as a growing list of transmembrane proteins including TMEM67, TMEM216, TMEM17, TMEM231 and TMEM107, plus possibly others like TMEM237 and TMEM218 (*Barker et al., 2014; Chih et al., 2011; Garcia-gonzalo FR et al., 2011; Huang et al., 2011; Lambacher et al., 2017; C. Li et al., 2016; Roberson et al., 2015; Wood et al., 2012*) (**Figure 1.2**).

The NPHP module (nephronophthisis): The other transition zone protein complex is the NPHP module, which includes NPHP1, NPHP4, and RPGRIP1L. Mutations in these components mostly result in nephronophthisis (NPHP) (*Arts et al., 2007; Mollet et al., 2005; Sang et al., 2011*). Super-resolution imaging reveals spatial segregation of these modules within the transition zone; the MKS complex proteins are closer to the ciliary membrane, whereas the NPHP complex proteins are closer to axoneme, with CEP290 (NPHP6) connecting both of the complexes (*Garcia-Gonzalo FR and Reiter, 2017*) (**Figure 1.2**). Inversin is another such linker hub, connecting the MKS and NPHP modules to the inversin/NPHP3/NEK8/ANKS6/ANKS3 complex (*Czarnecki et al., 2015; Hoff et al., 2013; Leettola et al., 2014; Sang et al., 2011; Yakulov et al., 2015*). Other oligomeric proteins like SEPT2 and SEPT7 might also co-operate to regulate transition zone, where they have been proposed to form a diffusion barrier (*Fliegauf et al., 2014; Hu et al., 2010; Kim et al., 2010*).

In summary, the transition zone is a hub of a huge number of protein complexes, which are all mostly associated with ciliopathies. However, their functional significance in restricting or facilitating cilia-specific transport based on their biochemistry and their relative arrangement to each has only recently been possible with the advent of super-resolution and CLEM (correlative light and electron microscopy) imaging (*Shi et al., 2017*).

How does ciliary cargo cross these diffusion barriers? Depending on the type of cargo being imported, different mechanisms exist to allow for selective transport across. For example, lipid-modified membrane-associated proteins are transported

across the barrier by PDE6δ/UNC119b, ARL3, ARL13B, and RP2 mediated pathway (see **Section 3.1.8**). In contrast, transmembrane proteins are transported across the diffusion barrier by TULP3 and IFT-A complex or via the BBSome complex (see **Section 1.3.2**). Lastly, the transport of soluble proteins depends on microtubule motor proteins and their IFT adaptors. For ciliary entry, ciliary proteins can associate with heterotrimeric kinesin-2 (comprised of KIF3A, KIF3B, and KAP) or with monomeric KIF17, whereas ciliary exit is mediated by cytoplasmic dynein 2 (*Verhey et al., 2011*). Heterotrimeric kinesin-2 co-ordinates with IFT-B complex (see **Section 1.5**) to transport proteins from the ciliary base to tip. These include soluble cargos like tubulin, as well as outer dynein arms and partially pre-assembled radial spoke complexes, which are two large macromolecular assemblies required for flagellar motility in *Chlamydomonas (Bhogaraju et al., 2013; Craft et al., 2015; Hou et al., 2007; Qin H et al., 2004*). KIF17, however, is not required for ciliogenesis and in contrast, is imported into cilia by interactions with both Importin-β2 and RAB23 (*Dishinger et al., 2010; Leaf and Zastrow, 2015; Lim and Tang, 2015*). Involvement of Importin-β2 and presence of nucleoporins at the base of cilia has led to the model that protein transport into cilia may be biochemically and functionally similar to that through the nuclear pore complex (*Breslow et al., 2013; Dishinger et al., 2010; Kee et al., 2012; Takao et al., 2014*). However, nucleoporins arrange as an octameric ring at the nuclear pore, and no such organization is reported at cilia base in ultrastructure studies.

Apart from motor-dependent transport of soluble proteins, some small soluble proteins can also diffuse through the diffusion barrier. For example, proteins and dextrans of about 70kDa can passively diffuse into cilia (*Breslow et al., 2013; Calvert et al., 2010*). In a steady-state cilium, intake of material into the ciliary compartment must be further counterbalanced with the removal of proteins and membranes to allow for efficient signal transduction as well as structural integrity, which is in part regulated by retrograde IFT.

1.1.5 Intraflagellar transport (IFT) in regulation of ciliary content and structure

IFT is essential for the assembly, maintenance, and disassembly of cilia. IFT was first observed by differential interference contrast (DIC) microscopy in 1990 (*Pazour and Rosenbaum, 2002; Brazelton et al., 2001*) in *Chlamydomonas* flagella, where particles were seen moving along the axoneme at anterograde speeds of nearly 2μm/sec and 3.5μm/sec for retrograde traffic. Genetic mutants in either –B or -A components also have distinct phenotypes on cilial/flagellar structure: IFT-B mutants had reduced or no cilia formation (*Brazelton et al., 2001; Hou et al., 2007; Pazour et al., 2000*), whereas, temperature-sensitive IFT-A mutants had short swollen axoneme bulging with accumulations of IFT-B components (*Iomini et al., 2009; Piperno et al., 1998*), similar those observed for the cytoplasmic dynein-2 motors (*Pazour et al., 1999, 1998*). As such, IFT-B was designated to be required for anterograde transport along the axoneme whereas IFT-A was proposed to be involved in retrograde transport from the cilial tip back into the cell body, a model that holds true today (**Figure 1.3A**). However, defining overlapping and distinct functions for each IFT component within a particle remains unclear. Biochemical isolation of IFT–B and -A sub-complexes was also first done in algae (*Piperno and Mead, 1997*). Biochemical fractionation at a higher ionic salt concentration stripped IFT particles into the salt-stable inner "core" complex from the weaker-associated members of the complex, known as the "peripheral" components. In this manner, IFT-A is biochemically divided into 3 core (IFT140, IFT144, and IFT122) and 3 peripheral proteins (IFT121, IFT139, and IFT43). Similarly IFT-B is defined as a salt-stable core complex of 10 proteins (IFT88, -81, -74, -70, -52, -46, -27, -25, -56 and -22) and 6 peripheral members (IFT172, -80, -54, -57, -20 and -38) (*Follit et al., 2009; Lucker et al., 2005*). However, it how proteins within the IFT-B and IFT-A core and peripheral components interact with each other and specifically select hundreds of ciliary cargos remains largely unknown.

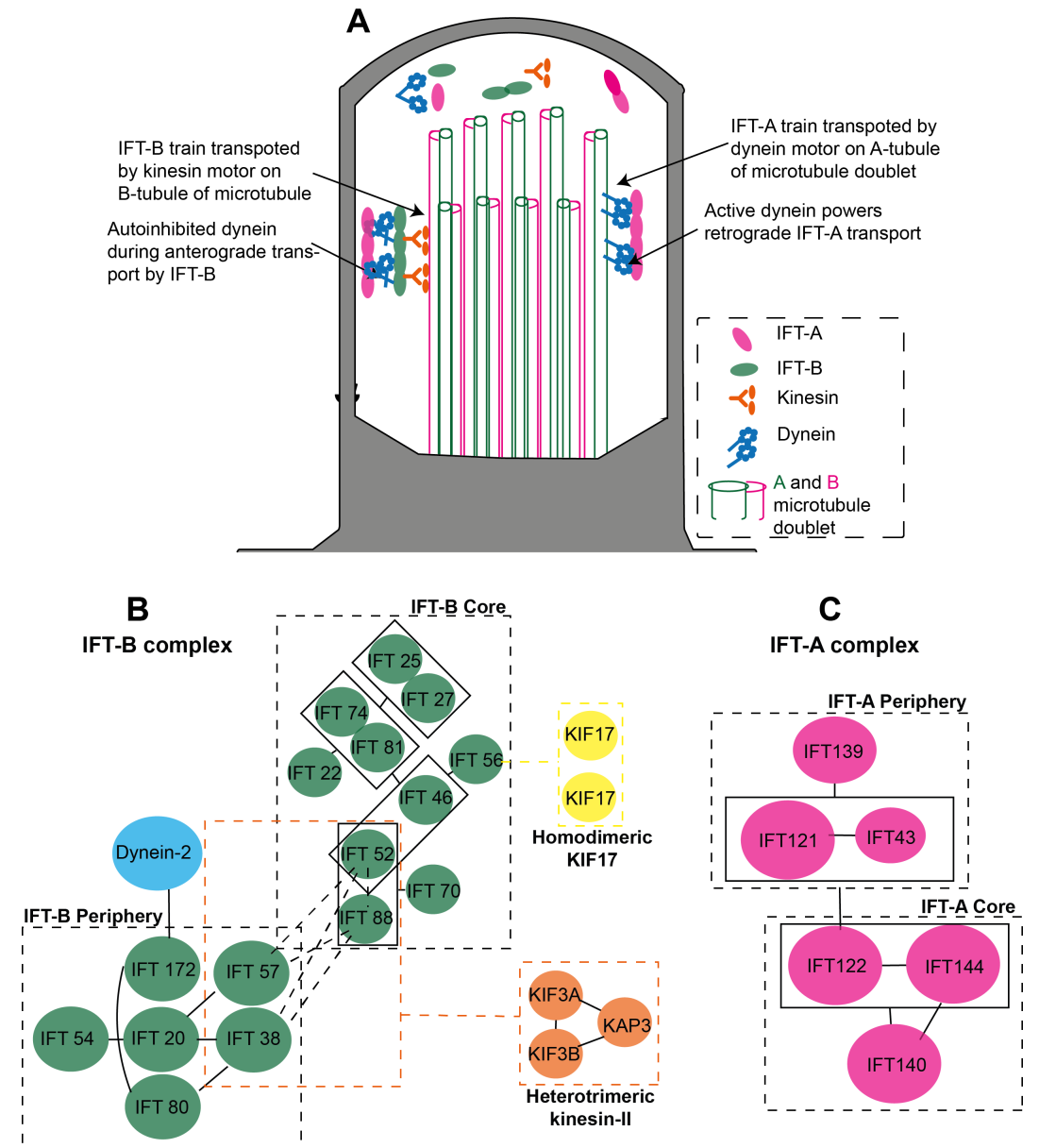

Figure 1.3. Schematic for intraflagellar transport (IFT) pathway in cilia. (A) IFT-B complex protein (green) aid in anterograde transport with the kinesin motor(s) (orange) and IFT-A complex proteins (magenta) help in retrograde transport from cilia along with dynein motor (blue). IFT-B and IFT-A train walk on B- and A- tubules of the doublet respectively to avoid a steric clash between trains moving in the opposite direction (*Stepanek and Pigino, 2016*). IFT-B complex also transports IFT-A proteins and dynein motors from base to tip of cilia and are seen in cryo-EM to have 11:6:18 periodicity of IFT-B:IFT-A: Dynein motors (*Jordan et al., 2018*). To avoid competition with kinesin binding to microtubules, dynein is transported in autoinhibited conformation during anterograde trafficking and takes an open and active conformation during retrograde transport (*Jordan et al., 2018*). Arrangements of subunits of IFT complexes has been extrapolated from (B) IFT-B complex *(Funabashi et al., 2018, 2017; Katoh et al., 2016; Mourão et al., 2016; Pedersen et al., 2006*) and (C) IFT-A complex (*Hirano et al., 2017*).

Broadly the IFT-B complex is sub-divided in two modules B1 and B2 interconnected by the IFT88-52-57-38 proteins and motor proteins interacting with specific complex proteins (**Figure 1.3B)** (*Funabashi et al., 2018, 2017; Katoh et al., 2016; Mourão et al., 2016; Pedersen et al., 2006; Taschner M et al., 2016*). In vitro biochemical experiments have provided a rough plan of IFT-A protein arrangement (*Takahara et al., 2018*) (**Figure 1.3C**). There are a few examples known for IFT cargo interactions. These include for IFT-B: outer dynein arm transport by IFT46 *(Ahmed et al., 2008*); tubulin transport by IFT81/74 (*Bhogaraju et al., 2013*) and IFTB2 complex (*Taschner M et al., 2016*); IFT172 interaction with dynein-2 (*Pedersen et al., 2006; Roberts, 2018; Tsao and Gorovsky, 2008; Williamson et al., 2012*); kinesin-II trimer KIF3A–KIF3B–KAP3 interaction with IFT-B connecting tetramer IFT38–IFT52–IFT57–IFT88 (*Funabashi et al., 2018*); KIF17 binding to the IFT-B complex via the IFT46–IFT56 dimer (*Funabashi et al., 2017*), IFT20 interaction with the Golgi protein GMAP210 (*Follit et al., 2008*)and Rabaptin-5 (*Omori et al., 2008*); and various motility-related factors by the IFT56 (*Ishikawa et al., 2014*). In the case of IFT-A, a role in the transport of membrane protein cargos has been suggested for IFT144 (*Liem KF et al., 2012*) , IFT122 (*Takahara et al., 2018*) and IFT121/WDR35 (*Caparrós-Martín JA et al., 2015; Fu W et al., 2016; Hirano et al., 2017*). The IFT-A complex as a whole has also been shown to be critical for import of many ciliary membrane proteins (*Badgandi HB et al., 2017; Mukhopadhyay et al., 2010; Ye F et al., 2018*). IFT-A has recently also been shown to interact with the IFT-B train *in situ*; a periodicity of 11nm:6nm for IFTB: IFTA was observed by cryo-EM of *C. reinhardtii* flagella (Jordan et al., 2018) (**Figure 1.3A**). It is proposed that IFT-As and dynein motor proteins are passively carried from base-to-cilia tip by IFT-B trains in association with kinesin motors. Interestingly, while kinesin and dynein bind to the complex at the same time, in order to avoid accessing the microtubules too early during anterograde transport, the dynein motors adopt an autoinhibited conformation *(Jordan et al., 2018*) (**Figure 1.3A**). The complex disassembles at the cilia tip, where the IFT-A complex proteins remodel to form a retrograde train to export cargo out of cilia. Interestingly, both the anterograde trains (IFT-B) and retrograde (IFT-A) trains are choreographed to walk on different microtubule tracks with IFT-B walking on B-tubule and IFT-A walking on A-tubule to avoid collisions between trains moving in

opposite directions (*Stepanek and Pigino, 2017*) **(Figure 1.3A)**. Deciphering individual interactions between IFT-B and IFT-A subunits, as well as their cargo specificities will be a key area of future research.

IFTs share a high degree of conservation among ciliated organisms, implying a universal role in protein trafficking in cilia and flagella (*Jékely G and Arendt D, 2006*). IFT components need to interact not only with each other to form IFT particles and then higher-order trains, but also with the appropriate molecular motors as well as cargo proteins. This would likely require a significant number of protein-protein interaction surfaces. Some structural studies of IFT complexes have been done to date. These include electron tomographic reconstructions of IFT trains *in vivo* (*Jordan et al., 2018; Pigino et al., 2009; Stepanek and Pigino, 2017*); cryo-EM Structure of the dynein-2 complex and its assembly with IFT trains (*Toropova et al., 2019*), high-resolution X-ray crystal structures of sub-complexes including IFT27/25 (*Bhogaraju et al., 2011*); IFT70/52 and IFT52/46 (*Taschner M et al., 2014*); individual domains such as the N-terminus of IFT81 (*Bhogaraju et al., 2013*); IFT52-N terminal domain and IFT54 CH domain (*Taschner M et al., 2016*); and IFT80 (*Taschner M et al., 2018*); and a proposed structure of IFT172 by negative stain EM (*Wang et al., 2018*). Moreover, bioinformatics analysis of IFT proteins shows clear enrichment of protein-protein interaction domains such as TPRs (tetratricopeptide repeats), WD40 repeats, and coiled-coils (*Taschner M et al., 2012*). No crystal structures have been yet reported for IFT-A proteins, but bioinformatics predictions show a similar enrichment of these interaction interfaces (i.e.WD40 repeats, TPR repeats and coiled-coil domains), importantly with no recognizable enzymatic activity domains. Further structural analysis of IFTs individually or in the complex will provide a great deal of mechanistic information.

Assignment to either IFT-B or -A complex has been done biochemically, but phenotypic analysis of some individual components suggests functional assignments may not be so clear cut. For example, the IFT-B component IFT172 has a retrograde IFT mutant phenotype (*Iomini et al., 2001*). Another IFT-B protein, IFT27, has been proposed to be involve in the export of BBSomes from cilia (*Liew et al. 2014*), what should be a retrograde function. Similarly, inactivation of the IFT-B component IFT22 results in the retrograde phenotype of short flagella packed with IFT material

(*Adhiambo et al., 2009*). Similarly, anterograde functions have been reported for IFT-A proteins (*Badgandi HB et al., 2017; Caparrós-Martín JA et al., 2015; Fu W et al., 2016; Hirano et al., 2017; Liem KF et al., 2012; Mukhopadhyay et al., 2010; Takahara et al., 2018; Ye F et al., 2018*) (see **Section 1.1.6** and **Section 1.3.2**). Defining the function(s) of individual IFT proteins remains an important open question towards understanding the transport pathways into and from cilia.

1.1.6 The emerging functions of IFT-A in the transport of ciliary membrane protein cargos into cilia

Intraflagellar transport proteins (IFT) are highly conserved trafficking modules required for the assembly and maintenance of cilia (*Cole, 2009; Rosenbaum and Witman, 2002*). They are classified in two different complexes: the IFT-B complex (consisting of 16 proteins) which helps in anterograde transport (from cell body to cilia tip) of cargo with the help of kinesin motors and the IFT-A complex (consisting of 6 proteins) which helps in retrograde transport (from cilia tip to cell body) of cargo driven by dynein motors. The IFT-A complex is composed of 3 biochemically defined core proteins (IFT144/WDR19, IFT140, IFT122/WDR10) and 3 peripheral proteins (IFT139/TTC21B/THM1, IFT121/WDR35, and IFT43). Some of the IFTA and IFTB structures and functions have been described both in-vitro and in-vivo before which forms an important basis for future research (see **section 1.5**).

Apart from retrograde defects (see **Section 1.1.5**), several IFT-A mutants show very severe ciliary and as a consequence, severe developmental defects. IFT144, IFT140, IFT121/WDR35, and IFT43 mutations result in either reduction in cilia length or complete loss of cilia (*Caparrós-Martín JA et al., 2015; Duran et al., 2017; Hirano et al., 2017; Liem KF et al., 2012; Mill et al., 2011; Takahara et al., 2018; Zhu et al., 2017*) which implies there importance in the transport of cargo to cilia. Our lab previously demonstrated that null mutations in human and mouse *Ift121*/*Wdr35* result in mid-gestation lethality due to loss of cilia and leading to a short-rib polydactyly syndrome (SRPS) (*Mill et al., 2011*). Wdr35 mutation in humans results in atypical short-rib polydactyly syndrome characterized by postaxial polydactyly, extreme micromelia, and short ribs (*Mill et al., 2011*). *Wdr35* null mice used in this thesis were generated by ENU screen for genes involved in embryonic patterning. They were found to have a G>A mutation in the splice acceptor of exon 22 and were shown in

our lab before to be null for WDR35 based on mRNA and protein levels. Mutant mice exhibited randomized laterality, craniofacial defects, and polysyndactyly, exhibited hedgehog signaling defects, were midgestational lethal, and died before E12.5 (*Mill et al., 2011*). Later WDR35 pathogenic variants were also found in patients with a distinct form of Ellis-van Creveld syndrome, which resulted from defects in the transport of critical ciliary proteins to cilia (*Caparrós-Martín JA et al., 2015*). Further on it was shown that *Wdr35*$^{-/-}$ cells fail to localize a range of ciliary membrane proteins like EVC1, EVC2, SMO, ARL13B, INPP5E, SSTR3 and serotonin to cilia (*Caparrós-Martín JA et al., 2015; Fu W et al., 2016*). All three core IFT-As have similarly been reported to disrupt the transport of membrane proteins into cilia. IFT144 helps in the transport of ARL13B to mammalian cilia (*Liem KF et al., 2012*) while IFT140 is required to transport guanylyl cyclase into *C. elegans* cilia (*Jensen et al., 2010*) and the ion channel TRPV to *Drosophila* cilia (*Lee et al., 2008*). IFT144 has been proposed to aid interactions between IFT-A and IFT-B during their turnaround at the tip and base of cilia (*Wei et al., 2012*). *IFT122* null RPE cells fail to accumulate Smoothened in cilia, even after Hh ligand stimulation (*Takahara et al., 2018*). Human disease mutations have been reported in every component of the IFT-A complex, with a range of severities likely reflected how much protein function remains **(Table 3.1)**. The multiorgan defects attest to the critical importance of IFTAs in cilia assembly and function in all mammalian tissues. Moreover, along with other defects, IFT-A mutations exhibit a set of similar etiology, indicating their co-ordinating function. (**Table 3.1**).

Table 1.1 Ciliopathies caused by mutations in IFT-A gene

IFT-A	ATD/ Jeune syndrome	SRPS/ SRTD	CED	Other ciliopathies
IFT144/ WDR19	Sensenbrenner and Jeune syndrome (Ashe et al., 2012)	SRTD	CED	Senior-loken Nephronophthisis
IFT140	Mainzer-Saldino and Jeune syndrome (Perrault et al., 2012)	SRTD		Retinitis Pigmentosa
IFT122/ WDR10			CED	
IFT121/ WDR35		SRPS (Mill et al., 2011) and SRTD	CED	
IFT139/ TTC21B	Jeune syndrome (Davis et al., 2011)			Nephronophthisis (Davis et al., 2011)
IFT43		SRPS (Duran et al., 2017)	CED (Duran et al., 2017)	

Where SRPS is short rib polydactyly syndrome, SRTD is short rib thoracic dysplasia, CED is cranioectodermal dysplasia, and ATD is asphyxiating thoracic dystrophy. Data is compiled from the OMIM database and references listed in the table.

Although the IFT complex is highly conserved in eukaryotes, the full repertoire of IFT components is not retained in all species. Least conserved amongst the IFT-As is IFT43 (*Jékely G and Arendt D, 2006*). IFT144, IFT140, IFT122, and IFT121/WDR35 have well-formed structures, whereas IFT139 and IFT43 are made only of TPR repeats (*Taschner M et al., 2012*). IFT121 from here on referred to as WDR35 is well conserved and is known to be part of peripheral IFT-A complex *(Hirano et al., 2017; Piperno et al., 1998*). Our lab has previously shown that WDR35 is essential for embryonic development (*Mill et al., 2011*). Wdr35 null mutant mice are embryonic lethal at E11.5, and loss of WDR35 results in short cilia (*Mill et al., 2011*). Further phenotypic analysis of *Wdr35*$^{-/-}$ MEFs showed short and stumpy cilia similar to retrograde dynein mutants with an additional defect in lack of localized membrane protein in cilia (*Caparrós-Martín JA et al., 2015; Fu W et al., 2016*). WDR35 is

ubiquitously expressed in all cell types and localizes as an enriched pool at the base of cilia extending from the transition zone to cilial tip (*Mill et al., 2011*). How WDR35 regulates cilial composition and transport of membrane proteins in cilia remains unclear. In **chapter 3**, I have characterized the transport defects in different ciliary proteins in *Wdr35*$^{-/-}$ cilia and the assembly defects in components of the IFT machinery. To distinguish canonical function IFT-A in retrograde transport, I compared the *Wdr35*$^{-/-}$ phenotype with a null mutant for the retrograde IFT dynein motor *Dync2h1* (*Criswell et al., 1996; Huangfu D and Anderson KV, 2005; Porter et al., 1999; Signor et al., 1999*).

Dync2h1 is the central ATPase subunit of the IFT dynein-2 complex, the principal minus-end directed microtubule motor (*Schmidt et al., 2015*). Dynein-2 complex drives retrograde transport (tip-to-base) transport in cilia (*Rajagopalan et al., 2013*). Dync2h1 mutations cause asphyxiating thoracic dystrophy and short rib-polydactyly syndrome, and cells derived from patients have short cilia (*Badiner et al., 2017*). Dync2h1 null mouse is mid-gestation lethal and displays loss of Shh dependent signaling in embryonic mouse neural tube (*Ocbina et al., 2011*). MEFs derived from embryos had short cilia with accumulated various Shh proteins and IFTs exhibiting typical retrograde defects (*Ocbina et al., 2011*). *Dync2h1*$^{-/-}$ being established as a model for retrograde defects in cilia, is used to distinguish anterograde and retrograde functions of WDR35 shown in Chapter-3.

1.2 Function of cilia

1.2.1 Ciliopathies associated with dysfunctional cilia

Cilia and flagella play essential motile and sensory function, which are not only crucial for normal physiological functions but are also critical for healthy embryonic development. Dysfunction of cilia results in a wide range of diseases including kidney disorders like polycystic kidney disease (PKD) and Nephronophthisis (NPHP), primary ciliary dyskinesia (PCD), retinitis pigmentosa (RP), short rib polydactyly (SRP), situs invertus, cognitive impairment, hepatic disease, brain defects and obesity. The first mammalian model to stablish connection between ciliopathies and cilia was the insertional mutation *Ift88* mouse model called Oak ridge polycystic kidney mouse, which was initially described as a model for human recessive polycystic kidney disease

(*Lehman et al., 2008*). It is a hypomorphic allele (*Tg737*) of *Ift88*, which disrupts IFT88 protein expression and function. Mutant phenotypes include growth retardation, hydrocephalus, cerebellar hypoplasia, skeletal defects including polydactyly, degenerated retina, hepatic and pancreatic ductal cysts, dishevelled fur and late-onset obesity (*Lehman et al., 2008*). Since then, the spectrum of ciliopathies has widened, and interestingly mutations in the same gene can give rise to different syndromes (*Baala et al., 2007; Bergmann et al., 2008; Hoefele et al., 2007; Leitch et al., 2008; Reiter and Leroux, 2017; Wheway and Mitchison, 2019*), which makes classification and diagnosis of ciliopathies tricky. However, attempts have been made to group them into classes with overlapping phenotypes and pathophysiology (*Badano et al., 2006; Baker and Beales, 2009*).

Classification of ciliopathies is mostly based on either cilia type (motile or sensory) or on phenotypic similarity (for example skeletal abnormalities, obesity). Another challenge is to identify novel ciliopathy phenotypes in clinic, which could be done by correlating them with existing defects. Almost 40 syndromes have been attributed to mutations in one of nearly 200 cilia genes, whose symptoms include RP, renal cysts, polydactyly or brain abnormalities (*Baker and Beales, 2009; Reiter and Leroux, 2017*). As ciliopathies are an extensive phenotypic group of overlapping syndromes arising from the disruption in cilia structure and/or function, understanding the functional and biochemical networks involved in these complex organelles is key to understanding disease mechanisms. Some ciliopathies affect only specific tissues like the kidney (i.e. PKD) or photoreceptors (i.e. RP), even though some of the genes affected by these mutations are very broadly expressed (*Reiter and Leroux, 2017; Waters and Beales, 2011*). This suggests cell-type specific functional redundancy or tissue-specific isoforms may exist for this category of ciliary disease products. Some ciliopathies result from mutations that disrupt lineage-specific cilial differentiation programs, like that for cilia motility in the case of assembly of axonemal dyneins mutated in PCD (*Horani et al., 2016*). As cilia are found in virtually every cell of the human body, mutations disrupting cilia formation can also be very severe, often embryonic or perinatal lethal, as they disrupt essential developmental signaling cascades like Hedgehog (Hh) required for proper neural, skeletal and heart development, as is the case in SRP (*Bangs and Anderson, 2017; Liem KF et al., 2012; Mill et al., 2011*).

Many signaling pathways are dependent on cilia including Hedgehog, Wnt (*Abdelhamed et al., 2013; Adams et al., 2012; Cano et al., 2004; Carvajal-Gonzalez et al., 2016; Dawe et al., 2009; Gómez-Orte et al., 2013; Huang and Schier, 2009; Jones et al., 2008; Lin et al., 2003; Ocbina et al., 2009; Park et al., 2008; Simons et al., 2005; Sorusch et al., 2014; Sugiyama et al., 2011; Valente et al., 2010; Wallingford et al., 2000; Wheway et al., 2013*); Notch (*Andersson et al., 2011; Ezratty et al., 2016, 2011; Grisanti et al., 2016; L. Li et al., 2016; Liu et al., 2019; Stasiulewicz et al., 2015*); Hippo (*Frank et al., 2013; Habbig et al., 2012, 2011; Kim et al., 2014; Lobo et al., 2017*), G-protein coupled receptors (GPCR), platelet-derived growth factor (PDGF) (*Christensen et al., 2012; Jacoby et al., 2009; Nielsen et al., 2015; Schneider et al., 2010, 2005*); as well as other RTKs including fibroblast growth factor receptor (FGFR) , mammalian target of rapamycin (mTOR) (*Boehlke et al., 2010; Qin et al., 2010; Shillingford et al., 2006; Tobin and Beales, 2008; Zullo et al., 2010*); and transforming growth factor beta signaling (TGF-β) to control developmental processes, tissue plasticity and organ function. To co-ordinate the signaling pathways, transmembrane proteins on the ciliary membrane receive the signal and transmit it through receptors at cilia base to the cytoplasm. In this section, I have briefly described Hedgehog signaling since the role of cilia in its signaling has been best described so far.

1.2.2 Regulation of Hedgehog signaling by primary cilia

One of the critical regulators of animal development is the Hedgehog (Hh) signaling pathway, which functions by sending signals to embryonic cells for proper cell differentiation and proliferation (*Varjosalo and Taipale, 2008*). Different parts of the embryo have different concentration of hedgehog signaling protein *(Varjosalo and Taipale, 2008*). It is present in all bilaterians (*Ingham et al., 2011*). Knockout mice lacking components of the pathway have defects in the brain, skeleton, muscle, gastrointestinal tract and lung development. The pathway derives its name from its ligand, an intercellular signaling molecule called hedgehog found in the fruit flies. Larvae with Hh signaling defect are short and spiny and resemble hedgehog animal (*Niisslein-Volhard and Wieschaus, 1980*). Mammals have three Hh homologs, Desert (DHH), Indian (IHH) and Sonic (SHH) of which best described it SHH (*Bangs and*

Anderson, 2017). Other than functions in embryonic development, new studies have shown that Hh signaling play role in regulating adult stem cells. Defects in the pathway have also been implicated in the development of some cancers (*Skoda et al., 2018*).

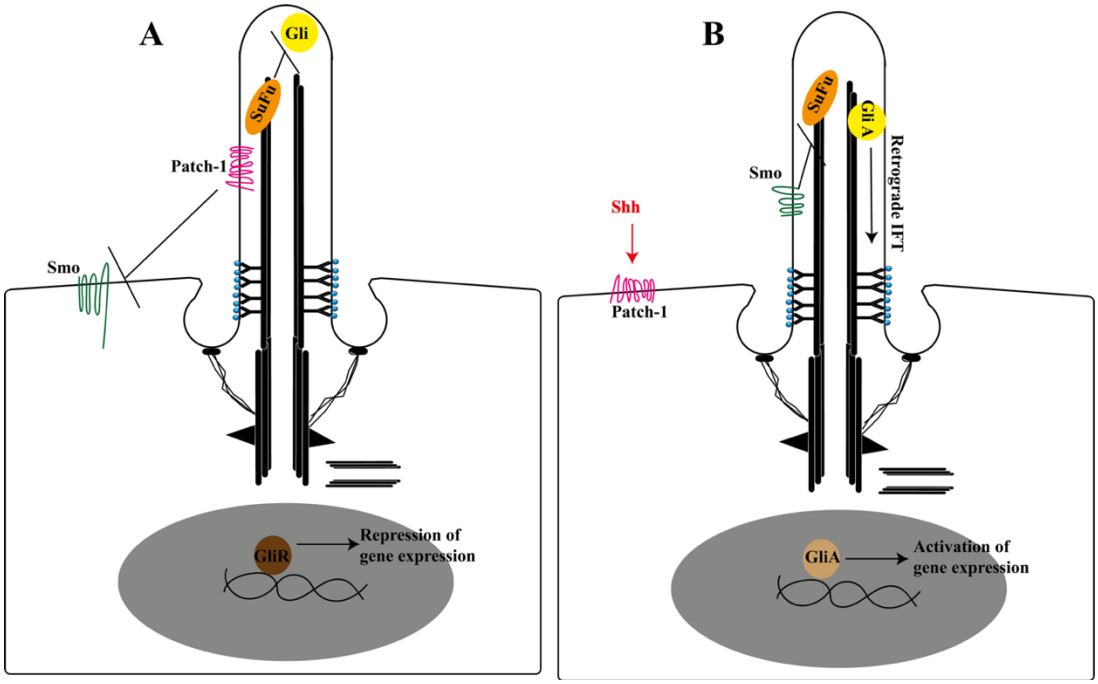

Figure 1.4. Overview of the Sonic hedgehog (SHH) signaling pathway in vertebrates. **(A)** In unstimulated cells Patched1 (PTCH1- magenta) sits at the ciliary membrane and restricts the entry of Smoothened (SMO- green) to cilia. The GLI transcription factors are proteolytically processed to their repressor (GLIR- dark brown)) to inhibit expression of target genes in the nucleus. **(B)** In cells stimulated with Hh ligand (red), PTCH1 is removed from cilia while SMO accumulates in ciliary membrane. Once inside the cilium, SMO activates the GLI transcription factor by repressing suppressor of fused (SUFU- orange). This results in post-translational modification of GLIs to their activator forms (GliA- light brown) and is transported to the nucleus to stimulate expression of downstream target genes.

The primary cilium is essential for regulation of the canonical Hedgehog (Hh) signaling pathway in vertebrates. Patched1 (PTCH1) and Smoothened (SMO) are the GPCRs which are two key components of the Hh signaling pathway that localize to the ciliary membrane. In the absence of ligand, PTCH1 resides in the ciliary membrane and restricts the entry of SMO to cilia. As a result, the GLI transcription factors are proteolytically processed to a repressor form (GLIR) and target genes are turned off. Upon stimulation with one of three vertebrate HH ligands, PTCH1 exits the cilium

whilst SMO accumulates in the ciliary membrane (*Corbit KC et al., 2005*). Once inside the cilium, SMO activates GLI transcription factors by repressing suppressor of fused (SuFu), which restricts GLI to the ciliary tip. GLI transcription factors are then post-translationally modified to potent activator forms (GliA) whereby they are transported to the nucleus to activate expression of downstream target genes (**Figure 1.4**) (*Corbit KC et al., 2005; Haycraft et al., 2005; Rohatgi R et al., 2007; Zeng et al., 2010*). More recently, an additional negative regulator of Hh signalling was identified and found to localize to primary cilia in a TULP3/IFT-A-dependent manner *(Mukhopadhyay et al., 2013*). Similar to PTCH1, this highly conserved G-protein-coupled receptor GPR161 is internalized from cilia on Hh ligand binding. In the absence of GPR161, levels of Shh signaling are ectopically activated whereas constitutive GPR161 activity increases cAMP levels via protein kinase A (PKA) promoting the processing of Gli3 to its potent repressor form. To date number of ciliary proteins have been reported to be essential for hedgehog signaling (*Bangs and Anderson, 2017*) and a genome-wide RNA interference (RNAi) screen revealed a number of Hh pathway genes which, when knocked down, led to cilia disassembly (*Jacob et al., 2011*).

Hedgehog signaling molecules are transported in and out of cilia with the help of IFT proteins and their associated motor proteins (*Huangfu D et al., 2003*). IFT proteins were subsequently shown to function upstream of Hh signaling gene target and downstream of PTCH1(*Huangfu D et al., 2003*). Loss of IFT122 proteins result in accumulation of GLI2 and GLI3 at the cilium tip (*Qin J et al., 2011*), and downregulation of *Patched1* target gene expression (*Beales et al., 2007*). Additionally, IFT80 has been shown to inhibit not only canonical hedgehog signaling by inhibiting Smoothened localization to cilium but to promote non-canonical Hh-Gαi-RhoA stress fiber signaling in differentiating osteoblast (*Yuan et al., 2016*). However, more recent studies suggest that activation of Gαi or RhoA by SMO in the non-canonical Hh signaling pathway is independent of primary cilia (*Ho Wei et al., 2018*).

Importantly defects in cilia result both in loss of GLI activator phenotypes like in the neural tube where Gli2 activator typically play a significant role in inducing ventral cell types, as well as loss of GLI repressor phenotypes like in the developing limb bud where Gli3 repressor regularly plays a significant role in patterning digit identity (*Bai et al., 2002; Haycraft et al., 2005; Huangfu D and Anderson KV, 2005; Wang et al.,*

2000). As primary cilia have both positive and negative effects on Hh signaling, loss of cilia may affect signaling outcomes differently including loss of induction of some Hh target genes, versus lack of repression of expression of others. The effect of this target gene misexpression will dependent on the cell type.

There also appears to be role for cilia in both promoting and suppressing Hh-dependent cancers. In some cancer types, where Hh signaling is upregulated, tumour cells are reported to have lost cilia compared to its surrounding tissue, which can have either a positive or negative effect on tumour growth depending if tumor is driven by SMO or GLI activation, respectively (*Han et al., 2009; Kim et al., 2011; Moser et al., 2009; Seeley et al., 2009; Wong et al., 2009; Yuan et al., 2010*). While functional cilia are required for vertebrate Hedgehog signal transduction during development, much less in known about how cilia function in these Hh dependent cancers and adult homeostasis and repair (*Petrova and Joyner 2014*). Further studies will be required to resolve these issues.

1.3 Vesicular trafficking and its role in the formation of functional cilia

1.3.1 Classic coatomers in vesicular trafficking: COPI, COPII, and clathrin

In eukaryotes, different spatially and functionally segregated cellular compartments exchange cargo by vesicular transport. Most transport vesicles form from specialized "coated" regions of the membrane that bud off as coated vesicles. The root mechanism for budding of small vesicles by respective coat proteins from the donor compartment is more or less the same (*Bonifacino and Lippincott-schwartz, 2003; Kirchhausen, 2000*). In general, the specific coat proteins polymerize on the donor membrane, generating membrane curvature and finally pinch off the vesicles containing cargo. Three mechanisms exist for generating membrane curvature: (a) membrane deformation by proteins exerting mechanical force ; (b) curvature generation by scaffolding protein (coat-proteins) and (C) curvature generation by insertion of hydrophobic domains of proteins, also known as wedging (*Shibata et al., 2009*). Next, these vesicles either diffuse or are transported along the microtubules to the acceptor compartment where they fuse with its membrane compartment. RAB GTPase and SNARE proteins facilitate the fusion of vesicles to the specific target organelle

membranes. COPI, COPII, and clathrin are the three archetypical protein coatomer complexes, which help the vesicle budding process (*Kirchhausen, 2000*) (**Figure 1.5)**.

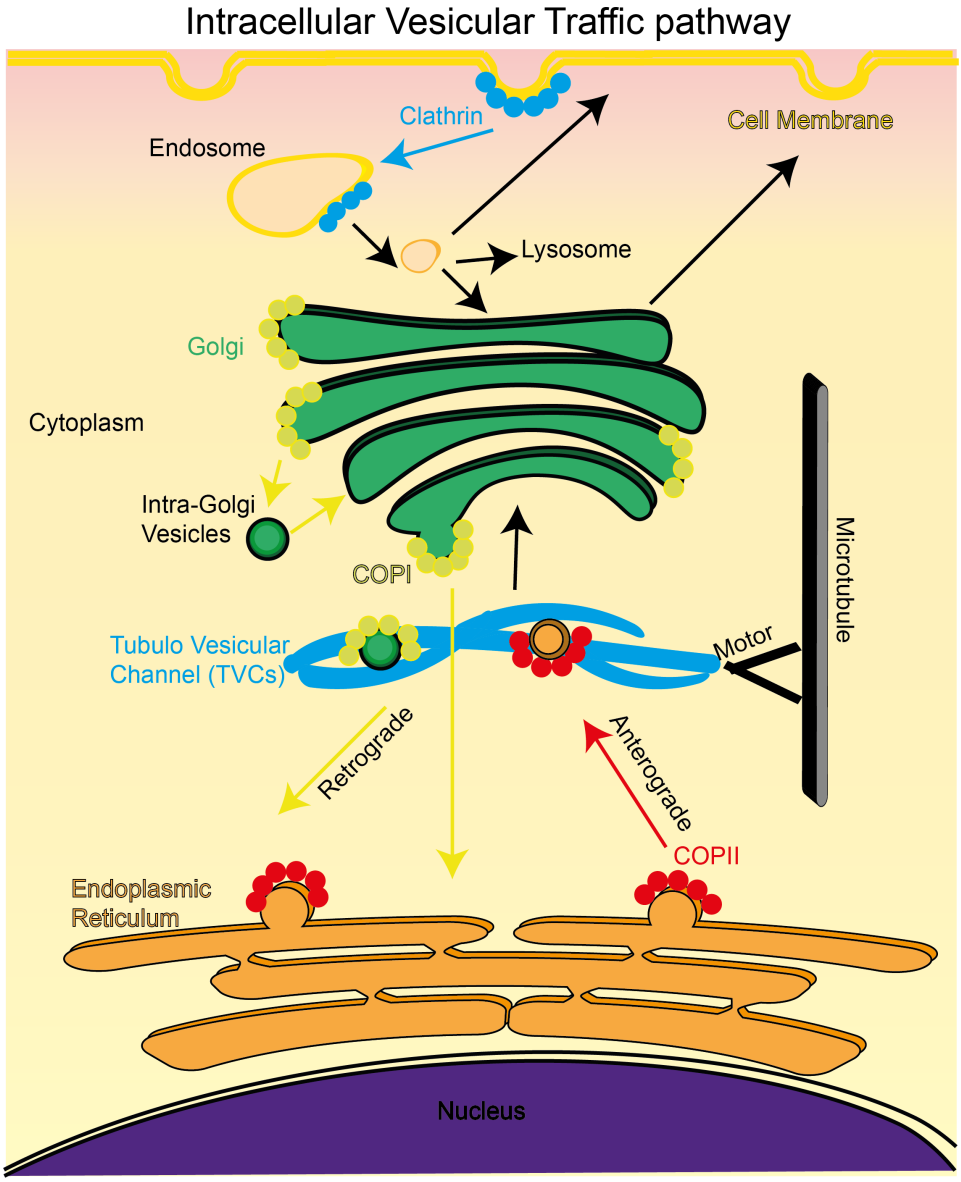

Figure 1.5. Three canonical coat protein complexes mediating the intracellular trafficking pathway: Diagrammatic representation of trafficking between functionally segregated membrane compartments- the ER, TVCs, the Golgi and cell membrane, highlighting the vesicular transport between them. COPII initiates vesicle budding from the ER and collects and transports cargo to the Golgi (anterograde transport). Between ER and Golgi, some COPII vesicles fuse to form TVCs. COPI coats bud off vesicles from the TVCs to return ER resident proteins to the ER. COPI also buds off vesicles from the Golgi to transport proteins between Golgi stacks (intra-Golgi) and to the ER (retrograde transport). Clathrin mediates transport between the cell membrane and the Golgi. Vesicles and TVCs can diffuse or walk along microtubules via motor proteins.

These different coated vesicles mediate distinct transport steps within the secretory pathway. COPII transports cargo from ER to Golgi (*Barlowe et al., 1994; Lee et al., 2004; Lord et al., 2013*). COPI transports intra-Golgi cargo as well as cargo in the retrograde Golgi to ER transport (*Letourneur et al., 1994; Malhotra et al., 1989*). And clathrin is known to bud off the cargo from the plasma membrane and Golgi to the endocytic pathway (*Ina Hinners and Tooze SA, 2003*) (**Figure 1.5**). The cytoplasmic proteins which form these coats not only play a role in pinching off the vesicles with cargo but also play a role in the initial recognition of specific cargo. In this section, I describe the structure, function, and evolutionary relation of these three coats.

COPII coat: Despite similar general principles underlying their functions, all three coat complexes are built of a different set of proteins arranged as distinct lattice structures. The COPII coat is made of five proteins SAR1, SEC23, SEC24, SEC13, and SEC31, which arrange sequentially in two layers, as shown in (**Figure 1.6**). SEC23, SEC24, and GTPase SAR1 make the inner adaptor layer and the outer cage forming layer is made of SEC13 and SEC31. SAR1, a RAS-superfamily small GTPase initiates the COPII coat assembly. ER resident protein SEC12 activates SAR1 by facilitating GDP to GTP exchange. Upon activation, the N-terminal amphipathic helix of SAR1 becomes free to be embedded in the lipid bilayer of the ER membrane (*Lee et al., 2005*). SAR1, while inserted in the ER membrane, recruits the SEC23-SEC24 heterodimer by interacting with SEC23 to the membrane completing the inner adaptor layer of the COPII complex (*Matsuoka et al., 1998*). SEC24 binds to membrane proteins in ER by directly interacting with their ER export signals as well as lumenal proteins in ER by interacting with cognate receptor proteins carrying ER luminal proteins (*Miller et al., 2002*). SEC24 and its isoforms have many different cargo binding domains to select and bind different types of sorting signals. This inner layer of SAR1-SEC23-SEC24 polymerizes as a bowtie-shaped structure on the ER membrane. Following this, a SEC13-SEC31 heterodimer forms the outer cage layer by SEC31 and SAR1-SEC23 interaction (*Bi et al., 2007*) (**Figure 1.6A**). SEC13 and SEC31 both have N-terminal amphipathic WD40 repeat domains which polymerizes to form a cage where four rods come together to form a vertex (*Bhattacharya et al., 2012; Noble et al., 2013; Stagg et al., 2008, 2006; Zanetti et al., 2013*) (**Figure 1.6A**). This outer tetraskelion cage is assumed to concentrate the inner layer. In order to pinch

off the vesicle by COPII coat assembly, the SAR1 amphipathic helix insert in the lipid bilayer. This curves the membrane by wedging which is further scaffolded by the SEC13-SEC31 heterodimer (*Noble et al., 2013; Zanetti et al., 2013*). COPII coated vesicles then travel to fuse directly with Golgi in plants and yeast, where the Golgi is close to the ER. In mammalian cells, in contrast, where the Golgi is at some distance from the ER, COPII vesicles take a stopover at an additional transient structure called vesicular-tubular channel (VTC) (**Figure 1.5**). The VTC is formed on the way to the Golgi when COPII vesicles fuse to form a series of a convoluted membranous structure as reported in EM (*Appenzeller-Herzog and Hauri, 2006; Schweizer et al., 1988*). The VTC is a separate compartment, biochemically different from the ER, which lacks proteins which function in ER and is meant to direct cargo transport from ER-to-Golgi and return ER resident proteins to ER in COPI coated vesicles. Thus soon after the VTC forms, it starts to bud of the vesicles which are no longer coated with COPII but are COPI-coated to direct transport of cargo back to ER for retrograde vesicular transport (**Figure 1.5**).

COPI coat: COPI functions in retrograde transport of cargo from Golgi-to-ER and between different cisternae of Golgi (intra-Golgi transport) (*Letourneur et al., 1994; Malhotra et al., 1989*). COPI coats capture ER resident proteins by ER retrieval signals, which are K(X)KXX in ER membrane proteins (*Jackson et al., 2012; Ma and Goldberg, 2013*) and K/HDEL in ER luminal proteins to return them to the ER (*Banfield, 2011; Pastor-Cantizano et al., 2017; Silva-Alvim et al., 2018*). Seven different proteins make up the COPI coat and are biochemically characterized into two categories.

1. A tetrameric complex made of β-COP, γ-COP, δ-COP, and ζ-COP, which are homologues of the AP1 and AP2 clathrin adaptor complexes (*Schledzewski et al., 1999*).
2. A trimeric cage formed of three proteins α-COP, β'-COP and ε-COP.

Although characterized to arrange as adaptors and cage interestingly, unlike the COPII complex, the COPI complex structure is not separated in an inner and outer complex (**Figure 1.6B**). Instead, it assembles on the membrane as a heptameric complex (*Dodonova et al., 2017, 2015; Faini et al., 2013*). Of the cage components, α-COP and β'-COP have N-terminal WD40 β–propellers with extended α–solenoids, which are

characteristic of a 'proto-coatomer' (*Dodonova et al., 2015; Hsia and Hoelz, 2010; Lee and Goldberg, 2010*). The similar structural organization is found in the COPII coat protein SEC31 (as explained above), in clathrin heavy chain and some nuclear pore components (*Devos et al., 2004; Lee and Goldberg, 2010*). Just like COPII coat initiation, COPI coat formation is initiated by the small GTPase ARF1, a small GTPase related to SAR1. Like SAR1, ARF1 also binds to the membrane by its N-terminal amphipathic domain resulting in wedging of the membrane (*Dodonova et al., 2017; Yu et al., 2012*). This is followed by assembly of the rest of the coat covering the entire membrane further providing a curved scaffold for more membrane curvature. α-COP and β'-COP form an arch-like heterodimer interacting with each other via their C-terminals and with the membrane via their N-terminal β propeller domain with is also the cargo-binding site. The tetrad formed by β-COP, γ-COP, δ-COP, and ζ-COP also forms an arch on the membrane and support the adjacent α-COP-β'-COP sub-complexes. Six copies of ARF1 and three copies of coatomer form a threefold triad structure which contacts the membrane surface to pinch off vesicles (*Dodonova et al., 2017, 2015*).

Clathrin coat: Clathrin-coated vesicles (CCVs) shuttle cargo in the endocytic pathway and late secretory pathway that is from the Golgi to endosomes. CCVs also assemble in two layers like a COPII coat (*Musacchio et al., 1999*). However, unlike COPI and COPII, a small GTPase is not required for initiation of clathrin coats. Instead, the AP2/AP1 adaptor complex is recruited to the membrane by phosphatidylinositol phosphates (PIPs) (*Gaidarov et al., 1996*). The clathrin triskelia then polymerize to form either hexagonal or pentagonal cages as a second layer. Three clathrin heavy chains and three clathrin light chains make up the cage-forming triskelia . The three heavy chains interact via their C-terminals to form the triskelia, which provide the structural backbone of clathrin lattice. The N-terminal WD40 domain of the heavy chain is amphipathic, which helps triskelia to interact with the N-terminal of other nearby heavy chain triskelia (*Kirchhausen et al., 2014*). The three light chains are thought to regulate this process and stick to the heavy chain close to the vertex point (*Fotin et al., 2004*) (**Figure 1.6C**). Once the clathrin coat scaffold carves out a vesicular structure from the membrane, conformational changes in the dynamin helix at the bud neck are triggered by the repeated cycle of GTP loading and hydrolysis

results in the scission of the vesicle (*Morlot et al., 2012*). EPSIN is another major contributor of scission, which inserts an amphipathic helix into the membrane after dynamin is disassembled in order to complete the scission process (*Boucrot et al., 2012*).

Summary: It is important to note that scission in all the three systems (COPI, COPII, and clathrin), are facilitated by the wedging of the membrane by insertion of amphipathic helices of ARF1, SAR1 and EPSIN respectively (**Figure 1.6**). Insertion of amphipathic helices in the lipid bilayer creates a high energy state, which is relaxed by separation of vesicles from the donor membrane (*Beck et al., 2011*). Soon after, the fresh clathrin coat is disassembled by ATP hydrolysis of HSC70 (*Böcking et al., 2011*), unlike COPI and COPII where the coat is disassembled by GTP hydrolysis. The vesicle is then free to travel to its target organelle, and removal of its coat renders the vesicular membrane competent for fusing with its target membrane.

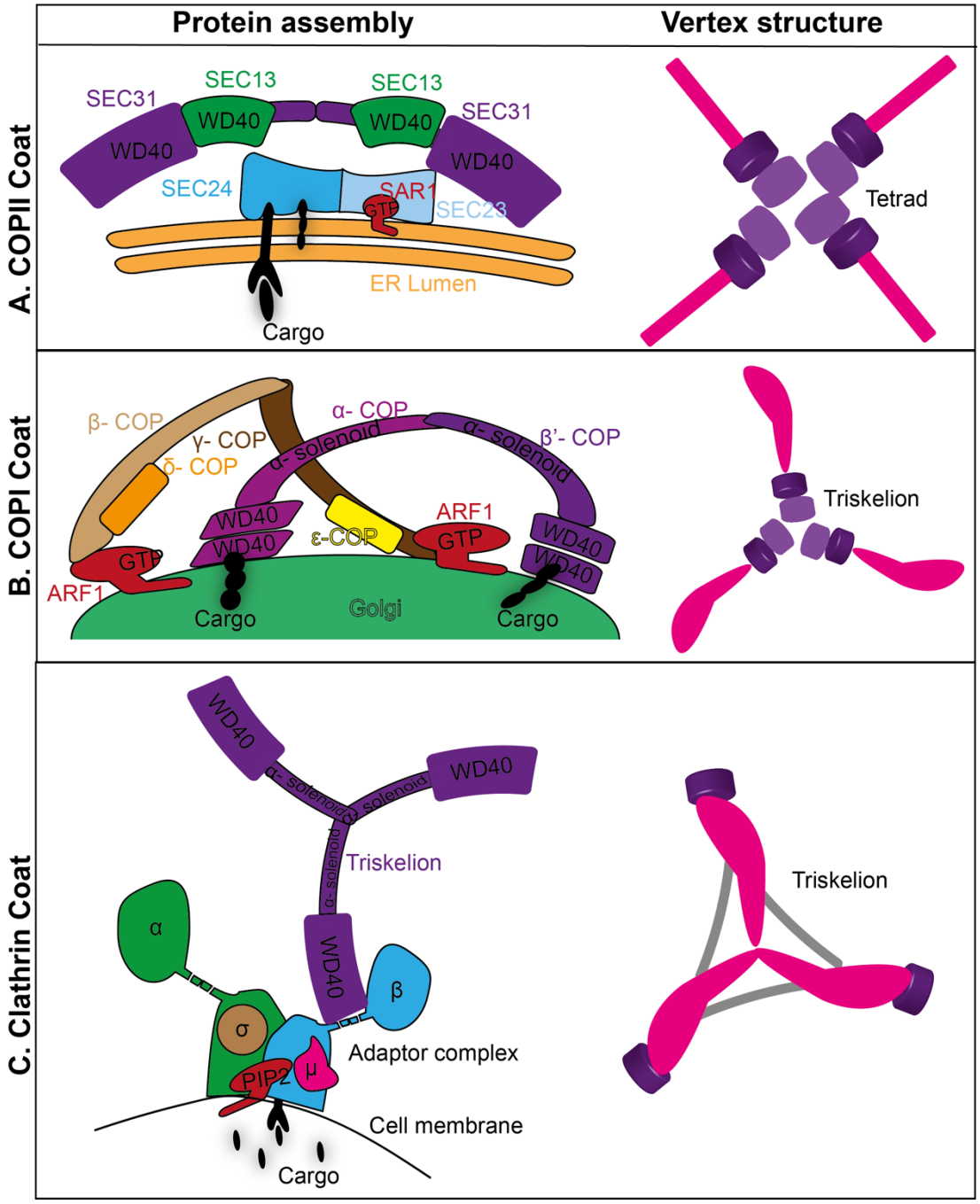

Figure 1.6. Diagrammatic representation of proteins arrangement in three coat systems. (A) COPII coat assembly on the ER membrane (left) and its vertex organization (right). The COPII coat is made of two layers. The inner layer is made of the GTPase SAR1-SEC23-SEC24 having SEC23-SEC24 arranged in a bowtie shape with the SAR1 amphipathic helix inserted in membrane. SEC24 interacts with both the membrane and cargo ER lumen protein. The outer layer is made of SEC13-SEC31, two units of both form a heterotetramer which then polymerizes to form the cage. **(B)** COPI coat assembly on the Golgi or TVCs membranes (left) and its vertex organization (right). COPI is not divided as an outer and inner layer but assembles as a heptameric complex on the membrane. ARF1 initiates membrane association. α and β' WD40 domains also directly interact with the membrane, bind with cargo, and form

a triskelion vertex which further polymerizes to a polyhedral structure. α and β'heterodimer and γ-ε-β-δ form a separate arch-like structure to complete the coat. **(C)** Clathrin coat assembly on the cell membrane (left) and its vertex organization (right). Four subunits of clathrin AP2 adaptor α, β2, μ2, σ2 form the lower layer with help from PIP2. The clathrin heavy chain polymerizes to form triskelia, which assemble to form upper polyhedral cage layer. Its vertex structure on the left illustrates its WD40 domains in purple and α- solenoid in magenta.

Structure, function, and evolutionary relationships of the coats: All three coat complexes perform similar functions but on the different membranes and follow different cellular routes. All three assemble coats with the help of a different set of proteins but having a similar division of labour between components, functionally characterized as adaptors and cage-forming proteins. Whilst the cage forming proteins do not have detectable sequence homology, they share significant structural homology, having at their N-terminal one or two WD40 repeat β-propellers followed by an elongated α-solenoid (**Figure 1.6**) (*Field et al., 2011*). The β-propeller is known to be involved in protein interactions and are ideal for cargo binding (*Eugster et al., 2004; Haar et al., 1998*). A α-solenoid is a flexible protein domain that can either have a bent conformation (as in clathrin (**Figure 1.6C**) and COPI (**Figure 1.6B**) or straight rods as SEC31 of COPII (**Figure 1.6A**). A similar structural arrangement with a β-propeller and α-solenoid is present in some nuclear complex proteins, which interact with curved membranes of the nuclear pore, supporting a common evolutionary origin of pores and coats (*Devos et al., 2004*). Here, an arrangement similar to SEC31 is observed; nuclear pore complex scaffold is made from membrane proximal lattice formed of NUP85-SEH1 complex (*Brohawn et al., 2008*). However, despite similar domain organization, the cage-forming proteins polymerize differently to assemble remarkably divergent cage lattice , suggesting substantial divergence (*Field et al., 2011*). Comparing the adaptor proteins, the clathrin tetrameric adaptors share sequence and structural homology to COPI- β, γ, δ , and ζ proteins (*Serafini et al., 1991; Yu et al., 2012*). β, γ-COP, and δ, ζ-COP also have sequence similarity suggesting that the adaptor subcomplex may originate from the duplication of a protodimer of a large and a small subunit (*Schledzewski et al., 1999*). In contrast, the COPII adaptor SEC23-SEC24 has no sequence or structural similarity to COPI or clathrin adaptors suggesting an independent origin. Similar domain organization has been reported for IFT and

BBsome proteins, suggesting a similar function (*Jékely G and Arendt D, 2006; Dam TJPV et al., 2013*).

1.3.2 Cilia-based trafficking modules - a 'cilia-specific' coat hypothesis involving BBSomes, TULP3/TUB, IFTs, and PDE6δ/UNC119a based system.

The diffusion barrier at the base of cilia allows specific and selective transport of cargo from the cytoplasm into cilia. BBSomes and IFTs are highly conserved protein complexes involved in cargo transport into and from cilia. BBSomes is mostly known to transport protein to and from cilia whereas IFTs mainly transport proteins inside cilia. Both are important for the transport of membrane proteins to or from cilia, have been proposed to be capable of forming vesicular coats like coatomer as explained in the previous section and have been shown to assemble on lipid vesicles in-vitro (*Jin H et al., 2010; Wang et al., 2018*). This introductory section explains the molecular, biological, structural, and evolutionary basis for an adaptor or coat-forming hypothesis for BBSomes and IFTs, which I have pursued in this work. Further, I describe the TULP3/TUB protein, which are other adaptor proteins for a broad range of ciliary membrane proteins and compare its role in cargo transport with BBSomes.

BBSomes: Ciliary membrane protein adaptor mainly for ciliary exports: The BBSome complex is made of eight BBS proteins BBS 1,2,4,5,7,8 9 and BBS18 (*Loktev et al., 2008; Nachury MV et al., 2007*). Three chaperonin-like BBS proteins exist, BBS6, BBS10 and BBS12. These have been proposed to initiate the assembly of the BBSome complex (*Seo et al., 2010; Zhang et al., 2012*). BBSomes concentrate at base of cilia and cycle through cilia attached to IFT trains and may regulate IFT train assembly (*Pan et al., 2006; Wei et al., 2012; Williams et al., 2014*). Mutations in BBS proteins result in a cilia-related, inherited pleiotropic disorder called Bardet-Biedel syndrome (BBS), whose symptoms include cystic kidney, obesity, blindness, and polydactyly (*Beales et al., 1997; Zaghloul and Katsanis, 2009*). These genetic conditions have been reported to be due to defects in assembly or localization of BBSomes, leading to ciliary transport defects. Unlike IFTs, BBSomes are dispensable for cilia assembly in most systems. *Bbs4-null* mice are viable, which indicates that it is not critical for global cilia formation (*Mykytyn et al., 2004; Uytingco et al., 2019*). BBS mutations surprisingly have very different defects in different organisms and

different cell phenotypes. *Bbs4*$^{-/-}$ mice phenocopy some aspects of the human phenotype, as they display obesity, retinal degeneration and male infertility due to lack of sperm flagella. However, there was no defect in size, number, and structure of motile cilia of the trachea and sensory cilia of retinal tubules (*Mykytyn et al., 2004*). Defects in cilia assembly has only recently been reported in *Bbs4*$^{-/-}$ mice which showed a reduction in the number of cilia in the multicilia on dendrites of olfactory neurons (*Uytingco et al., 2019*). Whilst BBSomes are highly conserved, different mutational defects are noted in different ciliated organisms. For example, in *Chlamydomonas bbs1*, *bbs4* and *bbs7* mutants assemble flagella, have no defects in IFT but have defects in the export of specific signalling molecules from cilia (*Lechtreck et al., 2009; Liu and Lechtreck, 2018*). *C. elegans bbs-7* and *bbs-8* mutants could assemble cilia but have destabilized IFT complexes (*Wei et al., 2012*). Similarly, in olfactory sensory neurons in mouse, a 1:1 stoichiometry of BBSome to IFT (*Williams et al., 2014*) is also disturbed in *Bbs4*$^{-/-}$ mice (*Uytingco et al., 2019*). Among cell lines, there is a drastic reduction in number and size of cilia after BBS knockdown in RPE cells (*Jin H et al., 2010; Nachury MV et al., 2007*) whilst no change in the size of cilia is observed in IMCD3 cells (*Nager et al., 2017*). Although most systems assemble cilia in BBS mutants, they do have many other trafficking defects, which can lead to disease etiology.

It has been suggested that the BBSome works as an adaptor for the selection of cargo by IFT proteins (*Berbari et al., 2008*). BBSomes, initially proposed to be adaptors for import of cargo to cilia (*Berbari et al., 2008; Jin H et al., 2010; Loktev and Jackson, 2013*) were later established to be adaptors for mostly export of cargo from cilia (*Domire et al., 2011; Eguether et al., 2014; Lechtreck et al., 2013, 2009; Liew et al., 2014; Xu et al., 2015*). Moreover, knockdown of BBS in IMCD3 cells resulted in defective cargo export triggering ectocytosis to get rid of excess cargo (*Nager et al., 2017*) which also points towards their role in cargo export from cilia. Part of the controversial role of BBSomes in import vs export of ciliary cargo is due to reports of specific membrane proteins missing in BBS mutant cilia while some others are enriched. Specific GPCRs like SSTR3, PKD1, and MCHR1 are depleted in BBSome mutants (*Berbari et al., 2008; Loktev and Jackson, 2013; Su et al., 2014*) whereas GPR161, SMO, PTCH1, and D1R fail to exit cilia (*Eguether et al., 2014;*

Liew et al., 2014; Nager et al., 2017; Ye F et al., 2018; Zhang et al., 2011). PLD also fails to get exported out of *Chlamydomonas* BBS mutant flagella (*Liu and Lechtreck, 2018*). *Bbs* null mice neuronal cilia also accumulate dopamine receptor (D1), and outer segment of rods in photoreceptor cells accumulates non-outer segment protein (*Datta et al., 2015; Domire et al., 2011*). SSTR3 and GPR161 directly interact with BBSome and β-Arrestin-2 and are retrieved in cilia in the absence of either of these; hence, BBSomes and β-Arrestin-2 work together to facilitate cargo exit from cilia (*Ye F et al., 2018*). ARL6, a small GTPase, helps assemble the BBSome complex on the donor membrane (*Jin H et al., 2010*) and binds BBSome-β-Arrestin-2 complex for cargo exit from cilia (*Ye F et al., 2018*). In the absence of BBSome assembly activator ARL6 GTPase, membrane proteins are retained in cilia (**Figure 1.7**).

How does the BBSome recognize and bind membrane proteins for transport? No universal ciliary targeting sequence (CTS) is known to interact with BBSome proteins, although a few interactions between the BBSome and membrane proteins have been described. For example, SSTR3 interacts with BBSome via third loop (*Berbari et al., 2008; Jin H et al., 2010*) but this interaction is dispensable for SSTR3 transport to cilia, likely via TULP3, another adaptor protein for SSTR3 transport to cilia (*Badgandi HB et al., 2017*). A liposome membrane association for the BBSome was shown to be ARL6/BBS3 dependent in vitro (*Jin H et al., 2010*), reminiscent of COPI and COPII assembly dependance on ARF1 and SAR1 GTPase, respectively. Along with sharing the similar GTPase-mediated membrane association of BBSome, the BBSome also has some protein domain similarity to COPI/COPII/clathrin and IFT proteins (*Jékely G and Arendt D, 2006; Jin H et al., 2010; Dam TJPV et al., 2013*) . Hence BBSomes have also been proposed to function like ciliary vesicular transport coats. ARL6-GMP-PNP binds to liposomes *in-vitro* with the help of multi phosphorylated PIPs similar to the COPI, COPII and clathrin adaptor binding to phospholipids and PIPs. BBSomes also bind Rabin-8, associated with the ciliary membrane and BBS-5 was also shown to bind PIPs on lipid-protein overlays (*Nachury MV et al., 2007*). Moreover, BBS proteins have also been shown to work in vesicular trafficking to and from the plasma membrane (*Guo et al., 2016; Langousis et al., 2016; Starks et al., 2015*). Several lines of circumstantial evidence suggest BBSomes may be working as adaptor proteins for many ciliary transport processes including a GTPase-dependent membrane binding

activity, some structural similarity to canonical coat proteins, and association with PIPs and Rab8-Rabin8. Whilst there has been no *in-vivo* or direct proof of vesicular coat forming function for BBSomes, they are necessary for the export of several ciliary membrane proteins with the help of ARL6-BBSome-β Arrestin-2 complex (**Figure 1.7**).

TULP3 and TUB proteins are adaptors for import of integral membrane proteins to cilia: Tubby protein is encoded by the *TUB* gene and shares homology with four Tubby-like paralogs, TULP1-4. They all share the common structural elements with 12 β-barrels packed around an α-helix. Mutant *tubby* mice develop retinal degeneration, sensorineural hearing loss and obesity (*Kleyn PW et al., 1996; Noben-Trauth K et al., 1996; Ohlemiller K et al., 1995*), from which the gene derives its name. Tubby proteins can bind to phosphoinositide (PIPs) and hence is capable of binding to membranes via PIPs. TULP3 binds with a subset of ciliary localized GPCRs and IFT-As, where it is proposed to act as an anchor between IFT-As and GPCRs. In turn, IFT-As help in the transport of TULP3 into cilia (*Mukhopadhyay et al., 2010*). Whilst work from *Chlamydomonas* had suggested IFT-As were solely responsible for retrograde transport from cilia, a growing body of evidence support a critical role in transport of cargo including many membrane proteins into cilia (Lee et al., 2008). At the transition zone, the TULP-3 and IFTA complex help in the transport of many membrane proteins to cilia (**Figure 1.7**). *TULP3* mutants which fails to bind either IFTA or PIPs have a dominant-negative effect on the transport of GPCRs into cilia (*Badgandi HB et al., 2017; Mukhopadhyay et al., 2010; Ye F et al., 2018*). TULP3 is a universal adaptor for the import of many ciliary membrane proteins: 16 class A cilia-related GPCRs; a single pass transmembrane protein Fibrocystin; proteins with ciliary localization signal (CLS) fusions; the TPR channel family; and the polycystic kidney disease-causing proteins PKD1 and PKD2. The GPCRs which are transported into cilia by TULP-3 include the Dopamine receptors (D1R, D2R short and D5R); the Galanin receptors (GAL2R, GAL3R); orphan GPCRs (Gpr161, GPR19, GPR83, GPR88); the Kisspeptin receptor (KISS1R); the melanin-concentrating hormone receptor-1 (MCHR1); Neuropeptide FF receptors (NPFFR1and NPY2R); the P2Y Purinoceptor 1 (P2RY1); the prolactin releasing hormone receptor (PRHLR) and the somatostatin receptor type 3 (SSTR3) (*Badgandi HB et al., 2017; Loktev and Jackson,*

2013; Mukhopadhyay et al., 2013, 2010; Ye F et al., 2018). Knockdown of *TULP3* results in low or non-detectable levels of all of these ciliary membrane proteins inside cilia. TUB is another Tubby domain protein, which is predominantly expressed in brain and photoreceptors, exclusively traffics a subset of GPCRs (MCHR1, SSTR3, and NPY2R) to neuronal cilia (*Loktev and Jackson, 2013; Sun et al., 2012*). In spite of not having structural similarity to coatomer adaptors, based on (1) the direct interaction of TULP3 with ciliary localization signals (CLS) to transport above mentioned ciliary membrane proteins and (2) it's interaction with PIPs, it has been proposed that TULP3 and TUB proteins are adaptors for integral ciliary membrane proteins to help in their transport into cilia.

An emerging theme from these two different types of adaptors discussed above suggests that the IFT-A/TULP3 complex is critical for import of integral membrane proteins whereas the ARL6-GTP/β-Arrestin-2/BBSome complex is vital for export out of cilia (*Badgandi HB et al., 2017; Ye F et al., 2018*) (**Figure 1.7**). TULP3 and BBSomes regulate import and export of ciliary membrane-integrated proteins, but there are another class of membrane-associated proteins (prenylated and myristoylated proteins) which are trafficked by PDE6δ and UNC119b by binding these lipid moieties (*Fansa et al., 2016; Ismail et al., 2012*) (see **Section 3.1.8**). IFTs are other candidates for being not only adaptors but also more related to coatomer cage forming units explained in next section.

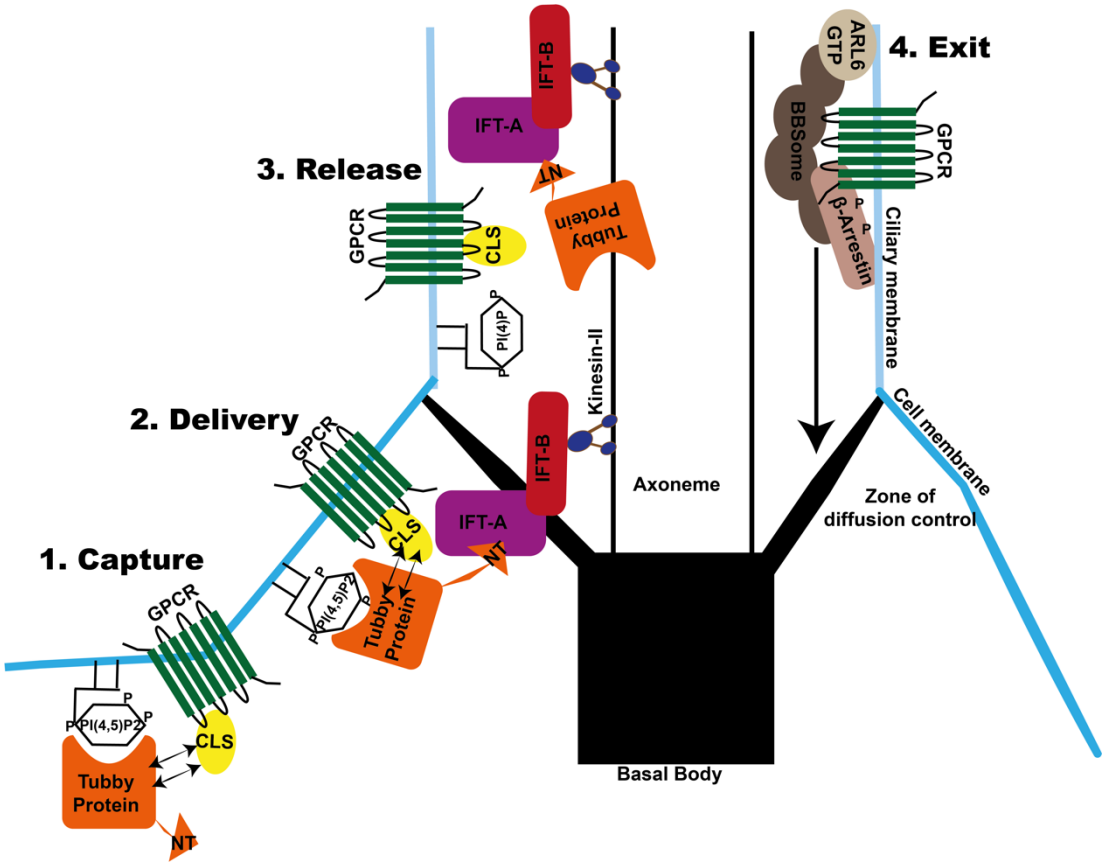

Figure 1.7. Ciliary integral membrane proteins are imported into cilia by the IFT-A complex with TUBBY adaptor proteins and exported out of cilia by ARL6-GTP-BBSome-βArrestin-2 complex. TUBBY and BBSome function as adaptors for ciliary import and export, respectively. STEP 1-Capture: TULP3 is attached to membranes via PI(4,5)P2 and binds to the ciliary localization signal (CLS) of ciliary integral membrane proteins. Cargo-binding through CLS to TULP3 depends on a PI(4,5)P2 membrane interaction, similar to clathrin adaptors AP2, AP180, or Epsin (see **Section 1.3.1**). **STEP 2-Delivery**: The IFT-A complex concentrated at the transition zone of cilia, associates with TULP3 and its interacting cargos via the CLS, helping to transfer cargo across the increased membrane density of the transition zone. In the absence of IFT-A, TULP3 and cargo fail to transfer across the transition zone. **STEP 3-Release**: The PI(4,5)P2 composition of the cell membrane is not present in the ciliary membrane. Upon entry inside cilia, PI(4,5)P2 is catalysed to PI(4) which weakens TULP3 binding to CLS-containing cargo leaving it at the ciliary membrane. **STEP 4-Exit**: The ARL6-GTP/BBSome/β-Arrestin-2 complex helps retrieve integral membrane proteins from the ciliary membrane for export into the cytoplasm. In the absence of any of the four components, proteins fail to exit cilia and are often exocytosed from the tip to get rid of excess cargo as 'default' clearance pathway.

1.3.3 IFTs are found close to ciliary membrane inside cilia and some IFTs are capable of membrane association

Intraflagellar complex (IFT) proteins constitute the most conserved method of cargo transport in cilia. The IFT-B complex along with kinesin motor helps in anterograde transport and the IFT-A complex along with dynein motors helps in retrograde transport of cargo from cilia. For details on structure, function and molecular assemblies of IFT proteins see **Section 1.1.5, 1.1.6** and **Figure 1.3**. This section explains previous studies in favour of membrane association of IFTs. IFT trains are observed by TEM to be in close apposition between axonemal microtubules and the ciliary membrane in *Chlamydomonas* (*Kozminski et al., 1993; Pazour et al., 1998; Pigino et al., 2009*) and in mammalian cells (*Rogowski M et al., 2013*). Their interaction with microtubules is mediated by the kinesin and dynein motor proteins, however whether there exists additional IFT interaction partner(s) to mediate binding to the ciliary membrane remains contentious. The IFT-A interactor TULP3 has been shown to bind directly to membrane phosphoinositides (*Mukhopadhyay et al., 2010*), and be required for ciliary GPCR localization (*Badgandi HB et al., 2017*) (**Figure 1.7**). However, stacked close to the ciliary membrane, IFTs might also have some direct affinity for membranes. Previous studies have shown IFT proteins localizing to various membranes and vesicular compartments in cells, summarized here.

Best characterized is IFT20, which localizes to the Golgi, as well as to the cilia base and cilia lumen (*Follit et al., 2006; Noda et al., 2016*). Here, IFT20 localizes as a fine thread extending from cis-Golgi to cilia (*Follit et al., 2006*). Depletion of *IFT20* interfered with transport of membrane cargo PKD2 to cilia (*Follit et al., 2008*), suggesting this localization marks a functional role for IFT in Golgi-to-cilia transport. In mammalian photoreceptors, immune-EM studies revealed IFT57, IFT52, IFT88, IFT140 and IFT20 staining to be clustered around vesicle-like structures towards the periciliary base, around the basal body and also centriole in inner segment of photoreceptor cells (*Sedmak and Wolfrum, 2010*). IFTs were also shown accumulating around vesicles in the dendritic process of retinal secondary neurons (*Sedmak and Wolfrum, 2010*). In *Chlamydomonas,* in-vitro and in-situ immuno-EM revealed both ciliary cargo proteins including PKD2, RSP1, RSP3 and α-tubulin as well as IFT46 to be accumulating around vesicles in the periciliary cytoplasm (*Wood and Rosenbaum,*

2014). Vesicular localization of IFT27 was also observed at the cleavage furrow of dividing *Chlamydomonas* cells by immuno-EM, with a similar localization of IFT172, IFT46 and IFT139 observed using light microscopy (*Wood et al., 2012*) . However, the best and most compelling evidence for IFT directly binding to membranes was the high affinity association of recombinant IFT172 with lipid vesicles (giant unilamellar vesicles- GUVs) with high affinity (*Wang et al., 2018*). This recombinant protein was observed to have a 10nm globular repeat with a rod-like extension, and associated with lipid vesicles via its globular domain. Moreover, excitingly, IFT172 itself was able to deform and pinch off smaller vesicles (~20nm), similar in size to COPI complex vesicles. This was the first report highlighting direct association of IFT (IFT172) with lipid vesicles in-vitro (*Wang et al., 2018*). Like BBSomes, IFTs have also not only evolved from coatomers (*Jékely G and Arendt D, 2006; Dam TJPV et al., 2013*), but a few IFTs (IFT172 and IF80) have been proven to have homologous domain arrangement to coatomer cage proteins (*Taschner M et al., 2018; Wang et al., 2018*). However there has been no direct in-vivo evidence of IFTs forming vesicular coats, which I aimed to address using my TEM results.

1.3.4 Vesicular transport to cilia: from the endocytic pathway or Golgi

In spite of the continuity between the ciliary membrane and cell membranes, the existence of a diffusion barrier at the base of cilia opposes free diffusion of ciliary cargo either from cell membrane or cytoplasm into the ciliary compartment (see **Chapter 1**). To establish and maintain this compartmentalization, three different transport pathways are proposed to move cargos across the transition zone selectively. The three different types of pathways include the (1) passive lateral diffusion from the plasma membrane to the ciliary membrane, (2) recycling of membrane proteins via endocytic pathway directed to cilia (3) selective cargo transport directly from Golgi-derived vesicles for both membrane and non-membrane proteins and lipids (**Figure 1.8**).

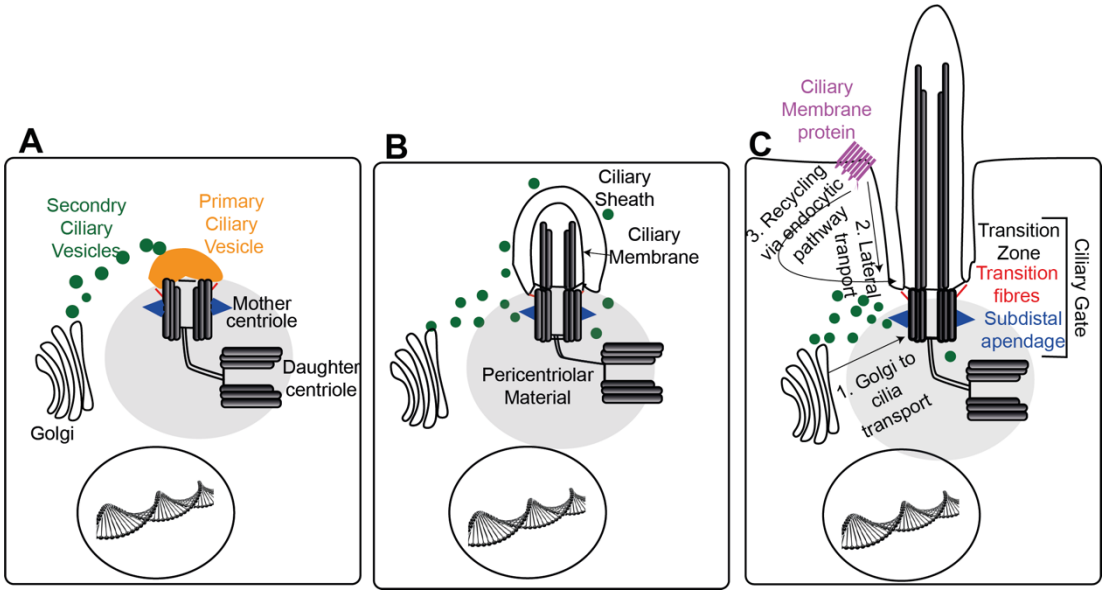

Figure 1.8. Schematic of vesicular transport system to ferry cargo to nascent cilia. **(A)** The primary ciliary vesicle (PCV) docks on the mother centriole. Distal appendage proteins (also known as transition fibres) are critical for primary ciliary vesicle docking. In mesenchymal cells, the Golgi stacks are found close to cilia throughout the process of ciliation. Secondary ciliary vesicles fuse with the PCV and help in elongation of cilia. **(B)** As the cilia elongate, basal body microtubules serve as the nucleation site for nascent ciliary axoneme. Secondary vesicles fuse with the ciliary sheath or cilia base to transport structural and functional units of cilia. **(C)** Finally, as the cilia elongate and emerge out of the cell, the ciliary sheath combines with the cell membrane. Transition zone and transition fibres form a ciliary gate to stop free diffusion of proteins and lipids between the cellular and ciliary compartments. **(C)** Also shows ciliary components are trafficked by three different pathway. 1. Vesicular transport from Golgi to cilia, 2. Lateral transport from the cell membrane, and 3. Recycling from cell membrane to cilia base by endocytic pathway.

Compartmentalization is established early in the process of ciliation, as demonstrated by Sorokin and Wheatley in the 1960s by electron microscopy studies in non-polarized cells showing the proximity of Golgi stacks to the mother centriole, before basal body docking. This suggests potential Golgi-derived vesicles carrying cilia building lipids and proteins allow ciliation and subsequent axoneme extension to occur. The mother centriole is distinguished from the daughter centriole by the presence of subdistal and distal appendages (or transition fibres at the ciliary base), the latter thought to be essential for linking basal bodies to the plasma membrane. The mother centriole recruits small most likely Golgi-derived vesicles (*Sorokin S, 1962*), which fuse to each other to form a large primary ciliary vesicle (PCV) attached at the distal appendages. More secondary vesicles fuse with the PCV, along with uncapping

of the mother centriole by degradation of the CP110/Cep97 inhibitory complex, allows the elongation of both the ciliary sheath and ciliary membrane (*Spektor et al., 2007*). The axonemal core of the cilia further polymerizes using basal body microtubules as a nucleation site. This extension process of the cilium from each basal body, and its subsequent maintenance, requires intraflagellar transport (IFT), a bidirectional transport system that tracks along the axonemal microtubules (*Rosenbaum and Witman, 2002*). During this entire elongation process, the secondary vesicles could be seen docking along the ciliary sheath and around the ciliary base (**Figure 1.8B and C**). Finally, the ciliary sheath fuses with the cell membrane. What is interesting is that vesicles could still be seen surrounding fully formed cilia, suggesting a continued exchange of materials from Golgi even during cilia maintenance.

The molecular mechanisms and components for ciliary vesicle formation are beginning to emerge, often which co-localize to both the Golgi and mother centrosome. Critical for the induction of ciliogenesis are several candidates involved in the initial attachment of vesicles to the distal appendages of mother centrioles; these include CCDC41, IFT20, HOOK2 and CEP164 (*Baron Gaillard et al., 2011; Follit et al., 2006; Graser et al., 2007; Joo et al., 2013; Schmidt et al., 2012; Tanos et al., 2013*) (**Figure 4.11**). The protein coiled-coil domain containing 41 protein CCDC41 (CEP83) localizes to distal appendages of the mother centriole. Mutant studies demonstrate that CCDC41 is critical for initial docking of primary ciliary vesicle on the basal body (*Joo et al., 2013; Tanos et al., 2013*). *CCDC41*-depleted cells fail to ciliate with ciliation blocked after mother centriole maturation in RPE cells and zebrafish embryos (*Joo et al., 2013*). Interestingly, CCDC41 also localizes to the Golgi complex where it interacts with IFT20, the intraflagellar transport component resident in the Golgi. IFT20 localizes to cis and medial Golgi, is recruited to centrioles throughout cell cycle, including the basal transition zone and ciliary axoneme (*Follit et al., 2006*). For the formation of functional cilia and transport of membrane proteins in cilia, IFT20 is also critical (*Follit et al., 2006*). Whilst localization of CCDC41 to cilia is independent of IFT20, IFT20 localization to cilia requires CCDC41 *(Joo et al., 2013*). Alternatively, it has been proposed that IFT20 recruits CCDC41 to the Golgi in order to transfer cargo destined for the ciliary vesicle (*Joo et al., 2013*). Like CCDC41, HOOK2 is also a distal appendage protein in cilia and is critical for docking of primary

ciliary vesicle on mother centriole (*Baron Gaillard et al., 2011*). It also localizes to the Golgi and centrosome/basal body, where it interacts and stabilizes PCM-1 and is required for recruitment of Rab8a, a GTPase implicated in membrane transport to nascent primary cilia (*Baron Gaillard et al., 2011*). Another distal appendage protein is CEP164 (*Tanos et al., 2013*) required for primary ciliary vesicle docking to mother centriole (*Graser et al., 2007; Schmidt et al., 2012*). CEP164 also interacts with Rab8 and its guanine nucleotide exchange factor (GEF) Rabin8 in order to promote ciliary membrane biogenesis (*Nachury MV et al., 2007*). Expression of a GDP-locked Rab8 in *Xenopus* photoreceptors leads to accumulation of Golgi-derived rhodopsin carrier vesicles at the base of connecting cilium (*Moritz et al., 2001*), implicating Rab8 and Rabin8 in docking and fusion of post-Golgi vesicles to the base of cilia.

Evidence supporting the existence of Golgi-to-cilia transport has mostly focused on cargo- or cell-type specific mechanisms. Best described are the mechanisms controlling trafficking of the vesicles containing the light-sensitive GPCR rhodopsin from the trans-Golgi network to the connecting cilium in photoreceptors in the retina (*Wang and Deretic, 2014*). In contrast, polycystin-2 (PKD2) a transmembrane protein mutated in polycystic kidney disease is transported from cis-Golgi to cilia (*Hoffmeister et al., 2011*). IFT20 also localizes to cis and median Golgi network and not to the trans Golgi network helping in transportation of PKD2 from Golgi-to-cilia, where it appears as a track of vesicles from the Golgi to cilia (*Follit et al., 2008, 2006; Noda et al., 2016*). Together these interaction studies of proteins required for primary ciliary vesicle docking, with their dual localizations to both Golgi and cilia, provide very compelling evidence for the existence of a bespoke vesicular trafficking of cargo from the Golgi to nascent cilia.

1.4 Thesis Hypothesis and Aims

Until now IFT-A complex proteins have been considered to be essential for mostly retrograde transport within cilia with an emerging role for the transport of some membrane proteins into cilia (*Caparrós-Martín JA et al., 2015; Duran et al., 2017; Hirano et al., 2017; Liem KF et al., 2012; Mill et al., 2011; Takahara et al., 2018; Zhu et al., 2017*). Except for few mechanistic insights for the role of IFT-A interactions with membrane proteins via Tubby proteins (*Badgandi HB et al., 2017; Ye F et al.,*

2018), very little is known about how exactly the IFT-A proteins mediate the process of transport of membrane proteins into cilia.

I hypothesized that WDR35 is required for the stability of the IFT-A complex and its function for trafficking cargos into mammalian cilia. In order to test this hypothesis, this project had two aims:

1. To phenotype defects of mammalian cilia from *Wdr35*$^{-/-}$ and retrograde dynein *Dync2h1*$^{-/-}$ mutants on ciliogenesis and assembly of ciliary protein complexes.
2. To investigate the molecular and cellular mechanisms underlying these defects using bioinformatics and electron tomography, and whether they form a novel ciliary shipping complex to direct select membrane cargos critical for building and maintaining cilia.

The fundamental requirement for WDR35 in vesicular trafficking to nascent cilia described in this novel work strengthens our understanding of the key principles of ciliation and what goes wrong in diseases when this process is disturbed.

Chapter 2. Material and Methods

2.1 Mouse Methods

2.1.1 Preparation of primary MEFs

Foetuses were harvested at embryonic (E)11.5 days of gestation and dissected from the uterus in sterile, cold PBS on dissection microscope. The following steps were done in the laminar flow hood. The embryo head and liver were removed and could be used for extracting DNA or for RNA. All blood was removed from the embryo, by washing with 1-2ml of PBS, before transferring to a fresh 60mm dish. The tissue was minced into small pieces with sterile razor blades (changing between samples) and then 2ml of trypsin: versine mix was added and incubated at 37℃ for 30mins. After incubation, the tissue mix was vigorously pipetted until it became a single-cell suspension. To neutralize the trypsin, 2ml of Opti-MEM-I (ThermoFisher Gibco 11995-065) supplemented with 10% foetal calf serum (FCS)/1% penicillin-streptomycin (P/S) and 0.026µl 2-mercaptoethanol, mixed well. Each embryo suspension was transferred to one T75 or two T25 flasks and supplemented with more media. This culture is considered passage number 1 (p1).

MEFs were incubated at 37℃ in a hypoxic incubator (3% O_2 and 5% CO2). MEFs are healthier in hypoxic incubator than in 5% O_2 incubator. Media was changed on the following day to remove dead cells. Cells were split every 3-4 days during early passages (p1-p6) after which their growth slows, and when they can be split or fed every week. In these studies, only primary MEFs were used and all characterization was done with passages less than p8, after which most cultures underwent a growth crisis. One flask should be frozen at passage-2 (see **Section 2.2.2**).

2.1.2 Genotyping

Genotyping *Wdr35* mutant (J4 mice). The *Wdr35*^{J4} null allele was generated previously in our lab (*Mill et al., 2011*). DNA was isolated from the tail of E11.5 embryos using an alkaline lysis method. Briefly, samples were incubated in 100µl of alkaline lysis solution (25mM NaOH pH 12, 0.2mM EDTA) on a thermocycler at 95℃ for 20mins to extract DNA. This was then neutralized by adding 100µl of 40mM Tris-

HCl (pH 5.0) and vortexed well. 2 µl of the DNA sample final mix was used in 20µl of following PCR reaction using primers listed in **Table 2.1**.

J4 Genotyping PCR reaction:

Template DNA = 2 µl
DreamTaq Green PCR Master Mix = 10.0 µl
Forward primer (20µM) =0.5 µl
Reverse Primer (20µM) =0.5 µl
dH_20 =7.0 µl
Reaction volume =20 µl

DreamTaq Green PCR Master Mix (2X) is from Thermo Scientific.

J4 thermocycler setting:

1. 94^0C 3mins
2. 94^0C 30secs;
3. 55^0C 45secs;
4. 68^0C 1min
5. Cycle to step 2 times 34
6. 68^0C 2 mins
7. 15^oC forever

The PCR reaction mix was subsequently digested with Bsl1 (NEB) with 10 µl reaction mix and incubated on the thermal block at 55℃ for 2hrs. The digested reaction mix was run on 2% agarose gel. As designed by (*Mill* et al*., 2011*), Bsl1 has a restriction site in wild type locus (C3H) and give 2 bands on the gel, and it does not cut *Wdr35*$^{-/-}$ DNA which runs as a single band of 428bp.

PCR product = 10 µl
Cut smart buffer 10X = 2 µl
Bsl1 enzyme = 0. 5 µl
dH_20 = 7.5 µl
Reaction volume = 10 µl

Genotyping *Dync2h1* mutant (named as D5 line): *Dync2h1*^{D5} (dynein cytoplasmic 2 heavy chain 1: MGI: 107736) null allele was previously produced by the lab (*Mill et al., 2011*) The mutation is found in exon 69 of *Dync2h1*, where the 15th base in exon 69 is changed from C to A resulting in a premature termination mutation (TAC tyrosine to TAA stop) and the product is degraded by nonsense mediated decay.

DNA was isolated the same as described in J4 line and genotyped by PCR using primers listed in **Table 2.1** and same reaction mix as above, followed by an enzyme digest with MluC1 at 37℃ for 2hrs. Digest with MluC1 gives a single band at 354bp for the wild type allele and 2 bands of 240bp and 114bp for the mutant.

D5-Thermocycler setting:

1. 94^{0}C 4mins
2. 94^{0}C 30secs
3. 55^{0}C 30secs
4. 72^{0}C 1min
5. Cycle to step 2 times 35
6. 72^{0}C 10 mins
7. 4^{o}C forever

Genotyping PCM1-SNAP mouse line: Dr. Emma Hall generated and validated this mouse line by CRISPR-Cas-9 editing (unpublished). DNA was isolated as above and PCR reaction mix was prepared the same as J4 line. Two sets of primer used are listed in **Table-2.1**.

PCM-1-SNAP Thermocycler setting:

1. 94^{0}C 5mins
2. 94^{0}C 30sec
3. 65^{0}C 30sec
4. 72^{0}C 45sec
5. Cycle to step 2 times 2.
6. 94^{0}C 30sec
7. 62^{0}C 30sec
8. 72^{0}C 45sec

9. Cycle to step 6 times 2
10. 94^0C 30sec
11. 59^0C 30sec
12. 72^0C 45sec
13. Cycle to step 10 times 2
14. 94^0C 30sec
15. 55^0C 30sec
16. 72^0C 45sec
17. Cycle to step 14 times 30
18. 72^0C 10min
19. 16^0C forever

2.2 Cell Culture

2.2.1 General cell culture

Two cell lines used in this thesis are MEFs and the hTERT-immortalized retinal pigment epithelial cell line(hTERT RPE-1: ATCC® CRL-4000™). RPE-1 cells were cultured in Gibco Dulbecco's modified eagle medium (DMEM (1X) + GlutaMAX™-1, Catalog number- 31966-021) and MEFs were grown in Opti-MEMI ® (1X) (Gibco Catalog number 31985-047). Both were supplemented with 10% FCS and 1% pen/strep. MEF culture additionally had 6.67µl 2-β mercaptoethanol. All cell culture work was done in a sterile laminar flow hood. Cells were maintained at 37˚C + 5% CO_2, and MEFs were cultured in hypoxic conditions of low 3% O_2. Cells were passaged when they attained nearly 80% confluency. This was 2-3 days for both MEFs and RPE cells. MEFs grow slightly slower than RPE cells. To passage the cells, they were treated with 1:1 mix of trypsin and versine and incubated in an incubator at 37℃ for 2-3 mins. Trypsin was inactivated with foetal calf serum (FCS). Cells were spun down at 3000rpm for 3mins and seeded at the desired density. MEFs used for all experiments in this thesis are never beyond passage no. 8.

2.2.2 Freezing cells

Trypsinised cells were spin down as explained in **Section 2.2.1** and resuspended in freezing medium containing 10% DMSO and 20% FCS while keeping the cryovials

on dry ice. Normally $4x10^6$ cells were frozen in one vial. Cells frozen in cryovials were stored in -80℃ for a short time and transferred to the liquid N_2 storage facility for long term storage.

2.2.3 Thawing cells

Cells are rapidly thawed from liquid nitrogen by dipping the cryovials in warm water (nearly 37℃) and seeded directly to desired flask size in their compatible media (**Section 2.2.1**). Fresh media was replaced the next day to get rid of dead cells. Seeding density for T25 flask is $0.7x10^6$, and T75 flask is $4.6 x10^6$.

2.2.4 Ciliogenesis

To induce ciliogenesis, 70-80% confluent cells were starved of serum and grown in an incubator maintained at 37℃ for 24hrs. Cells could also be induced for an extended period as per the requirement of experiments. In this thesis, most cilia studied was after 24hrs of serum starvation.

2.2.5 Neon system to electroporate primary cells

Unlike RPE cells, MEFs are challenging to transfect and need to be electroporated to express exogenous plasmids/constructs.

Reagents & Equipment: (1) Mouse embryonic fibroblasts (high density/near confluency: cells survive better), (2) PBS, (3) Trypsin/Versene (1:1), (4) Optimem-I (10% serum, no antibiotics) (5) Neon™ Transfection System, 10µL Kit (Invitrogen Cat. No. MPK-1096) (6) 24-well tissue culture plates (Corning, Cat. No. 3524).

Protocol: 24-well plates or 6-well plates were prepared by filling with 500µl or 2mL culture medium containing serum (without antibiotic), respectively and pre-incubated in a humidified 37°C/5% CO_2 incubator. Aliquots of plasmid(s) DNA (0.5-1.5µg/transfection) were prepared. Cells were trypsinized to a single-cell suspension, as described **Section 2.2.1** and trypsin was inactivated with Opti-MEM/FCS without antibiotics. The total number of cells was determined using the haemocytometer or the Scepter (Merck Millipore PHCC20040). $0.5x10^5$ cells/transfection reaction is needed, and 1-3 transfections per well of a 24 well plate or 4-6 transfections per well of a 6

well plate was used. Cells were centrifuged at 1200rpm for 5 minutes at room temperature, rinsed in PBS and spun again. The PBS supernatant discarded. Cells were resuspended in 10µl Resuspension Buffer R per transfection reaction. One NeonTM tube was filled with 3 ml Solution E and placed in the electroporation pipette station. Load 10µl of the cells and DNA mixture into electroporation tip using NeonTM pipette and insert into the pipette station. The instrument parameters were set for voltage 1350V, width 30ms and 1 pulse and the sample electroporated, as per the manufacturer's instructions. The electroporated sample was transferred into the prepared 24-well or 6- well plates. The samples were incubated in antibiotic-free media 37℃/5%CO_2/3%O_2 overnight. There is generally a lot of cell death following electroporation so the following day, cells were gently rinsed and dead cells aspirated off after 16 hours. Transfected cells are harvested or visualized 24-72 hours post-electroporation.

2.2.6 DNA transfection: Transfection protocol of RPE-1 cells with Lipofectamine

Reagents: (1) hTERT RPE-1 cells, (2) PBS, (3) Trypsin/Versene (1:1), (4) Gibco-Dulbecco's modified eagle medium, DMEM (1X) + GlutaMAX-1, Catalog number-31966-021, and (5) Lipofectamine® 2000 reagent , REF no. 11668-019 - Invitrogen Thermo Fischer Scientific.

Protocol: The cells were plated the day before in complete media to the desired confluency of 80-90%. The transfection mix was prepared: 3µg total DNA per well of 24 well plates, 5 µg for a 6 well plate or 10-20 µg for a 10cm petri dish. For the transfection, the DNA was mixed with 150µl Opti-MEM I per well of a 24 well plate, with 300 µl per well of a 6 well plate or 2 ml per 10cm dish. Mix lipofectamine 3 µl/24 well or 10µl/ 6 well/ or 15-20 µl/ 10cm dish in 150 µl OPTMEM/well of 24 well plate or 300 µl per well of a 6 well plate or 2 ml per 10cm dish. Cells were washed three times with warm PBS and any remaining liquid was aspirated off , before adding the lipofectamine+ DNA mix on top of the cells. The cells were incubated in the transfection mix for 4-5 hour. After this the transfection media was removed and replaced by new media either with or without serum, depending if you want to trigger ciliogenesis.

2.2.7 Kill curve for Zeocin sensitivity in hTERT RPE-1 cells

Cells were plated at 25% confluency and cultured at 37℃ for 24hrs. The next day, a series of dilution were added to fresh medium containing varying concentrations of Zeocin (Invitrogen, Cat No.: R250-01)- (0/50/100/200/400/600/800/1000) µg/ml of Zeocin were added to different plates. Selective media was replenished every 3-4 days and the percentage of surviving cells determined. The concentration was selected at which he majority of cells were killed within 1-2 weeks; most cells were found dead at 50µg/ml to 100µg/ml concentration of Zeocin in 2 weeks.

2.3 DNA methods

2.3.1 CRISPR based genome editing

To knock-out *WDR35* from hTERT RPE-1 cells using CRISPR Cas9, guides shown in **Table 2.2** were phosphorylated using T4 PNK (polynucleotide kinase) and 1X T4 ligation buffer. The guide was annealed using annealing buffer (10mM Tris, 50mM NaCl, and 1mM EDTA, pH 7.5). pSpCas9(BB)-2A-Puro(pX459) V2.0 (Plasmid# 62988) was digested with restriction enzyme Bbs1 at 37℃ for 1hr followed by incubation in SAP for additional 30mins to dephosphorylate the plasmid. DNA was cleaned-up using PureLink PCR Purification Kit (ThermoFisher Scientific), as per the instruction manual. Annealed and phosphorylated guides were diluted 1:200 in Tris-EDTA solution and ligated with vector T4 ligase and 1X suitable buffer. The ligation reaction was set up for 16hrs at 16℃. DH5α E. coli cells were transformed with 2µl of the ligated product and spread on LB-ampicillin plates and incubated at 37℃ overnight. DNA was extracted using the miniprep kit and sent for sequencing. Sequencing primers are listed in **Table 2.2**. Guide1 was found ligated to vector in sequencing result. Plasmid with guide-1 was transfected in hTERT-RPE cells using lipofectamine based transfection method as described in **Section 2.2.6**. Clones were selected with 10mg/ml puromycin (Invitrogen-A1113803), were sorted on FACs to get single-cell colonies. When confluent DNA was extracted as described in **Section 2.3.8** and sequenced. Sequencing primers are in **Table 2.2**. Unfortunately, I failed to succeed in isolating a clone knock-out for *WDR35*.

2.3.2 PCR (polymerase chain reaction)

DNA amplification was done using the polymerase chain reaction (PCR). Primers used for amplifying DNA for genotyping were already available in lab (**Section 2.1.2**), and the one used for *WDR35* cloning were designed on software (URL< http://frodo.wi.mit.edu/cgibin/primer3/primer3_www.cgi>) (**Table 2.1**). PCR reaction was set up using DreamTaq Green PCR master mix and respective primers (**Table 2.1**) with DNA template/clone. Thermocycler was set to amplify DNA for genotyping as described in **Section 2.1.2**. DNA from pcDNA6.2-EmGFP-Topo vector was amplified with 0.5U Pfu Ultra polymerase with Pfu Ultra buffer, 0.2mM dNTP, 2.5mM $MgCl_2$, and primers shown in **Table 2.1**.

2.3.3 Agarose gel electrophoresis

Agarose gels electrophoresis was used to separate nucleic acids. 0.8-2% agarose (Hi-Pure Low EEO agarose, Biogene) solution was prepared in TBE buffer (89mM Tris base, 89mM boric acid and 20mM EDTA) by heating in microwave until the agarose completely dissolved. 0.5µg/ml Ethidium bromide was added to the agarose solution Once solidified, nucleic acid samples were loaded with Blue Orange 6X loading dye (Promega) with a PhiX174/Hae III DNA ladder (Promega-REF no. G1761) to mark nucleic acid fragment sizes. 150-200V voltage was applied to aid nucleic acid shift towards the positive electrode in a gel electrophoresis tank filled with 1X TBE. Gels were imaged with UV transilluminator (BioDoc-It System, UVP).

2.3.4 Restriction enzyme digestion

In an attempt to change EmGFP tag to EGFP to use for GFP-Trap protocol, mouse *Wdr35* was amplified from the pcDNA6.2-EmGFP-WDR35-Topo (**Section 2.3.2**). pEGFP-1 (Catalog no. PT3027-5) vector was digested using HF-SalI restriction enzyme (Ref no. 3138L) and inactivated as per the manufacturer' instructions. the product was run on a gel, purified and dephosphorylated with SAP for 30mins at 37℃. SAP was than heat-inactivated by incubating reaction mix at 65℃ for 20min. Vector was then ligated and with amplified PCR product is explained in **Section 2.3.5**.

2.3.5 Ligation

200ng of the vector was mixed with 2.4 times molar amount of insert and incubated with 1U of T4 ligase (Roche) and 1X ligation buffer (Roche) and incubated overnight at 4℃. 1µg of ligation mixture was used to transform DH5α E coli cells.

2.3.6 Purification of DNA from *E coli* cells

A single bacterial colony was inoculated in 5ml LB for miniprep and 500ml LB medium for maxiprep with the relevant antibiotic. The culture is left shaking in 37℃ incubator overnight, pelleted down next day and DNA was isolated using Invitrogen Purelink HiPure Plasmid Miniprep or maxiprep Kit according to manufacturer's instructions.

2.3.7 DNA sequencing

The Institute of Genetics and Molecular Medicine (IGMM) core technical services used Dye terminator sequencing reactions (Applied Biosystems) and processed all sequencing samples using a 3130/3730 genetic analyser (Applied Biosystems). Electropherograms were analysed using Sequencer software 4.8 (Gene Codes Corp.). Primers used for sequencing are in **Table 2.1**.

2.3.8 DNA isolation from mammalian cells

Trypsinized cells were resuspended in 500µl of lysis buffer (100mM Tris HCL, 5mM EDTA, 0.2% SDS, and 200mM NaCl) and 10µl of proteinase K and incubated overnight at 55℃. Next day, 500µl of isopropanol was added and the sample mixed well. Samples were spun at maximum speed at 4℃ for 30mins and the DNA pellets were washed with 70% ethanol. Pellets were air dried and resuspended it in 50µl Tris-EDTA and concentration measured on a Nanodrop spectrophotometer (Therm Fischer Scientific).

2.4 Microbiology Methods

2.4.1 DNA transformation in E. coli cells

Library efficiency ® DH5α chemically competent cells from Invitrogen (Ref: 18263-012) were transfected with relevant plasmids by adding 1ng plasmid to 50µl of cells

and incubating on ice for 30mins. The vial was then heat shocked for 30 seconds at 42℃ and immediately placed back on ice. 1ml of warm LB (Luria-Bertani medium (10g/L NaCl, 10g/L Bacto-tryptone, 5g/L Yeast extract) media was then added to cells and left to grow in incubator shaker maintained at 37℃ for one hour. 20-100µl of this was then plated on L-agar (10g/L NaCl, 10g/L Bacto-tryptone, 5g/L Yeast extract, 15g/L Difco Agar) plates containing a relevant antibiotic. Plates were left upside down in incubator at 37℃ overnight.

2.4.2 Purification of DNA from E.coli cells

Single colonies were isolated from L-agar plates and used to inoculate 5ml LB media for minipreps or 500ml LB media for maxipreps. These were grown overnight in the shaker incubator at 37℃ with a suitable antibiotic (Ampicillin at 50µg/L, Kanamycin at 50µg/L). To prepare glycerol stocks, 500µl of transformed E. coli cultures were mixed with 500µl of 50% glycerol and stored in 2ml cryo-screw capped vials at -80℃. The remainder of the cultures were used to isolate DNA using Invitrogen Purelink HiPure Plasmid Miniprep kit (REF: K210011) or Maxiprep Kit (REF: K210007) as per the manufacturer's instructions. All plasmids were verified by sequencing.

2.5 Protein Methods

2.5.1 Protein isolation from mammalian cells and tissues

Buffers used:

- 1X Cell lysis buffer (Cell Signalling Technology: 20mM Tris-HCl (pH 7.5), 150mM NaCl, 1mM Na_2 EDTA, 1mM EGTA, 1% Triton-X100, 2.5mM sodium pyrophosphate, 1mM β-glycerophosphate, 1mM Na_3VO_4, 1µg/ml leupeptin).
- 1X RIPA buffer (Cell signalling Technology: 20mM Tris-HCl (pH 7.5), 150mM NaCl, 1mM Na_2 EDTA, 1mM EGTA, 1% NP-40, 1% sodium deoxycholate, 2.5mM sodium pyrophosphate, 1mM β-glycerophosphate, 1mM Na_3VO_4, 1µg/ml leupeptin).
- Immunoprecipitation lysis buffer (50mM Tris-HCl (pH 7.5), 100mM NaCl, 10% Glycerol, 0.5mM EDTA, 0.5% IGEPAL, and 0.15% Triton-X 100).

Cells or tissues were lysed in one of the above buffers with the addition of 1/100 Halt protease inhibitor cocktail solution (Thermo) and a tablet of protease inhibitor tablet (1 tablet per 10mL, Complete Mini, Roche). The lysate was either homogenized at 4℃ for 30mins or sonicated briefly (5x10 second pulses, Bioruptor Diagenode) to lyse the cells or tissue. The lysate was centrifuged at 14,000g at 4℃ for 30mins and the supernatant transferred to a fresh tube. For western blot experiments, samples were stored at -80℃. If samples were to be used for immunoprecipitation experiments, lysates were immediately used for the experiment to maximize chances of detecting transient interactors.

2.5.2 Endogenous immunoprecipitation to isolate interactors

Embryos were dissected and sample taken for genotyping. Embryos were weighed and lysed in 10µL IP lysis buffer per mg of each sample (**Section 2.5.1**). Samples were homogenised with the hand held tissue Biorupter and incubate at 4℃ on a rotator for 30 minutes. Lysates were clarified by spinning at 4℃ (14,000rpm) for 20 minutes and transferring the supernatant to a fresh tube. The protein concentration was determined using the BCA Protein Assay Kit (Thermo Fisher Scientific, **Section 2.5.5**). For each IP, 500µg of protein was used and 3µg of each antibody (**Table 2.2**) was added. Lysates were incubated with the antibody overnight at 4℃ with mild agitation (side-to-side). Immunoprecipitation of immunocomplexes was done using Pure Proteome beads (lot#2432495, REF: 030914). Before adding antibody-lysate mix, beads were resuspended by gently rotating on a roller. To a fresh tube, 30µl beads/IP was transferred and resuspended in 500µl IP lysis buffer/IP, followed by gentle agitation for 5mins to equilibrate the beads. Tubes were placed on a magnet for ~2min and any buffer was aspirated off with the fine pipette. 200µl antibody-lysate mix was added each tube of to 30µl equilibrated beads and incubated for 45mins with agitation, to concentrate immunoglobulin complexes on beads at 4℃. Washes (8 times) were performed, each lasting 2-5min. Beads were transferred to a fresh tube and spun as followed by a final magnetic separation to ensure all liquid is removed. Washes were as follows: 2x washes in Wash Buffer-1 (same as IP lysis buffer used); followed by 2x washes with Wash Buffer-2 (IP lysis buffer with reduced IGEPAL (0.2%)); and finally 4x washes with Wash Buffer-3 (IP lysis buffer without any IGEPAL

detergent). Dry beads were stored at -80℃ or samples were sent immediately for mass spec.

2.5.3 GFP-trap to pull down interactors of overexpressed WDR35

Given the lack of robust antibodies for WDR35 for an endogenous IP approach, I tried to use a transiently transfection approach with WDR35-EmGFP. GFP-trap system (Chromotek) is a high-affinity GFP-binding nanobodies coupled to magnetic or agarose beads, which helps to cleanly pull down overexpressed WDR35, which could be then analysed by mass spec to find out interactors. This experiment was done using RPE cells.

Protocol: hTERT RPE-1 cells were plated the day before in complete media to a desired confluency of 80%-90% ($2.2X10^6$ cells in 10cm dish). Cells were transfected as described in **Section 2.2.6** using either Wdr35-EmGFP and the other dish were transfected with control pEGFP-N1vector (**Table 2.3**). 10 times less DNA was used for control than test. Imaging confirmed success and efficiency of transfection. Cells were rinsed with warm PBS and aspirated thoroughly. Directly to the plate, 750µl lysis buffer (**Section 2.5.2**) was added and samples incubated on ice for 10mins. Cells were scraped off the plate into fresh tubes, spun down at 14000g at 4℃ for 20mins and the supernatant was transferred to a fresh tube. The protein concentration was determined using the BCA Protein Assay Kit (Thermo Fisher Scientific, **Section 2.5.5**). The sample was diluted with wash buffer to lower the IGEPAL concentration to 0.2%. 20µl of blocking beads per IP were equilibrated with 100µl (per IP) of wash buffer with 0.2% IGEPAL for 5mins at 4℃ with mixing. Samples were magnetically separated and the supernatant discarded. 1mg of lysate was added to equilibrated beads and incubated for 45-60mins at 4℃ with mixing. After blocking, magnetically separate the lysate from the blocking beads transferring it to GFP trap beads, equilibrated beforehand as per the blocking beads. Pre-cleared lysates were incubated with the GFP trap beads for 2-3hrs at 4℃ with mixing. Samples were magnetically separated and the supernatant frozen down as the unbound lysate at -80℃. Beads were washed two times with wash buffer with 0.2% IGEPAL. Beads were washed again twice with wash

buffer with no detergent. After the final wash, beads were given for mass spec or run on gel to check the protein bands by western blot.

2.5.4 Mass spectrometry

All mass spectrometry experiments were done in house at IGMM in the lab of Dr. Alex Von Kriegsheim by Jimi Wills, as per their published protocol (*Turriziani et al., 2014*). Briefly, the immunocomplexes collected on magnetic beads, as explained in **Section 2.5.2**, were processed to generate tryptic peptides. Proteins were eluted from beads by incubating at 27℃ for 30mins in elution buffer (2M urea, 50mM Tris-HCl pH 7.5 and 5µg/mL Trypsin). The sample was then centrifuged, bead pellets washed twice and the supernatant from samples digested overnight at room temperature. Iodoacetamide was added to the samples to inhibit disulphide bond formation and incubated for 30mins in the dark. This was followed by addition of trifluoroacetic acid (TFA) to stop tryptic digestion. Desalting and pre-fractionation of the digested peptides were done by manually using C18 pipette stage-tips filled with 3M empore disc activated with 50% acetonitrile and 0.1% TFA and then washed once with 0.1% TFA. The peptide mixtures were passed manually along to the column with a syringe to concentrate and purify the analytes. Peptides were subsequently eluted twice in 50% acetonitrile, and 0.1% TFA and both eluates were combined. Samples were concentrated and resuspended in 0.1% TFA. This was followed by chromatographic separation on a Reprosil column along a 3-32% acetonitrile gradient. The LC setup was attached to a Q-Exactive mass spectrometer, and ion mass spectra were obtained following HPLC during a tandem MS run. Mass spectra were analysed using Max-Quant software. Label-free quantification intensity (LFQ) values were obtained for analysis by identifying mass/charge ratio, and their intensities at a specific elution time for individual peptides. The data was collected for both control (GFP) and specific proteins IPs (i.e. IFT88, IFT140, and ARL13B). LFQ (label-free quantification intensity) values for the proteins were obtained by summing the ion intensities corresponding to peptides after assigning the unique peptides to proteins. The ratio of LEQ intensities of Test: control was taken, where higher the ratio better corresponds to a better enrichment of protein in complex.

2.5.5 Protein concentration determination by BCA kit

Protein concentration was determined using the Pierce Bicinchroninic Acid (BCA) Protein Assay Kit (ThermoScientific), as per manufacturer's instructions. Briefly, 10µl of the sample was mixed with 190µl working reagent (50 parts Reagent A to one part Reagent B) and incubated at 37°C for 30minutes. The samples change color after 30mins. The Thermo Multiskan Spectrum plate reader was used to measure absorbance at 562nm and compared to a bovine serum albumin (BSA, provided in the kit) standard curve to calculate the protein concentration in the lysates.

2.5.6 SDS-PAGE to resolve proteins

Ready-to-use SDS-PAGE gels (NuPage Novex precast gels, Life Technologies) were used to separate proteins for IPs of lysates. 3-8% Tris Acetate gels were used for high molecular weight proteins, whereas 4-12% Bis-Tris gels were used for medium to low molecular weight proteins. Gels were run in an XCell SureLock electrophoresis cell (Life Technologies) with either Tris-Acetate buffer, MOPS or MES buffers (Life Technologies) with antioxidant and diluted in water. Protein concentration was determined with BCA kit (**Section 2.5.5**), and the calculated amount of protein sample was reduced by adding 0.25 volume of 4X LDS buffer (contains lithium dodecyl sulphate) and 0.1 volume 1X reducing agent (Life Technologies) and incubating at 70°C for 10 min to denature the protein It was then loaded in wells and alongside Novex Sharp Protein Standard (range: ~31kDa - ~460kDa markers) was loaded as a protein molecular weight marker lane (Life Technologies). A 150V-200V potential was applied depending on the type of gel for around one hour or more, in order to get good quality electrophoretic separation.

2.5.7 Western blotting

The resolved proteins on the gel were transferred to nitrocellulose or PVDF (Hybond P, GE health care) membrane by western blot. Nitrocellulose membranes were pre-soaked in transfer solution and PVDF membrane in 100%methanol. The gel was layered over the transfer membrane and sandwiched between two Whatmann filter paper and sponges on either side. Whatmann and sponges were pre-equilibrated with transfer buffer (Novex transfer buffer 20X (Life Technologies), 10% methanol and

antioxidant up in water). The transfer was carried out in an XCell II Blot module. Protein transfer took about 10mins at 30V. The success of transfer was assessed by complete transfer of the high molecular weight markers of the protein ladder to the membrane. The membrane was then blocked with a 10% solution of dried skimmed milk (Marvel Premier Foods) made in 1X TBST (0.05% Tween-20 in TBS) for 1h at room temperature or overnight at 4°C on a shaker. It was then washed with PBS and incubated with primary antibody (**Table 2.3**) diluted in 1% skimmed milk solution in 1X TBST and incubated overnight at 4°C on shaker/roller. Membranes were washed in 1X TBST three times for 10mins followed, by a one-time wash with PBS. the membrane was incubated in HRP-conjugated secondary antibody from appropriate species (**Table 2.4**) for one hour at RT, diluted in a solution of 1X TBST and 1% milk. Blot was then washed with 1X TBST, three times and with PBS twice. After the washes, protein bands were detected by incubating the membrane in 1:1 reaction mix from Super Signal West Femto kit (ThermoScientific) or Super Signal West Pico kit (Thermo scientific). Protein bands were visualized digitally by transmission light imaging on ImageQuant LAS 4000 (GE Healthcare) and analysed using ImageQuant TL software. Membranes were stripped between successive primary antibody incubations with Restore PLUS stripping buffer (ThermoScientific) followed by washes and re-blocking. For long-term storage, membranes were air-dried between Whatmann filter papers and stored sealed in plastic. For re-use, PVDF membranes were first equilibrated in methanol and nitrocellulose membranes in transfer buffers.

2.5.8 Quantification of protein concentration by immunoblot densitometry

Images acquired, as explained above, were quantified with ImageJ/FIJI software, by measuring the intensity of individual bands and normalizing intensities with alpha-tubulin or beta-actin loading control bands on the same blot. Every quantification in this thesis is no less than an average of three to four different blots per antibody.

2.6 Immunostaining Dyes and Methods

2.6.1 Antibody staining

Cells were washed two times with warm PBS, then fixed in either 4% PFA in 1X PHEM/PBS 15mins at room temperature, 2% fresh glutaraldehyde/1X PHEM for

15mins, or 100% cold ethanol for 3mins.), according to the antigenicity compatibility as listed in **Table 2.2**, then washed twice in wash with PBS. (1X PHEM (pH 6.9) contains: 60mM PIPES, 25mM HEPES, 10mM EGTA, and 4mM MgSO4·7H20). To quench autofluorescence, cells were treated with 50mM NH_3Cl, two times, 15mins each for PFA fixed cells or 0.01mg of $NaBH_4$ in 1X PBS for 7mins for glutaraldehyde fixed cells. Cells were then washed twice with PBS. Cells were permeabilised with 0.25% Triton-X 100/TBS for 10mins at room temperature. Cells were rinsed twice in 1X TBS 5mins. Blocking for non-specific binding was done by incubating samples in 10% donkey serum/ 1X TBS (0.2% Tween-20) for 60mins at room temperature. Samples were washed twice with warm PBS. Primary antibodies (**Table 2.2**) were added to samples and incubated for 60mins at room temperature or 4℃ overnight, in dilutant made of 1% donkey serum/TBST (0.025% Triton X-100). Samples were washed with 0.25% Triton-X 100 in TBS 4-6 times 10mins each. Secondary antibodies diluted in 1% donkey serum and 0.025% triton-X100 in TBS (1:200) were incubated on samples for 60mins room temperature. Samples were washed with TBST 4-6 times 10mins then stained with DAPI (1:1000) in PBS for 5mins at room temperature. Samples were washed with PBS then either directly imaged or coverslips were added on slides using ProLong Gold antifade (Thermo Fisher Scientific), according to the manufacturer's instructions.

2.6.2 SIR-tubulin

From a SIR-tubulin kit (Spirochrome REF: SC002), a 1mM stock solution was prepared in anhydrous DMSO and stored at -20℃, without aliquoting. For staining, 1:5000 (200nm) of SiR-tubulin stock was diluted in low serum or complete serum media, cells were incubated in the hypoxic incubator for 1hrs, then live imaged without washing. The kit comes with Verapamil which is an efflux pump and calcium channel inhibitor. The two cell lines mentioned in this thesis RPE-1 cells (**movie 2.1**) and MEFs **movie 2.2**) were very efficiently stained without any Verapamil treatment included in the kit (*Lukinavičius et al., 2014*) (see **movie 2.1 and 2.2 and Appendix II**).

2.6.3 Tubulin nanobodies

Single domain antibodies or nanobodies are antibody fragment consisting of single monomeric variable antibody domain, making them very small (12KDa) as opposed to conventional antibodies (~150KDa). Therefore, their small size helps to avoid the linkage error of ~20-30nm when using primary and secondary antibodies (Ries et al., 2012). Tubulin nanobodies are specific for polymerised microtubule tubulin (Mikhaylova et al., 2015). This was a gift from Jonas Ries Lab (EMBL Heidelberg). I used 1:500 concentration of nanobodies along with other antibodies to stain other structure following the immunofluorescence protocol (**Section 2.6.1**). Microtubules are best preserved with glutaraldehyde staining; tubulin nanobodies worked with both paraformaldehyde and glutaraldehyde staining. Many other antibodies are not compatible with GA fixation. Interestingly, tubulin nanobodies worked well on RPE-1 cells but were gave high nonspecific staining on MEFS, so were not used in further experiments .

2.6.4 SNAP-tag dyes

SNAP-TMR staining protocol: A SNAP-Cell® TMR-Star (Bio Labs, REF No. S9105S) stock concentration was received at 30nmol. 24hrs serum-starved confluent cells in 24well plate were incubated with 1:1500 TMR-SNAP to low serum media in the hypoxic incubator for 30mins. 500ul of media with TMR-SNAP was added to each well. Give 2X wash with low serum media (for ciliated cells) 1hr each while incubating the samples in the incubator. Important to note SNAP-BG bond is a covalent bond. Hence it's highly stable. Unbound dye was washed out by two rounds of incubation in low serum media, but unlike SIR-SNAP, TMR was not very photostable and bleached after 24hrs of imaging. Samples were incubated for 1hr in 1:5000 SIR tubulin (**Section 2.6.2**) and a drop of Hoechst 344442 in the incubator. Live imaging was done using DAPI, rhodamine, and Cy5 filters.

SNAP-Cell® 647-SiR staining protocol: A SNAP-Cell® SiR-Star (Bio LabsREF: S9102S) was purchased from Bio Labs, with a stock concentration of 30nmol. Cells were treated with 1:200 SiR-SNAP diluted in complete media and incubated in a hypoxic incubator for 30mins. Cells were washed twice in complete media 1hr each while incubating the samples in the incubator. Nuclear staining was done by adding 1

drop of Hoescht33342 in 4ml of culture media. Live imaging was done using the DAPI and Cy5 channels on the Leica SP5.

2.7 Microscopy Methods

2.7.1 Light microscopy

Most confocal imaging for both fixed and live-cell samples was done on Leica SP5 (Leica Microsystems, Milton Keynes UK) at the Imaging Resource core facility of MRC Institute of Genetics and Molecular Medicine using the LAS-AF software. The microscope is equipped with 405nm diode, Argon and, 561 and 648nm laser lines, three Photomultiplier tubes and one HyD GaSP detector. Images were scanned using a 63X 1.4NA oil immersion objective and latter processed using ImageJ and Imaris software.

2.7.2 Super-resolution microscopy- STED

Stimulated emission depletion microscopy (STED) is a super-resolution technique capable of 50nm resolution through the selective deactivation of fluorescent molecules by two synchronized lasers (Hell and Wichmann, 1994). To further improve resolution, gated fluorescence detection (g-STED) was used, which further helps to reduce out of focus intensity in samples. gSTED methods were used for imaging cilia and endosomes in a 3D single color STED experiments. Single color gated STED experiments were done on Leica-SP5 STED based at Heriot-Watt University using 100 X, 1.4NA objectives. Samples were prepared as explained in **Section 2.6.1**.

2.7.3 Electron microscopy

Electron microscopy experiment was done at MPI-CBG Dresden, Germany, in collaboration with Dr. Gaia Pigino.

EM sample preparation: 24hr serum-starved MEFs were chemically fixed for flat embedding using the following protocol: (1) Cells were grown on 60mm dishes and ciliogenesis induced by serum starvation. (2) For prefixation under culture conditions, 25% glutaraldehyde was added to the growth medium to a final concentration of 1%, mixed gently and incubated for a few minutes at 37℃. (3) The growth medium (containing the glutaraldehyde) was replaced with 0.1M HEPES, 4mM $CaCl_2$, 1–2.5%

glutaraldehyde, pH 7.2 and incubated for 1hr at room temperature (replacing the fixation buffer with fresh one after 20 min). All prefixation solutions were prewarmed to 37℃ and all steps done at 37℃, to preserve microtubules polymerization. (4) The fixation buffer was replaced with fresh fixation buffer and incubated for 3–4hrs at 4℃. (5) Washes were done in the dish, once in 0.1M HEPES, 4mM $CaCl_2$, pH 7.2 and 2–3 times in distilled water, each for 5–10mins, gently removing and replacing the buffer. (6) Samples were incubated in 1% OsO_4 (EMS) (in distilled water) for 1h at 4℃. (7) Samples were washed 3–4 times for 10mins each in distilled water. (8) Samples were incubated in 1% uranyl acetate (EMS) (in distilled water) overnight at 4℃. (9) Samples were rinsed 3–4 times for 10mins each in distilled water. (10) Dehydration was performed using a graduated series of ethanol: 30%, 50%, 70%, 80%, 90%, 96% ethanol 5mins each step at 4°C, followed by twice rinsed in anhydrous 100% ethanol 10mins each at RT. (11) Infiltration was performed using a 1:1 mixture of LX112 (Ladd Research, USA; EMS) and ethanol 2hrs, followed by pure LX112 overnight and another 2hrs pure LX112, where all steps were performed at room temperature. (12) FLAT EMBEDDING: For flat embedding, the caps of BEEM embedding capsule (size, #3, EMS) were cut off and capsules filled with LX112. The capsules were inverted over a selected area of the cell monolayer the dish and the resin cured in 60°C oven for 48hr. The capsule is then removed by breaking off from dish leaving the monolayer cells embedded in the surface of the block. The top 1-2mm block surface with embedded cell monolayer was removed by sawing it off and remounting it on a dummy block for sectioning, in a perpendicular orientation in respect to the monolayer. (13) SECTIONING AND POST-STAINIG: For sectioning and post-staining, 300nm thick serial sections were cut by Leica Ultracut UCT (Leica microsystem, Wetzlar, Germany) with a diamond knife and sections picked up with a Formvar (EMS) coated 1x2 mm slot copper grid (EMS). Sections were post-stained with 2% uranyl acetate for 10mins, then with lead citrate 5mins.

Imaging: Sections were stained on the grid with fiducials (15nm gold nanoparticles, Sigma-Aldrich). Tilt series were acquired on Tecnai F30 (FEI) transmission electron microscope, operated at 300kV and attached with 2048x2048 Gatan CCD camera and Serial EM software (Mastronarde, 2005). Serial EM software was used for automatic

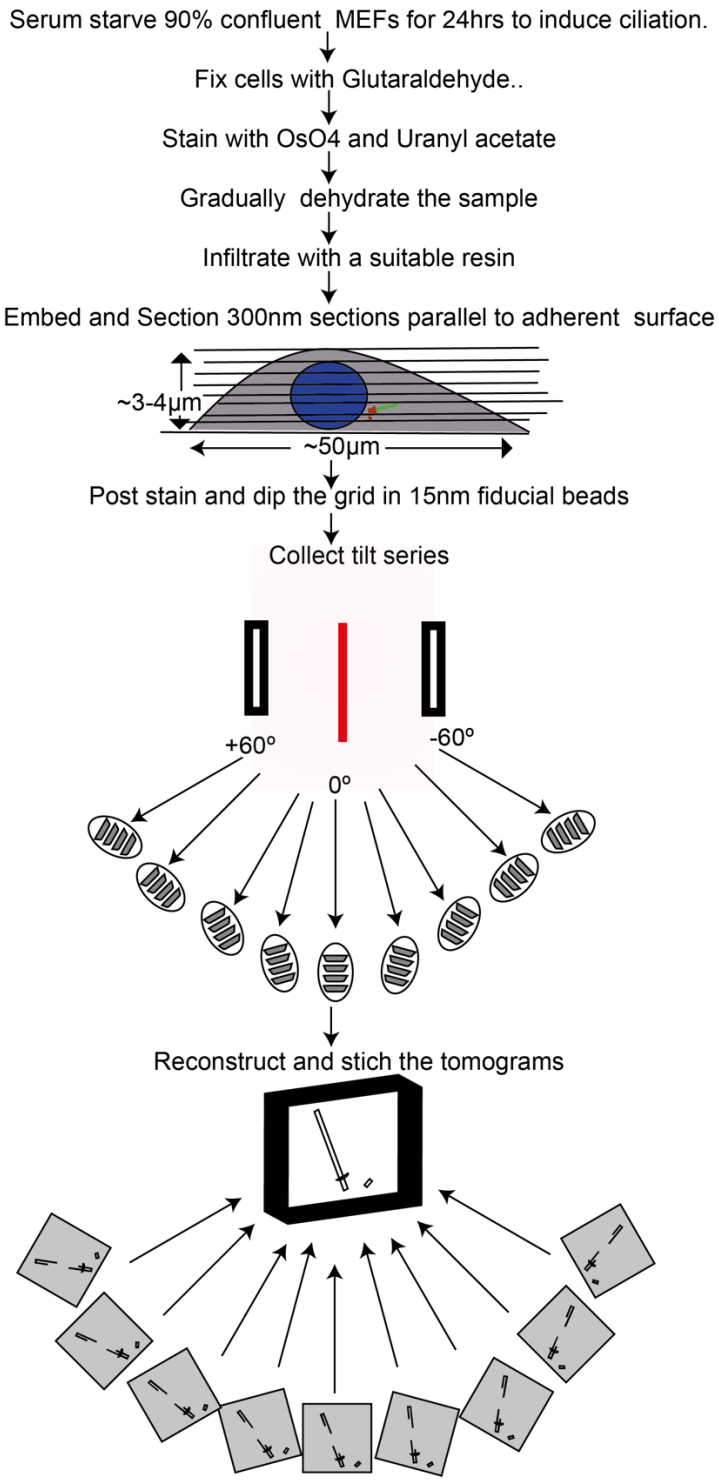

Figure 2.1. Summary of TEM and tomography workflow to reconstruct a 3D model of MEF cilia. Cells were serum-starved, fixed, stained, dehydrated, infiltrated, and embedded and sectioned, as explained in the protocol. 3-4 300nm sections were collected on each grid, and co-ordinates for cells marked. A dual tilt from +60º to -60º angle with an increment of 1º angle using Serial EM software was collected. The 2D image at each angle was aligned and reconstructed into 3D volume using ETOMO and IMOD software.

acquisition of double tilt series. Before setting up the automated high throughput imaging on Techei F30, cell co-ordinates were initially marked by imaging on the FEI Morgagni TEM (100kV) equipped with a side-entry Olympus Morada CCD Camera (11Mpixels). Since 300nm sections are too thick for electron beams, 3D density maps of cells were reconstructed from multiple 2D projections acquired at a tilt series, a series of different angles with an increment of 1º (**Figure 2.1**). Tomographic tilt series were recorded in single tilt axis geometry, with a pixel size of 1.235nm, a maximum tilt range of about 60° and tilt steps of 1°. MEFs are around 3-4µm thick from the adherent cell surface, and cilia were found to initiate mostly at the height of nearly 1µm. In 24hrs serum-starved MEFs, cilia were around 2-3µm in length and grew almost parallel to the cell. To get the complete 3D overview of cilia with its surrounding, two to three 300nm sections were needed. Complete 3D information of one cilium required reconstruction of two to three tomograms. For quantification, at least 3 cilia each for *wild type*, *Wdr35*$^{-/-}$ and *Dync2h1*$^{-/-}$ minimum of 27 tomograms were reconstructed. A total of 40 tomograms have been reconstructed for this thesis. Reconstruction, joining, segmentation, and visualization of the tomograms was done using the IMOD software package (*Kremer et al., 1996*).

2.7.4 CLEM (correlative light and electron microscopy):

In order to determine IFT121/WDR35 localization on vesicles around control cilia, CLEM (correlative light and electron microscopy) experiments were performed on MEFs. To bypass subpar endogenous WDR35 antibodies, we undertook an alternate approach using WDR35-EmGFP overexpressed in *Wdr35*$^{-/-}$ MEFs in order to have all WDR35 as the GFP-tagged version to maximize GFP labeling. Briefly, cells were seeded onto graded glass metric dishes. Although glutaraldehyde fixed cells gave best structural preservation in electron microscopy experiments, antibodies used for light microscopy could not survive their epitopes after GA treatment. Light microscopy-STED was performed on PFA fixed cells, with staining as described (**Section 2.6.1**). Cells were immunostained with a rabbit ARL13B antibody and a mouse GFP Ab (**Table 2.2**), followed by secondary antibodies anti-rabbit Alexa 594 and anti-mouse Alexa635P (**Table 2.3**). STED experiments were performed on a custom microscope

in Dr. Alf Honigmann's lab, MPI-CBG Dresden. Along with STED images, transmission bright field light microscopy images were also made to get the right co-ordinates to be cut out for electron microscopy imaging. Following STED imaging, cells were then fixed with 2% glutaraldehyde and processed for TEM as described (**Section 2.7.3**). This time 70nm sections were made, mounted on grids and scanned FEI Morgagni TEM (100kV) microscope to find the right cells. STED images are overlaid with TEM data later.

2.8 Statistics and Software

2.8.1 Swiss Model and Phyre^2 for protein structural modelling

SWISS-MODEL is a fully automated protein structure homology-modelling server, accessible via the ExPASy web server, or from the program DeepView (Swiss Pdb-Viewer). Phyre^2 (protein homology/anology recognition engine V2.0) is another open source structure prediction server. Both the servers were used to predict structures of IFTs and BBSomes and gave similar results, but the data shown in this thesis is from only the SWISS-MODEL server. Briefly, a template search with BLAST and HHblits was performed against the SWISS-MODEL template library. The target sequence was searched with BLAST against the primary amino acid sequence contained in the SMTL (**Appendix-IV**). A total templates were found in each case is shown in **Appendix-V** . An initial HHblits profile, followed by 1 iteration of HHblits against NR20, was run and the obtained profile then searched against all profiles of the SMTL. The total number of templates were found are detailed in **Appendix-V**. The top hit in all of IFTA searches was 3mkqA a coatomer β' subunit 2.5Å X-ray structure with 14-20% sequence identity and 25-30% sequence similarity with different IFT-A proteins (**Figure 4.2 chapter4**). Range and percentage of amino acids covered for all IFT-As in shown in (**Figure 4.2 chapter4**). A coatomer α subunit was also found within these top matches. Models were built on the target-template alignment using ProMod3. Coordinates which are conserved between the target and the template were copied from the template to the model. Insertions and deletions were remodelled using a fragment library. Side chains were then rebuilt. Finally, the geometry of the resulting model was regularized by using a force field. In case loop modelling with ProMod3 fails, an alternative model was built with PROMOD-II. The global and per-residue

model quality has been assessed using the QMEAN scoring function. BBSome swiss model search result is listed in **Appendix-V**.

2.8.2 ImageJ and Imaris:

For live and fixed cell image processing and statistics of cilia number and length, all image analysis was performed using, ImageJ and FIJI (open source software, (http://fiji.sc/Fiji) and Imaris software (https://imaris.oxinst.com/packages).

2.8.3 ETOMO and IMOD (https://bio3d.colorado.edu/imod/):

IMOD is a set of image processing, modelling and display programs used for tomographic reconstruction and 3D reconstruction of EM serial sections and optical sections. The package contains tools for assembling and aligning data within multiple types and sizes of image stacks, viewing 3-D data from any orientation, and modelling and display of the image files. IMOD was developed primarily by David Mastronarde, Rick Gaudette, Sue Held, Jim Kremer, Quanren Xiong, and John Heumann at the University of Colorado. Etomo provides a graphical user interface (GUI) to the IMOD Tomography package. All tomograms in this thesis were reconstructed and stitched using ETOMO and displayed and segmented using IMOD.

2.8.4 Databases

- CRAPome is a repository for contaminants found in affinity purification mass spectrometry (http://www.crapome.org). Some of the common contaminates found IP-mass spec data were curated with references from CRAPome repository.
- NCBI (National Centre for Biotechnology Information) (https://www.ncbi.nlm.nih.gov).
- Ensembl Genome Browser (https://www.ensembl.org/index.html) was used to browse vertebrate genomes.
- RSCB Protein Data Bank (https://www.rcsb.org) repository was used to access X-ray or cryoEM based structures.
- PANTHER (http://pantherdb.org) was used for protein analysis through evolutionary relationships.

- OrthoMLC (https://orthomcl.org/orthomcl/) was used to search the closest ortholog.
- Statistical analyses were performed using MS excel.
- HHblits: (https://toolkit.tuebingen.mpg.de/#/) was used by Jonathan Wells (the Marsh lab, MRC HGU) for high throughput protein sequence based proximity searches.

Table 2.1 Primers used in this thesis

Gene/ region to be amplified	**Primer**	**Sequence**
Primers used for genotyping J4, D5, and PCM1-SNAP mouse line.		
Wdr35	FP	CCAGTGATCAAAATGGGCTTA
	RP	CGATTGTTGATCATCTCCTCAT
Dync2h1	FP	GGTGGGACCAGAAGGATGT
	RP	CGGAGCTGAGAGAAGGCATA
PCM1-SNAP (Exon 2F and Exon 2R)	FP	CTCTGACCTCTGCACACATG
	RP	ACAATCGATGGGAGAGCCTC
PCM1-SNAP (Exon 2F and SNAP R)	FP	CTCTGACCTCTGCACACATG
	RP	AAAGTAGGCGTTGAGCCAGG
Primers used for *Wdr35* cloning		
Wdr35	FP	ACGCGTCCGACGATGTTCTTCTACCTGAGCAAG
	RP	CGGTACCGTCGACTGTTCTACCGAGCTGTGGCATAAAG
CMV forward	FP	CGCAAATGGGCGGTAGGCGTG
EGFP-N	RP	CGTCGCCGTCCAGCTCGACCAG
CRISPR guides		
h*WDR35* Gd1	Top	CACCGGCTCGAGTAACGGACAGTAC
h*WDR35* Gd1	Bottom	AAACGTACTGTCCGTTACTCGAGCC
h*WDR35* Gd8	Top	CACCGGAGATGTCTATGATAGCAAGA
h*WDR35* Gd8	Bottom	AAACTCTTGCTATCATAGACATCTCC
CRISPR vector primers for sequencing guide cloned in Bbs1site in pX330		
51377 pX330_2F	FP	AGGGCCTATTTCCCATGATTC
51378pX330_435R	FP	CCTCTAGAGCCATTTGTCTGC

Table 2.2 Primary antibodies used in this thesis

Antibody	Species	Source	Dilution	Fixation
ARL13b	Rabbit	Proteintech: 17711-1-AP, Stock-41 µg/150µl	1:100 IF 1:5000 WB	PFA
Ac α-tubulin	Mouse	Sigma T6793.	1:1000 IF	PFA/GA
Ac α-tubulin	Rabbit	ab179484	1:1000 IF	PFA/GA
γ-tubulin (GTU88)	Mouse	Sigma T6557	1:100 IF	PFA
γ-tubulin	Rabbit	ABCAM ab11317,	1:100 IF	PFA
Centrin-3	Mouse	Novus Biologicals-H00001070-M01,Stock-0.1 mg.	1:100 IF	PFA
GFP	Mouse	Roche (11814460001)	1:1000 IF 1:1000 WB	PFA
GFP	Rabbit	Abcam (ab6556)	1:1000 IF 1:1000 WB	PFA
GFP	Rabbit	Santa Cruz Sc8334. Stock-0.2µg/µl	3µg IP 1:5000 WB	-
IFT88	Rabbit	Proteintech 13967-1AP. Stock 0.23µg/µl	1:200 IF 1:1000 WB 3µg IP	PFA
IFT81	Rabbit	Proteintech 11744-1-AP.	1:200 IF 1:1000 WB	PFA
IFT144	Rabbit	Proteintech 1367-1-AP.	1:200 IF 1:1000WB	PFA
IFT140	Rabbit	Proteintech 17460-1-AP..	1:200 IF 1:1000 WB	PFA
IFT122	Rabbit	Proteintech 19304-1-AP	1:200 IF 1:1000 WB	PFA
IFT122	Rabbit	Aviva ARP 53817_P050	1:1000 WB Not for IF	-
IFT43	Rabbit	From Victor L. Ruiz-Perez lab, University of Madrid, Spain	1:200 IF 1:2000 WB	PFA
IFT139	Rabbit	Novus-NBP1-90416	1:1000 WB Not for IF	-
IFT121	Rabbit	Custom made from Proteintech (only Rabbit-2 worked on blots)	1:50 WB Not for IF	-

Antibody	Species	Source	Dilution	Fixation
PCM-1	Rabbit	Proteintech19856-1-AP. Stock-40µg/150µl	1:100 PFA	MeOH
SNAP	Rabbit	New England Biolabs-P9310S	1:300 IF	MeOH
Clathrin	Rabbit	Abcam ab21679	1:1000 IF	MeOH
α-adaptin 1/2 (C-8)	Mouse	Santa Cruz sc-17771 Stock-200 µg/ml	1:100 IF	MeOH
EEA1	Rabbit	Cell Signalling Technology 3288P	1:100 IF	PFA
GPSM-1	Mouse	Santa Cruz Sc271721. Stock-200µg/ml	1:100 WB	-
GPSM-1	Rabbit	Biorbyt orb338335.	1:1000WB	-
GPSM-1	Rabbit	Millipore ABS1531	1:500 WB	-

PFA: Paraformaldehyde, PE: Pre extraction, IF: Immunofluorescence, WB: Western Blot, IP: Immunoprecipitation. MeOH: Methanol. MEOH fixed cells were pre-extracted for 30 seconds on ice in 0.1 M PIPES pH 6.8, 2mM EGTA and 1mM $MgSO_4$, then cells were fixed in ice cold methanol on ice for 10 minutes.

Table 2.3 Secondary antibodies used in this thesis

Antibody	Host	Source	Dilution	Application
ECL α-Mouse IgG, HRP-conjugated	Sheep	GE Healthcare UK Ltd NA931-1ML	1:10,000	WB
ECL α-Rabbit IgG, HRP-conjugated	Goat	GE Healthcare UK Ltd RPN4301	1:10,000	WB
MsX α-Rabbit light chain specific HRP conjugated	Mouse	Merk-MAB201P	1:10,000	WB
α-Rabbit IgG Light-Chain Specific mAb	Mouse	Cell signalling technology-L57A3	1:10,000	WB
Alexa 488, 594,647conjugated-α-Mouse	Donkey	Molecular Probes	1:500	WB
Alexa 488, 594, 647conjugated-α-Rabbit	Donkey	Molecular Probes	1:500	WB
Alexa 488, 594, 647conjugated-α-Goat	Donkey	Molecular Probes	1:500	WB

Table 2.4 Clones used in this thesis

Plasmid	Description	Source
Wdr35-EmGFP	pcDNA6.2Wdr35::C-EmGFP-TOPO	Created by Peter Budd, Mill lab, IGMM HGU
pEGFP-N1	Cat no. 6085-1, Gen Bank # U55762	Mill lab- IGMM HGU
pCAG2-mCherry-C-ITF139	IFT139 Insert-Human; NM_024753. Antibiotic-Ampicillin, Cloning site-EcoRI-BamHI	Nakayama lab-Japan
pSpCas9(BB)-2A-Puro (PX459) V2.0	Antibiotic: Ampicillin	https://www.addgene.org/62988/
Arl13B EGFP	Antibiotic: Ampicillin	Clone in Lab from Japan

Chapter 3. Characterization of ciliary phenotypes in *Wdr35*$^{-/-}$ and *Dync2h1*$^{-/-}$ mutants.

3.1 Results

3.1.1 WDR35 is concentrated at the transition zone in diffraction-limited imaging, which can be resolved as a punctate circle in STED imaging

To determine the dynamic localization of WDR35, I transiently transfected WDR35-EmGFP into primary mouse embryonic fibroblasts (MEFs) and co-stained with the microtubule biosensor SIR-tubulin (*Lukinavičius et al., 2014*) for live-cell imaging. In wild-type cells, WDR35 was found to concentrate at the transition zone of cilia, which is implicated in selective cargo trafficking into the ciliary compartment, with sparse localization along the axoneme (**Figure 3.1 and 3.2A**). Ciliated MEFs transiently expressing WDR35-EmGFP were also fixed and stained with anti-polyglutamated tubulin to highlight stabilized tubulin staining in basal body and ciliary axoneme. Here, WDR35-EmGFP was concentrated at the transition zone (negative for polyglutamated tubulin staining) (*Wloga et al., 2017*) (**Figure 3.1B-** by Dr. Pleasantine Mill). Like other IFT-As, WDR35 concentrates at transition zone but is very sparse inside cilia.

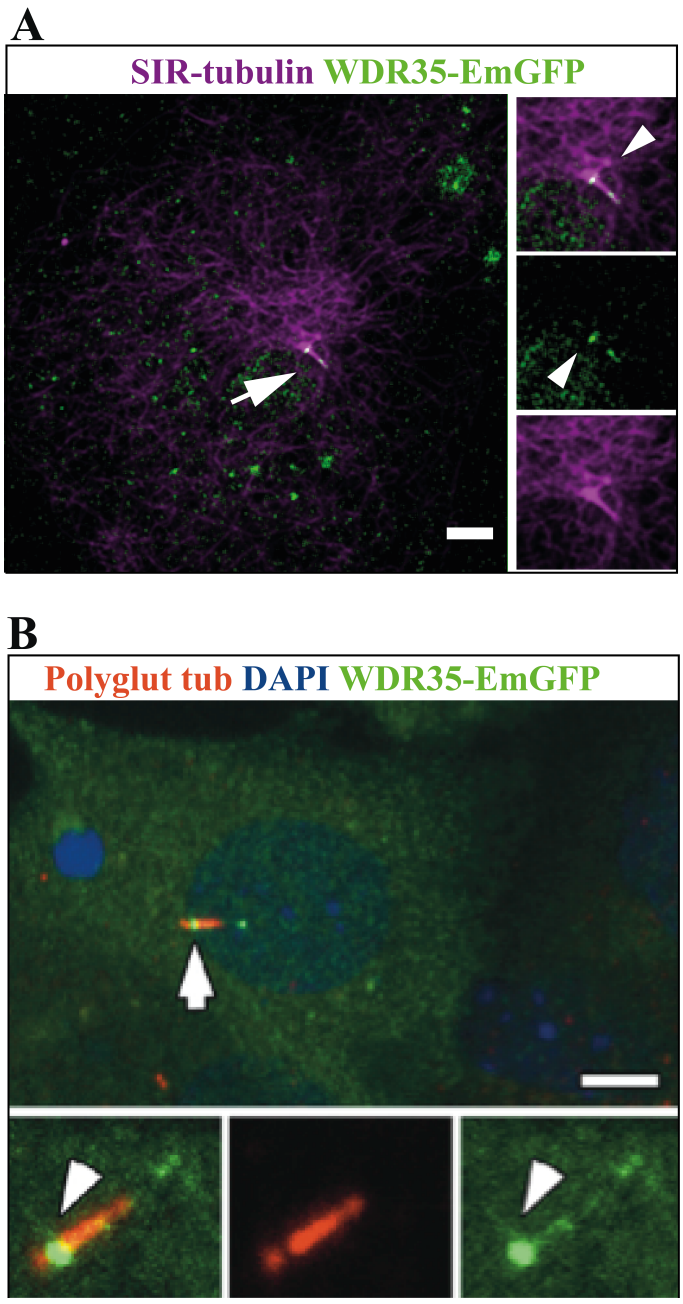

Figure 3.1. WDR35 concentrates at the transition zone and tip of cilia with faint localization along the cilia length. (A) Z-stack snapshot from live-cell imaging of MEFs stained with SIR-tubulin and electroporated with *Wdr35-EmGFP*. (B) MEFs electroporated with *Wdr35-EmGFP* followed by fixing and staining by poly-glutamylated tubulin. Scale bars: A & B=2μm. Arrows are pointing at cilia and arrowheads are pointing at the transition zone.

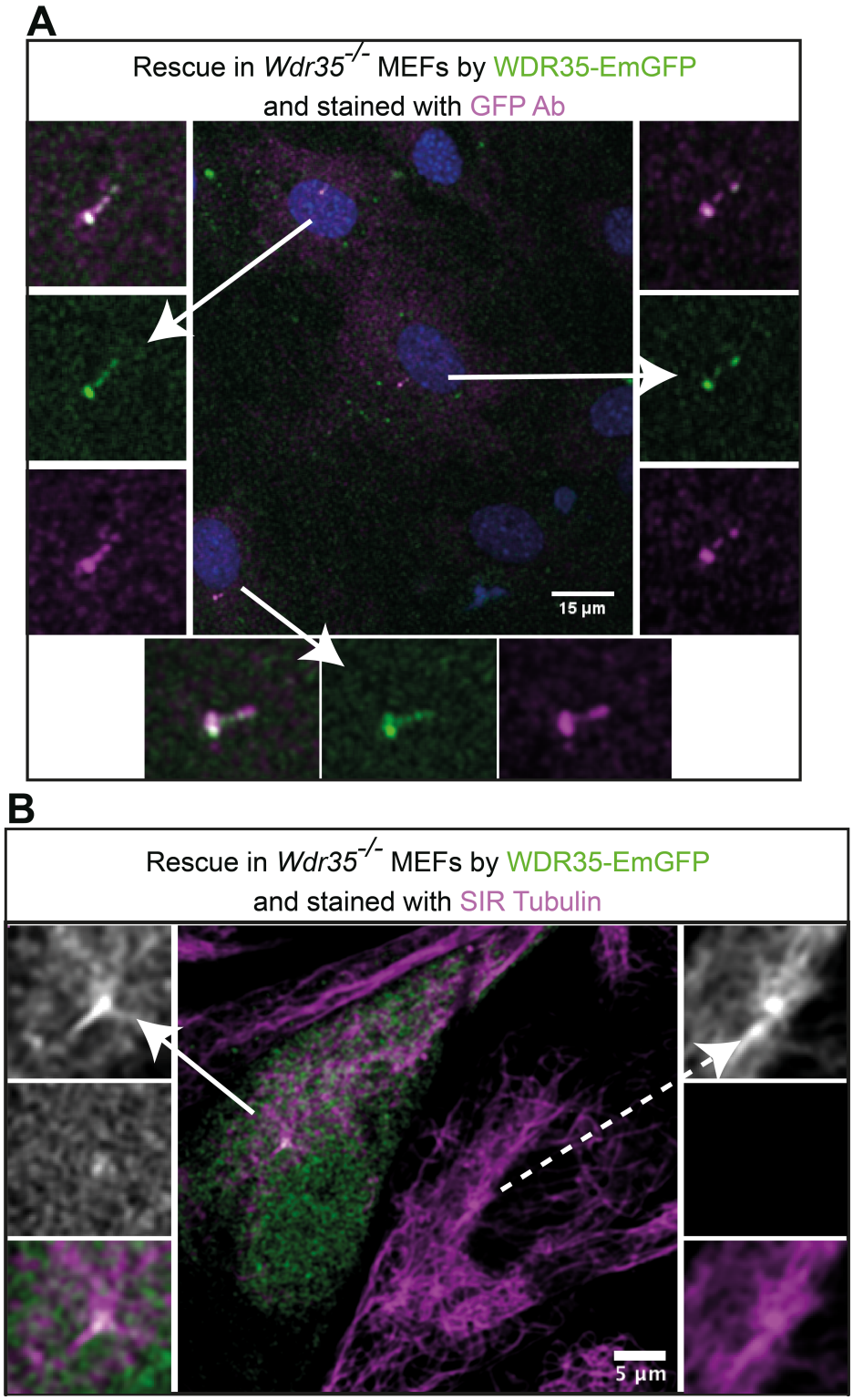

Figure 3.2. Rescue experiment of *Wdr35*$^{-/-}$ MEFs by WDR35-EmGFP followed by (A) fixing and staining with anti-GFP antibody and (B) Snapshot from live-cell imaging after SIR-tubulin staining after 24hrs of serum starvation. Arrow is pointing at zoomed out rescued cilia and dashed arrow points at small cilia of un-rescued cell in the same field of view. Scale bar: A =15µm and B =5µm.

To boost the signal, such that every molecule of WDR35 was GFP-tagged, I electroporated *Wdr35*$^{-/-}$ cells with WDR35-EmGFP to avoid competition from endogenous pools of unlabelled WDR35 and boosted the signal with anti-GFP staining. While again it was found to concentrate at the cilia base, it was much more visible as a track along cilia length (**Figure 3.2A**). Cilia are diffraction-limited structures which are challenging to image given the hundreds of proteins clustered within limited dimensions of 0.25µm in diameter and 2-4um in length. As a confocal image, WDR35 looks like diffraction-limited mass at the transition zone which has dimensions close to 0.25µm. To further refine the localization and distribution of WDR35 at transition zone, I used the stimulated emission depletion (STED) super-resolution method. STED can resolve structures 5-10nm apart in 2D and nearly 10-20nm in Z-direction; resolution of any conventional diffraction-limited imaging method is limited to 250nm in 2D and 500nm in Z-direction (*Hell and Wichmann, 1994*). I imaged MEFs transiently expressing WDR35-EmGFP and as a marker for cilia stained for membrane associated cilia marker ARL13B then imaged with single colour STED microscope to resolve WDR35 localization pattern (MPI-CBG, in-house STED microscope). I found it to resolve as a punctate ring rather than concentrating as single blob as seen in diffraction limited imaging (**Figure 3.3**).

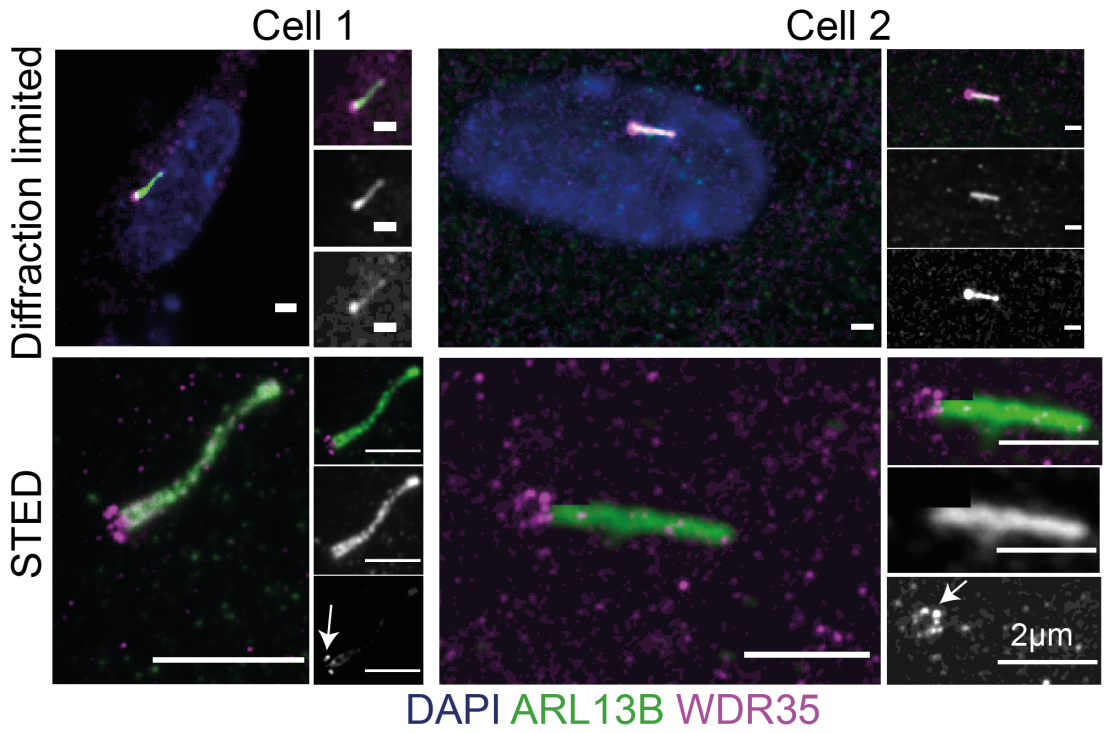

Figure 3.3. STED imaging reveals WDR35 localization to the base of cilia at the transition zone as a punctate ring. *Wdr35*$^{-/-}$ cells were electroporated with *Wdr35-EmGFP*, serum starved for 24hrs and was fixed and stained with rabbit anti-ARL13B antibody (Anti-rabbit secondary Alexa594) and anti-GFP antibody (Anti-mouse secondary Alexa647). Scale bars=2μm. Arrows point at punctate ring of WDR35 at cilia base.

3.1.2 *Wdr35*$^{-/-}$ and *Dync2h1*$^{-/-}$ cells have a drastic reduction in acetylated axoneme length, but have no difference in the number of acetylated cilia

Cilia are microtubule-based structures, and tubulin subunits in ciliary microtubules undergo highly conserved posttranslational modifications (PTMs) including acetylation, detyrosynation, glutamylation, and glycylation. This relays a 'tubulin code' that can be read by motors and other microtubule binding proteins to affect their functions. Most long-lived microtubules, like the ones present in cilia, flagella, and centrioles, have these PTMs to provide them extra stability. Acetylation is one of the most conserved PTM which marks the axoneme, transition zone, and the basal body (*Wloga et al., 2017*). To count the number of cilia and stability of axonemal microtubules in *Wdr35*$^{-/-}$ MEFs, I performed high-throughput imaging by staining with Ac- α tubulin and ϒ-tubulin antibodies. I found the length of axoneme drastically reduced from 2-4μm in *Wdr35*$^{+/+}$ cells to ~0.5μm in both *Wdr35*$^{-/-}$ and *Dync2h1*$^{-/-}$ mutant when quantifying Ac- α tubulin staining (**Figures 3.4B**). However, the total

tubulin expression level was unaltered in whole mouse E11.5 litter lysate in *Wdr35*$^{-/-}$ and MEF lysate in both *Wdr35*$^{-/-}$ and *Dync2h1*$^{-/-}$ (**Figure 3.15**). Since tubulin acetylating enzyme specifically in cilia tubulin acetyltransferase (αTAT1) prefers polymerized microtubules over tubulins (*Shida et al., 2010*), I propose that the tiny axoneme left in *Wdr35*$^{-/-}$ cilia has some polymerized microtubules which do not elongate further maybe because of the absence of enough αTAT1 or other ciliary microtubule modifying and assembling enzymes.

αTAT-1 acetylates K-40 of α-tubulin in the lumen of both central and peripheral microtubules. I also tried another tubulin marker SIR-tubulin, which is a Taxol derived small molecule conjugated to the silicon rhodamine dye, which binds to β-tubulin of polymerized microtubules irrespective of PTMs (*Lukinavičius et al., 2014*). SIR-tubulin staining also gave the same reduction in length of cilia in *Wdr35*$^{-/-}$ as Ac-α tubulin Ab-staining (**Figure 3.2B**).

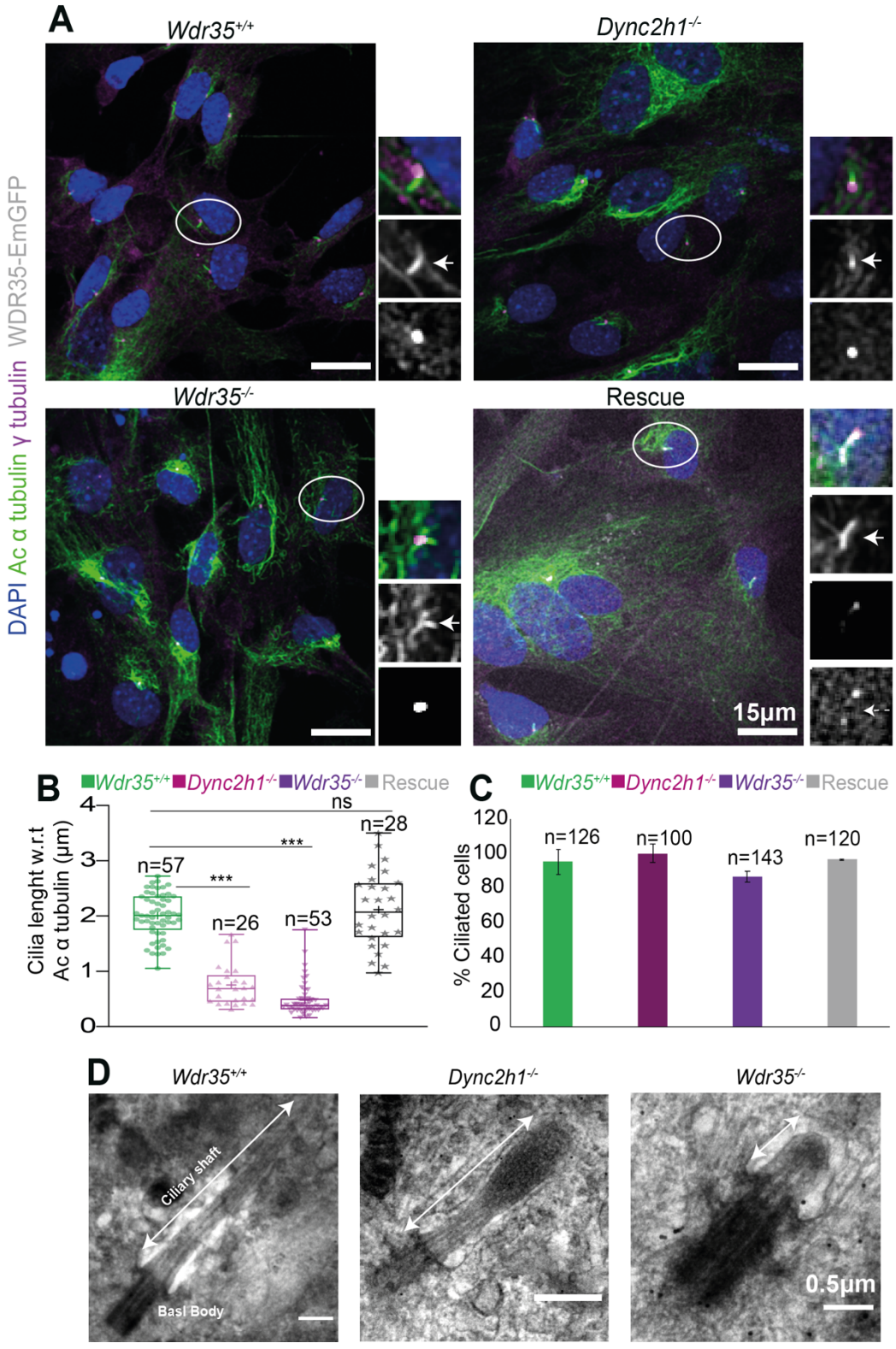

Figure 3.4. *Wdr35*$^{-/-}$ and *Dync2h1*$^{-/-}$ mutant cells have a drastic reduction in acetylated axoneme length, but have no difference in the number of cilia. After 24hrs serum-starvation *Wdr35*$^{+/+}$ and mutant MEFs, as well as those rescued by transiently expressing *Wdr35-EmGFP,* were fixed and stained with respective antibodies for Ac α tubulin (green) and γ tubulin (magenta). Nuclei were stained with

DAPI. Arrows point at ciliary axoneme stained for Ac α tubulin and dashed arrow points at WDR35-EmGFP localisation in rescued cell. (B) Quantification of Ac α tubulin positive staining of cilia length from the basal body to tip. (C) Percentage of Ac α tubulin positive ciliated cells. n= number of cells from three biological replicates). Asterisk denotes significant p-value from t-test: (*, P<0.05), (**, P<0.01), (***, P<0.001). (D) TEM images of 300nm sections of WT and *dync2h1*$^{-/-}$ and *Wdr35*$^{-/-}$ show reduction in overall length of cilia in the mutants. However while the reduction in cilia length w.r.t to Ac α tubulin staining was comparable with TEM data *Wdr35*$^{-/-}$, Ac α tubulin staining showed further reduction in cilia length when compared to TEM data of *dync2h1*$^{-/-}$ mutant. TEM images are representative of 30 each of WT , *dync2h1*$^{-/-}$ and *Wdr35*$^{-/-}$ MEFs serum starved for 24hrs, chemically fixed and processed into 300nm serial sections for TEM imaging. Scale bars, A= 15µm and D= 0.5 µm.

However staining for other ciliary proteins like IFT-B complex proteins for quantification for cilia length revealed mutant cilia to be longer than those measured with Ac- α tubulin as reference marker (**Figure 3.8-3.11** and explained in **Section 3.1.4**). Indeed, TEM analysis of *Wdr35*$^{-/-}$ cilia further confirmed the presence of a few short disorganized microtubules compared to (9+0) microtubule arrangement extending to the tip of cilia in *Wdr35*$^{+/+}$ cells (**Figure 4.3, 4.4 and 4.8**). Unexpectedly whilst *Dync2h1*$^{-/-}$ cells also possessed very tiny cilia with respect to Ac-α tubulin immunostaining (~0.5µm from basal body, TEM analysis revealed longer cilia (**Figure 3.4D**) with polymerised microtubules extending throughout the length of cilia (2-4um from basal body (**Figure 3.4D and 4.10**). This suggests that standard axonemal assembly is not affected in the absence of retrograde axonemal dynein function, albeit with a reduced level of acetylation limited to the most proximal end of the axoneme. Alterations in PTMs could result from stalled IFT- particles and motors which accumulate in *Dync2h1*$^{-/-}$ cilia.

3.1.3 Membrane protein cargos have an anterograde trafficking defect in *Wdr35*$^{-/-}$ and retrograde defect in dynein mutant *Dync2h1*$^{-/-}$.

In *Wdr35*$^{-/-}$ mutant cilia, endogenous ARL13B, a small membrane associated GTPase, fails to localize to cilia whereas the axonemal IFT-B subunit IFT88 accumulates inside short club-shaped structures (**Figure 3.5**). While the accumulation of IFT-B is consistent with a defect in retrograde IFT similar to *Dync2h1*$^{-/-}$ (**Figure 3.5 and 3.8-3.11)**), the lack of membrane cargo enrichment in cilia is distinct. This defect represents a defect in trafficking as the total levels of ARL13B, as shown by immunoblot, are unchanged (**Figure 3.5B**). Moreover, very high levels of transiently

transfected membrane cargos including fluorescently-tagged ARL13B (**Figure 3.6A**) and SMO (**Figure 3.6B**) also fail to localize to *Wdr35*$^{-/-}$ cilia, with some accumulation at the cilia base. Interestingly, overexpressed ARL13B, when not transported to cilia, becomes concentrated on other membranes, particularly the cell membrane whereas SMO which fails to enter cilia is localised in vesicles in cytoplasm of mutant cells (**Figure 3.6, Movie 3.1**).

To look more generally at ciliary membrane compartmentalization in *Wdr35*$^{-/-}$ MEFs, I examined the localization of lipidated motifs tagged to EGFP (*Williams et al., 2014*) to look at specialized membrane microdomains. While EGFP alone was found to diffuse freely in cilia in *Wdr35*$^{+/+}$ MEFs, efficient targeted delivery into control cilia was observed in EGFP tagged with either myristoylation and palmitoylation (MyrPalm) or dual palmitoylation (PalmPalm) motifs. No enrichment of dual geranylation (GerGer) modified EGFP was observed in control primary cilia of fibroblasts, whereas low level expression was reported previously in the most proximal portions of highly specialized olfactory sensory cilia (*Williams et al., 2014*). This suggests cell-type, cilia-specific differences likely exist. In contrast, in *Wdr35*$^{-/-}$ MEFs, both the myristoylation and palmitoylation (MyrPalm) or dual palmitoylation (PalmPalm) eGFP accumulated around centrioles (**Figure 3.7**). These results suggest that WDR35 plays a critical role in trafficking several broad categories of the membrane and membrane-associated cargos, necessary for the unique and specialized identity and function of the cilial compartment.

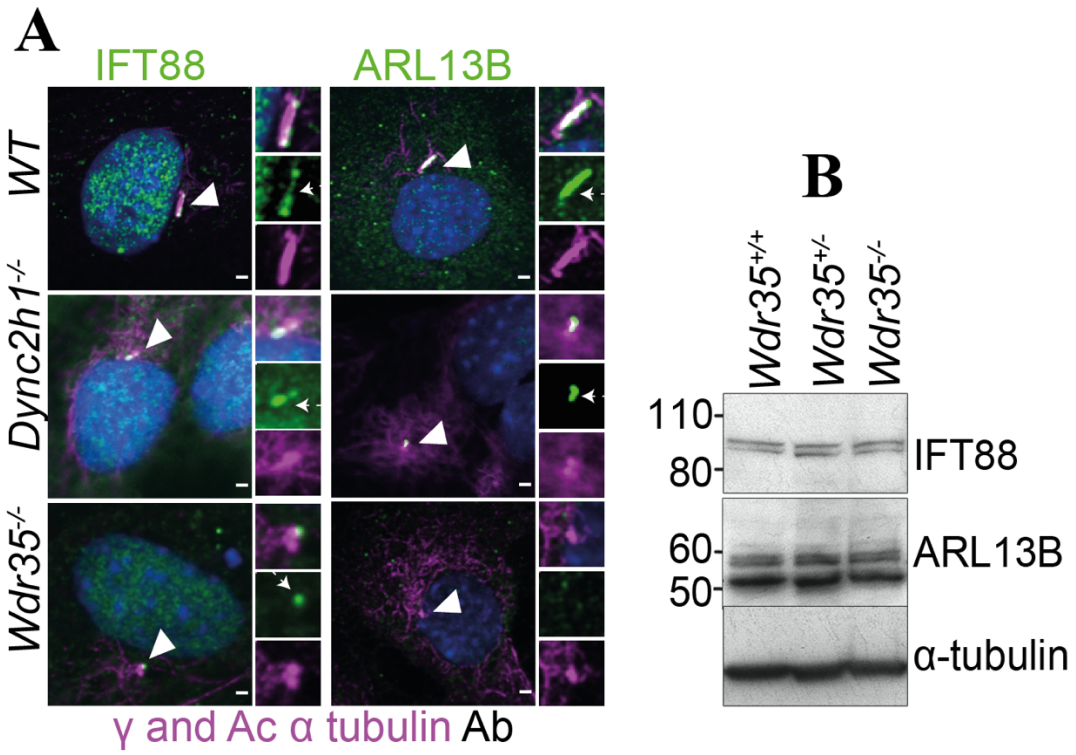

Figure 3.5. Defects in trafficking different types of cargo were observed between *Wdr35*$^{-/-}$ and *Dync2h1*$^{-/-}$ mutants. (A) 24 hr serum starved *Wdr35*$^{+/+}$, *Wdr35*$^{-/-}$ and *Dync2h1*$^{-/-}$ MEFs stained for ARL13B (right, magenta), IFT88 (left, magenta) and acetylated α- tubulin and γ-tubulin (green) and imaged with confocal imaging. The left panel shows IFT88 has a retrograde defect in both *Wdr35*$^{-/-}$ and retrograde dynein mutants, whereas the right panel shows ARL13B has a retrograde defect in dynein mutant only whereas no staining in *Wdr35*$^{-/-}$ suggests an anterograde defect. White arrowheads point at cilia and dashed arrows at IFT88 and ARL13B localised in WT and mutant cilia. (B) Western blot analysis of serum starved MEF lysates show no striking difference in total ARL13B and IFT88 levels, indicating defects lie in localization of these cargos.

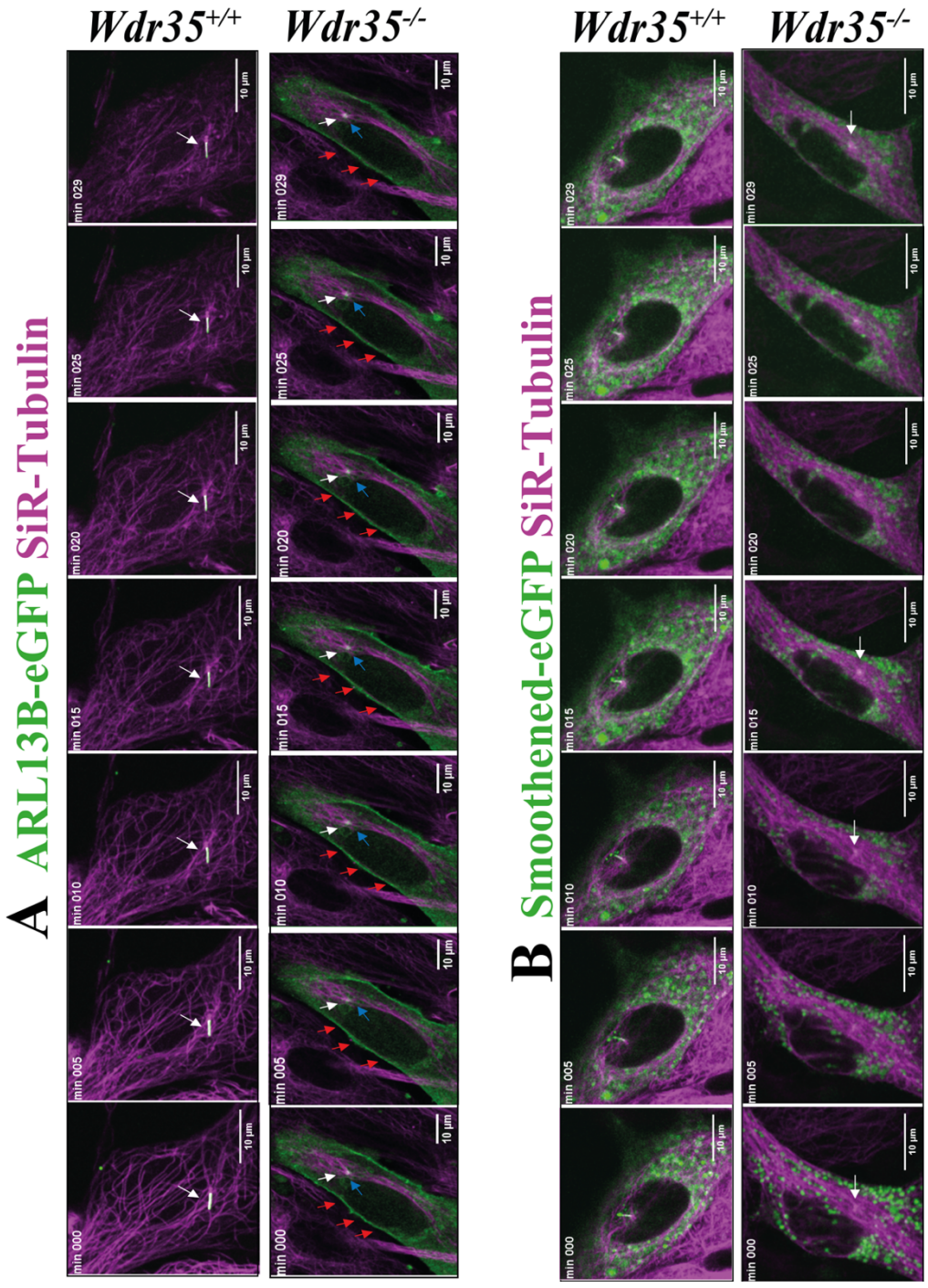

Figure 3.6. Cilia specific membrane-associated cargo (A) ARL13B and membrane-integrated cargo (B) SMO fail to localize in *Wdr35*$^{-/-}$ cilia. Primary MEFs were electroporated with the respective clones, serum starved for 24hrs, stained with SIR-tubulin and imaged live (**Movie 3.1**). The figure presents snapshots from live cell imaging. Red arrows indicate enrichment of ARL13B on the plasma membrane in *Wdr35*$^{-/-}$ mutants, blue arrows accumulation of ARL13B at the base of cilia in mutant and white arrows size of cilia in both wild type and mutant cells. ARL13B is highly enriched in WT cilia after 24hrs serum starvation as could be seen as white overlay from green code (for ARL13B) and magenta code (for SIR-tubulin) in first panel.

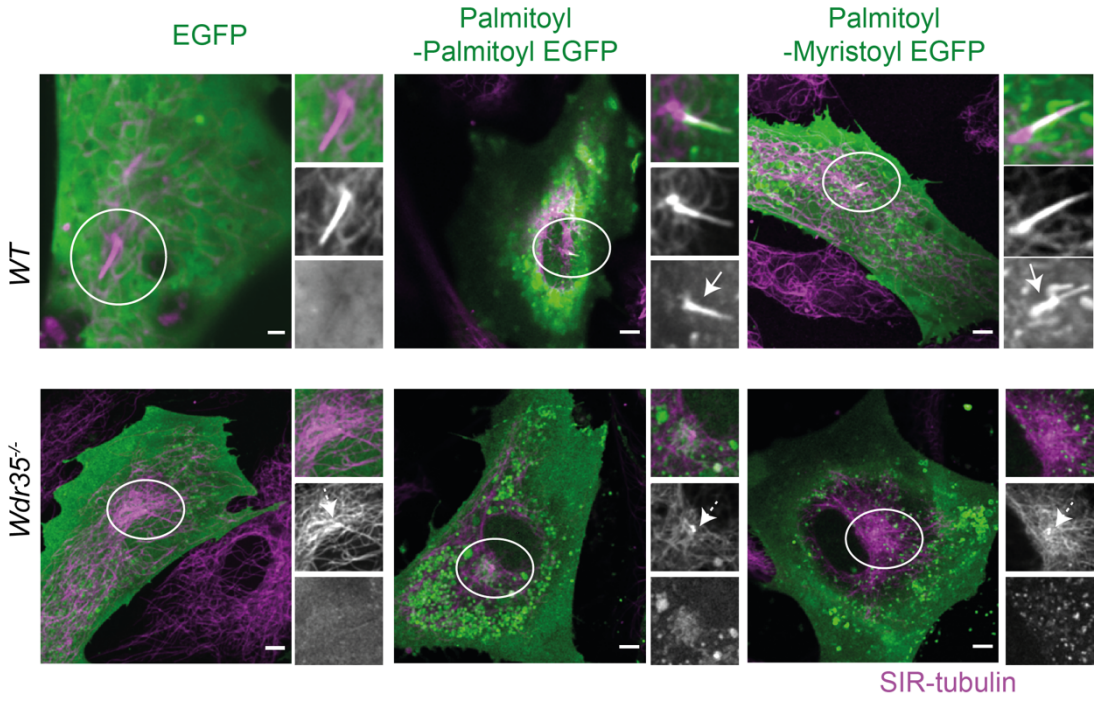

Figure 3.7. General lipidated protein cargo fails to localize *Wdr35*$^{-/-}$ cilia. Primary MEFs were electroporated with respective clones, serum starved for 24hrs, stained with SiR-tubulin (magenta) and imaged in live. Presented here is a representative snapshot from Z-stacks. (A) Cells electroporated with just eGFP expressing construct were found diffusing throughout the cytoplasm in both *Wdr35*$^{+/+}$ and *Wdr35*$^{-/-}$ cells. (B) GFP tagged with two sites for palmitoylation (PP-GFP) or sites for (C) palmitoylation and myristoylation (PM-GFP) were found to concentrate in cilia in *Wdr35*$^{+/+}$ cells. In *Wdr35*$^{-/-}$, they fail to localize to cilia. Arrows point at lipidated GFP localised in cilia of WT cells and dashed arrows point at mutant cell centrioles which have failed to form cilia . Scale bars= 2µm.

3.1.4 Despite its cilial accumulation, the composition of IFT-B complex is intact in *Wdr35*$^{-/-}$ mutants

To check trafficking defects of IFT-B complex in *Wdr35*$^{-/-}$ cilia, I performed high throughput imaging and quantification for the enrichment of IFT-B complex components IFT88 and IFT81 in *Wdr35*$^{-/-}$ and *Dyc2h1*$^{-/-}$, confirming a retrograde defect in the transport of IFT-Bs in both the mutants (**Figure 3.5, and Figure 3.8 - 3.11**). To ask whether there were qualitative differences in the composition of the IFT-B complex between controls and mutants, I performed an immunoprecipitation-mass spec (IP/MS) analysis of complex using endogenous IFT88 as a bait. Recent cryo-EM

work had suggested IFT-A is being carried by IFT-B trains inside the *Chlamydomonas* flagella (*Jordan et al., 2018*). In light of this, I hypothesized that some components of IFT-A might be interacting with IFT-B complex in order to assist in the transport of membrane proteins indirectly into cilia. The IFT-B complex is made of 16 proteins which control anterograde IFT transport into cilia. IFT88 is a link between peripheral and core IFT-B complex, interacting with IFT38 on the peripheral side and IFT52 on the core side (*Katoh et al., 2016; Mourão et al., 2016*). I performed an immunoprecipitation experiment using polyclonal anti-IFT88 and anti-GFP (control) antibodies on protein lysates extracted from E11.5 *Wdr35*$^{-/-}$ and *Wdr35*$^{+/+}$ embryos (n=4 embryos per genotype). After confirming robust enrichment for IFT88 by immunoblot (**Figure 3.12A**), the samples were sent for mass spectrometry. I isolated almost the entire IFT-B complex (14 out of 16 IFT-B components) purified in my IFT88 IP-mass spec dataset except for IFT70, which is not reported yet in mouse, as well as phosphoprotein IFT25 which binds as a heterodimer to IFT27 (*Wang et al., 2009*) and is necessary for Hh signalling (*Keady et al., 2012*). However, no significant differences in the IFT-B complex in *Wdr35*$^{-/-}$ lysates were detected in terms of composition or stoichiometry, although levels were slightly upregulated in null mutants (**Figure 3.12B**). I did not get any of IFT-As or BBSomes down with my IFT88 IP-mass spec, suggesting more transient interactions. Additional proteins associated with IFT88 IPs include Septins, CEP85, CEP131, and several myosin proteins. The only significant difference seen between *Wdr35*$^{+/+}$ and *Wdr35*$^{-/-}$ IPs was a reduced level of Myosin-6 (MYO6: **Figure 3.13**). MYO6 is mutated in the classical Snell's waltzer mouse mutant where animals display hearing loss caused by disruption of actin networks in the apical region of inner ear hair cells (*Seki et al., 2017*). However, due to lack of time this was not followed further.

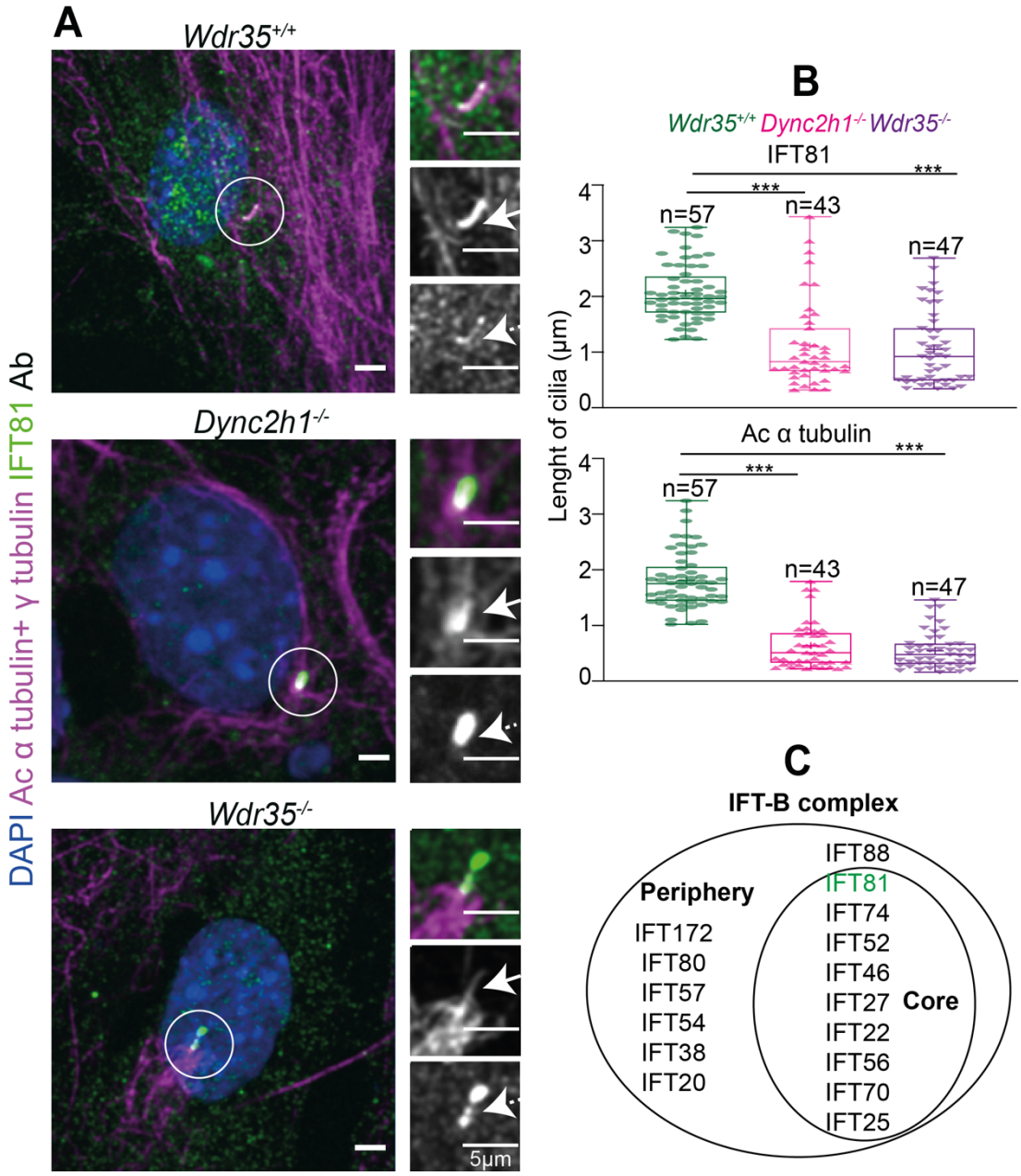

Figure 3.8: *Wdr35*$^{-/-}$ mutants have a similar retrograde defect in transporting IFT81 as *Dync2h1*$^{-/-}$ mutants. (A) Immunofluorescence of 24hr serum-starved MEFs, fixed and stained for Ac-α tubulin and γ tubulin (green) and IFT81 (magenta). Both *Dync2h1*$^{-/-}$ and *Wdr35*$^{-/-}$ mutant have IFT81 stuck inside cilia, consistent with defects in the retrograde pathway. Arrows point at acetylated tubulin and dashed arrows point at IFT81 in cilia. Scale bars are 5μm. (B) Length of cilia measured for IFT81and Ac α tubulin shows a drastic reduction in cilia length in both mutants. (C) Schematic overview of 16 IFT-B proteins in the core and periphery of the complex. Asterisk denotes significant p-value from t-test: (*, P<0.05), (**, P<0.01), (***, P<0.001). N is the number of cilia from three biological replicates each.

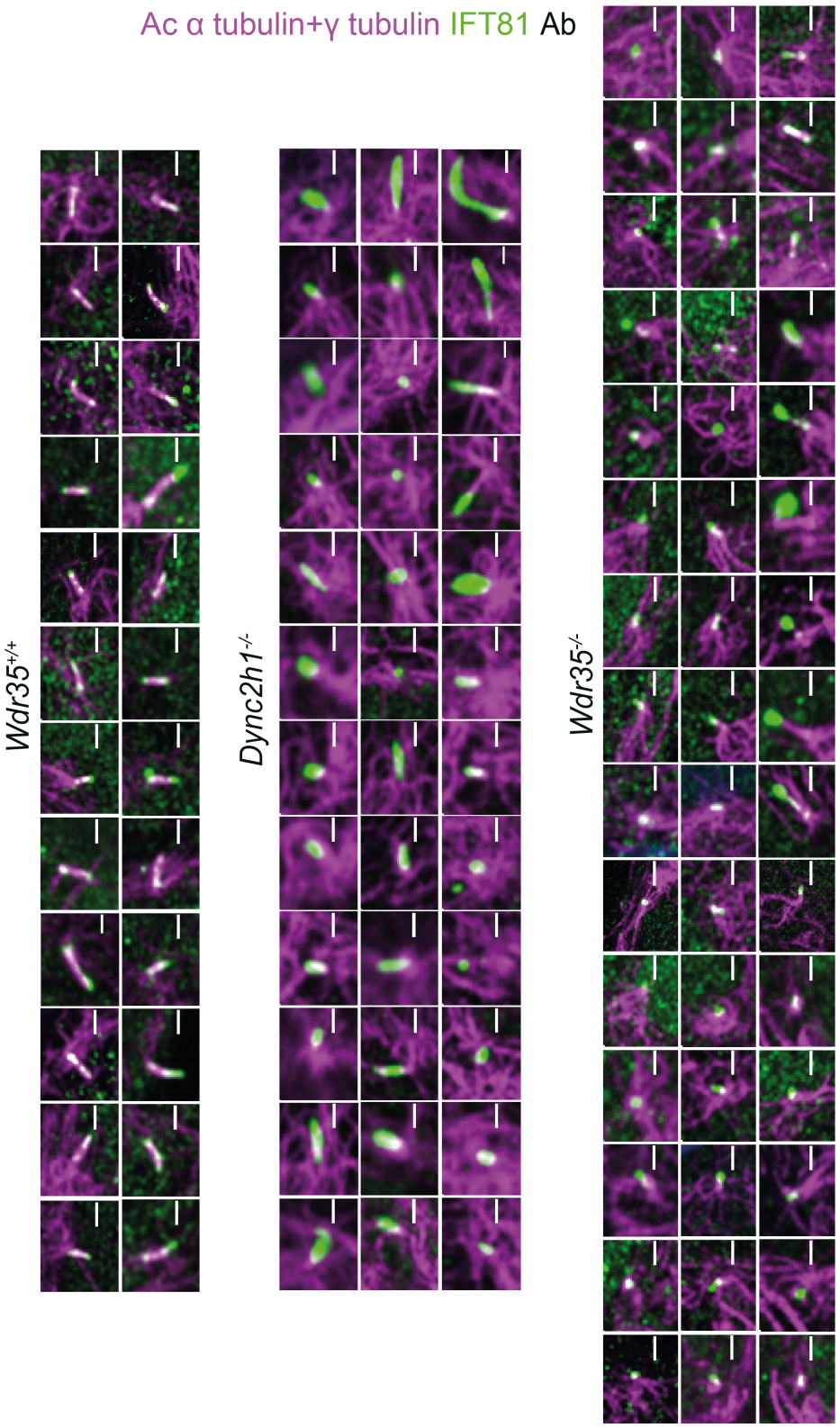

Figure 3.9: Similar cilia IFT81 accumulation is observed in *Dync2h1*$^{-/-}$ and *Wdr35*$^{-/-}$ mutants. As shown in Figure 3.8, *Wdr35*$^{-/-}$ mutants have a similar retrograde defect in transporting IFT81 as *Dync2h1*$^{-/-}$ mutants. IFT81 can be seen to accumulate in sac-like cilia in both the mutants. Scale bars = 1μm.

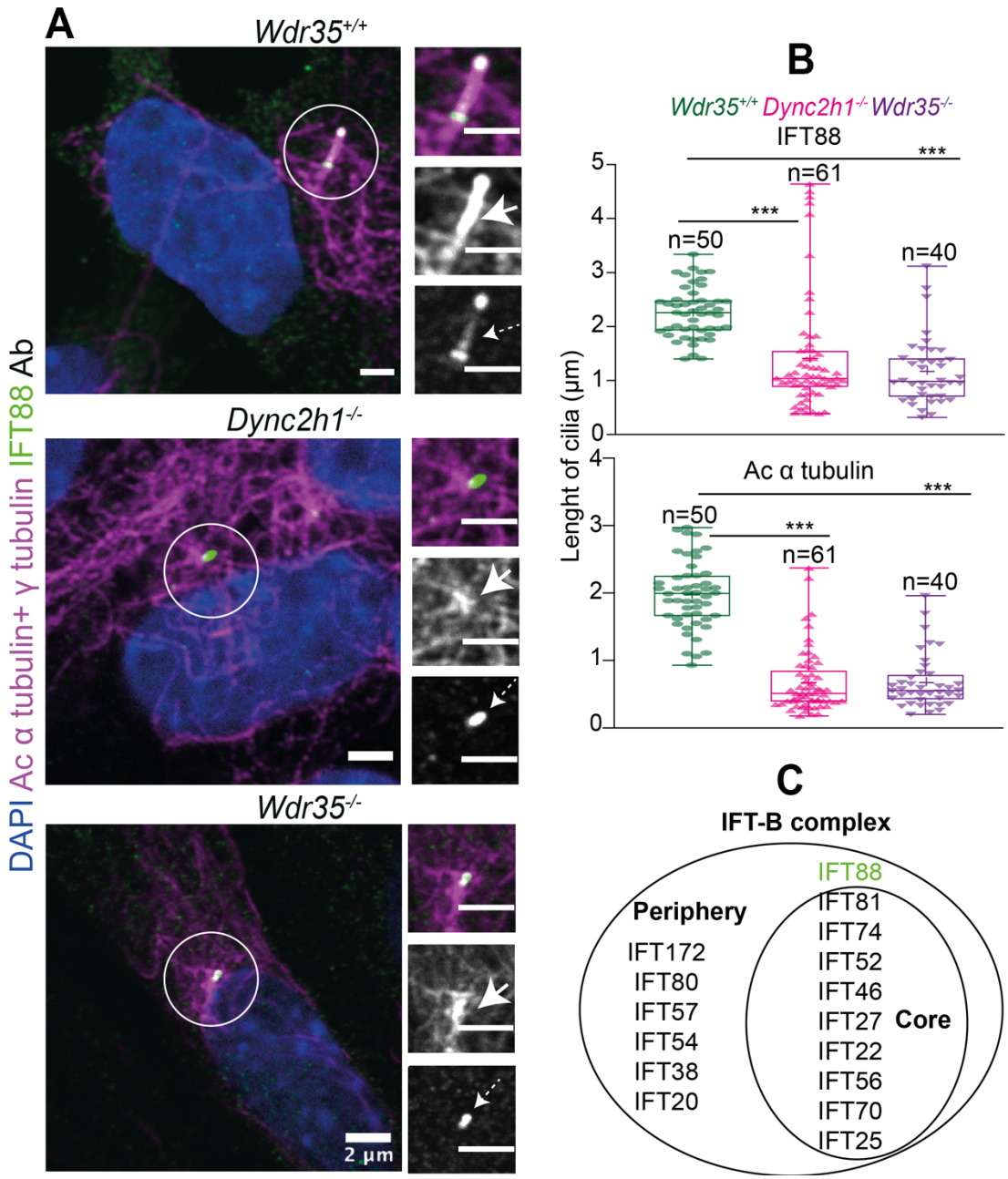

Figure 3.10. *Wdr35*$^{-/-}$ mutants have a similar retrograde defect in transporting IFT88 as *Dync2h1*$^{-/-}$ mutants. (A) IF of 24hr serum-starved MEFs, fixed and stained for Ac-α tubulin and γ tubulin (green) and IFT88 (magenta). IFT88 is stuck inside cilia in both *Dync2h1*$^{-/-}$ and *Wdr35*$^{-/-}$ mutant, consistent with a retrograde defect. Arrows point at acetylated tubulin and dashed arrows point at IFT88 in cilia. Scale bars are 2µm. (B) Length of cilia measured for IFT88 and Ac α tubulin shows a drastic reduction in cilia length. (C) Schematic overview of 16 IFT-B proteins in the core and periphery of the complex. Asterisk denotes significant p-value from t-test: (*, P<0.05), (**, P<0.01), (***, P<0.001). n is the number of cilia from three biological replicates each.

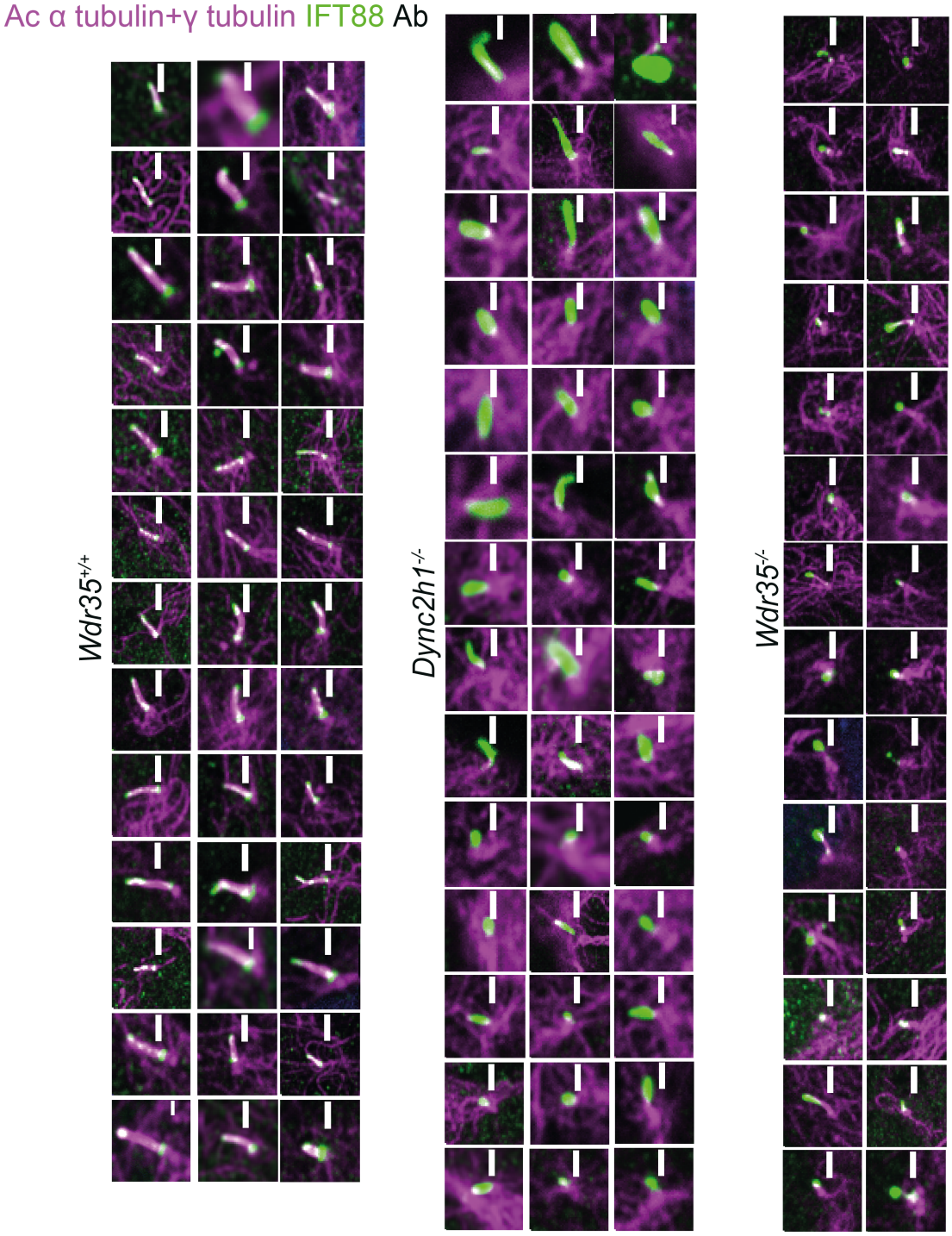

Figure 3.11. Similar cilia IFT88 accumulation is observed in *Dync2h1*$^{-/-}$ and *Wdr35*$^{-/-}$ mutants. As shown in Figure 3.10, *Wdr35*$^{-/-}$ mutants have a similar retrograde defect in transporting IFT88 as *Dync2h1*$^{-/-}$ mutants. IFT88 can be seen to accumulate in sac-like cilia in both the mutants. Scale bars are 1µm.

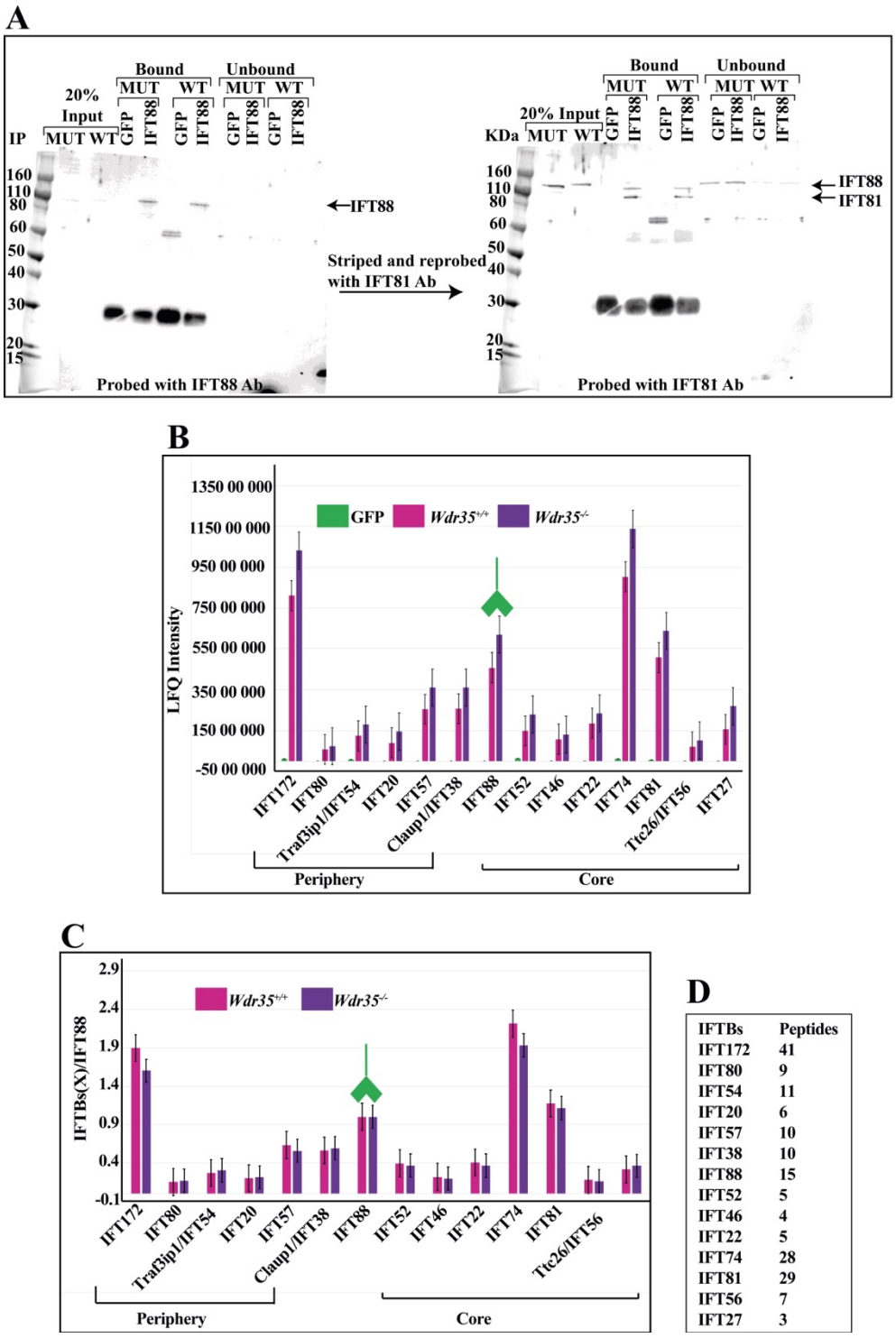

Figure 3.12. In spite of differences in localization, IP/MS analysis of E11.5 *Wdr35*$^{+/+}$ and *Wdr35*$^{-/-}$ littermates reveals no difference in composition of the IFT-B complex. (A) Efficacy of IFT88 IP was confirmed by immunoblot for IFT88 Ab (upper blot) and IFT81 (lower blot). (B) Mass spec label free quantification (LFQ) intensities in control GFP and IFT88 IP samples from *Wdr35*$^{+/+}$ and *Wdr35*$^{-/-}$ samples. (C) Normalized LFQs to IFT88 intensity reveals no difference between *Wdr35*$^{-/-}$ and

Wdr35$^{+/+}$ IFT-B complex composition. (D) The number of unique peptides identified in IP/MS. N= 4 embryos per genotype.

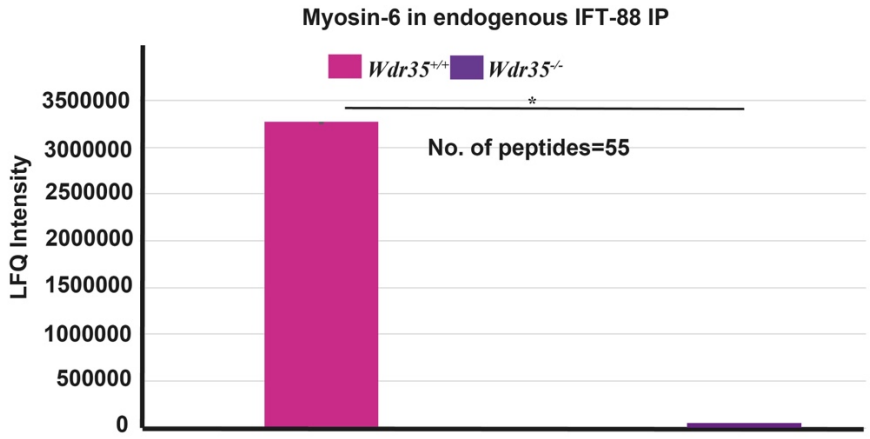

Figure 3.13. In *Wdr35*$^{+/+}$ extracts, IFT88 interacts with MYO6. Endogenous IFT88 IP-mass spec analysis of E11.5 littermates showed Myosin-6 interaction only in *Wdr35*$^{+/+}$ condition. N= 4 embryos per genotype. Asterisk denotes significant p-value from t-test: (*, P<0.1), (**, P<0.01), (***, P<0.001).

3.1.5 Differential defects in IFT-A complex assembly and trafficking is observed between *Wdr35*$^{-/-}$ and *Dync2h1*$^{-/-}$ mutants.

The IFT-A complex is composed of 6 proteins: three of which make the core (IFT144, IFT140, and IFT122) and three make the periphery (IFT139, IFT43, and IFT121/WDR35) (**Figure 1.3C**). After assaying assembly defects of the IFT-B complex, I next checked the stability of IFT-A complex by IP/MS and the localization of IFT-As by confocal imaging. I chose core IFT140 as the bait to pull down IFT-A complex and its interactors from E11.5 *Wdr35*$^{+/+}$ and *Wdr35*$^{-/-}$ embryonic lysates using polyclonal anti-IFT140 or anti-GFP (control) antibodies. After confirming robust enrichment for IFT140 by immunoblot (**Figure 3.14A**), the samples were sent for mass spectrometry. IFT140 immunoprecipitation successfully all 6 proteins of IFT-A complex from *Wdr35*$^{+/+}$ animal lysate but the two peripheral components IFT139 and IFT43 were missing in *Wdr35*$^{-/-}$ (**Figure 3.14B**). This suggested that WDR35 is critical for intact IFT-A complex stability.

In order to address whether loss of WDR35 affected stability and/or localization of individual IFT-A components, I undertook analysis of total protein levels by

immunoblot and immunofluorescence, respectively. Immunoblot analysis of whole cell lysates from both MEFs and E11.5 embryos revealed that whilst IFT-A core proteins though were nearly equally expressed in both *Wdr35*$^{+/+}$ and *Wdr35*$^{-/-}$ lysates, levels of the peripheral IFT139 and IFT43 components were undetectable (**Figure 3.15A and B**). This suggests that IFT121/WDR35 might be a link between IFT-A core and periphery proteins, required to protect them from degradation. To investigate this further, control and mutant MEFs were treated with 20μM MG-132 proteasome inhibitor with increasing period of time (**Figure 3.15C**). Treated cells rescued expression of some levels IFT43 but not IFT 139. This supports that in the absence of WDR35, these peripheral proteins are targeted by the proteasomal degradation pathway. Differences in biochemical assembly of IFT-A and IFT-B complexes in *Wdr35* mutants are summarised in (**Figure 3.23)**.

I next looked at localization and levels of the IFT-A components by immunofluorescence. In *Wdr35*$^{-/-}$ MEFs, I found components of the IFT-A core to be restricted at transition zone (**Figures 3.16- 3.20**). In contrast, peripheral proteins were undetectable, consistent with robust degradation (**Figures 3.21- 3.22**). All IFT-A components accumulated in the retrograde dynein mutant cilia (**Figures 3.16- 3.22**).

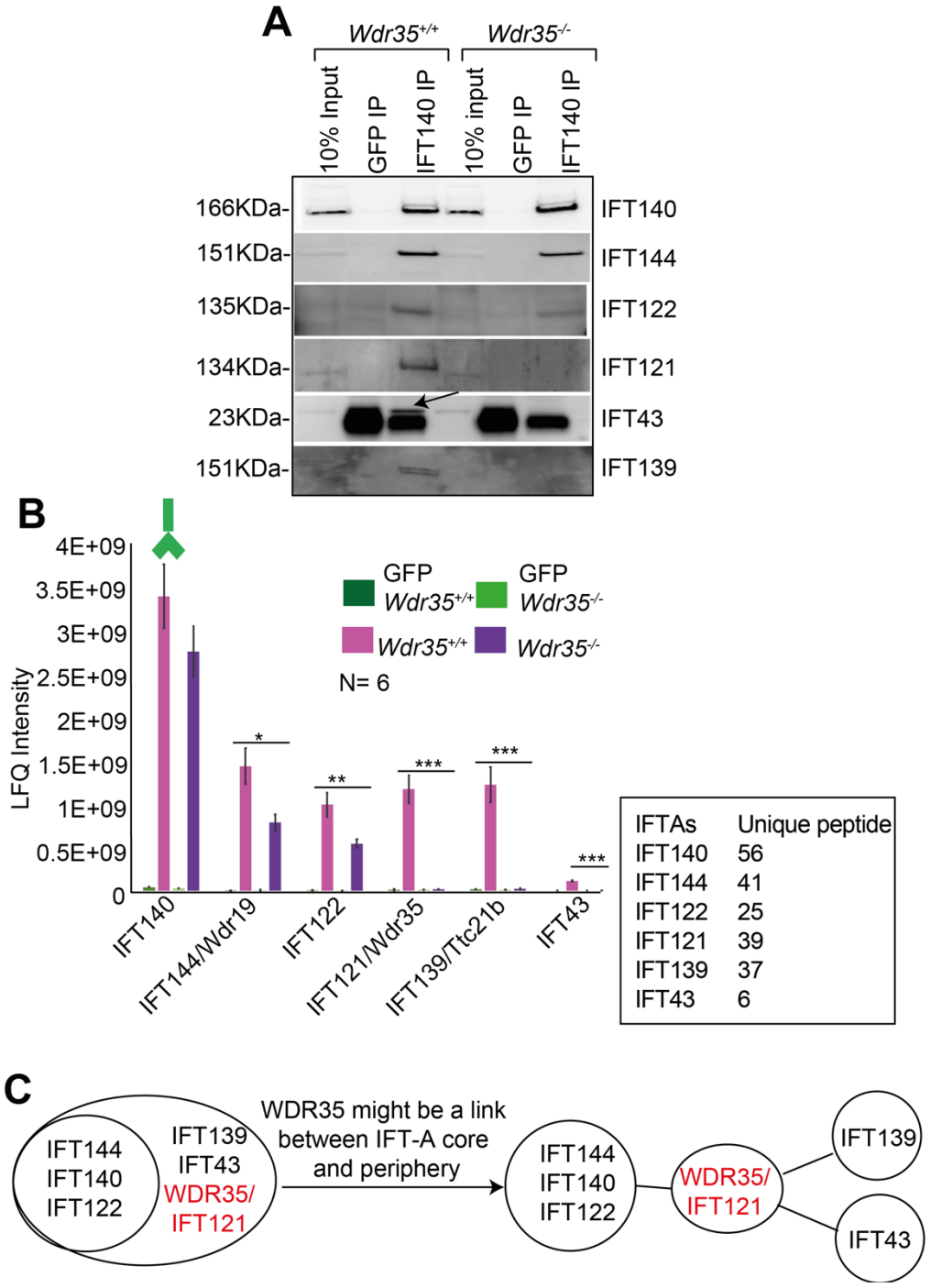

Figure 3.14. IFT140 IP/MS reveals WDR35 is required for stability of IFT-A complex. (A) IFT140 IP samples from E11.5 *Wdr35*$^{+/+}$ and *Wdr35*$^{-/-}$ embryo lysates were probed with respective IFT-A antibodies to show IFT43 and IFT139 are missing from the complex. IFT-43 runs close to the molecular weight of GFP, is shown by an arrow as IFT43 band over GFP band in *Wdr35*$^{+/+}$, whilst the corresponding band is absent in *Wdr35* mutants. (B) Summary of select hits in MS dataset for n=6 embryos per genotype. (C) Summary diagram showing IFT121/WDR35 to be link between IFT-A core and periphery proteins. Bait for IP is highlighted by a green Antibody. Asterisk denotes significant p-value from t-test (*, P<0.05), (**, P<0.01), (***, P<0.001).

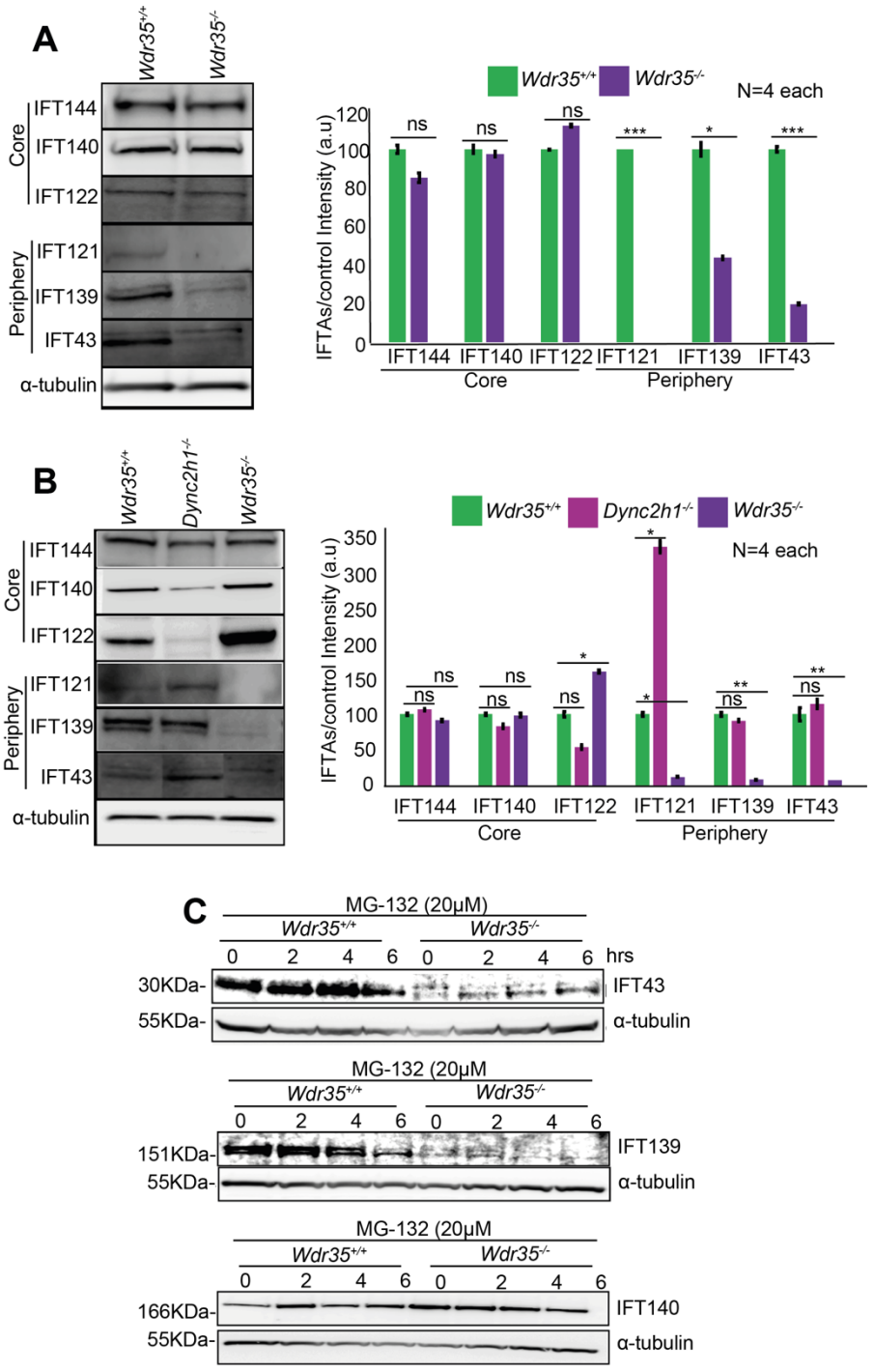

Figure 3.15. In the absence of WDR35, stability of peripheral components IFT139 and IFT43 is compromised. The total level of expression of IFT-A subunits in (A) E11.5 litter lysates and (B) MEF lysates revels reduced expression IFT139 and IFT43, whilst levels of core components are largely unaffected (IFT144, IFT140, and IFT122). (C) Inhibition of the proteasome by treatment with MG-132 partially rescues IFT43 and IFT139 stability in *Wdr35*$^{-/-}$ MEFs suggesting post-translational stability is affected in the absence of WDR35. N= number of embryos or MEF lines (biological replicates). Asterisk denotes significant p-value from t-test: (*, P<0.05), (**, P<0.01), (***, P<0.001).

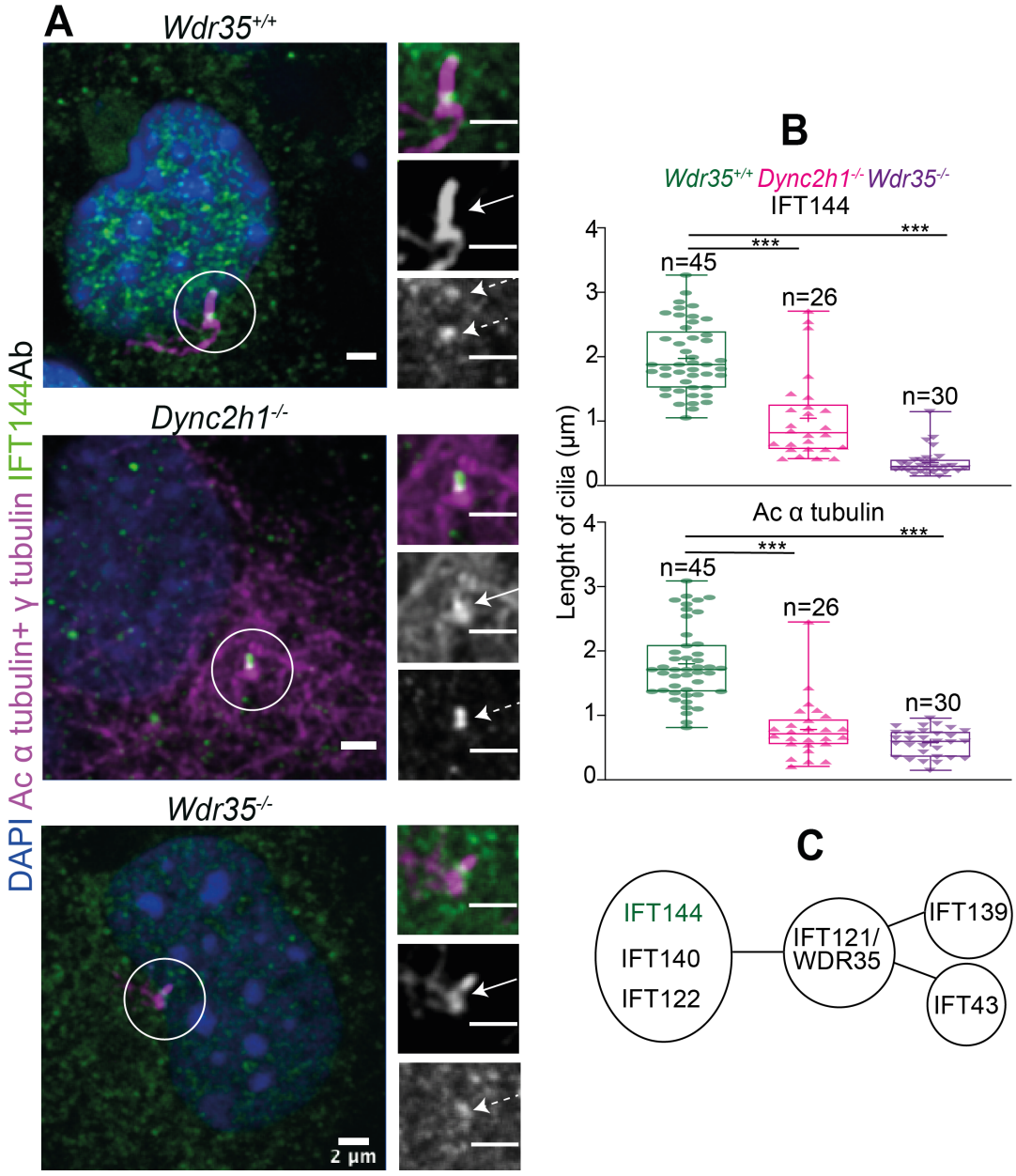

Figure 3.16. Anterograde defects are observed in IFT-A component IFT144 in *Wdr35*$^{-/-}$ cilia. (A) IFT144 concentrates at cargo loading point at transition zone and remodelling point at the tip of cilia along with faint localization along the length of cilia (green) in *Wdr35*$^{+/+}$ MEFs, concentrates in short club-shaped cilia in *Dync2h1*$^{-/-}$ mutant and is stuck in the transition zone in *Wdr35*$^{-/-}$. Ac α tubulin staining (Magenta) also shows a drastic reduction in the length of the axoneme in both the mutants. Arrows point at acetylated tubulin and dashed arrows point at IFT144 in cilia. Scale bars are 2µm. (B) Quantification of cilia length from 2 sets of experiments. Asterisk denotes significant p-value from t-test: (*, P<0.05), (**, P<0.01), (***, P<0.001). n=no. of cilia used to measure cilia length.(C) Summary diagram summarizing the proposed arrangement of 6 IFT-A proteins with respect to IFT121/WDR35 from my interaction and localization data. IFT144 is highlighted in green.

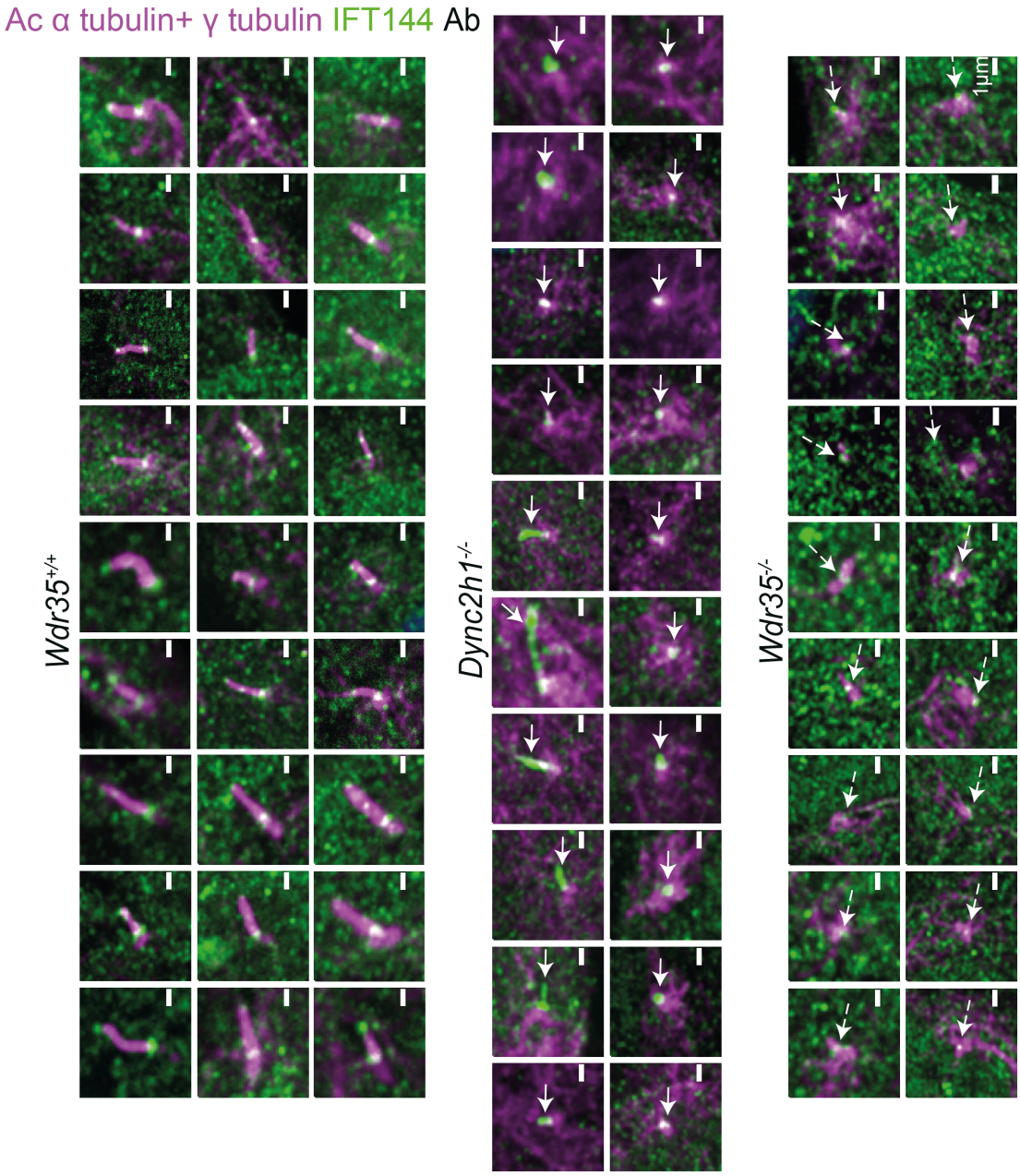

Figure 3.17: Overview of IFT-A IFT144 localization within cilia *Wdr35*$^{+/+}$, *Dync2h1*$^{-/-}$, and *Wdr35*$^{-/-}$ mutants. As shown in Figure 3.16, *Wdr35*$^{-/-}$ mutants have an anterograde defect in transporting IFT144 compared retrograde transport defect in *Dync2h1*$^{-/-}$ mutants. IFT144 can be seen stuck at the transition zone of tiny cilia in *Wdr35*$^{-/-}$ cells. Arrows point at IFT144 concentrated in *Dync2h1*$^{-/-}$ cilia and dashed arrows point at IFT144 localised at cilia base in *Wdr35*$^{-/-}$ cells. Scale bars are 1µm.

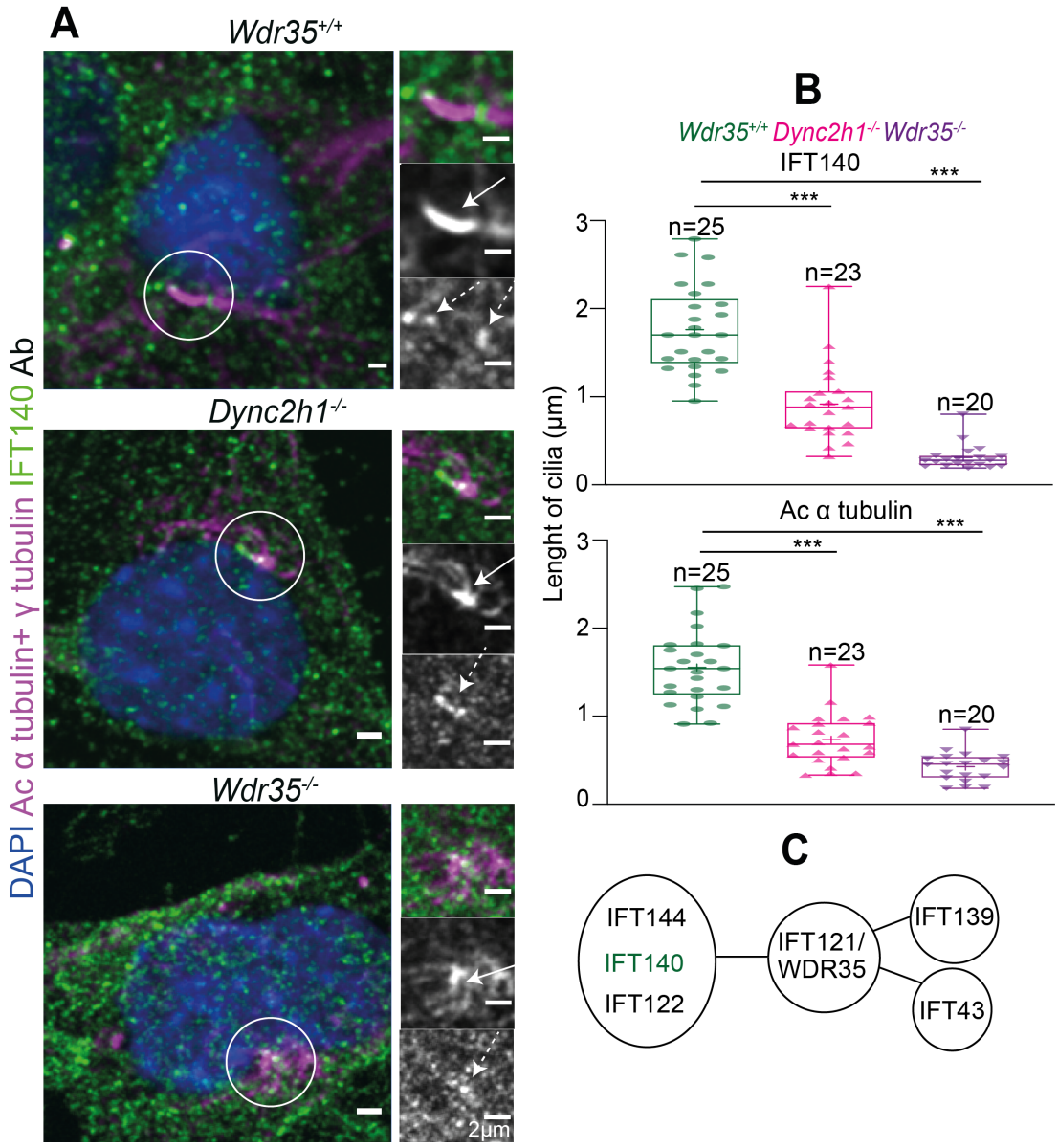

Figure 3.18. IFT140 has an anterograde transport defect in *Wdr35*$^{-/-}$ cilia. (A) IFT140 concentrates at cargo loading point at transition zone and remodelling point at the tip of cilia along with faint localization along the length of cilia (IFT140: green) in *Wdr35*$^{+/+}$ MEFs. In contrast, it concentrates in short club-shaped cilia in *Dync2h1*$^{-/-}$ mutants whilst being stuck in the transition zone in *Wdr35*$^{-/-}$ mutants. Ac α tubulin staining (magenta) also shows a drastic reduction in the length of the axoneme in both the mutants. Arrows point at acetylated tubulin and dashed arrows point at IFT140 in cilia. Scale bars are 2µm. (B) Quantification of cilia length from. Asterisk denotes significant p-value from t-test: (*, P<0.05), (**, P<0.01), (***, P<0.001). n= number of cilia used to measure cilia length from three biological replicates.(C) A diagram to show an arrangement of 6 IFT-A proteins with IFT121/WDR35 assigned as a link between periphery and core IFT-A complex. IFT140 component of IFT-A core is highlighted in green.

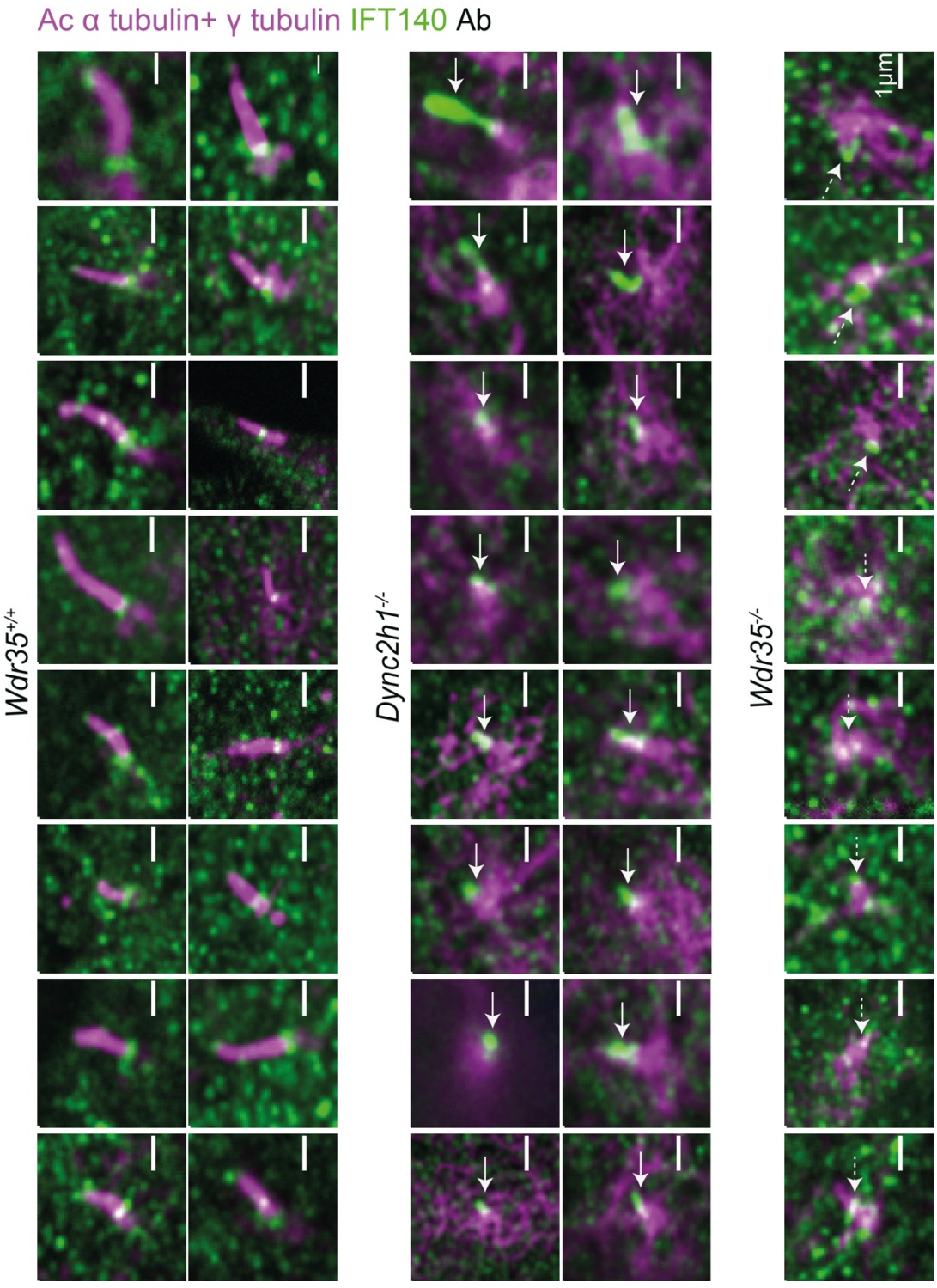

Figure 3.19. Overview of IFT-A IFT140 trafficking defects in cilia from *Wdr35*$^{+/+}$, *Dync2h1*$^{-/-}$, and *Wdr35*$^{-/-}$ mutants. As shown in Figure 3.18, *Wdr35*$^{-/-}$ mutants have an anterograde defect in transporting IFT140 where IFT140 can be seen stuck at the transition zone of tiny cilia in *Wdr35*$^{-/-}$ cells. Arrows point at IFT144 concentrated in *Dync2h1*$^{-/-}$ cilia and dashed arrows point at IFT144 localised at cilia base in *Wdr35*$^{-/-}$ cells. Scale bars are 1µm.

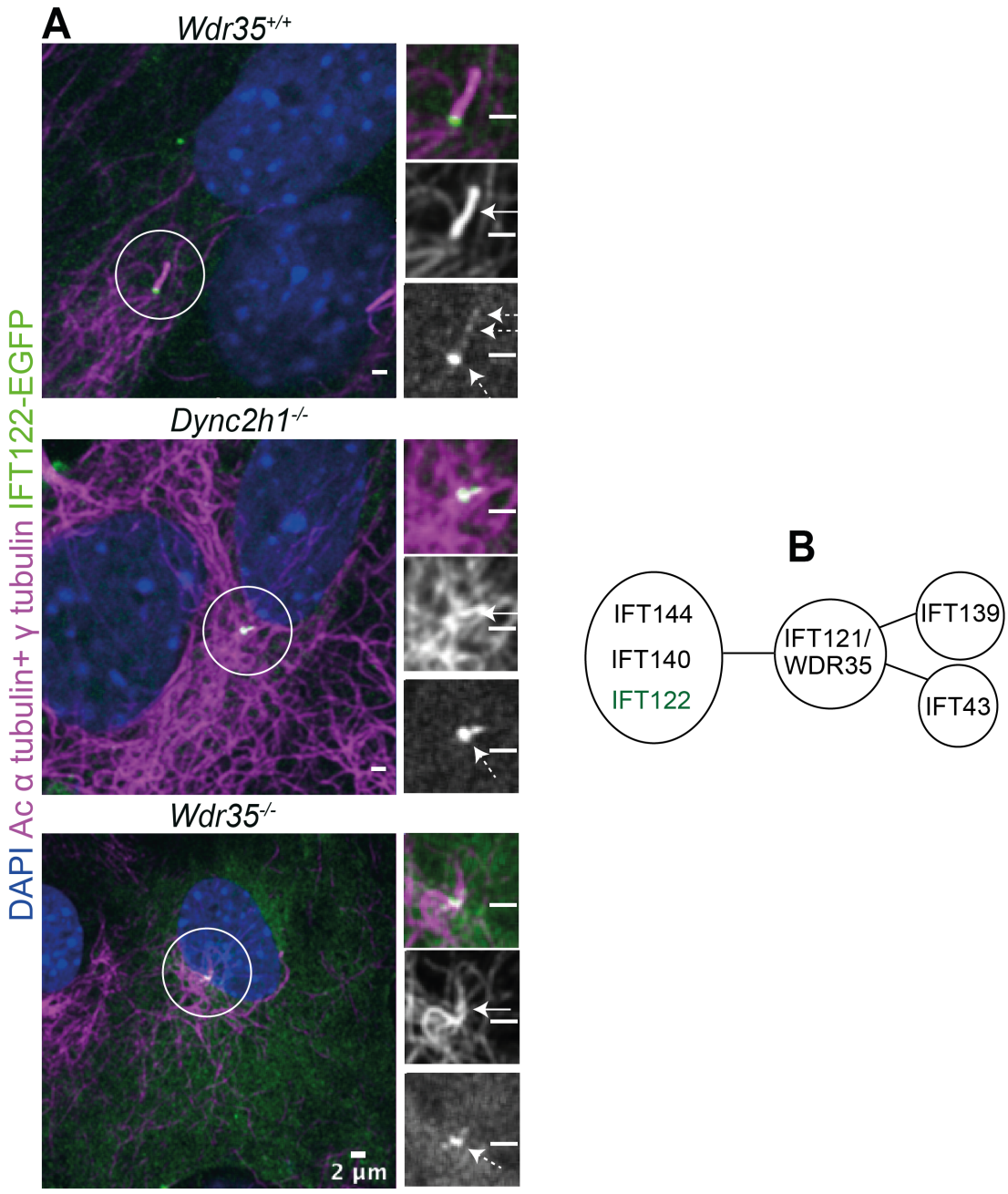

Figure 3.20. Anterograde defects in trafficking IFT-A IFT122 in *Wdr35*$^{-/-}$ cilia. (A) Tagged IFT122 concentrates at the cargo loading point at transition zone and remodelling point at the tip of cilia along with faint localization along the length of cilia (green) in control MEFs. In contrast, it concentrates in short club-shaped cilia of *Dync2h1*$^{-/-}$ mutants, whereas it is stuck in the transition zone in *Wdr35*$^{-/-}$ cilia. Ac α tubulin staining (magenta) reveals a drastic reduction in the length of the axoneme in both mutants. Arrows point at acetylated tubulin and dashed arrows point at IFT122 in cilia. (B) Summary of imaged component with relation to the other 5 IFT-A proteins, where IFT121/WDR35 is proposed be the link between peripheral and core components in the complex. IFT122 component of core complex is highlighted in gree.

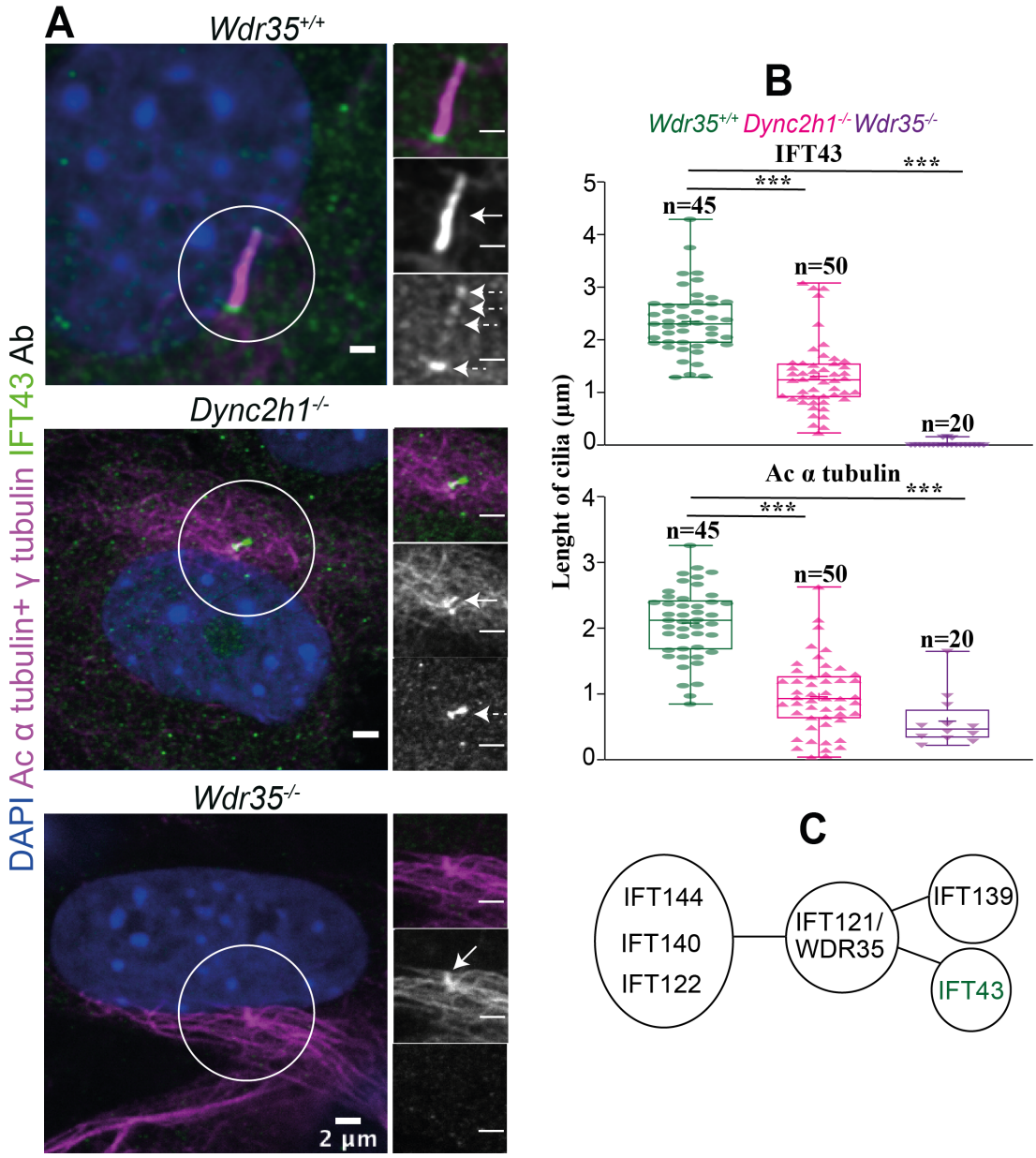

Figure 3.21. IFT43 is indetectable in or around *Wdr35*$^{-/-}$ cilia. (A) IFT43 concentrates at cargo loading point at transition zone and remodelling point at the tip of cilia along with faint localization along the length of cilia (green) in *Wdr35*$^{+/+}$ MEFs. Whilst in *Dync2h1*$^{-/-}$ mutants it concentrates in the short club-shaped cilia, it is undetectable in *Wdr35*$^{-/-}$ cells. Ac α tubulin staining (magenta) also shows a drastic reduction in the length of the axoneme in both the mutants. Arrows point at acetylated tubulin and dashed arrows point at IFT43 in cilia. Scale bars are 2µm. (B) Quantification of cilia length w.r.t IFT43 and Ac α tubulin staining. Asterisk denotes significant p-value from t-test: (*, P<0.05), (**, P<0.01), (***, P<0.001). n= number of cilia used to measure cilia length from three biological replicates.(C) Summary diagram of arrangement of 6 IFT-A protein interactions, with IFT43 is highlighted in green as peripheral component.

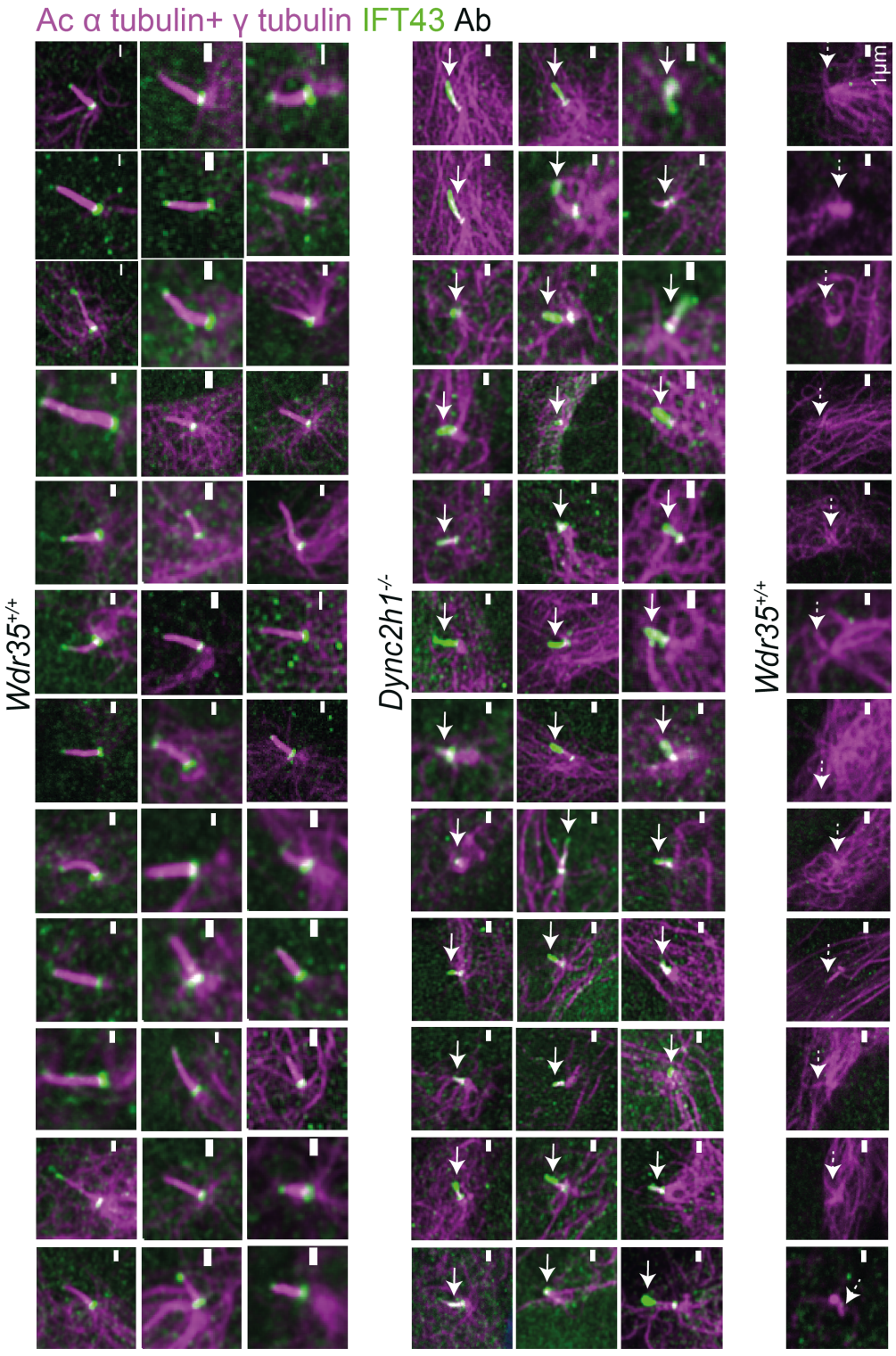

Figure 3.22. Summary of IFT43 localization in *Wdr35*$^{+/+}$, *Dync2h1*$^{-/-}$, and *Wdr35*$^{-/-}$ cells. As shown in Figure 3.21, *Wdr35*$^{-/-}$ mutants fail to express detectable IFT43 whilst it accumulates with a retrograde transport defect in *Dync2h1*$^{-/-}$ mutants. This is consistent with IFT43 being degraded in the absence of WDR35. Arrows point at IFT43 concentrated in *Dync2h1*$^{-/-}$ cilia and dashed arrows point at drastically reduced length of cilia in *Wdr35*$^{-/-}$ cells. Scale bars are 1μm.

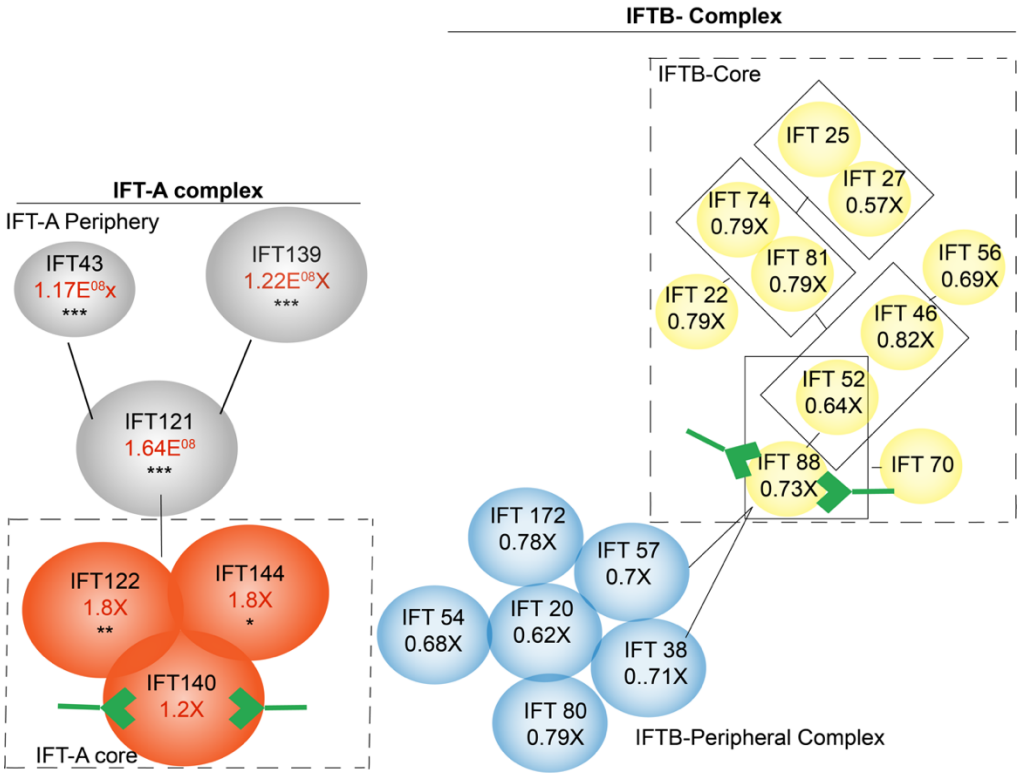

Figure 3.23. Summary of IFT complex analysis by IP/MS for (A) IFT-A and (B) IFT-B-complex in *Wdr35*$^{+/+}$ and *Wdr35*$^{-/-}$ lysates. Bait for affinity purification is marked in green in each case. Fold change of WT/MUT normalised L.F.Q is shown in red and flagged with one star for P<0.05, two star for P<0.01 and three stars for P<0.001.

3.1.6 Organization of centriolar satellites is unaltered in *Wdr35*$^{-/-}$ MEFs.

Centriolar satellites (CS) are dynamic, 70-100nm granular non-membranous structures trafficking to and from the centriole and basal body. CS are proposed to function to serve as 'on-demand' hubs for prompt delivery of both ciliary and centrosomal proteins via dynein/dynactin-driven movement along microtubules, as needed (*Bärenz et al., 2011; Hori and Toda, 2017; Kubo et al., 1999; Tollenaere et al., 2015*) (**Figure 3.24A**). Live cell imaging of ciliated MEFs showed PCM-1 localising at pericentriolar space at cilia base (**movie 3.2 and Figure 3.24A**) Though centriolar satellites are ubiquitous in mammalian cells, they are variable in number and size *(Nielsen et al., 2018; Rai et al., 2018; Villumsen et al., 2013*) and exhibit different mutant phenotypes in different cell types (*Odabasi et al., 2019; Wang et al., 2016*). Defects in CS components lead to ciliopathies- including primary microcephaly and schizophrenia (*Bradshaw and Porteous, 2012; Hori and Toda, 2017; Tabarés-Seisdedos and*

Rubenstein, 2009; Tollenaere et al., 2015). In certain cell types, CS proteins like CEP290 (*Kim et al., 2008; Tsang et al., 2008*), CEP131(*Hall et al., 2013*) and PCM1 are essential for cilia assembly (*Odabasi et al., 2019; Wang et al., 2016*).

PCM-1 is a critical component of the CS and functions as a chaperone stabilizing CS and ciliary proteins (*Joachim et al., 2017; Nachury MV et al., 2007; Wang et al., 2016*) and a scaffold to keep them in place (*Dammermann and Merdes, 2002; Gupta et al., 2015; Hori and Toda, 2017; Odabasi et al., 2019; Wang et al., 2016*). PCM1 is the 'gold standard' marker for studying satellite assembly and disassembly. Surprisingly PCM-1 mutants have different defects in different cell types. RPE1 cells fail to ciliate when *PCM1* is knocked out or knocked down (*Nachury MV et al., 2007; Wang et al., 2016*), resulting in mislocalization of CS proteins. Importantly, BBSomes fail to localize suggesting CS transiently function as adaptors for vesicular transport during ciliogenesis (*Chou et al., 2019; Nachury MV et al., 2007*). Moreover, PCM-1 tethers the E3 ligase Mib-1 to CS, restricting it from the centrioles and preventing degradation of Talpid-3, which in turn recruits ciliary vesicles to cilia in association with Rab8 to promote ciliogenesis (*Kobayashi et al., 2014; Wang et al., 2016*). PCM-1, along with CEP290 also helps in localization of RAB8 a small GTPase to cilia base (*Kim et al., 2008*), and Rab8 along with BBSome is proposed to promote ciliogenesis (*Nachury MV et al., 2007*). Importantly, recent results from the Dynlacht lab suggest PCM1 localization is disrupted in *WDR35* mutants (*Fu W et al., 2016*), and they went on to suggest that Wdr35-dependent centriolar satellite organization could be linked with its roles at cilia.

To independently test this, I crossed the *Wdr35*$^{+/-}$ mouse line with an endogenously tagged *Pcm-1-SNAP* line the lab had generated and isolated MEFs. I did not see any difference in the localization of PCM-1 around cilia in the absence of WDR35 (**Figure 3.24**). To validate this further, I measured PCM1 abundance around centrosome in 24hr serum-starved ciliated MEFs by both live cell (**Figure 3.24B; Movie 3.3**) and fixed cell (**Figure 3.24C**) imaging. In both cases, I saw no difference in PCM1 abundance or distribution at the cilia base [Dr. Emma Hall and Laura Murphy performed the fixed cell imaging and quantification]. Based on immunofluorescence imaging and quantification, I conclude that WDR35 is not essential for centriolar satellite organization.

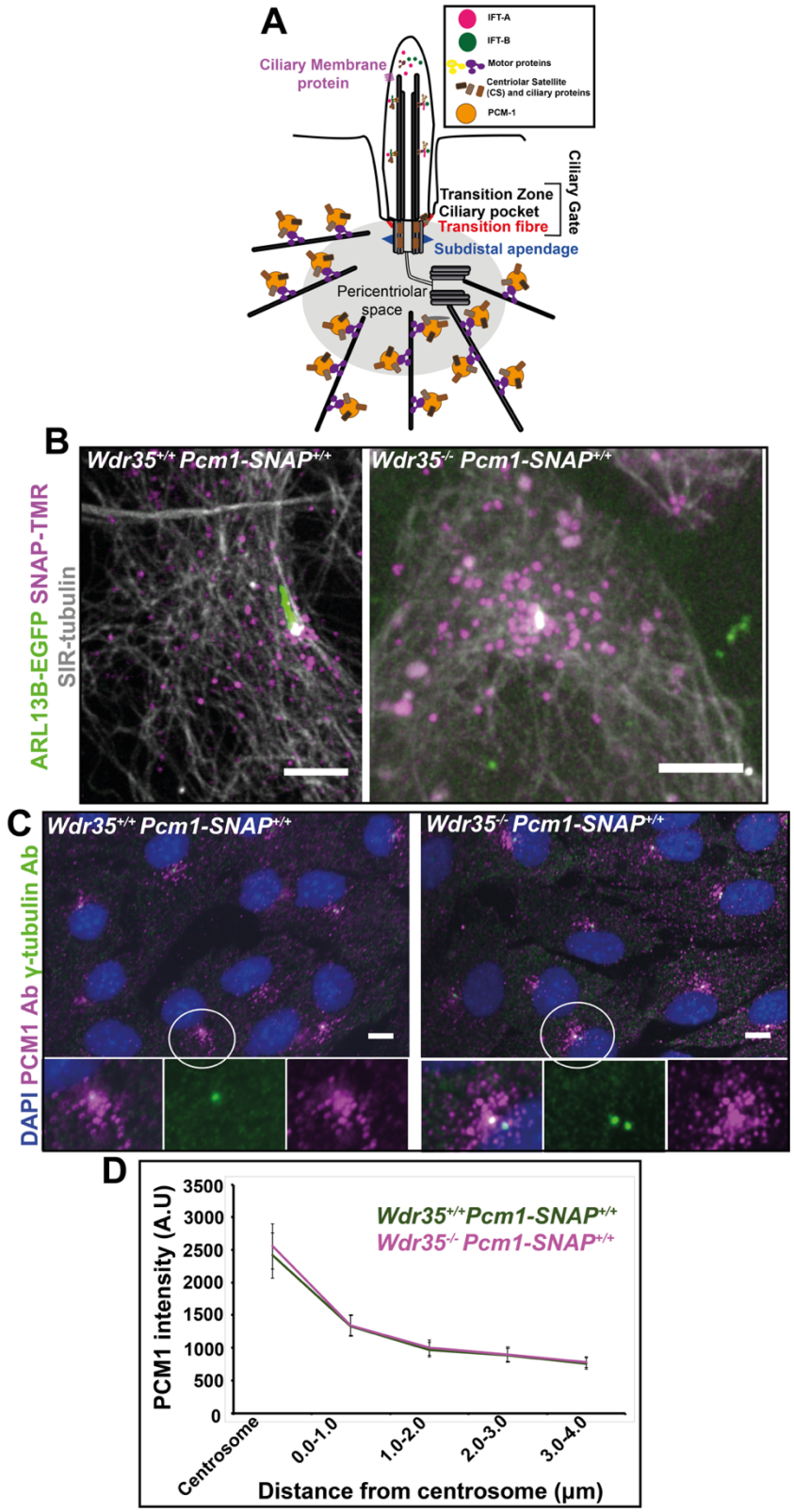

Figure 3.24. Organization of centriolar satellites is not disrupted in *Wdr35*$^{-/-}$. (A) Overview of centriolar satellites and cilia (CS= Centriolar satellite, DA= Distal appendage, TZ= transition zone). Diagrammatic representation of PCM-1 ferrying ciliary proteins on microtubules assisted by motor proteins. PCM1 is shown in yellow

and ciliary/CS proteins in shades of brown. (B) 24hr serum-starved MEFs derived from *Wdr35*$^{+/+}$;*Pcm1*$^{SNAP/SNAP}$ and *Wdr35*$^{-/-}$;*Pcm1* $^{SNAP/SNAP}$ E11.5 mouse embryos were imaged (A) live by staining with SNAP-TMR and SIR-Tubulin and (B) in fixed by staining with anti-PCM1 Ab and γ-tubulin. TMR staining in live cells and PCM1-Ab staining in fixed cells shows no localization difference of PCM1 in *Wdr35*$^{-/-}$ MEFs. Live cells were also electroporated with ARL13B-EGFP shown in green. (C) An automated bespoke script in ImageJ was written for the unbiased quantification of PCM1 intensity around centrosome in concentric rings of specific radius shown on X-axis. Data points show the average intensity at each radial point around centrosome in n=50 cells each from 3 biological replicates. Scale bars= 5µm. Asterisk denotes significant p-value from t-test: (*, P<0.05), (**, P<0.01), (***, P<0.001).

3.1.7 Clathrin organization remains unchanged around *Wdr35*$^{-/-}$ cilia.

Clathrin have been proposed to coat vesicles budding from cilia to assist in endocytosis from the cilia to the cytoplasm (*Kaplan et al., 2010; Molla-Herman A et al., 2010*). In order to test whether clathrin could be the coat observed in my TEM images, I quantified clathrin staining in WT and *Wdr35*$^{-/-}$ MEFs (experiments performed with Dr. Emma Hall and Dr. Laura Murphy). My TEM images showed uncoated vesicles clustering in a range of 2µm radius around cilia in *Wdr35*$^{-/-}$. Using an automated analysis algorithm, I found no difference in mean Clathrin intensity in a volume of 2µm around cilia base *Wdr35*$^{-/-}$ cilia compared to control MEFs (**Figure 3.25**). However, since clathrin is described to endocytose cargo from cilia to the cytoplasm (*Molla-Herman A et al., 2010*), one might expect to see the difference if any in the immediate vicinity of cilia and not in a range of 2µm. In the absence of any membrane proteins and many other ciliary materials in *Wdr35*$^{-/-}$ mutants, reduced Clathrin intensity could be expected in immediate vicinity (0.5µm- 1µm) of cilia which is to be analysed later.

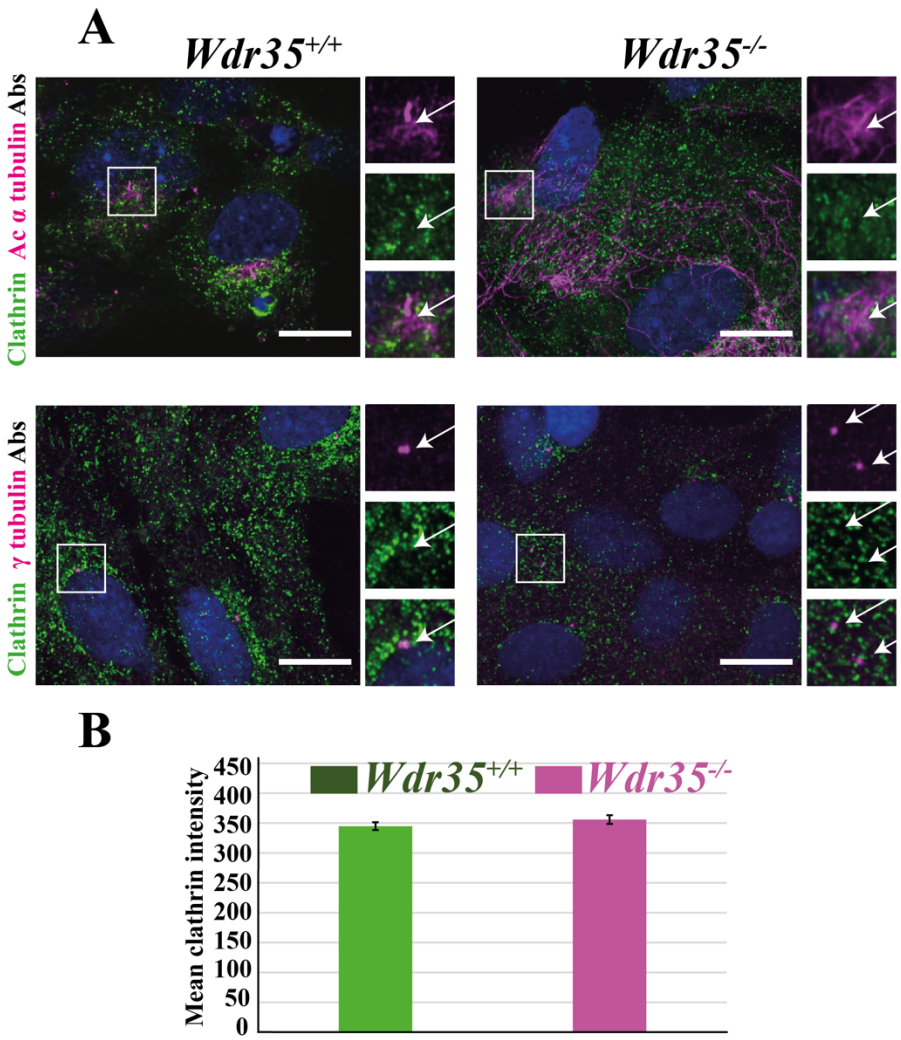

Figure 3.25. Mean clathrin localization in 2µm distance around cilia remains unchanged. (A) 24hr serum starved cells stained for clathrin antibody (green) and Ac α tubulin (upper panel) and γ-tubulin (lower panel) antibodies (magenta). (B) Mean intensity of clathrin quantified in a volume of 2µm radius around base of cilia shows no difference. n= 40cells each from 3 biological replicates.

3.1.8 Although the total levels of ARL13B is unchanged in *Wdr35*$^{-/-}$ a change in one interaction partner was detected consistent with change in localization in mutant

As a small GTPase, ARL13B is known to play a critical role in the formation and function of cilia (*Li et al., 2012*) including mice, humans and worms. In *C. elegans*, ARL13B has been proposed to bridge IFT-A and IFT-B particles (*Cevik et al., 2010*). ARL13B is specifically enriched in cilia and is a gold-standard cilial marker. However, its molecular function remains controversial. Characteristic of GTPases, ARL13B has been shown to cycle between GTP and GDP-bound forms where the GTP-bound

conformation is functional and membrane associated, whereas the inactive GDP-bound form is cytoplasmic (*Cherfils and Zeghouf, 2013*) . While not readily visible, it has been suggested that it resides on the cell membrane in non-conciliated cells and concentrates in cilia in ciliated cells. However, I saw ARL13B highly enriched on cell membrane after overexpressing it in the absence of ciliation (**Figure 3.6A, Movie 3.1**) Recently, it was proposed that ARL13B has GEF activity towards ARL3 in cilia (*Gotthardt et al., 2015*), where it interacts with ARL3 to helps in the release of lipid-modified membrane cargo into cilia. Given that ARL13B failed to enter cilia of *Wdr35* mutants (**Figure 3.6A)**, we asked whether interactors of ARL13B may inform on the cilia defects observed.

Using polyclonal anti-ARL13B and anti-GFP (control) antibodies for immunoprecipitation of E11.5 embryonic lysate, I was able to obtain a good purification of ARL13B (**Figure 3.26B**). However, by IP/MS I was unable to detect previously reported interactors including IFT-A (IFT-121/WDR35, IFT43, IFT139 and IFT122) (*Fu W et al., 2016*), IFT-B (including IFT70/TTC30A, IFT46, IFT74, IFT81, IFT27, IFT25, IFT22, IFT88, IFT52 and DYF-3) (*Cevik et al., 2013*), its target effector GTPase ARL3 (*Gotthardt et al., 2015*), the cilia inositol phospholipid regulator INPP5E (*Humbert et al., 2012*) or the planar cell polarity protein VANGL2 (*Song et al., 2016*). However, I did find a novel ARL13B interactor , the G-protein signalling modulator (GPSM1) with 6 fold WT/MUT enrichment ($p<0.01$) (**Figure 3.26A**).

GPSM1 is a GDP dissociation inhibitor (GDI) which binds to GTPases (like $G_i1\alpha$, $G_i2\alpha$ and $G_i3\alpha$) (*An et al., 2008*) to inhibit their release of GDP and hence removal of their target proteins from membranes, sequestering them in a cytoplasmic form . Given I see ARL13B enriched on the cell membrane and not in cilia in *Wdr35 mutant* cells (**Figure 3.6A**), I hypothesized that this ARL13B 'mislocalization' might be due to a lack of interaction with GPSM1, as suggested in the mass spec dataset (**Figure 3.26A**). May be directly or indirectly WDR35 might also assist release of ARL13B-GTP from cell membrane , once released from cell membrane When in a GDP bound conformation, ARL13B might be capable of binding to GPSM1. When in active GTP-bound conformation, GTPases are bound to membrane but in GDP-bound inactive conformation are released into the cytoplasm (**Figure 3.26D**). I hypothesize that in

absence of WDR35, ARL13B is not released from the cell membrane and as such, is not free in cytoplasm to bind with GPSM-1 and localize to cilia. Despite the robust hit by IP/MS, I was unable to confirm this interaction on immunoblots. Alternate approaches like FRET-based experiments could be carried out to confirm this interaction.

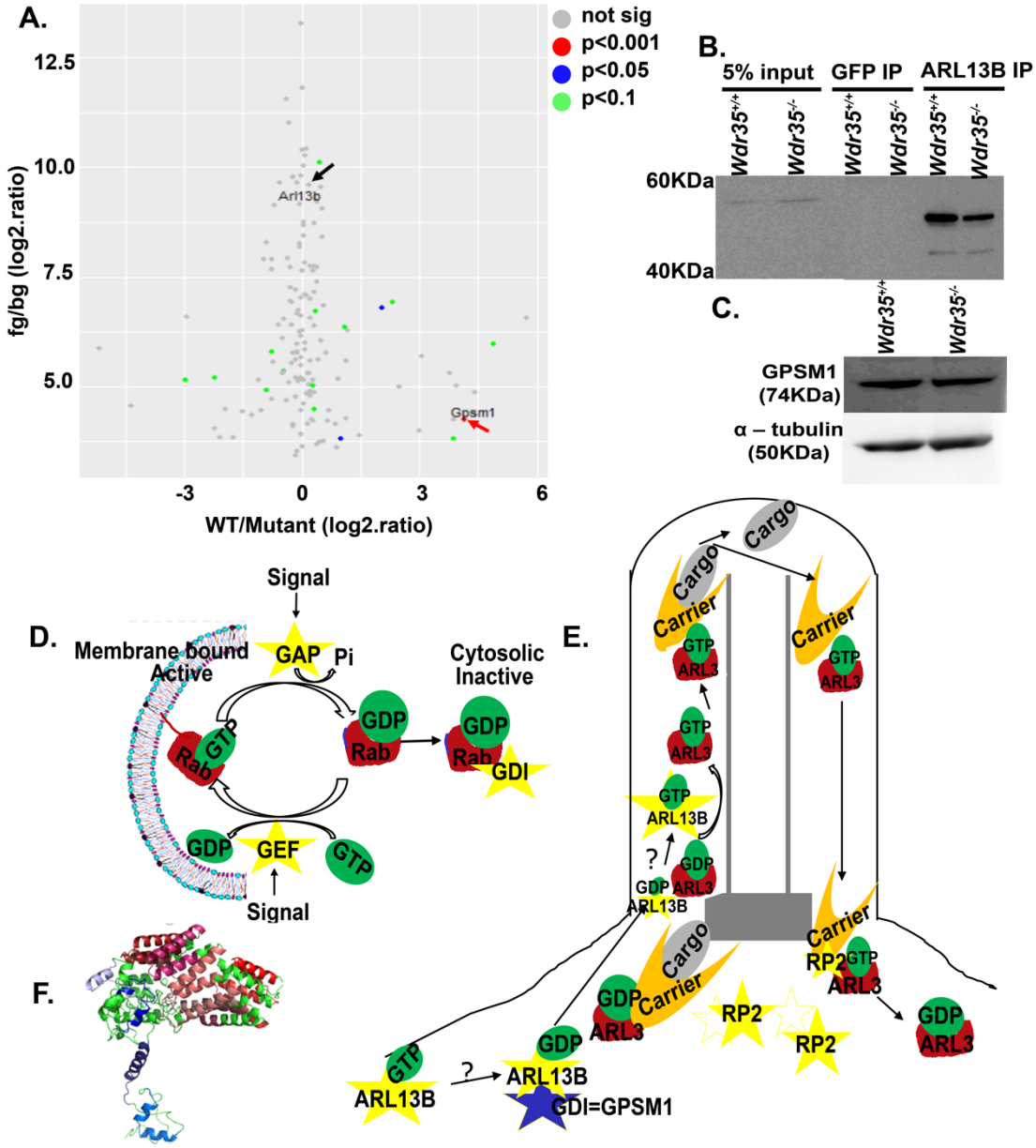

Figure 3.26. ARL13B-GPSM1 interaction is not detected in *Wdr35*$^{-/-}$ lysates. (A) IP/MS analysis of ARL13B in *Wdr35*$^{+/+}$ and *Wdr35*$^{-/-}$ shows GPSM-1–ARL13B interaction is not detected in *Wdr35*$^{-/-}$ mutants. The color key is the significance of Wdr35$^{+/+}$/Mutant ratio. (B) ARL13B IP samples probed for anti-ARL13B shows an equal level of protein in both *Wdr35*$^{+/+}$ and *Wdr35*$^{-/-}$ samples. (C) Total levels of

GPSM1 expression level are the same in *Wdr35*+/+ and *Wdr35*$^{-/-}$ extracts. (D) Basic Overview of the GTP/GDP GTPase cycle in cells. GTP-bound GTPases are in their active conformation and localize to the cell membrane and GDP-bound inactive forms localizes to the cytoplasm. (C) Outline for the role of GTPases in cilia: Carrier (UNC119a/b) ferries lipidated cargo into cilia, where ARL3-GTP allosterically interacts with the carrier to open up cargo binding pocket and release cargo within cilia. ARL3, in turn is activated by the GEF activity of ARL13B. I hypothesis ARL13B-GTP is stuck to the plasma membrane is not free to interact with GDI-GPSM-1, and could be the reason for failed transport of ARL13B to cilia. (F) GPSM1 modelled with 100% confidence with PINS, and GPSM2 template has two domains. One formed of 9TPR repeats (shades of red) and four GOLOCO/ GRP (G-protein regulating domain (shades of blue).

3.2 Discussion

3.2.1 WDR35 is required for stability and function of an intact IFT-A complex

The importance of IFT-A complex stability has been previously established to be critical for ciliogenesis in different model organisms and different IFT-A protein mutants (*Hirano et al., 2017; Liem KF et al., 2012; Picariello et al., 2019; Takahara et al., 2018; Zhu et al., 2017*). In *Chlamydomonas*, IFT43 mutants have no or very short flagella as a result of destabilized and degraded IFT139 and IFT121, which get rescued by inhibiting proteasomal degradation with MG-132 treatment (*Zhu et al., 2017*). IFT43 interacts with IFT121 directly shown in *Chlamydomonas* (*Zhu et al., 2017*) and RPE cells (*Hirano et al., 2017*) by biochemical assays. In *Chlamydomonas*, mutation of IFT140 prevented assembly of flagella severely affected total protein levels of at least two other IFT-A components, IFT122 and IFT139 the only two for which antibodies were available (*Picariello et al., 2019*). However, in mammalian cells, I determined that WDR35 is required for IFT139 and IFT43 stability (**Figure 3.14 and 3.15**). This is interesting because recent work from the Wallingford lab demonstrated that the assembly and function of the IFT-A complex required a series of cytoplasmic chaperone-like proteins in order to localize to cilia (*Toriyama et al., 2016*). It might be that all three peripheral IFT-As are more or less or equally critical for the formation of stable complex and transport. Mutation of any of them may result destabilization of the remaining peripheral components.

In spite of multiple experimental replicates of the IP/MS data for IFT-A interactors, I failed to detect published interactors like TULP-3 (*Mukhopadhyay et al., 2010;*

Toriyama et al., 2016) as well as any membrane protein cargos like ARL13B, INPP5E, and SSTR3 (*Fu W et al., 2016*). This could reflect the transient nature of these interactor which were mostly isolated using exogenously overexpressed proteins. Also what was missing were components from the CPLANE complex (ciliogenesis and planar cell polarity effectors) including planar cell polarity proteins- FUZ, WDPCP, and Inturn, as well as JBTS17. CPLANE is proposed to help to chaperone the peripheral IFT-A complements onto core and would thus not be incorporated into the final complex. In the absence of CPLANE components, the IFT-A complex is disrupted and IFT-A core proteins alone are transported inside cilia by IFT-B complex train (*Toriyama et al., 2016*). Similar to CPLANE mutant phenotypes, the IFT-A complex is disrupted in *Wdr35*$^{-/-}$ mutants and its peripheral proteins are degraded (**Figure 3.15**). However, unlike CPLANE mutants, the endogenous IFT-A core proteins do not localize inside cilia but have a restricted localisation at the transition zone in *Wdr35*$^{-/-}$ mutants (**Figures 3.16-3.20**). This is very interesting given that although IFT-B trains has been reported to ferry IFT-A during anterograde transport inside cilia (*Jordan et al., 2018*), in *Wdr35*$^{-/-}$ cilia which are filled with IFT-B particles, IFT-A core complex remains trapped at the transition zone (**Figures 3.16-3.20**) and IFT-B moves in cilia leaving IFT-A core proteins stuck at the transition zone. How WDR35 mediates this link between IFT-B and IFT-A complexes remains to be explored. Since CPLANE proteins also share some structural elements to coatomer adaptors, IFTs, and BBSomes (*Toriyama et al., 2016*), it would be interesting to explore more deeply the mechanism of action of CPLANE on IFT-A complex assembly and function.

3.2.2 IFT-A and regulation of ciliary membrane- a role for GTPases

I was interested to see how the interactions of ARL13B changed in the absence of IFT-A, given its failure to localize to cilia in *Wdr35 mutants*. Why I thought this may be informative was that ARL13B has been proposed to function as a GEF (GDP exchange factor) during transport of lipidated membrane associated proteins into cilia via the Unc119a/b-ARL3-ARL13B (*Ismail et al. 2012*), whereas transport of cilia- integral membrane proteins occurs via the TULP-3-IFT-A or BBSome-β-arrestin-2-ARL6 modules (explained in **Section 1.3.2**) (*Badgandi HB et al., 2017; Ye F et al., 2018*). In

the cytoplasm, UNC119a/b adaptor binds to lipidated domains of cargo proteins and transports them to cilia. Once inside cilia ARL3-GTP allosterically binds to Unc119a to release ciliary cargo inside cilia, protecting them to be released by effectors in cytoplasm (*Ismail et al. 2011, 2012*). ARL13B functions as GEF (GDP nucleotide exchange factor) for ARL3 (*Gotthardt et al., 2015*) and thus activates ARL3 to bind UN119a/b to release cargo inside cilia. ARL3-GTP then is cycled out of cilia where it's GAP (GTPase activating protein: RP-2) present at base of cilia hydrolyse GTP and inactivates ARL3 (*Ismail et al. 2012*) (**Figure 3.26E**). As I failed to see any transport of lipidated GFP (**Figure 3.7**) into *Wdr35 mutant* cilia, I hypothesized that these processes were likely affected. However, interactions with endogenous ARL13B in both control and mutant samples were a few suggesting more transient interactions requiring additional techniques such as proximity labelling approaches, such as turboBio-ID or APEX2, would be a way to circumvent these limitations.

3.2.3 WDR35 and vesicular trafficking appears to be independent of centriolar satellites (CSs)

After 24 hours serum starvation, I could not see differences between controls and *Wdr35* mutants in organization of centriolar satellites (**Figure 3.24**). At this stage, robust ciliogenesis is underway in control cells, whilst *Wdr35* mutants have very small, rudimentary cilia surrounded by small vesicles (**Chapter 4).** This phenotype suggests that the initial trafficking to the base of cilia occurs in *Wdr35* mutants, however subsequent docking/fusion of vesicles fails to occur during cilia elongation (shown in **Chapter 4**). This would be downstream of the role proposed for CS. In this model, CEP290 (another CS and transition zone protein) co-localises and interacts with PCM-1, and both PCM-1 and CEP290 are required for Rab8 localisation to initiate ciliogenesis in RPE1 cells (*Kim et al., 2008*). Indeed in the Dynlacht paper, it was suggested that Rab8 localized correctly, but CEP290 failed to colocalize to cilia in *WDR35*$^{-/-}$ RPE cells (*Fu W et al., 2016*). Another possible explanation is that whilst CS are not disrupted in *WDR35* mutant cells, trafficking of other cargos, like those destined for the transition zone like CEP290, are disrupted. Support for this comes from a recent report that *C. elegans* IFT-A genes function to regulate membrane transport of components of the MKS (Meckel-Gruber syndrome) module, which

includes CEP290, to cilia, thus maintaining composition of the TZ membrane diffusion barriers that ‘‘gate’’ ciliary protein entry and exit (*Scheidel and Blacque, 2018*).

Chapter 4. Identification of an IFT-dependent coat to transport cargo in vesicles from Golgi into cilia

4.1 Results

4.1.1 IFT144, IFT140, IFT122, and, IFT121 share significant sequence and structural similarity to COPI proteins α and ß'

Given the defects in cilial membrane content observed in the *Wdr35* mutant remnant cilia (see **Chapter 3**), I hypothesized that WDR35, in collaboration with other IFT-A complex members, may be required for moving ciliary cargos from donor membranes (like Golgi-derived vesicles and/or the ciliary pocket) to its destination ciliary membrane. My experiments suggested functions akin to a coatomer for WDR35, which had been previously hypothesized IFTs have evolved from a protocoatomer (*Jékely G and Arendt D, 2006; Dam TJPV et al., 2013*). To test this further, I undertook bioinformatics analysis to look at the similarity of IFT components at the global proteome level using deep sequence analysis and homology modeling.

It is challenging to establish evolutionary relationships in repeat proteins. And while there are previous reports of some IFTs having similarity to COPI and clathrin vesicles forming proteins (*Jékely G and Arendt D, 2006; Taschner M et al., 2012; Dam TJPV et al., 2013*), more advanced computational methods have been recently developed in order to make phylogenetic studies of protein families more robust. In collaboration with Dr. Jonathan Wells (laboratory of Dr. Joe Marsh, MRC HGU, IGMM), we undertook a highly sensitive method for detecting sequence relationships by carrying out multiple, iterative rounds of homology searches via alignment for sequence proximity-based clustering of IFT and COP proteins (*Wells et al., 2017; Wells and Marsh, 2019*). We used IFT-As (**Figure 4.1A**) and COP proteins (**Figure 4.1B**) as seeds to initiate the process. Briefly, using an open-source software HH-suite (https://toolkit.tuebingen.mpg.de) to detect close sequence relationships between IFT-As and COP proteins separately and the hits were clustered as graphs. Multiple iterations of homologous searches were done for generating a large cluster of related proteins using profile hidden Markov models. Protein sequences used as seeds in

(**Figure 4.1A**) are (IFTs: >sp|Q8NEZ3|WDR19_HUMAN,>sp|Q96RY7|IF140_HUMAN,>sp|Q9HBG6|IF122_HUMAN,>sp|Q9P2L0|WDR35_HUMAN) and (**Figure 4.1B**) are (COPI: >sp|P48444|COP D_HUMAN Coatomer subunit delta OS=Homo sapiens OX=9606 GN=ARCN1 PE=1 SV=1, >sp|P61923|COPZ1_HUMAN Coatomer subunit zeta-1 OS=Homo sapiens OX=9606 GN=COPZ1 PE=1 SV=1, >sp|O14579|COPE_HUMAN Coatomer subunit epsilon OS=Homo sapiens OX=9606 GN=COPE PE=1 SV=3. Summarized in (**Figure 4.1)**, our analysis revealed that COPα and COPβ' cluster with 6 IFT proteins (two IFT-B and four IFT-A components), both having TPR and WD40 repeats. In contrast, COPβ and COPϒ1/2 have HEAT/ARM repeats not found in IFT components, whilst COPε has highly diverged TPR repeats without any WD40 domains. COPδ and COP**ζ**1/2 have no identifiable repeat domains and are most closely related to adaptor protein complexes AP2 and AP3.

In summary, using multiple rounds of homology searches in HH-suite, we generated a large set of putatively related repeat proteins from those of initial interest the COPI or the IFT-A components as seeds. WD40 repeat containing proteins are an important and very large group of proteins sharing diverse biological functions. Simple alignment strategies with proteins such as these IFTs containing multiple copies of the same repeat motifs could erroneously align to suggest a close evolutionary relationship where none exists (i.e. false positives). Using our reciprocal search algorithm producing mutually high-ranking alignments for four of IFT-As (IFT144, IFT140, IFT122 and IFT121) and two of IFT-Bs (IFT80 and IFT172) with very close sequence proximity to α and β' COPI proteins.

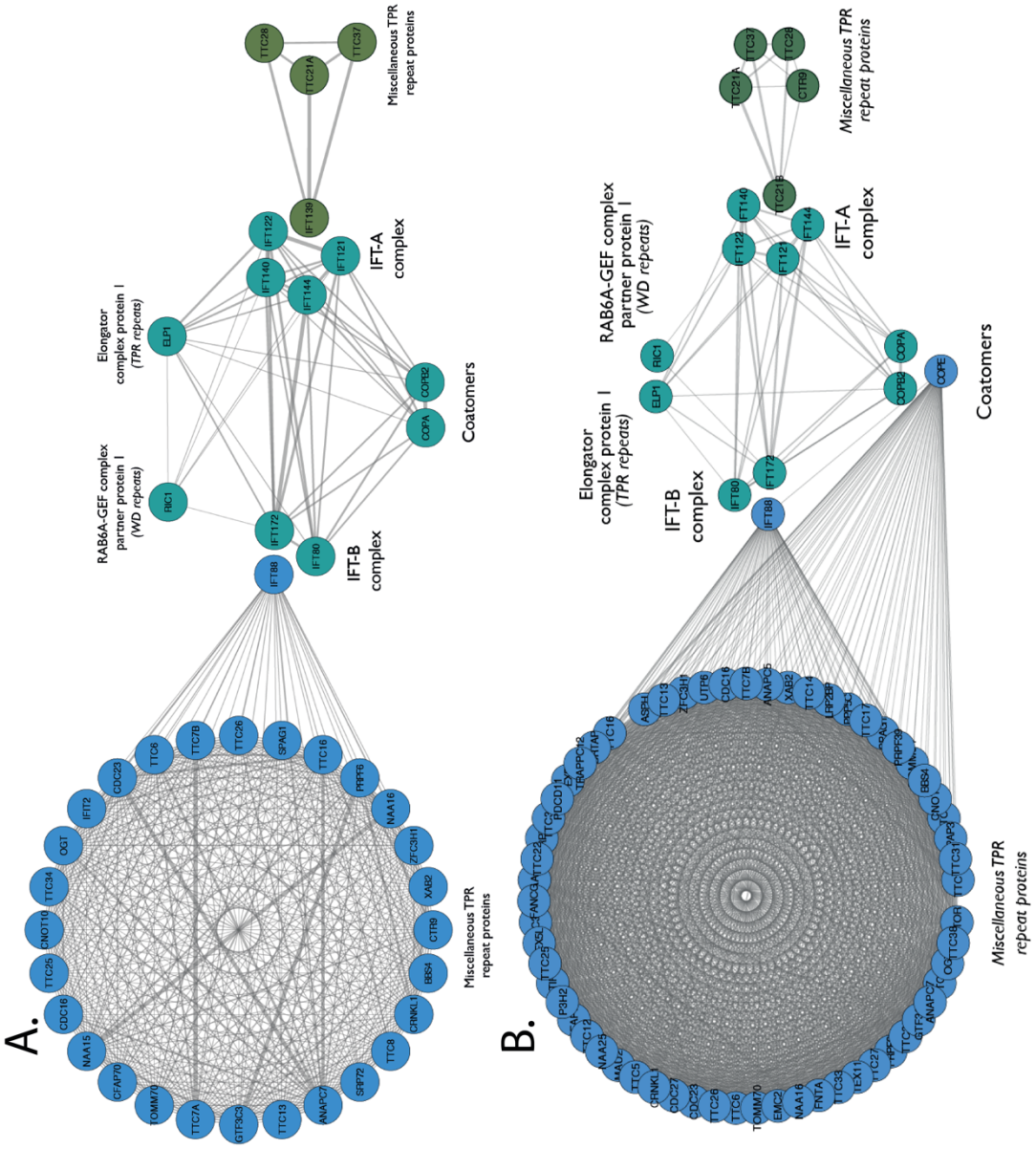

Figure 4.1. Multiple rounds of homology searches via alignment of profile hidden Markov model analysis reveal IFT-A subunits have very close sequence similarity to α and β' COPI subunits, supporting a relationship of conserved evolutionary function. Clusters of IFT and COP subunits generated based on sequence similarity using **(A)** IFT144/WDR19, IF140, IF122 and IFT121/WDR35 as seeds and **(B)** COPI proteins as seeds. These reciprocal high-ranking alignments suggest very close similarity exists between a subset of IFTs and the COPI α and β' subunits, suggesting a functional evolutionary relationship may exist between COPI and IFT. Clusters are color-coded according to protein structural motifs. TPR repeat proteins are highlighted in blue and dual WD40 repeat, and TPR repeat containing proteins are shown in bluish-green. Lines between clusters indicate sequence based proximity.

Next, I used SWISS-MODEL, a fully automated protein structure homology-modeling tool (https://swissmodel.expasy.org/) to predict structures of IFT-A proteins. Template search with BLAST and HHblits was performed against the SWISS-MODEL template library. With the help of the BLAST, the target sequence was searched against the primary amino acid sequence contained in the SWISS-MODEL Template Library (SMTL), a large structural database of experimentally determined protein structures derived from the Protein Data Bank (PDB). Subsequently, the obtained profile was searched against all profiles of the SMTL. With 12%-15% sequence identity and 25%-30% sequence similarity to 4 of IFT-A complex proteins (IFT144, IFT140, IFT122, and IFT121/WDR35), COPI α and β′ structures were top hits (**Appendix-V**). Based on the target-template alignment models are built using ProMod3, ribbon diagrams of all these 4 IFT-A subunits modeled structures with two N-terminal seven-bladed WD40 β propellers and C-terminal extended TPR repeats, also found in α and β' COPI proteins **(Figure 4.2**), and previously modeled for WDR35/IFT121 from our lab (*Mill et al., 2011*). I have extended this analysis to the rest of the IFT-As, where the structure was possible. Reassuringly, while undertaking this work, a crystal structure for IFT80 was published highlighting the same domain organization (*Taschner M et al., 2018*) as our modeling and reciprocal search algorithm above predicted. We found 4 IFT-As (IFT144, IFT140, IFT122, and IFT121) have very high sequence and structural similarity to COPI α and β′ sub units with N-terminal WD40 repeats and C-terminus TPR region. The remaining 2 IFT-A subunits were not possible to model accurately. IFT139 contains only TPR repeats with some sequence similarity to COPε subunit of COPI vesicle proteins. IFT43 is the smallest and most unstructured protein, as such could not be modeled and is presumed to be made of α-helices.

Given the proximity of the Golgi to cilia (*Sorokin S, 1962*) and the dynamic exchange of many proteins critical for ciliation between the Golgi and distal appendages (see **Section 1.3.4**) (*Baron Gaillard et al., 2011; Follit et al., 2006; Graser et al., 2007; Joo et al., 2013*), and the structural homology of IFT-As to COPI proteins which derive vesicles from Golgi, it is tempting to speculate that IFT-As may function similar to COPI vesicle coats assisting Golgi-to-cilia vesicular transport.

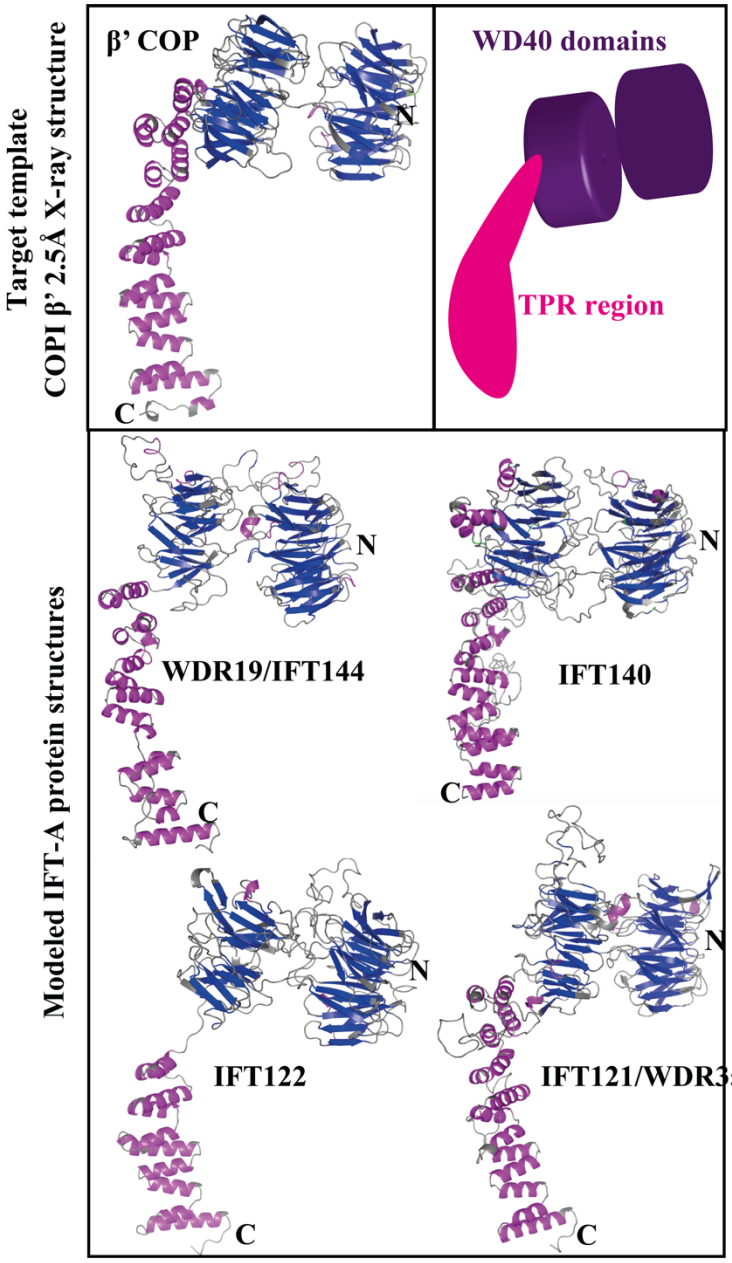

	IFT144	IFT140	IFT122	IFT121
%Sequence Identity	14.58	13.38	14.11	12.11
% Sequence similarity	27	27	27	26
%Sequence coverage	51	47	52	60

Figure 4.2. IFT-A complex proteins IFT144/WDR19, IFT140, IFT122, and IFT121/WDR35 have strong structural homology to α and β' COPI coat proteins. Analysis of the SWISS Model template library revealed α and β' COPI coat proteins to be top sequence match for four of IFT-A proteins IFT144, IFT140, IFT122, and IFT121. Ribbon diagram of modeled structures shows N-terminal seven-bladed WD40-like β propeller and C-terminal TPR domain. β-sheets are shown in blue, α-helix in magenta and loops in grey. Sequence coverage for modeling, similarity, and

Identity of respective IFT-As to β' COPI is in a box at the bottom. Details of the analysis methods are provided in the Material and Methods sections, and the complete template hit library and sequence blast analysis is available as an Appendix V.

4.1.2 Ultrastructural analysis of ciliation in MEFs reveals a deep-seated ciliary pocket in the cell

To further investigate the hypothesis of IFT-As functioning as coatomer proteins, I undertook TEM (transmission electron microscopy) analysis of ciliated MEFs in collaboration with Dr. Gaia Pigino at MPI CBG Dresden. I did this by two methods. In the first, I directly imaged thin sections (70nm) with TEM. In the second, since cilia are around 250nm in diameter and 2-4μm in length and electron beam can't directly pass through the entire thickness of a cell, I also made serial, thick (300nm) sections. I then imaged sections by making TEM tilt series, reconstructing tomograms and stitching the tomograms of serial sections to get the complete view of the cell, focusing on the area around cilia (see **Materials and Methods**). This work was to landmark the position and orientation of cilia in wild type cells during ciliogenesis and determine how it is perturbed in mutants (**Section 4.1.3**).

After 24hr serum starvation, when imaging TEM sections perpendicular with the adherent surface, we could not readily find cilia. Next, I scanned sections parallel to the adherent surface, and I found 80% of cilia in fully confluent cultures. In 300nm sections, all observed cilia have their basal body and proximal part of cilia in a single section, with the nearly entire 3-5μm long cilia in the following section. This suggests cilia grow almost parallel to the cell surface in MEFs. Cilia were most prevalent at the height of 1-2μm from the adherent surface with a height of the free surface of the cell being 5-6μm from the base (**Figure 4.3A**) indicating that cilia are not randomly originating with respect to the Z-axis.

The process of ciliation was observed to start very close to the nucleus, and remains in close proximity to the Golgi stacks throughout. Surprisingly, even after 24 hours, only ~1% of cilia were observed to emerge from the cell (**Figure 4.3-4.10**), highlighting how deep-seated the ciliary pocket is in MEFs and how long it takes to emerge out of the cell. A similar process has been described in RPE cells (*Molla-Herman A et al., 2010*), where when 80% of cells were confirmed to be ciliated by

immunofluorescence, whilst scanning electron microscopy was unable to detect any cilia. Upon transmission electron microscopy, 80% of cells were observed to have cilia (*Molla-Herman A et al., 2010*). In the majority of the cases, the tip was found to be pointing towards the cell membrane and base in very close proximity to the nucleus (**Figures 4.4, 4.8, 4.10a& c**), occasionally a cilia tip was also found protruding into the nucleus (**Figure 4.10b**). In control MEFs, a (9+0) arrangement of microtube ran the length of the axoneme (**Figure 4.3-4.4**). Additionally, 25nm microtubule filaments can be seen attached at the base of cilia and subsequently radiating in different directions in the cell (**Figure 4.3**). This was further very clearly seen in immunofluorescence imaging of SIR-tubulin stained ciliated MEFs (**movie-2.1 and 2.2**). Around 6nm actin filaments could also be seen present at the tip, base and along the length of cilia in the cytoplasm (**Figure 4.3**). Intriguingly coated vesicles (having a regular patterned electron density) were observed bulging from ciliary pockets and ciliary sheaths in WT MEFs (**Figure 4.3**).

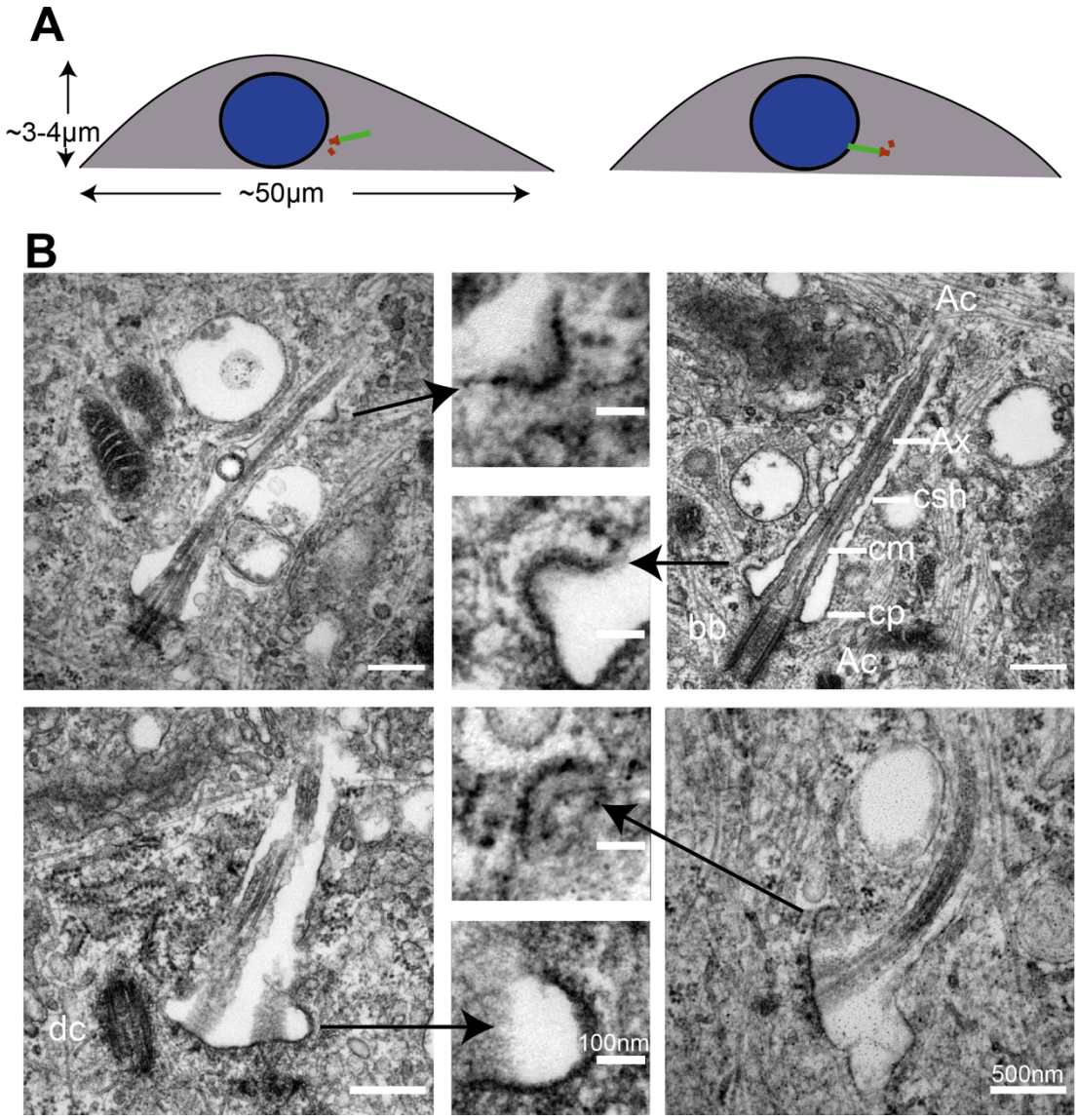

Figure 4.3. Vesicles with electron dense coats could be seen bulging from the ciliary sheath in wild type MEFs. (A) Arrangement of cilia in wild type MEFs. Cilia in MEFs grow at the height of 1-2µm from the adherent surface and run almost parallel to the adherent surface as shown, so for TEM analysis transverse sections parallel to surface were made. **(B)** TEM micrographs demonstrate vesicles fusing with ciliary sheath mostly at the base of the ciliary pocket and less along the length (shown by arrows). Other structures highlighted by straight lines are Actin filaments (Ac), Axoneme (Ax), Ciliary sheath (csh), Ciliary membrane (cm), ciliary pocket (cp), basal body (bb), daughter centriole (dc). Scale bars: 500nm and 100nm.

4.1.3 Differences in vesicle numbers and electron densities around them are observed around *Wdr35*$^{-/-}$ MEF cilia

The high sequence and structural homology between IFT-As to COPI subunits we found coupled with the defects in the establishment and/or maintenance of ciliary membrane in *Wdr35*$^{-/-}$ I observed by immunofluorescence led us to ask whether we could observe differences in the early stages of ciliogenesis by TEM in Golgi-to-cilia vesicular trafficking. In immunofluorescence experiments, we saw no membrane proteins trafficked into *Wdr35*$^{-/-}$ cilia, whilst IFT-As have restricted localisation only in the transition zone and IFT-Bs accumulated in short stubby cilia. In contrast, retrograde dynein motor mutant cilia accumulated all three type of ciliary proteins in short stubby cilia, consistent with a retrograde phenotype (**Chapter 3**). Next, we compared TEM data of WT, *Dync2h1*$^{-/-}$, and *Wdr35*$^{-/-}$ MEFs. Short club shaped cilia were observed in *Wdr35*$^{-/-}$ (up to 0.5µm) and *Dync2h1*$^{-/-}$ (2µm- 4µm) compared to normal 2-4µm long cilia in control cells (**Figure 3.4D, 4.3, 4.4, 4.6, 4.8 and 4.10**). In comparison to the well-defined ciliary membrane and well polymerized microtubules in a (9+0) arrangement of the control axoneme, *Wdr35*$^{-/-}$ cilia have 'wavy' membranes and disorganized microtubules (**Figure 4.8**). Surprisingly, *Dync2h1* mutants retained a well-defined ciliary membrane and a well-formed axoneme present throughout (**Figures 4.9** and **4.10**). This 'wavy' nature of the flagellar membrane in the absence of retrograde IFT (*fla-14*) was previously reported in *Chlamydomonas* (*Pigino et al., 2009*).

After 24hrs of serum starvation, electron-dense invaginations from ciliary sheath towards the cytoplasmic side in wild type MEFs were observed. These invaginations were predominantly found at the base of cilia at the ciliary pocket but are also occasionally present along the length of the ciliary sheath (**Figure 4.3**). Additionally, small electron-dense vesicles could also be seen predominantly clustering around the base of wild type MEF cilia (**Figures 4.3,4.4, and Movie 4.1**). In all of these images, Golgi stacks can be seen in close proximity of the growing cilia with a clear track of electron-dense vesicles extending between the Golgi and the cilia base in Z-stacks of reconstituted tomograms (**Figure 4.5, Movie 4.2**).

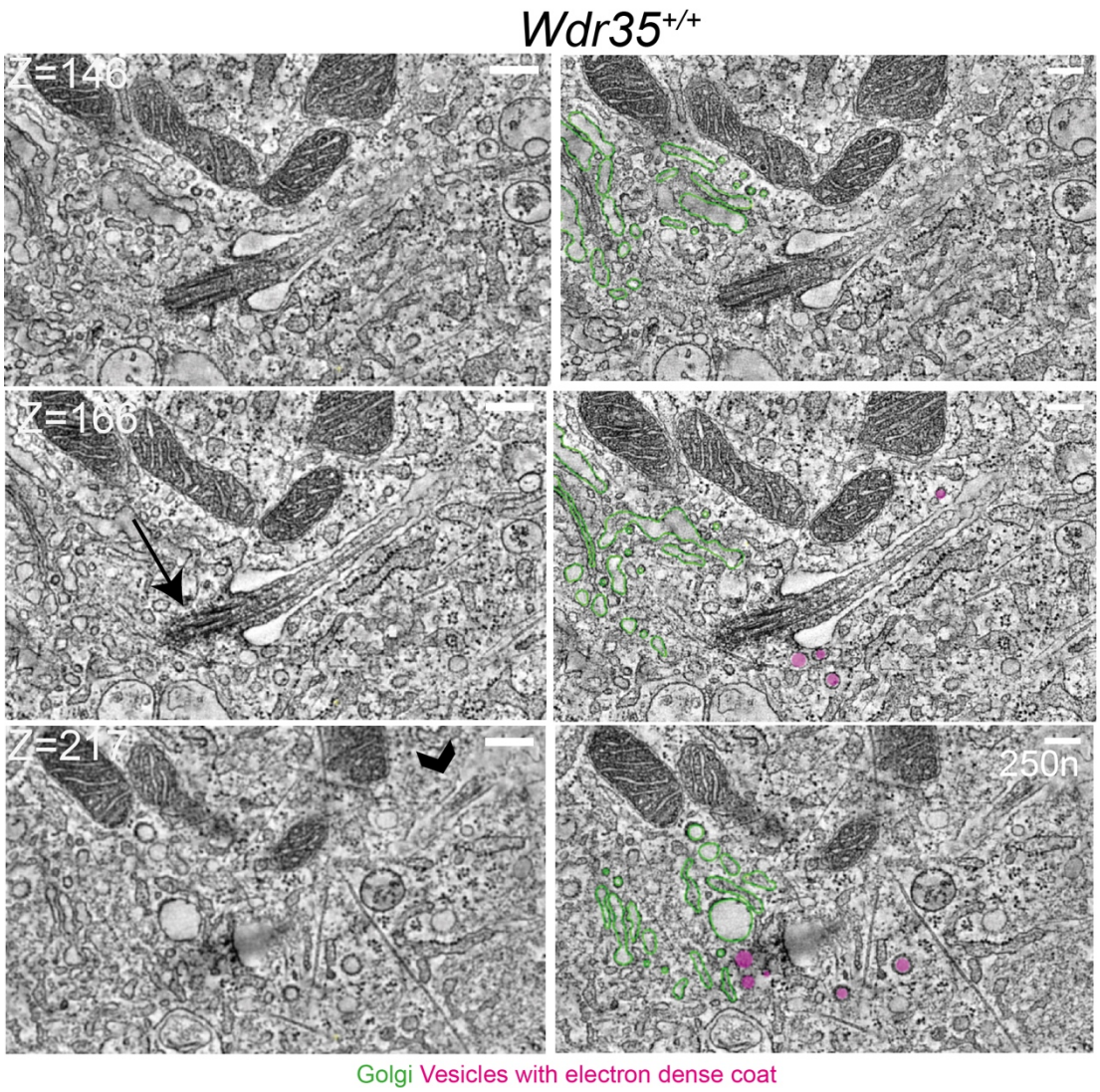

Figure 4.4a. Electron-dense vesicles could be seen at the base of cilia in wild type MEFs. After 24 hours of serum starvation, Z-stacks through the slice of 300nm TEM tomograms were color-coded to highlight the Golgi (green) and electron-dense coated vesicles within a 2µm radius of the cilia (magenta). Images in the right panel are segmented in the left panel. Electron-dense vesicles are found prominently around the base of cilia. Arrow points at cilia base and arrowhead points at cilia tip. Zoomed in image for segmented data is shown in **Figure 4.4b** and for the morphology of vesicles is shown in **Figure 4.9**. Scale bar= 250nm.

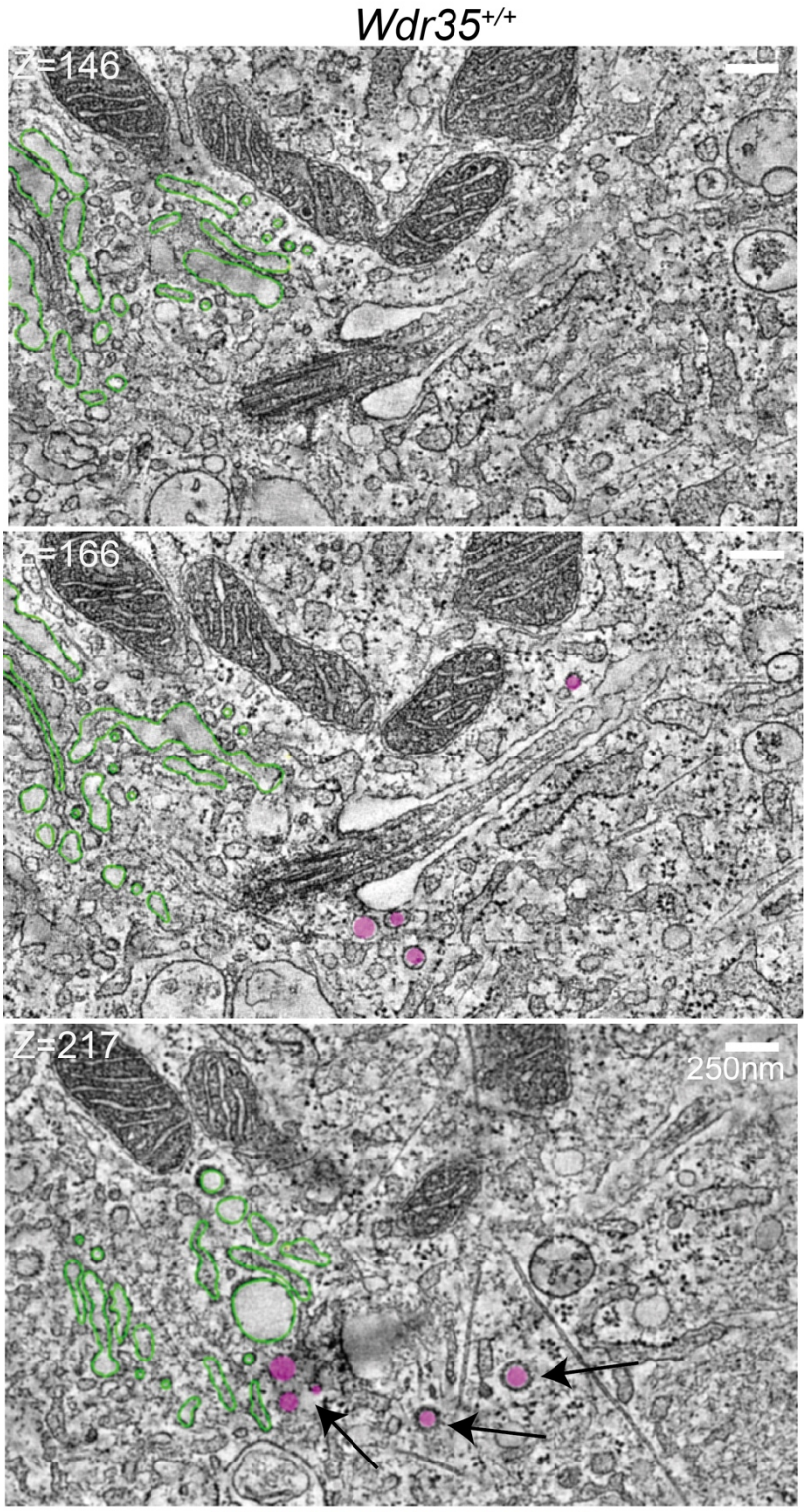

Figure 4.4b. Electron-dense vesicles could be seen at the base of cilia in wild type MEFs (zoomed-in region-of-interest from 4.4a image): Golgi stacks shown in green can be seen close to cilia and vesicles with electron-dense coats could be seen clustering prominently around the base of cilia. Arrows point at the vesicles. Scale bar: 250nm.

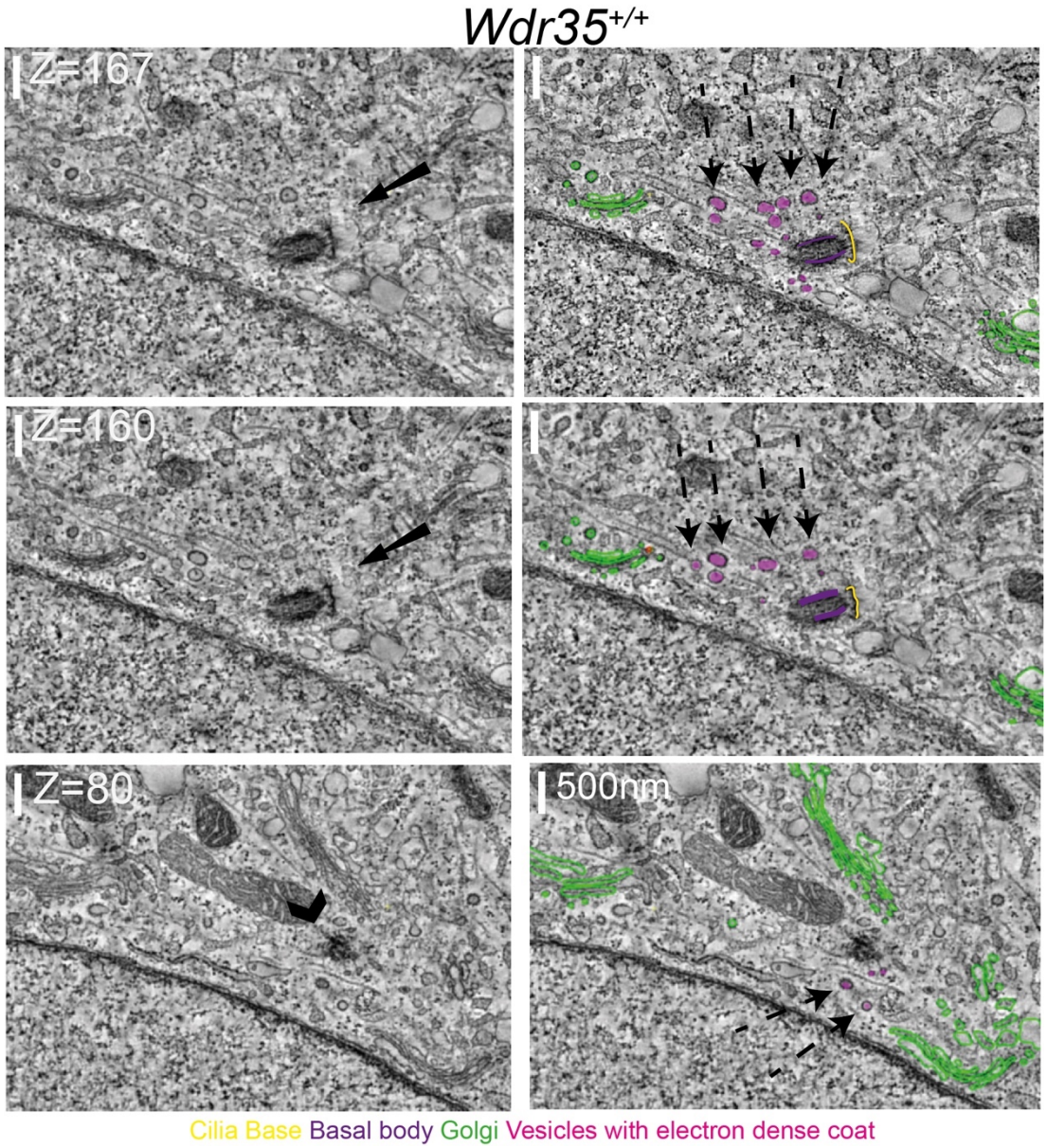

Figure 4.5a. Electron-dense vesicles tracking between Golgi and cilia are present in wild type fibroblasts. After 24 hours of serum starvation, Z-stacks through the slice of 600nm TEM tomograms were color-coded to highlight the Golgi (green) and electron-dense coated vesicles within a 2µm radius of the cilia (magenta). Images in the right panel are segmented in the left panel. Electron-dense vesicles are found prominently around the base of cilia. Arrow points at cilia in the upper section and arrowhead point at daughter centriole in the lower section. Few vesicles could also be seen around daughter centriole as well. Zoomed in region-of-interest for segmented data is shown in **Figure 4.5b** and for the morphology of vesicles in **Figure 4.9**. Scale bar 500nm.

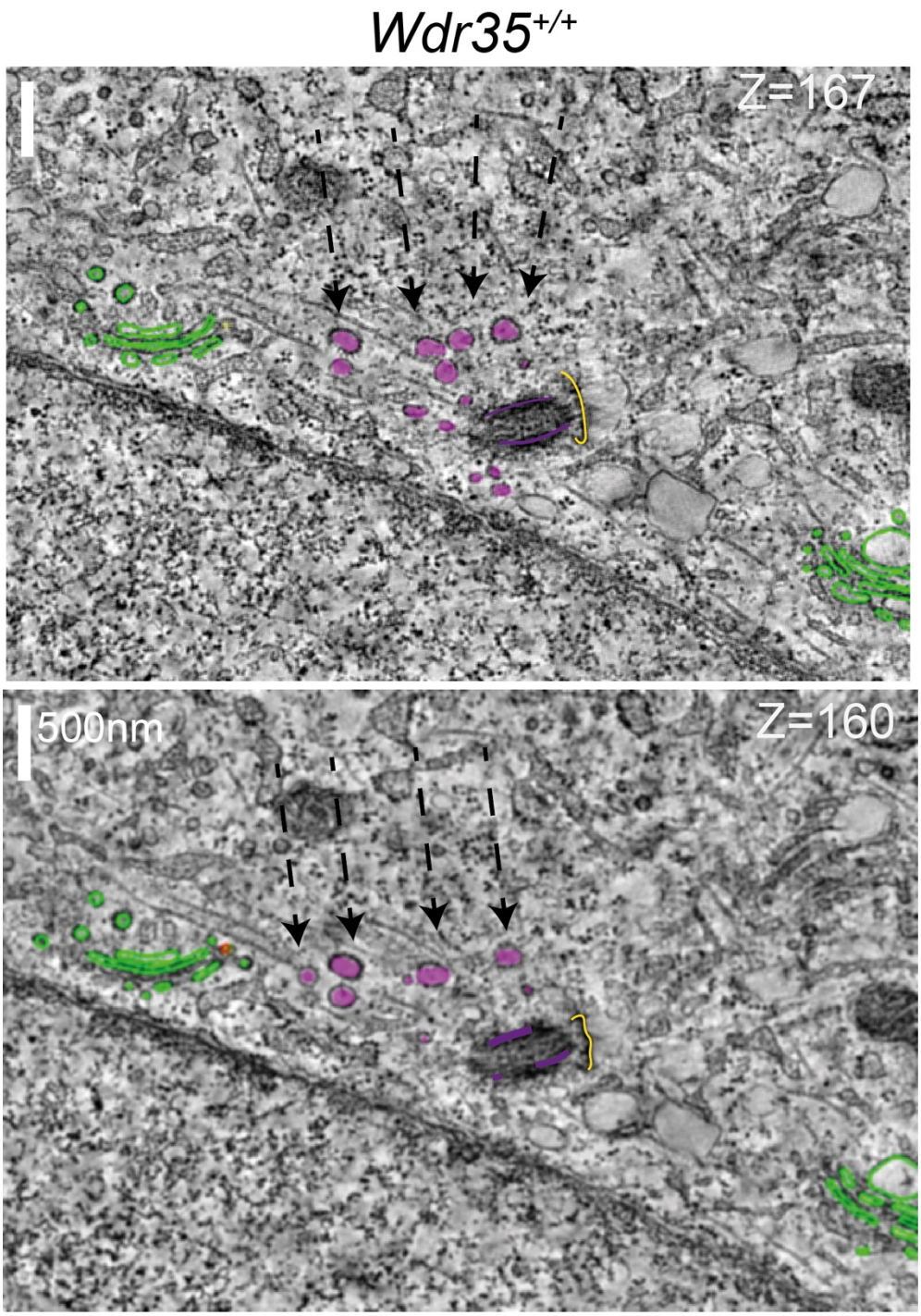

Figure 4.5b. Electron-dense vesicles tracking between Golgi and cilia are present in wild type fibroblasts (Zoomed-in region of interest from Figure 4.5a image). The Golgi is shown in green surrounds cilia and tracks of electron-dense vesicles (magenta) is present between the Golgi and cilia base. Arrows point at the path of vesicles between Golgi and cilia. Scale bar is 500nm.

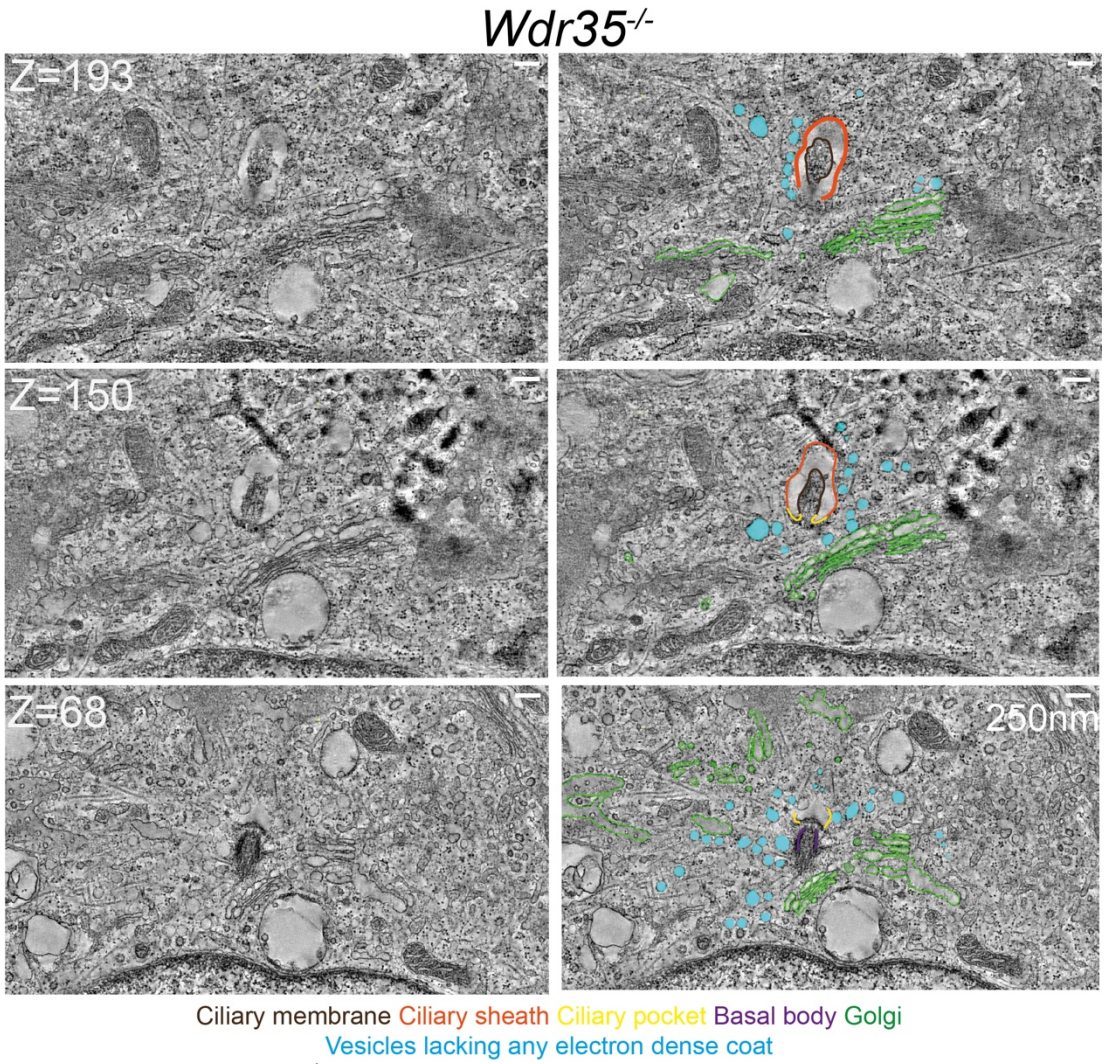

Figure 4.6a. In *Wdr35*$^{-/-}$ fibroblasts, an accumulation of small noncoated vesicles is observed around short and stumpy cilia. After 24 hours of serum starvation, Z-stacks through the slice of 600nm TEM tomograms were color-coded to highlight the Golgi (green) and vesicles within a 2µm radius of the cilia (blue). Images in the right panel are segmented in the left panel. Zoomed in region-of-interest for segmented data is shown in **Figure 4.10b** and for the morphology of vesicles in **Figure 4.9**. Scale bar= 250nm.

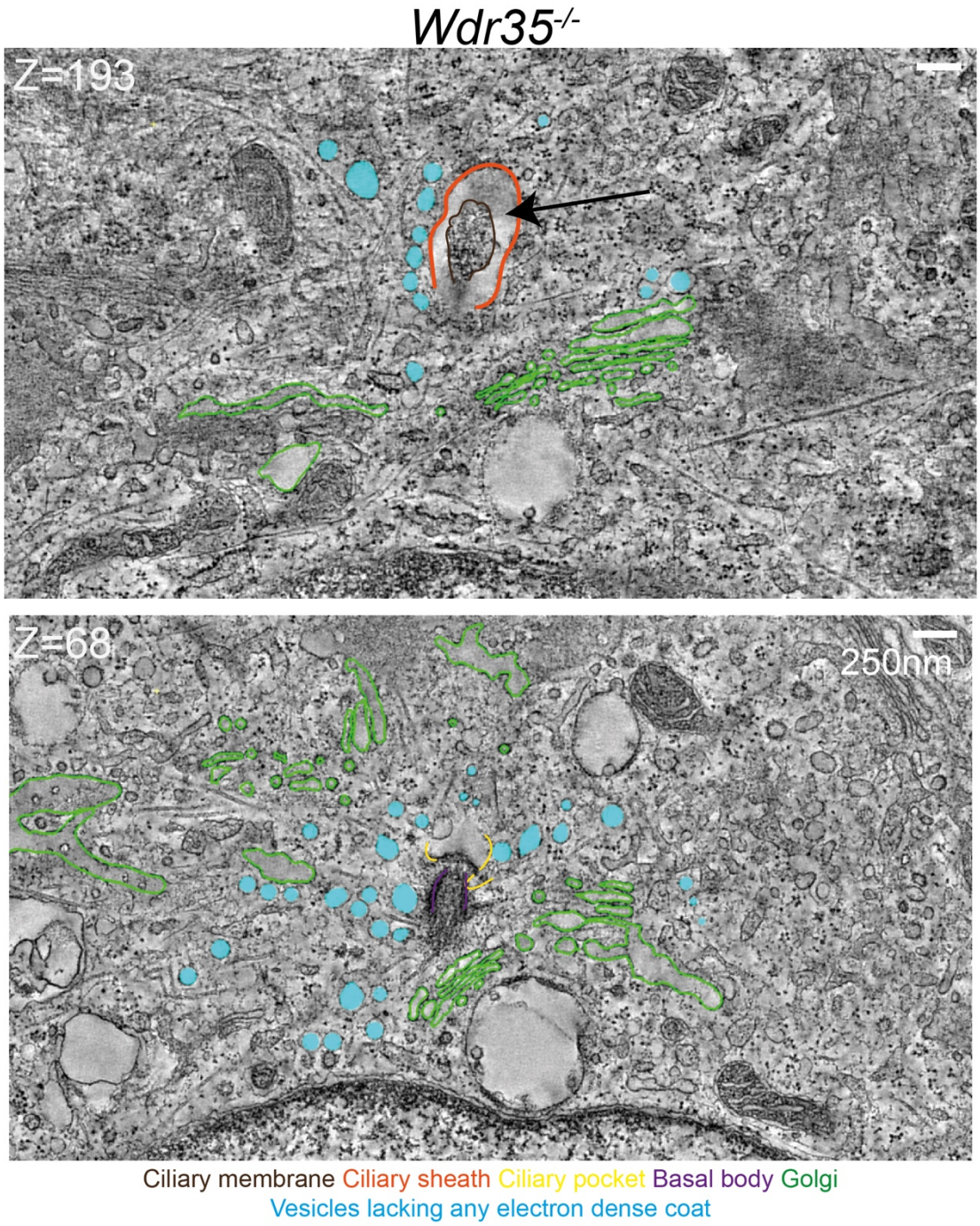

Figure 4.6b. In *Wdr35*$^{-/-}$ fibroblasts, an accumulation of small noncoated vesicles is observed around mutant cilia (Zoomed in region-of-interest from Figure 4.6a). Golgi stacks are shown in green and uncoated vesicles are shown in the blue colors clustering around cilia. Arrow points at the floppy ciliary membrane observed in *Wdr35*$^{-/-}$ MEFs. Scale bar: 250nm.

However, in *Wdr35*$^{-/-}$ mutant cells, there is a 10 fold increase in the average number of vesicles around the cilia base (**Figure 4.9, 4.6;Movie 4.3 and 4.7;Movie 4.4**) and all of these vesicles completely lack electron dense coats observed in controls (**Figure 4.3, 4.4; Movie 4.1, 4.5; Movie 4.2 and 4.9**). An increased number of Golgi stacks clustering around the rudimentary cilia in *Wdr35*$^{-/-}$ mutants is also observed. In mutant cells, it is as if the cell senses a failure to ciliate fully and tries to increase cargo through the Golgi-to-cilia route. These uncoated vesicles are spread in a radius 1-2μm, but do not cluster near or pile up on ciliary sheath. Together this TEM analysis suggests that *Wdr35*$^{-/-}$ MEFs are blocked at the later stages of ciliogenesis, after the PCV has fused but before elongation can occur. Our studies raise an interesting question into the nature of what are these electron dense vesicles at the base of wild type cilia, are they involved in the import or export cargo from cilia?

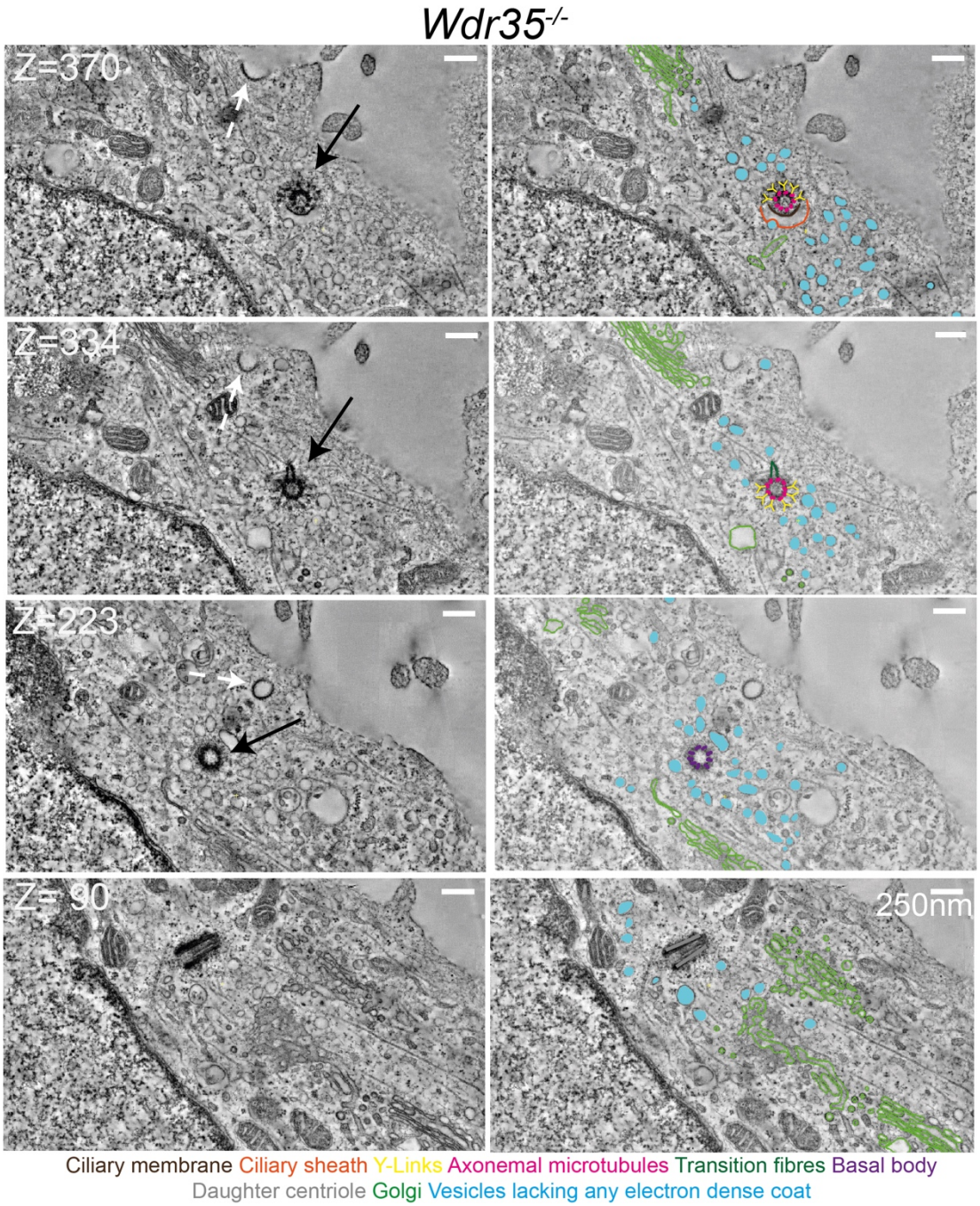

Figure 4.7a. Transition zone is unaltered in *Wdr35*$^{-/-}$ MEFs. After 24 hours of serum starvation, Z-stacks through the slice of 900nm TEM tomograms were color-coded to highlight the Golgi (green) and vesicles within a 2µm radius of the cilia (blue). Images in the right panel are segmented in the left panel. Arrows point at transition zone and dashed arrow points at one clathrin coated vesicle budding in from the cell membrane. Zoomed in regions-of-interest of segmented data are shown in **Figure 4.7b** and for the morphology of vesicles in **Figure 4.9**. Scale bars = 250nm.

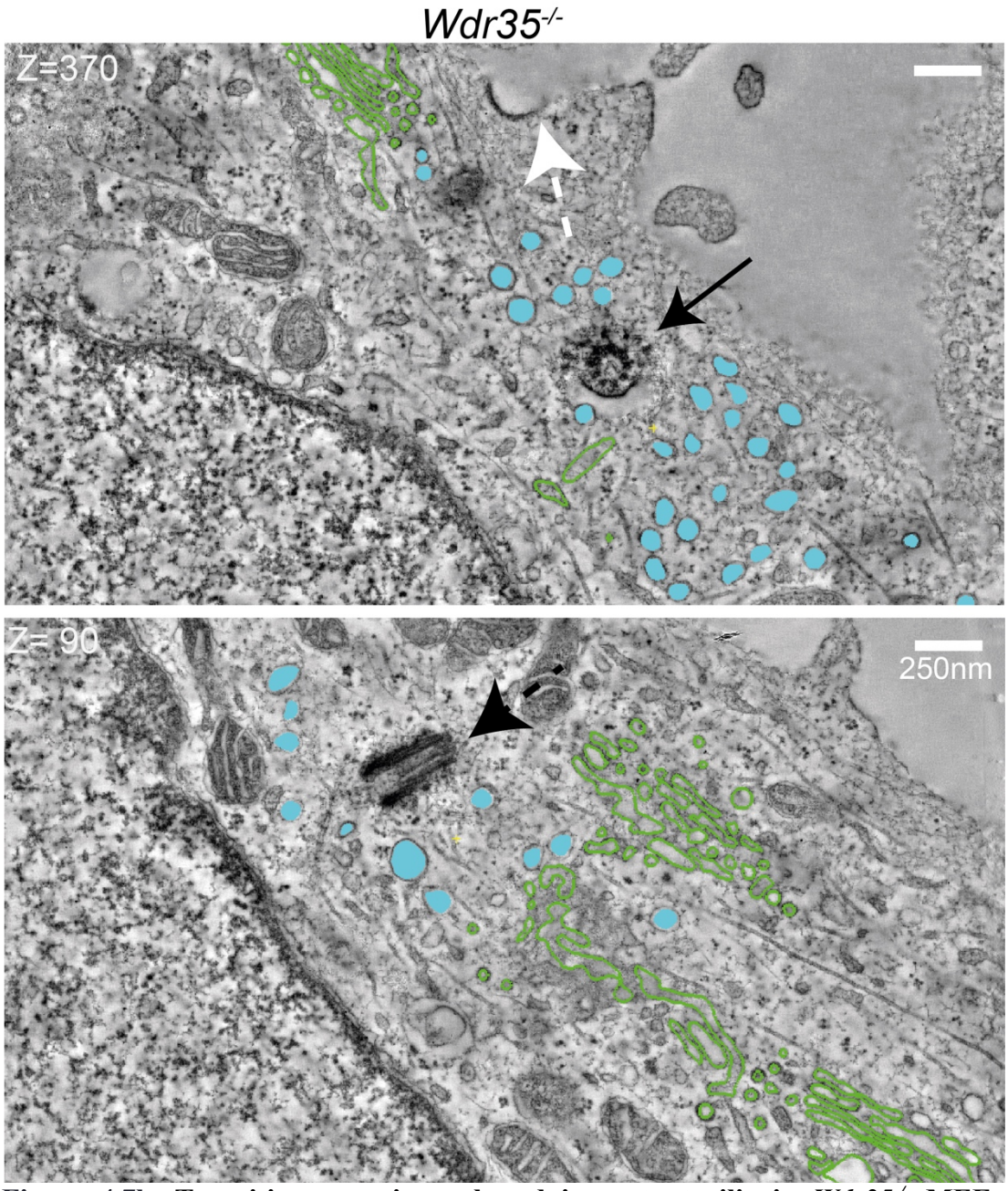

Figure 4.7b. Transition zone is unaltered in mutant cilia in *Wdr35*$^{-/-}$ MEFs (Zoomed in region-of-interest from Figure 4.7a stacks). Golgi stacks are shown in green and vesicles are shown in the blue colors cluster around cilia. Black dashed arrow points at the daughter centriole, black arrow points at ciliary transition zone in *Wdr35*$^{-/-}$ MEFs. White arrow shows one clathrin coated vesicle invaginating from the cell membrane. Scale bar: 250nm.

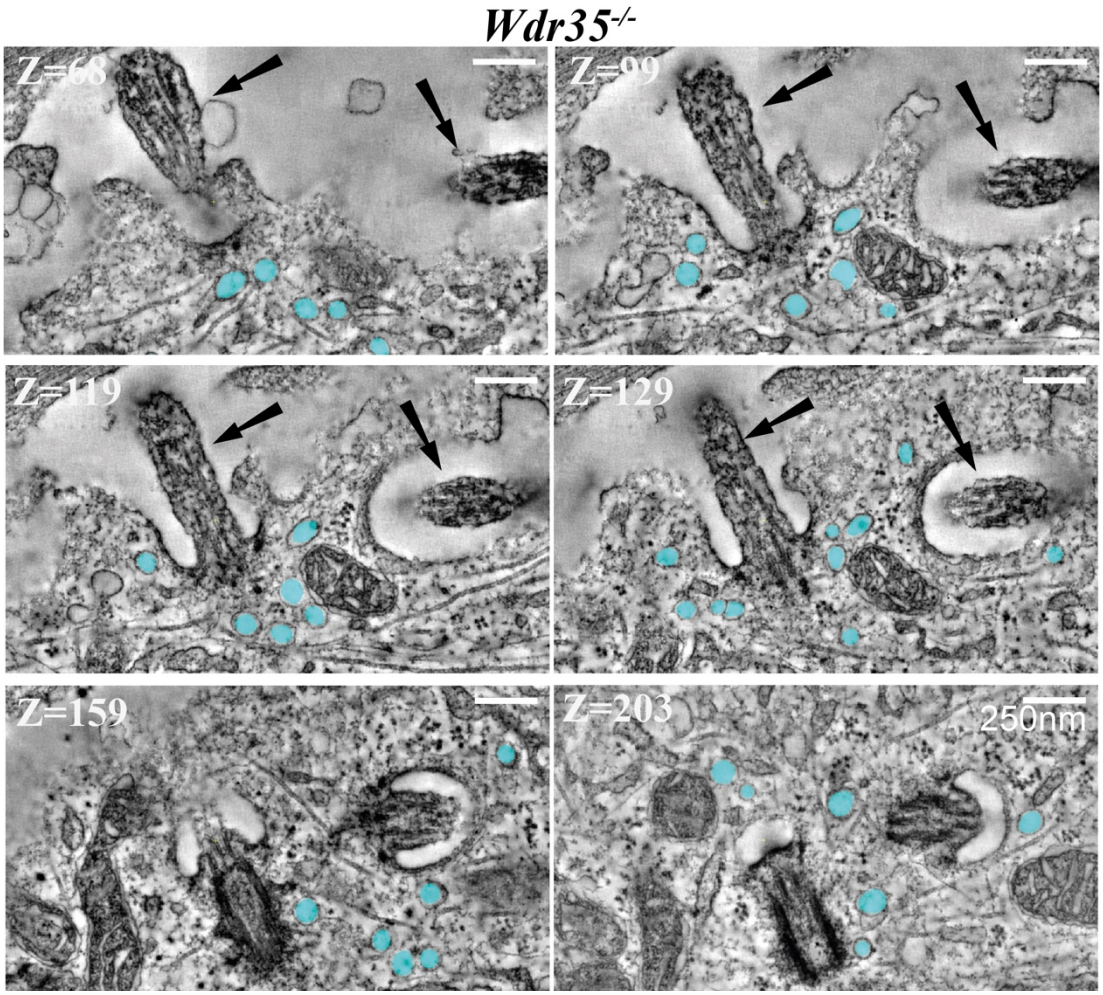

Figure 4.8. In *Wdr35*$^{-/-}$ MEFs, the ciliary membrane is less well-defined and microtubules are not typical (9+0) axonemal arrangement. Z-stack from a tomogram reconstructed from TEM tilt series. Arrows point at the floppy ciliary membrane. Periciliary vesicles are color-coded in blue. Scale bar=250nm.

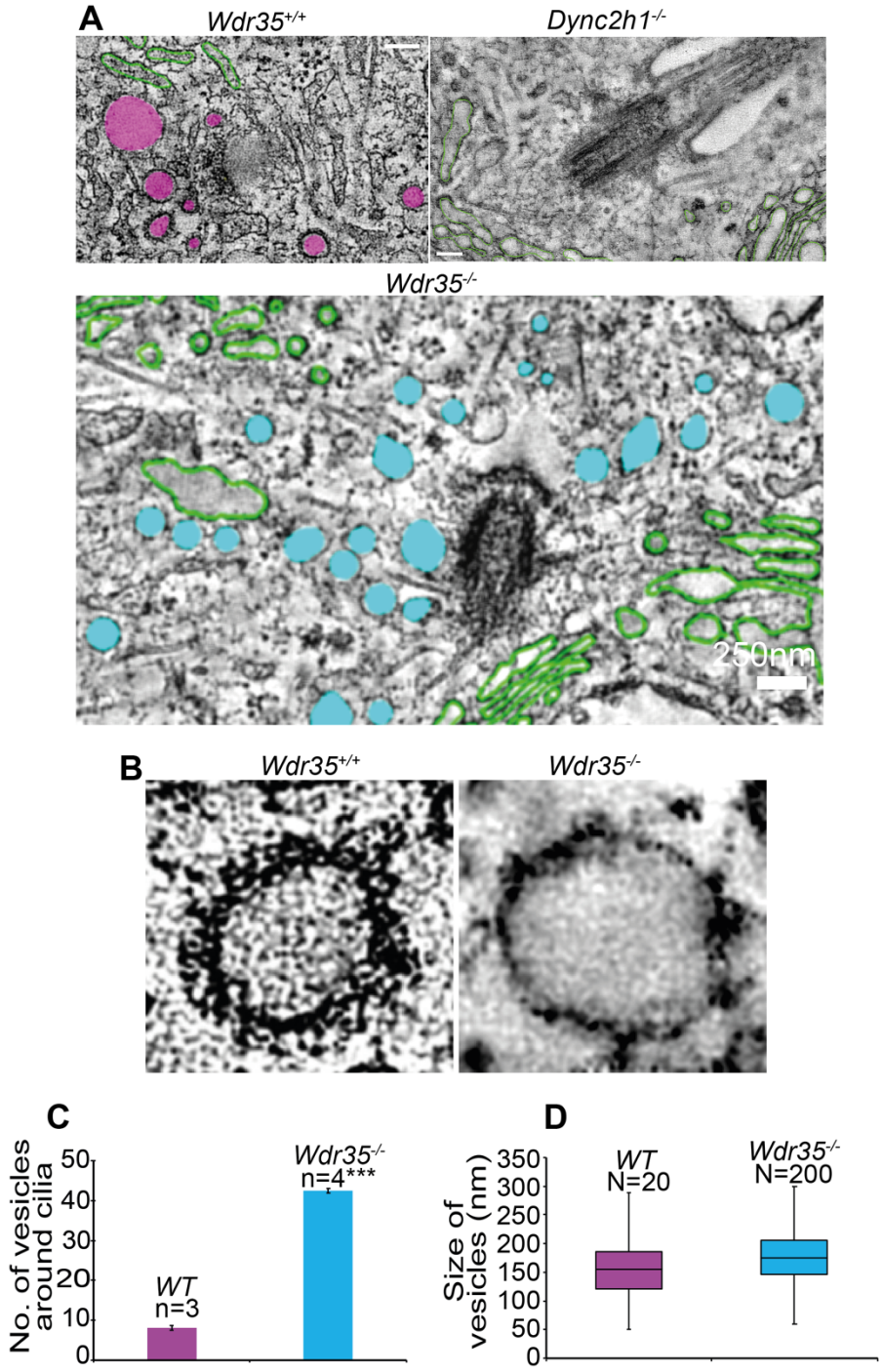

Figure 4.9. Quantitation of periciliary vesicle number, size and electron density as observed around wild type, *Dync2h1*$^{-/-}$ and *Wdr35*$^{-/-}$ mutant MEF cilia. (A) Representative images of zoomed-in views of periciliary vesicles observed in *Wdr35*$^{+/+}$, *Wdr35*$^{-/-}$, *Dync2h1*$^{-/-}$ MEFs 24 hours post-serum starvation. Coated vesicles in *Wdr35*$^{+/+}$ are coded in magenta and vesicles in *Wdr35*$^{-/-}$ are coded in blue. Too few/no vesicles were observed in *Dync2h1* mutants. (B) Electron dense coats are present around periciliary vesicles in *Wdr35*$^{+/+}$ cilia and are absent in *Wdr35*$^{-/-}$ MEFs. (C) The average number of vesicles around cilia in control and *Wdr35*$^{-/-}$ cells, counted in a volume of 2µm radius around cilia in tomograms reconstructed from TEM tilt

series. Ten times more vesicles in *Wdr35*$^{-/-}$ compared to *Wdr35*$^{+/+}$ control cilia were observed. (D) Size of periciliary vesicles did not show a significant difference between control and *Wdr35*$^{-/-}$ MEFs. The paucity of vesicles around *Dync2h1* mutant cilia prohibited quantification. Scale bars= 250nm. Asterisk denotes significant p-value from t-test: (*, P<0.05), (**, P<0.001), (***, P<0.0001). n= number of tomograms per genotype reconstructed for quantification.

4.1.4 TEM analysis of *Dync2h1*$^{-/-}$ MEF cilia show IFT trains stacked at a periodicity of 40nm inside the axoneme

In order to test whether the electron dense vesicles observed around cilia in control cells were involved in import or export of ciliary cargo, we examined cells where ciliary export was inhibited, using a mutant for the retrograde IFT motor *Dync2h1* (*Criswell et al., 1996; Huangfu D and Anderson KV, 2005; Porter et al., 1999; Signor et al., 1999*).

In the absence of retrograde transport out of cilia, no accumulation of vesicles is observed in *Dync2h1*$^{-/-}$ cilia. Too few vesicles, either coated or uncoated, around *Dync2h1*$^{-/-}$ cilia were observed by scanning through around 100 cells, in both 70nm and 300nm sections in TEM, prohibiting quantification. Since *Dync2h1*$^{-/-}$ mutant cilia are sack-like structures overloaded with ciliary material (See **Chapter 3**, **Figure 3.5, and Figure 3.8-3.11**) from defects in ciliary export, one could explain an accumulation of small vesicles around cilia as a means to get rid of excess ciliary material, but this is not observed in *Dync2h1*$^{-/-}$ mutants (**Figure 4.9** and **4.10)**. This suggests that 'coated' vesicles around the base of wild type cilia are responsible for the import of cargo from the cytoplasm into cilia, and the non-coated vesicles accumulated in *Wdr35*$^{-/-}$ marks a failure in this process.

Another difference between the IFT protein and dynein motor mutants was that although both mutants accumulated IFT-B by immunofluorescence (see **Chapter 3** - **Figure 3.8-3.11**), only *Dync2h1*$^{-/-}$ cilia displayed a striped pattern with a regular periodicity of 40nm on ultrastructural TEM analysis (**Figure 4.10**). These striped patterns were consistently present in all of *Dync2h1*$^{-/-}$ cilia, irrespective of cilia length (**Figure 4.10**). Periodicity of IFT-A and IFT-B particles has been reported in *Chlamydomonas* flagella as 11nm and 6nm, respectively (*Jordan et al., 2018*). The existence of standing trains, having a particle periodicity of 40 nm, was identified by TIRF confocal and TEM imaging (*Stepanek and Pigino, 2016*). These are caused by

'traffic jams' in the absence of retrograde transport, which could explain this striped pattern observed in *Dync2h1*$^{-/-}$ cilia where 'standing trains' are piling on top of each other. Similar stalled trains with the same periodicity of 40nm have been reported in the absence of another dynein motor protein *fla14* in *Chlamydomonas*. In the absence of the dynein light chain gene product *fla14,* retrograde IFT trains were also absent, so this striped pattern was claimed to be made of anterograde IFT train only with a periodicity of 40nm (*Pigino et al., 2009*). However, given (**Chapter 3)** both IFT-As **(Figure 3.16 to 3.22)** and IFT-Bs **(Figure 3.8 to 3.11)** were seen filling up the sack-like cilia in *Dync2h1*$^{-/-}$ by immunofluorescence, it is likely the stripes are composed of both IFT-A or IFT-B particles. The composition of these stripes in *Dync2h1*$^{-/-}$ mutants could be explored using correlative light-electron microscopy (CLEM).

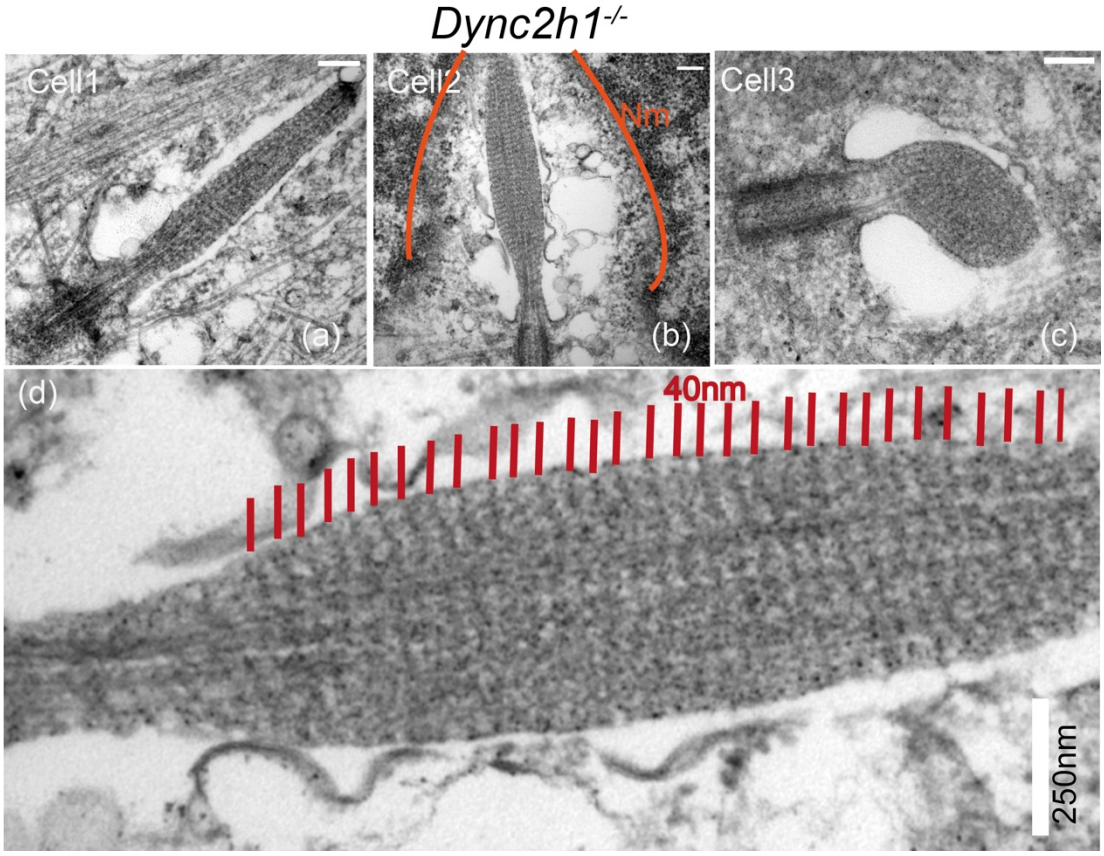

Figure 4.10. Standing IFT trains are stacked in *Dync2h1*$^{-/-}$ mutant cilia with a periodicity of 40nm. After 24hr serum starvation, *Dync2h1*$^{-/-}$ MEFs were chemically fixed and processed for TEM. 70nm sections shown for 3 different cells (a-c) and (d) zoomed in image of b is shown. Unlike *Wdr35*$^{-/-}$ cilia, dynein mutant axonemes were apparent throughout the length of cilia. Unlike WT cilia, *Dync2h1*$^{-/-}$ mutants displayed

a stripe pattern with a periodicity of 40nm (shown by red lines), which may be standing IFT trains stacked on top of each other. Scale bars= 250nm.

4.2 Discussion

4.2.1 Electron-dense coat on vesicles around cilia is most probably made of WDR35/IFT-A proteins and not clathrin or BBSomes

Based on the close sequence and structural similarity of IFTs to COPI cage forming proteins, the absence of electron-dense cloud on periciliary vesicles and the absence of localized membrane proteins in *Wdr35*$^{-/-}$ cilia, I propose a coatomer function for WDR35/IFT-A that is critical for transport of ciliary membrane and membrane cargo into cilia. Two other protein complexes have been proposed before to form vesicular coats implicated in cilia biology, including clathrin (*Kaplan et al., 2010; Molla-Herman A et al., 2010*) and the BBSome complex (*Jin H et al., 2010*). I examined evidence supporting a proposed role for clathrin and BBSomes in forming vesicular coats on periciliary vesicles.

The importance of the ciliary pocket was best described in an elegant study from the Bastin and Benmerah labs (*Molla-Herman A et al., 2010*) describing electron-dense invaginations from ciliary pocket into the cytoplasm. This study functionally investigated nature of these invaginations, similar to what I have described in MEFs (**Figure 4.3**), which they observed on both sensory/primary cilia *in-vitro* in RPE-1, IMCD-3 and MEFs, as well as sensory cilia of cumulus cells and motile cilia of ependymal cells and developing spermatid flagella (*Molla-Herman A et al., 2010*). By diffraction-limited immunofluorescence, they characterized staining for clathrin and standard markers for clathrin-coated pits (CCPs), like adaptor complex AP-2, Epsin, Eps15 and CALM, around cilia and ciliary pocket. These CCPs were found to be active sites for endocytosis since they could internalize transferrin, which is a widely used marker for clathrin-mediated endocytosis (CME). However, none of the cilia specific cargos so far are shown to be internalized by employing this mechanism. The association of actin cables close to CCPs around cilia indicates the similar mechanism of endocytosis as the plasma membrane. However, in spite of the enrichment of CCPs at the ciliary pocket in comparison to the plasma membrane, knock-down of either clathrin or AP-2 in RPE-1 cells (*Molla-Herman A et al., 2010*), and *C. elegans* (*Kaplan*

et al., 2010) did not result in a reduction of cilia. Moreover, treatment with Dynasore a small molecule inhibiting dynamin and therefore clathrin-coated vesicle (CCV) formation also did not reveal striking modification of the ciliary pocket or cilia formation (*Molla-Herman A et al., 2010*). Together, this suggests that CME is not essential for ciliogenesis, and that these CCPs might be responsible for removing excess cargo from cilia. Indeed, live-cell imaging followed these clathrin-positive vesicles as arising from cilia and disappear in the cytoplasm, consistent with a role in removing excess cargo from cilia. The electron-dense vesicles observed in our control TEM images (**Figure 4.3**) may look similar to those reported in Molla-Herman (*Molla-Herman A et al., 2010*), we suggest they are a functionally different population.

While knock-down of clathrin and clathrin-associated proteins result in a normal number and size of cilia as control RPE1 cells (*Molla-Herman A et al., 2010*), the size of cilia is drastically reduced in *Wdr35*$^{-/-}$ MEFs [(*Caparrós-Martín JA et al., 2015; Fu W et al., 2016; Mill et al., 2011*) and **Chapter 3**] with a massive enrichment of uncoated vesicles around mutant cilia (**Figure 4.10-4.9**). This leads me to propose that the electron density observed on vesicles around cilia in wild type MEFs is made of WDR35/ IFT-As and not clathrin, and that this 'coatomer' is functionally required for transportation of cargo from the cytoplasm into cilia. In the absence of WDR35, none of the cilia specific membrane protein cargos (**Chapter 3**) get transported to cilia and the cilia are also very short, as if too little membrane 'building blocks' were available for axoneme extension. Moreover, I found no difference in mean Clathrin intensity in a volume of 2µm around cilia base *Wdr35*$^{-/-}$ cilia compared to control MEFs (**Figure 3.25**) further confirming coats on vesicles around WT cilia are not clathrin.

Alternately, WDR35 and other IFTAs (IFT122, IFT140, and IFT144) and two IFTB (IFT172 and IFT80), which have the same domain organization, could function as coatomer cage proteins. They all have an interacting motif WD40 domain, which being amphipathic can also insert in lipid bilayer resulting in membrane curvature. Based on the structural similarities and the absence of an identifiable 'coat' on the numerous periciliary vesicles in *Wdr35*$^{-/-}$ mutants, I propose that WDR35 coated vesicles could ferry cargo to cilia. It would likely be working together with other IFT-As and/or the two IFT-B proteins IFT80 and IFT172 to import membrane cargo into cilia, whereas clathrin might be necessary for exporting cargo from cilia via endocytosing them to

cytoplasm. A definitive test to determine whether an IFT coat does exist would be either a CLEM or immunogold experiment, showing IFT-A localization on vesicles. A preliminary attempt at these experiments was done with Dr. Gaia Pigino, MPI CDG, using WDR35-GFP in *Wdr35*$^{-/-}$, such that the entire pool of WDR35 in a cell is GFP-labeled and there is increased signal-to-noise-ratio.

Another proposed ciliary coat complex is the BBSome. The BBSome complex was first discovered by a pull-down of BBS4 as bait in RPE1 cells, where it formed a stable heptameric complex with BBS1, 2, 5, 7, 8 and 9 (*Nachury MV et al., 2007*). Initial studies had suggested that the role for the BBSome was in import of some cargo (*Berbari et al., 2008; Jin H et al., 2010; Loktev et al., 2008*), but it was later more firmly established to be critical for export of a greater number of proteins from cilia (*Domire et al., 2011; Eguether et al., 2014; Lechtreck et al., 2013, 2009; Liew et al., 2014; Nager et al., 2017; Xu et al., 2015; Ye F et al., 2018*), (see **Section 1.3.2**). The BBSome complex was also proposed to evolve from coatomer proteins (*Jékely G and Arendt D, 2006; Dam TJPV et al., 2013*). It was shown to assemble on liposomes in-vitro in an ARL6-GTP dependent manner, similar to coatomer adaptor assembly by the ARF1 and SAR1 GTPases. Several membrane proteins, like SSTR3, mislocalized accumulating in cilia in BBS depleted cells (*Jin H et al., 2010*). Protein-protein interaction motif perceived in BBSome proteins are different from the classic coatomers. For example, while only few structural elements similar to coatomer proteins in BBSomes are ß propeller repeats are found in BBS1, BBS2, BBS7 and BBS9, and only TPR repeats are found in BBS4, and BBS8. Comparatively the three core IFT-A proteins IFT144, IFT140, and IFT122 and the linker between periphery and core proteins IFT121/WDR35, were found to have closer structural homology to COPI cage proteins having N- terminal WD40 ß-propeller domain and C-terminal TPR region (**Figure 4.2**). My attempts at homology modeling of BBS proteins using SWISS MODEL did not find clathrin or COP complex proteins as putative sequence matches (except for BBS7 which found sequence match with COPß' with a sequence identity of 12.8%). The complete list of sequence match hits for BBSome complex is shown in **Appendix-V**. The differences in the function of IFTs and BBSomes in vesicular transport can be summarized as follows:

1. I found components of the IFT-A (140, 144, 122 and 121) and IFT-B (80 and 172) to be closer sequence and structural relatives of the COPI proteins.
2. The BBSome and ARL6 are not critical for global cilia assembly, whereas IFT-As described in this section are. This implies IFT-As as a stronger candidates for cargo import to cilia. Indeed a growing body of evidence supports a stronger role for the BBSome has in export of most ciliary proteins.
3. The donor compartment for BBSome mediated vesicular transport of membrane proteins to cilia remains unclear. BBSomes have never been shown to localize to any endomembrane or plasma membrane. In contrast, IFT20 has been demonstrated to localize to Golgi stacks (*Follit et al., 2008; Noda et al., 2016*).
4. In our TEM tomograms, we observe a track of electron-dense coated vesicles between Golgi and cilia in controls (**Figure 4.5a & b**), which was absent in *Wdr35*$^{-/-}$. This suggests WDR35 may be involved in Golgi-to-cilia trafficking of cargo.
5. BBSomes cluster on in-vitro assembled liposomes in TEM images but these clusters were unable to deform the liposome membrane (*Jin H et al., 2010*). On the other hand, it was recently reported that IFT172, which is one of the structural homologs of COPI α and ß' like WDR35, not only assemble on in-vitro liposomes but can also bud 50nm vesicles from them at a concentration as low as 50nM (*Wang et al., 2018*).

Keeping in mind the BBSome functions with the ARF-like GTPase ARL6 for transportation of some membrane proteins in cilia and also physically interacts with phospholipids, it might be working as an adaptor for IFT-A mediated cage formation similar to clathrin (AP1/AP2) or COP coat adaptors. While I was writing this section, a study reported BBSome complex crystal structure and showed it to adopt an auto-inhibited closed conformation in solution. On binding to ARL6-GTP on membranes, it can switch to an open conformation in a mechanism similar to COPI, AP1, and AP2 adaptors. Thus I propose that while BBSomes are suitable adaptors for export of membrane cargo (*Chou et al., 2019; Ye F et al., 2018*) (see **Section 1.3.2**), IFT-As might form vesicular coat for import of cargo to cilia. I am further completing CLEM to finally further confirm this proposed vesicular coat forming function of WDR35.

4.2.2 Model for WDR35's role in the ciliary vesicular transport pathway

Several other genes have been shown to accumulate vesicles around cilia at various stages of ciliogenesis when deleted or depleted. For example, depletion of Eps15 homology domain (Eps15HD) containing proteins EHD1 and EHD3 in RPE-1 cells inhibits ciliogenesis, and smaller distal appendage vesicles (DAV) accumulate in the periciliary space. As the Eps15HD domain is critical for membrane curvature, EHD1 and EHD3 depletion impairs membrane curvature and inhibits fusion of DAVs needed to form the preciliary vesicle (PCV) (*Q. Lu et al., 2015*). During the first morphological event of ciliogenesis (**Figure 1.8** and **Figure 4.11**), the interaction of the membrane PCV, formed by the fusion of DAVs, docks onto the distal end of the mother centriole. In the case of deletion or depletion of distal appendage proteins CCDC41, CEP164 and RAB8, this initial step of ciliogenesis is inhibited at PCV docking point. In RPE-1 cells, electron micrographs of RAB8 (*Q. Lu et al., 2015*) or CCDC41 (*Joo et al., 2013*) depletion show ciliogenesis to be arrested at the PCV docking stage. In the case of depletion of HOOK-2 (*Baron Gaillard et al., 2011*) or CEP164 (*Schmidt et al., 2012*), numerous small vesicles are accumulating around centrioles before PCV formation. In the case of RAB34, the small GTPase is required for the successive fusion of small preciliary vesicles to form the PCV and subsequent migration of the mother centriole from the perinuclear area to the plasma membrane (*Xu et al., 2018*). In the case of ciliogenesis in *Wdr35*$^{-/-}$ MEFs, I have shown that ciliogenesis proceeds past all these early stages of DAV fusion to form the PCV and subsequent PCV docking. Cilia of nearly 0.5µm length is seen in *Wdr35*$^{-/-}$ in comparison to 2-4µm MEF cilia in controls indicating that WDR35 plays a significant role in the subsequent elongation of cilia following the initial vesicle docking steps (**Figure 4.11**). BBSomes in the cytoplasm have intrinsic nature to aggregate and are shielded from degradation by the centriolar satellite protein PCM-1, whilst being transported from cytoplasm to basal body. They are released by PCM1 at the basal body in order to be transported inside cilia (*Nachury MV et al., 2007*). Along with BBSomes, PCM-1 is important for transport of many other pericentriolar proteins and is used as marker of centriolar satellite and pericentriolar material stability (*Dammermann and Merdes, 2002; Gupta et al., 2015; Hori and Toda, 2017; Odabasi et al., 2019; Wang et al., 2016*). Although defects in PCM1 organization had been previously reported in *WDR35* mutant RPE-1

cells (*Fu W et al., 2016*) , we did not see any difference in localization of PCM-1 at the base of cilia in between wild type and *Wdr35*$^{-/-}$ (see **Chapter 3- Figure 3.24**). PCM-1 being the landmark for structural stability of pericentriolar material around cilia, not being disturbed in *Wdr35*$^{-/-}$ strengthens our proposal of WDR35 important for cilia elongation at later stages of ciliogenesis and not initial pericentriolar material assembly (**Figure 3.24**).

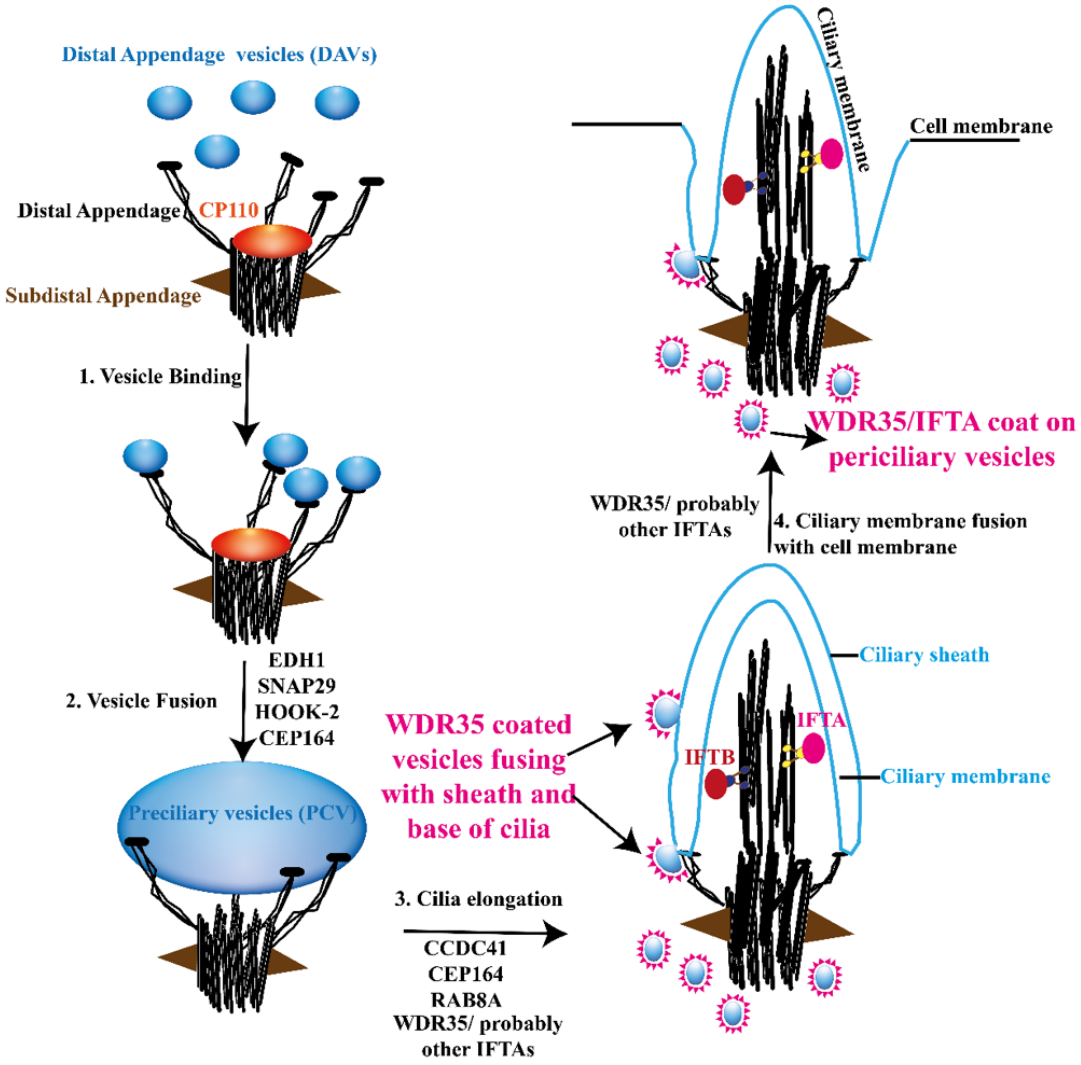

Figure 4.11. WDR35 functions to transport cargo at the later stage of cilia elongation. Four steps of ciliation- STEP 1: Vesicle binding: Smaller distal appendage vesicles (DAVs) dock on the distal appendage of mother centriole. The older centriole (called the mother centriole) is recognized and distinguished from the daughter centriole by vesicles because of the presence of distal appendages and subdistal appendages/basal foot. **STEP 2: Vesicle fusion:** DAVs fuse to form one preciliary vesicle (PCV) with the help of EHD1 and SNAP29 proteins. EHD1 tubulates and SNAP29 fuses the vesicles. Two other distal appendage proteins HOOK-2 and CEP164 help in vesicle fusion. CP110 which blocks microtubule elongation of the axoneme is removed/degraded at this stage. **STEP 3: cilia elongation:** Periciliary vesicles then fuse with more secondary vesicles resulting in cilia elongation. WDR35 coated vesicles (magenta coats shown on blue vesicles) with cargo derived from Golgi fuse with cilia to help in further elongation. Other proteins which help in cilia elongation are CCDC41, CEP164, and RAB8A. **STEP 4: Ciliary membrane fusion with cell membrane:** Ciliary pocket being deep in MEF cilia keeps growing inside ciliary sheath till it emerges out of the cell, and ciliary sheath now fuses with the cell membrane.

Chapter 5. Conclusions and Future Work

From my thesis work, I propose that WDR35 functions as a novel coatomer complex to transport membrane proteins into cilia. In **Chapter 3**, I demonstrate that many membrane proteins fail to get transported into cilia in the absence of WDR35. Moreover, without WDR35, the IFT-A complex is unstable, completely lacking the peripheral components, and any core components gets trapped at the transition zone, whilst anterograde IFT continues and IFT-B accumulate in the runted mutant axonemes. The work described in **Chapter 4** goes on to strongly suggest that IFT-A may be functioning as a novel cilia bound coatomer complex necessary for the transfer of Golgi-originated vesicles to the developing ciliary pocket. My EM tomograms clearly show electron-dense vesicles fusing with ciliary pocket and sheath as well accumulating at cilia base in controls. On the contrary, *Wdr35*$^{-/-}$ mutant cells have 10 times more vesicles which lack any electron density clustered around the cilia, whose axoneme fails to extend. In wild type cells, vesicles follow a near linear track between the Golgi and cilia base, whereas in *Wdr35*$^{-/-}$ mutants they appear to be randomly accumulating around the ciliary base (**Figure 5.1**). This accumulation of coatless vesicles which fail to fuse is not observed in *Dync2h1* mutants, which suggests this process is not a result of defective retrograde transport, nor from decreased endocytosis which may be a knock-on effect if ciliary trafficking is impaired. This novel discovery marks the beginning of a new field of study in cilia biology, opening many new questions as well. More work is needed to understand the role of other IFT-A components in this vesicular transport, particularly where and when the IFT-A coatomer is assembling, as well as the identity of the requisite GTPases as well as GTPase- regulators (GDIs/GEFs/GAPs) involved in this dynamic process.

5.1 Explore the role of WDR35 in GPSM-1 and ARL13B interaction

In **Chapter 3**, I deeply characterized the cellular and biochemical defects of *Wdr35* mutant cilia to show defects in the later steps of ciliogenesis, namely axoneme extension and cargo trafficking. Specifically, I found absence of membrane protein localisation to cilia, retrograde transport defect for IFT-B complex proteins and IFT-A core components to be stuck at transition zone. Intriguingly, when exogenously

expressed ARL13B was found to be enriched on membranes particularly cell membrane in *Wdr35* mutant. In an attempt to answer this, I undertook an IP/MS approach to compare interactors between control ARL13B (cilial) and mutant ARL13B (diffuse in plasma membrane), where I isolated one significant hit the G-protein signaling modulator 1 (GPSM1), which is lost in *Wdr35* mutants (see **Section 3.1.8)**. GPSM1 (also known as activator of G-protein signaling 3 (AGS3)) has diverse functional requirements for GPCR signalling in the cell and moves between different subcellular compartments in a regulated manner. It consists of a tetratricopeptide repeat (TPR) domain and a G-protein regulatory (GPR) domain, also termed a GoLoco motif of 19-amino-acids with guanine nucleotide dissociation inhibitor activity (*Bernard et al., 2001*). Interestingly, a mouse model reveals that loss of GPSM1 in a mouse model of autosomal dominant polycystic kidney disease (ADPKD) *Pkd1*$^{v/v}$ accelerates dynamics of cyst progression and decline in renal function (*Kwon et al., 2012*). Links to cilia are otherwise unknown.

Given I see ARL13B enriched on the cell membrane in *Wdr35*$^{-/-}$ MEFs (**Figure 3.6A; Movie 3.1**), I hypothesized that this ARL13B mislocalization might be due to a lack of interaction with GPSM-1, as determined by my mass spec data (see **Section 3.1.8, Figure 3.26)**. Without interaction with its GDI, ARL13B could remain in a GTP-bound form locked in the plasma membrane, unable to relocalize into the axonemal compartment in *Wdr35* mutant cilia. As ARL13B-GTP is thought to function as a GEF for ARL3 to facilitate release of ciliary cargo within cilia (*Gotthardt et al., 2015*), but passing through a GDP-bound intermediate may be necessary allow translocation to interact with the ciliary membrane compartment. Whilst overexpressed GDP-locked ARL13B can localize to cilia, it failed to elongate cilia in contrast to wild type ARL13B over-expression (*H. Lu et al., 2015; Nakayama, 2016*). It would be interesting to see if GDP locked version of ARL13B (which is proposed to be more cytoplasmic) also fails to interact with GPSM-1 in *Wdr35*$^{-/-}$. There are crucial questions remaining to be answered by this method are: (1) Is WDR35 important only for GPSM-1 and ARL13B interaction by regulating the GTP- or GDP-bound states of ARL13B? (2) Is the lack of ARL13B-GPSM-1 interaction in *Wdr35*$^{-/-}$ mutants responsible for the failure of ARL13B transport to cilia? Alternatively, (3) is this merely a reflection of a lack of proper trafficking of cargos into cilia?

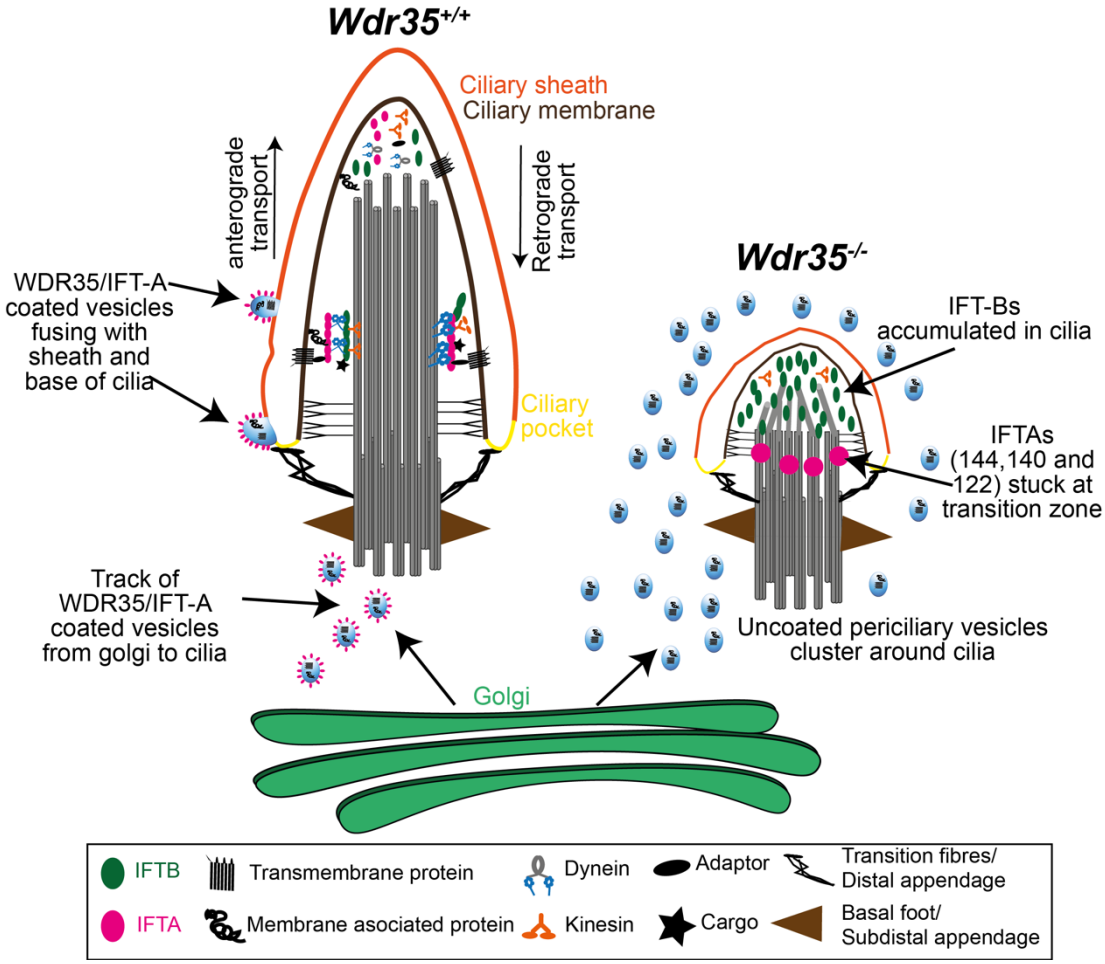

Figure 5.1. WDR35 packages microdomains of cargo-carrying vesicles destined for transport from the Golgi into cilia. Diagramatic representation of the TEM data showing electron-dense (magenta) vesicles fusing and localizing around cilia in wild type cells and uncoated vesicles (blue) clustering around cilia in *Wdr35*$^{-/-}$ MEFs. Vesicles follow a track between the Golgi and cilia base in wild type cells but are clustered randomly around cilia in *Wdr35*$^{-/-}$ cells, with the Golgi being close to cilia in both cases. IFT-Bs accumulated in short mutant cilia, whilst core IFT-As core components stuck at the transition zone and no membrane proteins accumulate inside *Wdr35*$^{-/-}$ cilia, suggesting an arrest at the late stages of ciliogenesis during axoneme accumulation.

5.2 Does WDR35 function like an adaptor for fusion or a coatomer complex for fission?

All three classic coatomer protein complexes (COPII, COPI, and clathrin) pinch off vesicles from donor membranes (ER, Golgi, and cell membrane, respectively) (**Section 1.3.1**). These vesicles then diffuse in the cytoplasm or move via motor

proteins to their target organelle membranes where SNARE proteins and Rab GTPases assist their fusion. Given that WDR35 shares significant and striking structural similarity to COPI proteins, which helps in the fission of vesicles, versus SNARES, which help in the fusion of vesicles to a target membrane, which action could WDR35 be promoting? In our TEM data, we see ten times more vesicles around the shortened cilia base of *Wdr35*$^{-/-}$ MEFs, which are all lacking an electron-dense coat. This suggests that vesicles are formed but are failing to fuse with either the ciliary pocket membrane or base in the absence of WDR35. Could WDR35, which shares structure homology to fission inducing proteins, function like a fusion facilitating protein? Although *Wdr35*$^{-/-}$ MEFs are missing one COPIα/β'-like member homolog, the other three structurally similar members WDR19, IFT140, and IFT122 may have compensated for loss of WDR35 by providing interaction motifs necessary for fission of vesicles from the source organelle the Golgi, which resulted in an accumulation of numerous vesicles around mutant cilia. Since the IFT-A complex is unstable in the absence of WDR35 (**Figure 3.14-3.15**), any core IFT-A coat assembled on periciliary vesicles might be unstable. Indeed, the peripheral IFT-A proteins IFT139 and IFT43 are degraded in the absence of WDR35 (**Figure 3.15**). In the absence of IFT139 and IFT43, which are helical proteins similar to SNARE proteins, that mediate vesicle fusion with target membranes, periciliary vesicles may fail to fuse with the ciliary pocket or base, and as such fail to transfer cargos and membrane to the growing cilia sheath. It would be interesting to investigate the difference in periciliary vesicles in the absence of other components of the IFT-A complex individually to answer this question, as well as identify the Rab-GTPase that might be acting in this process to organize the fusion site. The recently identified RAB34, which localize to Golgi and cilia, and whose knock-out disrupts ciliogenesis and Hh signaling is a good candidate (*Pusapati et al., 2018*).

5.3 Identifying the missing regulatory GTPase involved in IFT-A mediated coatomer assembly for Golgi to cilia transport

If IFT-A is functioning as a coatomer, as the complex lacks any regulatory enzymatic regulatory in any of its six subunits, we have still to identify the missing candidate small GTPase for catalyzing vesicle formation this model proposes. An important

regulator of vesicular transport in cilia are RAB and ARF family of small GTPases, where these act as regulatable switches that recruit effector molecules, in their GTP-bound form. They are part of the RAS superfamily of small GTPases mainly regulating intracellular membrane trafficking in the cell (*Donaldson JG et al., 2012; Pfeffer, 2017; Stenmark, 2009; Zhen and Stenmark, 2015*). Found on the cytosolic face of diverse intracellular membranes, these small GTPases cycle between -GTP and -GDP bound forms to regulate a wide range of trafficking process (see **Section 3.1.8**). Out of 66 known Rab GTPase, 10 (RAB-5, -8, -10, -11, -17, -23, -28, -29, -34 and -35) have been shown so far to be implicated in ciliogenesis (*Blacque et al., 2018; Hsiao et al., 2012; Pusapati et al., 2018; Xu et al., 2018; Yoshimura et al., 2007*). From the family of 29 members of mammalian ARF/ARL GTPases (6 ARFs, SAR1 and over 20 ARF-like proteins (ARLs)), four are known to localize to cilia (ARF4, ARL3, ARL6, and ARL13B) (*Li et al., 2012*). Mutations in several of them, most notably *ARL13B, ARL3, ARL6, RAB23*, and *RAB28,* result in defects in ciliary trafficking leading to ciliopathy disorders (*Alkanderi et al., 2018; Cantagrel et al., 2008; Fan et al., 2004; Roosing et al., 2013*).

Some RABs and ARFs are also known to regulate ciliary membrane protein localization. The best studied is the ARF4-Rab11-Rab8 pathway which helps rhodopsin transport to the outer segment of photoreceptor cilia from the trans Golgi network (*Knödler et al., 2010; Wang and Deretic, 2014*). Although the exact mechanisms is less clear, RAB35 has been recently reported to be an essential regulator of ARL13B, SMOOTHENED, and INPP5E trafficking into cilia (*Kuhns et al., 2019*). Moreover, it was also shown to be directly interacting with ARL13B (*Kuhns et al., 2019*). Functional studies suggest RAB35 may play much broader roles in the cell in terms of regulating actin protrusions in neurite outgrowth, as well as T-cell receptor recycling and cytokinesis (*Chua et al., 2010*). In contrast, RAB23 was initially identified in a mouse forward genetics screen as a critical regulator of Hh signalling (*Eggenschwiler et al., 2006; May et al., 2005*), where it has been shown to be essential for trafficking KIF17 (*Lim and Tang, 2015*) as well as dopamine receptors into ciliary membranes (*Leaf and Zastrow, 2015*). Similarly, ARF like GTPase ARL6/BBS-3 has been proposed to assemble BBSome coat on liposomes in-vitro (*Jin H et al., 2010*) (see **Section 1.3.2**) which might be necessary for SSTR-3 localization into cilia.

RABs and ARFs have been also described to regulate the early stages of ciliogenesis. The best described in cells is the Rab11-Rabin8-Rab8 pathway which regulates the initial stages of ciliary vesicle docking in ciliogenesis (*Vetter et al., 2015*). However, human and mouse mutations in some of these 'critical' regulators like RAB-8, -10, and -11 have not been reported to have cilia defects or ciliopathy phenotypes, suggesting compensation or functional redundancy exists *in vivo*. Another interesting candidate is RAB34, which has recently been shown independently by several groups to be required for early vesicle trafficking, and importantly fusion during ciliogenesis, as well Hh signaling in cells and *in vivo* (*Pusapati et al., 2018; Xu et al., 2018*). Intriguingly this GTPase is generally associated with the recycling endosome compartment which surrounds the base of the cilia in most cells, however it transiently localizes to cilia too (*Xu et al., 2018*). Of interest, the small GTPase RSG1 was found to also be required for the final steps in ciliogenesis initiation; mouse mutants die at E12.5 with reduced Hh signaling (*Agbu et al., 2018; Brooks and Wallingford, 2013*). Intriguingly, *Rsg1* mutant cells have fewer cilia, but those that form are of normal length and protein content. Those that fail to form have mother centrioles that properly recruit proteins required for cilia initiation and dock normally onto ciliary vesicles, but subsequently the axoneme fails to elongate, like was observed in *Wdr35* mutants. Indeed, RSG1 is recruited to the mother centriole in a manner that is dependent on the cytoplasmic C-PLANE chaperones, necessary for the IFT-A complex formation (*Agbu et al., 2018; Brooks and Wallingford, 2013*).

COPI and COPII vesicle formation are regulated by the small GTPases SAR-1 and ARF-1, respectively (see **Section 1.3.1**): does a similar regulatory GTPase exist for the IFT-A to function as a coatomer? Indeed three RAB-like GTPases (RABL) have been identified as part of the IFT-B complex (IFT27/RABL4), IFT22/RABL5) or as functionally required for assembly of cilia (RABL2) (*Kanie et al., 2017; Nishijima et al., 2017*). However, I have failed to pull out any RABs or ARFs in my endogenous IP/mass spec analysis of ARL13B (except for one GDI precipitated with ARL13B- see **Section 3.1.8**). Even with the robust IP/mass of IFT-Bs and IFT-As where I managed to isolate two of the GTPase in IFT-B complex no IFT-A associated GTPase were isolated. Isolation of transient interactors like RAB and ARF factors may require alternate techniques like proximity labeling proteomics based approaches via APEX2

or turboID with short kinetics to interrogate even the most transient interactors. Alternately locking some of these candidates like RAB34 in their GTP-bound state through site-directed mutagenesis may also support isolation of IFT-A bound complexes. For example, in an in vitro purified reconstitution experiment, can GTP-locked RAB34 alone recruit IFT-A components to artificial membranes like giant unilamellar vesicles more robustly. Does if form switches in the structures resembling the electron dense coats we observed at the ciliary based? Does it cause fusion or fission events? It will be important to systematically explore if any GTPases, as well as any associated regulators like GDI/GEFs/GAPs are essential to regulate IFT-A complex-mediated vesicular coat formation and thereby membrane protein trafficking to cilia.

5.4 Concluding remarks

In my phenotypic characterization of the cellular and biochemical defects in primary cells from *Wdr35*$^{-/-}$ mutants, I observed defects in the size of the acetylated axoneme as well as failure of localization of diverse ciliary membrane proteins. This suggest a failure at the later stages of ciliogenesis, perhaps from limiting amounts of membrane cargo necessary for axoneme extension as a result of defects in vesicle fusion. It is interesting, as whilst the IFT-B complex composition is unaltered and accumulates as predicted for a retrograde mutant, no endogenous core IFT-A members are detected in the mutant axoneme, rather core components are trapped at the transition zone and the peripheral components IFT139 and IFT43 are degraded in the absence of WDR35. Importantly, no electron-dense coat is observed on vesicles that accumulate in the periciliary membrane trafficking region of mutant cells. Given that IFT-As show a deep structural and sequence homology to COPI complex proteins, which mediate retrograde vesicular trafficking from the Golgi to the ER, it is tempting to posit that IFT-As may be playing a similar coatomer function in trafficking from Golgi-derived vesicles into cilia. Indeed, TEM tomograms of control ciliated MEFs showed the track of vesicles with some electron density between the Golgi and cilia, suggestive of this vesicular Golgi-to-cilia transport. Frequent fusion events with these control coated vesicles were observed with the ciliary pocket, but these events were entirely lacking in tomograms from *Wdr35*$^{-/-}$ cilia. In parallel, there was a 10x increase in vesicle number as compared to controls cells. Together, the lines of study suggested above

could test my hypothesis that WDR35 with other IFT-As function like novel coatomer complex to selectively transport cargo from the Golgi into cilia, necessary for protein localization but also late ciliogenesis/axoneme elongation. Understanding this IFT-A complex mediated trafficking mechanism to cilia is key to understanding their complex biology.

Bibliography

Abdelhamed ZA, Wheway G, Szymanska K, Natarajan S, Toomes C, Inglehearn C, Johnson CA. 2013. Variable expressivity of ciliopathy neurological phenotypes that encompass Meckel - Gruber syndrome and Joubert syndrome is caused by complex de-regulated ciliogenesis, Shh and wnt signalling defects. *Human Molecular Genetics* **22**:1358–1372. DOI: http://doi.org/10.1093/hmg/dds546, PMID: 23283079

Adams M, Simms RJ, Abdelhamed Z, Dawe HR, Szymanska K, Logan CV, Wheway G, Pitt E, Gull K, Knowles MA, Blair E, Cross SH, Sayer JA, Johnson CA. 2012. A meckelin-filamin A interaction mediates ciliogenesis. *Human Molecular Genetics* **21**:1272–1286. DOI: http://doi.org/10.1093/hmg/ddr557, PMID: 22121117

Adhiambo C, Blisnick T, Toutirais G, Delannoy E, Bastin P. 2009. A novel function for the atypical small G protein Rab-like 5 in the assembly of the trypanosome flagellum. *Journal of Cell Science* **122**:834–41. DOI: https://doi.org/10.1242/jcs.040444, PMID: 19240117

Agbu SO, Liang Y, Liu A, Anderson KV. 2018. The small GTPase RSG1 controls a final step in primary cilia initiation. *The Journal of Cell Biology* **217**:413–427. DOI: http://doi.org/10.1083/jcb.201604048, PMID: 29038301

Ahmed NT, Gao C, Lucker BF, Cole DG, Mitchell DR. 2008. ODA16 aids axonemal outer row dynein assembly through an interaction with the intraflagellar transport machinery. *The Journal of Cell Biology* **183**:313–322. DOI: http://doi.org/10.1083/jcb.200802025, PMID: 18852297

Alkanderi S, Molinari E, Shaheen R, Elmaghloob Y, Stephen LA, Sammut V, Ramsbottom SA, Srivastava S, Cairns G, Edwards N, Rice SJ, Ewida N, Alhashem A, White K, Miles CG, Steel DH, Alkuraya FS, Ismail S, Sayer JA. 2018. ARL3 Mutations Cause Joubert Syndrome by Disrupting Ciliary Protein Composition. *American Journal of Human Genetics* **103**:612–620. DOI: http://doi.org/10.1016/j.ajhg.2018.08.015, PMID: 30269812

An N, Blumer JB, Bernard ML, Lanier SM. 2008. The PDZ and band 4.1 containing protein Frmpd1 regulates the subcellular location of activator of G-protein

signaling 3 and its interaction with G-proteins. *Journal of Biological Chemistry* **283**:24718–24728. DOI: http://doi.org/10.1074/jbc.M803497200, PMID: 18566450

Andersson ER, Sandberg R, Lendahl U. 2011. Notch signaling: Simplicity in design, versatility in function. *Development* **138**:3593–3612. DOI: http://doi.org/10.1242/dev.063610, PMID: 21828089

Appenzeller-Herzog C, Hauri HP. 2006. The ER-Golgi intermediate compartment (ERGIC): in search of its identity and function. *Journal of Cell Science* **119**:2173–2183. DOI: http://doi.org/10.1242/jcs.03019, PMID: 16723730

Arts HH, Doherty D, Beersum SEV, Parisi MA, Letteboer SJF, Gordon NT, Peters TA, Märker T, Voesenek K, Kartono A, Ozyurek H, Farin FM, Kroes HY, Wolfrum U, Brunner HG, Cremers FP, Glass IA, Knoers NV, Roepman R. 2007. Mutations in the gene encoding the basal body protein RPGRIP1L , a nephrocystin-4 interactor , cause Joubert syndrome. *Nature Genetics* **39**:882–888. DOI: http://doi.org/10.1038/ng2069, PMID: 17558407

Ashe A, Butterfield NC, Town L, Courtney AD, Cooper AN, Ferguson C, Barry R, Olsson F, Liem KF, Parton RG, Wainwright BJ, Anderson KV, Whitelaw E, Wicking C. 2012. Mutations in mouse Ift144 model the craniofacial, limb and rib defects in skeletal ciliopathies. *Human Molecular Genetics* **21**:1808–1823. DOI: http://doi.org/10.1093/hmg/ddr613, PMID: 22228095

Attree O, Olivos IM, Okabe I, Bailey LC, Nelson DL, Lewis RA, Mclnnes RR, Nussbaum RL. 1992. The Lowe's oculocerebrorenal syndrome gene encodes a protein highly homologous to inositol polyphosphate-5-phosphatase. *Nature* **358**:239–242. DOI: http://doi.org/10.1038/358239a0, PMID: 1321346

Baala L, Audollent S, Martinovic J, Ozilou C, Babron MC, Sivanandamoorthy S, Saunier S, Salomon R, Gonzales M, Rattenberry E, Esculpavit C, Toutain A, Moraine C, Parent P, Marcorelles P, Dauge MC, Roume J, Merrer ML, Meiner V, Meir K, Menez F, Beaufrère A, Francannet C, Tantau J, Sinico M, Dumez Y, MacDonald F, Munnich A, Lyonnet S, Gubler MC, Génin E, Johnson CA, Vekemans M, Encha-Razavi F, Attié-Bitach T. 2007. Pleiotropic effects of CEP290 (NPHP6) mutations extend to Meckel syndrome. *Americal Journal of Human Genetics* **81**:170–179. DOI: http://doi.org/10.1086/519494,

PMID: 17564974

Badano JL, Mitsuma N, Beales PL, Katsanis N. 2006. The Ciliopathies: An Emerging Class of Human Genetic Disorders. *Annual Review of Genomics and Human Genetics* **7**:125–148. DOI: http://doi.org/10.1146/annurev.genom.7.080505.115610, PMID: 16722803

Badgandi HB, Hwang S, Shimada IS, Loriot E, Mukhopadhyay S. 2017. Tubby family proteins are adapters for ciliary trafficking of integral membrane proteins. *The Journal of Cell Biology* **216**:743–760. DOI: http://doi.org/10.1083/jcb.201607095, PMID: 28154160

Badiner N, Taylor SP, Forlenza K, Lachman RS, Bamshad M, Nickerson D, Cohn DH, Krakow D. 2017. Mutations in DYNC2H1, the cytoplasmic dynein 2, heavy chain 1 motor protein gene, cause short-rib polydactyly type I, Saldino–Noonan type. *Clinical Genetics* **92**:158–165. DOI: http://doi.org/10.1111/cge.12947, PMID: 27925158

Bai CB, Auerbach W, Lee JS, Stephen D, Joyner AL. 2002. Gli2, but not Gli1, is required for initial Shh signaling and ectopic activation of the Shh pathway. *Development* **129**:4753–4761. PMID: 12361967

Baker K, Beales PL. 2009. Making sense of cilia in disease: The human ciliopathies. *American Journal of Medical Genetics* **151C**:281–295. DOI: http://doi.org/10.1002/ajmg.c.30231, PMID: 19876933

Balla T. 2013. Phosphoinositides: Tiny lipids with giant impact on cell regulation. *Physiological Reviews* **93**:1019–1137. DOI: http://doi.org/10.1152/physrev.00028.2012, PMID: 23899561

Banfield DK. 2011. Mechanisms of protein retention in the Golgi. *Cold Spring Harbor Perspectives in Biology* **3**:a005264. DOI: http://doi.org/10.1101/cshperspect.a005264, PMID: 21525512

Bangs F, Anderson KV. 2017. Primary Cilia and Mammalian Hedgehog Signaling. *Cold Spring Harbor Perspective in Biology* **9**:a028175. DOI: http://doi.org/10.1101/cshperspect.a028175, PMID: 27881449

Bärenz F, Mayilo D, Gruss OJ. 2011. Centriolar satellites: Busy orbits around the centrosome. *European Journal of Cell Biology* **90**:983–989. DOI: http://doi.org/10.1016/j.ejcb.2011.07.007, PMID: 21945726

Barker AR, Renzaglia KS, Fry K, Dawe HR. 2014. Bioinformatic analysis of ciliary transition zone proteins reveals insights into the evolution of ciliopathy networks. *BMC Genomics* **15**:531. DOI: http://doi.org/10.1186/1471-2164-15-531, PMID: 24969356

Barlowe C, Orci L, Yeung T, Hosobuchi M, Hamamoto S, Salama N, Rexach MF, Ravazzola M, Amherdt M, Schekman R. 1994. COPII: A membrane coat formed by Sec proteins that drive vesicle budding from the endoplasmic reticulum. *Cell* **77**:895–907. DOI: http://doi.org/10.1016/0092-8674(94)90138-4, PMID: 8004676

Beales PL, Bland E, Tobin JL, Bacchelli C, Tuysuz B, Hill J, Rix S, Pearson CG, Kai M, Hartley J, Johnson C, Irving M, Elcioglu N, Winey M, Tada M, Scambler PJ. 2007. IFT80, which encodes a conserved intraflagellar transport protein, is mutated in Jeune asphyxiating thoracic dystrophy. *Nature Genetics* **39**:727–729. DOI: http://doi.org/10.1038/ng2038, PMID: 17468754

Beales PL, Warner AM, Hitman GA, Thakker R, Flinter FA. 1997. Bardet-Biedl syndrome: a molecular and phenotypic study of 18 families. *Journal of Medical Genetics* **34**:92–98. DOI: http://doi.org/10.1136/jmg.34.2.92, PMID: 9039982

Beck R, Prinz S, Diestelkötter-Bachert P, Röhling S, Adolf F, Hoehner K, Welsch S, Ronchi P, Brügger B, Briggs JAG, Wieland F. 2011. Coatomer and dimeric ADP ribosylation factor 1 promote distinct steps in membrane scission. *The Journal of Cell Biology* **194**:765–777. DOI: http://doi.org/10.1083/jcb.201011027, PMID: 21893600

Berbari NF, Lewis JS, Bishop GA, Askwith CC, Mykytyn K. 2008. Bardet-Biedl syndrome proteins are required for the localization of G protein-coupled receptors to primary cilia. *Proceedings of the National Academy of Sciences* **105**:4242–4246. DOI: http://doi.org/10.1073/pnas.0711027105, PMID: 18334641

Bergmann C, Fliegauf M, Brüchle NO, Frank V, Olbrich H, Kirschner J, Schermer B, Schmedding I, Kispert A, Kränzlin B, Nürnberg G, Becker C, Grimm T, Girschick G, Lynch SA, Kelehan P, Senderek J, Neuhaus TJ, Stallmach T, Zentgraf H, Nürnberg P, Gretz N, Lo C, Lienkamp S, Schäfer T, Walz G, Benzing T, Zerres K, Omran H. 2008. Loss of Nephrocystin-3 Function Can Cause

Embryonic Lethality, Meckel-Gruber-like Syndrome, Situs Inversus, and Renal-Hepatic-Pancreatic Dysplasia. *American Journal of Human Genetics* **82**:959–970. DOI: http://doi.org/10.1016/j.ajhg.2008.02.017, PMID: 18371931

Bernard ML, Peterson YK, Chung P, Jourdan J, Lanier SM. 2001. Selective interaction of AGS3 with G-proteins and the influence of AGS3 on the activation state of G-proteins. *Journal of Biological Chemistry* **276**:1585–1593. DOI: https://doi.org/10.1074/jbc.M005291200, PMID: 11042168

Bhattacharya N, O'Donnell J, Stagg SM. 2012. The structure of the Sec13/31 COPII cage bound to Sec23. *Journal of Molecular Biology* **420**:324–334. DOI: https://doi.org/10.1016/j.jmb.2012.04.024, PMID: 22543240

Bhogaraju S, Cajanek L, Fort C, Blisnick T, Weber K, Taschner M, Mizuno N, Lamla S, Bastin P, Nigg EA, Lorentzen E. 2013. Molecular basis of tubulin transport within the cilium by IFT74 and IFT81. *Science* **341**:1009–1012. DOI: http://doi.org/ 10.1126/science.1240985, PMID: 23990561

Bhogaraju S, Taschner M, Morawetz M, Basquin C, Lorentzen E. 2011. Crystal structure of the intraflagellar transport complex 25/27. *The EMBO Journal* **30**:1907–1918. DOI: http://doi.org/10.1038/emboj.2011.110, PMID: 21505417

Bi X, Mancias JD, Goldberg J. 2007. Insights into COPII Coat Nucleation from the Structure of Sec23•Sar1 Complexed with the Active Fragment of Sec31. *Developmental Cell* **13**:635–645. DOI: https://doi.org/10.1016/j.devcel.2007.10.006, PMID: 17981133

Blacque OE, Scheidel N, Kuhns S. 2018. Rab GTPases in cilium formation and function. *Small GTPases* **9**:76–94. DOI: https://doi.org/10.1080/21541248.2017.1353847, PMID: 29072526

Böcking T, Aguet F, Harrison SC, Kirchhausen T. 2011. Single-molecule analysis of a molecular disassemblase reveals the mechanism of Hsc70-driven clathrin uncoating. *Nature Structural and Molecular Biology* **18**:295–301. DOI: https://doi.org/10.1038/nsmb.1985, PMID: 21278753

Boehlke C, Kotsis F, Patel V, Braeg S, Voelker H, Bredt S, Beyer T, Janusch H, Hamann C, Gödel M, Müller K, Herbst M, Hornung M, Doerken M, Köttgen M, Nitschke R, Igarashi P, Walz G, Kuehn EW. 2010. Primary cilia regulate mTORC1 activity and cell size through Lkb1. *Nature Cell Biology* **12**:1115–

1122. DOI: https://doi.org/10.1038/ncb2117, PMID: 20972424

Bonifacino JS, Lippincott-schwartz J. 2003. Coat proteins: shaping membrane transport. *Nature Reviews Molecular Cell Biology* **4**:409–414. DOI: https://doi.org/10.1038/nrm1099, PMID: 12728274

Boucrot E, Pick A, Çamdere G, Liska N, Evergren E, McMahon HT, Kozlov MM. 2012. Membrane fission is promoted by insertion of amphipathic helices and is restricted by crescent BAR domains. *Cell* **149**:124–136. DOI: https://doi.org/10.1016/j.cell.2012.01.047, PMID: 22464325

Bradshaw NJ, Porteous DJ. 2012. DISC1-binding proteins in neural development, signalling and schizophrenia. *Neuropharmacology* **62**:1230–1241. DOI: https://doi.org/10.1016/j.neuropharm.2010.12.027, PMID: 21195721

Brazelton WJ, Amundsen CD, Silflow CD, Lefebvre PA. 2001. The bld1 mutation identifies the Chlamydomonas osm-6 homolog as a gene required for flagellar assembly. *Current Biology* **11**:1591–1594. DOI: https://doi.org/10.1016/S0960-9822(01)00485-7, PMID: 11676919

Breslow DK, Koslover EF, Seydel F, Spakowitz AJ, Nachury MV. 2013. An in vitro assay for entry into cilia reveals unique properties of the soluble diffusion barrier. *The Journal of Cell Biology* **203**:129–47. DOI: https://doi.org/10.1083/jcb.201212024, PMID: 24100294

Brohawn SG, Leksa NC, Spear ED, Rajashankar KR, Schwartz TU. 2008. Structural Evidence for Common Ancestry of the Nuclear Pore Complex and Vesicle Coats. *Science* **322**:1369–1373. DOI: https://doi.org/10.1126/science.1165886, PMID: **18974315**

Brooks ER, Wallingford JB. 2013. The Small GTPase Rsg1 is important for the cytoplasmic localization and axonemal dynamics of intraflagellar transport proteins. *Cilia* **2**:13. DOI: https://doi.org/10.1186/2046-2530-2-13, PMID: 24192041

Byrne EFX, Sircar R, Miller PS, Hedger G, Luchetti G, Nachtergaele S, Tully MD, Mydock-mcgrane L, Covey DF, Rambo RP, Sansom MSP, Newstead S, Rohatgi R, Siebold C. 2016. Structural basis for Smoothened regulation by its extracellular domains. *Nature* **535**:517–522. DOI: https://doi.org/10.1038/nature18934, PMID: 27437577

Calvert PD, Schiesser WE, Pugh Jr. EN. 2010. Diffusion of a soluble protein , photoactivatable GFP , through a sensory cilium. *Journal of General Physiology* **135**:173–196. DOI: https://doi.org/10.1085/jgp.200910322, PMID: 20176852

Cameron DA, Pennimpede T, Petkovich M. 2009. Tulp3 is a critical repressor of Mouse hedgehog signaling. *Developmental Dynamics* **238**:1140–1149. DOI: https://doi.org/10.1002/dvdy.21926, PMID: 19334287

Cano DA, Murcia NS, Pazour GJ, Hebrok M. 2004. Orpk mouse model of polycystic kidney disease reveals essential role of primary cilia in pancreatic tissue organization. *Development* **131**:3457–3467. DOI: https://doi.org/10.1242/dev.01189, PMID: 15226261

Cantagrel V, Silhavy JL, Bielas SL, Swistun D, Marsh SE, Bertrand JY, Audollent S, Attié-Bitach T, Holden KR, Dobyns WB, Traver D, Al-Gazali L, Ali BR, Lindner TH, Caspary T, Otto EA, Hildebrandt F, Glass IA, Logan CV, Johnson CA, Bennett C, Brancati F, Valente EM, Woods CG, Gleeson JG. 2008. Mutations in the Cilia Gene ARL13B Lead to the Classical Form of Joubert Syndrome. *American Journal of Human Genetics* **83**:170–179. DOI: https://doi.org/10.1016/j.ajhg.2008.06.023, PMID: 18674751

Caparrós-Martín JA, Luca AD, Cartault F, Aglan M, Temtamy S, Otaify GA, Mehrez M, Valencia M, Vázquez L, Alessandri J, Nevado J, Rueda-Arenas I, Heath KE, Digilio MC, Dallapiccola B, Goodship JA, Mill P, Lapunzina P, Ruiz-Perez VL. 2015. Specific variants in WDR35 cause a distinctive form of Ellis-van Creveld syndrome by disrupting the recruitment of the EvC complex and SMO into the cilium. *Human Molecular Genetics* **24**:4126–4137. DOI: https://doi.org/10.1093/hmg/ddv152, PMID: 25908617

Carvajal-Gonzalez JM, Roman AC, Mlodzik M. 2016. Positioning of centrioles is a conserved readout of Frizzled planar cell polarity signalling. *Nature Communication* **7**:11135. DOI: https://doi.org/10.1038/ncomms11135, PMID: 27021213

Cevik S, Hori Y, Kaplan OI, Kida K, Toivenon T, Foley-Fisher C, Cottell D, Katada T, Kontani K, Blacque OE. 2010. Joubert syndrome Arl13b functions at ciliary membranes and stabilizes protein transport in Caenorhabditis elegans. *The*

Journal of Cell Biology **189**:187. DOI: DOI: https://doi.org/10.1083/jcb.20090813320100323c,

Cevik S, Sanders AAMW, Wijk EV, Boldt K, Clarke L, Reeuwijk JV, Hori Y, Horn N, Hetterschijt L, Wdowicz A, Mullins A, Kida K, Kaplan OI, Beersum SECV, Wu KM, Letteboer SJF, Mans DA, Katada T, Kontani K, Ueffing M, Roepman R, Kremer H, Blacque OE. 2013. Active Transport and Diffusion Barriers Restrict Joubert Syndrome-Associated ARL13B/ARL-13 to an Inv-like Ciliary Membrane Subdomain. *PLoS Genetics* **9:**e1003977. DOI: https://doi.org/10.1371/journal.pgen.1003977, PMID: 24339792

Chávez M, Ena S, Sande JV, D'Exaerde ADK, Schurmans S, Schiffmann SN. 2015. Modulation of Ciliary Phosphoinositide Content Regulates Trafficking and Sonic Hedgehog Signaling Output. *Developmental Cell* **34**:338–350. DOI: http://doi.org/https://doi.org/10.1016/j.devcel.2015.06.016, PMID: 26190144

Cherfils J, Zeghouf M. 2013. Regulation of small GTPases by GEFs, GAPs, and GDIs. *American Physiological Society* **93**:269–309. DOI: https://doi.org/10.1152/physrev.00003.2012

Chih B, Liu P, Chinn Y, Chalouni C, Komuves LG, Hass PE, Sandoval W, Peterson AS. 2012. A ciliopathy complex at the transition zone protects the cilia as a privileged membrane domain. *Nature Cell Biology* **14**:61–72. DOI: https://doi.org/10.1038/ncb2410

Chou HT, Apelt L, Farrell DP, White SR, Woodsmith J, Svetlov V, Goldstein JS, Nager AR, Li Z, Muller J, Dollfus H, Nudler E, Stelzl U, DiMaio F, Nachury MV, Walz T. 2019. The Molecular Architecture of Native BBSome Obtained by an Integrated Structural Approach. *Structure* **27**:1384-1394.e4. DOI: https://doi.org/10.1016/j.str.2019.06.006, PMID: 31303482

Christensen ST, Morthorst SK, Mogensen JB, Pedersen LB. 2017. Primary cilia and coordination of receptor tyrosine kinase (RTK) and transforming growth factor β (TGF-β) signaling. *Cold spring harbor perspective biology*. **9**:a028167 DOI: http://doi.org/10.1101/cshperspect.a028167, PMID: 27638178

Chua CEL, Lim YS, Tang BL. 2010. Rab35 - A vesicular traffic-regulating small GTPase with actin modulating roles. *FEBS Letters* **584**:1–6. DOI: https://doi.org/10.1016/j.febslet.2009.11.051, PMID: 19931531

Cole DG. 2009. Chapter 4 - Intraflagellar Transport. *Chlamydomonas Sourcebook* **3**:71–113. DOI: https://doi.org/10.1016/B978-0-12-370873-1.00041-1

Corbit KC, Aanstad P, Singla V, Norman AR, Stainier DYR, Reiter JF. 2005. Vertebrate Smoothened functions at the primary cilium. *Nature* **437**:1018–1021. DOI: https://doi.org/10.1038/nature04117, PMID: 16136078

Craft JM, Harris JA, Hyman S, Kner P, Lechtreck KF. 2015. Tubulin transport by IFT is upregulated during ciliary growth by a cilium-autonomous mechanism. *The Journal of Cell Biology* **208**:223–237. DOI: https://doi.org/10.1083/jcb.201409036, PMID: 25583998

Criswell PS, Ostrowski LE, Asai DJ. 1996. A novel cytoplasmic dynein heavy chain: expression of DHC1b in mammalian ciliated epithelial cells. *Journal of Cell Science* **109**:1891–1898. PMID: 8832411

Czarnecki PG, Gabriel GC, Manning DK, Sergeev M, Lemke K, Klena NT, Liu X, Chen Y, Li Y, Agustin JTS, Garnaas MK, Francis RJ, Tobita K, Goessling W, Pazour GJ, Lo CW, Beier DR, Shah JV. 2015. ANKS6 is the critical activator of NEK8 kinase in embryonic situs determination and organ patterning. *Nature Communications* **6**:6023. DOI: https://doi.org/10.1038/ncomms7023

Dam TJPV, Townsend MJ, Turk M, Schlessinger A, Sali A, Field MC, Huynen MA. 2013. Evolution of modular intraflagellar transport from a coatomer-like progenitor. *Proceedings of the National Academy of Sciences* **110**:6943–6948. DOI: https://doi.org/10.1073/pnas.1221011110, PMID: 23569277

Dammermann A, Merdes A. 2002. Assembly of centrosomal proteins and microtubule organization depends on PCM-1. *The Journal of Cell Biology* **159**:255–266. DOI: https://doi.org/10.1083/jcb.200204023, PMID: 12403812

Datta P, Allamargot C, Hudson JS, Andersen EK, Bhattarai S, Drack AV, Sheffield VC, Seo S. 2015. Accumulation of non-outer segment proteins in the outer segment underlies photoreceptor degeneration in Bardet–Biedl syndrome. *Proceedings of the National Academy of Sciences* **112**:E4400–E4409. DOI: https://doi.org/10.1073/pnas.1510111112, PMID: 26216965

Davis EE, Zhang Q, Liu Q, Diplas BH, Davey LM, Hartley J, Stoetzel C, Szymanska K, Ramaswami G, Logan CV, Donna MM, Young AC, Wheeler DA, Cruz P,

Morgan M, Lewis LR, Cherukuri P, Maskeri B, Hansen NF, Mullikin JC, Blakesley RW, Bouffard GG, Gyapay G, Reiger S, Tönshoff B, Kern I, Soliman NA, Neuhaus TJ, Swoboda KJ, Kayserili H, Gallagher TE, Lewis RA, Bergmann C, Otto EA, Saunier S, Scambler PJ, Beales PL, Gleeson JG, Maher ER, Attié-Bitach T, Dollfus H, Johnson CA, Green ED, Gibbs RA, Hildebrandt F, Pierce EA, Katsanis N. 2011. TTC21B contributes both causal and modifying alleles across the ciliopathy spectrum. *Nautre Genetics* **43**:189–196. DOI: https://doi.org/10.1038/ng.756, PMID: 21258341

Dawe HR, Adams M, Wheway G, Szymanska K, Logan CV, Noegel AA, Gull K, Johnson CA. 2009. Nesprin-2 interacts with meckelin and mediates ciliogenesis via remodelling of the actin cytoskeleton. *Journal of Cell Science* **122**:2716–2726. DOI: https://doi.org/10.1242/jcs.043794, PMID: 19596800

De Matteis MA, Staiano L, Emma F, Devuyst O. 2017. The 5-phosphatase OCRL in Lowe syndrome and Dent disease 2. *Nature Reviews Nephrology* **13**:455–470. https://doi.org/10.1038/nrneph.2017.83, PMID: 28669993

Devos D, Dokudovskaya S, Alber F, Williams R, Chait BT, Sali A, Rout MP. 2004. Components of coated vesicles and nuclear pore complexes share a common molecular architecture. *PLoS Biology* **2**:e380. DOI: https://doi.org/10.1371/journal.pbio.0020380, PMID: 15523559

Dishinger JF, Kee HL, Jenkins PM, Fan S, Hurd TW, Hammond JW, Truong YN, Margolis B, Martens JR, Verhey KJ. 2010. Ciliary entry of the kinesin-2 motor KIF17 is regulated by importin-β2 and Ran-GTP. *Nature Cell Biology* **12**:703–710. DOI: https://doi.org/10.1038/ncb2073, PMID: 20526328

Dodonova SO, Aderhold P, Kopp J, Ganeva I, Röhling S, Hagen WJH, Sinning I, Wieland F, Briggs JAG. 2017. 9Å structure of the COPI coat reveals that the Arf1 GTPase occupies two contrasting molecular environments. *eLIFE* **6**:e26691. DOI: http://doi.org/10.7554/eLife.26691, PMID: 28621666

Dodonova SO, Diestelkoetter-Bachert P, Appen AV, Hagen WJH, Beck R, Beck M, Wieland F, Briggs JAG. 2015. A structure of the COPI coat and the role of coat proteins in membrane vesicle assembly. *Science* **349**:195–198. DOI: https://doi.org/10.1126/science.aab1121, PMID: 26160949

Domire JS, Green JA, Lee KG, Johnson AD, Askwith CC, Mykytyn K. 2011.

Dopamine receptor 1 localizes to neuronal cilia in a dynamic process that requires the Bardet-Biedl syndrome proteins. *Cellular and Molecular Life Sciences* **68**:2951–2960. DOI: 10.1007/s00018-010-0603-4, PMID: 21152952

Donaldson JG, Jackson CL. 2011. Arf Family G Proteins and their regulators: roles in membrane transport, development and disease. *Nature Reviews Molecular Cell Biology* **12**:362–375. DOI: https://doi.org/10.1038/nrm3117, PMID: 21587297

Dowdle WE, Robinson JF, Kneist A, Sirerol-Piquer MS, Frints SGM, Corbit KC, Zaghloul NA, Lijnschoten GV, Mulders L, Verver DE, Zerres K, Reed RR, Attié-Bitach T, Johnson CA, García-Verdugo JM, Katsanis N, Bergman C, Reiter JF. 2011. Disruption of a Ciliary B9 Protein Complex Causes Meckel Syndrome. *American Journal of Human Genetics* **89**:94–110. DOI: https://doi.org/10.1016/j.ajhg.2011.06.003, PMID: 21763481

Duran I, Taylor SP, Zhang W, Martin J, Qureshi F, Jacques SM, Wallerstein R, Lachman RS, Nickerson DA, Bamshad M, Cohn DH, Krakow D. 2017. Mutations in IFT-A satellite core component genes IFT43 and IFT121 produce short rib polydactyly syndrome with distinctive campomelia. *Cilia* **6**:7. DOI: https://doi.org/10.1186/s13630-017-0051-y, PMID: 28400947

Eggenschwiler JT, Bulgakov OV, Qin J, Li T, Anderson KV. 2006. Mouse Rab23 regulates Hedgehog signaling from Smoothened to Gli proteins. *Developmental Biology* **290**:1–12. DOI: https://doi.org/10.1016/j.ydbio.2005.09.022, PMID: 16364285

Eguether T, Agustin JTS, Keady BT, Jonassen JA, Liang Y, Francis R, Tobita K, Johnson CA, Abdelhamed ZA, Lo CW, Pazour GJ. 2014. IFT27 Links the BBSome to IFT for Maintenance of the Ciliary Signaling Compartment. *Developmental Cell* **31**:279–290. DOI: https://doi.org/10.1016/j.devcel.2014.09.011, PMID: 25446516

Eugster A, Frigerio G, Dale M, Duden R. 2004. The α- and β'-COP WD40 Domains Mediate Cargo- selective Interactions with Distinct Di-lysine Motifs. *Molecular Biology of the Cell* **15**:1011–1023. DOI: https://doi.org/10.1091/mbc.e03-10-0724, PMID: 14699056

Ezratty EJ, Pasolli HA, Fuchs E. 2016. A Presenilin-2-ARF4 trafficking axis modulates Notch signaling during epidermal differentiation. *The Journal of Cell*

Biology **214**:89–101. DOI: https://doi.org/10.1083/jcb.201508082, PMID: 27354375

Ezratty EJ, Stokes N, Chai S, Shah AS, Williams SE, Fuchs E. 2011. A role for the primary cilium in notch signaling and epidermal differentiation during skin development. *Cell* **145**:1129–1141. DOI: https://doi.org/10.1016/j.cell.2011.05.030, PMID: 21703454

Faini M, Beck R, Wieland FT, Briggs JAG. 2013. Vesicle coats: Structure, function, and general principles of assembly. *Trends in Cell Biology* **23**:279–288. DOI: https://doi.org/10.1016/j.tcb.2013.01.005, PMID: 23414967

Fan Y, Esmail MA, Ansley SJ, Blacque OE, Boroevich K, Ross AJ, Moore SJ, Badano JL, May-Simera H, Compton DS, Green JS, Lewis RA, Haelst MMV, Parfrey PS, Baillie DL, Beales PL, Katsanis N, Davidson WS, Leroux MR. 2004. Mutations in a member of the Ras superfamily of small GTP-binding proteins causes Bardet-Biedl syndrome. *Nature Genetics* **36**:989–993. DOI: https://doi.org/10.1038/ng1414, PMID: 15314642

Fansa EK, Kösling SK, Zent E, Wittinghofer A, Ismail S. 2016. PDE6δ-mediated sorting of INPP5E into the cilium is determined by cargo-carrier affinity. *Nature Communication* **7**:11366. DOI: https://doi.org/10.1038/ncomms11366, PMID: 27063844

Ferris PJ, Waffenschmidt S, Umen JG, Lin H, Lee J, Ishida K, Kubo T, Lau J, Goodenough UW. 2005. Plus and minus sexual agglutinins from Chlamydomonas reinhardtii. *The Plant Cell* **17**:597–615. DOI: 10.1105/tpc.104.028035, PMID: 15659633

Field MC, Sali A, Rout MP. 2011. On a bender-BARs, ESCRTs, COPs, and finally getting your coat. *The Journal of Cell Biology* **193**:963–972. DOI: https://doi.org/10.1083/jcb.201102042, PMID: 21670211

Fliegauf M, Kahle A, Häffner K, Zieger B. 2014. Distinct localization of septin proteins to ciliary sub-compartments in airway epithelial cells. *Biological Chemistry* **395**:151–156. DOI: https://doi.org/10.1515/hsz-2013-0252, PMID: 24317785

Follit JA, Agustin JTS, Xu F, Jonassen JA, Samtani R, Lo CW, Pazour GJ. 2008. The Golgin GMAP210/TRIP11 anchors IFT20 to the Golgi complex. *PLoS Genetics*

4:e1000315. DOI: https://doi.org/10.1371/journal.pgen.1000315, PMID: 19112494

Follit JA, Tuft RA, Fogarty KE, Pazour GJ. 2006. The Intraflagellar Transport Protein IFT20 Is Associated with the Golgi Complex and Is Required for Cilia Assembly. *Molecular Biology of the Cell* **17**:3781–3792. DOI: https://doi.org/10.1091/mbc.e06-02-0133, PMID: 16775004

Follit JA, Xu F, Keady BT, Pazour GJ. 2009. Characterisation of Mouse IFT Complex B. *Cell Motility Cytoskeleton* **66**:457–468. DOI: https://doi.org/10.1002/cm.20346, PMID: 19253336

Fotin A, Cheng Y, Sliz P, Grigorieff N, Harrison SC, Kirchhausen T, Walz T. 2004. Molecular model for a complete clathrin lattice from electron cryomicroscopy. *Nature* **432**:573–579. DOI: https://doi.org/10.1038/nature03079, PMID: 15502812

Frank V, Habbig S, Bartram MP, Eisenberger T, Veenstra-Knol HE, Decker C, Boorsma RA, Göbel H, Nürnberg G, Griessmann A, Franke M, Borgal L, Kohli P, Völker LA, Dötsch J, Nürnberg P, Benzing T, Bolz HJ, Johnson C, Gerkes EH, Schermer B, Bergmann C. 2013. Mutations in NEK8 link multiple organ dysplasia with altered Hippo signalling and increased c-MYC expression. *Human Molecular Genetics* **22**:2177–2185. DOI: https://doi.org/10.1093/hmg/ddt070, PMID: 23418306

Fu W, Wang L, Kim S, Li J, Dynlacht BD. 2016. Role for the IFT-A Complex in Selective Transport to the Primary Cilium. *Cell Reports* **17**:1505–1517. DOI: DOI: https://doi.org/10.1016/j.celrep.2016.10.018, PMID: 27806291

Funabashi T, Katoh Y, Michisaka S, Terada M, Sugawa M, Nakayama K. 2017. Ciliary entry of KIF17 is dependent on its binding to the IFT-B complex via IFT46-IFT56 as well as on its nuclear localization signal. *Molecular Biology of the Cell* **28**:624–633. DOI: https://doi.org/10.1091/mbc.e16-09-0648, PMID: 28077622

Funabashi T, Katoh Y, Okazaki M, Sugawa M, Nakayama K. 2018. Interaction of heterotrimeric kinesin-II with IFT-B-connecting tetramer is crucial for ciliogenesis. *The Journal of Cell Biology* **217**:2867–2876. DOI: https://doi.org/10.1083/jcb.201801039, PMID: 29903877

Gaidarov I, Chen Q, Falck JR, Reddy KK, Keen JH. 1996. A Functional Phosphatidylinositol 3,4,5-Trisphosphate/Phosphoinositide Binding Domain in the Clathrin Adaptor AP-2 α Subunit. Implications for the endocytic pathway. *Journal of Biological Chemistry* **271**:20922–20929. DOI: http://doi.org/10.1074/jbc.271.34.20922, PMID: 8702850

Gaillard CLB, Pallesi-Pocachard E, Massey-Harroche D, Richard F, Arsanto J, Chauvin J, Lecine P, Krämer H, Borg JP, Bivic AL. 2011. Hook2 is involved in the morphogenesis of the primary cilium. *Molecular Biology of the Cell* **22**:4549–4562. DOI: http://doi.org/10.1091/mbc.E11-05-0405, PMID: 21998199

Garcia-gonzalo FR, Corbit KC, Sirerol-piquer MS, Ramaswami G, Otto EA, Noriega TR, Seol AD, Robinson JF, Bennett CL, Josifova DJ, García-verdugo JM, Katsanis N, Hildebrandt F, Reiter JF. 2011. A transition zone complex regulates mammalian ciliogenesis and ciliary membrane composition. *Nature Genetics* **43**:776–784. DOI: https://doi.org/10.1038/ng.891, PMID: 21725307

Garcia-Gonzalo FR, Phua SC, Roberson EC, Garcia G, Abedin M, Schurmans S, Inoue T, Reiter JF. 2015. Phosphoinositides Regulate Ciliary Protein Trafficking to Modulate Hedgehog Signaling. *Developmental Cell* **34**:400–409. DOI: https://doi.org/10.1016/j.devcel.2015.08.001, PMID: 26305592

Garcia-Gonzalo FR, Reiter JF. 2017. Open Sesame: How transition fibers and the transition zone control ciliary composition. *Cold Spring Harbor Perspective in Biology* **9**: a028134. DOI: https://doi.org/10.1101/cshperspect.a028134, PMID: 27770015

Gómez-Orte E, Sáenz-Narciso B, Moreno S, Cabello J. 2013. Multiple functions of the noncanonical Wnt pathway. *Trends in Genetics* **29**:545–553. DOI: https://doi.org/10.1016/j.tig.2013.06.003, PMID: 23846023

Gotthardt K, Lokaj M, Koerner C, Falk N, Gießl A, Wittinghofer A. 2015. A G-protein activation cascade from Arl13B to Arl3 and implications for ciliary targeting of lipidated proteins. *eLIFE* **4**: e11859. DOI: http://doi.org/10.7554/eLife.11859, PMID: 26551564

Graser S, Stierhof YD, Lavoie SB, Gassner OS, Lamla S, Clech ML, Nigg EA. 2007. Cep164, a novel centriole appendage protein required for primary cilium formation. *The Journal of Cell Biology* **179**:321–330. DOI:

https://doi.org/10.1083/jcb.200707181, PMID: 17954613

Grisanti L, Revenkova E, Gordon RE, Iomini C. 2016. Primary cilia maintain corneal epithelial homeostasis by regulation of the Notch signaling pathway. *Development* **143**:2160–2171. DOI: https://doi.org/10.1242/dev.132704, PMID: 27122169

Guo DF, Cui H, Zhang Q, Morgan DA, Thedens DR, Nishimura D, Grobe JL, Sheffield VC, Rahmouni K. 2016. The BBSome Controls Energy Homeostasis by Mediating the Transport of the Leptin Receptor to the Plasma Membrane. *PLoS Genet* **12**: e1005890. DOI: https://doi.org/10.1371/journal.pgen.1005890, PMID: 26926121

Gupta GD, Coyaud É, Gonçalves J, Mojarad BA, Liu Y, Wu Q, Gheiratmand L, Comartin D, Tkach JM, Cheung SWT, Bashkurov M, Hasegan M, Knight JD, Lin ZY, Schueler M, Hildebrandt F, Moffat J, Gingras A, Raught B, Pelletier L. 2015. A dynamic protein interaction landscape of the human centrosome-cilium interface. *Cell* **163**:1484–1499. DOI: https://doi.org/10.1016/j.cell.2015.10.065 https://doi.org/10.1016/j.cell.2015.10.065, PMID: 26638075

Haar E, Musacchio A, Harrison SC, Kirchhausen T. 1998. Atomic Structure of Clathrin: A β Propeller Terminal Domain Joins an α Zigzag Linker. *Cell* **95**:563–573. DOI: https://doi.org/10.1016/S0092-8674(00)81623-2, PMID: 9827808

Habbig S, Bartram MP, Müller RU, Schwarz R, Andriopoulos N, Chen S, Sägmüller JG, Hoehne M, Burst V, Liebau MC, Reinhardt HC, Benzing T, Schermer B. 2011. NPHP4, a cilia-associated protein, negatively regulates the Hippo pathway. *The Journal of Cell Biology* **193**:633–642. DOI: https://doi.org/10.1083/jcb.201009069, PMID: 21555462

Habbig S, Bartram MP, Sägmüller JG, Griessmann A, Franke M, Müller RU, Schwarz R, Hoehne M, Bergmann C, Tessmer C, Reinhardt HC, Burst V, Benzing T, Schermer B. 2012. The ciliopathy disease protein NPHP9 promotes nuclear delivery and activation of the oncogenic transcriptional regulator TAZ. *Human Molecular Genetics* **21**:5528–5538. DOI: https://doi.org/10.1093/hmg/dds408, PMID: 23026745

Hall EA, Keighren M, Ford MJ, Davey T, Jarman AP, Smith LB, Jackson IJ, Mill P. 2013. Acute Versus Chronic Loss of Mammalian Azi1/Cep131 Results in

Distinct Ciliary Phenotypes. *PLoS Genetics* **9**:e1003928. DOI: https://doi.org/10.1371/journal.pgen.1003928, PMID: 24415959

Hammond GRV, Machner MP, Balla T. 2014. A novel probe for phosphatidylinositol 4-phosphate reveals multiple pools beyond the Golgi. *The Journal of Cell Biology* **205**:113–126. DOI: https://doi.org/10.1083/jcb.201312072, PMID: 24711504

Hammond GRV, Fischer MJ, Anderson KE, Holdich J, Koteci A, Balla T, Irvine RF. 2012. PI4P and PI(4,5)P2 Are Essential But Independent Lipid Determinants of Membrane Identity. *Science* **337**:727–730. DOI: https://doi.org/10.1126/science.1222483, PMID: 22722250

Han Y, Kim HJ, Dlugosz AA, Ellison DW, Gilbertson RJ, Alvarez-Buylla A. 2009. Dual and opposing roles of primary cilia in medulloblastoma development. *Nature Medicine* **15**:1062–1065. DOI: https://doi.org/10.1038/nm.2020, PMID: 19701203

Haycraft CJ, Banizs B, Aydin-Son Y, Zhang Q, Michaud EJ, Yoder BK. 2005. Gli2 and Gli3 localize to cilia and require the intraflagellar transport protein polaris for processing and function. *PLoS Genet* **1**:e53. DOI: https://doi.org/10.1371/journal.pgen.0010053, PMID: 16254602

Hell SW, Wichmann J. 1994. Breaking the diffraction resolution limit by stimulated emission: stimulated-emission-depletion fluorescence microscopy. *Optics Letters* **19**:780–782. DOI: https://doi.org/10.1364/OL.19.000780, PMID: 19844443

Hirano T, Katoh Y, Nakayama K. 2017. Intraflagellar transport-A complex mediates ciliary entry and retrograde trafficking of ciliary G protein–coupled receptors. *Molecular Biology of the Cell* **28**:429–439. DOI: https://doi.org/10.1091/mbc.e16-11-0813, PMID: 27932497

Hoefele J, Wolf MTF, O'Toole JF, Otto EA, Schultheiss U, Dêschenes G, Attanasio M, Utsch B, Antignac C, Hildebrandt F. 2007. Evidence of oligogenic inheritance in nephronophthisis. *Journal of American Society of Nephrology* **18**:2789–2795. DOI: https://doi.org/10.1681/ASN.2007020243, PMID:17855640

Hoff S, Halbritter J, Epting D, Frank V, Nguyen TM, Reeuwijk JV, Boehlke C, Schell C, Yasunaga T, Helmstädter M, Mergen M, Filhol E, Boldt K, Horn N, Ueffing M, Otto EA, Eisenberger T, Elting MW, Wijk JAEV, Bockenhauer D, Sebire NJ, Rittig S, Vyberg M, Ring T, Pohl M, Pape L, Neuhaus TJ, Elshakhs NAS, Koon

SJ, Harris PC, Grahammer F, Huber TB, Kuehn EW, Kramer-Zucker A, Bolz HJ, Roepman R, Saunier S, Walz G, Hildebrandt F, Bergmann C, Lienkamp SS. 2013. ANKS6 is a central component of a nephronophthisis module linking NEK8 to INVS and NPHP3. *Nature Genetics* **45**:951–956. DOI: https://doi.org/10.1038/ng.2681, PMID: 23793029

Hoffmeister H, Babinger K, Gürster S, Cedzich A, Meese C, Schadendorf K, Osten L, Vries UD, Rascle A, Witzgall R. 2011. Polycystin-2 takes different routes to the somatic and ciliary plasma membrane. *The Journal of Cell Biology* **192**:631–645. DOI: http://doi.org/10.1083/jcb.201007050, PMID: 21321097

Horani A, Ferkol TW, Dutcher SK, Brody SL. 2016. Genetics and Biology of Primary Ciliary Dyskinesia. *Paediatric Respiratory Reviews* **18**:18–24. DOI: https://doi.org/10.1016/j.prrv.2015.09.001, PMID: 26476603

Hori A, Toda T. 2017. Regulation of centriolar satellite integrity and its physiology. *Celular and Molecular Life Sciences.* **74**:213–229. DOI: http://doi.org/10.1007/s00018-016-2315-x, PMID: 27484406

Hou Y, Qin H, Follit JA, Pazour GJ, Rosenbaum JL, Witman GB. 2007. Functional analysis of an individual IFT protein: IFT46 is required for transport of outer dynein arms into flagella. *The Journal of Cell Biology* **176**:653–665. DOI: https://doi.org/10.1083/jcb.200608041, PMID: 17312020

Hsia K, Hoelz A. 2010. Crystal structure of α-COP in complex with ε-COP provides insight into the architecture of the COPI vesicular coat. *Proceedings of the National Academy of Sciences* **107**:11271–11276. DOI: https://doi.org/10.1073/pnas.1006297107, PMID: 20534429

Hsiao Y, Tuz K, Ferland RJ. 2012. Trafficking in and to the primary cilium. *Cilia* **1**:4. DOI: https://doi.org/10.1186/2046-2530-1-4,

Hu Q, Milenkovic L, Jin H, Scott MP, Nachury MV, Spiliotis ET, Nelson WJ. 2010. A septin diffusion barrier at the base of the primary cilium maintains ciliary membrane protein distribution. *Science* **329**:436–439. DOI: 10.1126/science.1191054, PMID: 20558667

Huang L, Szymanska K, Jensen VL, Janecke AR, Innes AM, Davis EE, Frosk P, Li C, Willer JR, Chodirker BN, Greenberg CR, Mcleod DR, Bernier FP, Chudley AE, Müller T, Shboul M, Logan CV, Loucks CM, Beaulieu CL, Bowie RV, Bell

SM, Adkins J, Zuniga FI, Ross KD, Wang J, Ban MR, Becker C, Nürnberg P, Douglas S, Craft CM, Akimenko M, Hegele RA, Ober C, Utermann G, Bolz HJ, Bulman DE, Katsanis N, Blacque OE, Doherty D, Parboosingh JS, Leroux MR, Johnson CA, Boycott KM. 2011. TMEM237 Is Mutated in Individuals with a Joubert Syndrome Related Disorder and Expands the Role of the TMEM Family at the Ciliary Transition Zone. *American Journal of Human Genetics* **89**:713–730. DOI: https://doi.org/10.1016/j.ajhg.2011.11.005, PMID: 22152675

Huang P, Schier AF. 2009. Dampened Hedgehog signaling but normal Wnt signaling in zebrafish without cilia. *Development* **136**:3089–3098. DOI: https://doi.org/10.1242/dev.041343, PMID: 19700616

Huangfu D, Anderson KV. 2005. Cilia and Hedgehog responsiveness in the mouse. *Proceedings of the National Academy of Sciences* **102**:11325–11330. DOI: https://doi.org/10.1073/pnas.0505328102, PMID: 16061793

Huangfu D, Liu A, Rakeman AS, Murcia NS, Niswander L, Anderson KV. 2003. Hedgehog signalling in the mouse requires intraflagellar transport proteins. *Nature* **426**:83–87. DOI: https://doi.org/10.1038/nature02061, PMID: 14603322

Humbert MC, Weihbrecht K, Searby CC, Li Y, Pope RM, Sheffield VC, Seo S. 2012. ARL13B, PDE6D, and CEP164 form a functional network for INPP5E ciliary targeting. *Proceedings of the National Academy of Sciences* **109**:19691–19696. DOI: https://doi.org/10.1073/pnas.1210916109, PMID: 23150559

Hunnicutt GR, Kosfiszer MG, Snell WJ. 1990. Cell body and flagellar agglutinins in Chlamydomonas reinhardtii: The cell body plasma membrane is a reservoir for agglutinins whose migration to the flagella is regulated by a functional barrier. *The Journal of Cell Biology* **111**:1605–1616. DOI: https://doi.org/10.1083/jcb.111.4.1605, PMID: 2170424

Ina Hinners, Tooze SA. 2003. Changing directions: clathrin-mediated transport between the Golgi and endosomes. *Journal of Cell Science* **116**:763–771. DOI: https://doi.org/10.1242/jcs.00270, PMID: 12571274

Ingham PW, Nakano Y, Seger C. 2011. Mechanisms and functions of Hedgehog signalling across the metazoa. *Nature Reviews Genetics* **12**:393–406. DOI: https://doi.org/10.1038/nrg2984, PMID: 21502959

Iomini C, Babaev-Khaimov V, Sassaroli M, Piperno G. 2001. Protein particles in

Chlamydomonas flagella undergo a transport cycle consisting of four phases. *The Journal of Cell Biology* **153**:13–24. DOI: https://doi.org/10.1083/jcb.153.1.13, PMID: 11285270

Iomini C, Li L, Esparza JM, Dutcher SK. 2009. Retrograde intraflagellar transport mutants identify complex A proteins with multiple genetic interactions in Chlamydomonas reinhardtii. *Genetics* **183**:885–896. DOI: https://doi.org/10.1534/genetics.109.101915, PMID: 19720863

Ishikawa H, Ide T, Yagi T, Jiang X, Hirono M, Sasaki H, Yanagisawa H, Wemmer KA, Stainier DYR, Qin H, Kamiya R, Marshall WF. 2014. TTC26/DYF13 is an intraflagellar transport protein required for transport of motility-related proteins into flagella. *eLIFE*. **3**:e01566. DOI: http://doi.org/10.7554/eLife.01566, PMID: 24596149

Ismail SA, Chen Y, Miertzschke M, Vetter IR, Koerner C, Wittinghofer A. 2012. Structural basis for Arl3-specific release of myristoylated ciliary cargo from UNC119. *The EMBO Journal* **31**:4085–4094. DOI: https://doi.org/10.1038/emboj.2012.257, PMID: 22960633

Ismail SA, Chen Y, Rusinova A, Chandra A, Bierbaum M, Gremer L, Triola G, Waldmann H, Bastiaens PIH, Wittinghofer A. 2011. Arl2-GTP and Arl3-GTP regulate a GDI-like transport system for farnesylated cargo. *Nature Chemical Biology* **7**:942–949. DOI: https://doi.org/10.1038/nchembio.686, PMID: 22002721

Jackson LP, Lewis M, Kent HM, Edeling MA, Evans PR, Duden R, Owen DJ. 2012. Molecular Basis for Recognition of Dilysine Trafficking Motifs by COPI. *Developmental Cell* **23**:1255–1262. DOI: https://doi.org/10.1016/j.devcel.2012.10.017, PMID: 23177648

Jacob LS, Wu X, Dodge ME, Fan C, Kulak O, Chen B, Tang W, Wang B, Amatruda JF, Lum L. 2011. Genome-wide RNAi screen reveals disease-associated genes that are common to Hedgehog and Wnt signaling. *Science Signaling* **4**:ra4. DOI: https://doi.org/10.1126/scisignal.2001225, PMID: 21266715

Jacoby M, Cox JJ, Gayral S, Hampshire DJ, Ayub M, Blockmans M, Pernot E, Kisseleva MV, Compère P, Schiffmann SN, Gergely F, Riley JH, Pérez-Morga D, Woods CG, Schurmans S. 2009. INPP5E mutations cause primary cilium

signaling defects, ciliary instability and ciliopathies in human and mouse. *Nature Genetics* **41**:1027–1031. DOI: https://doi.org/10.1038/ng.427, PMID: 19668215

Jékely G, Arendt D. 2006. Evolution of intraflagellar transport from coated vesicles and autogenous origin of the eukaryotic cilium. *BioEssays* **28**:191–198. DOI: https://doi.org/10.1002/bies.20369, PMID: 16435301

Jensen VL, Bialas NJ, Bishop-Hurley SL, Molday LL, Kida K, Nguyen PAT, Blacque OE, Molday RS, Leroux MR, Riddle DL. 2010. Localization of a guanylyl cyclase to chemosensory cilia requires the novel ciliary MYND domain protein DAF-25. *PLoS Genetics* **6**: e1001199. DOI: https://doi.org/10.1371/journal.pgen.1001199, PMID: 21124868

Jin H, White SR, Shida T, Schulz S, Aguiar M, Gygi SP, Bazan JF, Nachury MV. 2010. The conserved Bardet-Biedl Syndrome proteins assemble a coat that traffics membrane proteins to cilia. *Cell* **141**:1208–1219. DOI: https://doi.org/10.1016/j.cell.2010.05.015,

Joachim J, Razi M, Judith D, Wirth M, Calamita E, Encheva V, Dynlacht BD, Snijders AP, O'Reilly N, Jefferies HBJ, Tooze SA. 2017. Centriolar Satellites Control GABARAP Ubiquitination and GABARAP-Mediated Autophagy. *Current Biology* **27**:2123-2136.e7. DOI: https://doi.org/10.1016/j.cub.2017.06.021, PMID: 28712572

Jones C, Roper VC, Foucher I, Qian D, Banizs B, Petit C, Yoder BK, Chen P. 2008. Ciliary proteins link basal body polarization to planar cell polarity regulation. *Nature Genetics* **40**:69–77. DOI: https://doi.org/10.1038/ng.2007.54, PMID: 18066062

Joo K, Kim CG, Lee MS, Moon HY, Lee SH, Kim MJ, Kweon HS, Park WY, Kim CH, Gleeson JG, Kim J. 2013. CCDC41 is required for ciliary vesicle docking to the mother centriole. *Proceedings of the National Academy of Sciences* **110**:5987–5992. DOI: https://doi.org/10.1073/pnas.1220927110, PMID: 23530209

Jordan MA, Diener DR, Stepanek L, Pigino G. 2018. The Cryo-EM structure of Intraflagellar Transport Trains reveals how dynein is inactivated to ensure unidirectional anterograde movement in cilia. *Nature Cell Biology* **20**:1250–1255. DOI: https://doi.org/10.1038/s41556-018-0213-1, PMID: 30323187

Joubert M, Eisenring JJ, Robb JP, Andermann F. 1999. Familial Agenesis of the Cerebellar Vermis : A Syndrome of Episodic Hyperpnea , Abnormal Eye Movements, Ataxia, and Retardation. *Journal of Child Neurology* **14**:554–564. DOI: https://doi.org/10.1177/088307389901400902, PMID: 10488899

Kanie T, Abbott KL, Mooney NA, Plowey ED, Demeter J, Jackson PK. 2017. The CEP19-RABL2 GTPase complex binds IFT-B to initiate intraflagellar transport at the ciliary base. *Developmental Cell* **42**:22-36.e12. DOI: https://doi.org/10.1016/j.devcel.2017.05.016, PMID: 28625565

Kaplan OI, Molla-Herman A, Cevik S, Ghossoub R, Kida K, Kimura Y, Jenkins P, Martens JR, Setou M, Benmerah A, Blacque OE. 2010. The AP-1 clathrin adaptor facilitates cilium formation and functions with RAB-8 in C. elegans ciliary membrane transport. *Journal of Cell Science* **123**:3966–3977. DOI: https://doi.org/10.1242/jcs.073908, PMID: 20980383

Katoh Y, Terada M, Nishijima Y, Takei R, Nozaki S, Hamada H, Nakayama K. 2016. Overall architecture of the intraflagellar transport (IFT)-B complex containing cluap1/IFT38 as an essential component of the IFT-B peripheral subcomplex. *Journal of Biological Chemistry* **291**:10962–10975. DOI: http://doi.org/10.1074/jbc.M116.713883, PMID: 26980730

Keady BT, Samtani R, Tobita K, Tsuchya M, Agustin JTS, Follit JA, Jonassen JA, Subramanian R, Lo CW, Pazour GJ. 2012. IFT25 Links the Signal-Dependent Movement of Hedgehog Components to Intraflagellar Transport. *Developmental Cell* **22**:940–951. DOI: https://doi.org/10.1016/j.devcel.2012.04.009 https://doi.org/10.1016/j.devcel.2012.04.009, PMID: 22595669

Kee HL, Dishinger JF, Blasius TL, Liu C, Margolis B, Verhey KJ. 2012. A Size-Exclusion Permeability Barrier and Nucleoporins Characterize a Ciliary Pore Complex that Regulates Transport into Cilia. *Nature Cell Biology* **14**:431–437. DOI: https://doi.org/10.1038/ncb2450, PMID: 22388888

Kim J, Dabiri S, Seeley ES. 2011. Primary cilium depletion typifies cutaneous melanoma in situ and malignant melanoma. *PLoS One* **6**: e27410. DOI: https://doi.org/10.1371/journal.pone.0027410, PMID: 22096570

Kim J, Krishnaswami SR, Gleeson JG. 2008. CEP290 interacts with the centriolar

satellite component PCM-1 and is required for Rab8 localization to the primary cilium. *Human Molecular Genetics* **17**:3796–3805. DOI: https://doi.org/10.1093/hmg/ddn277, PMID: 18772192

Kim M, Kim M, Lee M, Kim C, Lim D. 2014. The MST1/2-SAV1 complex of the Hippo pathway promotes ciliogenesis. *Nature Communication* **5**:5370. DOI: https://doi.org/10.1038/ncomms6370, PMID: 25367221

Kim SK, Shindo A, Park TJ, Oh EC, Ghosh S, Gray RS, Lewis RA, Johnson CA, Attie-bittach T, Wallingford JB. 2010. Planar Cell Polarity Acts Through Septins to Control Collective Cell Movement and Ciliogenesis. *Science* **329**:1337–1340. DOI: http.//doi.org/10.1126/science.1191184, PMID: 20671153

Kirchhausen T. 2000. Three Ways to make a vesicle. *Nature Reviews Molecular Cell Biology* **1**:187–198. DOI: https://doi.org/10.1038/35043117, PMID: 11252894

Kirchhausen T, Owen D, Harrison SC. 2014. Molecular Structure, Function, and Dynamics of Clathrin-Mediated Membrane Traffic. *Cold Spring Harbor Perspective in Biology*. **6**:a016725. DOI: 10.1101/cshperspect.a016725, PMID: 24789820

Kleyn PW, Fan W, Kovats SG, Lee JJ, Pulido JC, Wu Y, Berkemeier LR, Misumi DJ, Holmgren L, Charlat O, Woolf EA, Tayber O, Brody T, Shu P, Hawkins F, Kennedy B, Baldini L, Ebeling C, Alperin GD, Deeds J, Lakey ND, Culpepper J, Chen H, Glücksmann-Kuis MA, Carlson GA, Duyk GM, Moore KJ. 1996. Identification and Characterization of the Mouse Obesity Gene tubby: A Member of a Novel Gene Family. *Cell* **85**:281–290. DOI: https://doi.org/10.1016/S0092-8674(00)81104-6, PMID: 8612280

Knödler A, Feng S, Zhang J, Zhang X, Das A, Peränen J, Guo W. 2010. Coordination of Rab8 and Rab11 in primary ciliogenesis. *Proceedings of the National Academy of Sciences* **107**:6346–6351. DOI: https://doi.org/10.1073/pnas.1002401107, PMID: 20308558

Kobayashi T, Kim S, Lin Y, Inoue T, Dynlacht BD. 2014. The CP110-interacting proteins talpid3 and cep290 play overlapping and distinct roles in cilia assembly. *The Journal of Cell Biology* **204**:215–229. DOI: https://doi.org/10.1083/jcb.201304153, PMID: 24421332

Kösling SK, Fansa EK, Maffini S, Wittinghofer A. 2018. Mechanism and dynamics

of INPP5E transport into and inside the ciliary compartment. *Biological Chemistry* **399**:277–292. DOI: https://doi.org/10.1515/hsz-2017-0226, PMID: 29140789

Kozminski KG, Johnson KA, Forscher P, Rosenbaum JL. 1993. A motility in the eukaryotic flagellum unrelated to flagellar beating. *Proceedings of the National Academy of Sciences* **90**:5519–5523. DOI: https://doi.org/10.1073/pnas.90.12.5519, PMID: 8516294

Kremer JR, Mastronarde DN, McIntosh JR. 1996. Computer visualization of three-dimensional image data using IMOD. *Journal of Structural Biology* **116**:71–76. DOI: https://doi.org/10.1006/jsbi.1996.0013, PMID: 8742726

Kubo A, Sasaki H, Yuba-Kubo A, Tsukita S, Shiina N. 1999. Centriolar satellites: Molecular characterization, ATP-dependent movement toward centrioles and possible involvement in ciliogenesis. *The Journal of Cell Biology* **147**:969–980. DOI: https://doi.org/10.1083/jcb.147.5.969, PMID: 10579718

Kuhns S, Seixas C, Pestana S, Tavares B, Nogueira R, Jacinto R, Ramalho JS, Simpson JC, Andersen JS, Echard A, Lopes SS, Barral DC, Blacque OE. 2019. Rab35 controls cilium length, function and membrane composition. *EMBO Reports* **20**:e47625. DOI: https://doi.org/10.15252/embr.201847625, PMID: 31432619

Kwon M, Pavlov TS, Nozu K, Rasmussen SA, Ilatovskaya DV, Lerch-Gaggl A, North LM, Kim H, Qian F, Sweeney WE, Avner ED, Blumer JB, Staruschenko A, Park F. 2012. G-protein signaling modulator 1 deficiency accelerates cystic disease in an orthologous mouse model of autosomal dominant polycystic kidney disease. *Proceedings of the National Academy of Sciences* **109**:21462–21467. DOI: https://doi.org/10.1073/pnas.1216830110 , PMID: 23236168

Lambacher NJ, Bruel A, Dam TJPV, Szymańska K, Slaats GG, Kuhns S, Mcmanus GJ, Kennedy JE, Gaff K, Wu M, Lee RVD, Burglen L, Doummar D, Rivière J, Faivre L, Attié-bitach T, Saunier S, Curd A, Peckham M, Giles RH, Johnson CA, Huynen MA, Thauvin-Robinet C, Blacque OE. 2016. TMEM107 recruits ciliopathy proteins to subdomains of the ciliary transition zone and causes Joubert syndrome. *Nature Cell Biologyl* **18**:122–131. DOI: 10.1038/ncb3273, PMID: 26595381

Langousis G, Shimogawa MM, Saada EA, Vashisht AA, Spreafico R, Nager AR, Barshop WD, Nachury MV, Wohlschlegel JA, Hill KL. 2016. Loss of the BBSome perturbs endocytic trafficking and disrupts virulence of Trypanosoma brucei . *Proceedings of the National Academy of Sciences* **113**:632–637. DOI: 10.1073/pnas.1518079113, PMID: 26721397

Leaf A, Zastrow MV. 2015. Dopamine receptors reveal an essential role of IFT-B , KIF17 , and Rab23 in delivering specific receptors to primary cilia. *eLIFE* **4**:e06996. DOI: 10.7554/eLife.06996, PMID: 26182404

Lechtreck KF, Brown JM, Sampaio JL, Craft JM, Shevchenko A, Evans JE, Witman GB. 2013. Cycling of the signaling protein phospholipase D through cilia requires the BBSome only for the export phase. *The Journal of Cell Biology* **201**:249–261. DOI: 10.1083/jcb.201207139, PMID: 23589493

Lechtreck KF, Johnson EC, Sakai T, Cochran D, Ballif BA, Rush J, Pazour GJ, Ikebe M, Witman GB. 2009. The Chlamydomonas reinhardtii BBSome is an IFT cargo required for export of specific signaling proteins from flagella. *The Journal of Cell Biology* **187**:1117–1132. DOI: 10.1083/jcb.200909183, PMID: 20038682

Lee C, Goldberg J. 2010. Structure of Coatomer Cage Proteins and the Relationship among COPI, COPII, and Clathrin Vesicle Coats. *Cell* **142**:123–132. DOI: 10.1016/j.cell.2010.05.030, PMID: 20579721

Lee E, Sivan-loukianova E, Eberl DF, Kernan MJ. 2008. An IFT-A protein is required to delimit functionally distinct zones in mechanosensory cilia. *The Journal of Cell Biology* **18**:1899–1906. DOI: 10.1016/j.cub.2008.11.020, PMID: 19097904

Lee MCS, Miller EA, Goldberg J, Orci L, Schekman R. 2004. Bi-Directional Protein Transport Between the ER and Golgi. *Annual Review of Cell and Developmental Biology* **20**:87–123. DOI: https://doi.org/10.1146/annurev.cellbio.20.010403.105307

Lee MCS, Orci L, Hamamoto S, Futai E, Ravazzola M, Schekman R. 2005. Sar1p N-terminal helix initiates membrane curvature and completes the fission of a COPII vesicle. *Cell* **122**:605–617. DOI: https://doi.org/10.1016/j.cell.2005.07.025, PMID: 16122427

Leettola CN, Knight MJ, Cascio D, Hoffman S, Bowie JU. 2014. Characterization of the SAM domain of the PKD-related protein ANKS6 and its interaction with

ANKS3. *BMC Structural Biology* **14**:1–15. DOI: 10.1186/1472-6807-14-17, PMID: 24998259

Lehman JM, Michaud EJ, Schoeb TR, Aydin-son Y, Miller M, Yoder BK. 2008. The Oak Ridge Polycystic Kidney Mouse: Modeling Ciliopathies of Mice and Men. *Developmental Dynamics* **237**:1960–1971. DOI: 10.1002/dvdy.21515, PMID: 18366137

Leitch CC, Zaghloul NA, Davis EE, Stoetzel C, Diaz-Font A, Rix S, Alfadhel M, Lewis RA, Eyaid W, Banin E, Dollfus H, Beales PL, Badano JL, Katsanis N. 2008. Hypomorphic mutations in syndromic encephalocele genes are associated with Bardet-Biedl syndrome. *Nature Genetics* **40**:443–448. DOI: https://doi.org/10.1038/ng.97

Letourneur F, Gaynor EC, Hennecke S, Démollière C, Duden R, Emr SD, Riezman H, Cosson P. 1994. Coatomer is essential for retrieval of dilysine-tagged proteins to the endoplasmic reticulum. *Cell* **79**:1199–207. DOI: 10.1016/0092-8674(94)90011-6, PMID: 8001155

Li C, Jensen VL, Park K, Kennedy J, Garcia-Gonzalo FR, Romani M, Mori RD, Bruel A, Gaillard D, Doray B, Lopez E, Rivière J, Faivre L, Thauvin-robinet C, Reiter JF, Blacque OE, Valente EM, Leroux MR. 2016. MKS5 and CEP290 Dependent Assembly Pathway of the Ciliary Transition Zone. *PLoS Biology* **14**:e1002416. DOI: 10.1371/journal.pbio.1002416, PMID: 26982032

Li L, Grausam KB, Wang J, Lun MP, Ohli J, Lidov HGW, Calicchio ML, Zeng E, Salisbury JL, Wechsler-Reya RJ, Lehtinen MK, Schüller U, Zhao H. 2016. Sonic Hedgehog promotes proliferation of Notch-dependent monociliated choroid plexus tumour cells. *Nature Cell Biology* **18**:418–430. DOI: 10.1038/ncb3327, PMID: 26999738

Li Y, Ling K, Hu J. 2012. The emerging role of Arf/Arl small GTPases in cilia and ciliopathies. *Journal of Cellular Biochemistry* **113**:2201–2207. DOI: 10.1002/jcb.24116, PMID: 22389062

Liem KF, Ashe A, He M, Satir P, Moran J, Beier D, Wicking C, Anderson K V. 2012. The IFT-A complex regulates Shh signaling through cilia structure and membrane protein trafficking. *The Journal of Cell Biology* **197**:789–800. DOI: 10.1083/jcb.201110049, PMID: 22689656

Liew GM, Ye F, Nager AR, Murphy JP, Lee JS, Aguiar M, Breslow DK, Gygi SP, Nachury MV. 2014. The intraflagellar transport protein ift27 promotes bbsome exit from cilia through the gtpase ARL6/BBS3. *Dev Cell* **31**:265–278. DOI: 10.1016/j.devcel.2014.09.004, PMID: 25443296

Lim YS, Tang BL. 2015. A role for Rab23 in the trafficking of Kif17 to the primary cilium. *Journal of Cell Science* **128**:2996–3008. DOI: 10.1242/jcs.163964, PMID: 26136363

Lin F, Hiesberger T, Cordes K, Sinclair AM, Goldstein LSB, Somlo S, Igarashi P. 2003. Kidney-specific inactivation of the KIF3A subunit of kinesin-II inhibits renal ciliogenesis and produces polycystic kidney disease. *Proceedings of the National Academy of Sciences* **100**:5286–5291. DOI: 10.1073/pnas.0836980100, PMID: 12672950

Liu P, Lechtreck KF. 2018. The Bardet–Biedl syndrome protein complex is an adapter expanding the cargo range of intraflagellar transport trains for ciliary export. *Proceedings of the National Academy of Sciences* **115**:E934–E943. DOI: 10.1073/pnas.1713226115, PMID: 29339469

Liu Z, Tu H, Kang Y, Xue Y, Ma D, Zhao C, Li H, Wang L, Liu F. 2019. Primary cilia regulate hematopoietic stem and progenitor cell specification through Notch signaling in zebrafish. *Nature Communication* **10**:1839. DOI: 10.1038/s41467-019-09403-7, PMID: 31015398

Lobo GP, Fulmer D, Guo L, Zuo X, Dang Y, Kim SH, Su Y, George K, Obert E, Fogelgren B, Nihalani D, Norris RA, Rohrer B, Lipschutz JH. 2017. The exocyst is required for photoreceptor ciliogenesis and retinal development. *Journal of Biological Chemistry* **292**:14814–14826. DOI: 10.1074/jbc.M117.795674, PMID: 28729419

Loktev AV, Jackson PK. 2013. Neuropeptide Y family receptors traffic via the bardet-biedl syndrome pathway to signal in neuronal primary cilia. *Cell Reports* **5**:1316–1329. DOI: 10.1016/j.celrep.2013.11.011, PMID: 24316073

Loktev AV., Zhang Q, Beck JS, Searby CC, Scheetz TE, Bazan JF, Slusarski DC, Sheffield VC, Jackson PK, Nachury MV. 2008. A BBSome Subunit Links Ciliogenesis, Microtubule Stability, and Acetylation. *Dev Cell* **15**:854–865. DOI: 10.1016/j.devcel.2008.11.001, PMID: 19081074

Lord C, Ferro-Novick S, Miller EA. 2013. The highly conserved COPII coat complex sorts cargo from the endoplasmic reticulum and targets it to the Golgi. *Cold Spring Harbor Perspectives in Bioliogy* **5**:a013367. DOI: 10.1101/cshperspect.a013367, PMID: 23378591

Lu H, Toh MT, Narasimhan V, Thamilselvam SK, Choksi SP, Roy S. 2015. A function for the Joubert syndrome protein Arl13b in ciliary membrane extension and ciliary length regulation. *Development Bioliogy* **397**:225–236. DOI: 10.1016/j.ydbio.2014.11.009, PMID: 25448689

Lu Q, Insinna C, Ott C, Stauffer J, Pintado PA, Rahajeng J, Baxa U, Walia V, Cuenca A, Hwang YS, Daar IO, Lopes S, Lippincott-Schwartz J, Jackson PK, Caplan S, Westlake CJ. 2015. Early steps in primary cilium assembly require EHD1/EHD3-dependent ciliary vesicle formation. *Nature Cell Biology* **17**:531. DOI: 10.1038/ncb3155, PMID: 25812525

Lucker BF, Behal RH, Qin H, Siron LC, Taggart WD, Rosenbaum JL, Cole DG. 2005. Characterization of the intraflagellar transport complex B core: Direct interaction of the IFT81 and IFT74/72 subunits. *Journal of Biological Chemistry* **280**:27688–27696. DOI: 10.1074/jbc.M505062200, PMID: 15955805

Lukinavičius G, Reymond L, ĎEste E, Masharina A, Göttfert F, Ta H, Güther A, Fournier M, Rizzo S, Waldmann H, Blaukopf C, Sommer C, Gerlich DW, Arndt HD, Hell SW, Johnsson K. 2014. Fluorogenic probes for live-cell imaging of the cytoskeleton. *Nature Methods* **11**:731–3. DOI: 10.1038/nmeth.2972, PMID: 24859753

Ma W, Goldberg J. 2013. Rules for the recognition of dilysine retrieval motifs by coatomer. *The EMBO Journal* **32**:926–937. DOI: https://doi.org/10.1038/emboj.2013.41, PMID: 23481256

Malhotra V, Serafini T, Orci L, Shepherd JC, Rothman JE. 1989. Purification of a novel class of coated vesicles mediating biosynthetic protein transport through the Golgi stack. *Cell* **58**:329–36. DOI: https://doi.org/10.1016/0092-8674(89)90847-7, PMID: 2752426

Mastronarde DN. 2005. Automated electron microscope tomography using robust prediction of specimen movements. *Journal of Structural Biology* **152**:36–51. DOI: https://doi.org/10.1016/j.jsb.2005.07.007, PMID: 16182563

Matsuoka K, Orci L, Amherdt M, Bednarek SY, Hamamoto S, Schekman R, Yeung T. 1998. COPII-coated vesicle formation reconstituted with purified coat proteins and chemically defined liposomes. *Cell* **93**:263–275. DOI: https://doi.org/10.1016/s0092-8674(00)81577-9, PMID: 9568718

May SR, Ashique AM, Karlen M, Wang B, Shen Y, Zarbalis K, Reiter J, Ericson J, Peterson AS. 2005. Loss of the retrograde motor for IFT disrupts localization of Smo to cilia and prevents the expression of both activator and repressor functions of Gli. *Developmental Biology* **287**:378–389. DOI: https://doi.org/10.1016/j.ydbio.2005.08.050, PMID: 16229832

McMahon HT, Boucrot E. 2015. Membrane curvature at a glance. *Journal of Cell Science* **128**:1065–1070. DOI: https://doi.org/10.1242/jcs.114454, PMID: 25774051

Mesland DAM, Hoffman JL, Caligor E, Goodenough UW. 1980. Flagellar tip activation stimulated by membrane adhesions in chlamydomonas gametes. *The Journal of Cell Biology* **84**:599–617. DOI: https://doi.org/10.1083/jcb.84.3.599, PMID: 7358792

Mikhaylova M, Cloin BMC, Finan K, Berg RVD, Teeuw J, Kijanka MM, Sokolowski M, Katrukha EA, Maidorn M, Opazo F, Moutel S, Vantard M, Perez F, van Henegouwen PMPVBE, Hoogenraad CC, Ewers H, Kapitein LC. 2015. Resolving bundled microtubules using anti-tubulin nanobodies. *Nature Communication* **6**:7933. DOI: https://doi.org/10.1038/ncomms8933, PMID: 26260773

Milenkovic L, Weiss LE, Yoon J, Roth TL, Su YS, Sahl SJ, Scotta MP, Moerne WE. 2015. Single-molecule imaging of Hedgehog pathway protein Smoothened in primary cilia reveals binding events regulated by Patched1. *Proceedings of the National Academy of Sciences* **112**:8320–8325. DOI: https://doi.org/10.1073/pnas.1510094112, PMID: 26100903

Mill P, Lockhart PJ, Fitzpatrick E, Mountford HS, Hall EA, Reijns MAM, Keighren M, Bahlo M, Bromhead CJ, Budd P, Aftimos S, Delatycki MB, Savarirayan R, Jackson IJ, Amor DJ. 2011. Human and mouse mutations in WDR35 cause short-rib polydactyly syndromes due to abnormal ciliogenesis. *American Journal of Human Genetics* **88**:508–515. DOI: https://doi.org/10.1016/j.ajhg.2011.03.015,

PMID: 21473986

Miller E, Antonny B, Hamamoto S, Schekman R. 2002. Cargo selection into COPII vesicles is driven by the Sec24p subunit. *The EMBO Journal* **21**:6105–6113. DOI: https://doi.org/10.1093/emboj/cdf605, PMID: 12426382

Molla-Herman A, Ghossoub R, Blisnick T, Meunier A, Serres C, Silbermann F, Emmerson C, Romeo K, Bourdoncle P, Schmitt A, Saunier S, Spassky N, Bastin P, Benmerah A. 2010. The ciliary pocket: an endocytic membrane domain at the base of primary and motile cilia. *J Cell Sci* **123**:1785–1795. DOI: https://doi.org/10.1242/jcs.059519, PMID: 20427320

Mollet G, Silbermann F, Delous M, Salomon R, Antignac C, Saunier S. 2005. Characterization of the nephrocystin / nephrocystin-4 complex and subcellular localization of nephrocystin-4 to primary cilia and centrosomes. *Human Molecular Genetics* **14**:645–656. DOI: https://doi.org/10.1093/hmg/ddi061, PMID: 15661758

Montesano R. 1979. Inhomogeneous distribution of filipin-sterol complexes in the ciliary membrane of rat tracheal epithelium. *American Journal of Anatomy* **156**:139–145. DOI: https://doi.org/10.1002/aja.1001560115, PMID: 517447

Moritz OL, Tam BM, Hurd LL, Peränen J, Deretic D, Papermaster DS. 2001. Mutant rab8 Impairs docking and fusion of rhodopsin-bearing post-Golgi membranes and causes cell death of transgenic Xenopus rods. *Molecular Biology of the Cell* **12**:2341–2351. DOI: https://doi.org/10.1091/mbc.12.8.2341, PMID: 11514620

Morlot S, Galli V, Klein M, Chiaruttini N, Manzi J, Humbert F, Dinis L, Lenz M, Cappello G, Roux A. 2012. Membrane shape at the edge of the dynamin helix sets location and duration of the fission reaction. *Cell* **151**:619–629. DOI: http://doi.org/10.1016/j.cell.2012.09.017, PMID: 23101629

Moser JJ, Fritzler MJ, Rattner JB. 2009. Primary ciliogenesis defects are associated with human astrocytoma/glioblastoma cells. *BMC Cancer* **9**:1–12. DOI: http://doi.org/10.1186/1471-2407-9-448, PMID: 20017937

Mourão A, Christensen ST, Lorentzen E. 2016. The intraflagellar transport machinery in ciliary signaling. *Current Opinion in Structural Biology* **41**:98–108. DOI: http://doi.org/10.1016/j.sbi.2016.07.018, PMID: 27546002

Mukhopadhyay S, Wen X, Chih B, Nelson CD, Lane WS, Scales SJ, Jackson PK.

2010. TULP3 bridges the IFT-A complex and membrane phosphoinositides to promote trafficking of G protein-coupled receptors into primary cilia. *Genes and Development* **24**:2180–2193. DOI: http://doi.org/10.1101/gad.1966210, PMID: 20889716

Mukhopadhyay S, Wen X, Ratti N, Loktev A, Rangell L, Scales SJ, Jackson PK. 2013. The ciliary G-protein-coupled receptor Gpr161 negatively regulates the sonic hedgehog pathway via cAMP signaling. *Cell* **152**:210–223. DOI: http://doi.org/10.1016/j.cell.2012.12.026, PMID: 23332756

Musacchio A, Smith CJ, Roseman AM, Harrison SC, Kirchhausen T, Pearse BM. 1999. Functional organization of clathrin in coats: Combining electron cryomicroscopy and x-ray crystallography. *Molecular Cell* **3**:761–770. DOI: http://doi.org/10.1016/s1097-2765(01)80008-3, PMID: 10394364

Musgrave A, De WP, Van EI, Pijst H, Scholma C, Kooyman R, Homan W, Van D EH. 1986. Evidence for a functional membrane barrier in the transition zone between the flagellum and cell body of Chlamydomonas eugametos gametes. *Planta* **167**:544–553. DOI: http://doi.org/10.1007/BF00391231, PMID: 24240371

Myers BR, Sever N, Chong YC, Kim J, Belani JD, Rychnovsky S, Bazan JF, Beachy PA. 2013. Hedgehog Pathway Modulation by Multiple Lipid Binding Sites on the Smoothened Effector of Signal Response. *Development Cell* **26**:346–357. DOI: http://doi.org/10.1016/j.devcel.2013.07.015, PMID: 23954590

Mykytyn K, Mullins RF, Andrews M, Chiang AP, Swiderski RE, Yang B, Braun T, Casavant T, Stone EM, Sheffield VC. 2004. Bardet-Biedl syndrome type 4 (BBS4)-null mice implicate Bbs4 in flagella formation but not global cilia assembly. *Proceedings of the National Academy of Sciences* **101**:8664–8669. DOI: http://doi.org/10.1073/pnas.0402354101, PMID: 15173597

Nachtergaele S, Whalen DM, Mydock LK, Zhao Z, Malinauskas T, Krishnan K, Ingham PW, Covey DF, Siebold C, Rohatgi R. 2013. Structure and function of the Smoothened extracellular domain in vertebrate Hedgehog signaling. *eLIFE* **2**:e01340. DOI: http://doi.org/10.7554/eLife.01340, PMID: 24171105

Nachury MV, Loktev AV., Zhang Q, Westlake CJ, Peränen J, Merdes A, Slusarski DC, Scheller RH, Bazan JF, Sheffield VC, Jackson PK. 2007. A Core Complex

of BBS Proteins Cooperates with the GTPase Rab8 to Promote Ciliary Membrane Biogenesis. *Cell* **129**:1201–1213. DOI: http://doi.org/10.1016/j.cell.2007.03.053, PMID: 17574030

Nager AR, Goldstein JS, Herranz-Pérez V, Portran D, Ye F, Garcia-Verdugo JM, Nachury MV. 2017. An Actin Network Dispatches Ciliary GPCRs into Extracellular Vesicles to Modulate Signaling. *Cell* **168**:252-263.e14. DOI: http://doi.org/10.1016/j.cell.2016.11.036, PMID: 28017328

Nozaki S, Kotah Y, Tereda M, Mishisaka S, Funabashi T, Takahashi S, Kontani K, Nakayama K. 2017. Regulation of ciliary retrograde protein trafficking by Joubert syndrome proteins ARL13B and INPP5E. Journal of Cell Science. DOI: http://doi.org/10.1242/jcs.197004, PMID: 27927754

Nedelcu D, Liu J, Xu Y, Jao C, Salic A. 2013. Oxysterol binding to the extracellular domain of Smoothened in Hedgehog signaling. *Nature Chemical Biology* **9**:557–564. DOI: http://doi.org/10.1038/nchembio.1290, PMID: 23831757

Nielsen BS, Malinda RR, Schmid FM, Pedersen SF, Christensen ST, Pedersen LB. 2015. PDGFRβ and oncogenic mutant PDGFRα D842V promote disassembly of primary cilia through a PLCγ- and AURKA-dependent mechanism. *Journal of Cell Science* **128**:3543–3549. DOI: http://doi.org/10.1242/jcs.173559, PMID: 26290382

Nielsen JC, Nordgaard C, Tollenaere MAX, Bekker-Jensen S. 2018. Osmotic Stress Blocks Mobility and Dynamic Regulation of Centriolar Satellites. *Cells* **7**:65. DOI: http://doi.org/10.3390/cells7070065, PMID: 29932434

Niisslein-Volhard C, Wieschaus E. 1980. Mutations affecting segment number and polarity in Drosophila. *Nature* **287**:795–801. DOI: http://doi.org/10.1038/287795a0, PMID: 6776413

Nishijima Y, Hagiya Y, Kubo T, Takei R, Katoh Y, Nakayama K. 2017. RABL2 interacts with the intraflagellar transport-B complex and CEP19 and participates in ciliary assembly. *Molecular Biology of the Cell* **28**:1652–1666. DOI: http://doi.org/10.1091/mbc.E17-01-0017, PMID: 28428259

Noben-Trauth K, Naggert JK, North MA, Nishina PM. 1996. A candidate gene for the mouse mutation tubby. *Nature* **380**:534–538. DOI: http://doi.org/10.1038/380534a0, PMID: 8606774

Noble AJ, Zhang Q, O'Donnell J, Hariri H, Bhattacharya N, Marshall AG, Stagg SM. 2013. A Pseudo-Atomic Model of the COPII Cage Obtained from CryoEM and Mass Spectrometry Analyses. *Nature Structural and Molecular Biology* **20**:167–173. DOI: http://doi.org/10.1038/nsmb.2467, PMID: 23262493

Noda K, Kitami M, Kitami K, Kaku M, Komatsu Y. 2016. Canonical and noncanonical intraflagellar transport regulates craniofacial skeletal development. P*roceedings of the National Academy of Sciences* **113**:E2589–E2597. DOI: http://doi.org/10.1073/pnas.1519458113, PMID: 27118846

Norman RX, Ko HW, Huang V, Eun CM, Abler LL, Zhang Z, Sun X, Eggenschwiler JT. 2009. Tubby-like protein 3 (TULP3) regulates patterning in the mouse embryo through inhibition of Hedgehog signaling. *Human Molecular Genetics* **18**:1740–1754. DOI: http://doi.org/10.1093/hmg/ddp113, PMID: 19286674

Ocbina PJR, Eggenschwiler JT, Moskowitz IP, Anderson KV. 2011. Complex interactions between genes controlling trafficking in primary cilia. *Nature Genetics* **43**:547–553. DOI: http://doi.org/10.1038/ng.832, PMID: 21552265

Ocbina PJR, Tuson M, Anderson KV. 2009. Primary cilia are not required for normal canonical Wnt signaling in the mouse embryo. *PLoS One* **4**:e6839. DOI: http://doi.org/10.1371/journal.pone.0006839, PMID: 19718259

Odabasi E, Gul S, Kavakli IH, Firat-Karalar EN. 2019. Centriolar satellites are required for efficient ciliogenesis and ciliary content regulation. *EMBO Reports* **20**:e47723. DOI: http://doi.org/10.15252/embr.201947723, PMID: 31023719

Ohlemiller KK, Hughes RM, Mosinger-Ogilvie J, Speck JD, Grosof DH, Silverman MS. 1995. Cochlear and retinal degeneration in the tubby mouse. *Neuroreport* **6**:845–849. DOI: http://doi.org/10.1097/00001756-199504190-00005, PMID: 7612867

Omori Y, Zhao C, Saras A, Mukhopadhyay S, Kim W, Furukawa T, Sengupta P, Veraksa A, Malicki J. 2008. Elipsa is an early determinant of ciliogenesis that links the IFT particle to membrane-associated small GTPase Rab8. *Nature Cell Biology* **10**:437–444. DOI: http://doi.org/10.1038/ncb1706, PMID: 18364699

Pan J, Snell WJ. 2000. Signal transduction during fertilization in the unicellular green alga, Chlamydomonas. *Current Opinion in Microbiology* **3**:596–602. DOI: http://doi.org/10.1016/s1369-5274(00)00146-6, PMID: 11121779

Pan X, Ou G, Civelekoglu-Scholey G, Blacque OE, Endres NF, Tao L, Mogilner A, Leroux MR, Vale RD, Scholey JM. 2006. Mechanism of transport of IFT particles in C. elegans cilia by the concerted action of kinesin-II and OSM-3 motors. *The Journal of Cell Biology* **174**:1035–1045. DOI: http://doi.org/10.1083/jcb.200606003, PMID: 17000880

Paolo GD, Camilli PD. 2006. Phosphoinositides in cell regulation and membrane dynamics. *Nature* **443**:651–657. DOI: https://doi.org/10.1038/nature05185, PMID: 17035995

Park TJ, Mitchell BJ, Abitua PB, Kintner C, Wallingford JB. 2008. Dishevelled controls apical docking and planar polarization of basal bodies in ciliated epithelial cells. *Nature Genetics* **40**:871–879. DOI: http://doi.org/10.1038/ng.104, PMID: 18552847

Pastor-Cantizano N, García-Murria MJ, Bernat-Silvestre C, Marcote MJ, Mingarro I, Aniento F. 2017. N-Linked Glycosylation of the p24 Family Protein p24δ5 Modulates Retrograde Golgi-to-ER Transport of K/HDEL Ligands in Arabidopsis. *Molecular Plant* **10**:1095–1106. DOI: http://doi.org/10.1016/j.molp.2017.07.007, PMID: 28735024

Patterson VL, Damrau C, Paudyal A, Reeve B, Grimes DT, Stewart ME, Williams DJ, Siggers P, Greenfield A, Murdoch JN. 2009. Mouse hitchhiker mutants have spina bifida, dorso-ventral patterning defects and polydactyly: Identification of Tulp3 as a novel negative regulator of the Sonic hedgehog pathway. *Human Molecular Genetics* **18**:1719–1739. DOI: http://doi.org/10.1093/hmg/ddp075, PMID: 19223390

Pazour GJ, Dickert BL, Vucica Y, Seeley ES, Rosenbaum JL, Witman GB, Cole DG. 2000. Chlamydomonas IFT88 and Its Mouse Homologue , Polycystic Kidney Disease Gene Tg 737 , Are Required for Assembly of Cilia and Flagella. *The Journal of Cell Biology* **151**:709–718. DOI: http://doi.org/10.1083/jcb.151.3.709, PMID: 11062270

Pazour GJ, Dickert BL, Witman GB. 1999. The DHC1b (DHC2) isoform of cytoplasmic dynein is required for flagellar assembly. *The Journal of Cell Biology* **144**:473–481. DOI: http://doi.org/10.1083/jcb.144.3.473, PMID: 9971742

Pazour GJ, Rosenbaum JL. 2002. Intraflagellar transport and cilia-dependent

diseases. *Trends in Cell Biology* **12**:551–555. DOI: http://doi.org/ 10.1016/s0962-8924(02)02410-8, PMID: 12495842

Pazour GJ, Wilkerson CG, Witman GB. 1998. A dynein light chain is essential for the retrograde particle movement of intraflagellar transport (IFT). *The Journal of Cell Biology* **141**:979–992. DOI: http://doi.org/10.1083/jcb.141.4.979, PMID: 9585416

Pedersen LB, Geimer S, Rosenbaum JL. 2006. Dissecting the molecular mechanisms of intraflagellar transport in Chlamydomonas. *Current Biology* **16**:450–459. DOI: http://doi.org/10.1016/j.cub.2006.02.020, PMID: 16527740

Pedersen LB, Schrøder JM, Satir P, Christensen ST. 2012. The ciliary cytoskeleton. *Comprehensive Physiology* **2**:779–803. DOI: http://doi.org/10.1002/cphy.c110043, PMID: 23728985

Perrault I, Saunier S, Hanein S, Filhol E, Bizet AA, Collins F, Salih MAM, Gerber S, Delphin N, Bigot K, Orssaud C, Silva E, Baudouin V, Oud MM, Shannon N, Le Merrer M, Roche O, Pietrement C, Goumid J, Baumann C, Bole-Feysot C, Nitschke P, Zahrate M, Beales P, Arts HH, Munnich A, Kaplan J, Antignac C, Cormier-Daire V, Rozet J. 2012. Mainzer-saldino syndrome is a ciliopathy caused by IFT140 mutations. *American Journal of Human Genetics* **90**:864–870. DOI: http://doi.org/10.1016/j.ajhg.2012.03.006, PMID: 22503633

Pfeffer SR. 2017. Rab GTPases: Master regulators that establish the secretory and endocytic pathways. *Molecular Biology of the Cell* **28**:712–715. DOI: http://doi.org/10.1091/mbc.E16-10-0737, PMID: 28292916

Picariello T, Brown JM, Hou Y, Swank G, Cochran DA, King OD, Lechtreck K, Pazour GJ, Witman GB. 2019. A global analysis of IFT-A function reveals specialization for transport of membrane-associated proteins into cilia. *Journal of Cell Science* **132**:jcs220749. DOI: http://doi.org/10.1242/jcs.220749, PMID: 30659111

Pigino G, Geimer S, Lanzavecchia S, Paccagnini E, Cantele F, Diener DR, Rosenbaum JL, Lupetti P. 2009. Electron-tomographic analysis of intraflagellar transport particle trains in situ. *The Journal of Cell Biology* **187**:135–148. DOI: http://doi.org/10.1083/jcb.200905103, **PMID:** 19805633

Piperno G, Mead K. 1997. Transport of a novel complex in the cytoplasmic matrix of

Chlamydomonas flagella. *Proceedings of the National Academy of Sciences* **94**:4457–4462. DOI: http://doi.org/10.1073/pnas.94.9.4457, PMID: 9114011

Piperno G, Siuda E, Henderson S, Segil M, Vaananen H, Sassaroli M. 1998. Distinct mutants of retrograde intraflagellar transport (IFT) share similar morphological and molecular defects. *The Journal of Cell Biology* **143**:1591–1601. DOI: http://doi.org/10.1083/jcb.143.6.1591, PMID: 9852153

Porter ME, Bower R, Knott JA, Byrd P, Dentler W. 1999. Cytoplasmic Dynein Heavy Chain 1b Is Required for Flagellar Assembly in Chlamydomonas. *Molecular Biology of the Cell* **10**:693–712. DOI: http://doi.org/10.1091/mbc.10.3.693, PMID: 10069812

Prosseda PP, Luo N, Wang B, Alvarado JA, Hu Y, Sun Y. 2017. Loss of OCRL increases ciliary PI(4,5)P 2 in Lowe oculocerebrorenal syndrome. *J Cell Sci* **130**:3447–3454. DOI: http://doi.org/https://doi.org/10.1242/jcs.200857, PMID: 28871046

Pusapati GV, Kong JH, Patel BB, Krishnan A, Sagner A, Kinnebrew M, Briscoe J, Aravind L, Rohatgi R. 2018. CRISPR Screens Uncover Genes that Regulate Target Cell Sensitivity to the Morphogen Sonic Hedgehog. *Developmental Cell* **44**:113-129.e8. DOI: http://doi.org/10.1016/j.devcel.2017.12.003, PMID: 29290584

Qin H, Diener DR, Geimer S, Cole DG, Rosenbaum JL. 2004. Intraflagellar transport (IFT) cargo : IFT transports flagellar precursors to the tip and turnover products to the cell body. *Journal of Cell Biology* **164**:255–266. DOI: http://doi.org/https://doi.org/10.1083/jcb.200308132

Qin J, Lin Y, Norman RX, Ko HW, Eggenschwiler JT. 2011. Intraflagellar transport protein 122 antagonizes Sonic Hedgehog signaling and controls ciliary localization of pathway components. *Proceedings of the National Academy of Sciences* **108**:1456–1461. DOI: http://doi.org/10.1073/pnas.1011410108, PMID: 21209331

Qin S, Taglienti M, Nauli SM, Contrino L, Takakura A, Zhou J, Kreidberg JA. 2010. Failure to ubiquitinate c-Met leads to hyperactivation of mTOR signaling in a mouse model of autosomal dominant polycystic kidney disease. *The Journal of Clinical Investigation* **120**:3617–3628. DOI: http://doi.org/10.1172/JCI41531,

PMID: 20852388

Rai AK, Chen JX, Selbach M, Pelkmans L. 2018. Kinase-controlled phase transition of membraneless organelles in mitosis. *Nature* **559**:211–216. DOI: http://doi.org/10.1038/s41586-018-0279-8, PMID: 29973724

Rajagopalan V, D'Amico JP, Wilkes DE. 2013. Cytoplasmic dynein-2: From molecules to human diseases. *Frontiers in Biology* **8**:119–126. DOI: http://doi.org/10.1007/s11515-012-1242-y

Reiter JF, Blacque OE, Leroux MR. 2012. The base of the cilium: Roles for transition fibres and the transition zone in ciliary formation, maintenance and compartmentalization. *EMBO Reports*. DOI: http://doi.org/10.1038/embor.2012.73, PMID: 22653444

Reiter JF, Leroux MR. 2017. Genes and molecular pathways underpinning ciliopathies. *Nature Reviews Molecular Cell Biology* **18**:533–547. DOI: http://doi.org/10.1038/nrm.2017.60, PMID: 28698599

Ries J, Kaplan C, Platonova E, Eghlidi H, Ewers H. 2012. A simple, versatile method for GFP-based super-resolution microscopy via nanobodies. *Nature Methods* **9**:582–584. DOI: http://doi.org/10.1038/nmeth.1991, PMID: 22543348

Roberson EC, Dowdle WE, Ozanturk A, Garcia-gonzalo FR, Li C, Halbritter J, Elkhartoufi N, Porath JD, Cope H, Ashley-koch A, Gregory S, Thomas S, Sayer JA, Saunier S, Otto EA, Katsanis N, Davis EE, Attié-bitach T, Hildebrandt F, Leroux MR, Reiter JF. 2015. TMEM231, mutated in orofaciodigital and Meckel syndromes, organizes the ciliary transition zone. *Journal of Cell Biology* **209**:129–142. DOI: http://doi.org/10.1083/jcb.201411087, PMID: 25869670

Roberts AJ. 2018. Emerging mechanisms of dynein transport in the cytoplasm versus the cilium. *Biochemical Society Transactions* **46**:967–982. DOI: http://doi.org/10.1042/BST20170568, PMID: 30065109

Rogowski M, Scholz D, Geimer S. 2013. Electron microscopy of flagella, primary cilia, and intraflagellar transport in flat-embedded cells. Methods in Enzymology **524**:243-263 DOI: http://doi.org/10.1016/B978-0-12-397945-2.00014-7, PMID: 23498744

Rohatgi R, Milenkovic L, Scott MP. 2007. Patched1 Regulates Hedgehog Signaling at the Primary Cilium. *Science* 317:372–376. DOI:

http://doi.org/https://doi.org/10.1126/science.1139740, PMID: 17641202

Roosing S, Rohrschneider K, Beryozkin A, Sharon D, Weisschuh N, Staller J, Kohl S, Zelinger L, Peters TA, Neveling K, Strom TM, Van Den Born LI, Hoyng CB, Klaver CCW, Roepman R, Wissinger B, Banin E, Cremers FPM, Den Hollander AI. 2013. Mutations in RAB28, encoding a farnesylated small gtpase, are associated with autosomal-recessive cone-rod dystrophy. *Americal Journal of Human Genetics* **93**:110–117. DOI: http://doi.org/ doi:10.1016/j.ajhg.2013.05.005 10.1016/j.ajhg.2013.05.005, PMID: 23746546

Rosenbaum JL, Witman GB. 2002. Intraflagellar transport. *Nature Reviews Molecular Cell Biol* **3**:813–825. DOI: http://doi.org/10.1038/nrm952, PMID: 12415299

Roth MG. 2008. Phosphoinositides in Constitutive Membrane Traffic. *Physiological Review* **84**:699–730. DOI: http://doi.org/ 10.1152/physrev.00033.2003, PMID: 15269334

Roux C, Wolf C, Mulliez N, Gaoua W, Cormier V, Chevy F, Citadelle D. 2000. Role of cholesterol in embryonic development. *The American Journal of Clinical Nutrition* **71**:1270S-1279S. DOI: http://doi.org/ doi:10.1093/ajcn/71.5.1270s 10.1093/ajcn/71.5.1270s, PMID: 10799401

Sang L, Miller JJ, Corbit KC, Giles RH, Brauer MJ, Otto EA, Baye LM, Wen X, Scales SJ, Kwong M, Huntzicker EG, Sfakianos MK, Sandoval W, Bazan JF, Kulkarni P, Garcia-gonzalo FR, Seol AD, Toole JFO, Held S, Reutter HM, Lane WS, Rafiq MA, Noor A, Ansar M, Devi ARR, Sheffield VC, Slusarski DC, Vincent JB, Doherty DA, Hildebrandt F, Reiter JF, Jackson PK. 2011. Mapping the NPHP-JBTS-MKS Protein Network Reveals Ciliopathy Disease Genes and Pathways. *Cell* **145**:513–528. DOI: http://doi.org/10.1016/j.cell.2011.04.019, PMID: 21565611

Scheidel N, Blacque OE. 2018. Intraflagellar Transport Complex A Genes Differentially Regulate Cilium Formation and Transition Zone Gating. *Current Biology* **28**:3279-3287.e2. DOI: http://doi.org/10.1016/j.cub.2018.08.017, PMID: 30293716

Schledzewski K, Brinkmann H, Mendel RR. 1999. Phylogenetic analysis of

components of the eukaryotic vesicle transport system reveals a common origin of adaptor protein complexes 1, 2, and 3 and the F subcomplex of the coatomer COPI. *Journal of Molecular Evolution* **48**:770–778. DOI: http://doi.org/doi:10.1007/PL00006521 10.1007/pl00006521, PMID: 10229581

Schmidt H, Zalyte R, Urnavicius L, Carter AP. 2015. Structure of human cytoplasmic dynein-2 primed for its power stroke. *Nature* **518**:435–438. DOI: http://doi.org/10.1038/nature14023, PMID: 25470043

Schmidt KN, Kuhns S, Neuner A, Hub B, Zentgraf H, Pereira G. 2012. Cep164 mediates vesicular docking to the mother centriole during early steps of ciliogenesis. *The Journal of Cell Biology* **199**:1083–1101. DOI: http://doi.org/10.1083/jcb.201202126, PMID: 23253480

Schneider L, Cammer M, Lehman J, Nielsen SK, Guerra CF, Veland IR, Stock C, Hoffmann EK, Yoder BK, Schwab A, Satir P, Christensen ST. 2010. Directional cell migration and chemotaxis in wound healing response to PDGF-AA are coordinated by the primary cilium in fibroblasts. *Cellular Physiology and Biochemistry* **25**:279–292. DOI: http://doi.org/10.1159/000276562, PMID: 20110689

Schneider L, Clement CA, Teilmann SC, Pazour GJ, Hoffmann EK, Satir P, Christensen ST. 2005. PDGFRαα signaling is regulated through the primary cilium in fibroblasts. *Current Biology* **15**:1861–1866. DOI: http://doi.org/10.1016/j.cub.2005.09.012, PMID: 16243034

Schweizer A, Fransen JA, Bächi T, Ginsel L, Hauri HP. 1988. Identification, by a monoclonal antibody, of a 53-kD protein associated with a tubulo-vesicular compartment at the cis-side of the Golgi apparatus. *The Journal of Cell Biology* **107**:1643–1653. DOI: http://doi.org/10.1083/jcb.107.5.1643, PMID: 3182932

Sedmak T, Wolfrum U. 2010. Intraflagellar transport molecules in ciliary and nonciliary cells of the retina. *The Journal of Cell Biology* **189**:171–186. DOI: http://doi.org/10.1083/jcb.200911095, PMID: 20368623

Seeley ES, Carrière C, Goetze T, Longnecker DS, Korc M. 2009. Pancreatic cancer and precursor pancreatic intraepithelial neoplasia lesions are devoid of primary cilia. *Cancer Research* **69**:422–430. DOI: http://doi.org/10.1158/0008-5472.CAN-08-1290, PMID: 19147554

Seki Y, Miyasaka Y, Suzuki S, Wada K, Yasuda SP, Matsuoka K, Ohshiba Y, Endo K, Ishii R, Shitara H, Kitajiri S ichiro, Nakagata N, Takebayashi H, Kikkawa Y. 2017. A novel splice site mutation of myosin VI in mice leads to stereociliary fusion caused by disruption of actin networks in the apical region of inner ear hair cells. *PLoS One* **12**:e0183477. DOI: http://doi.org/10.1371/journal.pone.0183477, PMID: 28832620

Seo S, Baye LM, Schulz NP, Beck JS, Zhang Q, Slusarski DC, Sheffield VC. 2010. BBS6, BBS10, and BBS12 form a complex with CCT/TRiC family chaperonins and mediate BBSome assembly. *Proceedings of the National Academy of Sciences* **107**:1488–1493. DOI: http://doi.org/10.1073/pnas.0910268107, PMID: 20080638

Serafini T, Stenbeck G, Brecht A, Lottspeich F, Orci L, Rothman JE, Wieland FT. 1991. A coat subunit of Golgi-derived non-clathrin-coated vesicles with homology to the clathrin-coated vesicle coat protein β-adaptin. *Nature* **349**:215–220. DOI: http://doi.org/10.1038/349215a0, PMID: 1898984

Sever N, Mann RK, Xu L, Snell WJ, Hernandez-lara CI, Porter NA, Beachy PA. 2016. Endogenous B-ring oxysterols inhibit the Hedgehog component Smoothened in a manner distinct from cyclopamine or side-chain oxysterols. *Proceedings of the National Academy of Sciences* **113**:5904–5909. DOI: http://doi.org/10.1073/pnas.1604984113, PMID: 27162362

Shi X, Garcia GIII, Van De Weghe JC, McGorty R, Pazour GJ, Doherty D, Huang B, Reiter JF. 2017. Super-resolution microscopy reveals that disruption of ciliary transition-zone architecture causes Joubert syndrome. *Nature Cell Biology* **19:**1178-1188. DOI: http://doi.org/10.1038/ncb3599, PMID: 28846093

Shibata Y, Hu J, Kozlov MM, Rapoport TA. 2009. Mechanisms Shaping the Membranes of Cellular Organelles. *Annual Review of Cell Developmental Biol*ogy **25**:329–354. DOI: http://doi.org/10.1146/annurev.cellbio.042308.113324

Shida T, Cueva JG, Xu Z, Goodman MB, Nachury M V. 2010. The major α-tubulin K40 acetyltransferase α TAT1 promotes rapid ciliogenesis and efficient mechanosensation. *Proceedings of the National Academy of Sciences* **107**:21517–21522. DOI: https://doi.org/10.1073/pnas.1013728107

Shillingford JM, Murcia NS, Larson CH, Low SH, Hedgepeth R, Brown N, Flask CA, Novick AC, Goldfarb DA, Kramer-Zucker A, Walz G, Piontek KB, Germino GG, Weimbs T. 2006. The mTOR pathway is regulated by polycystin-1, and its inhibition reverses renal cystogenesis in polycystic kidney disease. *Proceedings of the National Academy of Sciences* **103**:5466–5471. DOI: http://doi.org/10.1073/pnas.0509694103, PMID: 16567633

Signor D, Wedatman KP, Orozco JT, Dwyer ND, Bargmann CI, Rose LS, Scholey JM. 1999. Role of a class DHC1b dynein in retrograde transport of IFT motors and IFT raft particles along cilia, but not dendrites, in chemosensory neurons of living Caenorhabditis elegans. *The Journal of Cell Biology* **147**:519–530. DOI: http://doi.org/10.1083/jcb.147.3.519, PMID: 10545497

Siljee JE, Wang Y, Bernard AA, Ersoy BA, Zhang S, Marley A, Zastrow MV, Reiter JF, Vaisse C. 2018. Subcellular localization of MC4R with ADCY3 at neuronal primary cilia underlies a common pathway for genetic predisposition to obesity. *Nature Genetics* **50**:180–185. DOI: http://doi.org/10.1038/s41588-017-0020-9, PMID: 29311635

Silva-Alvim FAL, An J, Alvim JC, Foresti O, Grippa A, Pelgrom A, Adams TL, Hawes C, Denecke J. 2018. Predominant golgi residency of the plant K/HDEL receptor is essential for its function in mediating ER retention. *Plant Cell* **30**:2174–2196. DOI: http://doi.org/10.1105/tpc.18.00426, PMID: 30072420

Simons M, Gloy J, Ganner A, Bullerkotte A, Bashkurov M, Krönig C, Schermer B, Benzing T, Cabello OA, Jenny A, Mlodzik M, Polok B, Driever W, Obara T, Walz G. 2005. Inversin, the gene product mutated in nephronophthisis type II, functions as a molecular switch between Wnt signaling pathways. *Nature Genetics* **37**:537–543. DOI: http://doi.org/10.1038/ng1552, PMID: 158520

Skoda AM, Simovic D, Karin V, Kardum V, Vranic S, Serman L. 2018. The role of the Hedgehog signaling pathway in cancer: A comprehensive review. *Bosnian Journal of Basic Medical Sciences* **18**:8–20. DOI: http://doi.org/10.17305/bjbms.2018.2756, PMID: 29274272

Song P, Dudinsky L, Fogerty J, Gaivin R, Perkins BD. 2016. Arl13b interacts with vangl2 to regulate cilia and photoreceptor outer segment length in zebrafish. *Investigative Ophthalmology Visual Science* **57**:4517–4526. DOI: http://doi.org/

10.1167/iovs.16-19898, PMID: 27571019

Sorokin S. 1962. Centrioles and the Formation of Rudimentry Cilia by Fibroblasts and Smooth Muscle Cells. *The Journal of Cell Biology* **15**:363–377. DOI: http://doi.org/10.1083/jcb.15.2.363, PMID: 13978319

Sorusch N, Wunderlich K, Bauss K, Nagel-Wolfrum K, Wolfrum U. 2014. Usher syndrome protein network functions in the retina and their relation to other retinal ciliopathies. *Retinal Degerative Deseases. Advances in Experimental Medicine and Biology* **801**:527–533. DOI: http://doi.org/10.1007/978-1-4614-3209-8_67, PMID: 24664740

Spektor A, Tsang WY, Khoo D, Dynlacht BD. 2007. Cep97 and CP110 Suppress a Cilia Assembly Program. *Cell* **130**:678–690. DOI: http://doi.org/10.1016/j.cell.2007.06.027, PMID: 17719545

Stagg SM, Gürkan C, Fowler DM, LaPointe P, Foss TR, Potter CS, Carragher B, Balch WE. 2006. Structure of the Sec13/31 COPII coat cage. *Nature* **439**:234–238. DOI: http://doi.org/10.1038/nature04339, PMID: 16407955

Stagg SM, LaPointe P, Razvi A, Gürkan C, Potter CS, Carragher B, Balch WE. 2008. Structural Basis for Cargo Regulation of COPII Coat Assembly. *Cell* **134**:474–484. DOI: http://doi.org/10.1016/j.cell.2008.06.024, PMID: 18692470

Starks RD, Beyer AM, Guo DF, Boland L, Zhang Q, Sheffield VC, Rahmouni K. 2015. Regulation of Insulin Receptor Trafficking by Bardet Biedl Syndrome Proteins. *PLoS Genet* **11**:e1005311. DOI: http://doi.org/10.1371/journal.pgen.1005311, PMID: 26103456

Stasiulewicz M, Gray SD, Mastromina I, Silva JC, Björklund M, Seymour PA, Booth D, Thompson C, Green RJ, Hall EA, Serup P, Dale JK. 2015. A conserved role for Notch signaling in priming the cellular response to Shh through ciliary localisation of the key Shh transducer Smo. *Development* **142**:2291–2303. DOI: http://doi.org/10.1242/dev.125237, PMID: 25995356

Stenmark H. 2009. Rab GTPases as coordinators of vesicle traffic. *Nature Reviews Molecular Cell Biology* **10**:513–525. DOI: http://doi.org/10.1038/nrm2728, PMID: 19603039

Stepanek L, Pigino G. 2017. Millisecond time resolution correlative light and electron microscopy for dynamic cellular processes. *Methods in Cell Biology* **140**:1–20.

DOI: http://doi.org/10.1016/bs.mcb.2017.03.003, PMID: 28528628

Stepanek L, Pigino G. 2016. Microtubule doublets are double-track railways for intraflagellar transport trains. *Science* **352**:721–724. DOI: http://doi.org/10.1126/science.aaf4594, PMID: 27151870

Su X, Driscoll K, Yao G, Raed A, Wu M, Beales PL, Zhou J. 2014. Bardet-Biedl syndrome proteins 1 and 3 regulate the ciliary trafficking of polycystic kidney disease 1 protein. *Human Molecular Genetics* **23**:5441–5451. DOI: http://doi.org/10.1093/hmg/ddu267, PMID: 24939912

Sugiyama N, Tsukiyama T, Yamaguchi TP, Yokoyama T. 2011. The canonical Wnt signaling pathway is not involved in renal cyst development in the kidneys of inv mutant mice. *Kidney International* **79**:957–965. DOI: http://doi.org/10.1038/ki.2010.534, PMID: 21248711

Sun X, Haley J, Bulgakov OV, Cai X, McGinnis J, Li T. 2012. Tubby is required for trafficking G protein-coupled receptors to neuronal cilia. *Cilia* **1**:21. DOI: http://doi.org/10.1186/2046-2530-1-21, PMID: 23351594

Tabarés-Seisdedos R, Rubenstein JL. 2009. Chromosome 8p as a potential hub for developmental neuropsychiatric disorders: Implications for schizophrenia, autism and cancer. *Molecular Psychiatry* **14**:563–589. DOI: http://doi.org/10.1038/mp.2009.2, PMID: 19204725

Takahara M, Katoh Y, Nakamura K, Hirano T, Sugawa M, Tsurumi Y, Nakayama K. 2018. Ciliopathy-associated mutations of IFT122 impair ciliary protein trafficking but not ciliogenesis. *Human Molecular Genetics* **27**:516–528. DOI: http://doi.org/ https://doi.org/10.1093/hmg/ddx421, PMID: 29220510

Takao D, Dishinger JF, Kee HL, Pinskey JM, Allen BL, Verhey KJ. 2014. An assay for clogging the ciliary pore complex distinguishes mechanisms of cytosolic and membrane protein entry. *Current Biol* **24**:2288–2294. DOI: http://doi.org/10.1016/j.cub.2014.08.012, PMID: 25264252

Tanos BE, Yang HJ, Soni R, Wang WJ, Macaluso FP, Asara JM, Tsou MFB. 2013. Centriole distal appendages promote membrane docking, leading to cilia initiation. *Genes and Development* **27**:163–168. DOI: http://doi.org/10.1101/gad.207043.112, PMID: 23348840

Taschner M, Bhogaraju S, Lorentzen E. 2012. Architecture and function of IFT

complex proteins in ciliogenesis. *Differentiation* **83**:S12–S22. DOI: http://doi.org/10.1016/j.diff.2011.11.001, PMID: 22118932

Taschner M, Kotsis F, Braeuer P, Kuehn EW, Lorentzen E. 2014. Crystal structures of IFT70/52 and IFT52/46 provide insight into intraflagellar transport B core complex assembly. *The Journal of Cell Biology* **207**:269–282. DOI: http://doi.org/10.1083/jcb.201408002, PMID: 25349261

Taschner M, Lorentzen A, Mourão A, Collins T, Freke GM, Moulding D, Basquin J, Jenkins D, Lorentzen E. 2018. Crystal structure of intraflagellar transport protein 80 reveals a homo-dimer required for ciliogenesis. *eLIFE* **7**:e33067. DOI: http://doi.org/10.7554/eLife.33067, PMID: 29658880

Taschner M, Weber K, Mourão A, Vetter M, Awasthi M, Stiegler M, Bhogaraju S, Lorentzen E. 2016. Intraflagellar transport proteins 172, 80, 57, 54, 38, and 20 form a stable tubulin-binding IFT-B2 complex. *The EMBO Journal* **35**:773-790. DOI: https://doi.org/10.15252/embj.201593164, PMID: 26912722

Thomas S, Wright KJ, Corre S Le, Micalizzi A, Romani M, Abhyankar A, Saada J, Perrault I, Amiel J, Litzler J, Filhol E, Elkhartoufi N, Kwong M, Casanova JL, Boddaert N, Baehr W, Lyonnet S, Munnich A, Burglen L, Chassaing N, Encha-Ravazi F, Vekemans M, Gleeson JG, Valente EM, Jackson PK, Drummond IA, Saunier S, Attié-Bitach T. 2014. A Homozygous PDE6D Mutation in Joubert Syndrome Impairs Targeting of Farnesylated INPP5E Protein to the Primary Cilium. *Human Mutation* **35**:137–146. DOI: http://doi.org/10.1002/humu.22470, PMID: 24166846

Tobin JL, Beales PL. 2008. Restoration of renal function in zebrafish models of ciliopathies. *Pediatric Nephrology* **23**:2095–2099. DOI: http://doi.org/10.1007/s00467-008-0898-7, PMID: 18604564

Tollenaere MAX, Mailand N, Bekker-Jensen S. 2015. Centriolar satellites: Key mediators of centrosome functions. *Cellular and Molecular Life Sciences* **72**:11–23. DOI: http://doi.org/10.1007/s00018-014-1711-3, PMID: 25173771

Toriyama M, Lee C, Taylor SP, Duran I, Cohn DH, Bruel A, Tabler JM, Drew K, Kelly MR, Kim S, Park TJ, Braun D, Pierquin G, Biver A, Wagner K, Malfroot A, Panigrahi I, Franco B, Al-lami HA, Yeung Y, Choi YJ, Duffourd Y, Faivre L, Rivière JB, Chen J, Liu KJ, Marcotte EM, Hildebrandt F, Thauvin-Robinet C,

Krakow D, Jackson PK, Wallingford JB. 2016. The ciliopathy-associated CPLANE proteins direct basal body recruitment of intraflagellar transport machinery. *Nature Genetics* **48**:648–656. DOI: http://doi.org/ doi:10.1038/ng.3558 10.1038/ng.3558, PMID: 27158779

Toropova K, Zalyte R, Mukhopadhyay AG, Mladenov M, Carter AP, Roberts AJ. 2019. Structure of the dynein-2 complex and its assembly with intraflagellar transport trains. *Nature Structural and Molecular Biology* **26**:823–829. DOI: http://doi.org/10.1038/s41594-019-0286-y, PMID: 31451806

Tran PV, Haycraft CJ, Besschetnova TY, Turbe-Doan A, Stottmann RW, Herron BJ, Chesebro AL, Qiu H, Scherz PJ, Shah JV, Yoder BK, Beier DR. 2008. THM1 negatively modulates mouse sonic hedgehog signal transduction and affects retrograde intraflagellar transport in cilia. *Nature Genetics* **40**:403–410. DOI: http://doi.org/10.1038/ng.105, PMID: 18327258

Tsang WY, Bossard C, Khanna H, Peranen J, Swaroop A, Malhotra V, Dynlacht BD. 2008. CP110 Suppresses Primary Cilia Formation through its Interaction with CEP290, a Protein Deficient in Human Ciliary Disease. *Development Cell* **15**:187–197. DOI: http://doi.org/10.1016/j.devcel.2008.07.004, PMID: 18694559

Tsao C, Gorovsky MA. 2008. Different Effects of Tetrahymena IFT172 Domains on Anterograde and Retrograde Intraflagellar Transport. *Molecular Biology of the Cell* **19**:1450–1461. DOI: http://doi.org/10.1091/mbc.E07-05-0403, PMID: 18199688

Turriziani B, Garcia-Munoz A, Pilkington R, Raso C, Kolch W, Kriegsheim AV. 2014. On-Beads Digestion in Conjunction with Data-Dependent Mass Spectrometry: A Shortcut to Quantitative and Dynamic Interaction Proteomics. *Biology (Basel)* **3**:320–332. DOI: http://doi.org/10.3390/biology3020320, PMID: 24833512

Tyler KM, Fridberg A, Toriello KM, Olson CL, Cieslak JA, Hazlett TL, Engman DM. 2009. Flagellar membrane localization via association with lipid rafts. *Journal of Cell Science* **122**:859–866. DOI: http://doi.org/10.1242/jcs.037721, PMID: 19240119

Uytingco CR, Williams CL, Xie C, Shively DT, Green WW, Ukhanov K, Zhang L,

Nishimura DY, Sheffield VC, Martens JR. 2019. BBS4 is required for IFT coordination and basal body number in mammalian olfactory cilia. *Journal of Cell Science* **132**:jcs222331. DOI: https://doi.org/10.1242/jcs.222331, PMID: 30665891

Valente EM, Logan CV, Mougou-Zerelli S, Lee JH, Silhavy JL, Brancati F, Iannicelli M, Travaglini L, Romani S, Illi B, Adams M, Szymanska K, Mazzotta A, Lee JE, Tolentino JC, Swistun D, Salpietro CD, Fede C, Gabriel S, Russ C, Cibulskis K, Sougnez C, Hildebrandt F, Otto EA, Held S, Diplas BH, Davis E, Mikula M, Strom CM, Ben-Ze'ev B, Lev D, Sagie TL, Michelson M, Yaron Y, Krause A, Boltshauser E, Elkhartoufi N, Roume J, Shalev S, Munnich A, Saunier S, Inglehearn C, Saad A, Alkindy A, Thomas S, Vekemans M, Dallapiccola B, Katsanis N, Johnson CA, Attié-Bitach T, Gleeson JG. 2010. Mutations in TMEM216 perturb ciliogenesis and cause Joubert, Meckel and related syndromes. *Nature Genetics* **42**:619–625. DOI: http://doi.org/10.1038/ng.594, PMID: 20512146

Varjosalo M, Taipale J. 2008. Hedgehog: Functions and mechanisms. *Genes and Development* **22**:2454–2472. DOI: http://doi.org/10.1101/gad.1693608, PMID: 18794343

Verhey KJ, Dishinger J, Kee HL. 2011. Kinesin Motors and Primary Cilia. *Biochemical Society Transactions* **39**:1120–1125. DOI: http://doi.org/doi:10.1042/BST0391120. 10.1042/BST0391120, PMID: 21936775

Vetter M, Wang J, Lorentzen E, Deretic D. 2015. Novel topography of the rab 11-effector interaction network within a ciliary membrane targeting complex. *Small GTPases* **6**:165–173. DOI: http://doi.org/10.1080/21541248.2015.1091539, PMID: 26399276

Villumsen BH, Danielsen JR, Povlsen L, Sylvestersen KB, Merdes A, Beli P, Yang YG, Choudhary C, Nielsen ML, Mailand N, Bekker-Jensen S. 2013. A new cellular stress response that triggers centriolar satellite reorganization and ciliogenesis. *The EMBO Journal* **32**:3029–3040. DOI: http://doi.org/10.1038/emboj.2013.223, PMID: 24121310

Wallingford JB, Rowning BA, Vogell KM, Rothbächer U, Fraser SE, Harland RM. 2000. Dishevelled controls cell polarity during Xenopus gastrulation. *Nature*

405:81–85. DOI: http://doi.org/10.1038/35011077, PMID: 10811222

Wang B, Fallon JF, Beachy PA. 2000. Hedgehog-Regulated Processing of Gli3 Produces an Anterior / Posterior Repressor Gradient in the Developing Vertebrate Limb. *Cell* **100**:423–434. DOI: http://doi.org/ 10.1016/s0092-8674(00)80678-9, PMID: 10693759

Wang J, Deretic D. 2014. Molecular complexes that direct rhodopsin transport to primary cilia. *Progress in Retinal and Eye Research* **38**:1-19. DOI: http://doi.org/10.1016/j.preteyeres.2013.08.004, PMID: 24135424

Wang L, Lee K, Malonis R, Sanchez I, Dynlacht BD. 2016. Tethering of an E3 ligase by PCM1 regulates the abundance of centrosomal KIAA0586/Talpid3 and promotes ciliogenesis. *eLIFE* **5**:e12950. DOI: http://doi.org/10.7554/eLife.12950, PMID: 27146717

Wang Q, Taschner M, Ganzinger KA, Kelley C, Villasenor A, Heymann M, Schwille P, Lorentzen E, Mizuno N. 2018. Membrane association and remodeling by intraflagellar transport protein IFT172. *Nature Communication* **9**:4684. DOI: http://doi.org/10.1038/s41467-018-07037-9, PMID: 30409972

Wang Z, Fan ZC, Williamson SM, Qin H. 2009. Intraflagellar transport (IFT) protein IFT25 is a phosphoprotein component of IFT complex B and physically interacts with IFT27 in Chlamydomonas. *PLoS One* **4**.e5384. DOI: http://doi.org/10.1371/journal.pone.0005384, PMID: 19412537

Waters AM, Beales PL. 2011. Ciliopathies: An expanding disease spectrum. *Pediatric Nephrology* **26**:1039–1056. DOI: http://doi.org/10.1007/s00467-010-1731-7, PMID: 21210154

Wei LH, Arastoo M, Georgiou I, Manning DR, Galdo NAR. 2018. Activation of the Gi protein-RHOA axis by non-canonical Hedgehog signaling is independent of primary cilia. *PLoS One* **13**: e0203170. DOI: https://doi.org/10.1371/journal.pone.0203170, PMID: 30148884

Wei Q, Zhang Y, Li Y, Zhang Q, Ling K, Hu J. 2012. The BBSome controls IFT assembly and turnaround in cilia. *Nature Cell Biology* **14**:950–957. DOI: http://doi.org/10.1038/ncb2560, PMID: 22922713

Wells JN, Gligoris TG, Nasmyth KA, Marsh JA. 2017. Evolution of condensin and cohesin complexes driven by replacement of Kite by Hawk proteins. *Current*

Biology **27**:R17–R18. DOI: http://doi.org/10.1016/j.cub.2016.11.050, PMID: 28073014

Wells JN, Marsh JA. 2019. A Graph-Based Approach for Detecting Sequence Homology in Highly Diverged Repeat Protein Families. *Computational Methods in Protein Evolution. Methods in Molecular Biology* **1851**:251–261. DOI: http://doi.org/10.1007/978-1-4939-8736-8_13, PMID: 30298401

Wheway G, Abdelhamed Z, Natarajan S, Toomes C, Inglehearn C, Johnson CA. 2013. Aberrant Wnt signalling and cellular over-proliferation in a novel mouse model of Meckel-Gruber syndrome. *Developmental Biology* **377**:55–66. DOI: http://doi.org/10.1016/j.ydbio.2013.02.015, PMID: 23454480

Wheway G, Mitchison HM. 2019. Opportunities and challenges for molecular understanding of ciliopathies–the 100,000 genomes project. *Frontiers in Genetics* **10**:127. DOI: http://doi.org/10.3389/fgene.2019.00127, PMID: 30915099

Williams CL, Li C, Kida K, Inglis PN, Mohan S, Semenec L, Bialas NJ, Stupay RM, Chen N, Blacque OE, Yoder BK, Leroux MR. 2011. MKS and NPHP modules cooperate to establish basal body/transition zone membrane associations and ciliary gate function during ciliogenesis. *Journal of Cell Biology* **192**:1023–1041. DOI: http://doi.org/10.1083/jcb.201012116, PMID: 21422230

Williams CL, McIntyre JC, Norris SR, Jenkins PM, Zhang L, Pei Q, Verhey K, Martens JR. 2014. Direct evidence for BBSome-associated intraflagellar transport reveals distinct properties of native mammalian cilia. *Nature Communications* **5**:5813. DOI: http://doi.org/10.1038/ncomms6813, PMID: 25504142

Williamson SM, Silva DA, Richey E, Qin H. 2012. Probing the role of IFT particle complex A and B in flagellar entry and exit of IFT-dynein in Chlamydomonas. *Protoplasma* **249**:851–856. DOI: http://doi.org/10.1007/s00709-011-0311-4, PMID: 21853389

Wloga D, Joachimiak E, Louka P, Gaertig J. 2017. Posttranslational modifications of Tubulin and cilia. *Cold Spring Harbor Perspective Biology* **9:**piia028159. DOI: http://doi.org/10.1101/cshperspect.a028159, PMID: 28003186

Wong SY, Seol AD, So PL, Ermilov AN, Bichakjian CK, Epstein EH, Dlugosz AA, Reiter JF. 2009. Primary cilia can both mediate and suppress Hedgehog pathway-

dependent tumorigenesis. *Nature Medicine* **15**:1055–1061. DOI: http://doi.org/10.1038/nm.2011, PMID: 19701205

Wood CR, Rosenbaum JL. 2014. Proteins of the ciliary axoneme are found on cytoplasmic membrane vesicles during growth of cilia. *Current Biology* **24**:1114–1120. DOI: http://doi.org/10.1016/j.cub.2014.03.047, PMID: 24814148

Wood CR, Wang Z, Diener D, Zones JM, Rosenbaum J, Umen JG. 2012. IFT proteins accumulate during cell division and localize to the cleavage furrow in chlamydomonas. *PLoS One* **7**:e30729 DOI: http://doi.org/10.1371/journal.pone.0030729, PMID: 22328921

Xu L, Mirnics K, Bowman AB, Liu W, Da J, Porter N, Korade Z. 2012. DHCEO accumulation is a critical mediator of pathophysiology in a Smith – Lemli – Opitz syndrome model. *Neurobiology of Disease* **45**:923–929. DOI: http://doi.org/10.1016/j.nbd.2011.12.011, PMID: 22182693

Xu Q, Zhang Y, Wei Q, Huang Y, Li Y, Ling K, Hu J. 2015. BBS4 and BBS5 show functional redundancy in the BBSome to regulate the degradative sorting of ciliary sensory receptors. *Scientific Reports* **5**:11855. DOI: http://doi.org/10.1038/srep11855, PMID: 26150102

Xu S, Liu Y, Meng Q, Wang B. 2018. Rab34 small GTPase is required for Hedgehog signaling and an early step of ciliary vesicle formation in mouse. *Journal of Cell Science* **131**:jcs213710. DOI: http://doi.org/10.1242/jcs.213710, PMID: 30301781

Yakulov TA, Yasunaga T, Ramachandran H, Engel C, Mu B, Hoff S. 2015. Anks3 interacts with nephronophthisis proteins and is required for normal renal development. *Kidney International* **87**:1191–1200. DOI: http://doi.org/10.1038/ki.2015.17, PMID: 25671767

Ye F, Nager AR, Nachury MV. 2018. BBSome trains remove activated GPCRs from cilia by enabling passage through the transition zone. *The Journal of Cell Biology* **217**:1847–1868. DOI: http://doi.org/10.1083/jcb.201709041, PMID: 29483145

Yee LE, Garcia-gonzalo FR, Bowie RV, Li C, Kennedy JK, Ashrafi K, Blacque OE, Leroux MR, Reiter JF. 2015. Conserved Genetic Interactions between Ciliopathy Complexes Cooperatively Support Ciliogenesis and Ciliary Signaling. *PLoS Genet* **11**:e1005627. DOI: http://doi.org/10.1371/journal.pgen.1005627,

PMID: 26540106

Yoder BK, Hou X, Guay-Woodford LM. 2002. The polycystic kidney disease proteins, polycystin-1, polycystin-2, polaris, and cystin, are co-localized in renal cilia. *Journal of American Society of Nephrology* **13**:2508–2516. DOI: http://doi.org/10.1097/01.asn.0000029587.47950.25, PMID: 12239239

Yoshimura S, Egerer J, Fuchs E, Haas AK, Barr FA. 2007. Functional dissection of Rab GTPases involved in primary cilium formation. *The Journal of Cell Biology* **178**:363–369. DOI: http://doi.org/10.1083/jcb.200703047, PMID: 17646400

Yu X, Breitman M, Goldberg J. 2012. A Structure-based mechanism for Arf1-dependent recruitment of coatomer to membranes. *Cell* **148**:530–542. DOI: http://doi.org/10.1016/j.cell.2012.01.015, PMID: 22304919

Yuan K, Frolova N, Xie Y, Wang D, Cook L, Kwon YJ, Steg AD, Serra R, Frost AR. 2010. Primary cilia are decreased in breast cancer: Analysis of a collection of human breast cancer cell lines and tissues. *Journal of Histochemistry and Cytochemistry* **58**:857–870. DOI: http://doi.org/10.1369/jhc.2010.955856, PMID: 20530462

Yuan X, Cao J, He X, Serra R, Qu J, Cao X, Yang S. 2016. Ciliary IFT80 balances canonical versus non-canonical hedgehog signalling for osteoblast differentiation. *Nature Communications* **7**:11024. DOI: http://doi.org/10.1038/ncomms11024, PMID: 26996322

Zaghloul NA, Katsanis N. 2009. Mechanistic insights into Bardet-Biedl syndrome, a model ciliopathy. *The Journal of Clinical Investigation* **119**:428–437. DOI: http://doi.org/10.1172/JCI37041, PMID: 19252258

Zanetti G, Prinz S, Daum S, Meister A, Schekman R, Bacia K, Briggs JAG. 2013. The structure of the COPII transport-vesicle coat assembled on membranes. *eLIFE* **2**:e00951. DOI: http://doi.org/10.7554/eLife.00951, PMID: 24062940

Zeng H, Jia J, Liu A. 2010. Coordinated translocation of mammalian Gli proteins and suppressor of fused to the primary cilium. *PLoS One* **5**:e15900. DOI: http://doi.org/10.1371/journal.pone.0015900, PMID: 21209912

Zhang Q, Nishimura D, Seo S, Vogel T, Morgan DA, Searby C, Bugge K, Stone EM, Rahmouni K, Sheffield VC. 2011. Bardet-Biedl syndrome 3 (Bbs3) knockout mouse model reveals common BBS-associated phenotypes and Bbs3 unique

phenotypes. *Proceedings of the National Academy of Sciences* **108**:20678–20683. DOI: http://doi.org/10.1073/pnas.1113220108, PMID: 22139371

Zhang Q, Yu D, Seo S, Stone EM, Sheffield VC. 2012. Intrinsic protein-protein interaction-mediated and chaperonin-assisted sequential assembly of stable Bardet-Biedl syndrome protein complex, the BBSome. *Journal of Biological Chemistry* **287**:20625–20635. DOI: http://doi.org/10.1074/jbc.M112.341487, PMID: 22500027

Zhen Y, Stenmark H. 2015. Cellular functions of Rab GTPases at a glance. *Journal of Cell Science* **128**:3171–3176. DOI: http://doi.org/https://doi.org/10.1242/jcs.166074, PMID: 26272922

Zhu B, Zhu X, Wang L, Liang Y, Feng Q, Pan J. 2017. Functional exploration of the IFT-A complex in intraflagellar transport and ciliogenesis. *PLoS Genetics* **13**:e1006627. DOI: http://doi.org/10.1371/journal.pgen.1006627, PMID: 28207750

Zullo A, Iaconis D, Barra A, Cantone A, Messaddeq N, Capasso G, Dollé P, Igarashi P, Franco B. 2010. Kidney-specific inactivation of Ofd1 leads to renal cystic disease associated with upregulation of the mTOR pathway. *Human Molecular Genetics* **19**:2792–2803. DOI: http://doi.org/10.1093/hmg/ddq180, PMID: 20444807

Appendix I: Movie legends

1. **Movie 2.1.** SiR-tubulin: Tubulin marker for live cell imaging of RPE-1 cilia.

24hrs serum starved RPE-1 cells are transfected with respective clones (shown in green) and stained for SiR-Tubulin (see **Section 2.6.2)** and imaged live on LEICA SP5 microscope using an 63X, 1.4 oil immersion objective. Movie is compiled as 5fps.

2. **Movie 2.2.** SiR-tubulin: Tubulin marker for live cell imaging of MEFs cilia.

24hrs serum starved MEF cells are electroporated with respective clones (shown in green) and stained for SiR-Tubulin (see 2.6.2) and imaged live on LEICA SP5 microscope using an 63X, 1.4 oil immersion objective. The movie is compiled as 5fps.

3. **Movie 3.1.** Cilia specific membrane-associated cargo (A) ARL13B and membrane-integrated cargo (B) SMO fail to localize in *Wdr35*$^{-/-}$ cilia (**related to Figure 3.6**).

Wdr35$^{+/+}$ and *Wdr35*$^{-/-}$ MEFs electroporated with ARL13B-EGFP and SMOOTHENED-GFP, serum starved for 24hrs, stained with SiR-tubulin and imaged live on LEICA SP5 microscope using an 63X, 1.4 oil immersion objective. The movie is compiled as 5fps.

4. **Movie 3.2.** PCM-1 localizes in pericentriolar space around cilia.

PCM1-SNAP expressing MEFs were electroporated with ARL13B-EGFP, serum starved for 24hrs and stained for SNAP-SIR647 (see **Section 2.6.4**) and imaged live on LEICA SP5 microscope using an 63X, 1.4 oil immersion objective. The movie is compiled as 5fps.

5. **Movie 3.3.** Organization of centriolar satellites is not disrupted in *Wdr35*$^{-/-}$(**related to Figure 3.24**).

Wdr35$^{+/+}$*;PCM1*$^{SNAP/SNAP}$ and *Wdr35*$^{-/-}$*;PCM1*$^{SNAP/SNAP-}$ MEFs electroporated with ARL13B-EGFP (green), serum starved for 24hrs and stained for SiR-tubulin (grey) and SNAP-TMR (magenta) and imaged live on LEICA SP5 microscope using an 63X, 1.4 oil immersion objective. The movie is compiled as 5fps.

6. **Movie 4.1.** Electron-dense vesicles could be seen at base of cilia in wild type MEFs (**related to figure 4.4a and 4.4b**).

Z-stack through TEM-tomogram of 300nm wild type ciliated MEFs compiled as 5fps. The Golgi is shown in green and vesicles around cilia in magenta.

7. **Movie 4.2.** Electron-dense vesicles tracking between the Golgi and cilia are present in wild type fibroblasts (**related to figure 4.5a and 4.5b**).

Z-stack through TEM-tomogram of 600nm wild type ciliated MEFs compiled as 5fps. The Golgi is shown in green and vesicles around cilia in magenta.

8. **Movie 4.3.** In *Wdr35*$^{-/-}$ fibroblasts, an accumulation of small uncoated vesicles is observed around mutant cilia (**related to figure 4.6a and 4.6b**).

Z-stack through TEM-tomogram of 600nm *Wdr35*$^{-/-}$ ciliated MEFs compiled as 5fps. The Golgi is shown in green and vesicles around cilia in blue.

9. **Movie 4.4.** Transition zone is unaltered in *Wdr35*$^{-/-}$ MEFs (**related to figure 4.7a and 4.7b**).

Z-stack through TEM-tomogram of 900nm *Wdr35*$^{-/-}$ ciliated MEFs compiled as 5fps. The Golgi is shown in green and vesicles around cilia in blue.

All movies are .avi files.

Appendix II: Images

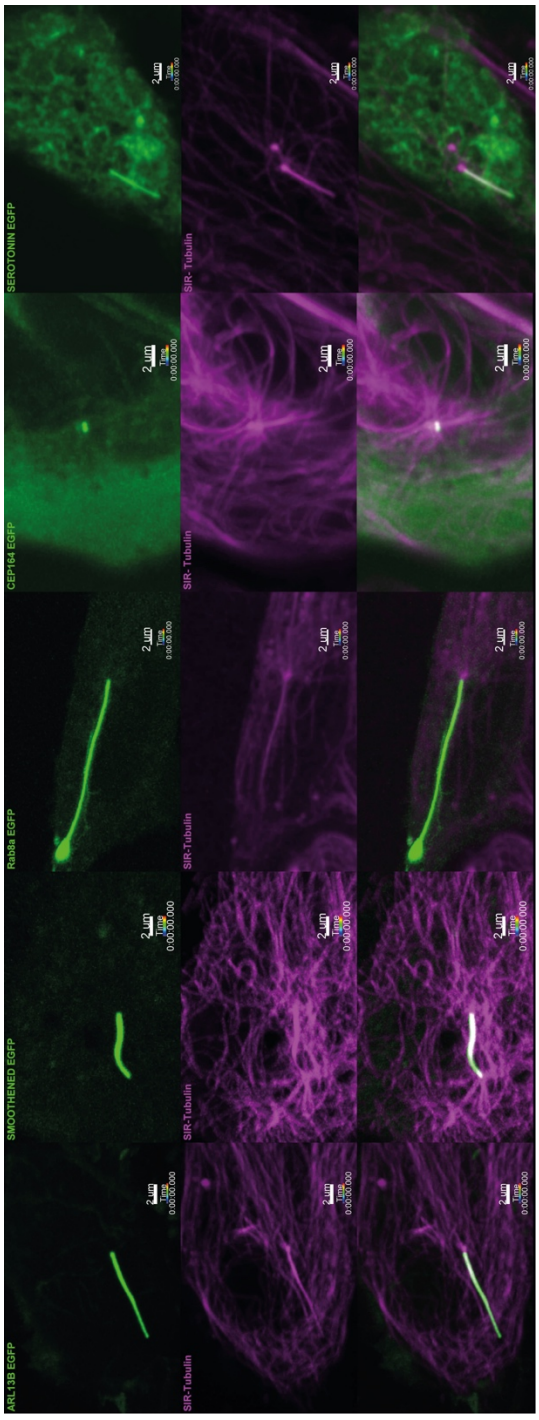

Figure A1. SiR-tubulin: Tubulin marker for live cell imaging of RPE-1 cilia (snapshot from **Movie 2.1**).

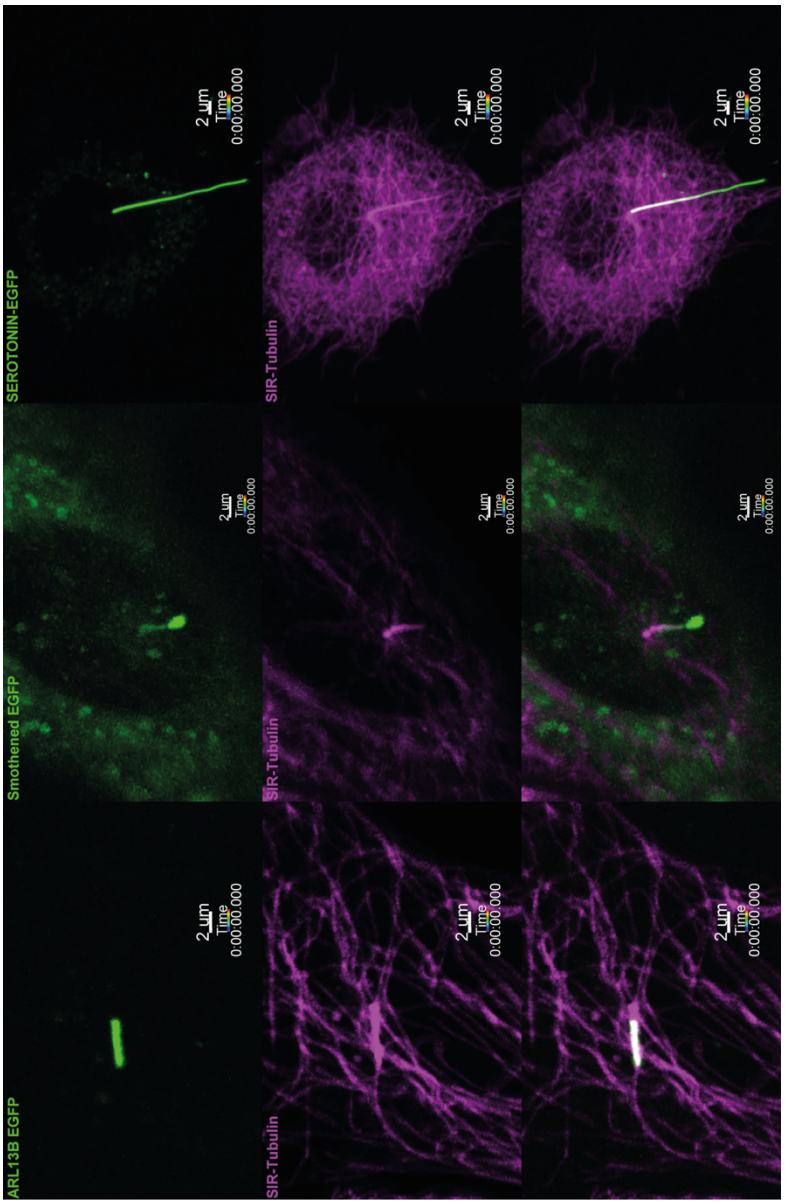

Figure A2. SiR-tubulin: Tubulin marker for live cell imaging of MEFs cilia (snapshot from Movie **2.2**).

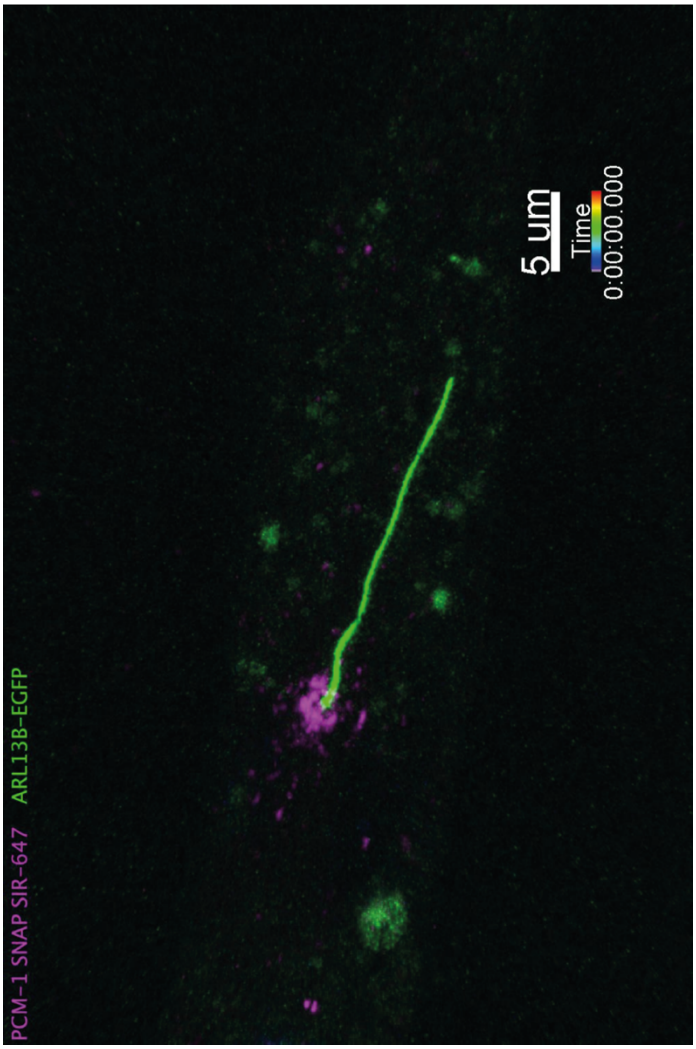

Figure A3. PCM-1 localisation at cilia base (snapshot from **Movie 3.2**).

Appendix III: publications

1. PLAA Mutations Cause a Lethal Infantile Epileptic Encephalopathy by Disrupting Ubiquitin-Mediated Endolysosomal Degradation of Synaptic Proteins. Hall EA, Nahorski MS, Murray LM, Shaheen R, Perkins E, Dissanayake KN, Kristaryanto Y, Jones RA, Vogt J, Rivagorda M, Handley MT, Mali GR, **Quidwai T**, Soares DC, Keighren MA, McKie L, Mort RL, Gammoh N, Garcia-Munoz A, Davey T, Vermeren M, Walsh D, Budd P, Aligianis IA, Faqeih E, Quigley AJ, Jackson IJ, Kulathu Y, Jackson M, Ribchester RR, von Kriegsheim A, Alkuraya FS, Woods CG, Maher ER, Mill P. Am J Hum Genet. May 2017. Doi: http://dx.doi.org/10.1016/j.ajhg.2017.03.008.

Appendix IV: Sequence blast result between IFT-A proteins and COPI-β'

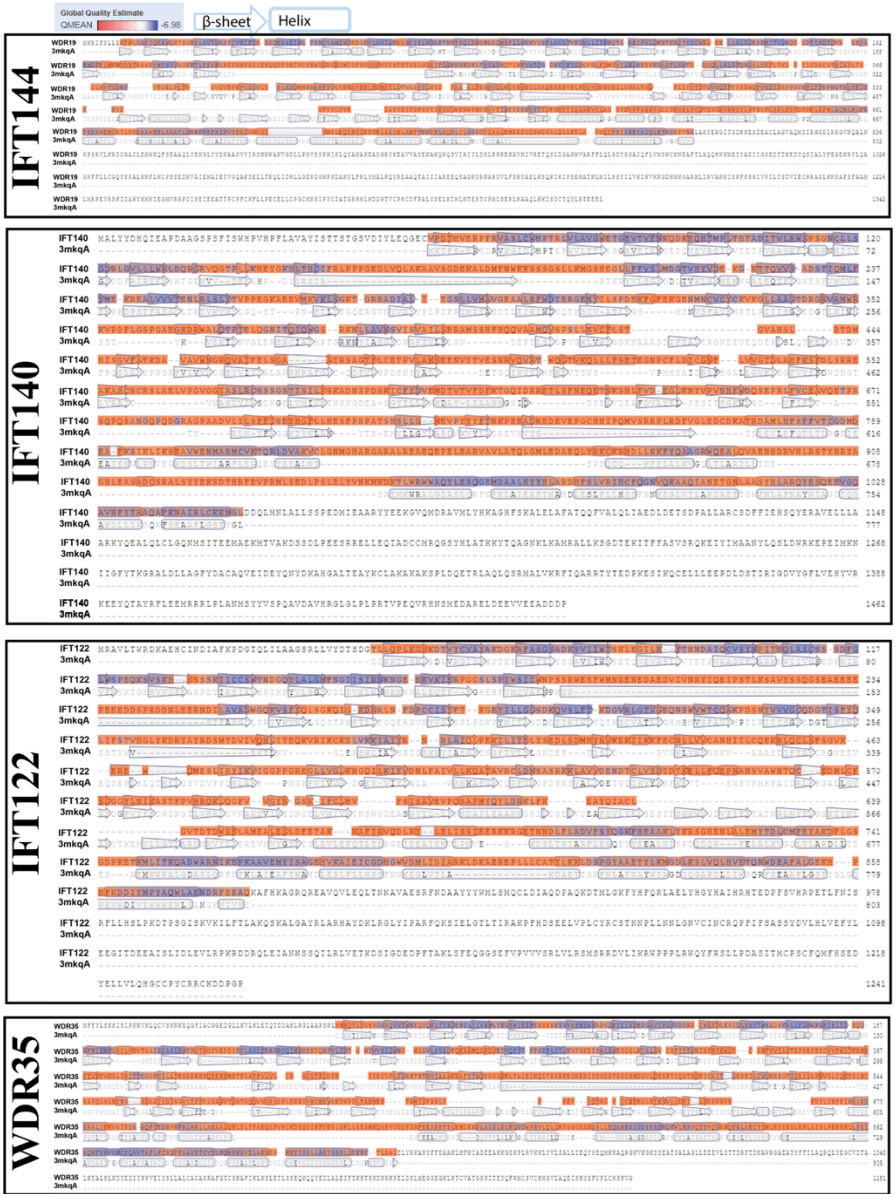

Related to fig: 4.1. Sequence blast result between IFT-As and COPIβ' received from SWISS MODEL server.

Appendix V: List of sequence matched to IFTAs as obtained from SWISS MODEL server

SWISS-MODEL Homology Modelling Report

Model Building Report

This document lists the results for the homology modelling project "WDR19_HUMAN Q8NEZ3 WD repeat-containing protein 19" submitted to SWISS-MODEL workspace on Feb. 25, 2018, 4:31 p.m..The submitted primary amino acid sequence is given in Table T1.

If you use any results in your research, please cite the relevant publications:

- Biasini, M., Bienert, S., Waterhouse, A., Arnold, K., Studer, G., Schmidt, T., Kiefer, F., Cassarino, T.G., Bertoni, M., Bordoli, L., Schwede, T. SWISS-MODEL: modelling protein tertiary and quaternary structure using evolutionary information. Nucleic Acids Res. 42, W252-W258 (2014). doi
- Guex, N., Peitsch, M.C., Schwede, T. Automated comparative protein structure modeling with SWISS-MODEL and Swiss-PdbViewer: A historical perspective. Electrophoresis 30, S162-S173 (2009). doi
- Bienert, S., Waterhouse, A., de Beer, T.A., Tauriello, G., Studer, G., Bordoli, L., Schwede, T. The SWISS-MODEL Repository - new features and functionality. Nucleic Acids Res. 45, D313-D319 (2017). doi
- Benkert, P., Biasini, M., Schwede, T. Toward the estimation of the absolute quality of individual protein structure models. Bioinformatics 27, 343-350 (2011). doi
- Bertoni, M., Kiefer, F., Biasini, M., Bordoli, L., Schwede, T. Modeling protein quaternary structure of homo- and hetero-oligomers beyond binary interactions by homology. Scientific Reports 7 (2017). doi

Results

The SWISS-MODEL template library (SMTL version 2018-02-21, PDB release 2018-02-16) was searched with BLAST (Camacho et al.) and HHBlits (Remmert, et al.) for evolutionary related structures matching the target sequence in Table T1. For details on the template search, see Materials and Methods. Overall 4217 templates were found (Table T2).

Models

The following model was built (see Materials and Methods "Model Building"):

Model #01	File	Built with	Oligo-State	Ligands	GMQE	QMEAN
	PDB	ProMod3 Version 1.1.0.	monomer (matching prediction)	None	0.27	-6.98

QMEAN	-6.98
Cβ	-4.43
All Atom	-3.06
Solvation	-1.32
Torsion	-5.67

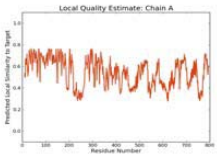

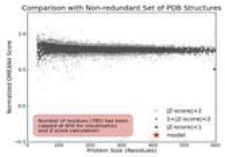

Template	Seq Identity	Oligo-state	QSQE	Found by	Method	Resolution	Seq Similarity	Range	Coverage	Description
3mkq.1.A	14.58	homo-trimer	0.05	HHblits	X-ray	2.50Å	0.27	10 - 794	0.51	Coatomer beta'-subunit

The template contained no ligands.

```
Target    MKRIFSLLEKTWLGAPIQFAWQKTSGNYLAVTGADYIVKIFDR-HGQKRSEINL-PGNCVAMDWDKDGDVLAVIAEKSSC
3mkq.1.A  ---------SNRSDRVKGIDFHP-TEPWVLTTLYSGRVEIWNYETQVEVRSIQVTETPVRAGKFIARKNWIIVGSD-DFR

Target    IYLWDANTNKTSQLDNGMRDQMSFLLWSKVGSFLAVGTVKGNLLIYNHQTS-RKIPVLGKHTKRITCGCWNA-EN-LLAL
3mkq.1.A  IRVFNYNTGEKVVDFEAHPDYIRSIAVHPTKPYVLSGSDDLTVKLWNWENNWALEQTFEGHEHFVMCVAFNPKDPSTFAS

Target    GGEDKMITVSNQE-GDTIRQTQVR--SEPSNMQFFLMKMDDRTSAAESMISVVLGKKTLFFLNLNEPDNPADLEFQQDFG
3mkq.1.A  GCLDRTVKVWSLGQSTPNFTLTTGQERGVNYVDYYPLP------DKPYMITASDD-LTIKIWDYQTK------------

Target    NIVCYNWYGDGRIMIGFSCGHFVVISTHTGELGQEIFQARNHKDNLTSIAVSQTLNKVATCG-DNCIKIQDLVDLKDMYV
3mkq.1.A  ---------------------------------SCVATLEGHMSNVSFAVFHPTLPIIISGSEDGTLKIWNSSTYKV---

Target    ILNLDEENKGLGTLSWTD--DGQLLALSTQRGSLHVFLTKL-P-ILGDACSTRIAYLTS---LLEVTVANP------VEG
3mkq.1.A  EKTLNVGLERSWCIATHPTGRKNYIASGFDNGFTVLSLGNDEPTLSLDPVGKLVWSGGKNAAASDIFTAVIRGNEEVEQD

Target    ELPITV-----SVDVEPNFVAVGLY--HLAVGMNNRAWFYVLGENAVKKLKDMEYLGTVASICLHSD--YAA-ALFEGKV
3mkq.1.A  EPLSLQTKELGSVDVFPQSLAHSPNGRFVTVVGDGEYVIYTALAWR------NKAFGKCQDFVWGPDSNSYALIDETGQI

Target    QLHLIESEILDAQEERETRLFPAVDDKCRILCHALTSD-----FLIYGTDTGVVQYFYIEDWQFVNDYRHPVSVKKIFPD
```

```
3mkq.1.A  KYYKNFK---------------E--VTSWSVPMHSAIDRLFSGALLGVKSDGFVYFFDWDNGTLVRRIDVN--AKDVIWS

Target    PNGTRLVFIDE------KSD---------------------------------------------GFVYCPVN-----
3mkq.1.A  DNGELVMIVNTNSNGDEASGYTLLFNKDAYLEAANNGNIDDSEGVDEAFDVLYELSESITSGKWVGDVFIFTTATNRLNY

Target    ---DATYEIPDFSPTIKGVLWENWPMDKGVFIAYDDDKVYTYVFHKDTIQGAKVILAG-STKVPFAHKPLLLYNGELTCQ
3mkq.1.A  FVGGKTYNLAHYTKEMYLLGYLA--RDNKVYLADREVHVYGYEISLEVLEFQTLTLRGEIEEAIENVLPNVEGKDSLT--

Target    TQSGKVNNIYLSTHGFLSNLKDTGPDELRPMLAQNLMLKRFSDAWEMCRILNDEAAWNELARACLHHMEVEFAIRVYRRI
3mkq.1.A  ----KIARF-LEGQEYYEEALNISPDQDQK-FELALKVGQLTLARDLLTDESAEMKWRALGDASLQRFNFKLAIEAFTNA

Target    GNVGI-------------VMSLEQIKGIEDYNLLAGHLAMFTNDYNLAQDLYLASSCPIAALEMRRDLQHWDSALQLAKH
3mkq.1.A  HDLESLFLLHSSFNNKEGLVTLAKDAETTGKFNLAFNAYWIAGDIQGAKDLLIKSQRFSEAAFL-------------GST

Target    LA--PDQIPFISKEYAIQLEFAGDYVNALAHYEKGITGDNKEHDEACLAGVAQMSIRMGDIRRGVNQALKHPSRVLKRDC
3mkq.1.A  YGLGDNEVNDIVTKWKENLILNGKNTVS-----------------------------------------------------

Target    GAILENMKQFSEAAQLYEKGLYYDKAASVYIRSKNWAKVGDLLPHVSSPKIHLQYAKAKEADGRYKEAVVAYENAKQWQS
3mkq.1.A  ----------------------------------------------------------------------------------

Target    VIRIYLDHLNNPEKAVNIVRETQSLDGAKMVARFFLQLGDYGSAIQFLVMSKCNNEAFTLAQQHNKMEIYADIIGSEDTT
3mkq.1.A  ----------------------------------------------------------------------------------

Target    NEDYQSIALYFEGEKRYLQAGKFFLLCGQYSRALKHFLKCPSSEDNVAIEMAIETVGQAKDELLTNQLIDHLLGENDGMP
3mkq.1.A  ----------------------------------------------------------------------------------

Target    KDAKYLFRLYMALKQYREAAQTAIIIAREEQSAGNYRNAHDVLFSMYAELKSQKIKIPSEMATNLMILHSYILVKIHVKN
3mkq.1.A  ----------------------------------------------------------------------------------

Target    GDHMKGARMLIRVANNISKFPSHIVPILTSTVIECHRAGLKNSAFSFAAMLMRPEYRSKIDAKYKKKIEGMVRRPDISEI
3mkq.1.A  ----------------------------------------------------------------------------------

Target    EEATTPCPFCKFLLPECELLCPGCKNSIPYCIATGRHMLKDDWTVCPHCDFPALYSELKIMLNTESTCPMCSERLNAAQL
3mkq.1.A  ----------------------------------------------------------------------------------

Target    KKISDCTQYLRTEEEL
3mkq.1.A  ----------------
```

Materials and Methods

Template Search

Template search with BLAST and HHBlits has been performed against the SWISS-MODEL template library (SMTL, last update: 2018-02-21, last included PDB release: 2018-02-16).

The target sequence was searched with BLAST against the primary amino acid sequence contained in the SMTL. A total of 8 templates were found.

An initial HHblits profile has been built using the procedure outlined in (Remmert, et al.), followed by 1 iteration of HHblits against NR20. The obtained profile has then be searched against all profiles of the SMTL. A total of 4301 templates were found.

Template Selection

For each identified template, the template's quality has been predicted from features of the target-template alignment. The templates with the highest quality have then been selected for model building.

Model Building

Models are built based on the target-template alignment using ProMod3. Coordinates which are conserved between the target and the template are copied from the template to the model. Insertions and deletions are remodelled using a fragment library. Side chains are then rebuilt. Finally, the geometry of the resulting model is regularized by using a force field. In case loop modelling with ProMod3 fails, an alternative model is built with PROMOD-II (Guex, et al.).

Model Quality Estimation

The global and per-residue model quality has been assessed using the QMEAN scoring function (Benkert, et al.) . For improved performance, weights of the individual QMEAN terms have been trained specifically for SWISS-MODEL.

Ligand Modelling

Ligands present in the template structure are transferred by homology to the model when the following criteria are met: (a) The ligands are annotated as biologically relevant in the template library, (b) the ligand is in contact with the model, (c) the ligand is not clashing with the protein, (d) the residues in contact with the ligand are conserved between the target and the template. If any of these four criteria is not satisfied, a certain ligand will not be included in the model. The model summary includes information on why and which ligand has not been included.

Oligomeric State Conservation

The quaternary structure annotation of the template is used to model the target sequence in its oligomeric form. The method (Bertoni et al.) is based on a supervised machine learning algorithm, Support Vector Machines (SVM), which combines interface conservation, structural clustering, and other template features to provide a quaternary structure quality estimate (QSQE). The QSQE score is a number between 0 and 1, reflecting the expected accuracy of the interchain contacts for a model built based a given alignment and template. Higher numbers indicate higher reliability. This complements the GMQE score which estimates the accuracy of the tertiary structure of the resulting model.

References

- **BLAST**
  Camacho, C., Coulouris, G., Avagyan, V., Ma, N., Papadopoulos, J., Bealer, K., Madden, T.L. BLAST+: architecture and applications. BMC Bioinformatics 10, 421-430 (2009). doi
- **HHblits**
  Remmert, M., Biegert, A., Hauser, A., Söding, J. HHblits: lightning-fast iterative protein sequence searching by HMM-HMM alignment. Nat Methods 9, 173-175 (2012). doi

Table T1:

Primary amino acid sequence for which templates were searched and models were built.

```
MKRIFSLLEKTWLGAPIQFAWQKTSGNYLAVTGADYIVKIFDRHGQKRSEINLPGNCVAMDWDKDGDVLAVIAEKSSCIYLWDANTNKTSQLDNGMRDQM
SFLLWSKVGSFLAVGTVKGNLLIYNHQTSRKIPVLGKHTKRITCGCWNAENLLALGGEDKMITVSNQEGDTIRQTQVRSEPSNMQFFLMKMDDRTSAAES
MISVVLGKKTLFFLNLNEPDNPADLEFQQDFGNIVCYNWYGDGRIMIGFSCGHFVVISTHTGELGQEIFQARNHKDNLTSIAVSQTLNKVATCGDNCIKI
QDLVDLKDMYVILNLDEENKGLGTLSWTDDGQLLALSTQRGSLHVFLTKLPILGDACSTRIAYLTSLLEVTVANPVEGELPITVSVDVEPNFVAVGLYHL
AVGMNNRAWFYVLGENAVKKLKDMEYLGTVASICLHSDYAAALFEGKVQLHLIESEILDAQEERETRLFPAVDDKCRILCHALTSDFLIYGTDTGVVQYF
YIEDWQFVNDYRHPVSVKKIFPDPNGTRLVFIDEKSDGFVYCPVNDATYEIPDFSPTIKGVLWENWPMDKGVFIAYDDDKVYTYVFHKDTIQGAKVILAG
STKVPFAHKPLLLYNGELTCQTQSGKVNNIYLSTHGFLSNLKDTGPDELRPMLAQNLMLKRFSDAWEMCRILNDEAAWNELARACLHHMEVEFAIRVYRR
IGNVGIVMSLEQIKGIEDYNLLAGHLAMFTNDYNLAQDLYLASSCPIAALEMRRDLQHWDSALQLAKHLAPDQIPFISKEYAIQLEFAGDYVNALAHYEK
GITGDNKEHDEACLAGVAQMSIRMGDIRRGVNQALKHPSRVLKRDCGAILENMKQFSEAAQLYEKGLYYDKAASVYIRSKNWAKVGDLLPHVSSPKIHLQ
YAKAKEADGRYKEAVVAYENAKQWQSVIRIYLDHLNNPEKAVNIVRETQSLDGAKMVARFFLQLGDYGSAIQFLVMSKCNNEAFTLAQQHNKMEIYADII
GSEDTTNEDYQSIALYFEGEKRYLQAGKFFLLCGQYSRALKHFLKCPSSEDNVAIEMAIETVGQAKDELLTNQLIDHLLGENDGMPKDAKYLFRLYMALK
QYREAAQTAIIIAREEQSAGNYRNAHDVLFSMYAELKSQKIKIPSEMATNLMILHSYILVKIHVKNGDHMKGARMLIRVANNISKFPSHIVPILTSTVIE
CHRAGLKNSAFSFAAMLMRPEYRSKIDAKYKKKIEGMVRRPDISEIEEATTPCPFCKFLLPECELLCPGCKNSIPYCIATGRHMLKDDWTVCPHCDFPAL
YSELKIMLNTESTCPMCSERLNAAQLKKISDCTQYLRTEEEL
```

Table T2:

Template	Seq Identity	Oligo-state	QSQE	Found by	Method	Resolution	Seq Similarity	Coverage	Description
5a1u.1.S	11.76	monomer		HHblits	EM	13.00Å	0.25	0.54	COATOMER SUBUNIT ALPHA
5nzu.1.A	11.76	monomer		HHblits	EM	NA	0.25	0.54	Coatomer subunit alpha
5a1u.1.S	11.87	monomer		HHblits	EM	13.00Å	0.26	0.52	COATOMER SUBUNIT ALPHA
5nzu.1.A	11.87	monomer		HHblits	EM	NA	0.26	0.52	Coatomer subunit alpha
3mkq.1.A	14.58	homo-trimer	0.05	HHblits	X-ray	2.50Å	0.27	0.51	Coatomer beta'-subunit
3mkq.1.C	14.58	homo-trimer	0.05	HHblits	X-ray	2.50Å	0.27	0.51	Coatomer beta'-subunit
3mkq.1.E	14.58	homo-trimer	0.05	HHblits	X-ray	2.50Å	0.27	0.51	Coatomer beta'-subunit
5a1u.1.T	13.66	monomer		HHblits	EM	13.00Å	0.27	0.51	COATOMER SUBUNIT BETA'
5nzu.1.C	13.66	monomer		HHblits	EM	NA	0.27	0.51	Coatomer subunit beta'
5a1u.1.T	11.48	monomer		HHblits	EM	13.00Å	0.26	0.51	COATOMER SUBUNIT BETA'
5nzu.1.C	11.48	monomer		HHblits	EM	NA	0.26	0.51	Coatomer subunit beta'
3mkq.1.A	11.63	homo-trimer	0.03	HHblits	X-ray	2.50Å	0.26	0.51	Coatomer beta'-subunit
3mkq.1.C	11.63	homo-trimer	0.03	HHblits	X-ray	2.50Å	0.26	0.51	Coatomer beta'-subunit
3mkq.1.E	11.63	homo-trimer	0.03	HHblits	X-ray	2.50Å	0.26	0.51	Coatomer beta'-subunit
5wyj.18.A	12.06	monomer		HHblits	EM	NA	0.26	0.49	U3 small nucleolar RNA-associated protein 13
4bzj.1.A	9.95	homo-dimer		HHblits	EM	40.00Å	0.26	0.47	PROTEIN TRANSPORT PROTEIN SEC31
4bzj.1.C	9.95	homo-dimer		HHblits	EM	40.00Å	0.26	0.47	PROTEIN TRANSPORT PROTEIN SEC31
5h1j.1.A	14.08	monomer		HHblits	X-ray	2.00Å	0.27	0.41	Gem-associated protein 5
5h1k.1.A	14.08	monomer		HHblits	X-ray	1.90Å	0.27	0.41	Gem-associated protein 5
5h3s.1.A	14.08	monomer		HHblits	X-ray	3.00Å	0.27	0.41	Gem-associated protein 5
5tee.1.A	13.49	monomer		HHblits	X-ray	1.65Å	0.27	0.41	Gem-associated protein 5
5gxh.1.A	13.51	monomer		HHblits	X-ray	1.80Å	0.27	0.41	Gem-associated protein 5

Template	Seq Identity	Oligo-state	QSQE	Found by	Method	Resolution	Seq Similarity	Coverage	Description
5oql.1.D	13.61	monomer		HHblits	EM	NA	0.27	0.41	Utp4
4xfv.1.A	10.95	monomer		HHblits	X-ray	3.20Å	0.25	0.42	Elongator complex protein 2
5oql.1.O	11.92	monomer		HHblits	EM	NA	0.25	0.42	Putative U3 snoRNP protein
5n1a.1.A	13.66	monomer		HHblits	X-ray	2.15Å	0.27	0.41	utp4
5m2n.1.A	11.21	monomer		HHblits	X-ray	2.81Å	0.25	0.42	Elongator complex protein 2
5wyj.17.A	14.26	monomer		HHblits	EM	NA	0.27	0.41	U3 small nucleolar RNA-associated protein 12
5wlc.22.A	14.08	monomer		HHblits	EM	NA	0.27	0.41	Utp12
3j2t.1.A	12.64	monomer		HHblits	EM	NA	0.27	0.41	Apoptotic protease-activating factor 1
3shf.1.A	12.29	monomer		HHblits	X-ray	3.55Å	0.27	0.41	Apoptotic peptidase activating factor 1
2ymu.1.A	14.77	monomer		HHblits	X-ray	1.79Å	0.28	0.40	WD-40 REPEAT PROTEIN
3jbt.1.A	12.48	monomer		HHblits	EM	NA	0.27	0.41	Apoptotic protease-activating factor 1
3sfz.1.A	12.29	monomer		HHblits	X-ray	3.00Å	0.27	0.41	Apoptotic peptidase activating factor 1
5wve.1.K	12.68	monomer		HHblits	EM	NA	0.27	0.41	Apoptotic protease-activating factor 1
5juy.1.B	12.68	monomer		HHblits	EM	NA	0.27	0.41	Apoptotic protease-activating factor 1
5juy.1.G	12.68	monomer		HHblits	EM	NA	0.27	0.41	Apoptotic protease-activating factor 1
5juy.1.D	12.68	monomer		HHblits	EM	NA	0.27	0.41	Apoptotic protease-activating factor 1
5juy.1.E	12.68	monomer		HHblits	EM	NA	0.27	0.41	Apoptotic protease-activating factor 1
5wlc.19.A	11.97	monomer		HHblits	EM	NA	0.26	0.40	Utp4
5wyj.18.A	12.18	monomer		HHblits	EM	NA	0.26	0.40	U3 small nucleolar RNA-associated protein 13
1pev.1.A	11.96	monomer		HHblits	X-ray	2.00Å	0.26	0.40	Actin interacting protein 1
5tzs.1.1	12.73	monomer		HHblits	EM	NA	0.26	0.40	Utp21
4nsx.1.A	12.71	monomer		HHblits	X-ray	2.10Å	0.26	0.40	U3 small nucleolar RNA-associated protein 21
5wlc.13.A	8.87	monomer		HHblits	EM	NA	0.25	0.40	Utp17
5wyj.20.A	12.41	monomer		HHblits	EM	NA	0.26	0.40	U3 small nucleolar RNA-associated protein 21
5wyk.1.V	12.41	monomer		HHblits	EM	NA	0.26	0.40	U3 small nucleolar RNA-associated protein 21
5jpq.1.I	12.41	monomer		HHblits	EM	NA	0.26	0.40	U3 small nucleolar RNA-associated protein 21
5wlc.25.A	12.41	monomer		HHblits	EM	NA	0.26	0.40	Utp21
4uzy.1.A	11.47	monomer		HHblits	X-ray	2.48Å	0.26	0.40	FLAGELLAR ASSOCIATED PROTEIN

The table above shows the top 50 filtered templates. A further 2,279 templates were found which were considered to be less suitable for modelling than the filtered list.
3fgb.1.A, 5gm6.1.4, 3vl1.1.A, 4a1s.1.A, 2ff4.2.A, 5cvo.2.A, 3fm0.1.A, 2g5p.1.A, 5ukl.1.B, 1x81.1.A, 4nox.1.A, 4di3.1.D, 4a0a.1.B, 1ft1.1.A, 5gm6.1.2, 5vgz.1.K, 5vgz.1.J, 5vgz.1.H, 5vgz.1.M, 2ysm.1.A, 2qx5.1.A, 4ui9.1.P, 4ui9.1.Q, 4ui9.1.V, 4ui9.1.W, 4ui9.1.J, 4ui9.1.K, 4ui9.1.H, 4ui9.1.I, 4ui9.1.O, 4ui9.1.B, 4ui9.1.C, 4ui9.1.F, 3ask.2.A, 3q15.1.A, 3ieg.2.A, 2xyi.1.A, 2kc7.1.A, 5cwm.1.A, 5gm6.1.Y, 2y4u.1.A, 1aof.1.A, 1aof.1.B, 1pc2.1.A, 1g25.1.A, 3ium.1.A, 4yhc.2.A, 5fqd.1.A, 5dse.1.A, 5n4d.1.A, 3hxe.1.A, 3sre.1.A, 1jmz.1.B, 5opt.1.A, 3mv3.1.B, 2ifu.2.A, 2lo2.1.A, 2qt9.1.A, 5k0m.1.A, 4i1a.1.A, 4uer.1.b, 2f2f.1.A, 4cvc.1.A, 3s2k.1.B, 5vgz.1.G, 3s2k.1.A, 3j7p.78.A, 1hxi.1.A, 5edv.1.A, 2ce9.2.B, 4s3o.1.B, 4s3o.1.C, 5wyk.1.U, 5gjr.12.A, 5wyk.1.V, 5wyk.1.R, 5jrl.1.B, 5b26.2.B, 2ijq.2.A, 2kwj.1.B, 5mqf.1.O, 5a7d.8.A, 5mqf.1.M, 4v5z.1.A, 5mqf.1.F, 5n4e.1.A, 5mqf.1.D, 5mqf.1.E, 3re2.1.A, 4v6w.2.A, 1jtd.1.B, 3kci.1.A, 5uw7.1.A, 5l4k.1.E, 3ffl.2.B, 5l4k.1.G, 5l4k.1.F, 5l4k.1.I, 3mbr.1.A, 5l4k.1.J, 4a2l.1.B, 2ku3.1.A, 2j9q.1.B, 2j9q.1.A, 5k1a.2.B, 6au8.1.A, 2ma6.1.A, 1xwh.1.A, 2y1m.4.A, 4yg8.1.B, 5h19.1.A, 5sv7.1.D, 3odt.1.A, 5sv7.1.A, 5a7d.4.A, 5sv7.1.C, 2fi7.1.A, 2fi7.1.B, 5gmk.1.0, 3li4.1.A, 5n4f.1.A, 2bkl.1.A, 6eos.1.B, 5wlc.27.A, 5mpq.1.A, 3hlh.1.A, 1o6f.1.A, 5b79.1.A, 1vz2.1.A, 4ri8.1.A, 3mv2.1.A, 5nd8.1.I, 1z68.1.B, 5cqr.1.A, 1z68.1.A, 5i1y.1.C, 3kif.1.C, 3kif.1.A, 2bed.1.A, 4x3e.1.A, 2be1.1.A, 5wvi.1.K, 5gmk.1.J, 5kkl.1.A, 3ly9.1.A, 5luq.2.A, 5gmk.1.X, 5u2j.2.A, 5gmk.1.R, 5a7d.6.A, 5gmk.1.W, 5iy8.1.Q, 2ooe.1.A, 3cv0.1.A, 5m72.1.A, 3rib.1.A, 2hes.1.A, 2gw1.1.A, 2gw1.1.B, 4eqf.1.A, 2iav.1.A, 4kvm.1.A, 2ecv.1.A, 5li0.1.j, 4j8e.1.A, 5wyj.19.A, 5v4b.1.B, 1sly.1.A, 2vz1.1.A, 3j8b.1.C, 1t1h.1.A, 1c9l.1.A, 5lpi.3.A, 3jck.1.A, 3jck.1.B, 1b9y.1.A, 3jck.1.D, 5o3u.1.A, 4ja7.1.A, 4ymr.1.A, 2p9w.1.A, 4ymr.1.B, 1n87.1.A, 3txn.1.A, 2pqr.2.A, 5kjk.1.A, 5guw.3.A, 3rtr.3.B, 5jj7.1.A, 5gm6.1.F, 5jj7.1.B, 5ulh.1.C, 3i7k.1.A, 5n4b.1.A, 2iat.1.A, 1tl2.1.A, 5eio.1.F, 2iax.1.A, 4ccg.2.B, 3edt.1.A, 3edt.1.B, 3u5m.1.A, 2ebs.1.A, 5c2w.1.E, 4lg8.1.A, 5juu.45.A, 5o85.2.B, 2kr4.1.A, 1hzu.1.A, 4q66.2.C, 2yhc.1.A, 5lj5.1.V, 5nrg.1.X, 3zfw.1.A, 2vjf.1.B, 4hou.2.A, 3jro.1.A, 1e96.1.B, 5k0y.1.8, 2k17.1.B, 3zgc.1.A, 5a1y.1.U, 4wne.1.A, 4i9e.1.A, 3cvq.1.A, 4d18.1.D, 4d18.1.B, 4d18.1.C, 3ow8.1.A, 5lpi.1.A, 4nc4.1.A, 4yde.1.A, 4cy1.1.A, 1vyh.1.C, 3kd7.1.A, 3bee.1.A, 5v3o.1.A, 2mwx.1.A, 5vhj.1.H, 5m5r.1.A, 4hhq.1.A, 4llb.1.A, 2l0b.1.A, 4kbq.2.A, 5aiu.1.A, 1n6f.1.A, 5wyj.17.A, 4hoq.1.A, 3gz1.1.A, 3sf4.1.A, 3jb9.1.3, 2uy1.1.A, 5vhf.1.J, 4wn4.2.A, 4bt8.1.B, 4bt8.1.A, 4buj.1.C, 4q6f.1.A, 2ynn.1.A, 2ecl.1.A,

4ld1.1.A, 3li3.1.A, 5jk7.2.A, 3jb9.1.K, 5oql.1.3, 5k1c.1.C, 5k1c.1.B, 6epc.1.S, 4l7b.1.A, 5igo.1.A, 6epc.1.T, 6epc.1.W, 6epc.1.V, 6epc.1.X, 6epc.1.Z, 2yql.1.A, 5oql.1.X, 4r5o.1.A, 2gop.1.A, 2gop.1.B, 6exn.1.J, 5i9d.1.A, 5oql.1.N, 5oql.1.O, 5oql.1.L, 6exn.1.S, 2xgs.1.A, 5oql.1.A, 3lvh.1.B, 3lrq.1.A, 5oql.1.D, 3lvh.1.A, 6exn.1.a, 6emk.1.D, 6emk.1.B, 6emk.1.C, 5ijn.1.U, 4v7h.1.Q, 5ijn.1.K, 5ijn.1.l, 5wbu.1.B, 3pbp.4.A, 5wbu.1.A, 5ijn.1.C, 1jju.1.B, 4uzy.1.A, 3no2.1.A, 5d0i.1.A, 2csy.1.A, 4n5c.5.A, 5yp1.1.B, 5yp1.1.A, 5i1y.1.A, 5m2n.1.A, 5i1y.1.B, 4bxr.1.A, 4hot.1.A, 2ep4.1.A, 4n5c.3.A, 5hgv.1.A, 5jul.1.A, 4l9p.1.A, 5cxb.1.B, 5cxb.1.A, 5ln3.1.0, 4p04.1.A, 4n5c.1.A, 3mzl.1.B, 4le7.2.A, 2co0.1.A, 5vlj.1.B, 5vlj.1.C, 5bt1.1.B, 6f9n.1.A, 5b4x.1.B, 3q4a.1.A, 5ln3.1.Y, 5ln3.1.X, 3as8.1.A, 5mgx.1.A, 2p4o.1.A, 4bzj.1.D, 4bzj.1.C, 4bzj.1.B, 4bzj.1.A, 2d8t.1.A, 4hw6.1.A, 3i7l.1.A, 4ynw.1.A, 5ln3.1.A, 3ww8.1.A, 5mc6.35.A, 3qdn.2.A, 4asc.1.A, 5nxq.1.A, 5ic8.3.A, 3va6.2.A, 1qsa.1.A, 5a9q.1.N, 3gd1.3.A, 5ic8.1.A, 5a9q.1.H, 5lyb.33.A, 5g05.1.l, 5yz0.1.A, 5jzz.2.A, 4ybm.2.A, 4fhl.1.A, 5vh9.1.B, 2ifu.3.A, 5d0m.1.B, 2ovr.1.B, 3j80.1.7, 3oxf.1.A, 1mda.1.A, 4wjw.1.B, 2iar.1.A, 3ivm.1.A, 3jco.1.8, 4wsn.4.D, 3acp.1.A, 1aoq.1.A, 1f62.1.A, 6epf.1.Z, 2pl2.1.A, 2c2l.2.A, 3flo.1.B, 2hz6.1.A, 3e0c.1.A, 3jrp.1.A, 5nrl.1.Q, 5nrl.1.W, 4x60.1.B, 5nrl.1.O, 2ro1.1.A, 3rpg.1.C, 4aez.1.A, 4aez.1.C, 5d0i.2.A, 3j78.45.A, 4aez.3.C, 2gvx.1.A, 5djs.1.A, 3vl1.2.A, 2yin.1.A, 5mps.1.U, 4zox.1.A, 5mps.1.Q, 5mps.1.R, 5lj3.1.L, 1qz2.1.C, 1qz2.1.B, 1qz2.1.A, 3vu4.1.A, 4a0a.1.A, 5lj3.1.U, 5lj3.1.T, 3iiw.1.A, 2i3s.2.A, 5olj.1.A, 5bv0.1.B, 3vu4.2.A, 3ade.1.A, 3tg5.1.A, 2qic.1.A, 2vyi.1.A, 1g72.1.A, 2xcc.1.A, 2rfo.1.A, 4zb4.2.A, 3kya.1.A, 5txc.1.A, 2jny.1.A, 5jz6.1.A, 1sr4.1.A, 3fvz.1.A, 2b5m.1.A, 1gjq.1.A, 2ovp.1.B, 3nol.1.A, 3li5.1.A, 5nd9.1.l, 4ggd.1.A, 5lj5.1.M, 5b75.1.A, 2xzg.1.A, 5lj5.1.U, 3mzk.1.A, 3mzk.1.B, 5o09.1.C, 5ftp.1.A, 5ftp.1.B, 3fw0.1.A, 3si5.1.A, 5lj5.1.d, 5diz.1.A, 4g2v.1.A, 5cqs.1.A, 3jct.1.n, 3lrq.1.B, 4o2w.1.A, 2eic.1.A, 4g56.1.B, 4v0m.1.B, 3n71.1.A, 5wlc.13.A, 4hnw.1.A, 3jzn.1.A, 5l0y.1.B, 5l0y.1.A, 5fkt.1.A, 2kwk.1.B, 1yr2.1.A, 3hym.1.B, 1jm7.1.A, 5n61.1.P, 5t0c.35.A, 2ece.1.A, 1zgk.1.A, 1klx.1.A, 5mc6.37.A, 1gxr.1.B, 1gxr.1.A, 4h7x.1.A, 3e4b.1.A, 3ott.1.B, 3ott.1.A, 5jqy.1.A, 4a09.1.A, 4nq0.1.A, 3zpj.1.A, 4r40.2.A, 4cgv.1.A, 4abn.1.A, 3as4.1.A, 5hb0.4.A, 5ulk.1.B, 1y8m.1.A, 1bpo.1.C, 5lvv.1.A, 3hli.1.A, 2hu5.1.B, 5i5i.1.A, 5c2v.1.B, 5wyj.20.A, 4d0k.1.A, 4lg9.1.A, 2l75.1.A, 1sqj.1.A, 2fpb.2.A, 5juy.1.G, 5d0q.1.C, 2e2e.1.A, 2yno.1.A, 5i5m.1.A, 5d0k.1.B, 3byc.1.A, 2ldr.1.A, 3v64.1.A, 5ndv.147.A, 3v64.1.D, 5o3v.1.A, 4av8.1.A, 3kae.1.A, 5tbk.1.B, 5o01.1.A, 3hrp.1.A, 2xcb.2.A, 4g1f.4.A, 2crb.1.A, 4n3c.1.A, 4qpl.2.A, 4xyh.1.A, 4bl0.2.A, 3zwu.1.A, 3i4r.1.B, 4j87.1.A, 3vk6.1.A, 5fnr.1.A, 5wvi.1.N, 2ecn.1.A, 1lrw.1.C, 1lrw.1.A, 4ja9.1.A, 4gpq.1.A, 2faw.1.A, 4gpk.1.D, 4gpk.1.A, 4gpk.1.C, 4gpk.1.B, 3fwv.2.A, 5nnz.1.A, 3zwl.1.A, 4gpk.3.D, 4gpk.3.C, 4gpk.3.B, 4gpk.3.A, 3lku.1.A, 3emh.1.A, 1ouv.1.A, 4kvo.1.A, 1wm5.1.A, 2hf1.1.A, 5igo.2.A, 5ife.1.D, 5ijo.1.Q, 5buz.2.B, 5ijo.1.W, 5gjq.1.Z, 5jpz.1.B, 3lvg.1.C, 5jpz.1.A, 5ijo.1.E, 4ozs.1.A, 5hkx.1.A, 3zvy.1.A, 4aow.1.A, 2i0r.1.C, 5a31.1.F, 5gjq.1.j, 2y0s.1.K, 4btb.1.A, 4imm.1.A, 3mmy.1.A, 5ltd.1.A, 3ii7.1.A, 3ng2.1.A, 3ng2.1.B, 2y1n.1.A, 5mpb.1.e, 2iaq.1.A, 5mpb.1.g, 5mpb.1.f, 3sfx.1.A, 5gjq.1.7, 5ctr.1.A, 5gjq.1.5, 3u4t.1.A, 2iwa.1.A, 1u6d.1.A, 5mpb.1.h, 4a1g.2.A, 1iyg.1.A, 4l9o.1.A, 2co0.2.A, 3ww9.1.A, 5obm.152.A, 1fpp.1.B, 5cvl.1.A, 4czv.1.A, 1ihg.1.A, 3soq.1.A, 5bw8.1.C, 3r9a.1.D, 5naf.1.A, 2h13.1.A, 3r9a.1.B, 1tnu.1.A, 3sn6.1.B, 6c23.1.D, 5tzs.1.e, 6c23.1.F, 1qqe.1.A, 6bq1.1.B, 2dg1.1.A, 5din.1.B, 1r5m.1.A, 4gq1.1.A, 3gj4.1.B, 5w65.1.O, 5c13.1.A, 4cc9.1.A, 5w5h.2.E, 3wwa.1.A, 5gvb.1.A, 5tzs.1.1, 2pm9.1.A, 2q7f.1.A, 5diz.2.A, 5nkp.2.A, 4o6f.1.A, 3w15.1.A, 3bws.1.A, 2bug.1.A, 5an3.1.A, 5vyc.4.I, 4o5t.1.A, 4jsn.1.A, 4jsn.1.B, 5ein.1.F, 3elq.1.A, 4pjq.1.A, 5cxc.1.B, 5cxc.1.A, 5b26.1.B, 1jof.1.A, 6em3.1.E, 3h7n.1.A, 2ias.1.A, 4m59.1.B, 3sfz.1.A, 4m59.1.A, 5jcs.1.3, 3hx6.1.A, 5yc3.1.A, 4yvd.1.A, 2y43.1.A, 5fjy.1.B, 5fjy.1.A, 2y43.1.B, 5l0y.6.A, 3fmo.1.A, 1o1r.1.A, 5sum.1.A, 1fwx.1.A, 5a5t.1.A, 5a5t.1.C, 4i9c.1.A, 4xmm.1.C, 5jjx.1.A, 2qxv.1.A, 4xmm.1.E, 5jut.45.A, 3shf.1.A, 3jcp.1.Z, 3jcp.1.Y, 4pxw.1.A, 5fks.1.A, 2vgy.1.A, 5nnr.1.A, 3jcp.1.1, 3jcp.1.0, 5wrw.1.A, 5wrw.1.B, 2eep.1.A, 3jcp.1.8, 2c0l.1.A, 3dsm.1.A, 1x4j.1.A, 4wjv.1.A, 5sv7.1.B, 3wwn.1.B, 5wrw.3.A, 3nf1.1.A, 1xfd.1.A, 4d4q.1.A, 5mpe.2.H, 5mpe.2.E, 5mpe.2.F, 2hu8.1.A, 3rjv.1.A, 4g55.1.A, 5n5y.1.P, 5trb.1.A, 3gj7.1.B, 4m57.1.A, 5a6c.1.A, 2lah.1.A, 4i17.1.A, 6eoq.1.A, 5afu.1.C, 6em5.1.5, 2b5l.1.A, 2kiz.1.A, 2miq.1.A, 5a7d.2.A, 5h64.1.A, 5h64.1.B, 5h64.1.C, 4lzf.1.A, 5fkq.1.A, 6em5.1.h, 5t0h.1.V, 2w18.1.A, 4fsc.2.B, 5en7.2.C, 5fww.1.A, 3fhc.1.A, 4kr0.1.A, 4in4.1.A, 3k1l.1.A, 5ic7.1.A, 4d0p.1.A, 5en8.1.B, 4zoy.1.A, 5xw7.2.A, 2d8s.1.A, 5xw7.4.A, 3lrq.2.A, 3lrq.2.B, 4lad.1.B, 5din.1.A, 3pe7.1.A, 5j3x.5.A, 5wlc.25.A, 5t88.1.A, 5uw5.1.A, 4zlh.1.B, 4wjs.1.A, 2mny.1.A, 2pzi.2.A, 3cfs.1.A, 5wlc.41.A, 5haz.1.A, 2eci.1.A, 3vty.4.A, 5nuv.1.A, 1kb0.1.A, 4yd8.1.A, 3wwl.1.A, 3tgo.1.A, 2wfx.1.B, 4og3.1.A, 5hay.2.A, 2bay.2.A, 4a49.1.A, 2kcl.1.A, 5c86.1.A, 5szb.2.C, 3i2n.1.A, 3azq.1.A, 5hb3.2.A, 1kt1.1.A, 5gjq.1.3, 4in3.1.D, 4yzy.1.A, 4l9o.2.A, 4p5o.1.B, 3e4b.4.A, 3f3g.1.C, 3f3g.1.D, 3f3g.1.E, 3prw.1.A, 3i5p.1.A, 4lea.2.A, 4o9d.1.A, 1w6s.1.A, 2qc5.1.A, 2b5n.2.A, 4hdj.1.A, 4jhn.1.A, 2r5s.1.A, 3kd7.2.A, 2xev.3.A, 5a9q.1.5, 3dqv.1.C, 2jr6.1.A, 2xev.1.A, 2y4t.1.A, 3asf.2.A, 3j96.1.J, 3j96.1.H, 5wwm.1.A, 4ax4.1.A, 3j96.1.G, 5n60.1.P, 4i9e.1.B, 1hzv.1.A, 3jb9.1.4, 2q7f.2.A, 4yvq.1.B, 5sui.1.A, 4buj.1.B, 3jb9.1.L, 5vhf.1.H, 3v1s.1.A, 2lni.1.A, 4buj.1.D, 5k0y.1.P, 5vhf.1.S, 5bt1.1.A, 2bbk.1.A, 3jb9.1.S, 3v9f.4.A, 3v9f.2.A, 4gcn.1.A, 4xfv.1.A, 5yz0.1.B, 3uvo.1.A, 3dpl.1.B, 5mr8.1.A, 2y4t.3.A, 4v0n.2.B, 2ct2.1.A, 5vbg.1.A, 1rwl.1.A, 5cvo.1.A, 2jne.1.A, 5mq0.1.I, 2qe8.1.A, 5fmf.1.T, 3upv.1.A, 3q5m.1.A, 5l4k.1.H, 5t0i.1.Y, 5t0i.1.X, 5t0i.1.W, 5t0i.1.V, 5t0i.1.U, 2kcv.1.A, 1rwi.1.A, 4hny.2.A, 4ppe.1.A, 5f72.1.A, 5dka.1.A, 3c9c.1.A, 5nnp.1.A, 4u0s.1.A, 4a11.1.B, 4a11.1.A, 3q15.2.A, 3q7o.1.A, 4wjl.1.A, 4ayc.1.A, 4ayc.1.B, 1l0q.3.A, 2xn4.1.A, 2gnq.1.A, 2ct0.1.A, 1u6g.1.B, 5vhi.1.S, 5hrm.1.A, 1q7f.2.A, 4wsn.6.D, 4g1t.1.A, 4qzv.2.A, 4g1t.1.B, 4j73.1.A, 5tqb.1.B, 4z8l.1.A, 5uw3.1.A, 3h0c.1.A, 3jpx.1.A, 4zey.1.A, 6b3j.1.D, 1ft2.1.A, 2ho1.1.B, 2ho1.1.A, 2n8w.1.A, 3vgz.1.A, 5ola.2.C, 3s94.1.A, 4amy.1.A, 2fbn.1.A, 3q6k.1.A, 5edv.2.B, 2ymu.1.A, 5mpd.1.F, 2i0s.1.C, 5flc.1.F, 2agl.1.C, 3ww7.1.A, 4zoz.1.A, 5k2m.1.E, 5hi7.1.A, 2mta.1.A, 3j9m.72.A, 3ffl.1.A, 1mm3.1.A, 5a01.1.A, 2ojy.1.C, 4rg6.1.A, 4rg6.1.B, 4hho.1.A, 4czy.1.A, 3dwl.1.B, 4me2.1.A, 5iww.1.D, 3ffl.1.B, 4qf3.2.A, 4orh.2.C, 5ljo.1.C, 2y1m.1.A, 4n5c.7.A, 4xmn.1.A, 4xmn.1.B, 4xmn.1.D, 4xmn.1.E, 2y1m.3.A, 5c2v.1.A, 1fbv.1.A, 3hxj.2.A, 3hxj.2.B, 2mhk.1.A, 4yc9.1.A, 3dza.1.A, 2hye.1.A, 5a7d.5.A, 5fa5.1.B, 2hye.1.D, 4ci8.1.A, 5k1a.1.B, 5cww.1.B, 4wz1.1.A, 3ro2.1.A, 5aja.1.A, 2vjf.2.B, 3uzs.1.B, 4amf.1.A, 4nlm.1.A, 4q1v.1.A, 5v1d.1.C, 5v1d.1.A, 4jhr.1.A, 3iax.1.A, 6eoj.1.A, 2dba.1.A, 6eoj.1.C, 5luq.1.A, 4p29.1.A, 3lvg.1.A, 6ez8.1.B, 5a7d.1.A, 5a7d.7.A, 3lvg.1.B, 2c0m.1.A, 3u0s.1.A, 4h5i.1.A, 5t2c.73.A, 4lct.2.B, 4lct.2.A, 4owr.1.A, 4aif.1.A, 3jd5.1.3, 3uux.1.A, 3e37.1.A, 1zbd.1.B, 5chb.1.A, 1weo.1.A, 3jd5.1.U, 5bpt.1.A, 5xyi.1.6, 3gj8.1.B, 5mc6.15.A, 3as5.2.A, 5wxg.1.A, 5jjo.1.A, 3j2t.1.A, 5hb1.1.A, 2vq2.1.A, 1zu2.1.A, 5gwn.1.A, 4rea.1.A, 4cy3.1.A, 5lyb.108.A, 5cyk.1.A, 2aqc.1.A, 4kmo.1.B, 3pz4.1.A, 5jhe.1.A, 3gw4.1.B, 1erj.1.A, 3gw4.1.A, 6bk8.1.V, 6bk8.1.W, 6bk8.1.P, 4n14.1.A, 3u5o.1.A, 4b94.1.A, 3mkq.1.B, 6bk8.1.H, 3mkq.1.D, 3mkq.1.F, 5kdo.1.B, 5bwk.1.D, 5v7v.1.A, 2ond.1.A, 4ccg.1.B, 5m23.1.A, 1kv9.1.A, 3ho5.2.A, 4uuy.1.A, 1ldk.1.C, 4q66.1.D, 3q7f.1.A, 4n2q.1.A, 4jml.1.A, 5it7.77.A, 3sz7.1.A, 3a9g.1.A, 5ait.1.A, 5o85.1.B, 2w8b.1.A, 4l1m.1.A, 3rtr.4.B, 5c1d.1.A, 4r7s.1.A, 4v7r.20.A, 2g9a.1.A, 3spa.1.A, 3vtx.2.A, 5gxh.1.A, 5h3s.1.A, 4apo.1.A, 5l0w.1.A, 5lpi.2.A, 1dce.2.A, 1e8m.1.A, 1tjc.1.A, 4v16.1.A, 4bxr.2.A, 3wxx.1.A, 5wyj.16.A, 5jjw.1.A, 4pk1.1.A, 3gj4.2.B, 5hb0.2.A, 1xnf.1.A, 3f3p.3.D, 4zgc.1.A, 3cik.1.B, 3jck.1.C, 2ecw.1.A, 4u1f.1.A, 3o36.2.A, 4niq.1.A, 5t0j.1.V, 1h2y.1.A, 3jbz.1.A, 5jpq.1.Y, 4qzv.1.A, 6epd.1.V, 6epd.1.W, 6epd.1.T, 6epd.1.U, 6epd.1.S, 6epe.1.X, 6epe.1.W, 6epe.1.V, 3j97.1.H, 6epe.1.T, 6epe.1.S, 1e5t.1.A, 4g23.1.A, 3esl.2.A, 3rfg.1.A, 2h9l.1.A, 2pm7.1.D, 2pm7.1.C, 4ap4.1.A, 2pm7.1.A, 3q7m.1.A, 5iy7.1.Q, 2lsu.1.A, 4kbq.1.A, 4r2y.2.A, 2bgr.1.A, 5aaq.1.A, 4wn4.1.A, 1gq1.1.A, 4hny.1.A, 5gjq.1.9, 4cr3.1.6, 3o37.1.A, 3gre.1.A, 4n5c.4.A, 4n5c.2.A, 4a1g.4.A, 5wql.2.A, 5lqi.1.A, 3wj9.2.A, 3gz2.1.B, 3gz2.1.A, 1q7f.1.A, 4ga1.1.A, 4v3p.1.A, 1yxr.1.A, 5waq.1.A, 5mc6.36.A, 5w5i.1.A, 2ism.1.A, 4mhc.1.A, 4pdt.1.A, 4ljn.1.A, 2j57.1.C, 3pz1.1.A, 3p5c.1.C, 4cr3.1.Z, 4cr3.1.Y, 3iun.1.A, 4l72.3.A, 1u8e.1.B, 1u8e.1.A, 3t6r.2.A, 5lyn.1.A, 5c13.2.C, 2c2l.1.A, 2lri.1.A, 4a0b.2.A, 2hr2.1.A, 2ynp.1.A, 3dxm.1.C, 4tqo.1.A, 4bt9.1.B, 4bt9.1.A, 3o4g.1.B, 4aif.2.A, 1ri6.1.A, 6fbs.1.A, 6fbs.1.B, 2iao.1.A, 4u0u.1.A, 5k1h.1.A, 5en7.2.A, 4eba.1.A, 2if4.1.A, 5efr.1.A, 4gy5.1.A, 4imm.2.A, 3hfq.1.A, 5em2.2.B, 5k2m.1.F, 1wen.1.A, 5bjs.1.A, 5iwb.1.B, 5jzz.1.A, 4cr4.1.U, 4cr4.1.W, 5k19.2.A, 4bp8.1.A, 4cr4.1.X, 4cr4.1.Y, 4cr4.1.Z, 5naf.3.A, 4c8h.1.C, 4c8h.1.A, 4a0l.1.A, 5izw.1.A, 4aez.2.C, 1nex.2.B, 4aez.2.A, 5wsg.1.R, 5en6.1.A, 3lya.1.A, 5wsg.1.U, 5wsg.1.T, 4d6v.1.A, 3jbt.1.A, 5g05.1.K, 5g05.1.O, 5g05.1.C, 4v3k.1.C, 5g05.1.F, 5mpd.1.K, 5mpd.1.J, 5mpd.1.I, 5mpd.1.H, 2i3s.1.A, 4ga2.1.A, 2ect.1.A, 4wz1.2.A, 5mpd.1.G, 5n5z.1.P, 5vab.1.A, 2yq8.1.A, 4cr4.1.6, 5vai.1.D, 3j6x.75.A, 3cvl.1.A, 5b4x.2.B, 3s8z.1.A, 5nus.1.B, 4fhn.1.B, 4a2m.2.A, 5jrk.1.A, 5l0y.7.A, 5jrk.1.B, 5jk7.1.B, 5cqs.2.A, 4qf2.2.B, 2js4.1.A, 1fch.1.A, 5wql.1.A, 1a0r.1.A, 2n8i.1.A, 5m1j.14.A, 1yiq.1.A, 5ft9.2.A, 3ma5.3.A, 4fhm.1.B, 2rfo.2.A, 4fhm.1.A, 2ajl.1.A, 2ajl.1.B, 5wrv.1.B, 5a31.1.O, 5a31.1.J, 5a31.1.H, 2ecf.1.A, 5a31.1.C, 4iqk.1.A, 2lsv.1.A, 1qbi.1.A, 1mm2.1.A, 3jap.1.i, 5a31.1.W, 5a31.1.V, 5x54.1.A, 5a31.1.R, 5a31.1.P, 5j3j.1.A, 5u5h.1.A, 3ei3.1.A, 5yp4.2.A, 3ho5.1.A, 5shb.1.A, 5b26.1.A, 5bpw.1.A, 4a0l.2.A, 4v8m.8.A, 2q7q.1.C, 2v5f.1.A, 5l0y.2.A, 3s8v.2.A, 2z2n.1.A, 5t0h.1.W, 5t0h.1.U, 1hz4.1.A, 2l5u.1.A, 5k18.1.A, 5t0h.1.Y, 4d4o.1.B,

4d4o.1.A, 3e4b.2.A, 1pi6.1.A, 5mpe.1.H, 2yba.1.A, 5tf2.1.A, 5xjc.1.W, 5xjc.1.T, 4qam.1.A, 4j8d.1.A, 2iaa.1.A, 5xjc.1.E, 5mpc.1.e, 5xjc.1.J, 5xjc.1.I, 1p22.1.A, 2jrj.1.A, 5mpc.1.f, 1mg2.1.A, 4cgv.2.A, 5c9s.1.A, 4abn.2.A, 3rkv.1.A, 6b3x.1.A, 5vfc.1.A, 4wju.1.A, 5w1r.1.A, 6az1.1.6, 5oj8.1.A, 5wuk.1.A, 1s4u.1.A, 3j77.45.A, 2yms.1.C, 2ecy.1.A, 3urz.1.A, 5vat.1.A, 5gap.1.F, 5gap.1.G, 3u4y.1.A, 3qqz.1.A, 3p5b.1.C, 4qrj.1.A, 5hqg.1.A, 5tbk.2.B, 3m0c.1.C, 5aem.1.A, 4qpl.1.A, 4dnv.1.A, 4zcn.1.A, 4zcn.1.C, 1sq9.1.A, 5fzs.1.A, 3o48.1.A, 5lyp.1.A, 5dbk.1.B, 5dbk.1.A, 4zb4.1.A, 5o01.2.A, 2pqn.1.A, 5ayw.1.B, 3qky.1.A, 2fo7.1.A, 5ayw.1.D, 2yur.1.A, 4ptb.1.A, 4wfb.1.Y, 5wxh.1.A, 4gpk.2.B, 4gpk.2.C, 4gpk.2.A, 4cgw.1.A, 4gpk.2.D, 3zvz.1.A, 4whv.1.B, 4whv.1.C, 5a2q.1.8, 5wyj.33.A, 1p5q.1.B, 2vsy.1.A, 5kc2.1.B, 4a08.1.A, 4a08.1.B, 3ah8.1.B, 4uqy.1.A, 2avp.1.A, 2xu7.1.A, 5flx.1.7, 3u64.2.H, 3lca.1.A, 5mpc.1.h, 5mpc.1.i, 5mpc.1.d, 5ioj.1.A, 3asg.1.A, 5mpc.1.g, 4ifl.1.A, 5ccl.1.A, 5jjt.1.A, 1c5k.1.A, 3s94.2.A, 5ojf.1.A, 2eid.1.A, 3f7f.1.A, 1p5q.1.A, 4hnx.1.A, 1p5q.1.C, 4hxg.1.A, 4hxf.1.F, 4ycz.1.A, 3mxx.1.A, 4reb.1.C, 4reb.1.D, 4gcn.2.A, 1ve7.1.A, 4ozu.1.A, 4a1g.1.A, 3c75.1.A, 5t0c.44.A, 3dqv.3.C, 5fxy.2.A, 5fey.1.B, 3mks.1.D, 4a1g.3.A, 4v7e.7.A, 2ckl.1.B, 5ctr.2.A, 4y6c.1.A, 5iy6.1.Q, 2jmd.1.A, 5ctq.1.A, 5ctq.1.B, 5n1a.1.A, 5ukm.1.B, 5h1t.1.A, 5u69.1.A, 5a31.1.B, 2k4d.1.A, 2iwf.1.A, 5mpb.1.d, 5udj.1.A, 5hrz.1.A, 4y49.1.A, 3frx.1.A, 5uzw.1.A, 3j9m.81.A, 5v1d.2.A, 1h4i.1.A, 4f3v.1.A, 6bw3.1.A, 5k04.1.A, 6eoo.1.A, 4v5o.1.0, 2h0d.1.A, 1elw.1.A, 2xl2.1.A, 3ru0.1.A, 2d0v.1.A, 4le7.1.A, 1xip.1.A, 3t6r.1.A, 5fsb.1.A, 3ei4.1.A, 5ekq.1.B, 4rea.1.B, 5n4w.1.C, 4gco.1.A, 2lgv.1.A, 5h1j.1.A, 5f30.1.A, 2pbi.2.B, 3qou.1.A, 1n9a.1.A, 6epf.1.T, 6epf.1.U, 6epf.1.V, 6epf.1.W, 6epf.1.S, 4gyw.1.A, 5fvm.1.C, 5fvm.1.A, 3iuj.1.A, 4xf2.1.C, 5m11.1.A, 5vzt.1.B, 4ga0.1.A, 2ckl.1.A, 1l0q.1.A, 5cgj.1.A, 2g8s.1.A, 5cvn.1.A, 4unm.1.A, 1iym.1.A, 5wve.1.K, 3dm0.1.A, 3sob.1.B, 4ffv.1.A, 4bp9.1.A, 4i1a.2.A, 3v43.1.A, 4bzk.1.D, 2md8.1.A, 1c9i.1.A, 4aah.1.A, 3ieg.1.A, 5tga.33.A, 5g04.1.Q, 5g04.1.P, 5g04.1.U, 2aq5.1.A, 5mpb.1.i, 5mzu.1.A, 5g04.1.C, 4o5s.1.A, 5g04.1.F, 5g04.1.I, 5g04.1.H, 5g04.1.K, 5g04.1.J, 5g04.1.O, 2kft.1.A, 5wp3.1.A, 1dy7.1.A, 4it4.1.A, 2g99.1.A, 3ho4.1.A, 3gz1.1.B, 5ln3.1.V, 4cgu.1.A, 1e2r.1.A, 5a7d.3.A, 3sjl.1.D, 5xgs.1.B, 2ojh.1.A, 3dr2.1.A, 5en7.1.C, 4dg6.1.A, 5hy7.2.A, 2lxp.1.C, 5b78.1.A, 4w9r.1.A, 2dcm.1.A, 4rib.1.A, 4ric.1.A, 5xw7.3.A, 5xw7.5.A, 1e4u.1.A, 5wlc.17.A, 5l8s.1.A, 5wvi.1.c, 5wlc.15.A, 4gm9.2.A, 2vsy.2.A, 5o9z.1.L, 5wvi.1.O, 5wvi.1.L, 3mv2.1.B, 5mwj.1.A, 5o9z.1.F, 5o9z.1.G, 5lfl.1.A, 3mun.1.A, 2ea6.1.A, 3s7f.1.A, 5wvi.1.V, 3q75.1.A, 3b13.1.A, 5jkp.1.A, 5m5g.1.A, 3hkz.1.L, 4wuy.1.A, 5en6.2.A, 4wju.2.A, 5hay.1.A, 1k8k.1.C, 2vgx.1.A, 2vgx.1.B, 1k3i.1.A, 4v3l.1.C, 2eib.1.A, 4gnb.1.A, 4raa.1.A, 3qwp.1.A, 2qzp.1.A, 5u2j.1.B, 3vty.1.A, 5wlc.28.A, 5a9q.1.T, 5a9q.1.W, 6f1t.1.b, 6f1t.1.c, 5wlc.19.A, 1crz.1.A, 5a9q.1.L, 3lpz.1.A, 5a9q.1.I, 5sxm.1.A, 5a9q.1.E, 5a9q.1.G, 5a9q.1.F, 1b89.1.A, 5a9q.1.C, 5a9q.1.B, 4jhp.1.B, 1nzn.1.A, 5t88.2.A, 5wlc.26.A, 5l8e.1.A, 3s9j.1.A, 4j8e.2.A, 4ljp.1.A, 2kwo.1.B, 6epc.1.U, 5a9q.1.a, 4v6i.1.A, 4v3k.2.C, 3ewe.1.A, 3ewe.1.B, 4n2s.1.A, 3j6y.75.A, 5hxb.1.B, 6f1t.1.4, 6f1t.1.3, 4tkp.1.B, 1w3b.1.B, 1bpo.1.B, 1bpo.1.A, 1w3b.1.A, 5igq.1.A, 2uy1.1.B, 5a9q.1.2, 3o4h.2.A, 4q1u.1.A, 3jam.1.7, 5fz5.1.U, 3pdn.1.A, 3uq3.1.A, 4psw.1.B, 5lpi.4.A, 3asf.1.A, 3azo.1.A, 2gbg.1.A, 2wvi.1.A, 2qfc.1.A, 3dw8.1.B, 1vz3.1.A, 4a0p.1.A, 4ynd.1.A, 2k16.1.A, 5ojs.1.A, 5bv1.2.B, 2woz.1.A, 6f38.1.3, 6f38.1.4, 4bxp.1.A, 2mq1.1.A, 5oej.1.A, 3i1c.1.A, 5aio.1.A, 1h4j.1.A, 6f38.1.b, 6f38.1.c, 3wdz.1.A, 1bor.1.A, 4xmm.1.D, 3o4j.1.A, 3o4j.1.B, 3kih.1.A, 1tbg.1.E, 3kih.1.C, 3kih.1.E, 1tbg.1.A, 1zbp.1.A, 4ci1.1.A, 3lrv.1.A, 5d9b.1.A, 1e2r.1.B, 5t0g.1.Y, 5t0g.1.X, 2ke1.1.A, 6exn.1.R, 4r5o.4.A, 3n0d.1.A, 1wao.1.A, 3asg.2.A, 5t0g.1.V, 2yh3.1.A, 5vtb.1.A, 1xhm.1.A, 1wao.3.A, 5j3x.1.A, 4xpd.1.A, 3u5n.2.A, 3smr.1.A, 1orv.1.A, 5oql.1.F, 4j79.1.A, 3sf4.2.A, 5ola.1.C, 5gva.1.A, 5lg7.1.A, 5oql.1.E, 5hh7.1.A, 4r7e.1.A, 5fb0.1.A, 5hb3.1.A, 5vhi.1.H, 4gn7.1.A, 5vdc.1.A, 5oql.1.M, 2djb.1.A, 4r2y.4.A, 4zql.1.A, 4xnh.1.A, 3sox.4.B, 4xi0.1.A, 5t0g.1.5, 4jsp.1.A, 3mkr.1.B, 3mkr.1.A, 1yfq.1.A, 5ij7.1.B, 5ljo.1.A, 4r89.1.A, 2mt5.1.A, 4hou.1.A, 5ex7.1.A, 4am9.1.A, 5jw7.1.B, 2ff4.1.A, 6emk.1.A, 1wgm.1.A, 2mnz.1.A, 1n7d.1.A, 5lg0.1.A, 4u04.1.A, 2kck.1.A, 4zov.2.A, 3c12.1.A, 2xcc.1.B, 4wng.1.A, 4a0k.1.C, 4a0k.1.D, 4f52.2.B, 4rec.1.A, 3ks2.1.A, 3sbp.1.A, 3i4r.1.A, 3hxj.1.B, 3hxj.1.A, 3qil.1.B, 3qil.1.C, 3qil.1.A, 2md7.1.A, 4a4c.1.A, 5hy7.1.A, 1a17.1.A, 3q54.1.A, 4e54.1.B, 4e54.1.A, 4tz4.1.A, 3j81.1.5, 5h1k.1.A, 1z6u.2.A, 5iy9.1.Q, 4orh.1.D, 3ho3.1.A, 4orh.1.C, 3ei4.1.B, 4n5c.8.A, 4lk9.1.A, 1r9m.1.A, 2oaj.1.A, 2yms.1.D, 2h6k.1.A, 2yms.1.B, 4n5c.6.A, 2yms.1.A, 4e85.1.A, 4x33.1.B, 5wft.1.A, 5cyk.1.B, 3ulq.1.A, 5vhs.1.H, 5vhr.1.H, 3ask.1.A, 4y5r.1.C, 3q8w.1.A, 3ash.1.A, 4r8a.1.A, 1hh8.1.A, 5lfm.1.A, 5lks.64.A, 1z6u.1.A, 5yp1.2.A, 4leu.1.A, 5yp1.2.B, 5h13.1.A, 1nl4.1.A, 5v1d.2.B, 2y1m.6.A, 6bll.1.A, 4hvt.1.A, 6bll.1.B, 1gp2.1.B, 2vdu.1.A, 5a5b.1.Z, 5a5b.1.Y, 4rid.2.A, 5a5b.1.W, 4jxm.1.A, 3euv.1.A, 3ho4.2.A, 6bcx.1.A, 6bcx.1.C, 6f3a.1.3, 6f3a.1.2, 1npe.1.A, 3va6.1.A, 4nsx.1.A, 3c72.1.A, 2r2l.1.A, 5ukk.1.B, 3das.1.A, 3qdn.1.A, 5tdh.1.B, 5wvk.1.k, 5wvk.1.d, 5wvk.1.a, 5wvk.1.b, 5wvk.1.c, 4gyo.1.A, 5o75.1.A, 4lct.1.A, 4lct.1.B, 3g4e.1.A, 1b2p.1.A, 2qzp.2.A, 3k9i.1.A, 4ybm.1.A, 4y6w.1.A, 3oxl.1.A, 4wce.1.Y, 5i3l.1.A, 5ndv.73.A, 5wvk.1.8, 4q6f.4.A, 6epf.1.X, 3o35.1.A, 6f9n.1.B, 4mae.1.A, 4oe1.1.A, 4oe1.1.B, 5ln3.1.Z, 2zir.1.A, 3ma5.1.A, 5hax.1.A, 5njx.1.A, 2rip.1.A, 4bwr.1.A, 2bay.3.B, 1elr.1.A, 2puy.1.A, 4nrh.1.B, 5gje.1.B, 5gje.1.A, 4fa4.1.D, 1flg.1.A, 4d9s.1.A, 5ogs.1.A, 4pjr.1.A, 5kcn.1.A, 5o7x.4.A, 3kqi.1.A, 4bta.1.B, 4bta.1.A, 3as5.1.A, 3si5.2.A, 4h7y.3.A, 2b5n.4.A, 3hxr.1.A, 6ek0.64.A, 4cgq.1.A, 1ijq.1.A, 3ww8.1.B, 5jus.45.A, 3esl.1.A, 5i9g.1.A, 5min.1.A, 4qf3.1.A, 3cvn.1.A, 4a5s.1.A, 1dce.1.A, 2xzh.1.A, 5hb0.1.A, 5oa1.1.S, 5ex0.1.A, 4j0u.1.A, 5hb0.3.A, 3ro3.1.A, 5l8w.1.B, 4wsl.1.A, 3f3p.2.B, 5omp.1.A, 4f52.1.B, 1pfq.1.A, 4cr2.1.X, 1pfq.1.B, 4cr2.1.W, 4cr2.1.U, 5wbk.1.A, 4v7f.1.j, 4gm3.1.A, 3jcm.1.D, 3jcm.1.B, 3v7d.1.B, 2bcj.1.B, 4d10.1.D, 4d10.1.B, 4d10.1.C, 4d10.1.A, 5w5y.1.O, 5gpy.1.A, 5jj6.1.A, 5jj6.1.B, 1qbq.1.A, 1mzc.1.A, 3o33.1.A, 5t2a.48.A, 2wpv.1.A, 2kwn.1.B, 3nok.1.A, 5arf.1.A, 4r40.1.A, 3iuq.1.A, 3mvd.1.K, 4cr2.1.6, 3sww.1.A, 2xpi.1.C, 2xpi.1.A, 2hqs.1.A, 3o4i.1.A, 3zn3.1.A, 4cy2.1.A, 3wj9.1.A, 2fpb.1.A, 4v92.1.8, 2xeu.1.A, 5en8.1.A, 2i3t.1.A, 5vhm.1.H, 5o3w.1.A, 2l43.1.A, 3ly7.1.A, 1utc.1.A, 3jan.80.A, 6epe.1.Z, 4og6.1.A, 4wnd.1.A, 3rtr.1.B, 5a9q.1.A, 4ry3.1.A, 5jpq.1.I, 4bxq.1.A, 2fp9.1.A, 6epe.1.U, 4bts.27.A, 5hb2.1.A, 1wy6.1.A, 2iap.1.A, 2o9k.1.A, 3esk.1.A, 2xgm.2.A, 4e5z.1.A, 6epd.1.X, 5udl.1.A, 4e5z.1.B, 3pz2.1.A, 3osv.1.A, 2e6r.1.A, 2z2p.1.A, 2w8b.2.A, 4a0b.1.B, 3asd.1.A, 4a0b.1.A, 2wb7.1.A, 4eba.2.A, 5wbi.1.A, 5tee.1.A, 3bg0.1.A, 3fwv.1.A, 3bg0.1.H, 5nnz.2.A, 2v6x.1.A, 5y3r.1.F, 5juy.1.B, 5d0o.1.B, 5d0o.1.D, 5juy.1.D, 5juy.1.E, 3v65.1.C, 3v65.1.B, 2m85.1.A, 3tkn.1.A, 3hac.1.A, 5lxz.1.A, 2ivz.1.A, 5hyn.2.B, 5juo.45.A, 4ehm.1.A, 3rfh.1.A, 3rfh.1.B, 5ccm.1.A, 5fzp.1.A, 2pk7.1.A, 3fp2.1.A, 2pk7.1.B, 5em2.1.B, 5em2.1.A, 4xgl.1.A, 5ams.1.A, 2hf1.2.A, 5mzh.1.A, 3i7p.1.A, 4fhn.2.B, 5wg4.1.B, 5m32.1.a, 5m32.1.b, 5m32.1.c, 4wsn.6.B, 4xmb.1.A, 4a0c.2.C, 6f5d.1.J, 6f5d.1.K, 6f5d.1.L, 2ysl.1.A, 4wsn.2.B, 4wsn.2.C, 4wsn.2.A, 4wsn.2.D, 1chc.1.A, 2ifu.1.A, 4c8s.1.A, 2wqh.1.A, 2xe4.1.A, 3asl.1.A, 4ld3.1.A, 5a5u.1.B, 4u7a.1.A, 5lcw.1.Q, 5lcw.1.R, 5lcw.1.S, 4pv7.1.A, 1ltx.1.A, 4boc.1.A, 5m32.1.9, 2dso.1.A, 2f0y.1.A, 5lcw.1.B, 5lcw.1.C, 5lcw.1.O, 5lcw.1.I, 4i2w.1.A, 4yvo.1.A, 5lwv.1.A, 5buz.1.B, 4yhc.1.A, 5i1z.5.C, 2wq8.1.A, 2lxh.1.A, 3ma5.4.A, 4exv.1.A, 3qww.1.A, 3ddu.1.A, 4gq2.1.B, 4gq2.1.A, 1fch.2.A, 3qbj.1.A, 4i79.1.A, 2b5n.1.A, 2vpj.1.A, 2z2o.1.A, 1ur6.1.B, 5w64.1.O, 1qni.1.A, 4o9d.2.A, 3oxg.1.A, 1fp0.1.A, 4ria.1.A, 4zov.1.A, 3wqh.1.A, 3wqh.1.B, 3ei4.3.A, 3dra.1.A, 4zlh.1.A, 3qhy.1.B, 4d4p.1.A, 1r9n.1.A, 2nc9.1.A, 3bg0.1.D, 5xi8.1.A, 4j0x.1.A, 3o34.1.A, 1na3.1.A, 4zlr.1.A, 2xbg.1.A, 1ldj.1.B, 2gvu.1.A, 4pjq.2.A, 4xei.1.C, 5ft9.1.A, 4j8f.1.A, 2kat.1.A, 5xw7.1.A, 2jid.1.A, 2b5n.3.A, 2z2o.3.A, 4xga.1.A, 2ghs.1.A, 3rrm.1.C, 5wcg.1.A, 5g04.1.T, 1iip.1.A, 5uz5.1.D, 5uz5.1.E, 4gqb.1.B, 4a0l.1.B, 5fzq.1.C, 5lls.1.A, 5fzq.1.A, 6epd.1.Z, 5x6o.1.A, 1o6g.1.A, 6bcu.1.A, 5l0y.5.B, 5l0y.5.A, 6bcu.1.B, 4mh1.1.A, 4mh1.1.B, 5vat.2.A, 5l0y.3.A, 3s8v.1.A, 3iur.1.A, 5hq8.1.A, 5g04.1.B, 5fyw.1.U, 4yzs.1.A, 1x2r.1.A, 4pwz.1.A, 5mpe.1.J, 5mpe.1.K, 5dse.2.A, 2j04.1.A, 5o3x.1.A, 3n0e.1.A, 2j04.1.B, 3ei2.1.A, 3ei2.1.B, 1na0.1.A, 2wg3.1.B, 4j0w.1.A, 2vsn.1.A, 2v91.1.A, 2h0d.1.B, 4d4q.2.A, 3u3w.1.B, 2iaw.1.A, 1t2x.1.A, 3scy.1.A, 1kt0.1.A, 4ptb.2.A, 2b5l.2.A, 5wxh.2.A, 3jco.1.Y, 3jco.1.Z, 3jco.1.W, 2onc.1.A, 5grs.1.A, 2z3z.1.A, 4a7j.1.A, 4pwx.1.C, 5tbk.5.B, 4kzz.1.6, 2ijq.1.A, 3jco.1.0, 3jco.1.1, 3k1l.2.A, 2ln0.1.A, 2oit.1.A, 3tc9.1.A, 4i0o.1.A, 5a6c.2.A, 3jaq.1.i, 2bay.1.B, 2bay.1.A, 1pev.1.A, 2iau.1.A, 3e4b.3.A, 5n4c.1.A, 5wlc.24.A, 2pm6.1.C, 5dfz.1.C, 5wlc.22.A, 2puy.1.B, 2qr5.1.A, 2l6j.1.A, 5che.1.E, 5che.1.F, 5wlc.20.A, 1a12.1.B, 1a12.1.C, 1a12.1.A, 3ly8.1.A, 2cnx.1.A, 1k32.1.A, 5i9f.1.A, 3vty.3.A, 3g4h.1.B, 3g4h.1.A, 4dnw.1.A, 2bay.3.A, 5ttw.2.A, 4zn4.1.A, 4u1e.1.A, 1d8d.1.A, 4ayb.1.L, 5i2t.1.A, 5txe.1.A, 4gga.1.A, 3f3p.2.C, 4bh6.1.A, 1got.1.B, 4wzx.1.A, 3s25.1.A, 3p1l.1.A, 5ctq.2.B, 5ctq.2.A, 4e6h.1.A, 3vnh.1.A, 2egp.1.A, 5lzz.77.A, 3j98.1.I, 3j98.1.H, 4buj.2.B, 3vng.1.A, 3ceq.1.A, 3ceq.1.B, 4naa.1.A, 4ay5.1.A, 2wb7.2.A, 1wee.1.A, 2xev.2.A, 4cr2.1.Z, 3bee.2.A, 5fzr.1.A, 5fzr.1.B, 3wwb.1.A, 4cr2.1.Y, 4r8p.1.K, 4d5l.1.7, 4ri9.1.A, 5xgs.1.A, 4ggc.1.A, 4ynv.1.A, 3iiy.1.A, 5fzq.1.B, 2pbi.1.B, 3jai.77.A, 2ecm.1.A, 2pzi.1.A, 3f3f.1.A, 3f8s.1.A, 3f3f.1.C, 4yzs.1.B, 3f3f.1.D, 3f3f.1.G, 4r2y.1.A, 5i9h.1.A, 5sva.1.7, 3fp3.1.A, 5nnp.2.A, 2pm6.1.B, 5vhq.1.H, 2pm6.1.A, 2wft.1.A, 4rid.1.A, 4dnu.1.A, 3v9f.3.A, 5ex3.1.A, 3c5m.1.A, 5jg6.1.A, 5uz7.1.B, 3e5z.1.A, 5ic8.4.A, 1wcy.1.A, 1u4c.1.A, 3v9f.1.A, 4ci8.2.A

SWISS-MODEL Homology Modelling Report

Model Building Report

This document lists the results for the homology modelling project "IF140_HUMAN Q96RY7 Intraflagellar transport protein 140 homolog" submitted to SWISS-MODEL workspace on Feb. 25, 2018, 7:40 p.m..The submitted primary amino acid sequence is given in Table T1.

If you use any results in your research, please cite the relevant publications:

- Biasini, M., Bienert, S., Waterhouse, A., Arnold, K., Studer, G., Schmidt, T., Kiefer, F., Cassarino, T.G., Bertoni, M., Bordoli, L., Schwede, T. SWISS-MODEL: modelling protein tertiary and quaternary structure using evolutionary information. Nucleic Acids Res. 42, W252-W258 (2014). doi
- Guex, N., Peitsch, M.C., Schwede, T. Automated comparative protein structure modeling with SWISS-MODEL and Swiss-PdbViewer: A historical perspective. Electrophoresis 30, S162-S173 (2009). doi
- Bienert, S., Waterhouse, A., de Beer, T.A., Tauriello, G., Studer, G., Bordoli, L., Schwede, T. The SWISS-MODEL Repository - new features and functionality. Nucleic Acids Res. 45, D313-D319 (2017). doi
- Benkert, P., Biasini, M., Schwede, T. Toward the estimation of the absolute quality of individual protein structure models. Bioinformatics 27, 343-350 (2011). doi
- Bertoni, M., Kiefer, F., Biasini, M., Bordoli, L., Schwede, T. Modeling protein quaternary structure of homo- and hetero-oligomers beyond binary interactions by homology. Scientific Reports 7 (2017). doi

Results

The SWISS-MODEL template library (SMTL version 2018-02-21, PDB release 2018-02-16) was searched with BLAST (Camacho et al.) and HHBlits (Remmert, et al.) for evolutionary related structures matching the target sequence in Table T1. For details on the template search, see Materials and Methods. Overall 3643 templates were found (Table T2).

Models

The following models were built (see Materials and Methods "Model Building"):

Model #01	File	Built with	Oligo-State	Ligands	GMQE	QMEAN
	PDB	ProMod3 Version 1.1.0.	monomer (matching prediction)	None	0.25	-6.43

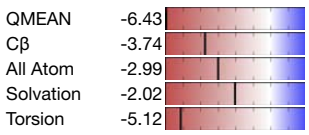

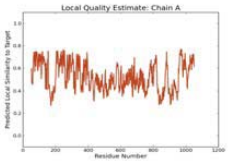

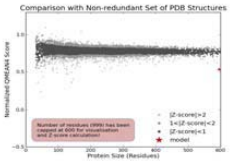

Template	Seq Identity	Oligo-state	QSQE	Found by	Method	Resolution	Seq Similarity	Range	Coverage	Description
3mkq.1.A	13.33	homo-trimer	0.00	HHblits	X-ray	2.50Å	0.27	53 - 1051	0.49	Coatomer beta'-subunit

The template contained no ligands.

```
Target    MALYYDHQIEAPDAAGSPSFISWHPVHPFLAVAYISTTSTGSVDIYLEQGECVPDTHVERPFRVASLCWHPTRLVLAVGW
3mkq.1.A  ----------------------------------------------------KKTFS-NRSDRVKGIDFHPTEPWVLTTL

Target    ETGEVTVFNKQDKEQHTMPLTHTADITVLRWSPSGNCLLSGDRLGVLLLWRLDQRGRVQGTPLLKHEYGKHLTHCIFRLP
3mkq.1.A  YSGRVEIWNYETQVEVRSIQVTETPVRAGKFIARKNWIIVGSDDFRIRVFNYNTGEKVV--DFEAHP--DYIRSIA----

Target    PPGEDLVQLAKAAVSGDEKALDMFNWKKSSSGSLLKMGSHEGLLFFVSLMDGTVHYVDE-KG-KTTQVVS-ADSTIQMLF
3mkq.1.A  -------------------------VH------------PTKPYVLSGSDDLTVKLWNWENNWALEQTFEGHEHFVMCVA

Target    YME-KREALVVVTENLRLSLYTVPPEGKAEEVMKVKLSGKT-GRRADIAL-I--EGSLLVMAVGEAALRFWDIERGENYI
3mkq.1.A  FNPKDPSTFASGCLDRTVKVWSLGQ-ST---PN-FTLTTGQERGVNYVDYYPLPDKPYMITASDDLTIKIWDYQTKSCV-
```

```
Target    LSPDEKFGFEKGENMNCVCYCKVKGLLAAGTDRGRVAMWRKVPDFLGSPGAEGKDRWALQTPTELQGNITQIQWGS--RK
3mkq.1.A  ATLEGH-----MSNVSFAVFHPTLPIIISGSEDGTLKIWNSST---------YK---VEKTLNVGLERSWCIATHPTGRK

Target    NLLAVNSVISVAILSERAMSSHFHQQVAAMQVSPSLLNVCFLST--------------------GVAHSL------RTDM
3mkq.1.A  NYIASGFDNGFTVLSLGN-------DEPTLSLDPVGKLVWSGGKNAAASDIFTAVIRGNEEVEQDEPLSLQTKELGSVDV

Target    HISGVFATKDA--VAVWNGRQVAIFELSGA------AIRSAGTFLCETPVLAMHEENVYTVESNRVQVRT-WQGTVKQLL
3mkq.1.A  FPQSLAHSPNGRFVTVVGDGEYVIYTALAWRNKAFGKC-QDFVWGPDSNSYALI------DETGQIKYYKNFKEVTSWS-

Target    LFSETEGNPCFLDICGNF---LVVGTDLAHFKSFDLSRREAKAHCSCRSLAELVPGVGGIASLRCSSSGSTISILPSKAD
3mkq.1.A  -------VPMHSAIDRLFSGALLGVKSDGFVYFFDWDNGTLVRRID----------VNAKDVIWSDNGELVMIVNTNSN

Target    NSPDSKICFYDVEMDTVTVFDFKTGQIDRRETLSFNEQETNKSHLFVD-EGLKNYVPVNHFWDQSEPRLFVCEAVQETPR
3mkq.1.A  GDEA-SGYTLLFNKDAY-LEAANNGNID---------DSEGVDEAFDVLYEL-SESITSGKWVGD---VFIFTT--A---

Target    SQPQSANGQPQDGRAGPAADVLILSFFISEEHGFLLHESFPRPATSHSLLG--MEVPYYYFTRKPEEADREDEVEPGCHH
3mkq.1.A  --------------TN-----RLN-YFVGGKTYNLAH----YTK-EMYLLGYLARDNKVYLADREVHVYG----------

Target    IPQMVSRRPLRDFVGLEDCDKATRDAMLHFSFFVTIGDMDEA-FKSIKLIKSEAVWENMARMCVKTQRLDVAKVCLGNMG
3mkq.1.A  ------------YE--------ISLEVLEFQTLTLRGEIEEAIENVLPNVEGKDSLTKIARFLEGQEYYEEALNI-----

Target    HARGARALREAEQEPELEARVAVLATQLGMLEDAEQLYRKCKRHDLLNKFYQAAGRWQEALQVAEHHDRVHLRSTYHRYA
3mkq.1.A  ------------------------------------SPDQDQ---KFELALKVGQLTLARDLLTDE-------------

Target    GHLEASADCSRALSYYEKSDTHRFEVPRMLSEDLPSLELYVNKMKDKTLWRWWAQYLESQGEMDAALHYYELARDHFSLV
3mkq.1.A  ----------------------------------------------SAEMKWRALGDASLQRFNFKLAIEAFTNAHDLESLF

Target    RIHCFQGNVQKAAQIANETGNLAASYHLARQYESQEEVGQAVHFYTRAQAFKNAIRLCKENGLDDQLMNLALLSSPEDMI
3mkq.1.A  LLHSSFNNKEGLVTLAKDAETTGKFNLAFNAYWIAGDIQGAKDLLIKSQRFSEAAFLGSTYGL-----------------

Target    EAARYYEEKGVQMDRAVMLYHKAGHFSKALELAFATQQFVALQLIAEDLDETSDPALLARCSDFFIEHSQYERAVELLLA
3mkq.1.A  ----------------------------------------------------------------------------------

Target    ARKYQEALQLCLGQNMSITEEMAEKMTVAKDSSDLPEESRRELLEQIADCCMRQGSYHLATKKYTQAGNKLKAMRALLKS
3mkq.1.A  ----------------------------------------------------------------------------------

Target    GDTEKITFFASVSRQKEIYIMAANYLQSLDWRKEPEIMKNIIGFYTKGRALDLLAGFYDACAQVEIDEYQNYDKAHGALT
3mkq.1.A  ----------------------------------------------------------------------------------

Target    EAYKCLAKAKAKSPLDQETRLAQLQSRMALVKRFIQARRTYTEDPKESIKQCELLLEEPDLDSTIRIGDVYGFLVEHYVR
3mkq.1.A  ----------------------------------------------------------------------------------

Target    KEEYQTAYRFLEEMRRRLPLANMSYYVSPQAVDAVHRGLGLPLPRTVPEQVRHNSMEDARELDEEVVEEADDDP
3mkq.1.A  ---------------------------------------------------------------------------
```

Model #02	File	Built with	Oligo-State	Ligands	GMQE	QMEAN
	PDB	ProMod3 Version 1.1.0.	monomer	None	0.24	-7.79

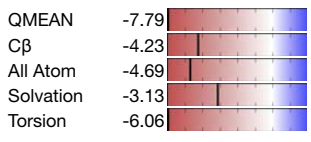

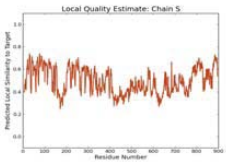

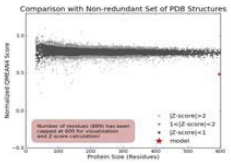

Template	Seq Identity	Oligo-state	Found by	Method	Resolution	Seq Similarity	Range	Coverage	Description
5a1u.1.S	13.38	monomer	HHblits	EM	13.00Å	0.27	7 - 895	0.47	COATOMER SUBUNIT ALPHA

The template contained no ligands.

```
Target    MALYYDHQIEAPDAAGSPSFISWHPVHPFLAVAYISTTSTGSVDIYL-EQGECVPDTHVERPFRVASLCWHPTRLVLAVG
5a1u.1.S  ------TKFETKS--ARVKGLSFHPKRPWILTSL----HNGVIQLWDYRMCTLIDKFD-EHDGPVRGIDFHKQQPLFVSG

Target    WETGEVTVFNKQDKEQHTMPLTHTADITVLRWSPSGNCLLSGDRLGVLLLWRLDQRGRVQGTPLLKHEYGKHLTHCIFRL
5a1u.1.S  GDDYKIKVWNYKLRRCLFTLLGHLDYIRTTFFHHEYPWILSASDDQTIRVWNWQSRTCVC--VLTGHN--HYVMCAQ---

Target    PPPGEDLVQLAKAAVSGDEKALDMFNWKKSSSGSLLKMGSHEGLLFFVSLMDGTVHYVDEKG-K----------------
5a1u.1.S  --------------------------FH------------PSEDLVVSASLDQTVRVWDISGLRKKNLSPGAVESDVRGI

Target    ------------TTQVVS-ADSTIQMLFYMEKREALVVVTENLRLSLYTVPPEGKAEEVMKVKLSGKTGRRADIAL-IEG
5a1u.1.S  TGVDLFGTTDAVVKHVLEGHDRGVNWAAFHPTMPLIVSGADDRQVKIWRMNE-SKA--WEVDTCRGHYNNVSCAVFHPRQ

Target    SLLVMAVGEAALRFWDIERGENYILSPDEKFGFEKGENMNCVCYCKVKGLLAAGTD------------------------
5a1u.1.S  ELILSNSEDKSIRVWDMSKRTGV-QTFRRD-----HDRFWVLAAHPNLNLFAAGHDGGMIVFKLERERPAYAVHGNMLHY

Target    --RGRVAMWRKVPDFLGSPGAEGKDRWALQTPTELQGNITQIQWGSRKNLLAV-----NSVISVAILSERAMSSHFHQQV
5a1u.1.S  VKDRFLRQLDFNS---------SKDVAVMQLRSGSKFPVFNMSYNPAENAVLLCTRASNLENSTYDLYTIPKDADSQ---

Target    AAMQVSPSLLNVCFLSTGVAHSLRTDMHISGVFATKDAVAVWNGRQVAIFELSGAAIRSAGTFLCETPVLAMHEENVYTV
5a1u.1.S  -----NPDA--------------------PEGK---RSS------------------G-LTAVWVARNRFA-------VLD

Target    ESNRVQVRTWQGTVKQLLLFSETEGNPCFLDICGNFLVVGTDLAHFKSFDLSRREAKAHCSCRSLAELVPGVGGIASLRC
5a1u.1.S  RMHSLLIKNLKNEITKKIQVPN--CDEIFYAGTGNLLLR--DADSITLFDVQQKRTLASV----------KISKVKYVIW

Target    SSSGSTISILPSKADNSPDSKICFYDVEMDTVTVFDFKTGQIDRRETLSFNEQETNKSHLFVDEGLKNYVPVNHFWDQSE
5a1u.1.S  SADMSHVALLA-------KHAIVICNRKLDALCNIHEN------------------------------IRVKSGAWDE-S

Target    PRLFVCEAVQETPRSQPQSANGQPQDGRAGPAADVLILSFFISEEHGFLLHESFPRPATSHSLLGMEVPYYYFTRKPEEA
5a1u.1.S  GVFIYTTS--------------------------NHIKYAVTTGDHGIIRTL----D-LPIYVTRVKGNNVYCLDRECRP

Target    DREDEV-----------EPGCHHIPQMVSRR-----PLRDF---VGLE-DCDKATRDAMLHFSFFVTIGDMDEAFKSIKL
5a1u.1.S  RVLTIDPTEFKFKLALINRKYDEVLHMVRNAKLVGQSIIAYLQKKGYPEVALHFVKDEKTRFSLALECGNIEIALEAAKA

Target    IKSEAVWENMARMCVKTQRLDVAKVCLGNMGHARGARALREAEQEPELEARVAVLATQLGMLEDAEQLYRKCKRHDLLNK
5a1u.1.S  LDDKNCWEKLGEVALLQGNHQIVEMCYQRTKNFDKLSFLYLITGNLEKLRKMMKIAEIRKDMSGHYQNALYLGDVSERVR

Target    FYQAAGRWQEALQVAEHHDRVHLRSTYHRYAGHLEASADCSRALSYYEKSDTHRFEVPRMLSEDLPSLELYVNKMKDKTL
5a1u.1.S  ILKNCGQKSLAYLSAATH------------------------------------------------------------

Target    WRWWAQYLESQGEMDAALHYYELARDHFSLVRIHCFQGNVQKAAQIANETGNLAASYHLARQYESQEEVGQAVHFYTRAQ
5a1u.1.S  ------------------------------------------------------------------------------

Target    AFKNAIRLCKENGLDDQLMNLALLSSPEDMIEAARYYEEKGVQMDRAVMLYHKAGHFSKALELAFATQQFVALQLIAEDL
5a1u.1.S  ------------------------------------------------------------------------------

Target    DETSDPALLARCSDFFIEHSQYERAVELLLAARKYQEALQLCLGQNMSITEEMAEKMTVAKDSSDLPEESRRELLEQIAD
5a1u.1.S  ------------------------------------------------------------------------------

Target    CCMRQGSYHLATKKYTQAGNKLKAMRALLKSGDTEKITFFASVSRQKEIYIMAANYLQSLDWRKEPEIMKNIIGFYTKGR
5a1u.1.S  ------------------------------------------------------------------------------

Target    ALDLLAGFYDACAQVEIDEYQNYDKAHGALTEAYKCLAKAKAKSPLDQETRLAQLQSRMALVKRFIQARRTYTEDPKESI
5a1u.1.S  ------------------------------------------------------------------------------

Target    KQCELLLEEPDLDSTIRIGDVYGFLVEHYVRKEEYQTAYRFLEEMRRRLPLANMSYYVSPQAVDAVHRGLGLPLPRTVPE
5a1u.1.S  ------------------------------------------------------------------------------

Target    QVRHNSMEDARELDEEVVEEADDDP
5a1u.1.S  -------------------------
```

Materials and Methods

Template Search

Template search with BLAST and HHBlits has been performed against the SWISS-MODEL template library (SMTL, last update: 2018-02-21, last included PDB release: 2018-02-16).

The target sequence was searched with BLAST against the primary amino acid sequence contained in the SMTL.

An initial HHblits profile has been built using the procedure outlined in (Remmert, et al.), followed by 1 iteration of HHblits against NR20. The obtained profile has then be searched against all profiles of the SMTL. A total of 3698 templates were found.

Template Selection

For each identified template, the template's quality has been predicted from features of the target-template alignment. The templates with the highest quality have then been selected for model building.

Model Building

Models are built based on the target-template alignment using ProMod3. Coordinates which are conserved between the target and the template are copied from the template to the model. Insertions and deletions are remodelled using a fragment library. Side chains are then rebuilt. Finally, the geometry of the resulting model is regularized by using a force field. In case loop modelling with ProMod3 fails, an alternative model is built with PROMOD-II (Guex, et al.).

Model Quality Estimation

The global and per-residue model quality has been assessed using the QMEAN scoring function (Benkert, et al.) . For improved performance, weights of the individual QMEAN terms have been trained specifically for SWISS-MODEL.

Ligand Modelling

Ligands present in the template structure are transferred by homology to the model when the following criteria are met: (a) The ligands are annotated as biologically relevant in the template library, (b) the ligand is in contact with the model, (c) the ligand is not clashing with the protein, (d) the residues in contact with the ligand are conserved between the target and the template. If any of these four criteria is not satisfied, a certain ligand will not be included in the model. The model summary includes information on why and which ligand has not been included.

Oligomeric State Conservation

The quaternary structure annotation of the template is used to model the target sequence in its oligomeric form. The method (Bertoni et al.) is based on a supervised machine learning algorithm, Support Vector Machines (SVM), which combines interface conservation, structural clustering, and other template features to provide a quaternary structure quality estimate (QSQE). The QSQE score is a number between 0 and 1, reflecting the expected accuracy of the interchain contacts for a model built based a given alignment and template. Higher numbers indicate higher reliability. This complements the GMQE score which estimates the accuracy of the tertiary structure of the resulting model.

References

- **BLAST**
  Camacho, C., Coulouris, G., Avagyan, V., Ma, N., Papadopoulos, J., Bealer, K., Madden, T.L. BLAST+: architecture and applications. BMC Bioinformatics 10, 421-430 (2009). doi
- **HHblits**
  Remmert, M., Biegert, A., Hauser, A., Söding, J. HHblits: lightning-fast iterative protein sequence searching by HMM-HMM alignment. Nat Methods 9, 173-175 (2012). doi

Table T1:

Primary amino acid sequence for which templates were searched and models were built.

```
MALYYDHQIEAPDAAGSPSFISWHPVHPFLAVAYISTTSTGSVDIYLEQGECVPDTHVERPFRVASLCWHPTRLVLAVGWETGEVTVFNKQDKEQHTMPL
THTADITVLRWSPSGNCLLSGDRLGVLLLWRLDQRGRVQGTPLLKHEYGKHLTHCIFRLPPPGEDLVQLAKAAVSGDEKALDMFNWKKSSSGSLLKMGSH
EGLLFFVSLMDGTVHYVDEKGKTTQVVSADSTIQMLFYMEKREALVVVTENLRLSLYTVPPEGKAEEVMKVKLSGKTGRRADIALIEGSLLVMAVGEAAL
RFWDIERGENYILSPDEKFGFEKGENMNCVCYCKVKGLLAAGTDRGRVAMWRKVPDFLGSPGAEGKDRWALQTPTELQGNITQIQWGSRKNLLAVNSVIS
VAILSERAMSSHFHQQVAAMQVSPSLLNVCFLSTGVAHSLRTDMHISGVFATKDAVAVWNGRQVAIFELSGAAIRSAGTFLCETPVLAMHEENVYTVESN
RVQVRTWQGTVKQLLLFSETEGNPCFLDICGNFLVVGTDLAHFKSFDLSRREAKAHCSCRSLAELVPGVGGIASLRCSSSGSTISILPSKADNSPDSKIC
FYDVEMDTVTVFDFKTGQIDRRETLSFNEQETNKSHLFVDEGLKNYVPVNHFWDQSEPRLFVCEAVQETPRSQPQSANGQPQDGRAGPAADVLILSFFIS
EEHGFLLHESFPRPATSHSLLGMEVPYYYFTRKPEEADREDEVEPGCHHIPQMVSRRPLRDFVGLEDCDKATRDAMLHFSFFVTIGDMDEAFKSIKLIKS
EAVWENMARMCVKTQRLDVAKVCLGNMGHARGARALREAEQEPELEARVAVLATQLGMLEDAEQLYRKCKRHDLLNKFYQAAGRWQEALQVAEHHDRVHL
RSTYHRYAGHLEASADCSRALSYYEKSDTHRFEVPRMLSEDLPSLELYVNKMKDKTLWRWWAQYLESQGEMDAALHYYELARDHFSLVRIHCFQGNVQKA
AQIANETGNLAASYHLARQYESQEEVGQAVHFYTRAQAFKNAIRLCKENGLDDQLMNLALLSSPEDMIEAARYYEEKGVQMDRAVMLYHKAGHFSKALEL
AFATQQFVALQLIAEDLDETSDPALLARCSDFFIEHSQYERAVELLLAARKYQEALQLCLGQNMSITEEMAEKMTVAKDSSDLPEESRRELLEQIADCCM
RQGSYHLATKKYTQAGNKLKAMRALLKSGDTEKITFFASVSRQKEIYIMAANYLQSLDWRKEPEIMKNIIGFYTKGRALDLLAGFYDACAQVEIDEYQNY
DKAHGALTEAYKCLAKAKAKSPLDQETRLAQLQSRMALVKRFIQARRTYTEDPKESIKQCELLLEEPDLDSTIRIGDVYGFLVEHYVRKEEYQTAYRFLE
EMRRRLPLANMSYYVSPQAVDAVHRGLGLPLPRTVPEQVRHNSMEDARELDEEVVEEADDDP
```

Table T2:

Template	Seq Identity	Oligo-state	QSQE	Found by	Method	Resolution	Seq Similarity	Coverage	Description

5a1u.1.T	13.15	monomer		HHblits	EM	13.00Å	0.27	0.54	COATOMER SUBUNIT BETA'
5nzu.1.C	13.15	monomer		HHblits	EM	NA	0.27	0.54	Coatomer subunit beta'
5a1u.1.T	14.02	monomer		HHblits	EM	13.00Å	0.27	0.52	COATOMER SUBUNIT BETA'
5nzu.1.C	14.02	monomer		HHblits	EM	NA	0.27	0.52	Coatomer subunit beta'
3mkq.1.A	11.73	homo-trimer		HHblits	X-ray	2.50Å	0.26	0.51	Coatomer beta'-subunit
3mkq.1.C	11.73	homo-trimer		HHblits	X-ray	2.50Å	0.26	0.51	Coatomer beta'-subunit
3mkq.1.E	11.73	homo-trimer		HHblits	X-ray	2.50Å	0.26	0.51	Coatomer beta'-subunit
5a1u.1.S	13.54	monomer		HHblits	EM	13.00Å	0.27	0.50	COATOMER SUBUNIT ALPHA
5nzu.1.A	13.54	monomer		HHblits	EM	NA	0.27	0.50	Coatomer subunit alpha
3mkq.1.A	13.33	homo-trimer		HHblits	X-ray	2.50Å	0.27	0.49	Coatomer beta'-subunit
3mkq.1.C	13.33	homo-trimer		HHblits	X-ray	2.50Å	0.27	0.49	Coatomer beta'-subunit
3mkq.1.E	13.33	homo-trimer		HHblits	X-ray	2.50Å	0.27	0.49	Coatomer beta'-subunit
5a1u.1.S	13.38	monomer		HHblits	EM	13.00Å	0.27	0.47	COATOMER SUBUNIT ALPHA
5nzu.1.A	13.38	monomer		HHblits	EM	NA	0.27	0.47	Coatomer subunit alpha
4m57.1.A	10.73	homo-dimer		HHblits	X-ray	2.86Å	0.26	0.38	Chloroplast pentatricopeptide repeat protein 10
3j2t.1.A	14.55	monomer		HHblits	EM	NA	0.28	0.37	Apoptotic protease-activating factor 1
6bq1.1.B	13.00	monomer		HHblits	EM	NA	0.25	0.38	Tetratricopeptide repeat protein 7B
5h1j.1.A	13.47	monomer		HHblits	X-ray	2.00Å	0.27	0.37	Gem-associated protein 5
5h1k.1.A	13.47	monomer		HHblits	X-ray	1.90Å	0.27	0.37	Gem-associated protein 5
5dse.1.A	13.19	monomer		HHblits	X-ray	2.90Å	0.26	0.37	Tetratricopeptide repeat protein 7B
5dse.2.A	13.19	monomer		HHblits	X-ray	2.90Å	0.26	0.37	Tetratricopeptide repeat protein 7B
5wve.1.K	14.61	monomer		HHblits	EM	NA	0.28	0.36	Apoptotic protease-activating factor 1
5juy.1.B	14.61	monomer		HHblits	EM	NA	0.28	0.36	Apoptotic protease-activating factor 1
5juy.1.G	14.61	monomer		HHblits	EM	NA	0.28	0.36	Apoptotic protease-activating factor 1
5juy.1.D	14.61	monomer		HHblits	EM	NA	0.28	0.36	Apoptotic protease-activating factor 1
5juy.1.E	14.61	monomer		HHblits	EM	NA	0.28	0.36	Apoptotic protease-activating factor 1
3sfz.1.A	15.18	monomer		HHblits	X-ray	3.00Å	0.28	0.36	Apoptotic peptidase activating factor 1
3shf.1.A	15.18	monomer		HHblits	X-ray	3.55Å	0.28	0.36	Apoptotic peptidase activating factor 1
5wyj.18.A	15.97	monomer		HHblits	EM	NA	0.27	0.36	U3 small nucleolar RNA-associated protein 13
5oql.1.M	12.17	monomer		HHblits	EM	NA	0.26	0.37	Utp17
5wyj.17.A	14.89	monomer		HHblits	EM	NA	0.27	0.35	U3 small nucleolar RNA-associated protein 12
3jbt.1.A	14.65	monomer		HHblits	EM	NA	0.28	0.35	Apoptotic protease-activating factor 1
3j2t.1.A	13.51	monomer		HHblits	EM	NA	0.27	0.35	Apoptotic protease-activating factor 1
5wve.1.K	13.57	monomer		HHblits	EM	NA	0.27	0.35	Apoptotic protease-activating factor 1
5juy.1.B	13.57	monomer		HHblits	EM	NA	0.27	0.35	Apoptotic protease-activating factor 1
5juy.1.G	13.57	monomer		HHblits	EM	NA	0.27	0.35	Apoptotic protease-activating factor 1
5juy.1.D	13.57	monomer		HHblits	EM	NA	0.27	0.35	Apoptotic protease-activating factor

									1
5juy.1.E	13.57	monomer		HHblits	EM	NA	0.27	0.35	Apoptotic protease-activating factor 1
3jbt.1.A	13.35	monomer		HHblits	EM	NA	0.27	0.35	Apoptotic protease-activating factor 1
3sfz.1.A	12.77	monomer		HHblits	X-ray	3.00Å	0.27	0.35	Apoptotic peptidase activating factor 1
5wyj.17.A	15.04	monomer		HHblits	EM	NA	0.27	0.35	U3 small nucleolar RNA-associated protein 12
5gxh.1.A	14.48	monomer		HHblits	X-ray	1.80Å	0.27	0.35	Gem-associated protein 5
3shf.1.A	12.40	monomer		HHblits	X-ray	3.55Å	0.27	0.35	Apoptotic peptidase activating factor 1
5tee.1.A	14.51	monomer		HHblits	X-ray	1.65Å	0.27	0.35	Gem-associated protein 5
5wlc.22.A	14.84	monomer		HHblits	EM	NA	0.27	0.35	Utp12
4xfv.1.A	10.31	monomer		HHblits	X-ray	3.20Å	0.25	0.36	Elongator complex protein 2
5oql.1.D	10.69	monomer		HHblits	EM	NA	0.25	0.36	Utp4
5fqd.1.A	13.20	monomer		HHblits	X-ray	2.45Å	0.26	0.35	DNA DAMAGE-BINDING PROTEIN 1
2b5l.1.A	11.84	monomer		HHblits	X-ray	2.85Å	0.26	0.35	damage-specific DNA binding protein 1
2b5l.2.A	11.84	monomer		HHblits	X-ray	2.85Å	0.26	0.35	damage-specific DNA binding protein 1

The table above shows the top 50 filtered templates. A further 1,836 templates were found which were considered to be less suitable for modelling than the filtered list.
3fgb.1.A, 5gm6.1.4, 3vl1.1.A, 4a1s.1.A, 2ff4.2.A, 5cvo.2.A, 3fm0.1.A, 2g5p.1.A, 5ukl.1.B, 1x81.1.A, 4nox.1.A, 4a0a.1.B, 1ft1.1.A, 5gm6.1.2, 5vgz.1.K, 5vgz.1.J, 5vgz.1.H, 2qx5.1.A, 4ui9.1.P, 4ui9.1.Q, 4ui9.1.V, 4ui9.1.W, 4ui9.1.J, 4ui9.1.K, 4ui9.1.H, 4ui9.1.I, 4ui9.1.O, 4ui9.1.C, 4ui9.1.F, 3q15.1.A, 3ieg.2.A, 2xyi.1.A, 2kc7.1.A, 5cwm.1.A, 5olj.1.A, 1aof.1.A, 1aof.1.B, 1pc2.1.A, 3ium.1.A, 4yhc.2.A, 5fqd.1.A, 5dse.1.A, 5n4d.1.A, 3hxe.1.A, 3sre.1.A, 1jmz.1.B, 5opt.1.A, 3mv3.1.B, 4bt9.1.A, 2qt9.1.A, 5k0m.1.A, 4i1a.1.A, 4uer.1.b, 4cvc.1.A, 3s2k.1.B, 5vgz.1.G, 3s2k.1.A, 3j7p.78.A, 1hxi.1.A, 2ce9.2.B, 5wyk.1.U, 5gjr.12.A, 5wyk.1.V, 5wyk.1.R, 5jrl.1.B, 2ymb.1.A, 5mqf.1.O, 5a7d.8.A, 5mqf.1.M, 4v5z.1.A, 5mqf.1.F, 5n4e.1.A, 5mqf.1.D, 5mqf.1.E, 4v6w.2.A, 1jtd.1.B, 1wm5.1.A, 5np1.1.A, 5uw7.1.A, 5l4k.1.E, 4e85.1.A, 5l4k.1.G, 5l4k.1.F, 5l4k.1.I, 3mbr.1.A, 5l4k.1.J, 4a2l.1.B, 2j9q.1.B, 2j9q.1.A, 5k1a.2.B, 6au8.1.A, 4yg8.1.B, 5h19.1.A, 5sv7.1.D, 3odt.1.A, 5sv7.1.A, 5a7d.4.A, 5sv7.1.C, 2fi7.1.A, 2fi7.1.B, 5gmk.1.0, 3li4.1.A, 5n4f.1.A, 2bkl.1.A, 6eos.1.B, 5wlc.27.A, 5mpq.1.A, 3hlh.1.A, 1o6f.1.A, 1vz2.1.A, 5wvi.1.N, 1z68.1.B, 5cqr.1.A, 1z68.1.A, 5i1y.1.C, 2bed.1.A, 4x3e.1.A, 2be1.1.A, 5mwj.1.A, 5gmk.1.J, 5kkl.1.A, 3ly9.1.A, 3q5m.1.A, 5gmk.1.X, 5gmk.1.R, 5a7d.6.A, 5gmk.1.W, 2ooe.1.A, 3cv0.1.A, 5m72.1.A, 3rib.1.A, 2hes.1.A, 2gw1.1.A, 2gw1.1.B, 4eqf.1.A, 2iav.1.A, 4kvm.1.A, 4j8e.1.A, 5wyj.19.A, 5v4b.1.B, 1sly.1.A, 2vz1.1.A, 3j8b.1.C, 3ly7.1.A, 3jck.1.B, 1b9y.1.A, 3jck.1.D, 5o3u.1.A, 4ja7.1.A, 4ymr.1.A, 2p9w.1.A, 4ymr.1.B, 3txn.1.A, 2pqr.2.A, 5kjk.1.A, 5guw.3.A, 5jj7.1.A, 5gm6.1.F, 5jj7.1.B, 3i7k.1.A, 5n4b.1.A, 2iat.1.A, 1tl2.1.A, 2iax.1.A, 3edt.1.A, 3edt.1.B, 2ebs.1.A, 5c2w.1.E, 4lg8.1.A, 5juu.45.A, 1hzu.1.A, 4q66.2.C, 2yhc.1.A, 5lj5.1.V, 3zfw.1.A, 4hou.2.A, 1e96.1.B, 4i9e.1.B, 3zgc.1.A, 5a1y.1.U, 4wne.1.A, 4i9e.1.A, 3cvq.1.A, 4d18.1.D, 4d18.1.B, 4bp8.1.A, 3ow8.1.A, 4nc4.1.A, 4yde.1.A, 4cy1.1.A, 1vyh.1.C, 3kd7.1.A, 5v3o.1.A, 5vhj.1.H, 4hhq.1.A, 4kbq.2.A, 1n6f.1.A, 4hoq.1.A, 3gz1.1.A, 3sf4.1.A, 3jb9.1.3, 5vhf.1.J, 4wn4.2.A, 4bt8.1.B, 4bt8.1.A, 3jb9.1.L, 2ynn.1.A, 3li3.1.A, 5jk7.2.A, 3jb9.1.K, 5oql.1.3, 5k1c.1.C, 5k1c.1.B, 6epc.1.S, 4l7b.1.A, 5igo.1.A, 6epc.1.T, 6epc.1.W, 6epc.1.V, 6epc.1.X, 5oql.1.X, 4r5o.1.A, 2gop.1.A, 2gop.1.B, 6exn.1.J, 5i9d.1.A, 5oql.1.N, 1e2r.1.B, 1e2r.1.A, 6exn.1.S, 2xgs.1.A, 5oql.1.A, 5oql.1.F, 5oql.1.D, 3lvh.1.A, 6exn.1.a, 6emk.1.D, 6emk.1.B, 6emk.1.C, 5ijn.1.U, 6emk.1.A, 5ijn.1.K, 5ijn.1.I, 5wbu.1.B, 3pbp.4.A, 5wbu.1.A, 5ijn.1.C, 1jju.1.B, 4uzy.1.A, 3no2.1.A, 4n5c.5.A, 5yp1.1.B, 5yp1.1.A, 5i1y.1.A, 5m2n.1.A, 5i1y.1.B, 4hot.1.A, 4n5c.3.A, 5hgv.1.A, 5jul.1.A, 5cxb.1.B, 5cxb.1.A, 5ln3.1.0, 4n5c.1.A, 3mzl.1.B, 2co0.1.A, 5vlj.1.B, 5vlj.1.C, 5bt1.1.B, 6f9n.1.A, 5b4x.1.B, 3q4a.1.A, 5ln3.1.Y, 5ln3.1.X, 3as8.1.A, 5mgx.1.A, 2p4o.1.A, 4bzj.1.D, 4bzj.1.C, 4bzj.1.B, 4bzj.1.A, 4hw6.1.A, 3i7l.1.A, 4ynw.1.A, 5ln3.1.A, 3ww8.1.A, 5mc6.35.A, 3qdn.2.A, 5nxq.1.A, 5ic8.3.A, 3va6.2.A, 1qsa.1.A, 5ic8.1.A, 5sxm.1.A, 5lyb.33.A, 5yz0.1.A, 5jzz.2.A, 4fhl.1.A, 5vh9.1.B, 2ifu.3.A, 2ovr.1.B, 3j80.1.7, 3oxf.1.A, 1mda.1.A, 4wjw.1.B, 2iar.1.A, 3ivm.1.A, 3jco.1.8, 4wsn.4.D, 3acp.1.A, 1aoq.1.A, 2pl2.1.A, 2c2l.2.A, 2hz6.1.A, 3e0c.1.A, 3jrp.1.A, 5nrl.1.Q, 5nrl.1.W, 4x60.1.B, 5nrl.1.O, 2y4u.1.A, 4aez.1.A, 4aez.1.C, 3j78.45.A, 4aez.3.C, 2gvx.1.A, 5djs.1.A, 3vl1.2.A, 2yin.1.A, 5mps.1.U, 4zox.1.A, 5mps.1.Q, 5mps.1.R, 5lj3.1.L, 1qz2.1.C, 1qz2.1.B, 1qz2.1.A, 3vu4.1.A, 4a0a.1.A, 5lj3.1.U, 5lj3.1.T, 4a0b.1.B, 2i3s.2.A, 5bv0.1.B, 3j6x.75.A, 3ade.1.A, 3tg5.1.A, 2vyi.1.A, 1g72.1.A, 2xcc.1.A, 2rfo.1.A, 4zb4.2.A, 5b26.2.B, 5txc.1.A, 5jz6.1.A, 3fvz.1.A, 2b5m.1.A, 1gjq.1.A, 2ovp.1.B, 3nol.1.A, 3li5.1.A, 4ggd.1.A, 5lj5.1.M, 3bg0.1.D, 5lj5.1.U, 3mzk.1.A, 5o09.1.C, 5ftp.1.A, 5ftp.1.B, 3fw0.1.A, 3si5.1.A, 5lj5.1.d, 5diz.1.A, 4g2v.1.A, 5cqs.1.A, 3jct.1.n, 2eic.1.A, 4g56.1.B, 4v0m.1.B, 3n71.1.A, 4hnw.1.A, 5jrk.1.B, 5l0y.1.B, 5l0y.1.A, 1yr2.1.A, 3hym.1.B, 5t0c.35.A, 1zgk.1.A, 1klx.1.A, 5mc6.37.A, 1gxr.1.B, 1gxr.1.A, 4h7x.1.A, 3e4b.1.A, 3ott.1.B, 3ott.1.A, 5jqy.1.A, 4a09.1.A, 4nq0.1.A, 3zpj.1.A, 4r40.2.A, 4cgv.1.A, 4abn.1.A, 3as4.1.A, 1y8m.1.A, 1w3b.1.B, 5lvv.1.A, 3hli.1.A, 2hu5.1.B, 5c2v.1.B, 5wyj.20.A, 2uy1.1.A, 4lg9.1.A, 1sqj.1.A, 2fpb.2.A, 5d0q.1.C, 2e2e.1.A, 2yno.1.A, 5obm.152.A, 3byc.1.A, 3v64.1.A, 5ndv.147.A, 3v64.1.D, 3fmo.1.A, 3kae.1.A, 5o01.1.A, 3hrp.1.A, 3a0f.1.A, 4g1f.4.A, 4xyh.1.A, 4bl0.2.A, 3zwu.1.A, 3i4r.1.B, 3cfs.1.A, 5fnr.1.A, 1lrw.1.C, 1lrw.1.A, 4ja9.1.A, 2faw.1.A, 4gpk.1.D, 4gpk.1.A, 4gpk.1.C, 4gpk.1.B, 3fwv.2.A, 5nnz.1.A, 3zwl.1.A, 4gpk.3.D, 4gpk.3.C, 4gpk.3.B, 4gpk.3.A, 3lku.1.A, 3emh.1.A, 5jub.1.A, 1ouv.1.A, 5jub.1.B, 4kvo.1.A, 4d0k.1.A, 5igo.2.A, 5ife.1.D, 5ijo.1.Q, 5buz.2.B, 5ijo.1.W, 5gjq.1.Z, 3lvg.1.A, 6ez8.1.B, 5jpz.1.A, 5ijo.1.E, 4ozs.1.A, 3ffl.2.B, 4aow.1.A, 2i0r.1.C, 5a31.1.F, 5gjq.1.j, 4btb.1.A, 4imm.1.A, 3mmy.1.A, 5ltd.1.A, 3ii7.1.A, 2iaq.1.A, 5mpb.1.g, 3sfx.1.A, 5gjq.1.7, 5ctr.1.A, 5gjq.1.5, 3u4t.1.A, 2iwa.1.A, 1u6d.1.A, 5mpb.1.h, 4a1g.2.A, 1iyg.1.A, 4l9o.1.A, 2co0.2.A, 3ww9.1.A, 5i5m.1.A, 1fpp.1.B, 5cvl.1.A, 4czv.1.A, 1ihg.1.A, 3soq.1.A, 5bw8.1.C, 3r9a.1.D, 5naf.1.A, 2h13.1.A, 3r9a.1.B, 1tnu.1.A, 3sn6.1.B, 6c23.1.D, 5tzs.1.e, 6c23.1.F, 1qqe.1.A, 6bq1.1.B, 2dg1.1.A, 1r5m.1.A, 4gq1.1.A, 4cc9.1.A, 5w5h.2.E, 3wwa.1.A, 5gvb.1.A, 5tzs.1.1, 2pm9.1.A, 2q7f.1.A, 5yp4.2.A, 5nkp.2.A, 4o6f.1.A, 3w15.1.A, 3bws.1.A, 2bug.1.A, 5an3.1.A, 5vyc.4.I, 4o5t.1.A, 4jsn.1.A, 4jsn.1.B, 4pjq.1.A, 5cxc.1.B, 5cxc.1.A, 5b26.1.B, 1jof.1.A, 6em3.1.E, 3h7n.1.A, 2ias.1.A, 4m59.1.B, 4m59.1.A, 5jcs.1.3, 4yvd.1.A, 5fjy.1.B, 5fjy.1.A, 5l0y.6.A, 1o1r.1.A, 5sum.1.A, 1fwx.1.A, 5a5t.1.C, 4i9c.1.A, 4xmm.1.C, 5jjx.1.A, 2qxv.1.A, 4xmm.1.E, 5jut.45.A, 3jcp.1.Z, 3jcp.1.Y, 4pxw.1.A, 2vgy.1.A, 5nnr.1.A, 3jcp.1.0, 5wrw.1.A,

5wrw.1.B, 2eep.1.A, 3jcp.1.8, 2c0l.1.A, 3dsm.1.A, 4wjv.1.A, 5sv7.1.B, 5wrw.3.A, 3nf1.1.A, 1xfd.1.A, 5mpe.2.H, 5mpe.2.E, 2hu8.1.A, 3rjv.1.A, 4j87.1.A, 4m57.1.A, 5a6c.1.A, 2lah.1.A, 4i17.1.A, 6eoq.1.A, 5afu.1.C, 6em5.1.5, 2b5l.1.A, 5a7d.2.A, 5h64.1.A, 5h64.1.B, 5h64.1.C, 6em5.1.h, 5t0h.1.V, 2w18.1.A, 5cwo.1.A, 4fsc.2.B, 5fww.1.A, 3fhc.1.A, 4kr0.1.A, 4in4.1.A, 5ic7.1.A, 4d0p.1.A, 4zoy.1.A, 5xw7.2.A, 5xw7.4.A, 1i2m.2.B, 3pe7.1.A, 5wlc.25.A, 5t88.1.A, 5uw5.1.A, 4zlh.1.B, 4wjs.1.A, 2pzi.2.A, 5wlc.41.A, 5wlc.21.A, 3vty.4.A, 5nuv.1.A, 1kb0.1.A, 3tgo.1.A, 2wfx.1.B, 2kcl.1.A, 5c86.1.A, 3i2n.1.A, 3azq.1.A, 5hb3.2.A, 1kt1.1.A, 5gjq.1.3, 2ymu.1.A, 4yzy.1.A, 4l9o.2.A, 3e4b.4.A, 2xcb.2.A, 3f3g.1.E, 3prw.1.A, 3i5p.1.A, 4o9d.1.A, 1w6s.1.A, 2qc5.1.A, 4j8d.1.A, 4hdj.1.A, 2r5s.1.A, 3kd7.2.A, 2xev.3.A, 2xev.1.A, 2y4t.1.A, 3asf.2.A, 3j96.1.J, 3j96.1.H, 5wwm.1.A, 4ax4.1.A, 3j96.1.G, 5k0y.1.8, 1hzv.1.A, 3jb9.1.4, 2q7f.2.A, 4yvq.1.B, 5sui.1.A, 4buj.1.B, 4buj.1.C, 5vhf.1.H, 3v1s.1.A, 2lni.1.A, 3iiy.1.A, 5k0y.1.P, 5vhf.1.S, 5bt1.1.A, 2bbk.1.A, 3jb9.1.S, 3v9f.4.A, 3v9f.2.A, 3o10.1.A, 4gcn.1.A, 4xfv.1.A, 5yz0.1.B, 3uvo.1.A, 2y4t.3.A, 4v0n.2.B, 1rwl.1.A, 5cvo.1.A, 5mq0.1.I, 2qe8.1.A, 3upv.1.A, 3ly8.1.A, 5l4k.1.H, 5t0i.1.Y, 5t0i.1.X, 5t0i.1.W, 5t0i.1.V, 5t0i.1.U, 2kcv.1.A, 1rwi.1.A, 4hny.2.A, 3c9c.1.A, 5nnp.1.A, 4u0s.1.A, 4a11.1.B, 4a11.1.A, 3q15.2.A, 3q7o.1.A, 4wjl.1.A, 1l0q.3.A, 2xn4.1.A, 2gnq.1.A, 5vhi.1.S, 5hrm.1.A, 1q7f.2.A, 4wsn.6.D, 4g1t.1.A, 4qzv.2.A, 4g1t.1.B, 4j73.1.A, 5tqb.1.B, 4z8l.1.A, 5uw3.1.A, 3h0c.1.A, 3jpx.1.A, 6b3j.1.D, 1ft2.1.A, 2ho1.1.B, 2ho1.1.A, 2n8w.1.A, 3vgz.1.A, 3s94.1.A, 4amy.1.A, 2fbn.1.A, 3q6k.1.A, 4in3.1.D, 2i0s.1.C, 5flc.1.F, 2agl.1.C, 3ww7.1.A, 4zoz.1.A, 5hi7.1.A, 2mta.1.A, 2jqk.1.A, 3j9m.72.A, 3ffl.1.A, 5a01.1.A, 2ojy.1.C, 4rg6.1.A, 4rg6.1.B, 4hho.1.A, 4czy.1.A, 3dwl.1.B, 4me2.1.A, 5iww.1.D, 3ffl.1.B, 5ij7.1.B, 4n5c.7.A, 4xmn.1.A, 4xmn.1.D, 4xmn.1.E, 5c2v.1.A, 3hxj.2.A, 3hxj.2.B, 2mhk.1.A, 2hye.1.A, 5a7d.5.A, 5fa5.1.B, 4ci8.1.A, 5k1a.1.B, 5cww.1.B, 3ro2.1.A, 5aja.1.A, 3uzs.1.B, 4amf.1.A, 4nlm.1.A, 2cpt.1.A, 4q1v.1.A, 5v1d.1.C, 5v1d.1.A, 4jhr.1.A, 3iax.1.A, 6eoj.1.A, 2dba.1.A, 6eoj.1.C, 4p29.1.A, 5jpz.1.B, 3lvg.1.C, 5a7d.1.A, 5a7d.7.A, 3lvg.1.B, 2c0m.1.A, 2ymb.1.B, 3u0s.1.A, 4h5i.1.A, 5t2c.73.A, 4lct.2.B, 4lct.2.A, 4owr.1.A, 4aif.1.A, 3jd5.1.3, 3uux.1.A, 3e37.1.A, 5chb.1.A, 5wyj.18.A, 3jd5.1.U, 5bpt.1.A, 5xyi.1.6, 5mc6.15.A, 3as5.2.A, 5jjo.1.A, 2vq2.1.A, 1zu2.1.A, 5gwn.1.A, 4cy3.1.A, 5lyb.108.A, 5o3v.1.A, 4kmo.1.B, 3pz4.1.A, 5jhe.1.A, 5np0.1.A, 3gw4.1.B, 1erj.1.A, 3gw4.1.A, 6bk8.1.V, 6bk8.1.W, 6bk8.1.P, 4n14.1.A, 4b94.1.A, 2jq9.1.A, 3mkq.1.B, 6bk8.1.H, 3mkq.1.D, 3mkq.1.F, 5kdo.1.B, 5bwk.1.D, 5v7v.1.A, 2ond.1.A, 5m23.1.A, 1kv9.1.A, 3ho5.2.A, 4uuy.1.A, 4q66.1.D, 3q7f.1.A, 4n2q.1.A, 4jml.1.A, 5it7.77.A, 3sz7.1.A, 3a9g.1.A, 2w8b.1.A, 4l1m.1.A, 5c1d.1.A, 4r7s.1.A, 4v7r.20.A, 2g9a.1.A, 5fvl.2.A, 3vtx.2.A, 5gxh.1.A, 5h3s.1.A, 4apo.1.A, 4pjq.2.A, 1e8m.1.A, 1tjc.1.A, 4v16.1.A, 3wxx.1.A, 5wyj.16.A, 5jjw.1.A, 4pk1.1.A, 1xnf.1.A, 4zgc.1.A, 3cik.1.B, 3jck.1.C, 4u1f.1.A, 4niq.1.A, 5t0j.1.V, 1h2y.1.A, 3jbz.1.A, 5jpq.1.Y, 4qzv.1.A, 6epd.1.V, 6epd.1.W, 6epd.1.T, 6epd.1.U, 6epd.1.S, 6epe.1.X, 6epe.1.W, 6epe.1.V, 3j97.1.H, 6epe.1.T, 6epe.1.S, 1e5t.1.A, 4g23.1.A, 3esl.2.A, 3rfg.1.A, 2h9l.1.A, 2pm7.1.D, 2pm7.1.C, 2pm7.1.A, 3q7m.1.A, 2lsu.1.A, 4kbq.1.A, 2bgr.1.A, 4wn4.1.A, 1gq1.1.A, 4hny.1.A, 5gjq.1.9, 4cr3.1.6, 3gre.1.A, 4n5c.4.A, 4n5c.2.A, 4a1g.4.A, 5wql.2.A, 5lqi.1.A, 3wj9.2.A, 3gz2.1.B, 1na0.1.A, 1q7f.1.A, 4ga1.1.A, 4v3p.1.A, 1yxr.1.A, 5waq.1.A, 5mc6.36.A, 5w5i.1.A, 2ism.1.A, 2j57.1.C, 3pz1.1.A, 3p5c.1.C, 4cr3.1.Y, 3iun.1.A, 4l72.3.A, 1u8e.1.B, 1u8e.1.A, 5hfs.1.A, 5lyn.1.A, 2c2l.1.A, 4a0b.2.A, 2hr2.1.A, 2ynp.1.A, 3dxm.1.C, 4tqo.1.A, 4bt9.1.B, 2ifu.2.A, 3o4g.1.B, 4aif.2.A, 1ri6.1.A, 6fbs.1.A, 6fbs.1.B, 2iao.1.A, 4u0u.1.A, 5k1h.1.A, 4eba.1.A, 2if4.1.A, 5efr.1.A, 4imm.2.A, 3hfq.1.A, 5em2.2.B, 5bjs.1.A, 5iwb.1.B, 5jzz.1.A, 4cr4.1.W, 5k19.2.A, 5f72.1.A, 4cr4.1.X, 4cr4.1.Y, 4a5x.1.A, 5naf.3.A, 4c8h.1.C, 4c8h.1.A, 4a0l.1.A, 5izw.1.A, 4aez.2.C, 1nex.2.B, 4aez.2.A, 5wsg.1.R, 3lya.1.A, 5wsg.1.U, 5wsg.1.T, 4d6v.1.A, 5g05.1.I, 5g05.1.K, 5g05.1.O, 5g05.1.C, 5g05.1.F, 5mpd.1.K, 5mpd.1.J, 5mpd.1.I, 2i3s.1.A, 4ga2.1.A, 5mpd.1.F, 2yq8.1.A, 4cr4.1.6, 5vai.1.D, 3vu4.2.A, 3cvl.1.A, 5b4x.2.B, 3s8z.1.A, 4fhn.1.B, 4a2m.2.A, 5jrk.1.A, 5l0y.7.A, 3jzn.1.A, 5jk7.1.B, 5cqs.2.A, 1fch.1.A, 5wql.1.A, 1a0r.1.A, 2n8i.1.A, 5m1j.14.A, 1yiq.1.A, 5ft9.2.A, 3ma5.3.A, 4fhm.1.B, 2rfo.2.A, 4fhm.1.A, 2ajl.1.A, 2ajl.1.B, 5wrv.1.B, 3kya.1.A, 5a31.1.O, 5a31.1.J, 5a31.1.H, 2ecf.1.A, 5a31.1.C, 4iqk.1.A, 2lsv.1.A, 3jap.1.i, 5a31.1.W, 5a31.1.V, 5x54.1.A, 5a31.1.R, 5a31.1.P, 5j3j.1.A, 5u5h.1.A, 3ei3.1.A, 5diz.2.A, 3ho5.1.A, 5b26.1.A, 5bpw.1.A, 4a0l.2.A, 4v8m.8.A, 2q7q.1.C, 2v5f.1.A, 5l0y.2.A, 3s8v.2.A, 2z2n.1.A, 5t0h.1.W, 5t0h.1.U, 1hz4.1.A, 5k18.1.A, 5t0h.1.Y, 3e4b.2.A, 1pi6.1.A, 2yba.1.A, 5tf2.1.A, 5xjc.1.W, 5xjc.1.T, 2b5n.2.A, 2iaa.1.A, 5xjc.1.E, 5xjc.1.J, 5xjc.1.I, 1p22.1.A, 1mg2.1.A, 4cgv.2.A, 5c9s.1.A, 4abn.2.A, 3rkv.1.A, 6b3x.1.A, 5vfc.1.A, 4wju.1.A, 6az1.1.6, 5oj8.1.A, 5wuk.1.A, 1s4u.1.A, 3j77.45.A, 3urz.1.A, 5gap.1.F, 5gap.1.G, 3u4y.1.A, 3qqz.1.A, 3p5b.1.C, 4qrj.1.A, 5hqg.1.A, 3m0c.1.C, 5aem.1.A, 4dnv.1.A, 4zcn.1.A, 4zcn.1.C, 1sq9.1.A, 5fzs.1.A, 3o48.1.A, 5lyp.1.A, 5dbk.1.B, 5dbk.1.A, 4zb4.1.A, 5o01.2.A, 2pqn.1.A, 5ayw.1.B, 3qky.1.A, 2fo7.1.A, 5ayw.1.D, 4gpk.2.B, 4gpk.2.C, 4gpk.2.A, 4cgw.1.A, 4gpk.2.D, 5a2q.1.8, 5wyj.33.A, 4hnx.1.A, 2vsy.1.A, 5kc2.1.B, 4a08.1.A, 4a08.1.B, 3ah8.1.B, 4uqy.1.A, 2avp.1.A, 2xu7.1.A, 5flx.1.7, 3lca.1.A, 5mpc.1.h, 5mpc.1.i, 5mpc.1.d, 5ioj.1.A, 3asg.1.A, 5mpc.1.g, 4ifl.1.A, 5ccl.1.A, 5jjt.1.A, 1c5k.1.A, 3s94.2.A, 5ojf.1.A, 3f7f.1.A, 1p5q.1.A, 1p5q.1.B, 1p5q.1.C, 4hxg.1.A, 4hxf.1.F, 4ycz.1.A, 3mxx.1.A, 4gcn.2.A, 1ve7.1.A, 4ozu.1.A, 4a1g.1.A, 3c75.1.A, 2xl2.1.A, 5fxy.2.A, 3mks.1.D, 4a1g.3.A, 4v7e.7.A, 5ctr.2.A, 4y6c.1.A, 5mzu.1.A, 5ctq.1.B, 5n1a.1.A, 5ukm.1.B, 5u69.1.A, 2iwf.1.A, 5mpb.1.d, 5udj.1.A, 5hrz.1.A, 4y49.1.A, 3frx.1.A, 5uzw.1.A, 3j9m.81.A, 5juf.1.A, 5v1d.2.A, 1h4i.1.A, 4f3v.1.A, 4e5z.1.B, 6bw3.1.A, 5k04.1.A, 6eoo.1.A, 4v5o.1.0, 1elw.1.A, 5t0c.44.A, 3ru0.1.A, 2d0v.1.A, 1xip.1.A, 5fsb.1.A, 3ei4.1.A, 5ekq.1.B, 4gco.1.A, 5h1j.1.A, 5f30.1.A, 2pbi.2.B, 3qou.1.A, 1n9a.1.A, 5w4n.1.B, 5w4n.1.A, 6epf.1.T, 6epf.1.U, 6epf.1.V, 6epf.1.W, 6epf.1.S, 6exn.1.R, 4gyw.1.A, 5fvm.1.C, 5fvm.1.A, 3iuj.1.A, 4xf2.1.C, 5m11.1.A, 4ga0.1.A, 1l0q.1.A, 5cgj.1.A, 2g8s.1.A, 5cvn.1.A, 4unm.1.A, 3dm0.1.A, 3sob.1.B, 4ffv.1.A, 4bp9.1.A, 4i1a.2.A, 4bzk.1.D, 1wr0.1.A, 4aah.1.A, 3ieg.1.A, 5tga.33.A, 5g04.1.Q, 5g04.1.P, 5g04.1.U, 5g04.1.T, 5mpb.1.i, 5ctq.1.A, 5g04.1.C, 4o5s.1.A, 5g04.1.F, 5mpe.1.J, 5g04.1.H, 5g04.1.K, 5g04.1.J, 5g04.1.O, 5wp3.1.A, 1dy7.1.A, 4it4.1.A, 2g99.1.A, 3ho4.1.A, 3gz1.1.B, 5ln3.1.V, 4cgu.1.A, 5a7d.3.A, 3sjl.1.D, 2ojh.1.A, 3dr2.1.A, 4dg6.1.A, 5hy7.2.A, 4w9r.1.A, 2dcm.1.A, 5xw7.3.A, 5xw7.5.A, 5wlc.17.A, 5l8s.1.A, 5wvi.1.c, 5wlc.15.A, 4gm9.2.A, 2vsy.2.A, 5o9z.1.L, 5wvi.1.O, 3mv2.1.B, 5wlc.13.A, 5o9z.1.F, 5o9z.1.G, 5lfl.1.A, 3mun.1.A, 3s7f.1.A, 5wvi.1.V, 3q75.1.A, 5jkp.1.A, 5m5g.1.A, 4wuy.1.A, 4wju.2.A, 1k8k.1.C, 2vgx.1.A, 2vgx.1.B, 1k3i.1.A, 2eib.1.A, 4gnb.1.A, 4raa.1.A, 1i2m.1.B, 3qwp.1.A, 2qzp.1.A, 3vty.1.A, 5wlc.28.A, 5a9q.1.T, 6f1t.1.b, 6f1t.1.c, 5wlc.19.A, 1crz.1.A, 5a9q.1.L, 3lpz.1.A, 5a9q.1.H, 5a9q.1.G, 5a9q.1.F, 1b89.1.A, 5a9q.1.C, 5a9q.1.B, 1nzn.1.A, 5t88.2.A, 5wlc.26.A, 5l8e.1.A, 4j8e.2.A, 6epc.1.U, 5a9q.1.a, 4v6i.1.A, 3ewe.1.A, 4n2s.1.A, 3j6y.75.A, 5hxb.1.B, 6f1t.1.4, 6f1t.1.3, 1bpo.1.C, 1bpo.1.B, 1bpo.1.A, 1w3b.1.A, 5igq.1.A, 2uy1.1.B, 5a9q.1.2, 3o4h.2.A, 4q1u.1.A, 3jam.1.7, 3pdn.1.A, 3uq3.1.A, 4psw.1.B, 3asf.1.A, 3azo.1.A, 2gbg.1.A, 2qfc.1.A, 3dw8.1.B, 1vz3.1.A, 4a0p.1.A, 4ynd.1.A, 5ojs.1.A, 5bv1.2.B, 6f38.1.3, 6f38.1.4, 5oej.1.A, 3i1c.1.A, 5aio.1.A, 1h4j.1.A, 6f38.1.b, 6f38.1.c, 3wdz.1.A, 4xmm.1.D, 3o4j.1.A, 3o4j.1.B, 3kih.1.A, 1tbg.1.E, 3kih.1.C, 3kih.1.E, 1tbg.1.A, 1qbi.1.A, 4ci1.1.A, 3lrv.1.A, 5d9b.1.A, 5oql.1.O, 5t0g.1.Y, 5t0g.1.X, 5oql.1.L, 4r5o.4.A, 3n0d.1.A, 1wao.1.A, 3asg.2.A, 5t0g.1.V, 2yh3.1.A, 5vtb.1.A, 1xhm.1.A, 1wao.3.A, 4xpd.1.A, 3smr.1.A, 1orv.1.A, 3lvh.1.B, 4j79.1.A, 3sf4.2.A, 5gva.1.A, 5oql.1.E, 5hb3.1.A, 5vhi.1.H, 4gn7.1.A, 5oql.1.M, 4xnh.1.A, 4xi0.1.A, 5t0g.1.5, 4jsp.1.A, 3mkr.1.A, 1yfq.1.A, 5ljo.1.C, 5ljo.1.A, 4r89.1.A, 4hou.1.A, 5ex7.1.A, 4am9.1.A, 2ff4.1.A, 4v7h.1.Q, 1n7d.1.A, 4u04.1.A, 2kck.1.A, 4zov.2.A, 3c12.1.A, 2xcc.1.B, 4wng.1.A, 4a0k.1.C, 4a0k.1.D, 3ks2.1.A, 3sbp.1.A, 3hxj.1.B, 3hxj.1.A, 3qil.1.B, 3qil.1.C, 3qil.1.A, 5hy7.1.A, 1a17.1.A, 3q54.1.A, 4e54.1.B, 4e54.1.A, 4tz4.1.A, 3j81.1.5, 5h1k.1.A, 3ho3.1.A, 3ei4.1.B, 4n5c.8.A, 1r9m.1.A, 2oaj.1.A, 2yms.1.D, 2h6k.1.A, 2yms.1.B, 4n5c.6.A, 2yms.1.A, 5cyk.1.A, 5cyk.1.B, 3ulq.1.A, 5vhs.1.H, 5vhr.1.H, 4y5r.1.C, 3q8w.1.A, 3ash.1.A, 4r8a.1.A, 1hh8.1.A, 5lfm.1.A, 5lks.64.A, 1a12.1.C, 5yp1.2.A, 4leu.1.A, 5yp1.2.B, 5h13.1.A, 1nl4.1.A, 5v1d.2.B, 6bll.1.A, 4hvt.1.A, 6bll.1.B, 1gp2.1.B, 2vdu.1.A, 5a5b.1.Z, 5a5b.1.Y, 4jxm.1.A, 3euv.1.A, 3ho4.2.A, 6bcx.1.A, 6bcx.1.C, 6f3a.1.3, 6f3a.1.2, 1npe.1.A, 3va6.1.A, 4nsx.1.A, 3c72.1.A, 2r2l.1.A, 5ukk.1.B, 3das.1.A, 3qdn.1.A, 5tdh.1.B, 5wvk.1.k, 5wvk.1.a, 5wvk.1.b, 5wvk.1.c, 4gyo.1.A, 4lct.1.A, 4lct.1.B, 3g4e.1.A, 2qzp.2.A, 3k9i.1.A, 5fvk.2.A, 4y6w.1.A, 3oxl.1.A, 5ndv.73.A, 6epf.1.X, 6f9n.1.B, 4mae.1.A, 4oe1.1.A, 4oe1.1.B, 5ln3.1.Z, 2zir.1.A, 3ma5.1.A, 5hax.1.A, 5njx.1.A, 2rip.1.A, 4bwr.1.A, 1elr.1.A, 4nrh.1.B, 5gje.1.B, 5gje.1.A, 4fa4.1.D, 1flg.1.A, 4d9s.1.A, 5ogs.1.A,

4pjr.1.A, 4bta.1.B, 4bta.1.A, 3as5.1.A, 3si5.2.A, 4h7y.3.A, 2b5n.4.A, 3hxr.1.A, 6ek0.64.A, 4cgq.1.A, 1ijq.1.A, 3ww8.1.B, 5jus.45.A, 2jqh.1.A, 3esl.1.A, 5fvl.1.A, 5i9g.1.A, 5min.1.A, 3cvn.1.A, 4a5s.1.A, 5ex0.1.A, 4j0u.1.A, 3ro3.1.A, 5l8w.1.B, 4wsl.1.A, 5txe.1.A, 5omp.1.A, 1pfq.1.A, 4cr2.1.X, 1pfq.1.B, 4cr2.1.W, 5wbk.1.A, 4v7f.1.j, 4gm3.1.A, 3jcm.1.D, 3jcm.1.B, 3v7d.1.B, 2bcj.1.B, 4d10.1.D, 4d10.1.B, 4d10.1.A, 5jj6.1.A, 5jj6.1.B, 1qbq.1.A, 1mzc.1.A, 5t2a.48.A, 2wpv.1.A, 3nok.1.A, 5arf.1.A, 4r40.1.A, 3iuq.1.A, 4cr2.1.6, 3sww.1.A, 2xpi.1.C, 2xpi.1.A, 2hqs.1.A, 3o4i.1.A, 3zn3.1.A, 4cy2.1.A, 3wj9.1.A, 2fpb.1.A, 4v92.1.8, 2i3t.1.A, 5vhm.1.H, 5o3w.1.A, 3jro.1.A, 3jan.80.A, 4wnd.1.A, 5a9q.1.A, 5jpq.1.I, 2fp9.1.A, 6epe.1.U, 4bts.27.A, 5hb2.1.A, 1wy6.1.A, 2iap.1.A, 2o9k.1.A, 3esk.1.A, 2xgm.2.A, 4e5z.1.A, 6epd.1.X, 5udl.1.A, 4av8.1.A, 3pz2.1.A, 3osv.1.A, 2z2p.1.A, 2w8b.2.A, 3iiw.1.A, 3asd.1.A, 4a0b.1.A, 4eba.2.A, 5wbi.1.A, 5tee.1.A, 3bg0.1.A, 3fwv.1.A, 3bg0.1.H, 5nnz.2.A, 5y3r.1.F, 5i5i.1.A, 5d0o.1.B, 5d0o.1.D, 3v65.1.C, 3v65.1.B, 3tkn.1.A, 3hac.1.A, 5lxz.1.A, 2ivz.1.A, 5hyn.2.B, 5juo.45.A, 4ehm.1.A, 3rfh.1.A, 3rfh.1.B, 5ccm.1.A, 3fp2.1.A, 5em2.1.B, 5em2.1.A, 4xgl.1.A, 5ams.1.A, 5mzh.1.A, 3i7p.1.A, 4fhn.2.B, 5wg4.1.B, 5m32.1.a, 5m32.1.b, 5m32.1.c, 4wsn.6.B, 4xmb.1.A, 6f5d.1.J, 6f5d.1.K, 2k3w.1.A, 6f5d.1.L, 4wsn.2.B, 4wsn.2.A, 4wsn.2.D, 2ifu.1.A, 4c8s.1.A, 2wqh.1.A, 2xe4.1.A, 5a5u.1.B, 4u7a.1.A, 5lcw.1.Q, 5lcw.1.R, 4pv7.1.A, 5m32.1.9, 2dso.1.A, 2f0y.1.A, 5lcw.1.C, 5lcw.1.O, 5lcw.1.I, 4i2w.1.A, 4yvo.1.A, 5lwv.1.A, 5buz.1.B, 4yhc.1.A, 5i1z.5.C, 2wq8.1.A, 3ma5.4.A, 4exv.1.A, 3qww.1.A, 3ddu.1.A, 4gq2.1.B, 4gq2.1.A, 1fch.2.A, 3qbj.1.A, 4i79.1.A, 2b5n.1.A, 2vpj.1.A, 2z2o.1.A, 1qni.1.A, 4o9d.2.A, 2d2s.1.A, 3oxg.1.A, 4zov.1.A, 3wqh.1.A, 3wqh.1.B, 3ei4.3.A, 3dra.1.A, 4zlh.1.A, 3qhy.1.B, 1r9n.1.A, 2nc9.1.A, 5xi8.1.A, 4j0x.1.A, 1na3.1.A, 4zlr.1.A, 2xbg.1.A, 5cwo.2.A, 2gvu.1.A, 5l0w.1.A, 4xei.1.C, 5ft9.1.A, 4j8f.1.A, 2kat.1.A, 5xw7.1.A, 2jid.1.A, 2b5n.3.A, 2z2o.3.A, 4xga.1.A, 2ghs.1.A, 3rrm.1.C, 5wcg.1.A, 2aq5.1.A, 1iip.1.A, 5uz5.1.D, 5uz5.1.E, 4gqb.1.B, 4a0l.1.B, 5fzq.1.C, 5lls.1.A, 5fzq.1.A, 5x6o.1.A, 1o6g.1.A, 6bcu.1.A, 5l0y.5.B, 5l0y.5.A, 6bcu.1.B, 4mh1.1.A, 4mh1.1.B, 5l0y.3.A, 3s8v.1.A, 3iur.1.A, 5hq8.1.A, 3f3f.1.A, 1x2r.1.A, 4pwz.1.A, 5g04.1.I, 5mpe.1.K, 5dse.2.A, 2j04.1.A, 5o3x.1.A, 3n0e.1.A, 2j04.1.B, 3ei2.1.A, 3ei2.1.B, 5ag8.1.A, 3gz2.1.A, 2wg3.1.B, 4j0w.1.A, 2vsn.1.A, 2v91.1.A, 2v6x.1.A, 3u3w.1.B, 2iaw.1.A, 1t2x.1.A, 3scy.1.A, 1kt0.1.A, 2b5l.2.A, 3jco.1.Y, 3jco.1.Z, 2onc.1.A, 5grs.1.A, 2z3z.1.A, 4a7j.1.A, 4pwx.1.C, 4kzz.1.6, 3jco.1.0, 2oit.1.A, 5fvk.1.A, 3tc9.1.A, 4i0o.1.A, 5a6c.2.A, 3jaq.1.i, 1pev.1.A, 2iau.1.A, 3e4b.3.A, 5n4c.1.A, 5wlc.24.A, 5vhq.1.H, 5dfz.1.C, 5wlc.22.A, 2qr5.1.A, 2l6j.1.A, 5che.1.E, 5che.1.F, 5wlc.20.A, 1a12.1.B, 4n3c.1.A, 1a12.1.A, 2cnx.1.A, 1k32.1.A, 5i9f.1.A, 3vty.3.A, 3g4h.1.B, 3g4h.1.A, 4dnw.1.A, 5ttw.2.A, 4zn4.1.A, 4u1e.1.A, 1d8d.1.A, 5i2t.1.A, 3f3p.2.B, 4gga.1.A, 4bh6.1.A, 1got.1.B, 3s25.1.A, 3p1l.1.A, 5ctq.2.B, 5ctq.2.A, 4e6h.1.A, 3vnh.1.A, 5lzz.77.A, 3j98.1.I, 3j98.1.H, 4buj.2.B, 3vng.1.A, 3ceq.1.A, 3ceq.1.B, 4ay5.1.A, 2xev.2.A, 5fzr.1.A, 5fzr.1.B, 3wwb.1.A, 4cr2.1.Y, 4d5l.1.7, 4ggc.1.A, 4ynv.1.A, 4buj.1.D, 5fzq.1.B, 2pbi.1.B, 3jai.77.A, 2pzi.1.A, 4yzs.1.A, 3f8s.1.A, 4yzs.1.B, 5i9h.1.A, 3fp3.1.A, 5nnp.2.A, 2pm6.1.B, 2pm6.1.C, 2pm6.1.A, 2wft.1.A, 4dnu.1.A, 3v9f.3.A, 5ex3.1.A, 3c5m.1.A, 3o10.2.B, 5uz7.1.B, 3e5z.1.A, 5ic8.4.A, 1wcy.1.A, 1u4c.1.A, 3v9f.1.A, 4ci8.2.A

SWISS-MODEL Homology Modelling Report

Model Building Report

This document lists the results for the homology modelling project "IF122_HUMAN Q9HBG6 Intraflagellar transport protein 122 homolog" submitted to SWISS-MODEL workspace on Feb. 26, 2018, 6:12 a.m..The submitted primary amino acid sequence is given in Table T1.

If you use any results in your research, please cite the relevant publications:

- Biasini, M., Bienert, S., Waterhouse, A., Arnold, K., Studer, G., Schmidt, T., Kiefer, F., Cassarino, T.G., Bertoni, M., Bordoli, L., Schwede, T. SWISS-MODEL: modelling protein tertiary and quaternary structure using evolutionary information. Nucleic Acids Res. 42, W252-W258 (2014). doi
- Guex, N., Peitsch, M.C., Schwede, T. Automated comparative protein structure modeling with SWISS-MODEL and Swiss-PdbViewer: A historical perspective. Electrophoresis 30, S162-S173 (2009). doi
- Bienert, S., Waterhouse, A., de Beer, T.A., Tauriello, G., Studer, G., Bordoli, L., Schwede, T. The SWISS-MODEL Repository - new features and functionality. Nucleic Acids Res. 45, D313-D319 (2017). doi
- Benkert, P., Biasini, M., Schwede, T. Toward the estimation of the absolute quality of individual protein structure models. Bioinformatics 27, 343-350 (2011). doi
- Bertoni, M., Kiefer, F., Biasini, M., Bordoli, L., Schwede, T. Modeling protein quaternary structure of homo- and hetero-oligomers beyond binary interactions by homology. Scientific Reports 7 (2017). doi

Results

The SWISS-MODEL template library (SMTL version 2018-02-21, PDB release 2018-02-16) was searched with BLAST (Camacho et al.) and HHBlits (Remmert, et al.) for evolutionary related structures matching the target sequence in Table T1. For details on the template search, see Materials and Methods. Overall 3940 templates were found (Table T2).

Models

The following model was built (see Materials and Methods "Model Building"):

Model #01	File	Built with	Oligo-State	Ligands	GMQE	QMEAN
	PDB	ProMod3 Version 1.1.0.	monomer (matching prediction)	None	0.28	-7.23

QMEAN	-7.23
Cβ	-4.35
All Atom	-3.61
Solvation	-1.72
Torsion	-5.82

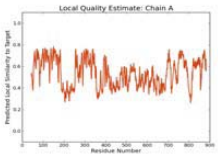

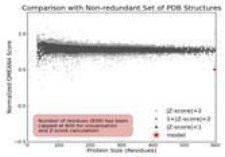

Template	Seq Identity	Oligo-state	QSQE	Found by	Method	Resolution	Seq Similarity	Range	Coverage	Description
3mkq.1.A	12.03	homo-trimer	0.00	HHblits	X-ray	2.50Å	0.26	44 - 882	0.56	Coatomer beta'-subunit

The template contained no ligands.

```
Target    MRAVLTWRDKAEHCINDIAFKPDGTQLILAAGSRLLVYDTSDGTLLQPLKGHKDTVYCVAYAKDGKRFASGSADKSVIIW
3mkq.1.A  -------------------------------------------DIKKTFSNRSDRVKGIDFHPTEPWVLTTLYSGRVEIW

Target    TSKLEGILK--YTHNDAIQCVSYNPITHQLASCSS-SDFGLWSPEQKSVSKH--KSSSKIICCSWTNDGQYLALGMFNGI
3mkq.1.A  NYETQVEVRSIQVTETPVRAGKFIARKNWIIVGSDDFRIRVFNYNTGEKVVDFEAHPDYIRSIAVHPTKPYVLSGSDDLT

Target    ISIRNKNGE-EKVKIERPGGSLSPIWSICWNPSSRWESFWMNRENEDAEDVIVNRYIQEIPSTLKSAVYSSQGSEAEEEE
3mkq.1.A  VKLWNWENNWALEQTF--EGHEHFVMCVAFNPKDP-------------------------------------------

Target    PEEEDDSPRDDNLEERNDILAVADWGQKVSFYQLSGKQIG-KDRALN-FDPCCISYFT--KGEYILLGGSDKQVSLFT-K
3mkq.1.A  -----------------STFASGCLDRTVKVWSLGQSTPNFTLTTGQERGVNYVDYYPLPDKPYMITASDDLTIKIWDYQ

Target    DGVRLGTVGEQNSWVWTCQAKPDSNYVVVGCQDGTISFYQLIFSTVHGLYKDRYAYRDSMTDVIVQHLITEQKVRIKCKE
3mkq.1.A  TKSCVATLEGHMSNVSFAVFHPTLPIIISGSEDGTLKIWNSSTYKV------------------EKTLNV-------GLE

Target    LVKKIAIYR--N--RLAIQLPEKILIYELYSEDLSDMHYRVKEKIIKKFECNLLVVCANHIILCQEKRLQCLSFSGVK--
3mkq.1.A  RSWCIATHPTGRKNYIASGFDNGFTVLSLGNDEP---TLSLD------PVGKLVWSGGKN---AAASDIFTAVIRGNEEV

Target    --ERE--W------QMESLIRYIKVIGGPPGREGLLVGLKNGQILKIFVDNLFAIVLLKQATAVRCLDMSASRKKLAVVD
```

```
3mkq.1.A  EQDEPLSLQTKELGSVDVFPQSLAHS---PNGRFVTVVG-DGEY-VIYTALA---WRNKAFGKCQDFVWGPDSNSYALID

Target    ENDTCLVYDIDTKELLFQEPNANSVAWNTQC---EDMLCFSGGGYLNIKASTFPVHRQKLQGFV--VGYN-GSK-IFCLH
3mkq.1.A  ETGQIKYYKNFKEVT----SWSVPMHSAIDRLFSGALLGVKSDGFVYFFDWDNGTLVRRIDVNAKDVIWSDNGELVMIVN

Target    V------FSISAVEVPQSAPMYQYLDRKLFK------EAYQIACL----------------------------------
3mkq.1.A  TNSNGDEASGYTL-LFNKDAYLEAANNGNIDDSEGVDEAFDVLYELSESITSGKWVGDVFIFTTATNRLNYFVGGKTYNL

Target    -------------GVTDTDWRELAMEALEGLDFETAK---KAFIRVQDLRY--LELISSIEERKKRGETNNDLFLADVFS
3mkq.1.A  AHYTKEMYLLGYLARDNKVYLADREVHVYGYEISLEVLEFQTLTLRGEIEEAIENVLPNVE---G---KDSLTKIARFLE

Target    YQGKFHEAAKLYKRSGHENLALEMYTDLCMFEYAKDFLGSGDPKETKMLITKQADWARNIKEPKAAVEMYISAGEHVKAI
3mkq.1.A  GQEYYEEALNISPDQDQK---FELALKVGQLTLARDLLTDES---AEMKWRALGDASLQRFNFKLAIEAFTNAHDLESLF

Target    EICGDHGWVDMLIDIARKLDKAEREPLLLCATYLKKLDSPGYAAETYLKMGDLKSLVQLHVETQRWDEAFALGEKH---P
3mkq.1.A  LLHSSFNNKEGLVTLA--------------KDAETTGKFNLAFNAYWIAGDIQGAKDLLIKSQRFSEAAFLGSTYGLGD

Target    EFKDDIYMPYAQWLAENDRFEEAQKAFHKAGRQREAVQVLEQLTNNAVAESRFNDAAYYYWMLSMQCLDIAQDPAQKDTM
3mkq.1.A  NEVNDIVTKWKENLILNGKNTVSE------------------------------------------------------

Target    LGKFYHFQRLAELYHGYHAIHRHTEDPFSVHRPETLFNISRFLLHSLPKDTPSGISKVKILFTLAKQSKALGAYRLARHA
3mkq.1.A  ------------------------------------------------------------------------------

Target    YDKLRGLYIPARFQKSIELGTLTIRAKPFHDSEELVPLCYRCSTNNPLLNNLGNVCINCRQPFIFSASSYDVLHLVEFYL
3mkq.1.A  ------------------------------------------------------------------------------

Target    EEGITDEEAISLIDLEVLRPKRDDRQLEIANNSSQILRLVETKDSIGDEDPFTAKLSFEQGGSEFVPVVVSRLVLRSMSR
3mkq.1.A  ------------------------------------------------------------------------------

Target    RDVLIKRWPPPLRWQYFRSLLPDASITMCPSCFQMFHSEDYELLVLQHGCCPYCRRCKDDPGP
3mkq.1.A  ------------------------------------------------------------
```

Materials and Methods

Template Search

Template search with BLAST and HHBlits has been performed against the SWISS-MODEL template library (SMTL, last update: 2018-02-21, last included PDB release: 2018-02-16).

The target sequence was searched with BLAST against the primary amino acid sequence contained in the SMTL. A total of 95 templates were found.

An initial HHblits profile has been built using the procedure outlined in (Remmert, et al.), followed by 1 iteration of HHblits against NR20. The obtained profile has then be searched against all profiles of the SMTL. A total of 3904 templates were found.

Template Selection

For each identified template, the template's quality has been predicted from features of the target-template alignment. The templates with the highest quality have then been selected for model building.

Model Building

Models are built based on the target-template alignment using ProMod3. Coordinates which are conserved between the target and the template are copied from the template to the model. Insertions and deletions are remodelled using a fragment library. Side chains are then rebuilt. Finally, the geometry of the resulting model is regularized by using a force field. In case loop modelling with ProMod3 fails, an alternative model is built with PROMOD-II (Guex, et al.).

Model Quality Estimation

The global and per-residue model quality has been assessed using the QMEAN scoring function (Benkert, et al.) . For improved performance, weights of the individual QMEAN terms have been trained specifically for SWISS-MODEL.

Ligand Modelling

Ligands present in the template structure are transferred by homology to the model when the following criteria are met: (a) The ligands are annotated as biologically relevant in the template library, (b) the ligand is in contact with the model, (c) the ligand is not clashing with the protein, (d) the residues in contact with the ligand are conserved between the target and the template. If any of these four criteria is not satisfied, a certain ligand will not be included in the model. The model summary includes information on why and which ligand has not been included.

Oligomeric State Conservation

The quaternary structure annotation of the template is used to model the target sequence in its oligomeric form. The method (Bertoni et al.) is based on a supervised machine learning algorithm, Support Vector Machines (SVM), which combines interface conservation, structural clustering, and other template features to provide a quaternary structure quality estimate (QSQE). The

QSQE score is a number between 0 and 1, reflecting the expected accuracy of the interchain contacts for a model built based a given alignment and template. Higher numbers indicate higher reliability. This complements the GMQE score which estimates the accuracy of the tertiary structure of the resulting model.

References

- **BLAST**
  Camacho, C., Coulouris, G., Avagyan, V., Ma, N., Papadopoulos, J., Bealer, K., Madden, T.L. BLAST+: architecture and applications. BMC Bioinformatics 10, 421-430 (2009). doi
- **HHblits**
  Remmert, M., Biegert, A., Hauser, A., Söding, J. HHblits: lightning-fast iterative protein sequence searching by HMM-HMM alignment. Nat Methods 9, 173-175 (2012). doi

Table T1:

Primary amino acid sequence for which templates were searched and models were built.

```
MRAVLTWRDKAEHCINDIAFKPDGTQLILAAGSRLLVYDTSDGTLLQPLKGHKDTVYCVAYAKDGKRFASGSADKSVIIWTSKLEGILKYTHNDAIQCVS
YNPITHQLASCSSSDFGLWSPEQKSVSKHKSSSKIICCSWTNDGQYLALGMFNGIISIRNKNGEEKVKIERPGGSLSPIWSICWNPSSRWESFWMNRENE
DAEDVIVNRYIQEIPSTLKSAVYSSQGSEAEEEEPEEEDDSPRDDNLEERNDILAVADWGQKVSFYQLSGKQIGKDRALNFDPCCISYFTKGEYILLGGS
DKQVSLFTKDGVRLGTVGEQNSWVWTCQAKPDSNYVVVGCQDGTISFYQLIFSTVHGLYKDRYAYRDSMTDVIVQHLITEQKVRIKCKELVKKIAIYRNR
LAIQLPEKILIYELYSEDLSDMHYRVKEKIIKKFECNLLVVCANHIILCQEKRLQCLSFSGVKEREWQMESLIRYIKVIGGPPGREGLLVGLKNGQILKI
FVDNLFAIVLLKQATAVRCLDMSASRKKLAVVDENDTCLVYDIDTKELLFQEPNANSVAWNTQCEDMLCFSGGGYLNIKASTFPVHRQKLQGFVVGYNGS
KIFCLHVFSISAVEVPQSAPMYQYLDRKLFKEAYQIACLGVTDTDWRELAMEALEGLDFETAKKAFIRVQDLRYLELISSIEERKKRGETNNDLFLADVF
SYQGKFHEAAKLYKRSGHENLALEMYTDLCMFEYAKDFLGSGDPKETKMLITKQADWARNIKEPKAAVEMYISAGEHVKAIEICGDHGWVDMLIDIARKL
DKAEREPLLLCATYLKKLDSPGYAAETYLKMGDLKSLVQLHVETQRWDEAFALGEKHPEFKDDIYMPYAQWLAENDRFEEAQKAFHKAGRQREAVQVLEQ
LTNNAVAESRFNDAAYYYWMLSMQCLDIAQDPAQKDTMLGKFYHFQRLAELYHGYHAIHRHTEDPFSVHRPETLFNISRFLLHSLPKDTPSGISKVKILF
TLAKQSKALGAYRLARHAYDKLRGLYIPARFQKSIELGTLTIRAKPFHDSEELVPLCYRCSTNNPLLNNLGNVCINCRQPFIFSASSYDVLHLVEFYLEE
GITDEEAISLIDLEVLRPKRDDRQLEIANNSSQILRLVETKDSIGDEDPFTAKLSFEQGGSEFVPVVVSRLVLRSMSRRDVLIKRWPPPLRWQYFRSLLP
DASITMCPSCFQMFHSEDYELLVLQHGCCPYCRRCKDDPGP
```

Table T2:

Template	Seq Identity	Oligo-state	QSQE	Found by	Method	Resolution	Seq Similarity	Coverage	Description
5a1u.1.T	14.70	monomer		HHblits	EM	13.00Å	0.28	0.59	COATOMER SUBUNIT BETA'
5nzu.1.C	14.70	monomer		HHblits	EM	NA	0.28	0.59	Coatomer subunit beta'
5a1u.1.S	13.39	monomer		HHblits	EM	13.00Å	0.27	0.59	COATOMER SUBUNIT ALPHA
5nzu.1.A	13.39	monomer		HHblits	EM	NA	0.27	0.59	Coatomer subunit alpha
3mkq.1.A	12.03	homo-trimer		HHblits	X-ray	2.50Å	0.26	0.56	Coatomer beta'-subunit
3mkq.1.C	12.03	homo-trimer		HHblits	X-ray	2.50Å	0.26	0.56	Coatomer beta'-subunit
3mkq.1.E	12.03	homo-trimer		HHblits	X-ray	2.50Å	0.26	0.56	Coatomer beta'-subunit
5a1u.1.T	14.14	monomer		HHblits	EM	13.00Å	0.28	0.54	COATOMER SUBUNIT BETA'
5nzu.1.C	14.14	monomer		HHblits	EM	NA	0.28	0.54	Coatomer subunit beta'
4bzj.1.A	14.00	homo-dimer		HHblits	EM	40.00Å	0.27	0.52	PROTEIN TRANSPORT PROTEIN SEC31
4bzj.1.C	14.00	homo-dimer		HHblits	EM	40.00Å	0.27	0.52	PROTEIN TRANSPORT PROTEIN SEC31
3mkq.1.A	14.11	homo-trimer	0.11	HHblits	X-ray	2.50Å	0.27	0.52	Coatomer beta'-subunit
3mkq.1.C	14.11	homo-trimer	0.11	HHblits	X-ray	2.50Å	0.27	0.52	Coatomer beta'-subunit
3mkq.1.E	14.11	homo-trimer	0.11	HHblits	X-ray	2.50Å	0.27	0.52	Coatomer beta'-subunit
5a1u.1.S	13.47	monomer		HHblits	EM	13.00Å	0.27	0.51	COATOMER SUBUNIT ALPHA
5nzu.1.A	13.47	monomer		HHblits	EM	NA	0.27	0.51	Coatomer subunit alpha
4bzj.1.A	12.39	homo-dimer		HHblits	EM	40.00Å	0.26	0.46	PROTEIN TRANSPORT PROTEIN SEC31
4bzj.1.C	12.39	homo-dimer		HHblits	EM	40.00Å	0.26	0.46	PROTEIN TRANSPORT PROTEIN SEC31
5oql.1.J	11.92	monomer		HHblits	EM	NA	0.26	0.45	Utp13
5h1j.1.A	14.29	monomer		HHblits	X-ray	2.00Å	0.27	0.45	Gem-associated protein 5
5h1k.1.A	14.29	monomer		HHblits	X-ray	1.90Å	0.27	0.45	Gem-associated protein 5
5h3s.1.A	14.34	monomer		HHblits	X-ray	3.00Å	0.27	0.44	Gem-associated protein 5
2ymu.1.A	18.13	monomer		HHblits	X-ray	1.79Å	0.30	0.42	WD-40 REPEAT PROTEIN
3jbt.1.A	15.73	monomer		HHblits	EM	NA	0.28	0.43	Apoptotic protease-activating factor 1
5wyj.16.A	13.04	monomer		HHblits	EM	NA	0.27	0.43	Periodic tryptophan protein 2

Template	Seq Identity	Oligo-state	QSQE	Found by	Method	Resolution	Seq Similarity	Coverage	Description
5wyk.1.R	13.04	monomer		HHblits	EM	NA	0.27	0.43	Periodic tryptophan protein 2
5wlc.20.A	13.04	monomer		HHblits	EM	NA	0.27	0.43	Utp1
3j2t.1.A	15.82	monomer		HHblits	EM	NA	0.28	0.43	Apoptotic protease-activating factor 1
5wve.1.K	15.85	monomer		HHblits	EM	NA	0.28	0.43	Apoptotic protease-activating factor 1
5juy.1.B	15.85	monomer		HHblits	EM	NA	0.28	0.43	Apoptotic protease-activating factor 1
5juy.1.G	15.85	monomer		HHblits	EM	NA	0.28	0.43	Apoptotic protease-activating factor 1
5juy.1.D	15.85	monomer		HHblits	EM	NA	0.28	0.43	Apoptotic protease-activating factor 1
5juy.1.E	15.85	monomer		HHblits	EM	NA	0.28	0.43	Apoptotic protease-activating factor 1
3shf.1.A	15.09	monomer		HHblits	X-ray	3.55Å	0.28	0.43	Apoptotic peptidase activating factor 1
3sfz.1.A	15.09	monomer		HHblits	X-ray	3.00Å	0.27	0.43	Apoptotic peptidase activating factor 1
5tee.1.A	15.04	monomer		HHblits	X-ray	1.65Å	0.27	0.43	Gem-associated protein 5
5gxh.1.A	15.04	monomer		HHblits	X-ray	1.80Å	0.27	0.43	Gem-associated protein 5
5wve.1.K	15.52	monomer		HHblits	EM	NA	0.28	0.42	Apoptotic protease-activating factor 1
5juy.1.B	15.52	monomer		HHblits	EM	NA	0.28	0.42	Apoptotic protease-activating factor 1
5juy.1.G	15.52	monomer		HHblits	EM	NA	0.28	0.42	Apoptotic protease-activating factor 1
5juy.1.D	15.52	monomer		HHblits	EM	NA	0.28	0.42	Apoptotic protease-activating factor 1
5juy.1.E	15.52	monomer		HHblits	EM	NA	0.28	0.42	Apoptotic protease-activating factor 1
5i2t.1.A	12.88	monomer		HHblits	X-ray	2.54Å	0.27	0.43	Periodic tryptophan protein 2
3shf.1.A	16.31	monomer		HHblits	X-ray	3.55Å	0.28	0.41	Apoptotic peptidase activating factor 1
5oql.1.A	11.41	monomer		HHblits	EM	NA	0.27	0.42	Periodic tryptophan protein 2-like protein
3jbt.1.A	15.53	monomer		HHblits	EM	NA	0.28	0.41	Apoptotic protease-activating factor 1
3sfz.1.A	16.34	monomer		HHblits	X-ray	3.00Å	0.28	0.41	Apoptotic peptidase activating factor 1
3j2t.1.A	15.34	monomer		HHblits	EM	NA	0.28	0.41	Apoptotic protease-activating factor 1
5m2n.1.A	11.30	monomer		HHblits	X-ray	2.81Å	0.25	0.43	Elongator complex protein 2
4xfv.1.A	11.39	monomer		HHblits	X-ray	3.20Å	0.25	0.42	Elongator complex protein 2

The table above shows the top 50 filtered templates. A further 2,072 templates were found which were considered to be less suitable for modelling than the filtered list.
3fgb.1.A, 5gm6.1.4, 3vl1.1.A, 4a1s.1.A, 2ff4.2.A, 5cvo.2.A, 3fm0.1.A, 2g5p.1.A, 5ukl.1.B, 1x81.1.A, 4nox.1.A, 4a0a.1.B, 1ft1.1.A, 5gm6.1.2, 5vgz.1.K, 5vgz.1.J, 5vgz.1.H, 5c4x.1.L, 5j4z.78.A, 2qx5.1.A, 4ui9.1.P, 4ui9.1.Q, 4ui9.1.V, 4ui9.1.W, 4ui9.1.J, 4ui9.1.K, 4ui9.1.H, 4ui9.1.I, 4ui9.1.O, 5wbh.3.A, 4ui9.1.C, 4ui9.1.F, 3q15.1.A, 3ieg.2.A, 2xyi.1.A, 2kc7.1.A, 3u85.1.A, 5olj.1.A, 4v6u.63.A, 1aof.1.A, 1aof.1.B, 3ium.1.A, 4yhc.2.A, 5fqd.1.A, 5dse.1.A, 3po3.1.L, 5n4d.1.A, 5iy9.1.L, 3sre.1.A, 1jmz.1.B, 5opt.1.A, 3mv3.1.B, 4bt9.1.A, 2qt9.1.A, 5m5w.1.L, 5k0m.1.A, 4i1a.1.A, 2y69.1.F, 4uer.1.b, 4cvc.1.A, 3s2k.1.B, 3s2k.1.A, 3j7p.78.A, 1hxi.1.A, 2ce9.2.B, 4s3o.1.C, 5wyk.1.U, 5gjr.12.A, 5wyk.1.V, 5wyk.1.R, 5jrl.1.B, 5mqf.1.O, 5a7d.8.A, 5mqf.1.M, 4v5z.1.A, 5mqf.1.F, 5n4e.1.A, 5mqf.1.D, 5mqf.1.E, 4v6w.2.A, 1jtd.1.B, 1wm5.1.A, 5uw7.1.A, 5l4k.1.E, 3ffl.2.B, 5l4k.1.G, 5l4k.1.F, 5l4k.1.I, 3mbr.1.A, 5l4k.1.J, 4a2l.1.B, 2j9q.1.B, 2j9q.1.A, 5k1a.2.B, 6au8.1.A, 3l1z.2.B, 2ma6.1.A, 4yg8.1.B, 3dqv.1.C, 5h19.1.A, 5sv7.1.D, 3odt.1.A, 5sv7.1.A, 5sv7.1.B, 5sv7.1.C, 2fi7.1.A, 2fi7.1.B, 5gmk.1.0, 3li4.1.A, 5n4f.1.A, 2bkl.1.A, 3j92.1.n, 6eos.1.B, 5wlc.27.A, 5mpq.1.A, 3hlh.1.A, 1o6f.1.A, 1vz2.1.A, 5o9z.1.L, 1z68.1.B, 5cqr.1.A, 1z68.1.A, 1z2z.1.A, 5i1y.1.C, 2bed.1.A, 4x3e.1.A, 2be1.1.A, 5wlc.13.A, 5gmk.1.J, 5kkl.1.A, 3ly9.1.A, 3ly8.1.A, 5gmk.1.X, 5gmk.1.R, 5a7d.6.A, 5a9q.1.A, 2ooe.1.A, 4ui9.1.B, 5mnj.1.D, 3cv0.1.A, 5m72.1.A, 3rib.1.A, 2hes.1.A, 2gw1.1.A, 2gw1.1.B, 3o4i.1.A, 4eqf.1.A, 2iav.1.A, 4kvm.1.A, 4y7n.1.J, 4j8e.1.A, 5wyj.19.A, 5v4b.1.B, 3gtk.1.J, 1sly.1.A, 2vz1.1.A, 3j8b.1.C, 1c9l.1.A, 3ly7.1.A, 3jck.1.B, 1b9y.1.A, 3jck.1.D, 5o3u.1.A, 4ja7.1.A, 4ymr.1.A, 2p9w.1.A, 4ymr.1.B, 3txn.1.A, 4a3d.1.L, 5kjk.1.A, 5guw.3.A, 3rtr.3.B, 5jj7.1.A, 2y4u.1.A, 5jj7.1.B, 5ulh.1.C, 3i7k.1.A, 5n4b.1.A, 2iat.1.A, 1tl2.1.A, 2iax.1.A, 3edt.1.A, 3edt.1.B, 2ebs.1.A, 5c2w.1.E, 4lg8.1.A, 5juu.45.A, 2kr4.1.A, 1hzu.1.A, 4q66.2.C, 4bxz.1.L, 2yhc.1.A, 5lj5.1.V, 3zfw.1.A, 4hou.2.A, 3jro.1.A, 1e96.1.B, 5k0y.1.8, 5wbh.4.A, 5a1y.1.U, 5eya.1.C, 5eya.1.B, 4wne.1.A, 4i9e.1.A, 3cvq.1.A, 4d18.1.D, 4d18.1.B, 3ow8.1.A, 4yde.1.A, 4cy1.1.A, 1vyh.1.C, 3kd7.1.A, 5m5x.1.L, 3bee.1.A, 5v3o.1.A, 5vhj.1.H, 5m5r.1.A, 4hhq.1.A, 2l0b.1.A, 4kbq.2.A, 5aiu.1.A, 1n6f.1.A, 5wyj.17.A, 5iya.1.L, 4hoq.1.A, 3gz1.1.A, 3sf4.1.A, 3gz1.1.B, 5vhf.1.J, 4wn4.2.A, 4bt8.1.B, 4bt8.1.A, 4buj.1.C, 2ynn.1.A, 2ecl.1.A, 3li3.1.A, 5cqs.1.A, 3jb9.1.K, 5oql.1.3, 5k1c.1.C, 5k1c.1.B, 6epc.1.S, 5igo.1.A, 6epc.1.T, 6epc.1.W, 6epc.1.V, 6epc.1.X, 5oql.1.X, 4r5o.1.A, 2gop.1.A, 2gop.1.B, 6exn.1.J, 5i9d.1.A, 5oql.1.N, 5oql.1.O, 5oql.1.L, 5oql.1.M, 2xgs.1.A, 5oql.1.A, 5oql.1.F, 5oql.1.D, 5oql.1.E, 6exn.1.a, 6emk.1.D, 6emk.1.B, 6emk.1.C, 5ijn.1.U, 4v7h.1.Q, 5ijn.1.K, 5ijn.1.I, 5wbu.1.B, 3pbp.4.A, 5wbu.1.A, 5ijn.1.C, 1jju.1.B, 4uzy.1.A, 3no2.1.A, 5d0i.1.A, 2csy.1.A, 4n5c.5.A, 5yp1.1.B, 5yp1.1.A, 5i1y.1.A, 5m2n.1.A, 5i1y.1.B, 4hot.1.A,

2ep4.1.A, 4n5c.3.A, 5hgv.1.A, 5jul.1.A, 5cxb.1.B, 5cxb.1.A, 5lvv.1.A, 4n5c.1.A, 3mzl.1.B, 2co0.1.A, 3j0k.1.L, 5vlj.1.B, 5vlj.1.C, 5bt1.1.B, 6f9n.1.A, 5b4x.1.B, 3q4a.1.A, 5ln3.1.Y, 5ln3.1.X, 3as8.1.A, 5mgx.1.A, 2p4o.1.A, 4bzj.1.D, 4bzj.1.B, 2d8t.1.A, 4hw6.1.A, 3i7l.1.A, 3ww8.1.B, 5ln3.1.A, 3ww8.1.A, 5mc6.35.A, 3qdn.2.A, 5ic8.3.A, 3va6.2.A, 5vny.1.A, 1qsa.1.A, 3gd1.3.A, 5ic8.1.A, 5fer.1.D, 5wsg.1.T, 5fer.1.A, 5sxm.1.A, 5lyb.33.A, 3jbt.1.A, 5yz0.1.A, 5jzz.2.A, 5flm.1.L, 4fhl.1.A, 5vh9.1.B, 2ifu.3.A, 5d0m.1.B, 2ovr.1.B, 4uic.1.A, 3j80.1.7, 3oxf.1.A, 1mda.1.A, 4wjw.1.B, 2iar.1.A, 3ivm.1.A, 3jco.1.8, 4wsn.4.D, 6b41.1.A, 3acp.1.A, 1aoq.1.A, 2pl2.1.A, 2c2l.2.A, 2hz6.1.A, 3e0c.1.A, 3jrp.1.A, 5nrl.1.Q, 5nrl.1.W, 4x60.1.B, 5nrl.1.O, 4aez.1.A, 4aez.1.C, 5d0i.2.A, 3j78.45.A, 4aez.3.C, 2gvx.1.A, 5m64.1.L, 5djs.1.A, 5mq0.1.I, 2yin.1.A, 5mps.1.U, 4zox.1.A, 5mps.1.Q, 5lj3.1.L, 1qz2.1.C, 1qz2.1.B, 1qz2.1.A, 3po2.1.L, 3vu4.1.A, 4a0a.1.A, 5lj3.1.U, 5lj3.1.T, 4a0b.1.B, 2i3s.2.A, 5gm6.1.F, 5a9q.1.a, 3vu4.2.A, 3tg5.1.A, 2vyi.1.A, 1g72.1.A, 2xcc.1.A, 2rfo.1.A, 4zb4.2.A, 5b26.2.B, 5txc.1.A, 5jz6.1.A, 3fvz.1.A, 2b5m.1.A, 1gjq.1.A, 2ovp.1.B, 3nol.1.A, 4u7y.1.A, 3li5.1.A, 4ggd.1.A, 5lj5.1.M, 2xzg.1.A, 5lj5.1.U, 3mzk.1.A, 3mzk.1.B, 5o09.1.C, 5ftp.1.A, 5ftp.1.B, 3fw0.1.A, 5fja.1.L, 3si5.1.A, 5lj5.1.d, 5diz.1.A, 4g2v.1.A, 5iy5.1.F, 5jk7.2.A, 3jct.1.n, 3lrq.1.B, 3lrq.1.A, 2eic.1.A, 4g56.1.B, 4v0m.1.B, 3n71.1.A, 3zwl.1.A, 4hnw.1.A, 5jrk.1.B, 5l0y.1.B, 5l0y.1.A, 1yr2.1.A, 3hym.1.B, 5t0c.35.A, 2ece.1.A, 1klx.1.A, 5mc6.37.A, 1gxr.1.B, 1gxr.1.A, 4h7x.1.A, 3e4b.1.A, 3ott.1.B, 3ott.1.A, 5jqy.1.A, 4a09.1.A, 4nq0.1.A, 3zpj.1.A, 4r40.2.A, 4cgv.1.A, 4abn.1.A, 3as4.1.A, 5hb0.4.A, 5ulk.1.B, 2occ.1.F, 5c2v.1.A, 5wql.1.A, 1bpo.1.B, 3hli.1.A, 2hu5.1.B, 5juy.1.B, 5c2v.1.B, 5wyj.20.A, 2uy1.1.A, 4lg9.1.A, 1sqj.1.A, 2fpb.2.A, 5d0o.1.D, 5d0q.1.C, 2e2e.1.A, 2yno.1.A, 5i5m.1.A, 5d0k.1.B, 3byc.1.A, 3s1r.1.J, 3v64.1.A, 5ndv.147.A, 3v64.1.D, 3gto.1.J, 3fmo.1.A, 4av8.1.A, 3kae.1.A, 3s25.1.A, 3hrp.1.A, 2xcb.2.A, 4g1f.4.A, 3cqz.1.J, 4qpl.2.A, 4xyh.1.A, 4bl0.2.A, 3zwu.1.A, 3cfs.1.A, 5wvi.1.N, 2ecn.1.A, 4r2y.1.A, 1lrw.1.C, 1lrw.1.A, 4ja9.1.A, 2faw.1.A, 4gpk.1.D, 4gpk.1.A, 4gpk.1.C, 4gpk.1.B, 3fwv.2.A, 5nnz.1.A, 3s94.2.A, 4gpk.3.D, 4gpk.3.C, 4gpk.3.B, 4gpk.3.A, 2lsu.1.A, 3emh.1.A, 1ouv.1.A, 4kvo.1.A, 4d0k.1.A, 5igo.2.A, 5ife.1.D, 5ijo.1.Q, 5buz.2.B, 5ijo.1.W, 5gjq.1.Z, 5jpz.1.B, 6ez8.1.B, 5jpz.1.A, 5ijo.1.E, 4c2m.1.L, 4ozs.1.A, 4aow.1.A, 2i0r.1.C, 5l4k.1.H, 5gjq.1.j, 2y0s.1.K, 4btb.1.A, 5em2.1.A, 3mmy.1.A, 5ltd.1.A, 3ng2.1.A, 3ng2.1.B, 2iaq.1.A, 5mpb.1.g, 3sfx.1.A, 5gjq.1.7, 5ctr.1.A, 5gjq.1.5, 3u4t.1.A, 2iwa.1.A, 5mpb.1.i, 5mpb.1.h, 4a1g.2.A, 4l9o.1.A, 2co0.2.A, 3ww9.1.A, 5obm.152.A, 1fpp.1.B, 5cvl.1.A, 4czv.1.A, 1ihg.1.A, 3soq.1.A, 5bw8.1.C, 3r9a.1.D, 5naf.1.A, 2h13.1.A, 3r9a.1.B, 1tnu.1.A, 3sn6.1.B, 6c23.1.D, 5tzs.1.e, 6c23.1.F, 1qqe.1.A, 6bq1.1.B, 2dg1.1.A, 1r5m.1.A, 4gq1.1.A, 5w65.1.L, 5xog.1.L, 1p22.1.A, 5w5h.2.E, 3wwa.1.A, 5tzs.1.1, 2pm9.1.A, 2q7f.1.A, 5yp4.2.A, 4o6f.1.A, 3w15.1.A, 3bws.1.A, 3h0g.1.L, 2bug.1.A, 5an3.1.A, 5vyc.4.I, 4o5t.1.A, 4jsn.1.A, 4jsn.1.B, 4pjq.1.A, 5cxc.1.B, 5cxc.1.A, 5b26.1.B, 1jof.1.A, 6em3.1.E, 3h7n.1.A, 5t2c.73.A, 2ias.1.A, 4m59.1.B, 3sfz.1.A, 4m59.1.A, 5jcs.1.3, 4yvd.1.A, 2y43.1.A, 5fjy.1.B, 5fjy.1.A, 2y43.1.B, 5l0y.6.A, 1o1r.1.A, 5igq.1.A, 1fwx.1.A, 5a5t.1.C, 3s16.1.J, 4i9c.1.A, 4xmm.1.C, 5jjx.1.A, 2qxv.1.A, 4xmm.1.E, 5jut.45.A, 3shf.1.A, 3jcp.1.Z, 3jcp.1.Y, 4pxw.1.A, 2vgy.1.A, 5nnr.1.A, 3jcp.1.0, 5wrw.1.A, 5wrw.1.B, 2eep.1.A, 3jcp.1.8, 2c0l.1.A, 3dsm.1.A, 1x4j.1.A, 4wjv.1.A, 5a7d.4.A, 5wrw.3.A, 3nf1.1.A, 1xfd.1.A, 4d4q.1.A, 5mpe.2.H, 5mpe.2.E, 2hu8.1.A, 3rjv.1.A, 2vdu.1.A, 4rid.2.A, 4m57.1.A, 5a6c.1.A, 2lah.1.A, 4i17.1.A, 6eoq.1.A, 5afu.1.C, 6em5.1.5, 3u84.3.B, 4ym7.3.L, 3u84.3.A, 2b5l.1.A, 2kiz.1.A, 5a7d.2.A, 5h64.1.A, 5h64.1.B, 5h64.1.C, 6em5.1.h, 5t0h.1.V, 2w18.1.A, 4fsc.2.B, 5en7.2.C, 5fww.1.A, 3fhc.1.A, 4kr0.1.A, 5ic7.1.A, 4d0p.1.A, 5en8.1.B, 4zoy.1.A, 5xw7.2.A, 2d8s.1.A, 5xw7.4.A, 3lrq.2.A, 3lrq.2.B, 4lad.1.B, 3pe7.1.A, 5wlc.25.A, 5t88.1.A, 5uw5.1.A, 4zlh.1.B, 4wjs.1.A, 2pzi.2.A, 5wlc.41.A, 5wlc.21.A, 5haz.1.A, 4v4n.48.A, 3vty.4.A, 5nuv.1.A, 1kb0.1.A, 4yd8.1.A, 3tgo.1.A, 2wfx.1.B, 5hay.2.A, 2nvz.1.M, 5ot2.1.L, 2kcl.1.A, 5c86.1.A, 3i2n.1.A, 5tf2.1.A, 4ri8.1.A, 5ip7.1.L, 1kt1.1.A, 5gjq.1.3, 2ymu.1.A, 4yzy.1.A, 4l9o.2.A, 4p5o.1.B, 3e4b.4.A, 3f3g.1.C, 3f3g.1.D, 3f3g.1.E, 4x67.1.J, 3prw.1.A, 4o9d.1.A, 1w6s.1.A, 2qc5.1.A, 2b5n.2.A, 4hdj.1.A, 2r5s.1.A, 3kd7.2.A, 2xev.3.A, 4by1.1.L, 2w2u.1.A, 5m3f.1.J, 2xev.1.A, 2y4t.1.A, 3asf.2.A, 3j96.1.J, 3j96.1.H, 5wwm.1.A, 4ax4.1.A, 3j96.1.G, 5o01.1.A, 4i9e.1.B, 1hzv.1.A, 3jb9.1.4, 2q7f.2.A, 4yvq.1.B, 3jb9.1.3, 4buj.1.B, 3jb9.1.L, 3v1s.1.A, 2lni.1.A, 3iiy.1.A, 5u5q.1.L, 5lg7.1.A, 5k0y.1.P, 5vhf.1.S, 5bt1.1.A, 2bbk.1.A, 3jb9.1.S, 3v9f.4.A, 3v9f.2.A, 4gcn.1.A, 4xfv.1.A, 5yz0.1.B, 3uvo.1.A, 3dpl.1.B, 2y4t.3.A, 4v0n.2.B, 2ct2.1.A, 5vbg.1.A, 1rwl.1.A, 5cvo.1.A, 3vl1.2.A, 2qe8.1.A, 3upv.1.A, 3q5m.1.A, 5fmf.1.N, 3lku.1.A, 5t0i.1.Y, 5t0i.1.X, 5t0i.1.W, 5t0i.1.V, 5t0i.1.U, 2kcv.1.A, 1rwi.1.A, 4hny.2.A, 4ppe.1.A, 5hb3.1.A, 5nnp.1.A, 4u0s.1.A, 4a11.1.B, 4a11.1.A, 3k1f.1.L, 3q15.2.A, 3q7o.1.A, 4wjl.1.A, 5wbh.2.A, 4ayc.1.A, 4ayc.1.B, 1l0q.3.A, 2gnq.1.A, 5gmk.1.W, 2ct0.1.A, 1u6g.1.B, 5hrm.1.A, 5nqv.2.A, 1q7f.2.A, 4wsn.6.D, 4g1t.1.A, 4qzv.2.A, 4g1t.1.B, 4j73.1.A, 5tqb.1.B, 4z8l.1.A, 5uw3.1.A, 3h0c.1.A, 3jpx.1.A, 4zey.1.A, 5jhp.1.A, 6b3j.1.D, 1ft2.1.A, 2ho1.1.B, 2ho1.1.A, 2n8w.1.A, 3vgz.1.A, 3s94.1.A, 4amy.1.A, 2fbn.1.A, 5jgc.1.A, 3q6k.1.A, 4in3.1.D, 3b7f.1.A, 2i0s.1.C, 5flc.1.F, 2agl.1.C, 3ww7.1.A, 4zoz.1.A, 5hi7.1.A, 2mta.1.A, 3s1n.1.J, 2jqk.1.A, 3j9m.72.A, 3ffl.1.A, 5a01.1.A, 2ojy.1.C, 4rg6.1.A, 4rg6.1.B, 4hho.1.A, 4czy.1.A, 3dwl.1.B, 4me2.1.A, 5iww.1.D, 3ffl.1.B, 4orh.2.C, 5ljo.1.C, 4n5c.7.A, 4xmn.1.A, 4xmn.1.B, 4xmn.1.D, 4xmn.1.E, 3hxj.2.A, 3hxj.2.B, 2mhk.1.A, 2hye.1.A, 5a7d.5.A, 5fa5.1.B, 2hye.1.D, 4ci8.1.A, 5k1a.1.B, 5cww.1.B, 1r5u.1.J, 3ro2.1.A, 5aja.1.A, 3uzs.1.B, 4amf.1.A, 4nlm.1.A, 2cpt.1.A, 4q1v.1.A, 5v1d.1.C, 5v1d.1.A, 4jhr.1.A, 3iax.1.A, 6eoj.1.A, 2dba.1.A, 6eoj.1.C, 2yu9.1.M, 4p29.1.A, 3lvg.1.A, 3lvg.1.C, 5a7d.1.A, 5a7d.7.A, 3lvg.1.B, 2c0m.1.A, 2ymb.1.B, 3u0s.1.A, 5wau.1.S, 4h5i.1.A, 5gap.1.G, 2ecf.1.A, 4lct.2.B, 4lct.2.A, 4owr.1.A, 4aif.1.A, 3jd5.1.3, 3e37.1.A, 5chb.1.A, 5wyj.18.A, 3jd5.1.U, 5bpt.1.A, 5xyi.1.6, 5mc6.15.A, 3as5.2.A, 5ijo.1.A, 3j2t.1.A, 2vq2.1.A, 1zu2.1.A, 4rea.1.A, 4cy3.1.A, 5lyb.108.A, 5o3v.1.A, 4kmo.1.B, 3pz4.1.A, 5jhe.1.A, 5lg0.1.A, 3gw4.1.B, 1erj.1.A, 3gw4.1.A, 6bk8.1.V, 6bk8.1.W, 6bk8.1.P, 4n14.1.A, 4b94.1.A, 2jq9.1.A, 3mkq.1.B, 6bk8.1.H, 3mkq.1.D, 3mkq.1.F, 5kdo.1.B, 5bwk.1.D, 5v7v.1.A, 2ond.1.A, 5m23.1.A, 1kv9.1.A, 3ho5.2.A, 4uuy.1.A, 1ldk.1.C, 4q66.1.D, 3l1x.1.A, 3q7f.1.A, 4n2q.1.A, 4jml.1.A, 5it7.77.A, 3sz7.1.A, 3a9g.1.A, 5ait.1.A, 2w8b.1.A, 4l1m.1.A, 3rtr.4.B, 5c1d.1.A, 4r7s.1.A, 4v7r.20.A, 2g9a.1.A, 3mps.2.A, 3qvd.1.A, 5fvl.2.A, 5c6v.1.D, 5c6v.1.A, 5c6v.1.C, 5c6v.1.B, 3vtx.2.A, 5gxh.1.A, 5h3s.1.A, 4apo.1.A, 5l0w.1.A, 1e8m.1.A, 1tjc.1.A, 4v16.1.A, 3wxx.1.A, 5wyj.16.A, 5jjw.1.A, 4pk1.1.A, 5hb0.2.A, 1xnf.1.A, 3f3p.3.D, 1occ.1.F, 3cik.1.B, 5x1b.2.F, 3jck.1.C, 4u1f.1.A, 4niq.1.A, 5t0j.1.V, 1h2y.1.A, 3jbz.1.A, 5jpq.1.Y, 4qzv.1.A, 6epd.1.V, 6epd.1.W, 6epd.1.T, 6epd.1.U, 6epd.1.S, 6epe.1.X, 6epe.1.W, 6epe.1.V, 3j97.1.H, 6epe.1.T, 6epe.1.S, 1e5t.1.A, 4g23.1.A, 3esl.2.A, 3rfg.1.A, 2h9l.1.A, 2pm7.1.D, 2pm7.1.C, 4ap4.1.A, 2pm7.1.A, 3q7m.1.A, 4kbq.1.A, 4r2y.2.A, 2bgr.1.A, 4wn4.1.A, 5x50.1.L, 1gq1.1.A, 4hny.1.A, 5gjq.1.9, 4cr3.1.6, 3gre.1.A, 4n5c.4.A, 4n5c.2.A, 4a1g.4.A, 5wql.2.A, 5lqi.1.A, 3wj9.2.A, 3s1q.1.J, 3gz2.1.B, 3gz2.1.A, 1q7f.1.A, 4ga1.1.A, 4v3p.1.A, 1yxr.1.A, 5waq.1.A, 5mc6.36.A, 5w5i.1.A, 2ism.1.A, 2j57.1.C, 3p5c.1.C, 4cr3.1.Y, 3iun.1.A, 4l72.3.A, 1u8e.1.B, 1u8e.1.A, 5lyn.1.A, 2c2l.1.A, 4a0b.2.A, 2hr2.1.A, 2ynp.1.A, 3dxm.1.C, 4tqo.1.A, 4bt9.1.B, 2ifu.2.A, 3o4g.1.B, 4aif.2.A, 1ri6.1.A, 6fbs.1.A, 6fbs.1.B, 2iao.1.A, 4u0u.1.A, 5k1h.1.A, 5en7.2.A, 4eba.1.A, 2if4.1.A, 5iy8.1.L, 5efr.1.A, 4imm.2.A, 3hfq.1.A, 5em2.2.B, 5k2m.1.F, 5k2m.1.E, 5bjs.1.A, 5iwb.1.B, 5jzz.1.A, 4cr4.1.W, 5k19.2.A, 4bp8.1.A, 4cr4.1.X, 4cr4.1.Y, 4a5x.1.A, 5naf.3.A, 5izw.1.A, 4aez.2.C, 1nex.2.B, 4aez.2.A, 5wsg.1.R, 5en6.1.A, 3lya.1.A, 5wsg.1.U, 4gqb.1.B, 4d6v.1.A, 5g05.1.I, 5g05.1.K, 5g05.1.O, 5g05.1.C, 4v3k.1.C, 5g05.1.F, 5mpd.1.K, 5mpd.1.J, 5mpd.1.I, 2i3s.1.A, 4ga2.1.A, 3rpg.1.B, 5mpd.1.F, 2yq8.1.A, 4cr4.1.6, 1k83.1.J, 5vai.1.D, 3j6x.75.A, 3cvl.1.A, 5b4x.2.B, 3s8z.1.A, 4fhn.1.B, 4a2m.2.A, 5jrk.1.A, 5l0y.7.A, 3jzn.1.A, 5jk7.1.B, 5cqs.2.A, 1fch.1.A, 2xcc.1.B, 1a0r.1.A, 2n8i.1.A, 5m1j.14.A, 1yiq.1.A, 5ft9.2.A, 3ma5.3.A, 4fhm.1.B, 2rfo.2.A, 4fhm.1.A, 2ajl.1.A, 2ajl.1.B, 5wrv.1.B, 5a31.1.O, 5a31.1.J, 5a31.1.H, 5a31.1.F, 5a31.1.C, 5a31.1.B, 2lsv.1.A, 3jap.1.i, 5a31.1.W, 5a31.1.V, 5a31.1.R, 5a31.1.P, 5j3j.1.A, 5u5h.1.A, 3ei3.1.A, 5diz.2.A, 3ho5.1.A, 5b26.1.A, 5bpw.1.A, 5wau.1.F, 4a0l.2.A, 1yuz.1.A, 4v8m.8.A, 2q7q.1.C, 2v5f.1.A, 5l0y.2.A, 3s8v.2.A, 2z2n.1.A, 5t0h.1.W, 5t0h.1.U, 1hz4.1.A, 5k18.1.A, 5t0h.1.Y, 4d4o.1.B, 4d4o.1.A, 3e4b.2.A, 1pi6.1.A, 3abm.1.F, 2yba.1.A, 3azq.1.A, 5xjc.1.W, 5xjc.1.T, 4j8d.1.A, 2iaa.1.A, 5xjc.1.E, 5xjc.1.J, 5xjc.1.I, 4cc9.1.A, 2jrj.1.A, 1mg2.1.A, 4cgv.2.A, 5c9s.1.A, 5vvr.1.L, 5c7e.1.A, 5c7e.1.C, 4abn.2.A, 3rkv.1.A, 6b3x.1.A, 5vfc.1.A, 4wju.1.A, 6az1.1.6, 5oj8.1.A, 5wuk.1.A, 1s4u.1.A, 3j77.45.A, 2yms.1.C, 3urz.1.A, 5vat.1.A, 5gap.1.F, 5cyk.1.A, 3u4y.1.A, 3qqz.1.A, 3p5b.1.C, 4qrj.1.A, 5hqg.1.A, 3m0c.1.C, 5aem.1.A, 4qpl.1.A, 4zcn.1.A, 4zcn.1.C, 1sq9.1.A, 2kre.1.A, 5fzs.1.A, 5lyp.1.A, 5dbk.1.B, 5dbk.1.A, 4zb4.1.A, 5o01.2.A, 6eu2.1.L, 5ayw.1.B, 3qky.1.A, 2fo7.1.A, 5ayw.1.D, 4gpk.2.B, 4gpk.2.C, 4gpk.2.A, 4cgw.1.A, 4gpk.2.D, 3hoy.1.L, 4whv.1.B, 4whv.1.C, 5a2q.1.8, 5fey.1.A, 5wyj.33.A, 4hnx.1.A, 2vsy.1.A, 5kc2.1.B, 4a08.1.A, 4a08.1.B, 3ah8.1.B, 4uqy.1.A, 2avp.1.A, 2xu7.1.A, 5flx.1.7, 3lca.1.A, 5mpc.1.h, 5mpc.1.i, 5mpc.1.d, 5ioj.1.A, 3asg.1.A, 5mpc.1.g, 5ccl.1.A, 5jjt.1.A, 1c5k.1.A, 6eu0.1.L, 5ojf.1.A, 5dse.2.A, 3f7f.1.A, 1p5q.1.A, 1p5q.1.B, 1p5q.1.C, 4hxg.1.A, 4hxf.1.F, 4ycz.1.A, 2jrr.1.A, 3mxx.1.A, 4reb.1.C, 4reb.1.D, 4gcn.2.A, 1ve7.1.A, 4ozu.1.A, 4a1g.1.A, 3c75.1.A, 2xl2.1.A, 3dqv.3.C, 5fxy.2.A, 5fey.1.B, 3mks.1.D, 4a1g.3.A, 4v7e.7.A, 2ckl.1.B, 5ctr.2.A, 4y6c.1.A, 2nvt.1.L, 5ctq.1.A, 5ctq.1.B, 2g99.1.A, 5ukm.1.B, 5u69.1.A, 2iwf.1.A, 5mpb.1.d, 5udj.1.A, 5hrz.1.A, 4y49.1.A, 3frx.1.A, 5uzw.1.A, 3j9m.81.A, 1nl4.1.A, 1h4i.1.A,

4f3v.1.A, 6bw3.1.A, 5k04.1.A, 6eoo.1.A, 4v5o.1.0, 2h0d.1.A, 1elw.1.A, 5t0c.44.A, 3ru0.1.A, 2d0v.1.A, 1xip.1.A, 5fsb.1.A, 3ei4.1.A, 5ekq.1.B, 4rea.1.B, 5n4w.1.C, 4gco.1.A, 2lgv.1.A, 5h1j.1.A, 5f30.1.A, 2pbi.2.B, 3qou.1.A, 1n9a.1.A, 3sbp.1.A, 6epf.1.T, 6epf.1.U, 6epf.1.V, 6epf.1.W, 6epf.1.S, 4gyw.1.A, 5fvm.1.C, 5fvm.1.A, 3iuj.1.A, 4xf2.1.C, 5m11.1.A, 4ga0.1.A, 6exn.1.S, 2ckl.1.A, 1l0q.1.A, 5min.1.A, 2g8s.1.A, 5cvn.1.A, 4bbs.1.L, 4unm.1.A, 1iym.1.A, 5wve.1.K, 3dm0.1.A, 3sob.1.B, 4ffv.1.A, 4bp9.1.A, 4i1a.2.A, 4bzk.1.D, 1c9i.1.A, 1wr0.1.A, 4aah.1.A, 3ieg.1.A, 5tga.33.A, 5g04.1.Q, 5g04.1.P, 5g04.1.U, 2aq5.1.A, 5mzu.1.A, 5g04.1.C, 4o5s.1.A, 5g04.1.F, 5mpe.1.J, 5g04.1.H, 5g04.1.K, 5g04.1.J, 5g04.1.O, 5wp3.1.A, 1dy7.1.A, 5n1a.1.A, 3ho4.1.A, 5x19.1.F, 2kdx.1.A, 1twa.1.J, 2akl.1.A, 5ln3.1.V, 4cgu.1.A, 1e2r.1.A, 5a7d.3.A, 3sjl.1.D, 2ojh.1.A, 3dr2.1.A, 5en7.1.C, 4dg6.1.A, 5hy7.2.A, 2lxp.1.C, 4w9r.1.A, 2dcm.1.A, 4rib.1.A, 4ric.1.A, 5xw7.3.A, 5xw7.5.A, 5wlc.17.A, 5l8s.1.A, 5wvi.1.c, 5wlc.15.A, 4gm9.2.A, 2vsy.2.A, 3mv2.1.A, 5wvi.1.O, 3mv2.1.B, 5mwj.1.A, 5o9z.1.F, 5o9z.1.G, 5lfl.1.A, 3mun.1.A, 2ea6.1.A, 5vvs.1.L, 3s7f.1.A, 5wvi.1.V, 3q75.1.A, 3b13.1.A, 5jkp.1.A, 5m5g.1.A, 3hkz.1.L, 4wuy.1.A, 5en6.2.A, 4wju.2.A, 5hay.1.A, 1k8k.1.C, 2vgx.1.A, 2vgx.1.B, 5ja5.1.A, 1k3i.1.A, 4v3l.1.C, 2eib.1.A, 5c3e.1.L, 4gnb.1.A, 6f40.1.L, 3qwp.1.A, 2qzp.1.A, 3vty.1.A, 5wlc.28.A, 5a9q.1.T, 5a9q.1.V, 6f1t.1.b, 6f1t.1.c, 5wlc.19.A, 5a9q.1.M, 5a9q.1.L, 3lpz.1.A, 5a9q.1.I, 5a9q.1.H, 5a9q.1.D, 5a9q.1.G, 5a9q.1.F, 1b89.1.A, 5a9q.1.C, 5a9q.1.B, 5t88.2.A, 5wlc.26.A, 5l8e.1.A, 4j8e.2.A, 6epc.1.U, 5bv0.1.B, 4v6i.1.A, 4v3k.2.C, 3kya.1.A, 4zhe.1.D, 4zhe.1.B, 4zhe.1.C, 4zhe.1.A, 3a0f.1.A, 4n2s.1.A, 3j6y.75.A, 5hxb.1.B, 6f1t.1.4, 6f1t.1.3, 1bpo.1.C, 5a9q.1.4, 1bpo.1.A, 1w3b.1.A, 5sum.1.A, 2uy1.1.B, 5a9q.1.2, 3o4h.2.A, 4q1u.1.A, 3jam.1.7, 3pdn.1.A, 3uq3.1.A, 4psw.1.B, 3asf.1.A, 3azo.1.A, 1crz.1.A, 2gbg.1.A, 2wvi.1.A, 2qfc.1.A, 3dw8.1.B, 1vz3.1.A, 4a0p.1.A, 4ynd.1.A, 5ojs.1.A, 5bv1.2.B, 6f38.1.3, 6f38.1.4, 5oej.1.A, 3i1c.1.A, 5aio.1.A, 1h4j.1.A, 6f38.1.b, 6f38.1.c, 5xdq.1.F, 4xmm.1.D, 3o4j.1.A, 3o4j.1.B, 1tbg.1.E, 1tbg.1.A, 1qbi.1.A, 4ci1.1.A, 3lrv.1.A, 5d9b.1.A, 1e2r.1.B, 5t0g.1.Y, 5t0g.1.X, 6exn.1.R, 4r5o.4.A, 2v6y.2.A, 3fki.1.L, 3n0d.1.A, 1wao.1.A, 3asg.2.A, 5t0g.1.V, 2yh3.1.A, 5vtb.1.A, 1xhm.1.A, 1wao.3.A, 4xpd.1.A, 3smr.1.A, 1orv.1.A, 3lvh.1.B, 4j79.1.A, 3sf4.2.A, 5gva.1.A, 5c7f.1.C, 3lvh.1.A, 3c9c.1.A, 5vhi.1.H, 4gn7.1.A, 5vhi.1.S, 2djb.1.A, 4r2y.4.A, 4xnh.1.A, 4xi0.1.A, 5t0g.1.5, 4jsp.1.A, 3mkr.1.B, 3mkr.1.A, 1yfq.1.A, 5ij7.1.B, 5ljo.1.A, 4r89.1.A, 2mt5.1.A, 4hou.1.A, 5sui.1.A, 5wbh.1.A, 5ex7.1.A, 4am9.1.A, 2ff4.1.A, 6emk.1.A, 3u88.1.A, 1n7d.1.A, 5wbh.5.A, 4u04.1.A, 2kck.1.A, 4zov.2.A, 5c4j.1.J, 2v6y.1.A, 4wng.1.A, 4a0k.1.C, 4a0k.1.D, 4f52.2.B, 4rec.1.A, 3ks2.1.A, 3i4r.1.B, 3hxj.1.B, 3hxj.1.A, 3qil.1.B, 3qil.1.C, 3qil.1.A, 5hy7.1.A, 1a17.1.A, 3q54.1.A, 4e54.1.B, 4e54.1.A, 4tz4.1.A, 3j81.1.5, 5h1k.1.A, 3rzd.1.J, 4orh.1.D, 3ho3.1.A, 4orh.1.C, 3ei4.1.B, 4n5c.8.A, 1r9m.1.A, 2oaj.1.A, 2yms.1.D, 2h6k.1.A, 2yms.1.B, 4n5c.6.A, 2yms.1.A, 4e85.1.A, 5cyk.1.B, 3ulq.1.A, 5vhs.1.H, 5vhr.1.H, 4y5r.1.C, 3q8w.1.A, 3ash.1.A, 4r8a.1.A, 1hh8.1.A, 5lfm.1.A, 5lks.64.A, 5yp1.2.A, 4leu.1.A, 5yp1.2.B, 5h13.1.A, 4by7.1.L, 5v1d.2.A, 5v1d.2.B, 6bll.1.A, 4hvt.1.A, 6bll.1.B, 1gp2.1.B, 4j87.1.A, 5a5b.1.Z, 5a5b.1.Y, 4jxm.1.A, 3euv.1.A, 3ho4.2.A, 6bcx.1.A, 6bcx.1.C, 6f3a.1.3, 6f3a.1.2, 1npe.1.A, 3va6.1.A, 4nsx.1.A, 2r2l.1.A, 5ukk.1.B, 3das.1.A, 3qdn.1.A, 5tdh.1.B, 5ln3.1.0, 5wvk.1.k, 5wvk.1.a, 5wvk.1.b, 5wvk.1.c, 4gyo.1.A, 5o75.1.A, 4lct.1.A, 4lct.1.B, 3g4e.1.A, 2qzp.2.A, 3k9i.1.A, 5fvk.2.A, 4y6w.1.A, 3oxl.1.A, 3ewe.1.A, 1ryt.1.A, 5ndv.73.A, 6epf.1.X, 6f9n.1.B, 4mae.1.A, 4oe1.1.A, 4oe1.1.B, 5nqv.1.A, 5ln3.1.Z, 2zir.1.A, 3ma5.1.A, 5njx.1.A, 2rip.1.A, 4bwr.1.A, 1elr.1.A, 4nrh.1.B, 5gje.1.B, 5gje.1.A, 4fa4.1.D, 1flg.1.A, 3m3y.1.J, 5iy5.2.F, 4pjr.1.A, 5kcn.1.A, 3as5.1.A, 3si5.2.A, 4h7y.3.A, 2b5n.4.A, 3hxr.1.A, 6ek0.64.A, 4cgq.1.A, 1ijq.1.A, 4ynw.1.A, 5jus.45.A, 2jqh.1.A, 5nqs.1.A, 3esl.1.A, 5fvl.1.A, 5i9g.1.A, 5x1f.1.F, 3cvn.1.A, 4a5s.1.A, 4c3j.1.L, 2xzh.1.A, 5hb0.1.A, 5ex0.1.A, 4j0u.1.A, 5hb0.3.A, 3ro3.1.A, 5l8w.1.B, 4wsl.1.A, 3f3p.2.B, 5omp.1.A, 4f52.1.B, 1pfq.1.A, 4cr2.1.X, 1pfq.1.B, 4cr2.1.W, 5wbk.1.A, 4v7f.1.j, 4gm3.1.A, 3jcm.1.D, 3jcm.1.B, 3v7d.1.B, 2bcj.1.B, 4d10.1.D, 4d10.1.B, 4d10.1.A, 5jj6.1.A, 5jj6.1.B, 1qbq.1.A, 1mzc.1.A, 5t2a.48.A, 2wpv.1.A, 2crb.1.A, 3nok.1.A, 1w3b.1.B, 5arf.1.A, 4r40.1.A, 3iuq.1.A, 5x4z.1.L, 4cr2.1.6, 3sww.1.A, 2xpi.1.C, 2xpi.1.A, 2hqs.1.A, 4g55.1.A, 3zn3.1.A, 4cy2.1.A, 3wj9.1.A, 2fpb.1.A, 4v92.1.8, 2xeu.1.A, 5en8.1.A, 2i3t.1.A, 5vhm.1.H, 5o3w.1.A, 3s15.1.J, 1z2z.2.A, 5w97.1.F, 1utc.1.A, 3jan.80.A, 4wnd.1.A, 3rtr.1.B, 4ry3.1.A, 5jpq.1.I, 2fp9.1.A, 6epe.1.U, 4bts.27.A, 5hb2.1.A, 1wy6.1.A, 2iap.1.A, 2o9k.1.A, 3esk.1.A, 2xgm.2.A, 4e5z.1.A, 6epd.1.X, 5udl.1.A, 4e5z.1.B, 2z2p.1.A, 2w8b.2.A, 3iiw.1.A, 3asd.1.A, 4a0b.1.A, 2wb7.1.A, 4eba.2.A, 5wbi.1.A, 5tee.1.A, 3bg0.1.A, 5iy7.1.L, 3fwv.1.A, 3bg0.1.H, 5jno.1.B, 5nnz.2.A, 2v6x.1.A, 5i5i.1.A, 5d0o.1.B, 5juy.1.G, 5juy.1.D, 5juy.1.E, 3v65.1.C, 3v65.1.B, 3tkn.1.A, 3hac.1.A, 5lxz.1.A, 2ivz.1.A, 5hyn.2.B, 5juo.45.A, 3rfh.1.A, 3rfh.1.B, 5ccm.1.A, 3fp2.1.A, 5em2.1.B, 4imm.1.A, 4xgl.1.A, 5ams.1.A, 5mzh.1.A, 3i7p.1.A, 4fhn.2.B, 5wg4.1.B, 5m32.1.a, 5m32.1.b, 5m32.1.c, 4wsn.6.B, 4a0c.2.C, 6f5d.1.J, 6f5d.1.K, 2k3w.1.A, 6f5d.1.L, 2ysl.1.A, 4wsn.2.B, 4wsn.2.A, 4wsn.2.D, 1chc.1.A, 2ifu.1.A, 2wqh.1.A, 2xe4.1.A, 5a5u.1.B, 4u7a.1.A, 5lcw.1.Q, 5lcw.1.R, 4pv7.1.A, 5m32.1.9, 2dso.1.A, 2f0y.1.A, 5lcw.1.B, 5lcw.1.C, 5lcw.1.O, 5lcw.1.I, 4i2w.1.A, 4yvo.1.A, 5lwv.1.A, 5buz.1.B, 4yhc.1.A, 5i1z.5.C, 2wq8.1.A, 2lxh.1.A, 1yux.1.A, 3ma5.4.A, 4exv.1.A, 3qww.1.A, 3ddu.1.A, 4gq2.1.B, 4gq2.1.A, 1fch.2.A, 3qbj.1.A, 3s2h.1.J, 4i79.1.A, 2b5n.1.A, 2ect.1.A, 2z2o.1.A, 1ur6.1.B, 1qni.1.A, 4o9d.2.A, 3gtm.1.J, 3oxg.1.A, 4ria.1.A, 4zov.1.A, 3wqh.1.A, 3wqh.1.B, 3ei4.3.A, 3dra.1.A, 4zlh.1.A, 3qhy.1.B, 4d4p.1.A, 1r9n.1.A, 2nc9.1.A, 3bg0.1.D, 5xi8.1.A, 4j0x.1.A, 1na3.1.A, 4zlr.1.A, 2xbg.1.A, 1ldj.1.B, 2hr5.1.A, 2gvu.1.A, 4pjq.2.A, 4xei.1.C, 5ft9.1.A, 4j8f.1.A, 2kat.1.A, 5xw7.1.A, 2jid.1.A, 2b5n.3.A, 2z2o.3.A, 4xga.1.A, 2ghs.1.A, 3rrm.1.C, 5wcg.1.A, 5g04.1.T, 1iip.1.A, 3hox.1.L, 5uz5.1.D, 5uz5.1.E, 4a0l.1.A, 4a0l.1.B, 5fzq.1.C, 5lls.1.A, 5fzq.1.A, 5x6o.1.A, 1o6g.1.A, 6bcu.1.A, 5l0y.5.B, 5l0y.5.A, 6bcu.1.B, 4mh1.1.A, 4mh1.1.B, 5fyw.1.L, 5vat.2.A, 5l0y.3.A, 3s8v.1.A, 3iur.1.A, 5hq8.1.A, 5g04.1.B, 3f3f.1.A, 4pwz.1.A, 5g04.1.I, 5mpe.1.K, 2eid.1.A, 2j04.1.A, 5o3x.1.A, 3n0e.1.A, 2j04.1.B, 3ei2.1.A, 3ei2.1.B, 1na0.1.A, 2uwj.1.C, 2wg3.1.B, 4j0w.1.A, 2vsn.1.A, 2v91.1.A, 4d4q.2.A, 3u3w.1.B, 2iaw.1.A, 6eu1.1.L, 1t2x.1.A, 3scy.1.A, 1kt0.1.A, 2b5l.2.A, 3jco.1.Y, 3jco.1.Z, 2onc.1.A, 5grs.1.A, 2z3z.1.A, 4a7j.1.A, 4pwx.1.C, 4kzz.1.6, 5m5y.1.L, 3jco.1.0, 2oit.1.A, 5fvk.1.A, 3tc9.1.A, 4i0o.1.A, 5a6c.2.A, 3jaq.1.i, 1pev.1.A, 2iau.1.A, 3e4b.3.A, 5n4c.1.A, 5wlc.24.A, 2pm6.1.C, 5dfz.1.C, 5wlc.22.A, 2qr5.1.A, 2l6j.1.A, 5che.1.E, 5che.1.F, 5wlc.20.A, 4n3c.1.A, 2cnx.1.A, 1k32.1.A, 5i9f.1.A, 3vty.3.A, 3g4h.1.B, 3g4h.1.A, 2p58.1.C, 5ttw.2.A, 4zn4.1.A, 4u1e.1.A, 1d8d.1.A, 4ayb.1.L, 5i2t.1.A, 5txe.1.A, 4gga.1.A, 3f3p.2.C, 4bh6.1.A, 1got.1.B, 4wzx.1.A, 3p1l.1.A, 5ctq.2.B, 5ctq.2.A, 4e6h.1.A, 5lzz.77.A, 3j98.1.I, 3j98.1.H, 4buj.2.B, 3ceq.1.A, 3ceq.1.B, 4ay5.1.A, 2wb7.2.A, 5xon.1.L, 2xev.2.A, 3bee.2.A, 5fzr.1.A, 5fzr.1.B, 3wwb.1.A, 4cr2.1.Y, 4r8p.1.K, 4d5l.1.7, 4ri9.1.A, 1ocz.1.F, 4ggc.1.A, 4ynv.1.A, 4buj.1.D, 5fzq.1.B, 2pbi.1.B, 3jai.77.A, 2ecm.1.A, 2pzi.1.A, 4yzs.1.A, 3f8s.1.A, 3f3f.1.C, 4yzs.1.B, 3f3f.1.D, 3f3f.1.G, 5hb3.2.A, 5i9h.1.A, 3fp3.1.A, 5nnp.2.A, 1wfd.1.A, 2pm6.1.B, 5vhq.1.H, 2pm6.1.A, 2wft.1.A, 4rid.1.A, 3v9f.3.A, 5ex3.1.A, 3c5m.1.A, 5jg6.1.A, 5uz7.1.B, 3e5z.1.A, 5ic8.4.A, 1wcy.1.A, 1u4c.1.A, 3v9f.1.A, 4ci8.2.A

SWISS-MODEL Homology Modelling Report

Model Building Report

This document lists the results for the homology modelling project "WDR35_HUMAN Q9P2L0 WD repeat-containing protein 35" submitted to SWISS-MODEL workspace on Feb. 24, 2018, 3:34 p.m..The submitted primary amino acid sequence is given in Table T1.

If you use any results in your research, please cite the relevant publications:

- Biasini, M., Bienert, S., Waterhouse, A., Arnold, K., Studer, G., Schmidt, T., Kiefer, F., Cassarino, T.G., Bertoni, M., Bordoli, L., Schwede, T. SWISS-MODEL: modelling protein tertiary and quaternary structure using evolutionary information. Nucleic Acids Res. 42, W252-W258 (2014). doi
- Guex, N., Peitsch, M.C., Schwede, T. Automated comparative protein structure modeling with SWISS-MODEL and Swiss-PdbViewer: A historical perspective. Electrophoresis 30, S162-S173 (2009). doi
- Bienert, S., Waterhouse, A., de Beer, T.A., Tauriello, G., Studer, G., Bordoli, L., Schwede, T. The SWISS-MODEL Repository - new features and functionality. Nucleic Acids Res. 45, D313-D319 (2017). doi
- Benkert, P., Biasini, M., Schwede, T. Toward the estimation of the absolute quality of individual protein structure models. Bioinformatics 27, 343-350 (2011). doi
- Bertoni, M., Kiefer, F., Biasini, M., Bordoli, L., Schwede, T. Modeling protein quaternary structure of homo- and hetero-oligomers beyond binary interactions by homology. Scientific Reports 7 (2017). doi

Results

The SWISS-MODEL template library (SMTL version 2018-02-21, PDB release 2018-02-16) was searched with BLAST (Camacho et al.) and HHBlits (Remmert, et al.) for evolutionary related structures matching the target sequence in Table T1. For details on the template search, see Materials and Methods. Overall 3838 templates were found (Table T2).

Models

The following models were built (see Materials and Methods "Model Building"):

Model #02	File	Built with	Oligo-State	Ligands	GMQE	QMEAN
	PDB	ProMod3 Version 1.1.0.	monomer (matching prediction)	None	0.32	-6.57

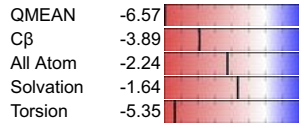

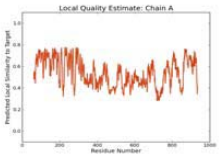

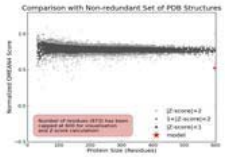

Template	Seq Identity	Oligo-state	QSQE	Found by	Method	Resolution	Seq Similarity	Range	Coverage	Description
3mkq.1.A	12.11	homo-trimer	0.00	HHblits	X-ray	2.50Å	0.26	62 - 934	0.60	Coatomer beta'-subunit

The template contained no ligands.

```
Target    MFFYLSKKISIPNNVKLQCVSWNKEQGFIACGGEDGLLKVLKLETQTDDAKLRGLAAPSNLSMNQTLEGHSGSVQVVTWN
3mkq.1.A  ------------------------------------------------------------DIKKTFSNRSDRVKGIDFH

Target    EQYQKLTTSDENGLIIVWMLYKGSWIEEMINNRNKSVVRSMSWNADGQKICIVYEDGAVIVGSVDGNR-IWGKDLKGIQL
3mkq.1.A  PTEPWVLTTLYSGRVEIWNYETQVEVRSIQ--VTETPVRAGKFIARKNWIIVGSDDFRIRVFNYNTGEKVVDFEAHPDYI

Target    SHVTWSADSKVLLFGMANGEIHIYD-NQG-NFMIKMKLSCLVNVTGAISIAGIHWYHGTEGYVEPDCPCLAVCFDNGRCQ
3mkq.1.A  RSIAVHPTKPYVLSGSDDLTVKLWNWENNWALEQTFE-------GHEHFVMCVAFNPKD-------PSTFASGCLDRTVK

Target    IMRHENDQNPVLIDT-G-MYVVGIQWNH--MGSVLAVAGFQKAAMQDKDVNIVQFYT-PFGEHLGTLKVPGKEISALSWE
3mkq.1.A  VWSLGQSTPNFTLTTGQERGVNYVDYYPLPDKPYMITASDD---------LTIKIWDYQTKSCVATLEGHMSNVSFAVFH

Target    GGGLKIALAV-DSFIYFANIRPNYKWGY---C-SNTVVYAYTRPDRPEYCVVFWDTKNNEKYVKYVKGLISITTCGDFCI
3mkq.1.A  PTLPIIISGSEDGTLKIWNSSTYKVEKTLNVGLERSWCIATHPT--GRKNYIASGFDNGFTVLSLGNDEPTLSLDPVGKL

Target    LATKADENHPQEENEMETFGATFVLVL--CN--SIGTPLDPK-------YIDIVPLFVAMTKTHVIAASKEAFYTWQYRV
3mkq.1.A  VWSGGKNAAA---------SDIFTAVIRGNEEVEQDEPLSLQTKELGSVDVFPQSLAHSPNGRFVTVVGDGEYVIYTALA

Target    AKKLTALEINQITRSRKEGRERIYHVDDTPSGSMDGVLDYSKTIQGTRDPICAIT--ASDKILIVGRESGTIQRYSLPNV
```

```
3mkq.1.A  WRN---K-------------------------------------AFGKCQDFVWGPDSNSYALIDETGQIKYYKNFKE

Target    GLIQKYSLNCRAYQLSLNCNS---SRLAIIDISGVLTFFDLDARVTDSTGQQVVGELLKLERRDVWDMKWAKDNPDLFAM
3mkq.1.A  -------VTSWSVPMHSAIDRLFSGALLGVKSDGFVYFFDWDNG------TLV----RRIDVN-AKDVIWSDNGELVMIV

Target    MEK-----TRMYVFRNLD----------------------P-----EEP---IQTSG-Y-ICNFEDLEIKSVLLDEI--L
3mkq.1.A  NTNSNGDEASGYTLLFNKDAYLEAANNGNIDDSEGVDEAFDVLYELSESITSGKWVGDVFIFTTATNRLNYFVGGKTYNL

Target    KDPEHPN------------------KDYLINFEIRSLRDSRALIEKVGIKDA-SQFIEDNPHPRLWRLLAEAALQKLDL
3mkq.1.A  AHYTKEMYLLGYLARDNKVYLADREVHVYGYEI-SLEVLEFQTLTLRGEIEEAIENVLPNVEGKDSLTKIARFLEGQ---

Target    YTAEQAFVRCKDYQGIKFVKRLGKLLSESMKQAEVVGYFGRFEEAERTYLEMDRRDLAIGLRLKLGDWFRVLQLLKTGSG
3mkq.1.A  -------------------------------------EYYEEALNISPDQ---DQKFELALKVGQLTLARDLLTDES-

Target    DADDSLLEQANNAIGDYFADRQKWLNAVQYYVQGRNQERLAECYYMLEDYEGLENLAISLPENHKLLPEIAQMFVRVGMC
3mkq.1.A  ---AEM---KWRALGDASLQRFNFKLAIEAFTNAHDLESLFLLHSSFNNKE-------------GLVTLAKDAETTGKF

Target    EQAVTAFLKCSQPKAAVDTCVHLNQWNKAVELAKNHS--MKEIGSLLARYASHLLEKNK--TLDAIELYRKANYFFDAAK
3mkq.1.A  NLAFNAYWIAGDIQGAKDLLIKSQRFSEAAFLGSTYGLGDNEVNDIVTKWKENLILNGKNTVSERV--------------

Target    LMFKIADEEAKKGSKPLRVKKLYVLSALLIEQYHEQMKNAQRGKVKGKSSEATSALAGLLEEEVLSTTDRFTDNAWRGAE
3mkq.1.A  ------------------------------------------------------------------------------

Target    AYHFFILAQRQLYEGCVDTALKTALHLKDYEDIIPPVEIYSLLALCACASRAFGTCSKAFIKLKSLETLSSEQKQQYEDL
3mkq.1.A  ------------------------------------------------------------------------------

Target    ALEIFTKHTSKDNRKPELDSLMEGGEGKLPTCVATGSPITEYQFWMCSVCKHGVLAQEISHYSFCPLCHSPVG
3mkq.1.A  ---------------------------------------------------------------------------
```

Model #01	File	Built with	Oligo-State	Ligands	GMQE	QMEAN
	PDB	ProMod3 Version 1.1.0.	monomer (matching prediction)	None	0.32	-6.57

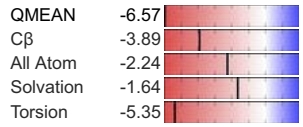

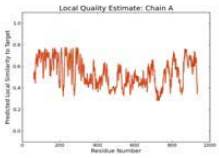

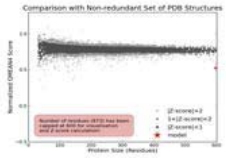

Template	Seq Identity	Oligo-state	QSQE	Found by	Method	Resolution	Seq Similarity	Range	Coverage	Description
3mkq.1.A	12.11	homo-trimer	0.00	HHblits	X-ray	2.50Å	0.26	62 - 934	0.60	Coatomer beta'-subunit

The template contained no ligands.

```
Target    MFFYLSKKISIPNNVKLQCVSWNKEQGFIACGGEDGLLKVLKLETQTDDAKLRGLAAPSNLSMNQTLEGHSGSVQVVTWN
3mkq.1.A  ------------------------------------------------------------DIKKTFSNRSDRVKGIDFH

Target    EQYQKLTTSDENGLIIVWMLYKGSWIEEMINNRNKSVVRSMSWNADGQKICIVYEDGAVIVGSVDGNR-IWGKDLKGIQL
3mkq.1.A  PTEPWVLTTLYSGRVEIWNYETQVEVRSIQ--VTETPVRAGKFIARKNWIIVGSDDFRIRVFNYNTGEKVVDFEAHPDYI

Target    SHVTWSADSKVLLFGMANGEIHIYD-NQG-NFMIKMKLSCLVNVTGAISIAGIHWYHGTEGYVEPDCPCLAVCFDNGRCQ
3mkq.1.A  RSIAVHPTKPYVLSGSDDLTVKLWNWENNWALEQTFE-------GHEHFVMCVAFNPKD-------PSTFASGCLDRTVK

Target    IMRHENDQNPVLIDT-G-MYVVGIQWNH--MGSVLAVAGFQKAAMQDKDVNIVQFYT-PFGEHLGTLKVPGKEISALSWE
3mkq.1.A  VWSLGQSTPNFTLTTGQERGVNYVDYYPLPDKPYMITASDD---------LTIKIWDYQTKSCVATLEGHMSNVSFAVFH

Target    GGGLKIALAV-DSFIYFANIRPNYKWGY---C-SNTVVYAYTRPDRPEYCVVFWDTKNNEKYVKYVKGLISITTCGDFCI
3mkq.1.A  PTLPIIISGSEDGTLKIWNSSTYKVEKTLNVGLERSWCIATHPT--GRKNYIASGFDNGFTVLSLGNDEPTLSLDPVGKL

Target    LATKADENHPQEENEMETFGATFVLVL--CN--SIGTPLDPK-------YIDIVPLFVAMTKTHVIAASKEAFYTWQYRV
3mkq.1.A  VWSGGKNAAA---------SDIFTAVIRGNEEVEQDEPLSLQTKELGSVDVFPQSLAHSPNGRFVTVVGDGEYVIYTALA

Target    AKKLTALEINQITRSRKEGRERIYHVDDTPSGSMDGVLDYSKTIQGTRDPICAIT--ASDKILIVGRESGTIQRYSLPNV
3mkq.1.A  WRN---K-------------------------------------AFGKCQDFVWGPDSNSYALIDETGQIKYYKNFKE

Target    GLIQKYSLNCRAYQLSLNCNS---SRLAIIDISGVLTFFDLDARVTDSTGQQVVGELLKLERRDVWDMKWAKDNPDLFAM
3mkq.1.A  -------VTSWSVPMHSAIDRLFSGALLGVKSDGFVYFFDWDNG------TLV----RRIDVN-AKDVIWSDNGELVMIV
```

```
Target    MEK-----TRMYVFRNLD----------------------P-----EEP---IQTSG-Y-ICNFEDLEIKSVLLDEI--L
3mkq.1.A  NTNSNGDEASGYTLLFNKDAYLEAANNGNIDDSEGVDEAFDVLYELSESITSGKWVGDVFIFTTATNRLNYFVGGKTYNL

Target    KDPEHPN-------------------KDYLINFEIRSLRDSRALIEKVGIKDA-SQFIEDNPHPRLWRLLAEAALQKLDL
3mkq.1.A  AHYTKEMYLLGYLARDNKVYLADREVHVYGYEI-SLEVLEFQTLTLRGEIEEAIENVLPNVEGKDSLTKIARFLEGQ---

Target    YTAEQAFVRCKDYQGIKFVKRLGKLLSESMKQAEVVGYFGRFEEAERTYLEMDRRDLAIGLRLKLGDWFRVLQLLKTGSG
3mkq.1.A  ---------------------------------------EYYEEALNISPDQ---DQKFELALKVGQLTLARDLLTDES-

Target    DADDSLLEQANNAIGDYFADRQKWLNAVQYYVQGRNQERLAECYYMLEDYEGLENLAISLPENHKLLPEIAQMFVRVGMC
3mkq.1.A  ---AEM---KWRALGDASLQRFNFKLAIEAFTNAHDLESLFLLHSSFNNKE-------------GLVTLAKDAETTGKF

Target    EQAVTAFLKCSQPKAAVDTCVHLNQWNKAVELAKNHS--MKEIGSLLARYASHLLEKNK--TLDAIELYRKANYFFDAAK
3mkq.1.A  NLAFNAYWIAGDIQGAKDLLIKSQRFSEAAFLGSTYGLGDNEVNDIVTKWKENLILNGKNTVSERV--------------

Target    LMFKIADEEAKKGSKPLRVKKLYVLSALLIEQYHEQMKNAQRGKVKGKSSEATSALAGLLEEEVLSTTDRFTDNAWRGAE
3mkq.1.A  ----------------------------------------------------------------------------

Target    AYHFFILAQRQLYEGCVDTALKTALHLKDYEDIIPPVEIYSLLALCACASRAFGTCSKAFIKLKSLETLSSEQKQQYEDL
3mkq.1.A  ----------------------------------------------------------------------------

Target    ALEIFTKHTSKDNRKPELDSLMEGGEGKLPTCVATGSPITEYQFWMCSVCKHGVLAQEISHYSFCPLCHSPVG
3mkq.1.A  ---------------------------------------------------------------------
```

Materials and Methods

Template Search

Template search with BLAST and HHBlits has been performed against the SWISS-MODEL template library (SMTL, last update: 2018-02-21, last included PDB release: 2018-02-16).

The target sequence was searched with BLAST against the primary amino acid sequence contained in the SMTL. A total of 1 template was found.

An initial HHblits profile has been built using the procedure outlined in (Remmert, et al.), followed by 1 iteration of HHblits against NR20. The obtained profile has then be searched against all profiles of the SMTL. A total of 3905 templates were found.

Template Selection

For each identified template, the template's quality has been predicted from features of the target-template alignment. The templates with the highest quality have then been selected for model building.

Model Building

Models are built based on the target-template alignment using ProMod3. Coordinates which are conserved between the target and the template are copied from the template to the model. Insertions and deletions are remodelled using a fragment library. Side chains are then rebuilt. Finally, the geometry of the resulting model is regularized by using a force field. In case loop modelling with ProMod3 fails, an alternative model is built with PROMOD-II (Guex, et al.).

Model Quality Estimation

The global and per-residue model quality has been assessed using the QMEAN scoring function (Benkert, et al.) . For improved performance, weights of the individual QMEAN terms have been trained specifically for SWISS-MODEL.

Ligand Modelling

Ligands present in the template structure are transferred by homology to the model when the following criteria are met: (a) The ligands are annotated as biologically relevant in the template library, (b) the ligand is in contact with the model, (c) the ligand is not clashing with the protein, (d) the residues in contact with the ligand are conserved between the target and the template. If any of these four criteria is not satisfied, a certain ligand will not be included in the model. The model summary includes information on why and which ligand has not been included.

Oligomeric State Conservation

The quaternary structure annotation of the template is used to model the target sequence in its oligomeric form. The method (Bertoni et al.) is based on a supervised machine learning algorithm, Support Vector Machines (SVM), which combines interface conservation, structural clustering, and other template features to provide a quaternary structure quality estimate (QSQE). The QSQE score is a number between 0 and 1, reflecting the expected accuracy of the interchain contacts for a model built based a given alignment and template. Higher numbers indicate higher reliability. This complements the GMQE score which estimates the accuracy of the tertiary structure of the resulting model.

References

- **BLAST**
  Camacho, C., Coulouris, G., Avagyan, V., Ma, N., Papadopoulos, J., Bealer, K., Madden, T.L. BLAST+: architecture and

applications. BMC Bioinformatics 10, 421-430 (2009). doi

- **HHblits**
  Remmert, M., Biegert, A., Hauser, A., Söding, J. HHblits: lightning-fast iterative protein sequence searching by HMM-HMM alignment. Nat Methods 9, 173-175 (2012). doi

Table T1:

Primary amino acid sequence for which templates were searched and models were built.

```
MFFYLSKKISIPNNVKLQCVSWNKEQGFIACGGEDGLLKVLKLETQTDDAKLRGLAAPSNLSMNQTLEGHSGSVQVVTWNEQYQKLTTSDENGLIIVWML
YKGSWIEEMINNRNKSVVRSMSWNADGQKICIVYEDGAVIVGSVDGNRIWGKDLKGIQLSHVTWSADSKVLLFGMANGEIHIYDNQGNFMIKMKLSCLVN
VTGAISIAGIHWYHGTEGYVEPDCPCLAVCFDNGRCQIMRHENDQNPVLIDTGMYVVGIQWNHMGSVLAVAGFQKAAMQDKDVNIVQFYTPFGEHLGTLK
VPGKEISALSWEGGGLKIALAVDSFIYFANIRPNYKWGYCSNTVVYAYTRPDRPEYCVVFWDTKNNEKYVKYVKGLISITTCGDFCILATKADENHPQEE
NEMETFGATFVLVLCNSIGTPLDPKYIDIVPLFVAMTKTHVIAASKEAFYTWQYRVAKKLTALEINQITRSRKEGRERIYHVDDTPSGSMDGVLDYSKTI
QGTRDPICAITASDKILIVGRESGTIQRYSLPNVGLIQKYSLNCRAYQLSLNCNSSRLAIIDISGVLTFFDLDARVTDSTGQQVVGELLKLERRDVWDMK
WAKDNPDLFAMMEKTRMYVFRNLDPEEPIQTSGYICNFEDLEIKSVLLDEILKDPEHPNKDYLINFEIRSLRDSRALIEKVGIKDASQFIEDNPHPRLWR
LLAEAALQKLDLYTAEQAFVRCKDYQGIKFVKRLGKLLSESMKQAEVVGYFGRFEEAERTYLEMDRRDLAIGLRLKLGDWFRVLQLLKTGSGDADDSLLE
QANNAIGDYFADRQKWLNAVQYYVQGRNQERLAECYYMLEDYEGLENLAISLPENHKLLPEIAQMFVRVGMCEQAVTAFLKCSQPKAAVDTCVHLNQWNK
AVELAKNHSMKEIGSLLARYASHLLEKNKTLDAIELYRKANYFFDAAKLMFKIADEEAKKGSKPLRVKKLYVLSALLIEQYHEQMKNAQRGKVKGKSSEA
TSALAGLLEEEVLSTTDRFTDNAWRGAEAYHFFILAQRQLYEGCVDTALKTALHLKDYEDIIPPVEIYSLLALCACASRAFGTCSKAFIKLKSLETLSSE
QKQQYEDLALEIFTKHTSKDNRKPELDSLMEGGEGKLPTCVATGSPITEYQFWMCSVCKHGVLAQEISHYSFCPLCHSPVG
```

Table T2:

Template	Seq Identity	Oligo-state	QSQE	Found by	Method	Resolution	Seq Similarity	Coverage	Description
5a1u.1.T	12.60	monomer		HHblits	EM	13.00Å	0.27	0.62	COATOMER SUBUNIT BETA'
5nzu.1.C	12.60	monomer		HHblits	EM	NA	0.27	0.62	Coatomer subunit beta'
3mkq.1.A	12.11	homo-trimer	0.00	HHblits	X-ray	2.50Å	0.26	0.60	Coatomer beta'-subunit
3mkq.1.C	12.11	homo-trimer	0.00	HHblits	X-ray	2.50Å	0.26	0.60	Coatomer beta'-subunit
3mkq.1.E	12.11	homo-trimer	0.00	HHblits	X-ray	2.50Å	0.26	0.60	Coatomer beta'-subunit
3mkq.1.A	10.16	homo-trimer		HHblits	X-ray	2.50Å	0.26	0.58	Coatomer beta'-subunit
3mkq.1.C	10.16	homo-trimer		HHblits	X-ray	2.50Å	0.26	0.58	Coatomer beta'-subunit
3mkq.1.E	10.16	homo-trimer		HHblits	X-ray	2.50Å	0.26	0.58	Coatomer beta'-subunit
5a1u.1.S	11.71	monomer		HHblits	EM	13.00Å	0.26	0.58	COATOMER SUBUNIT ALPHA
5nzu.1.A	11.71	monomer		HHblits	EM	NA	0.26	0.58	Coatomer subunit alpha
5a1u.1.T	13.04	monomer		HHblits	EM	13.00Å	0.26	0.57	COATOMER SUBUNIT BETA'
5nzu.1.C	13.04	monomer		HHblits	EM	NA	0.26	0.57	Coatomer subunit beta'
5a1u.1.S	10.39	monomer		HHblits	EM	13.00Å	0.26	0.56	COATOMER SUBUNIT ALPHA
5nzu.1.A	10.39	monomer		HHblits	EM	NA	0.26	0.56	Coatomer subunit alpha
4bzj.1.A	10.87	homo-dimer		HHblits	EM	40.00Å	0.26	0.55	PROTEIN TRANSPORT PROTEIN SEC31
4bzj.1.C	10.87	homo-dimer		HHblits	EM	40.00Å	0.26	0.55	PROTEIN TRANSPORT PROTEIN SEC31
5oql.1.J	11.71	monomer		HHblits	EM	NA	0.26	0.50	Utp13
2ymu.1.A	14.69	monomer		HHblits	X-ray	1.79Å	0.29	0.45	WD-40 REPEAT PROTEIN
5n1a.1.A	14.00	monomer		HHblits	X-ray	2.15Å	0.27	0.46	utp4
3jbt.1.A	11.72	monomer		HHblits	EM	NA	0.26	0.46	Apoptotic protease-activating factor 1
3sfz.1.A	11.42	monomer		HHblits	X-ray	3.00Å	0.27	0.46	Apoptotic peptidase activating factor 1
5tee.1.A	13.08	monomer		HHblits	X-ray	1.65Å	0.27	0.46	Gem-associated protein 5
3shf.1.A	11.40	monomer		HHblits	X-ray	3.55Å	0.26	0.46	Apoptotic peptidase activating factor 1
5wve.1.K	11.58	monomer		HHblits	EM	NA	0.26	0.46	Apoptotic protease-activating factor 1
5juy.1.B	11.58	monomer		HHblits	EM	NA	0.26	0.46	Apoptotic protease-activating factor 1
5juy.1.G	11.58	monomer		HHblits	EM	NA	0.26	0.46	Apoptotic protease-activating factor 1
5juy.1.D	11.58	monomer		HHblits	EM	NA	0.26	0.46	Apoptotic protease-activating factor 1
5juy.1.E	11.58	monomer		HHblits	EM	NA	0.26	0.46	Apoptotic protease-activating factor 1

Template	Seq Identity	Oligo-state	QSQE	Found by	Method	Resolution	Seq Similarity	Coverage	Description
3j2t.1.A	11.79	monomer		HHblits	EM	NA	0.26	0.46	Apoptotic protease-activating factor 1
5gxh.1.A	12.89	monomer		HHblits	X-ray	1.80Å	0.26	0.46	Gem-associated protein 5
5oql.1.M	11.80	monomer		HHblits	EM	NA	0.25	0.47	Utp17
5h3s.1.A	13.36	monomer		HHblits	X-ray	3.00Å	0.27	0.46	Gem-associated protein 5
1pi6.1.A	12.22	monomer		HHblits	X-ray	2.50Å	0.26	0.46	Actin interacting protein 1
5wlc.19.A	12.48	monomer		HHblits	EM	NA	0.27	0.45	Utp4
5h1j.1.A	13.99	monomer		HHblits	X-ray	2.00Å	0.28	0.45	Gem-associated protein 5
5h1k.1.A	13.99	monomer		HHblits	X-ray	1.90Å	0.28	0.45	Gem-associated protein 5
5wyj.18.A	12.38	monomer		HHblits	EM	NA	0.27	0.45	U3 small nucleolar RNA-associated protein 13
5h1j.1.A	13.72	monomer		HHblits	X-ray	2.00Å	0.26	0.45	Gem-associated protein 5
5h1k.1.A	13.72	monomer		HHblits	X-ray	1.90Å	0.26	0.45	Gem-associated protein 5
5wlc.22.A	11.55	monomer		HHblits	EM	NA	0.27	0.45	Utp12
5m2n.1.A	10.71	monomer		HHblits	X-ray	2.81Å	0.26	0.44	Elongator complex protein 2
4xfv.1.A	10.71	monomer		HHblits	X-ray	3.20Å	0.26	0.44	Elongator complex protein 2
5wyj.17.A	11.99	monomer		HHblits	EM	NA	0.27	0.44	U3 small nucleolar RNA-associated protein 12
5oql.1.D	11.20	monomer		HHblits	EM	NA	0.25	0.45	Utp4
5wlc.13.A	13.51	monomer		HHblits	EM	NA	0.26	0.44	Utp17
5oql.1.A	13.53	monomer		HHblits	EM	NA	0.27	0.43	Periodic tryptophan protein 2-like protein
2oaj.1.A	13.50	monomer		HHblits	X-ray	2.40Å	0.27	0.43	Protein SNI1
5wyj.17.A	12.30	monomer		HHblits	EM	NA	0.27	0.43	U3 small nucleolar RNA-associated protein 12
5i2t.1.A	11.94	monomer		HHblits	X-ray	2.54Å	0.27	0.43	Periodic tryptophan protein 2
5wyj.16.A	11.96	monomer		HHblits	EM	NA	0.27	0.43	Periodic tryptophan protein 2

The table above shows the top 50 filtered templates. A further 1,984 templates were found which were considered to be less suitable for modelling than the filtered list.
3fgb.1.A, 5gm6.1.4, 3vl1.1.A, 4a1s.1.A, 2ff4.2.A, 5cvo.2.A, 3fm0.1.A, 2g5p.1.A, 5ukl.1.B, 1x81.1.A, 4nox.1.A, 4a0a.1.B, 5vgz.1.G, 5gm6.1.2, 5vgz.1.K, 5vgz.1.J, 5vgz.1.H, 2qx5.1.A, 4ui9.1.P, 4ui9.1.Q, 4ui9.1.V, 4ui9.1.W, 4ui9.1.J, 4ui9.1.K, 4ui9.1.H, 4ui9.1.I, 4ui9.1.O, 4ui9.1.C, 4ui9.1.F, 3q15.1.A, 3ieg.2.A, 2xyi.1.A, 2kc7.1.A, 5gm6.1.F, 1aof.1.A, 1aof.1.B, 1pc2.1.A, 3ium.1.A, 4yhc.2.A, 5fqd.1.A, 5dse.1.A, 3po3.1.N, 5n4d.1.A, 3sre.1.A, 1jmz.1.B, 5opt.1.A, 3mv3.1.B, 4asc.1.A, 2qt9.1.A, 5k0m.1.A, 4i1a.1.A, 4uer.1.b, 4cvc.1.A, 3s2k.1.B, 1ft1.1.A, 3s2k.1.A, 3j7p.78.A, 1hxi.1.A, 2ce9.2.B, 5wyk.1.U, 5wyk.1.V, 5wyk.1.R, 5jrl.1.B, 5mqf.1.O, 5a7d.8.A, 5mqf.1.M, 4v5z.1.A, 5mqf.1.F, 5n4e.1.A, 5mqf.1.D, 5mqf.1.E, 4v6w.2.A, 2lsu.1.A, 1wm5.1.A, 5uw7.1.A, 5l4k.1.E, 3ffl.2.B, 5l4k.1.G, 5l4k.1.F, 5l4k.1.I, 3mbr.1.A, 5l4k.1.J, 4a2l.1.B, 2j9q.1.B, 2j9q.1.A, 5k1a.2.B, 6au8.1.A, 4yg8.1.B, 5h19.1.A, 5sv7.1.D, 3odt.1.A, 5sv7.1.A, 5sv7.1.B, 5sv7.1.C, 2fi7.1.A, 2fi7.1.B, 5gmk.1.0, 3li4.1.A, 5n4f.1.A, 2bkl.1.A, 6eos.1.B, 5wlc.27.A, 5mpq.1.A, 3hlh.1.A, 1o6f.1.A, 1vz2.1.A, 5wvi.1.N, 1z68.1.B, 5cqr.1.A, 1z68.1.A, 1z2z.1.A, 5i1y.1.C, 3kif.1.C, 3kif.1.A, 2bed.1.A, 4x3e.1.A, 2be1.1.A, 5wvi.1.K, 5gmk.1.J, 5kkl.1.A, 3ly9.1.A, 5luq.2.A, 5gmk.1.X, 5gmk.1.R, 5a7d.6.A, 5a9q.1.A, 2ooe.1.A, 3cv0.1.A, 5m72.1.A, 3rib.1.A, 2hes.1.A, 2gw1.1.A, 2gw1.1.B, 4eqf.1.A, 2iav.1.A, 4kvm.1.A, 4j8e.1.A, 5wyj.19.A, 5v4b.1.B, 1sly.1.A, 2vz1.1.A, 3j8b.1.C, 1c9l.1.A, 5lpi.3.A, 3ly7.1.A, 3jck.1.B, 1b9y.1.A, 3jck.1.D, 5o3u.1.A, 4ja7.1.A, 4ymr.1.A, 2p9w.1.A, 4ymr.1.B, 3txn.1.A, 5kjk.1.A, 5guw.3.A, 5jj7.1.A, 5olj.1.A, 5jj7.1.B, 5ulh.1.C, 3i7k.1.A, 5n4b.1.A, 2iat.1.A, 1tl2.1.A, 2iax.1.A, 3edt.1.A, 3edt.1.B, 2ebs.1.A, 5c2w.1.E, 4lg8.1.A, 2xzg.1.A, 5juu.45.A, 1hzu.1.A, 3j80.1.7, 4q66.2.C, 2yhc.1.A, 5lj5.1.V, 3zfw.1.A, 4hou.2.A, 1e96.1.B, 5k0y.1.8, 3zgc.1.A, 4lgn.1.A, 5a1y.1.U, 4wne.1.A, 4i9e.1.A, 3cvq.1.A, 1yjn.1.1, 4d18.1.D, 4d18.1.B, 5f72.1.A, 3ow8.1.A, 5lpi.1.A, 4nc4.1.A, 4yde.1.A, 4cy1.1.A, 1vyh.1.C, 3kd7.1.A, 5v3o.1.A, 5vhj.1.H, 5m5r.1.A, 4hhq.1.A, 2l0b.1.A, 4kbq.2.A, 5aiu.1.A, 1n6f.1.A, 4hoq.1.A, 3gz1.1.A, 3sf4.1.A, 5sui.1.A, 5vhf.1.J, 4wn4.2.A, 4bt8.1.B, 4bt8.1.A, 3jb9.1.L, 2ynn.1.A, 2ecl.1.A, 3li3.1.A, 5jk7.2.A, 3jb9.1.K, 5oql.1.3, 5k1c.1.C, 5k1c.1.B, 6epc.1.S, 4l7b.1.A, 5igo.1.A, 6epc.1.T, 6epc.1.W, 6epc.1.V, 6epc.1.X, 5oql.1.X, 4r5o.1.A, 2gop.1.A, 2gop.1.B, 6exn.1.J, 5i9d.1.A, 5oql.1.N, 1e2r.1.B, 1e2r.1.A, 5oql.1.M, 2xgs.1.A, 5oql.1.A, 5oql.1.F, 5oql.1.D, 5oql.1.E, 6exn.1.a, 6emk.1.D, 6emk.1.B, 6emk.1.C, 5ijn.1.U, 4v7h.1.Q, 5ijn.1.K, 5ijn.1.I, 5wbu.1.B, 3pbp.4.A, 5wbu.1.A, 5ijn.1.C, 1jju.1.B, 4uzy.1.A, 3no2.1.A, 4n5c.5.A, 5yp1.1.B, 5yp1.1.A, 5i1y.1.A, 5m2n.1.A, 5i1y.1.B, 4hot.1.A, 4n5c.3.A, 5hgv.1.A, 5jul.1.A, 5cxb.1.B, 5cxb.1.A, 5ln3.1.0, 4p04.1.A, 4n5c.1.A, 3mzl.1.B, 2co0.1.A, 5vlj.1.B, 5vlj.1.C, 5bt1.1.B, 6f9n.1.A, 6f9n.1.B, 5ln3.1.Z, 5ln3.1.Y, 5ln3.1.X, 3as8.1.A, 5mgx.1.A, 2p4o.1.A, 4bzj.1.D, 4bzj.1.C, 4bzj.1.B, 4bzj.1.A, 4hw6.1.A, 3i7l.1.A, 3b7f.1.A, 5ln3.1.A, 3ww8.1.A, 5mc6.35.A, 5a9q.1.M, 5nxq.1.A, 5ic8.3.A, 1qsa.1.A, 3gd1.3.A, 5ic8.1.A, 5wsg.1.T, 5a9q.1.H, 5lyb.33.A, 5g05.1.I, 5yz0.1.A, 5jzz.2.A, 4fhl.1.A, 5vh9.1.B, 2ifu.3.A, 2ovr.1.B, 4bl0.2.A, 3oxf.1.A, 1mda.1.A, 4wjw.1.B, 2iar.1.A, 3ivm.1.A, 3jco.1.8, 4wsn.4.D, 3acp.1.A, 1aoq.1.A, 2pl2.1.A, 2c2l.2.A, 2hz6.1.A, 3e0c.1.A, 3jrp.1.A, 5nrl.1.Q, 5nrl.1.W, 4x60.1.B, 5nrl.1.O, 2y4u.1.A, 4aez.1.A, 4aez.1.C, 1s72.1.1, 5d0i.2.A, 3j78.45.A, 4aez.3.C, 2gvx.1.A, 5djs.1.A, 3vl1.2.A, 2yin.1.A, 5mps.1.U, 4zox.1.A, 5mps.1.Q, 5mps.1.R, 5lj3.1.L, 1qz2.1.C, 1qz2.1.B, 1qz2.1.A, 3vu4.1.A, 3n0d.1.A, 5ulm.1.A, 4a0a.1.A, 5lj3.1.U, 5lj3.1.T, 3iiw.1.A, 2i3s.2.A, 5a9q.1.a, 3vu4.2.A, 3ade.1.A, 3tg5.1.A, 2vyi.1.A, 1g72.1.A, 2xcc.1.A, 2rfo.1.A, 4zb4.2.A, 5b26.2.B, 5txc.1.A, 2jny.1.A, 5jz6.1.A, 3fvz.1.A, 2b5m.1.A, 1gjq.1.A, 2ovp.1.B, 3nol.1.A, 3li5.1.A, 4ggd.1.A, 5lj5.1.M, 3bg0.1.D, 5lj5.1.U, 3mzk.1.A, 3mzk.1.B, 5o09.1.C, 5ftp.1.A, 5ftp.1.B, 3fw0.1.A, 3si5.1.A, 5lj5.1.d, 5diz.1.A, 4g2v.1.A, 5cqs.1.A, 3jct.1.n, 3lrq.1.B, 3lrq.1.A, 2eic.1.A, 4g56.1.B, 4v0m.1.B, 3n71.1.A, 3zwl.1.A, 4hnw.1.A, 3jzn.1.A, 5l0y.1.B, 5l0y.1.A, 5fkt.1.A, 1yr2.1.A, 3hym.1.B, 5n61.1.P, 5t0c.35.A, 2ece.1.A, 1zgk.1.A, 1klx.1.A, 5mc6.37.A, 1gxr.1.B, 1gxr.1.A, 4h7x.1.A, 3e4b.1.A, 3ott.1.B, 3ott.1.A, 5jqy.1.A, 4a09.1.A, 4nq0.1.A, 3zpj.1.A, 4r40.2.A, 4cgv.1.A, 4abn.1.A, 3as4.1.A, 5hb0.4.A, 5ulk.1.B, 1bpo.1.C, 5lvv.1.A, 3hli.1.A, 2hu5.1.B, 5i5i.1.A, 5c2v.1.B, 5wyj.20.A, 4d0k.1.A, 4lg9.1.A, 1sqj.1.A, 2fpb.2.A, 5d0o.1.D, 5d0q.1.C, 2e2e.1.A, 2yno.1.A, 5i5m.1.A, 5d0k.1.B, 3byc.1.A, 3v64.1.A, 5ndv.147.A, 3v64.1.D, 3fmo.1.A, 3kae.1.A, 5tbk.1.B, 5o01.1.A, 3hrp.1.A, 2xcb.2.A, 4g1f.4.A, 4xyh.1.A, 3zwu.1.A, 3i4r.1.B, 3cfs.1.A, 3vk6.1.A, 5fnr.1.A, 1lrw.1.C, 1lrw.1.A, 4ja9.1.A, 2faw.1.A, 4gpk.1.D, 4gpk.1.A, 4gpk.1.C, 4gpk.1.B, 3fwv.2.A, 5nnz.1.A, 3s94.2.A, 4gpk.3.D, 4gpk.3.C, 4gpk.3.B, 4gpk.3.A, 3lku.1.A, 3emh.1.A, 1ouv.1.A, 4kvo.1.A, 2hf1.1.A, 5igo.2.A, 5ife.1.D, 5ijo.1.Q, 5buz.2.B, 5ijo.1.W, 5gjq.1.Z, 3lvg.1.A, 3lvg.1.C, 3lvg.1.B, 5ijo.1.E, 4ozs.1.A, 2k4x.1.A, 4cy3.1.A, 2i0r.1.C, 5a31.1.F, 5gjq.1.j, 4ynw.1.A, 2y0s.1.K, 4btb.1.A, 4imm.1.A, 3mmy.1.A, 5ltd.1.A,

3ii7.1.A, 5mpb.1.e, 2iaq.1.A, 5mpb.1.g, 3sfx.1.A, 5gjq.1.7, 5ctr.1.A, 5gjq.1.5, 3u4t.1.A, 2iwa.1.A, 5mpb.1.i, 5mpb.1.h, 4a1g.2.A, 4l9o.1.A, 2co0.2.A, 3ww9.1.A, 5obm.152.A, 1fpp.1.B, 5cvl.1.A, 4czv.1.A, 1ihg.1.A, 3soq.1.A, 5bw8.1.C, 3r9a.1.D, 5naf.1.A, 2h13.1.A, 3r9a.1.B, 1tnu.1.A, 3sn6.1.B, 6c23.1.D, 5tzs.1.e, 6c23.1.F, 1qqe.1.A, 6bq1.1.B, 2dg1.1.A, 1r5m.1.A, 4gq1.1.A, 5w65.1.O, 5xog.1.L, 4cc9.1.A, 5w5h.2.E, 3wwa.1.A, 5gvb.1.A, 5tzs.1.1, 2pm9.1.A, 2q7f.1.A, 5yp4.2.A, 5nkp.2.A, 4o6f.1.A, 3w15.1.A, 3bws.1.A, 2bug.1.A, 5jwz.1.A, 5an3.1.A, 5vyc.4.I, 4o5t.1.A, 4jsn.1.A, 4jsn.1.B, 3elq.1.A, 4pjq.1.A, 5cxc.1.B, 5cxc.1.A, 5b26.1.B, 1jof.1.A, 6em3.1.E, 3h7n.1.A, 2ias.1.A, 4m59.1.B, 3sfz.1.A, 4m59.1.A, 5jcs.1.3, 2m6n.1.A, 4yvd.1.A, 5fjy.1.B, 5fjy.1.A, 5l0y.6.A, 1o1r.1.A, 5igq.1.A, 1fwx.1.A, 5a5t.1.C, 4i9c.1.A, 4mpz.1.A, 4xmm.1.C, 5jjx.1.A, 2qxv.1.A, 4xmm.1.E, 5jut.45.A, 3shf.1.A, 3jcp.1.Z, 3jcp.1.Y, 4pxw.1.A, 5fks.1.A, 2vgy.1.A, 5nnr.1.A, 3jcp.1.0, 5wrw.1.A, 5wrw.1.B, 2eep.1.A, 3gtm.1.K, 3jcp.1.8, 2c0l.1.A, 3dsm.1.A, 1x4j.1.A, 4wjv.1.A, 5a7d.4.A, 5wrw.3.A, 3nf1.1.A, 1xfd.1.A, 5mpe.2.H, 5mpe.2.E, 5mpe.2.F, 2hu8.1.A, 3rjv.1.A, 2vdu.1.A, 5n5y.1.P, 4m57.1.A, 5a6c.1.A, 2lah.1.A, 4i17.1.A, 6eoq.1.A, 5afu.1.C, 6em5.1.5, 2b5l.1.A, 2kiz.1.A, 5a7d.2.A, 5h64.1.A, 5h64.1.B, 5h64.1.C, 5fkq.1.A, 6em5.1.h, 5t0h.1.V, 2w18.1.A, 4fsc.2.B, 5fww.1.A, 3fhc.1.A, 4kr0.1.A, 4in4.1.A, 5ic7.1.A, 4d0p.1.A, 4zoy.1.A, 5xw7.2.A, 5xw7.4.A, 1i2m.2.B, 3lrq.2.A, 3lrq.2.B, 2o10.1.A, 3pe7.1.A, 5wlc.25.A, 5t88.1.A, 5uw5.1.A, 3g4s.1.0, 4zlh.1.B, 4wjs.1.A, 2pzi.2.A, 5wlc.41.A, 5haz.1.A, 3vty.4.A, 5nuv.1.A, 1kb0.1.A, 4yd8.1.A, 3tgo.1.A, 2wfx.1.B, 2kcl.1.A, 5c86.1.A, 3i2n.1.A, 3azq.1.A, 4ri8.1.A, 1kt1.1.A, 5gjq.1.3, 4in3.1.D, 4yzy.1.A, 4l9o.2.A, 3e4b.4.A, 3f3g.1.C, 3f3g.1.D, 3f3g.1.E, 3prw.1.A, 3i5p.1.A, 4o9d.1.A, 1w6s.1.A, 2qc5.1.A, 4j8d.1.A, 4hdj.1.A, 4jhn.1.A, 2r5s.1.A, 3kd7.2.A, 2xev.3.A, 5a9q.1.5, 2jr6.1.A, 2xev.1.A, 5a9q.1.4, 2y4t.1.A, 3asf.2.A, 3j96.1.J, 3j96.1.H, 5wwm.1.A, 4ax4.1.A, 3j96.1.G, 5xjc.1.I, 4bt9.1.A, 4i9e.1.B, 1hzv.1.A, 3jb9.1.4, 2q7f.2.A, 4yvq.1.B, 3jb9.1.3, 4buj.1.B, 4buj.1.C, 5vhf.1.H, 3v1s.1.A, 2lni.1.A, 3iiy.1.A, 5k0y.1.P, 5vhf.1.S, 5bt1.1.A, 2bbk.1.A, 3jb9.1.S, 3v9f.4.A, 3v9f.2.A, 4gcn.1.A, 4xfv.1.A, 5yz0.1.B, 3uvo.1.A, 2y4t.3.A, 4v0n.2.B, 5vbg.1.A, 1rwl.1.A, 5cvo.1.A, 2jne.1.A, 5mq0.1.I, 2qe8.1.A, 3upv.1.A, 3q5m.1.A, 5fmf.1.B, 5l4k.1.H, 5t0i.1.Y, 5t0i.1.X, 5t0i.1.W, 5t0i.1.V, 5t0i.1.U, 2kcv.1.A, 1rwi.1.A, 4hny.2.A, 5hb3.1.A, 5nnp.1.A, 4u0s.1.A, 4a11.1.B, 4a11.1.A, 3q15.2.A, 3q7o.1.A, 4wjl.1.A, 1l0q.3.A, 2xn4.1.A, 2gnq.1.A, 5gmk.1.W, 2ct0.1.A, 5hrm.1.A, 5nqv.2.A, 1q7f.2.A, 4wsn.6.D, 4g1t.1.A, 4qzv.2.A, 4g1t.1.B, 4j73.1.A, 5tqb.1.B, 4z8l.1.A, 5uw3.1.A, 3h0c.1.A, 3jpx.1.A, 4zey.1.A, 6b3j.1.D, 1ft2.1.A, 2ho1.1.B, 2ho1.1.A, 2n8w.1.A, 3vgz.1.A, 3s94.1.A, 4amy.1.A, 1y1v.1.M, 2fbn.1.A, 5jgc.1.A, 3q6k.1.A, 2ymu.1.A, 5mpd.1.F, 2dpf.1.A, 2i0s.1.C, 2dpf.1.B, 5flc.1.F, 2agl.1.C, 3ww7.1.A, 4zoz.1.A, 5hi7.1.A, 2mta.1.A, 3j9m.72.A, 3ffl.1.A, 5a01.1.A, 2ojy.1.C, 4rg6.1.A, 4rg6.1.B, 4hho.1.A, 4czy.1.A, 3dwl.1.B, 4me2.1.A, 5iww.1.D, 3ffl.1.B, 5ljo.1.C, 4n5c.7.A, 4xmn.1.A, 4xmn.1.B, 4xmn.1.D, 4xmn.1.E, 1u6d.1.A, 3hxj.2.A, 3hxj.2.B, 2hye.1.A, 5a7d.5.A, 5fa5.1.B, 1utc.1.A, 4ci8.1.A, 5k1a.1.B, 1bwu.1.D, 5cww.1.B, 3ro2.1.A, 5aja.1.A, 3uzs.1.B, 4amf.1.A, 4nlm.1.A, 4q1v.1.A, 5v1d.1.C, 5v1d.1.A, 4jhr.1.A, 3iax.1.A, 6eoj.1.A, 2dba.1.A, 6eoj.1.C, 5luq.1.A, 4p29.1.A, 5jpz.1.B, 6ez8.1.B, 5a7d.1.A, 5a7d.7.A, 5jpz.1.A, 2c0m.1.A, 3u0s.1.A, 4h5i.1.A, 5gap.1.G, 2ecf.1.A, 4lct.2.B, 4lct.2.A, 4owr.1.A, 4aif.1.A, 3jd5.1.3, 3e37.1.A, 5chb.1.A, 1weo.1.A, 5wyj.18.A, 3jd5.1.U, 5bpt.1.A, 5xyi.1.6, 5mc6.15.A, 3as5.2.A, 5jjo.1.A, 4qrj.1.A, 2vq2.1.A, 1zu2.1.A, 4aow.1.A, 5lyb.108.A, 5o3v.1.A, 2aqc.1.A, 4kmo.1.B, 3pz4.1.A, 5jhe.1.A, 3gw4.1.B, 1erj.1.A, 3gw4.1.A, 6bk8.1.V, 6bk8.1.W, 6bk8.1.P, 4n14.1.A, 3mkq.1.B, 6bk8.1.H, 3mkq.1.D, 3mkq.1.F, 5kdo.1.B, 5bwk.1.D, 5v7v.1.A, 1qbi.1.A, 5m23.1.A, 1kv9.1.A, 3ho5.2.A, 4uuy.1.A, 1ldk.1.C, 4q66.1.D, 3q7f.1.A, 4n2q.1.A, 4jml.1.A, 5it7.77.A, 3sz7.1.A, 3a9g.1.A, 5ait.1.A, 2w8b.1.A, 4l1m.1.A, 5c1d.1.A, 4r7s.1.A, 4v7r.20.A, 2g9a.1.A, 2zwa.1.A, 3vtx.2.A, 5gxh.1.A, 5h3s.1.A, 4apo.1.A, 4pjq.2.A, 5lpi.2.A, 1e8m.1.A, 1tjc.1.A, 4v16.1.A, 3wxx.1.A, 5wyj.16.A, 5jjw.1.A, 4pk1.1.A, 5hb0.2.A, 1xnf.1.A, 3f3p.3.D, 4zgc.1.A, 3cik.1.B, 3jck.1.C, 4u1f.1.A, 5t0j.1.V, 1h2y.1.A, 3jbz.1.A, 5jpq.1.Y, 4qzv.1.A, 6epd.1.V, 6epd.1.W, 6epd.1.T, 6epd.1.U, 6epd.1.S, 6epe.1.X, 6epe.1.W, 6epe.1.V, 3j97.1.H, 6epe.1.T, 6epe.1.S, 1e5t.1.A, 4g23.1.A, 3esl.2.A, 3rfg.1.A, 2h9l.1.A, 2z3z.1.A, 2pm7.1.C, 4ap4.1.A, 2pm7.1.A, 3q7m.1.A, 4kbq.1.A, 2bgr.1.A, 5aaq.1.A, 4wn4.1.A, 5x50.1.L, 1gq1.1.A, 4hny.1.A, 5gjq.1.9, 4cr3.1.6, 3gre.1.A, 4n5c.4.A, 4n5c.2.A, 4a1g.4.A, 5wql.2.A, 5lqi.1.A, 3wj9.2.A, 3gz2.1.B, 3gz2.1.A, 1q7f.1.A, 5c2m.1.A, 4ga1.1.A, 4v3p.1.A, 5waq.1.A, 5mc6.36.A, 5w5i.1.A, 2ism.1.A, 4pdt.1.A, 2j57.1.C, 3p5c.1.C, 4cr3.1.Y, 3iun.1.A, 4l72.3.A, 1u8e.1.B, 1u8e.1.A, 5lyn.1.A, 2c2l.1.A, 4a0b.2.A, 2hr2.1.A, 2ynp.1.A, 3dxm.1.C, 4tqo.1.A, 4bt9.1.B, 4g55.1.A, 2ifu.2.A, 3o4g.1.B, 4aif.2.A, 1ri6.1.A, 6fbs.1.A, 6fbs.1.B, 2iao.1.A, 4u0u.1.A, 5k1h.1.A, 4eba.1.A, 2if4.1.A, 5efr.1.A, 4imm.2.A, 3hfq.1.A, 5em2.2.B, 5bjs.1.A, 5iwb.1.B, 5jzz.1.A, 4cr4.1.U, 4cr4.1.W, 5k19.2.A, 4bp8.1.A, 4cr4.1.X, 4cr4.1.Y, 5naf.3.A, 4c8h.1.C, 4c8h.1.A, 5izw.1.A, 4aez.2.C, 1nex.2.B, 4aez.2.A, 5wsg.1.R, 3lya.1.A, 5wsg.1.U, 4a0l.1.A, 4d6v.1.A, 3jbt.1.A, 5g05.1.K, 5g05.1.O, 5g05.1.C, 5g05.1.F, 5mpd.1.K, 5mpd.1.J, 5mpd.1.I, 3flo.1.B, 4ady.1.A, 2i3s.1.A, 4ga2.1.A, 5mpd.1.G, 5n5z.1.P, 2yq8.1.A, 4cr4.1.6, 5vai.1.D, 3j6x.75.A, 3cvl.1.A, 5b4x.2.B, 3s8z.1.A, 5nus.1.B, 4fhn.1.B, 4a2m.2.A, 5jrk.1.A, 5l0y.7.A, 5jrk.1.B, 5jk7.1.B, 5cqs.2.A, 2js4.1.A, 1fch.1.A, 5wql.1.A, 1a0r.1.A, 2n8i.1.A, 5m1j.14.A, 1yiq.1.A, 5ft9.2.A, 3ma5.3.A, 4fhm.1.B, 2rfo.2.A, 4fhm.1.A, 2ajl.1.A, 2ajl.1.B, 5wrv.1.B, 5a31.1.O, 5a31.1.J, 5a31.1.H, 5t2c.73.A, 5a31.1.C, 4iqk.1.A, 2lsv.1.A, 3jap.1.i, 5a31.1.W, 5a31.1.V, 5x54.1.A, 5a31.1.R, 5a31.1.P, 5j3j.1.A, 5u5h.1.A, 3ei3.1.A, 5diz.2.A, 3ho5.1.A, 5b26.1.A, 5bpw.1.A, 4a0l.2.A, 2wmn.1.A, 4v8m.8.A, 2q7q.1.C, 2v5f.1.A, 5l0y.2.A, 3s8v.2.A, 2z2n.1.A, 5t0h.1.U, 3lca.1.A, 5k18.1.A, 5t0h.1.Y, 4d4o.1.B, 4d4o.1.A, 3e4b.2.A, 1pi6.1.A, 2yba.1.A, 5tf2.1.A, 5xjc.1.W, 5xjc.1.T, 2ond.1.A, 4qam.1.A, 2b5n.2.A, 2iaa.1.A, 5xjc.1.E, 5ioj.1.A, 5xjc.1.J, 5n60.1.P, 1p22.1.A, 1mg2.1.A, 4cgv.2.A, 5c9s.1.A, 4abn.2.A, 3rkv.1.A, 6b3x.1.A, 2oaj.1.A, 4wju.1.A, 5w1r.1.A, 6az1.1.6, 5oj8.1.A, 5wuk.1.A, 1s4u.1.A, 3j77.45.A, 2yms.1.C, 3urz.1.A, 5vat.1.A, 5gap.1.F, 5cyk.1.A, 3u4y.1.A, 3qqz.1.A, 3p5b.1.C, 3j2t.1.A, 5hqg.1.A, 5tbk.2.B, 3m0c.1.C, 5aem.1.A, 4dnv.1.A, 4zcn.1.A, 4zcn.1.C, 1sq9.1.A, 2zet.2.B, 5fzs.1.A, 5lyp.1.A, 5dbk.1.B, 5dbk.1.A, 4zb4.1.A, 5o01.2.A, 5ayw.1.B, 3qky.1.A, 2fo7.1.A, 5ayw.1.D, 2nb9.1.A, 4gpk.2.B, 4gpk.2.C, 4gpk.2.A, 4cgw.1.A, 4gpk.2.D, 5a2q.1.8, 5wyj.33.A, 4hnx.1.A, 2vsy.1.A, 5kc2.1.B, 4a08.1.A, 4a08.1.B, 3ah8.1.B, 4uqy.1.A, 2avp.1.A, 2xu7.1.A, 5flx.1.7, 1hz4.1.A, 5mpc.1.h, 5mpc.1.i, 5mpc.1.d, 5mpc.1.e, 3asg.1.A, 5mpc.1.g, 4ifl.1.A, 5ccl.1.A, 5jjt.1.A, 1c5k.1.A, 5ojf.1.A, 5dse.2.A, 3f7f.1.A, 1p5q.1.A, 1p5q.1.B, 1p5q.1.C, 4hxg.1.A, 4hxf.1.F, 4ycz.1.A, 3mxx.1.A, 4gcn.2.A, 1ve7.1.A, 4ozu.1.A, 4a1g.1.A, 3c75.1.A, 2xl2.1.A, 5fxy.2.A, 3mks.1.D, 4a1g.3.A, 4v7e.7.A, 5ctr.2.A, 4y6c.1.A, 5mzu.1.A, 5ctq.1.B, 5n1a.1.A, 5ukm.1.B, 5u69.1.A, 4ady.2.A, 2iwf.1.A, 5mpb.1.d, 5udj.1.A, 5hrz.1.A, 4y49.1.A, 3frx.1.A, 5uzw.1.A, 3j9m.81.A, 1nl4.1.A, 1h4i.1.A, 4f3v.1.A, 4e5z.1.B, 6bw3.1.A, 5k04.1.A, 6eoo.1.A, 4v5o.1.0, 1elw.1.A, 5t0c.44.A, 3ru0.1.A, 2d0v.1.A, 1xip.1.A, 5fsb.1.A, 3ei4.1.A, 5ekq.1.B, 4gco.1.A, 5f30.1.A, 2pbi.2.B, 3qou.1.A, 1n9a.1.A, 6epf.1.T, 6epf.1.U, 6epf.1.V, 6epf.1.W, 6epf.1.S, 6exn.1.R, 4gyw.1.A, 5fvm.1.C, 5fvm.1.A, 3iuj.1.A, 4xf2.1.C, 5m11.1.A, 2pm7.1.D, 4ga0.1.A, 1l0q.1.A, 5min.1.A, 2g8s.1.A, 5cvn.1.A, 4unm.1.A, 5wve.1.K, 3dm0.1.A, 3sob.1.B, 4ffv.1.A, 4bp9.1.A, 4i1a.2.A, 4bzk.1.D, 1c9i.1.A, 4aah.1.A, 3ieg.1.A, 5tga.33.A, 5g04.1.Q, 5g04.1.P, 5g04.1.U, 5g04.1.T, 5ctq.1.A, 5g04.1.C, 4o5s.1.A, 5g04.1.F, 5mpe.1.J, 5g04.1.H, 5g04.1.K, 5g04.1.J, 5g04.1.O, 5wp3.1.A, 1dy7.1.A, 2g99.1.A, 3ho4.1.A, 3gz1.1.B, 5ln3.1.V, 4cgu.1.A, 5a7d.3.A, 3sjl.1.D, 5xgs.1.B, 2ojh.1.A, 3dr2.1.A, 4dg6.1.A, 5hy7.2.A, 2zzk.1.A, 4w9r.1.A, 4rib.1.A, 4ric.1.A, 5xw7.3.A, 5xw7.5.A, 5wlc.17.A, 5l8s.1.A, 5wvi.1.c, 5wlc.15.A, 4gm9.2.A, 2vsy.2.A, 5o9z.1.L, 5wvi.1.O, 3mv2.1.B, 5wlc.13.A, 5o9z.1.F, 5o9z.1.G, 5lfl.1.A, 3mun.1.A, 2ea6.1.A, 3s7f.1.A, 5wvi.1.V, 3q75.1.A, 3b13.1.A, 5jkp.1.A, 5m5g.1.A, 3hkz.1.L, 4wuy.1.A, 4wju.2.A, 1k8k.1.C, 2vgx.1.A, 2vgx.1.B, 1k3i.1.A, 2eib.1.A, 4gnb.1.A, 4raa.1.A, 1i2m.1.B, 3qwp.1.A, 2qzp.1.A, 3vty.1.A, 5wlc.28.A, 5a9q.1.T, 5a9q.1.W, 5a9q.1.V, 6f1t.1.b, 6f1t.1.c, 5wlc.19.A, 1crz.1.A, 5a9q.1.L, 5a9q.1.N, 5a9q.1.I, 5sxm.1.A, 5a9q.1.E, 5a9q.1.D, 5a9q.1.G, 5a9q.1.F, 1b89.1.A, 5a9q.1.C, 5a9q.1.B, 4jhp.1.B, 1nzn.1.A, 5t88.2.A, 5wlc.26.A, 5l8e.1.A, 4j8e.2.A, 6epc.1.U, 5bv0.1.B, 4v6i.1.A, 3kya.1.A, 3ewe.1.B, 4n2s.1.A, 3j6y.75.A, 5hxb.1.B, 6f1t.1.4, 6f1t.1.3, 5c2v.1.A, 1bpo.1.B, 1bpo.1.A, 1w3b.1.A, 2uy1.1.A, 2uy1.1.B, 5a9q.1.2, 3o4h.2.A, 4q1u.1.A, 3jam.1.7, 3pdn.1.A, 3uq3.1.A, 4psw.1.B, 5lpi.4.A, 3asf.1.A, 3azo.1.A, 2gbg.1.A, 2qfc.1.A, 3dw8.1.B, 1vz3.1.A, 4a0p.1.A, 4ynd.1.A, 5ojs.1.A, 5bv1.2.B, 1suu.1.A, 2woz.1.A, 6f38.1.3, 6f38.1.4, 2cn2.1.A, 5oej.1.A, 3i1c.1.A, 5aio.1.A, 1h4j.1.A, 6f38.1.b, 6f38.1.c, 3wdz.1.A, 6eho.1.A, 4xmm.1.D, 3o4j.1.A, 3o4j.1.B, 3kih.1.A, 1tbg.1.E, 3kih.1.C, 3kih.1.E, 1tbg.1.A, 4ci1.1.A, 3lrv.1.A, 5d9b.1.A, 5oql.1.O, 5t0g.1.Y, 5t0g.1.X, 5oql.1.L, 4r5o.4.A, 6exn.1.S, 1wao.1.A, 3asg.2.A, 5t0g.1.V, 2yh3.1.A, 5vtb.1.A, 1xhm.1.A, 1wao.3.A, 4xpd.1.A, 3smr.1.A, 1orv.1.A, 3lvh.1.B, 4j79.1.A, 3sf4.2.A, 5gva.1.A, 3lvh.1.A, 3c9c.1.A, 5vhi.1.H, 4gn7.1.A, 5vhi.1.S, 4xnh.1.A, 4xi0.1.A, 5t0g.1.5, 4jsp.1.A, 3mkr.1.A, 1yfq.1.A, 5ij7.1.B, 5ljo.1.A, 4r89.1.A, 4hou.1.A, 5vid.1.B, 5ex7.1.A, 4am9.1.A, 2ff4.1.A, 6emk.1.A, 1n7d.1.A, 5lg0.1.A, 4u04.1.A, 2kck.1.A, 4zov.2.A, 2xcc.1.B, 4wng.1.A, 4a0k.1.C, 4a0k.1.D, 3ks2.1.A, 3sbp.1.A, 3hxj.1.B, 3hxj.1.A, 3qil.1.B, 3qil.1.C, 3qil.1.A, 5hy7.1.A, 5t94.1.A, 1a17.1.A, 3q54.1.A, 4e54.1.B, 4e54.1.A, 4tz4.1.A, 3j81.1.5, 3ho3.1.A, 3ei4.1.B, 4n5c.8.A, 1r9m.1.A, 5vfc.1.A, 2yms.1.D, 2h6k.1.A, 2yms.1.B, 4n5c.6.A, 2yms.1.A, 4e85.1.A, 4x33.1.B, 5cyk.1.B, 3ulq.1.A, 5vhs.1.H, 5vhr.1.H, 4y5r.1.C, 3q8w.1.A, 3ash.1.A, 4r8a.1.A, 1hh8.1.A,

5lfm.1.A, 5lks.64.A, 1a12.1.C, 5yp1.2.A, 4leu.1.A, 5yp1.2.B, 5h13.1.A, 5v1d.2.A, 5v1d.2.B, 6bll.1.A, 4hvt.1.A, 6bll.1.B, 1gp2.1.B, 4j87.1.A, 5a5b.1.Z, 5a5b.1.Y, 4rid.2.A, 5a5b.1.W, 4jxm.1.A, 3euv.1.A, 3ho4.2.A, 6bcx.1.A, 6bcx.1.C, 6f3a.1.3, 6f3a.1.2, 1npe.1.A, 2dcm.1.A, 4nsx.1.A, 2r2l.1.A, 5ukk.1.B, 3das.1.A, 3qdn.1.A, 5tdh.1.B, 5wvk.1.k, 5wvk.1.a, 5wvk.1.b, 5wvk.1.c, 4gyo.1.A, 4lct.1.A, 4lct.1.B, 3g4e.1.A, 2qzp.2.A, 3k9i.1.A, 4y6w.1.A, 3oxl.1.A, 3ewe.1.A, 5ndv.73.A, 5wvk.1.8, 6epf.1.X, 5b4x.1.B, 4mae.1.A, 4oe1.1.A, 4oe1.1.B, 5nqv.1.A, 3q4a.1.A, 2zir.1.A, 3ma5.1.A, 5hax.1.A, 5njx.1.A, 2rip.1.A, 4bwr.1.A, 1elr.1.A, 4nrh.1.B, 5gje.1.B, 5gje.1.A, 4fa4.1.D, 1flg.1.A, 3mvd.1.K, 5ogs.1.A, 4pjr.1.A, 5kcn.1.A, 5o7x.4.A, 4bta.1.B, 4bta.1.A, 3as5.1.A, 3si5.2.A, 4h7y.3.A, 2b5n.4.A, 3hxr.1.A, 6ek0.64.A, 4cgq.1.A, 1ijq.1.A, 3ww8.1.B, 5jus.45.A, 2zwa.2.A, 5nqs.1.A, 3esl.1.A, 5i9g.1.A, 5cgj.1.A, 3qdn.2.A, 3cvn.1.A, 4a5s.1.A, 2xzh.1.A, 5hb0.1.A, 5oa1.1.S, 5ex0.1.A, 5sum.1.A, 4j0u.1.A, 5hb0.3.A, 3ro3.1.A, 5l8w.1.B, 4wsl.1.A, 3f3p.2.B, 5omp.1.A, 1pfq.1.A, 4cr2.1.X, 1pfq.1.B, 4cr2.1.W, 4cr2.1.U, 5wbk.1.A, 4v7f.1.j, 4gm3.1.A, 3jcm.1.D, 3jcm.1.B, 3v7d.1.B, 2bcj.1.B, 4d10.1.D, 4d10.1.B, 4d10.1.A, 5w5y.1.O, 5gpy.1.A, 5jj6.1.A, 5jj6.1.B, 1qbq.1.A, 1mzc.1.A, 5t2a.48.A, 2wpv.1.A, 2crb.1.A, 3nok.1.A, 1w3b.1.B, 5arf.1.A, 4r40.1.A, 3iuq.1.A, 2cn3.1.A, 5x4z.1.L, 4cr2.1.6, 3sww.1.A, 2xpi.1.C, 2xpi.1.A, 2hqs.1.A, 3o4i.1.A, 5mwj.1.A, 3zn3.1.A, 4cy2.1.A, 3wj9.1.A, 2fpb.1.A, 4v92.1.8, 2xeu.1.A, 2i3t.1.A, 5vhm.1.H, 5o3w.1.A, 1z2z.2.A, 3jro.1.A, 3jan.80.A, 4wnd.1.A, 5d0i.1.A, 5jpq.1.I, 2fp9.1.A, 6epe.1.U, 4bts.27.A, 5hb2.1.A, 1wy6.1.A, 2iap.1.A, 2o9k.1.A, 3esk.1.A, 2xgm.2.A, 4e5z.1.A, 6epd.1.X, 5udl.1.A, 4av8.1.A, 2z2p.1.A, 2w8b.2.A, 4a0b.1.B, 3asd.1.A, 4a0b.1.A, 2wb7.1.A, 4eba.2.A, 5wbi.1.A, 5tee.1.A, 3bg0.1.A, 3fwv.1.A, 3bg0.1.H, 5jno.1.B, 5nnz.2.A, 5y3r.1.F, 5juy.1.B, 5d0o.1.B, 5juy.1.G, 5juy.1.D, 5juy.1.E, 3v65.1.C, 3v65.1.B, 3tkn.1.A, 3hac.1.A, 5lxz.1.A, 2ivz.1.A, 5hyn.2.B, 5juo.45.A, 3rfh.1.A, 3rfh.1.B, 5ccm.1.A, 5fzp.1.A, 2pk7.1.A, 3fp2.1.A, 2pk7.1.B, 5em2.1.B, 5em2.1.A, 4xgl.1.A, 5ams.1.A, 2hf1.2.A, 5mzh.1.A, 3i7p.1.A, 4fhn.2.B, 5wg4.1.B, 5m32.1.a, 5m32.1.b, 5m32.1.c, 4wsn.6.B, 4xmb.1.A, 6f5d.1.J, 6f5d.1.K, 6f5d.1.L, 4wsn.2.B, 4wsn.2.A, 4wsn.2.D, 2ifu.1.A, 4c8s.1.A, 2wqh.1.A, 2xe4.1.A, 5a5u.1.B, 4u7a.1.A, 5lcw.1.Q, 5lcw.1.R, 4pv7.1.A, 5m32.1.9, 2dso.1.A, 2f0y.1.A, 5lcw.1.C, 5lcw.1.O, 5lcw.1.I, 4i2w.1.A, 4yvo.1.A, 5lwv.1.A, 5buz.1.B, 4yhc.1.A, 5i1z.5.C, 2wq8.1.A, 3ma5.4.A, 4exv.1.A, 3qww.1.A, 3ddu.1.A, 4gq2.1.B, 4gq2.1.A, 1fch.2.A, 3qbj.1.A, 4i79.1.A, 2b5n.1.A, 2vpj.1.A, 2z2o.1.A, 5w64.1.O, 1qni.1.A, 4o9d.2.A, 2d2s.1.A, 3oxg.1.A, 4ria.1.A, 4zov.1.A, 3wqh.1.A, 3wqh.1.B, 3ei4.3.A, 3dra.1.A, 4zlh.1.A, 4d4p.1.A, 1r9n.1.A, 2nc9.1.A, 5xi8.1.A, 4j0x.1.A, 1na3.1.A, 4zlr.1.A, 2xbg.1.A, 1ldj.1.B, 2hr5.1.A, 2gvu.1.A, 5l0w.1.A, 4xei.1.C, 5ft9.1.A, 4j8f.1.A, 2kat.1.A, 5xw7.1.A, 2jid.1.A, 2b5n.3.A, 1lv3.1.A, 2z2o.3.A, 4xga.1.A, 2ghs.1.A, 3rrm.1.C, 5wcg.1.A, 2aq5.1.A, 1iip.1.A, 5uz5.1.D, 5uz5.1.E, 4gqb.1.B, 4a0l.1.B, 5fzq.1.C, 5lls.1.A, 5fzq.1.A, 5x6o.1.A, 1o6g.1.A, 6bcu.1.A, 5l0y.5.B, 5l0y.5.A, 6bcu.1.B, 4mh1.1.A, 4mh1.1.B, 1spw.1.A, 5vat.2.A, 5l0y.3.A, 3s8v.1.A, 3iur.1.A, 5hq8.1.A, 3f3f.1.A, 1x2r.1.A, 4pwz.1.A, 5g04.1.I, 5mpe.1.K, 2eid.1.A, 2j04.1.A, 5o3x.1.A, 3n0e.1.A, 2j04.1.B, 3ei2.1.A, 3ei2.1.B, 1na0.1.A, 2uwj.1.C, 2wg3.1.B, 4j0w.1.A, 2zet.1.B, 2vsn.1.A, 2v91.1.A, 2h0d.1.A, 3u3w.1.B, 2iaw.1.A, 1t2x.1.A, 3scy.1.A, 1kt0.1.A, 2b5l.2.A, 3jco.1.Y, 3jco.1.Z, 3jco.1.W, 2onc.1.A, 5grs.1.A, 4a7j.1.A, 4pwx.1.C, 5tbk.5.B, 4kzz.1.6, 3jco.1.0, 2oit.1.A, 3tc9.1.A, 4i0o.1.A, 5a6c.2.A, 3jaq.1.i, 1pev.1.A, 2iau.1.A, 3e4b.3.A, 5n4c.1.A, 5wlc.24.A, 2pm6.1.C, 5dfz.1.C, 5wlc.22.A, 2qr5.1.A, 2l6j.1.A, 5che.1.E, 5che.1.F, 5wlc.20.A, 1a12.1.B, 4n3c.1.A, 1a12.1.A, 3ly8.1.A, 2cnx.1.A, 1k32.1.A, 5i9f.1.A, 3vty.3.A, 3g4h.1.B, 3g4h.1.A, 2p58.1.C, 4dnw.1.A, 5ttw.2.A, 4zn4.1.A, 4u1e.1.A, 1d8d.1.A, 4ayb.1.L, 5i2t.1.A, 5txe.1.A, 4gga.1.A, 3f3p.2.C, 4bh6.1.A, 1got.1.B, 3of7.1.A, 3s25.1.A, 3p1l.1.A, 5ctq.2.B, 5ctq.2.A, 4e6h.1.A, 3vnh.1.A, 5lzz.77.A, 3j98.1.I, 3j98.1.H, 4buj.2.B, 3vng.1.A, 3ceq.1.A, 3ceq.1.B, 4naa.1.A, 4ay5.1.A, 2wb7.2.A, 5xon.1.L, 4fzo.1.B, 4fzo.1.A, 2xev.2.A, 5fzr.1.A, 5fzr.1.B, 3wwb.1.A, 4cr2.1.Y, 4r8p.1.K, 4d5l.1.7, 4ri9.1.A, 5xgs.1.A, 4ggc.1.A, 4ynv.1.A, 4buj.1.D, 5fzq.1.B, 2pbi.1.B, 3jai.77.A, 2pzi.1.A, 4yzs.1.A, 3f8s.1.A, 3f3f.1.C, 4yzs.1.B, 3f3f.1.D, 3f3f.1.G, 5hb3.2.A, 5i9h.1.A, 3fp3.1.A, 5nnp.2.A, 2pm6.1.B, 5vhq.1.H, 2pm6.1.A, 2wft.1.A, 4rid.1.A, 4dnu.1.A, 3v9f.3.A, 5ex3.1.A, 3c5m.1.A, 5uz7.1.B, 3e5z.1.A, 5ic8.4.A, 1wcy.1.A, 1u4c.1.A, 3v9f.1.A, 4ci8.2.A

SWISS-MODEL Homology Modelling Report

Model Building Report

This document lists the results for the homology modelling project "TT21B_HUMAN Q7Z4L5 Tetratricopeptide repeat protein 21B" submitted to SWISS-MODEL workspace on Feb. 26, 2018, 9:40 a.m..The submitted primary amino acid sequence is given in Table T1.

If you use any results in your research, please cite the relevant publications:

- Biasini, M., Bienert, S., Waterhouse, A., Arnold, K., Studer, G., Schmidt, T., Kiefer, F., Cassarino, T.G., Bertoni, M., Bordoli, L., Schwede, T. SWISS-MODEL: modelling protein tertiary and quaternary structure using evolutionary information. Nucleic Acids Res. 42, W252-W258 (2014). doi
- Guex, N., Peitsch, M.C., Schwede, T. Automated comparative protein structure modeling with SWISS-MODEL and Swiss-PdbViewer: A historical perspective. Electrophoresis 30, S162-S173 (2009). doi
- Bienert, S., Waterhouse, A., de Beer, T.A., Tauriello, G., Studer, G., Bordoli, L., Schwede, T. The SWISS-MODEL Repository - new features and functionality. Nucleic Acids Res. 45, D313-D319 (2017). doi
- Benkert, P., Biasini, M., Schwede, T. Toward the estimation of the absolute quality of individual protein structure models. Bioinformatics 27, 343-350 (2011). doi
- Bertoni, M., Kiefer, F., Biasini, M., Bordoli, L., Schwede, T. Modeling protein quaternary structure of homo- and hetero-oligomers beyond binary interactions by homology. Scientific Reports 7 (2017). doi

Results

The SWISS-MODEL template library (SMTL version 2018-02-21, PDB release 2018-02-16) was searched with BLAST (Camacho et al.) and HHBlits (Remmert, et al.) for evolutionary related structures matching the target sequence in Table T1. For details on the template search, see Materials and Methods. Overall 2147 templates were found (Table T2).

Models

The following models were built (see Materials and Methods "Model Building"):

Model #01	File	Built with	Oligo-State	Ligands	GMQE	QMEAN
	PDB	ProMod3 Version 1.1.0.	monomer	None	0.36	-3.42

QMEAN	-3.42
Cβ	-1.94
All Atom	-0.47
Solvation	1.22
Torsion	-3.19

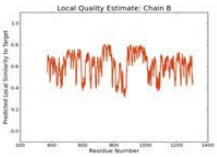

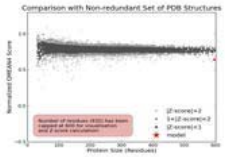

Template	Seq Identity	Oligo-state	Found by	Method	Resolution	Seq Similarity	Range	Coverage	Description
4buj.1.B	12.04	monomer	HHblits	X-ray	3.70Å	0.25	374 - 1305	0.64	SUPERKILLER PROTEIN 3

Ligand	Added to Model	Description
SO4	× - Not biologically relevant.	SULFATE ION
SO4	× - Not biologically relevant.	SULFATE ION
SO4	× - Not biologically relevant.	SULFATE ION
SO4	× - Not biologically relevant.	SULFATE ION
SO4	× - Not biologically relevant.	SULFATE ION
SO4	× - Not biologically relevant.	SULFATE ION
SO4	× - Not biologically relevant.	SULFATE ION
SO4	× - Not biologically relevant.	SULFATE ION
SO4	× - Not biologically relevant.	SULFATE ION
SO4	× - Not biologically relevant.	SULFATE ION
SO4	× - Not biologically relevant.	SULFATE ION

```
Target    MDSQELKTLINYYCQERYFHHVLLVASEGIKRYGSDPVFRFYHAYGTLMEGKTQEALREFEAIKNKQDVSLCSLLALIYA
4buj.1.B  ----------------------------------------------------------------------------------

Target    HKMSPNPDREAILESDARVKEQRKGAGEKALYHAGLFLWHIGRHDKAREYIDRMIKISDGSKQGHVLKAWLDITRGKEPY
4buj.1.B  ----------------------------------------------------------------------------------

Target    TKKALKYFEEGLQDGNDTFALLGKAQCLEMRQNYSGALETVNQIIVNFPSFLPAFVKKMKLQLALQDWDQTVETAQRLLL
4buj.1.B  ----------------------------------------------------------------------------------

Target    QDSQNVEALRMQALYYVCREGDIEKASTKLENLGNTLDAMEPQNAQLFYNITLAFSRTCGRSQLILQKIQTLLERAFSLN
4buj.1.B  ----------------------------------------------------------------------------------

Target    PQQSEFATELGYQMILQGRVKEALKWYKTAMTLDETSVSALVGFIQCQLIEGQLQDADQQLEFLNEIQQSIGKSAELIYL
4buj.1.B  ----------------------------------------------------EEEVVTVLTENIVKCK---NNILAHRI

Target    HAVLAMKKNKRQEEVINLLNDVLDTHFSQLEGLPLGIQYFEKLNPDFLLEIVMEYLSFCPMQPASPGQPLCPLLRRCISV
4buj.1.B  LCQYYLLTK-EYEAALPYIKNGISLIAYNIKDL--GVH-LPLTKREFSLDLATVYTYVD----------APKDHNAALKL

Target    LETVVRTVPGLLQTVFLIAKVKYLSGDIEAAFNNLQHCLEHNPSYADAHLLLAQVYLSQEKVKLCSQSLELCLSYDFKVR
4buj.1.B  YDNILSGDFSNIQAKMGKGIIFIERKNWKDAMTLLTQVHEQSPNNLEVLSELSWSKAHMGYMDEALAGLDTVIKGIKGMD

Target    D-----YPLYHLIKAQSQKK---------MGEIADAIKTLHMAMSLPGMKRIGASTKSKDRKTEVDTSHRLSIFLELIDV
4buj.1.B  LRSIDFRALNLWRQAKVYIMKHASINDAKQENVKCAFKLLIQSIKILD--------------------TFAPGFSTLGDI

Target    HRL-NGEQHEATKVLQDAIHEFSGTSEEVRVTIANADLALAQGDIERALSILQNVTAEQ------PYFIEAREKMADIYL
4buj.1.B  YCHYYKDHLRAFKCYFKAFDLDAGDYT---AAKYITETYASKPNWQAASSIASRLIKGEKAKAELRSNNWPFRVVGIAHL

Target    KHRKDKMLYITCFREIAERMAN-PRSFLLLGDAYMNILEPEEAIVAYEQALNQNPKDGTLASKMGKALIKTHNYSMAITY
4buj.1.B  EKQE-ESDSIEWFQSALRVDPNDVESWVGLGQAYHACGRIEASIKVFDKAIQLRPSHTFAQYFKAISLCDVGEYLESLDI

Target    YEAALKTGQKNY--------LCYDLAELLLKLKWYDKAEK-------VLQHAL-AHEPVNELSALMEDGRCQVLLAKVYS
4buj.1.B  LEKVCQEAATEESFQIGLVEVLMRCSLDLYSQGFLLKSVSIAKDTIERIKIIISELKCE--------NQQVWIYLSQVLR

Target    KMEKLGDAIT----------------------------------------------------ALQQARELQARVLKRVQME
4buj.1.B  LFIWIESKVDTLPVESLVSIFENSQFSGSEEIDSVDNIKIDTLLDSTTDDNVSIACKFLILASKYSVSDQ----------

Target    QPDAVPAQKHLAAEICAEIAKHSV-------AQRDYEKAIKFYREALVHCETDNKIMLELARLYLAQDDPDSCLRQCALL
4buj.1.B  -KFTDI-AGTVRASYWYNIGISELTAFITLKEPQYRDAAIFAFKKSIQLQSNTSETWIGLGIATMDI-NFRVSQHCFIKA

Target    LQSDQDNEAATMMMADLMFRKQDYEQAVFHLQQLLERKPDNYMTLSRLIDLLRRCGKLEDVPRFFSMAEKRNSRAKLEPG
4buj.1.B  TALEPKATNTWFNLAMLGLKKKDTEFAQQVLNKLQSLAPQDSSPWLGMALILEEQGDIIGSSKLFAHSFILSNGRSKAAQ

Target    FQYCKGLYLWY------------TGEPNDALRHFNKARKDRDWGQNALYNMIEICLNPDNETVGGEVFENLDGDLGNSTE
4buj.1.B  FMYAKNVLENHINNGDDERDIETVEKLTTASIALEQFFKKSPDSQFALQCALLTLER-----------------------

Target    KQESVQLAVRTAEKLLKELK-----PQTVQGHVQLR-IMENYCLMATKQKSNVEQALNTFTEIAASEKEH---------I
4buj.1.B  -LHHYENANELANRLIGILEKKFEKTQDERELFNFAIIKGQFA-RIHLGLGNFELSIENADLSQGIISESSDEKSMKTKI

Target    PALLGMATAYMILKQTPRARNQLKRIAKMNWNAIDAEEFEKSWLLLADIYIQSAKYD---MAEDLLKRCLRHNRSCCKAY
4buj.1.B  SNHICLGLSYFFLNDFDQTLNQFQELLSISKDS------KHLVVLIAKVLYDVGESDTKEIALQELTEYIATSGADLLVT

Target    EYMGYIMEKEQAYTDAALNYEMAWKYSNRTN-----PAVGYKLAFNYLKAKRYVDSIDICHQVLEAHPTYPKIRKDILDK
4buj.1.B  LTIAAMSILDDKREDLSIILEELKALPLSKQIIDKHKDAPYLIEEITKRLYRNDTGKQVWQRSAYFFPNNLKVWER----

Target    ARASLRP
4buj.1.B  -------
```

Model #02	File	Built with	Oligo-State	Ligands	GMQE	QMEAN
	PDB	ProMod3 Version 1.1.0.	monomer	None	0.16	-5.57

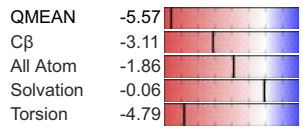

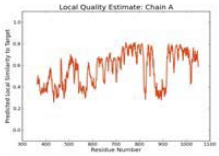

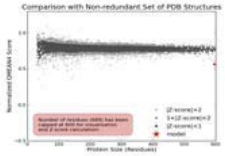

Template	Seq Identity	Oligo-state	Found by	Method	Resolution	Seq Similarity	Range	Coverage	Description

Template	Seq Identity	Oligo-state	Found by	Method	Resolution	Seq Similarity	Range	Coverage	Description
5dse.1.A	15.45	monomer	HHblits	X-ray	2.90Å	0.26	363 - 1051	0.55	Tetratricopeptide repeat protein 7B

The template contained no ligands.

```
Target    MDSQELKTLINYYCQERYFHHVLLVASEGIKRYGSDPVFRFYHAYGTLMEGKTQEALREFEAIKNKQDVSLCSLLALIYA
5dse.1.A  ------------------------------------------------------------------------------

Target    HKMSPNPDREAILESDARVKEQRKGAGEKALYHAGLFLWHIGRHDKAREYIDRMIKISDGSKQGHVLKAWLDITRGKEPY
5dse.1.A  ------------------------------------------------------------------------------

Target    TKKALKYFEEGLQDGNDTFALLGKAQCLEMRQNYSGALETVNQIIVNFPSFLPAFVKKMKLQLALQDWDQTVETAQRLLL
5dse.1.A  ------------------------------------------------------------SECQWERIPELVKQLSA

Target    QDSQNV-EALRMQALYYVCREGDIEKASTKLENLGNTLDAMEPQNAQLFYNITLAFSRTCGRSQLILQKIQTLLERAFSL
5dse.1.A  KLIANDDMAELLLGE-----------S--KLEQYLKE----HPLRQG----------ASPRGPKPQLTEVRKHLTAALDR

Target    ----NPQQSEFATELGYQMILQGRVKEALKWYKTAM----TLDETSVSALVGFIQCQLIEGQLQDADQQLEFLNEIQQSI
5dse.1.A  GNLKSEFLQESNLIMAKLNYVEGDYKEALNIYARVGLDDLPLTAVPPYRLRVIAEAYATKGLCL----------EKLPIS

Target    GKSAELIYLHAVLAMKKNKRQEEVINLLNDVLDTHFSQLEGLPLGIQYFEKLNPDFLLEIVMEYLSFCPMQPASPGQPLC
5dse.1.A  SSTS----------NLHVDREQDVITCYEKAGDIALL----------YLQEIERV--------ILSNIQNRSPKPG--PA

Target    PLLRRCISVLETVVRTVPGLLQTVFLIAKVKYLSGDIEAAFNNLQHCLEHNPSYAD------AHLLLAQVYLSQEK---V
5dse.1.A  PH-D---------QELGFFLETGLQRAHVLYFKNGNLTRGVGRFRELLRAVETRTTQNLRMTIARQLAEILLRGMCEQSY

Target    KLCSQSLELC-------LSYDFKVRDY---PLYHLIKAQSQKKMGEIADAIKTL---------HMAMSLPGMKRIGASTK
5dse.1.A  WNPLEDPPCQSPLDDPLRKGANTKTYTLTRRARVYSGENIFCPQENTEEALLLLLISESMANRDAVLSRIPEHKSD----

Target    SKDRKTEVDTSHRLSIFLELIDVHRLNGEQHEATKVLQDAIHEFSGTSEEVRVTIANADLALAQGDIERALSILQNVTAE
5dse.1.A  -----RLISLQSASVVYDLLTIALGRRGQYEMLSECLERAMKFAFEEF---HLWYQFALSLMAAGKSARAVKVLKECIRL

Target    QPYFIEAREKMADIYLKHRKDKMLYITCFREIAERMANP-R----SFLLLGDAYM-----------NILEPEEAIVAYEQ
5dse.1.A  KPDDATIPLLAAKLCMGSLHWLEEAEKFAKTVVDVGEKTSEFKAKGYLALGLTYSLQATDASLRGMQEVLQRKALLAFQR

Target    ALNQNPKDGTLASKMGKALIKTHNYSMAITYYEAALKTGQKNY-LCYDLAELLLKLKWYDKAEKVLQHALAHEPVNELSA
5dse.1.A  AHSLSPTDHQAAFYLALQLAISRQIPEALGYVRQALQLQGDDANSLHLLALLLSAQKHYHDALNIIDMALSEYPE-----

Target    LMEDGRCQVLLAKVYSKMEKLGDAITALQQARELQARVLKRVQMEQPDAVPAQKHLAAEI-------------------C
5dse.1.A  ---NFILLFSKVKLQSLCRGPDEALLTCKHMLQIWKSCYNL---TNPSDSGRGSSLLDRTIADRRQLNTITLPDFSDPET

Target    AEIAKHSVAQRDYEKAIKFYREALVHC-----ET-----DNKIMLELARLYLAQDDPDSCLRQCALLLQSDQDNEAATMM
5dse.1.A  GSVHATSVAASRVEQALSEVASSLQSSAPKQGPLHPWMTLAQIWLHAAEVYIGIGKPAEATACTQEAANLFPMSHNVLYM

Target    MADLMFRKQDYEQAVFHLQQLLERKPDNYMTLSRLIDLLRRCGKLEDVPRFFSMAEKRNSRAKLEPGFQYCKGLYLWYTG
5dse.1.A  RGQIAELRGSMDEARRWYEEALAISPTHVKSMQRLALILHQLGRYSLAEKILRDAVQVNS---TAHEVWNGLGEVLQAQG

Target    EPNDALRHFNKARKDRDWGQNALYNMIEICLNPDNETVGGEVFENLDGDLGNSTEKQESVQLAVRTAEKLLKELKPQTVQ
5dse.1.A  NDAAATECFLTALE------------------------------------------------------------------

Target    GHVQLRIMENYCLMATKQKSNVEQALNTFTEIAASEKEHIPALLGMATAYMILKQTPRARNQLKRIAKMNWNAIDAEEFE
5dse.1.A  ------------------------------------------------------------------------------

Target    KSWLLLADIYIQSAKYDMAEDLLKRCLRHNRSCCKAYEYMGYIMEKEQAYTDAALNYEMAWKYSNRTNPAVGYKLAFNYL
5dse.1.A  ------------------------------------------------------------------------------

Target    KAKRYVDSIDICHQVLEAHPTYPKIRKDILDKARASLRP
5dse.1.A  ---------------------------------------
```

Materials and Methods

Template Search

Template search with BLAST and HHBlits has been performed against the SWISS-MODEL template library (SMTL, last update: 2018-02-21, last included PDB release: 2018-02-16).

The target sequence was searched with BLAST against the primary amino acid sequence contained in the SMTL. A total of 10 templates were found.

An initial HHblits profile has been built using the procedure outlined in (Remmert, et al.), followed by 1 iteration of HHblits against NR20. The obtained profile has then be searched against all profiles of the SMTL. A total of 2149 templates were found.

Template Selection

For each identified template, the template's quality has been predicted from features of the target-template alignment. The templates with the highest quality have then been selected for model building.

Model Building

Models are built based on the target-template alignment using ProMod3. Coordinates which are conserved between the target and the template are copied from the template to the model. Insertions and deletions are remodelled using a fragment library. Side chains are then rebuilt. Finally, the geometry of the resulting model is regularized by using a force field. In case loop modelling with ProMod3 fails, an alternative model is built with PROMOD-II (Guex, et al.).

Model Quality Estimation

The global and per-residue model quality has been assessed using the QMEAN scoring function (Benkert, et al.) . For improved performance, weights of the individual QMEAN terms have been trained specifically for SWISS-MODEL.

Ligand Modelling

Ligands present in the template structure are transferred by homology to the model when the following criteria are met: (a) The ligands are annotated as biologically relevant in the template library, (b) the ligand is in contact with the model, (c) the ligand is not clashing with the protein, (d) the residues in contact with the ligand are conserved between the target and the template. If any of these four criteria is not satisfied, a certain ligand will not be included in the model. The model summary includes information on why and which ligand has not been included.

Oligomeric State Conservation

The quaternary structure annotation of the template is used to model the target sequence in its oligomeric form. The method (Bertoni et al.) is based on a supervised machine learning algorithm, Support Vector Machines (SVM), which combines interface conservation, structural clustering, and other template features to provide a quaternary structure quality estimate (QSQE). The QSQE score is a number between 0 and 1, reflecting the expected accuracy of the interchain contacts for a model built based a given alignment and template. Higher numbers indicate higher reliability. This complements the GMQE score which estimates the accuracy of the tertiary structure of the resulting model.

References

- **BLAST**
  Camacho, C., Coulouris, G., Avagyan, V., Ma, N., Papadopoulos, J., Bealer, K., Madden, T.L. BLAST+: architecture and applications. BMC Bioinformatics 10, 421-430 (2009). doi
- **HHblits**
  Remmert, M., Biegert, A., Hauser, A., Söding, J. HHblits: lightning-fast iterative protein sequence searching by HMM-HMM alignment. Nat Methods 9, 173-175 (2012). doi

Table T1:

Primary amino acid sequence for which templates were searched and models were built.

```
MDSQELKTLINYYCQERYFHHVLLVASEGIKRYGSDPVFRFYHAYGTLMEGKTQEALREFEAIKNKQDVSLCSLLALIYAHKMSPNPDREAILESDARVK
EQRKGAGEKALYHAGLFLWHIGRHDKAREYIDRMIKISDGSKQGHVLKAWLDITRGKEPYTKKALKYFEEGLQDGNDTFALLGKAQCLEMRQNYSGALET
VNQIIVNFPSFLPAFVKKMKLQLALQDWDQTVETAQRLLLQDSQNVEALRMQALYYVCREGDIEKASTKLENLGNTLDAMEPQNAQLFYNITLAFSRTCG
RSQLILQKIQTLLERAFSLNPQQSEFATELGYQMILQGRVKEALKWYKTAMTLDETSVSALVGFIQCQLIEGQLQDADQQLEFLNEIQQSIGKSAELIYL
HAVLAMKKNKRQEEVINLLNDVLDTHFSQLEGLPLGIQYFEKLNPDFLLEIVMEYLSFCPMQPASPGQPLCPLLRRCISVLETVVRTVPGLLQTVFLIAK
VKYLSGDIEAAFNNLQHCLEHNPSYADAHLLLAQVYLSQEKVKLCSQSLELCLSYDFKVRDYPLYHLIKAQSQKKMGEIADAIKTLHMAMSLPGMKRIGA
STKSKDRKTEVDTSHRLSIFLELIDVHRLNGEQHEATKVLQDAIHEFSGTSEEVRVTIANADLALAQGDIERALSILQNVTAEQPYFIEAREKMADIYLK
HRKDKMLYITCFREIAERMANPRSFLLLGDAYMNILEPEEAIVAYEQALNQNPKDGTLASKMGKALIKTHNYSMAITYYEAALKTGQKNYLCYDLAELLL
KLKWYDKAEKVLQHALAHEPVNELSALMEDGRCQVLLAKVYSKMEKLGDAITALQQARELQARVLKRVQMEQPDAVPAQKHLAAEICAEIAKHSVAQRDY
EKAIKFYREALVHCETDNKIMLELARLYLAQDDPDSCLRQCALLLQSDQDNEAATMMMADLMFRKQDYEQAVFHLQQLLERKPDNYMTLSRLIDLLRRCG
KLEDVPRFFSMAEKRNSRAKLEPGFQYCKGLYLWYTGEPNDALRHFNKARKDRDWGQNALYNMIEICLNPDNETVGGEVFENLDGDLGNSTEKQESVQLA
VRTAEKLLKELKPQTVQGHVQLRIMENYCLMATKQKSNVEQALNTFTEIAASEKEHIPALLGMATAYMILKQTPRARNQLKRIAKMNWNAIDAEEFEKSW
LLLADIYIQSAKYDMAEDLLKRCLRHNRSCCKAYEYMGYIMEKEQAYTDAALNYEMAWKYSNRTNPAVGYKLAFNYLKAKRYVDSIDICHQVLEAHPTYP
KIRKDILDKARASLRP
```

Table T2:

Template	Seq Identity	Oligo-state	QSQE	Found by	Method	Resolution	Seq Similarity	Coverage	Description
5mc6.35.A	12.04	monomer		HHblits	EM	NA	0.25	0.64	Superkiller protein 3
4buj.1.B	12.04	monomer		HHblits	X-ray	3.70Å	0.25	0.64	SUPERKILLER PROTEIN 3
4buj.2.B	12.04	monomer		HHblits	X-ray	3.70Å	0.25	0.64	SUPERKILLER PROTEIN 3
4buj.1.B	12.05	monomer		HHblits	X-ray	3.70Å	0.26	0.57	SUPERKILLER PROTEIN 3
4buj.2.B	12.05	monomer		HHblits	X-ray	3.70Å	0.26	0.57	SUPERKILLER PROTEIN 3
5mc6.35.A	11.92	monomer		HHblits	EM	NA	0.26	0.57	Superkiller protein 3
6bq1.1.B	14.99	monomer		HHblits	EM	NA	0.26	0.56	Tetratricopeptide repeat protein 7B
5dse.1.A	15.45	monomer		HHblits	X-ray	2.90Å	0.26	0.55	Tetratricopeptide repeat protein 7B
5dse.2.A	15.45	monomer		HHblits	X-ray	2.90Å	0.26	0.55	Tetratricopeptide repeat protein 7B
5xjc.1.I	12.09	monomer		HHblits	EM	3.60Å	0.26	0.53	Pre-mRNA-splicing factor SYF1
5mqf.1.M	12.09	monomer		HHblits	EM	NA	0.26	0.53	Pre-mRNA-splicing factor SYF1
5dse.1.A	14.16	monomer		HHblits	X-ray	2.90Å	0.26	0.53	Tetratricopeptide repeat protein 7B

Template	Seq Identity	Oligo-state	QSQE	Found by	Method	Resolution	Seq Similarity	Coverage	Description
5dse.2.A	14.16	monomer		HHblits	X-ray	2.90Å	0.26	0.53	Tetratricopeptide repeat protein 7B
4m59.1.A	13.72	homo-dimer		HHblits	X-ray	2.46Å	0.26	0.52	Chloroplast pentatricopeptide repeat protein 10
4m59.1.B	13.72	homo-dimer		HHblits	X-ray	2.46Å	0.26	0.52	Chloroplast pentatricopeptide repeat protein 10
5xjc.1.I	10.79	monomer		HHblits	EM	3.60Å	0.25	0.52	Pre-mRNA-splicing factor SYF1
5mqf.1.M	10.79	monomer		HHblits	EM	NA	0.25	0.52	Pre-mRNA-splicing factor SYF1
4kvo.1.A	13.63	monomer		HHblits	X-ray	3.15Å	0.26	0.51	N-terminal acetyltransferase A complex subunit nat1
6bq1.1.B	14.37	monomer		HHblits	EM	NA	0.26	0.51	Tetratricopeptide repeat protein 7B
4oe1.1.A	14.01	homo-dimer		HHblits	X-ray	2.80Å	0.26	0.51	Chloroplast pentatricopeptide repeat protein 10
4oe1.1.B	14.01	homo-dimer		HHblits	X-ray	2.80Å	0.26	0.51	Chloroplast pentatricopeptide repeat protein 10
5nnp.1.A	14.33	monomer		HHblits	X-ray	2.60Å	0.27	0.50	N-terminal acetyltransferase-like protein
5nnp.2.A	14.33	monomer		HHblits	X-ray	2.60Å	0.27	0.50	N-terminal acetyltransferase-like protein
5nnr.1.A	14.50	monomer		HHblits	X-ray	3.10Å	0.27	0.50	N-terminal acetyltransferase-like protein
5lj3.1.U	11.56	monomer		HHblits	EM	3.80Å	0.24	0.51	SYF1
5mps.1.R	11.85	monomer		HHblits	EM	3.85Å	0.24	0.51	Pre-mRNA-splicing factor SYF1
6exn.1.S	11.56	monomer		HHblits	EM	NA	0.24	0.51	Pre-mRNA-splicing factor SYF1
4m59.1.A	10.39	homo-dimer		HHblits	X-ray	2.46Å	0.25	0.50	Chloroplast pentatricopeptide repeat protein 10
4m59.1.B	10.39	homo-dimer		HHblits	X-ray	2.46Å	0.25	0.50	Chloroplast pentatricopeptide repeat protein 10
4oe1.1.A	10.39	homo-dimer		HHblits	X-ray	2.80Å	0.25	0.50	Chloroplast pentatricopeptide repeat protein 10
4oe1.1.B	10.39	homo-dimer		HHblits	X-ray	2.80Å	0.25	0.50	Chloroplast pentatricopeptide repeat protein 10
4m57.1.A	10.41	homo-dimer		HHblits	X-ray	2.86Å	0.25	0.50	Chloroplast pentatricopeptide repeat protein 10
4m57.1.A	14.31	homo-dimer		HHblits	X-ray	2.86Å	0.26	0.50	Chloroplast pentatricopeptide repeat protein 10
5lj5.1.V	12.13	monomer		HHblits	EM	3.80Å	0.25	0.51	Pre-mRNA-splicing factor SYF1
6bk8.1.W	12.13	monomer		HHblits	EM	NA	0.25	0.51	Pre-mRNA-splicing factor SYF1
5lj3.1.U	9.28	monomer		HHblits	EM	3.80Å	0.24	0.51	SYF1
6exn.1.S	9.45	monomer		HHblits	EM	NA	0.24	0.51	Pre-mRNA-splicing factor SYF1
5gap.1.G	11.69	monomer		HHblits	EM	3.60Å	0.26	0.49	Pre-mRNA-splicing factor 6
3jcm.1.D	11.69	monomer		HHblits	EM	NA	0.26	0.49	Pre-mRNA-splicing factor 6
5nrl.1.Q	11.69	monomer		HHblits	EM	NA	0.26	0.49	Pre-mRNA-splicing factor 6
5o9z.1.G	14.22	monomer		HHblits	EM	NA	0.26	0.48	Pre-mRNA-processing factor 6
5o9z.1.G	13.76	monomer		HHblits	EM	NA	0.26	0.47	Pre-mRNA-processing factor 6
5gap.1.G	12.16	monomer		HHblits	EM	3.60Å	0.26	0.47	Pre-mRNA-splicing factor 6
3jcm.1.D	12.16	monomer		HHblits	EM	NA	0.26	0.47	Pre-mRNA-splicing factor 6
5nrl.1.Q	12.16	monomer		HHblits	EM	NA	0.26	0.47	Pre-mRNA-splicing factor 6
5vhj.1.H	12.86	monomer		HHblits	EM	NA	0.25	0.44	26S proteasome non-ATPase regulatory subunit 2
5lj3.1.T	12.18	monomer		HHblits	EM	3.80Å	0.26	0.42	CLF1
5mps.1.Q	12.36	monomer		HHblits	EM	3.85Å	0.26	0.42	Pre-mRNA-splicing factor CLF1
5lj5.1.U	12.36	monomer		HHblits	EM	3.80Å	0.26	0.42	Pre-mRNA-splicing factor CLF1
6bk8.1.V	12.36	monomer		HHblits	EM	NA	0.26	0.42	Pre-mRNA-splicing factor CLF1

The table above shows the top 50 filtered templates. A further 1,086 templates were found which were considered to be less suitable for modelling than the filtered list.
5gm6.1.4, 5w66.1.Q, 5lyn.1.A, 5gm6.1.2, 2c2l.1.A, 1fpp.1.B, 4p29.1.A, 4a1s.1.A, 5efr.1.A, 1ihg.1.A, 1a17.1.A, 5a31.1.V, 3gw4.1.A, 1ya0.1.A, 4bt9.1.B, 1x81.1.A, 2ifu.2.A, 3r9a.1.D, 4di3.1.D, 2p58.1.C, 5vgz.1.G, 3r9a.1.B, 1tnu.1.A, 5vgz.1.J, 5vgz.1.H, 5vgz.1.M, 1qqe.1.A, 4u0u.1.A, 4mbq.2.A, 5en7.2.A, 5m32.1.b, 4eba.1.A, 4d10.1.C, 2n8w.1.A, 5oql.1.E, 1iip.1.A, 4ui9.1.P, 4n5c.8.A, 4ui9.1.V, 4ui9.1.W, 4ui9.1.J, 4ui9.1.K, 4ui9.1.H, 3oxf.1.A, 4ui9.1.O, 4ui9.1.C, 5oj8.1.A, 5w65.1.Q, 4ui9.1.F, 4n5c.6.A, 4e85.1.A, 3q15.1.A, 3ieg.2.A, 3ulq.1.A, 5vhs.1.H, 5iwb.1.B, 4rib.1.A, 5vhr.1.H, 5jzz.1.A, 2y4u.1.A, 2q7f.1.A, 3ash.1.A, 2o98.1.B, 4osr.2.A, 4r8a.1.A, 1hh8.1.A, 4cr4.1.U, 4cr4.1.W, 5lfm.1.A, 4yvq.1.B, 3pz2.1.A, 4y32.1.A, 4cr4.1.X, 3kd7.1.A, 4leu.1.A, 6f08.2.A, 2bug.1.A, 5lu1.1.A, 5lu1.1.B, 5xw7.3.A, 1nl4.1.A, 5wxn.1.A, 5uz5.1.E, 3hxe.1.A, 4jsn.1.A, 4yv6.2.B, 5izw.1.A, 4d10.1.A, 6f08.1.B, 5bw8.1.C, 1qbq.1.A, 5wsg.1.R, 3mv3.1.B, 3lya.1.A, 5wsg.1.T, 5a5b.1.Z, 2yhc.1.A, 5g05.1.K, 4rid.2.A, 4i1a.1.A, 5g05.1.C, 3lw1.1.A, 5a5b.1.W, 5g05.1.F,

5mpd.1.K, 3euv.1.A, 5mpd.1.I, 5mpd.1.H, 4ady.1.A, 4ga2.1.A, 1ft1.1.A, 5mpe.1.K, 5mpd.1.G, 6bcx.1.A, 6ejl.1.B, 3qou.1.A, 2yq8.1.A, 4cr4.1.6, 3uzd.1.A, 1hxi.1.A, 3spa.1.A, 3cvl.1.A, 2uwj.1.C, 1n9a.1.A, 5vgz.1.K, 4fhn.1.B, 3c72.1.A, 5gjr.12.A, 2r2l.1.A, 5fjy.1.B, 5fjy.1.A, 3bee.1.A, 5l0y.6.A, 4yv6.2.A, 5cqs.2.A, 5wvk.1.d, 1o1r.1.A, 5wvk.1.a, 5wvk.1.b, 5wvk.1.c, 1fch.1.A, 5mqf.1.O, 5a7d.8.A, 5wql.1.A, 5w4n.1.A, 5a5t.1.C, 4lct.1.A, 4lct.1.B, 4i9c.1.A, 5ft9.2.A, 2npm.1.A, 5jjx.1.A, 3ma5.3.A, 5w4m.1.A, 5w4m.1.B, 5jhp.1.A, 4fhm.1.B, 3jcp.1.Z, 2rfo.2.A, 2wqh.1.A, 5ok9.2.B, 5wrv.1.B, 4y6w.1.A, 3oxl.1.A, 3msv.1.A, 1wm5.1.A, 3jck.1.D, 5np1.1.A, 5a31.1.O, 5nnr.1.A, 3jcp.1.1, 3jcp.1.0, 5l4k.1.E, 5a31.1.J, 5wrw.1.B, 5l4k.1.F, 5l4k.1.I, 5a31.1.F, 3jcp.1.8, 5a31.1.C, 2c0l.1.A, 2lsv.1.A, 4fr3.1.A, 5wvk.1.8, 3kae.1.A, 5wrw.3.A, 5a31.1.W, 2j9q.1.B, 2j9q.1.A, 3nf1.1.A, 3zfw.1.A, 5a31.1.P, 6au8.1.A, 5mpe.2.H, 5mpe.2.E, 5diz.2.A, 5mpe.2.F, 3ual.1.A, 3rjv.1.A, 5n5y.1.R, 5b26.1.A, 5b26.1.B, 4yg8.1.B, 4lct.2.B, 5a6c.1.A, 2wpv.1.A, 5ln3.1.Z, 4boc.1.A, 4i17.1.A, 5ln3.1.Y, 5a7d.4.A, 2fi7.1.A, 2zir.1.A, 4n84.1.A, 2fi7.1.B, 2v5f.1.A, 3ma5.1.A, 5l0y.2.A, 5by9.1.B, 3u9x.1.A, 5njx.1.A, 5t0h.1.V, 5t0h.1.W, 5t0h.1.U, 4um2.1.A, 2qx5.1.A, 1hz4.1.A, 5k18.1.A, 5t0h.1.Y, 4bwr.1.A, 5okf.1.A, 5a7d.2.A, 3e4b.2.A, 4zhe.1.D, 5by9.1.A, 1elr.1.A, 5wvi.1.N, 4nrh.1.B, 3q4a.1.A, 5vat.2.A, 1o9c.1.A, 5cqr.1.A, 2xev.1.A, 4fsc.2.B, 4j8d.1.A, 5oeh.1.B, 5arf.1.A, 2vkj.1.A, 5n60.1.R, 5xjc.1.J, 2bed.1.A, 4pjr.1.A, 5mpc.1.f, 5kcn.1.A, 5w5h.2.E, 5o7x.4.C, 4cgv.2.A, 4bta.1.B, 3ly9.1.A, 3as5.1.A, 4q66.2.C, 5xw7.2.A, 3si5.2.A, 3si5.1.A, 3q5m.1.A, 4f7r.1.A, 4f7r.1.B, 5d3f.1.B, 5c9s.1.A, 4dx0.1.A, 5gmk.1.R, 5xw7.4.A, 3t5x.1.A, 5gmk.1.W, 2f0y.1.A, 5c7e.1.A, 5c7e.1.C, 4cgq.1.A, 2ooe.1.A, 4abn.2.A, 3rkv.1.A, 5lvz.1.B, 4j6s.2.A, 5mpq.1.A, 3cv0.1.A, 5m72.1.A, 3rib.1.A, 6erp.2.D, 4zlh.1.B, 4zlh.1.A, 2gw1.1.A, 2gw1.1.B, 4eqf.1.A, 4reb.1.C, 3efz.1.A, 5wlc.21.A, 1a38.1.A, 4kvm.1.A, 3fwv.2.A, 5i9g.1.A, 3urz.1.A, 6eww.2.A, 5vat.1.A, 4d18.1.C, 3vty.4.A, 5hq8.1.A, 3asf.2.A, 3cvn.1.A, 5wft.1.A, 4zdr.1.A, 1dce.1.A, 5h64.1.A, 3tgo.1.A, 3ubw.1.A, 5oa1.1.T, 5aem.1.A, 5o09.1.C, 1sly.1.A, 2kc7.1.A, 5oma.2.A, 5oma.2.B, 4j0u.1.A, 5an3.1.A, 3ro3.1.A, 5en8.1.B, 5fzs.1.A, 1qjb.1.A, 4wsl.1.A, 3ly7.1.A, 3jck.1.B, 5omp.1.A, 5lyp.1.A, 5dbk.1.B, 5dbk.1.A, 3efz.1.B, 5o01.2.A, 4cr2.1.Z, 4cr2.1.X, 4cr2.1.Y, 3qky.1.A, 2fo7.1.A, 5ayw.1.D, 4ymr.1.A, 4ymr.1.B, 4cr2.1.W, 4cr2.1.U, 2pqr.2.A, 1kt1.1.A, 2lah.1.A, 4bt9.1.A, 5t0h.1.0, 4bzj.1.C, 5jj7.1.A, 2ff4.2.A, 5jj7.1.B, 4gpk.2.B, 4gpk.2.C, 4d10.1.D, 4gpk.2.A, 4d10.1.B, 4cgw.1.A, 4gpk.2.D, 3e4b.4.A, 2xcb.2.A, 3p1o.1.A, 3axy.1.C, 1pc2.1.A, 5jj6.1.A, 5jj6.1.B, 3edt.1.A, 5wyj.33.A, 3edt.1.B, 1p5q.1.B, 1mzc.1.A, 6eih.1.A, 2vsy.1.A, 5en7.2.C, 1klx.1.A, 4ja9.1.A, 2vgx.1.A, 2r5s.1.A, 5en8.1.A, 2crb.1.A, 4uqy.1.A, 2xev.3.A, 4ryk.1.A, 5a1u.1.S, 5btv.1.A, 5a1u.1.T, 5xw7.5.A, 3u64.2.H, 3lca.1.A, 5mpc.1.h, 5mpc.1.i, 5ctq.2.B, 5mpc.1.d, 5mpc.1.e, 3asg.1.A, 5mpc.1.g, 4cr2.1.6, 4mal.1.A, 2xpi.1.C, 2xpi.1.A, 5ccl.1.A, 5jjt.1.A, 3zn3.1.A, 2y4t.1.A, 5ojf.1.A, 3j96.1.J, 3j96.1.H, 5wwm.1.A, 4hou.2.A, 3j96.1.G, 2vgx.1.B, 1e96.1.B, 1p5q.1.A, 4hnx.1.A, 1p5q.1.C, 5a1y.1.U, 4d0p.1.A, 4o6f.1.A, 4wne.1.A, 4i9e.1.B, 5vhm.1.H, 4i9e.1.A, 3cvq.1.A, 4yv6.1.A, 3jb9.1.4, 4d18.1.D, 2q7f.2.A, 4d18.1.B, 3gz1.1.A, 3jb9.1.3, 6epd.1.S, 5vhf.1.J, 4rec.1.A, 5vhf.1.H, 4gcn.2.A, 4wnd.1.A, 4yde.1.A, 5exa.1.B, 4ry3.1.A, 4cr4.1.Y, 4a1g.1.A, 5t0c.44.A, 4cr4.1.Z, 5c7f.1.C, 5vhf.1.S, 5bt1.1.A, 6epe.1.U, 4kbq.2.A, 5nas.1.A, 2wh0.1.A, 6epe.1.T, 5iqp.1.B, 6epe.1.S, 4bta.1.A, 4hoq.1.A, 4a5x.1.A, 5yz0.1.B, 3sf4.1.A, 2xgm.2.A, 6fel.1.A, 4gpk.3.A, 5udl.1.A, 2y4t.3.A, 5ctq.1.A, 5ctq.1.B, 5vbg.1.A, 5nwk.1.B, 4wn4.2.A, 4bt8.1.B, 4bt8.1.A, 5a5t.1.G, 4h7y.3.A, 3upv.1.A, 3asd.1.A, 5nwk.1.A, 3ly8.1.A, 5t0j.1.1, 5n10.1.C, 5n10.1.B, 4ady.2.A, 5lfl.1.A, 2lni.1.A, 4eba.2.A, 5mpb.1.d, 2vko.1.A, 5t0i.1.Y, 5t0i.1.X, 5udj.1.A, 5t0i.1.V, 5t0i.1.U, 5hrz.1.A, 4y49.1.A, 2kcv.1.A, 6epc.1.S, 5jno.1.B, 4hny.2.A, 6epc.1.T, 6epc.1.W, 6epc.1.V, 6epc.1.X, 3j9m.81.A, 6epc.1.Z, 5juf.1.A, 5nzu.1.C, 5nzu.1.A, 5nnp.1.A, 5d0o.1.D, 4u0s.1.A, 4f3v.1.A, 5i9d.1.A, 3q15.2.A, 6exn.1.R, 2xgs.1.A, 3lvh.1.B, 3lvh.1.A, 2bq0.1.B, 3mhr.1.A, 5k04.1.A, 3qtm.1.A, 5j31.1.A, 4ehm.1.A, 5a7d.6.A, 5ccm.1.A, 6emk.1.C, 5ijn.1.U, 5ctr.2.A, 3fp2.1.A, 5ijn.1.I, 2bq0.1.A, 5wbu.1.A, 5ijn.1.C, 4xgl.1.A, 2br9.1.A, 4uzy.1.A, 3ru0.1.A, 1a4o.1.A, 4fhn.2.B, 4zq0.1.A, 5m32.1.a, 4n5c.5.A, 5m32.1.c, 4wsn.6.B, 6f5d.1.J, 5ekq.1.B, 4wsn.6.D, 4rea.1.B, 4gco.1.A, 6f5d.1.L, 4g1t.1.A, 4hot.1.A, 4g1t.1.B, 4n5c.3.A, 5oma.1.A, 4gnt.1.A, 4wsn.2.B, 4wsn.2.C, 4reb.1.D, 4wsn.2.A, 5hgv.1.A, 5tqb.1.B, 4wsn.2.D, 4l9p.1.A, 2ifu.1.A, 3qtn.1.A, 5ln3.1.0, 4wrq.1.A, 5w4n.1.B, 4n5c.1.A, 6epf.1.T, 6epf.1.U, 6epf.1.V, 6epf.1.W, 6epf.1.S, 4gyw.1.A, 6epf.1.X, 5fvm.1.A, 1ft2.1.A, 3p1r.1.A, 2ho1.1.B, 2ho1.1.A, 5ln3.1.X, 3as8.1.A, 5mgx.1.A, 2btp.1.A, 4pjq.1.A, 5ola.2.C, 5ln3.1.V, 4bzj.1.A, 1ltx.1.A, 5m32.1.8, 5m32.1.9, 4a1g.3.A, 4ga0.1.A, 5mps.1.Q, 5lcw.1.C, 4ynw.1.A, 5ln3.1.A, 5lcw.1.O, 2fbn.1.A, 5en6.1.A, 1wy6.1.A, 3qdn.2.A, 4dat.1.A, 4i2w.1.A, 5ic8.3.A, 5ex0.1.A, 4yvo.1.A, 1qjb.1.B, 3uux.1.A, 5lwv.1.A, 4in3.1.D, 1qsa.1.A, 3lpz.1.A, 5ic8.1.A, 2c63.2.B, 3kd7.2.A, 5flc.1.F, 5l0y.1.B, 5bt1.1.B, 2kcl.1.A, 4yv9.2.A, 4y6c.1.A, 4yv6.1.B, 5jzz.2.A, 5fzr.1.A, 3esk.1.A, 5a5b.1.Y, 5n6n.1.B, 1ya0.2.A, 3ma5.4.A, 2ifu.3.A, 4jsp.1.A, 3qww.1.A, 5hi7.1.A, 6fel.1.B, 4gq2.1.A, 1fch.2.A, 4zhe.1.A, 3hym.1.B, 5g05.1.O, 3j9m.72.A, 4i1a.2.A, 4dnk.1.A, 4dnk.1.B, 3ffl.1.A, 4wjw.1.B, 3gw4.1.B, 5a01.1.A, 4rg6.1.A, 4rg6.1.B, 5y5a.1.A, 4me2.1.A, 3oxg.1.A, 5iww.1.D, 3ffl.1.B, 4ria.1.A, 1iyg.1.A, 5n6n.1.A, 3o8i.1.A, 4n5c.7.A, 5d2d.1.A, 5d2d.1.B, 3ieg.1.A, 4j6s.1.A, 4osr.1.A, 5g04.1.P, 3dra.1.A, 4r89.1.A, 5g04.1.U, 5g04.1.T, 5mpd.1.J, 6epf.1.Z, 2pl2.1.A, 3tg5.1.A, 5mzu.1.A, 2c2l.2.A, 5g04.1.C, 5fsh.1.A, 2mhk.1.A, 5jm4.1.B, 5g04.1.F, 5mpe.1.J, 5g04.1.H, 5g04.1.K, 5g04.1.J, 2nc9.1.A, 2pzi.2.A, 5g04.1.O, 5xi8.1.A, 2o98.1.A, 5a7d.5.A, 1na3.1.A, 5nwk.2.A, 5wlc.41.A, 5ln3.1.W, 4wsn.4.D, 3ro2.1.A, 5d3e.3.A, 5m35.1.A, 4pjq.2.A, 3p1p.1.A, 3gz1.1.B, 5ok9.2.A, 5ft9.1.A, 4xmn.1.D, 4j8f.1.A, 5mpd.1.F, 5djs.1.A, 4cgu.1.A, 2kat.1.A, 5n5z.1.R, 5xw7.1.A, 5mps.1.R, 4h7x.1.A, 4jhr.1.A, 4y5i.1.B, 6erp.1.D, 3jco.1.Z, 4gcn.1.A, 1qz2.1.C, 1qz2.1.B, 1qz2.1.A, 5d3e.1.B, 2if4.1.A, 4zq0.2.B, 5en7.1.C, 5ola.1.C, 5ulm.1.A, 5ok9.1.A, 5lj3.1.T, 5wcg.1.A, 4w9r.1.A, 3lvg.1.A, 3mkq.1.B, 4n5c.2.A, 4uqz.1.A, 3mkq.1.E, 2avp.1.A, 6ez8.1.B, 4ric.1.A, 5a7d.1.A, 5uz5.1.D, 5a7d.7.A, 5jpz.1.A, 2c0m.1.A, 2vyi.1.A, 5fsh.1.B, 3mkq.1.F, 2xcc.1.A, 2rfo.1.A, 2xcc.1.B, 5l0y.7.A, 5b26.2.B, 4zq0.2.A, 4fj3.1.A, 6epd.1.Z, 4o46.1.A, 2hr2.1.A, 5x6o.1.A, 5wql.2.A, 5wvi.1.c, 5ok9.1.B, 6bcu.1.A, 5l0y.5.B, 5l0y.5.A, 2mqw.1.A, 5jz6.1.A, 4lct.2.A, 4aif.2.A, 2vsy.2.A, 3mv2.1.A, 5wvi.1.O, 5wvi.1.L, 3mv2.1.B, 3jd5.1.3, 5wvi.1.K, 4hkc.1.A, 4j8e.1.A, 6ejl.1.A, 3e37.1.A, 3zhe.1.B, 5wvi.1.V, 3q75.1.A, 5jkp.1.A, 3jd5.1.U, 6epd.1.X, 4wuy.1.A, 5en6.2.A, 5lj5.1.U, 5lj5.1.V, 5ftp.1.A, 5ftp.1.B, 5ja5.1.A, 5mpe.1.H, 3as5.2.A, 5yqg.1.B, 5yqg.1.A, 5jjo.1.A, 1na0.1.A, 5diz.1.A, 5c1d.1.A, 4g2v.1.A, 2vq2.1.A, 5cqs.1.A, 5t0i.1.W, 2vsn.1.A, 3qdn.1.A, 3qwp.1.A, 2b05.1.A, 1zu2.1.A, 2vko.1.B, 4rea.1.A, 4f7r.2.B, 4f7r.2.A, 3n71.1.A, 3u3w.1.B, 3vty.1.A, 4zey.1.A, 5a9q.1.T, 3fwv.1.A, 4hnw.1.A, 5l0y.3.A, 3pz4.1.A, 5jhe.1.A, 5np0.1.A, 5l0y.1.A, 5oeg.1.D, 1b89.1.A, 5a9q.1.B, 3axy.1.D, 5n61.1.R, 6bk8.1.V, 6bk8.1.W, 5t0c.35.A, 1nzn.1.A, 3m50.1.A, 1kt0.1.A, 3jco.1.0, 5wvk.1.k, 3jco.1.1, 4j8e.2.A, 3jco.1.Y, 3e4b.1.A, 4b94.1.A, 3mkq.1.A, 6epc.1.U, 3mkq.1.C, 3jco.1.W, 5a9q.1.a, 3mkq.1.D, 5jqy.1.A, 4nq0.1.A, 5bwk.1.D, 4trq.1.B, 4zhe.1.B, 4zhe.1.C, 5v7v.1.A, 2ond.1.A, 4n7g.1.A, 3s7f.1.A, 4n2s.1.A, 3zpj.1.A, 4pwx.1.C, 5gjq.1.j, 3jco.1.8, 6epe.1.Z, 2ijq.1.A, 3o48.1.A, 2ijq.2.A, 4cgv.1.A, 4abn.1.A, 3as4.1.A, 4q66.1.D, 3q7f.1.A, 1w3b.1.B, 4n2q.1.A, 1w3b.1.A, 2uy1.1.A, 2uy1.1.B, 5a9q.1.2, 5ltw.1.A, 5d3e.1.A, 4gyo.1.A, 5lvv.1.A, 5a6c.2.A, 2pzi.1.A, 5ewz.1.B, 3pdn.1.A, 3uq3.1.A, 1y8m.1.A, 3sf4.2.A, 4r7s.1.A, 4aif.1.A, 3asf.1.A, 2wvi.1.A, 3j8b.1.C, 2qfc.1.A, 5c6v.1.D, 4ynd.1.A, 5d0q.1.C, 5c6v.1.C, 5c6v.1.B, 3vtx.2.A, 5ojs.1.A, 5d3e.3.B, 2l6j.1.A, 5che.1.E, 5che.1.F, 4apo.1.A, 5om0.1.B, 5l0w.1.A, 5om0.1.A, 4uqx.1.A, 3sz7.1.A, 1dce.2.A, 4e2e.1.A, 5oej.1.A, 1tjc.1.A, 5i9f.1.A, 3vty.3.A, 3gz2.1.B, 5aio.1.A, 5o01.1.A, 2wh0.1.B, 3e6y.1.B, 3wxx.1.A, 2pqn.1.A, 4xmm.1.E, 2vko.2.A, 5jjw.1.A, 3ffl.2.B, 4n3c.1.A, 3k9i.1.A, 4zq0.1.B, 1zbp.1.A, 3jcp.1.Y, 1d8d.1.A, 5t0g.1.Y, 5t0g.1.X, 2n8i.1.A, 1xnf.1.A, 4zdr.1.B, 1wao.1.A, 3asg.2.A, 5t0g.1.V, 2v7d.1.A, 2c23.1.A, 3jck.1.C, 4mal.2.A, 1elw.1.A, 3smo.1.A, 5ks5.1.A, 1wao.3.A, 5t0j.1.V, 4xpd.1.A, 3jbz.1.A, 4gpk.1.D, 5ctq.2.A, 4e6h.1.A, 4gpk.1.A, 4gpk.1.C, 4gpk.1.B, 6epd.1.V, 6epd.1.W, 6epd.1.T, 6epd.1.U, 3j98.1.I, 3j98.1.H, 2vko.2.B, 6epe.1.X, 6epe.1.W, 6epe.1.V, 3j97.1.H, 4gpk.3.D, 4gpk.3.C, 4gpk.3.B, 4g23.1.A, 3ceq.1.A, 3lku.1.A, 3ceq.1.B, 4ay5.1.A, 5vhi.1.H, 5jub.1.A, 1ouv.1.A, 5jub.1.B, 5vhi.1.S, 3j8b.1.G, 2vkj.1.B, 4kvo.1.A, 6eww.1.A, 2xev.2.A, 4xnh.1.A, 2lsu.1.A, 5ctr.1.A, 4kbq.1.A, 5t0g.1.0, 4xi0.1.A, 5t0g.1.5, 4ja7.1.A, 5fzr.1.B, 5a7d.3.A, 3mkr.1.B, 2c1n.1.A, 3mkr.1.A, 5f74.1.A, 4wn4.1.A, 4cr3.1.Z, 5ljo.1.C, 3jck.1.A, 4hny.1.A, 3bee.2.A, 4hou.1.A, 2vgy.1.A, 3rdh.1.A, 4ri9.1.A, 4cr3.1.6, 5gjq.1.Z, 6fel.2.A, 5mpb.1.f, 4n5c.4.A, 5jpz.1.B, 4ynv.1.A, 3lvg.1.C, 3lvg.1.B, 5fzq.1.C, 5fzq.1.B, 5fzq.1.A, 4a1g.4.A, 2ff4.1.A, 6emk.1.A, 4ozs.1.A, 5wrw.1.A, 5l4k.1.G, 3gz2.1.A, 1ib1.1.A, 5yz0.1.A, 5a31.1.H, 4qli.1.A, 4ga1.1.A, 4ri8.1.A, 4u04.1.A, 2kck.1.A, 5i9h.1.A, 5l4k.1.H, 3fp3.1.A, 3txn.1.A, 5nnp.2.A, 5waq.1.A, 4trq.1.E, 5w5i.1.A, 5l4k.1.J, 3e4b.3.A, 5vhq.1.H, 5ewz.1.A, 4btb.1.A, 5iqp.1.A, 4wng.1.A, 5l4k.1.L, 6f5d.1.K, 5c6v.1.A, 4rid.1.A, 5kjk.1.A, 5mpb.1.e, 5gjq.1.3, 5mpb.1.g, 5gjq.1.1, 3sfx.1.A, 5gjq.1.7, 3pz1.1.A, 5gjq.1.5, 3u4t.1.A, 3ks2.1.A, 4cr3.1.Y, 5gjq.1.9, 5mpb.1.i, 5mpb.1.h, 4a1g.2.A, 2e2e.1.A, 5ic8.4.A, 5lu2.1.A, 4am9.1.A, 5ex3.1.A, 2dba.1.A

SWISS-MODEL Homology Modelling Report

Model Building Report

This document lists the results for the homology modelling project "IFT43_HUMAN Q96FT9 Intraflagellar transport protein 43 homolog" submitted to SWISS-MODEL workspace on Jan. 29, 2018, 2:07 p.m..The submitted primary amino acid sequence is given in Table T1.

If you use any results in your research, please cite the relevant publications:

Marco Biasini; Stefan Bienert; Andrew Waterhouse; Konstantin Arnold; Gabriel Studer; Tobias Schmidt; Florian Kiefer; Tiziano Gallo Cassarino; Martino Bertoni; Lorenza Bordoli; Torsten Schwede. (2014). SWISS-MODEL: modelling protein tertiary and quaternary structure using evolutionary information. Nucleic Acids Research (1 July 2014) 42 (W1): W252-W258; doi: 10.1093/nar/gku340.
Arnold, K., Bordoli, L., Kopp, J. and Schwede, T. (2006) The SWISS-MODEL workspace: a web-based environment for protein structure homology modelling. Bioinformatics, 22, 195-201.
Benkert, P., Biasini, M. and Schwede, T. (2011) Toward the estimation of the absolute quality of individual protein structure models. Bioinformatics, 27, 343-350

Results

The SWISS-MODEL template library (SMTL version 2018-01-24, PDB release 2018-01-19) was searched with Blast (Altschul et al., 1997) and HHBlits (Remmert, et al., 2011) for evolutionary related structures matching the target sequence in Table T1. For details on the template search, see Materials and Methods. Overall 0 templates were found (Table T2).

Models

No models have been built for this project.

Materials and Methods

Template Search

Template search with Blast and HHBlits has been performed against the SWISS-MODEL template library (SMTL, last update: 2018-01-24, last included PDB release: 2018-01-19).

The target sequence was searched with BLAST (Altschul et al., 1997) against the primary amino acid sequence contained in the SMTL.

An initial HHblits profile has been built using the procedure outlined in (Remmert, et al., 2011), followed by 1 iteration of HHblits against NR20. The obtained profile has then be searched against all profiles of the SMTL. A total of 13 templates were found.

Template Selection

For each identified template, the template's quality has been predicted from features of the target-template alignment. The templates with the highest quality have then been selected for model building.

Model Building

Models are built based on the target-template alignment using ProMod3. Coordinates which are conserved between the target and the template are copied from the template to the model. Insertions and deletions are remodelled using a fragment library. Side chains are then rebuilt. Finally, the geometry of the resulting model is regularized by using a force field. In case loop modelling with ProMod3 fails, an alternative model is built with PROMOD-II (Guex, et al., 1997).

Model Quality Estimation

The global and per-residue model quality has been assessed using the QMEAN scoring function (Benkert, et al., 2011) . For improved performance, weights of the individual QMEAN terms have been trained specifically for SWISS-MODEL.

Ligand Modelling

Ligands present in the template structure are transferred by homology to the model when the following criteria are met (Gallo - Casserino, to be published): (a) The ligands are annotated as biologically relevant in the template library, (b) the ligand is in contact with the model, (c) the ligand is not clashing with the protein, (d) the residues in contact with the ligand are conserved between the target and the template. If any of these four criteria is not satisfied, a certain ligand will not be included in the model. The model summary includes information on why and which ligand has not been included.

Oligomeric State Conservation

Homo-oligomeric structure of the target protein is predicted based on the analysis of pairwise interfaces of the identified template structures. For each relevant interface between polypeptide chains (interfaces with more than 10 residue-residue interactions), the QscoreOligomer (Mariani et al., 2011) is predicted from features such as similarity to target and frequency of observing this interface in the identified templates (Kiefer, Bertoni, Biasini, to be published). The prediction is performed with a random forest regressor using these features as input parameters to predict the probability of conservation for each interface. The QscoreOligomer of the

whole complex is then calculated as the weight-averaged QscoreOligomer of the interfaces. The oligomeric state of the target is predicted to be the same as in the template when QscoreOligomer is predicted to be higher or equal to 0.5.

References

Altschul, S.F., Madden, T.L., Schaffer, A.A., Zhang, J., Zhang, Z., Miller, W. and Lipman, D.J. (1997) Gapped BLAST and PSI-BLAST: a new generation of protein database search programs. Nucleic Acids Res, 25, 3389-3402.
Remmert, M., Biegert, A., Hauser, A. and Soding, J. (2012) HHblits: lightning-fast iterative protein sequence searching by HMM-HMM alignment. Nat Methods, 9, 173-175.
Guex, N. and Peitsch, M.C. (1997) SWISS-MODEL and the Swiss-PdbViewer: an environment for comparative protein modeling. Electrophoresis, 18, 2714-2723.
Sali, A. and Blundell, T.L. (1993) Comparative protein modelling by satisfaction of spatial restraints. J Mol Biol, 234, 779-815.
Benkert, P., Biasini, M. and Schwede, T. (2011) Toward the estimation of the absolute quality of individual protein structure models. Bioinformatics, 27, 343-350.
Mariani, V., Kiefer, F., Schmidt, T., Haas, J. and Schwede, T. (2011) Assessment of template based protein structure predictions in CASP9. Proteins, 79 Suppl 10, 37-58.

Table T1:

Primary amino acid sequence for which templates were searched and models were built.

```
MEDLLDLDEELRYSLATSRAKMGRRAQQESAQAENHLNGKNSSLTLTGETSSAKLPRCRQGGWAGDSVKASKFRRKASEEIEDFRLRPQSLNGSDYGGDI
PIIPDLEEVQEEDFVLQVAAPPSIQIKRVMTYRDLDNDLMKYSAIQTLDGEIDLKLLTKVLAPEHEVREDDVGWDWDHLFTEVSSEVLTEWDPLQTEKED
PAGQARHT
```

Table T2:

Template	Seq Identity	Oligo-state	Found by	Method	Resolution	Seq Similarity	Coverage	Description

BIOZENTRUM
University of Basel
The Center for Molecular Life Sciences

SWISS-MODEL Homology Modelling Report

Model Building Report

This document lists the results for the homology modelling project "BBS1_HUMAN Q8NFJ9 Bardet-Biedl syndrome 1 protein" submitted to SWISS-MODEL workspace on July 23, 2018, 3:41 p.m..The submitted primary amino acid sequence is given in Table T1.

If you use any results in your research, please cite the relevant publications:

- Waterhouse, A., Bertoni, M., Bienert, S., Studer, G., Tauriello, G., Gumienny, R., Heer, F.T., de Beer, T.A.P., Rempfer, C., Bordoli, L., Lepore, R., Schwede, T. SWISS-MODEL: homology modelling of protein structures and complexes. Nucleic Acids Res. 46(W1), W296-W303 (2018). doi
- Guex, N., Peitsch, M.C., Schwede, T. Automated comparative protein structure modeling with SWISS-MODEL and Swiss-PdbViewer: A historical perspective. Electrophoresis 30, S162-S173 (2009). doi
- Bienert, S., Waterhouse, A., de Beer, T.A.P., Tauriello, G., Studer, G., Bordoli, L., Schwede, T. The SWISS-MODEL Repository - new features and functionality. Nucleic Acids Res. 45, D313-D319 (2017). doi
- Benkert, P., Biasini, M., Schwede, T. Toward the estimation of the absolute quality of individual protein structure models. Bioinformatics 27, 343-350 (2011). doi
- Bertoni, M., Kiefer, F., Biasini, M., Bordoli, L., Schwede, T. Modeling protein quaternary structure of homo- and hetero-oligomers beyond binary interactions by homology. Scientific Reports 7 (2017). doi

Results

The SWISS-MODEL template library (SMTL version 2018-07-12, PDB release 2018-07-06) was searched with BLAST (Camacho et al.) and HHBlits (Remmert et al.) for evolutionary related structures matching the target sequence in Table T1. For details on the template search, see Materials and Methods. Overall 1445 templates were found (Table T2).

Models

No models have been built for this project.

Materials and Methods

Template Search

Template search with BLAST and HHBlits has been performed against the SWISS-MODEL template library (SMTL, last update: 2018-07-12, last included PDB release: 2018-07-06).

The target sequence was searched with BLAST against the primary amino acid sequence contained in the SMTL. A total of 2 templates were found.

An initial HHblits profile has been built using the procedure outlined in (Remmert et al.), followed by 1 iteration of HHblits against NR20. The obtained profile has then be searched against all profiles of the SMTL. A total of 1483 templates were found.

Template Selection

For each identified template, the template's quality has been predicted from features of the target-template alignment. The templates with the highest quality have then been selected for model building.

Model Building

Models are built based on the target-template alignment using ProMod3. Coordinates which are conserved between the target and the template are copied from the template to the model. Insertions and deletions are remodelled using a fragment library. Side chains are then rebuilt. Finally, the geometry of the resulting model is regularized by using a force field. In case loop modelling with ProMod3 fails, an alternative model is built with PROMOD-II (Guex et al.).

Model Quality Estimation

The global and per-residue model quality has been assessed using the QMEAN scoring function (Benkert et al.) . For improved performance, weights of the individual QMEAN terms have been trained specifically for SWISS-MODEL.

Ligand Modelling

Ligands present in the template structure are transferred by homology to the model when the following criteria are met: (a) The ligands are annotated as biologically relevant in the template library, (b) the ligand is in contact with the model, (c) the ligand is not clashing with the protein, (d) the residues in contact with the ligand are conserved between the target and the template. If any of these four criteria is not satisfied, a certain ligand will not be included in the model. The model summary includes information on why and which ligand has not been included.

Oligomeric State Conservation

The quaternary structure annotation of the template is used to model the target sequence in its oligomeric form. The method (Bertoni et al.) is based on a supervised machine learning algorithm, Support Vector Machines (SVM), which combines interface conservation, structural clustering, and other template features to provide a quaternary structure quality estimate (QSQE). The QSQE score is a number between 0 and 1, reflecting the expected accuracy of the interchain contacts for a model built based a given alignment and template. Higher numbers indicate higher reliability. This complements the GMQE score which estimates the accuracy of the tertiary structure of the resulting model.

References

- **BLAST**
  Camacho, C., Coulouris, G., Avagyan, V., Ma, N., Papadopoulos, J., Bealer, K., Madden, T.L. BLAST+: architecture and applications. BMC Bioinformatics 10, 421-430 (2009). doi
- **HHblits**
  Remmert, M., Biegert, A., Hauser, A., Söding, J. HHblits: lightning-fast iterative protein sequence searching by HMM-HMM alignment. Nat Methods 9, 173-175 (2012). doi

Table T1:

Primary amino acid sequence for which templates were searched and models were built.

```
MAAASSSDSDACGAESNEANSKWLDAHYDPMANIHTFSACLALADLHGDGEYKLVVGDLGPGGQQPRLKVLKGPLVMTESPLPALPAAAATFLMEQHEPR
TPALALASGPCVYVYKNLRPYFKFSLPQLPPNPLEQDLWNQAKEDRIDPLTLKEMLESIRETAEEPLSIQSLRFLQLELSEMEAFVNQHKSNSIKRQTVI
TTMTTLKKNLADEDAVSCLVLGTENKELLVLDPEAFTILAKMSLPSVPVFLEVSGQFDVEFRLAAACRNGNIYILRRDSKHPKYCIELSAQPVGLIRVHK
VLVVGSTQDSLHGFTHKGKKLWTVQMPAAILTMNLLEQHSRGLQAVMAGLANGEVRIYRDKALLNVIHTPDAVTSLCFGRYGREDNTLIMTTRGGGLIIK
ILKRTAVFVEGGSEVGPPPAQAMKLNVPRKTRLYVDQTLREREAGTAMHRAFQTDLYLLRLRAARAYLQALESSLSPLSTTAREPLKLHAVVQGLGPTFK
LTLHLQNTSTTRPVLGLLVCFLYNEALYSLPRAFFKVPLLVPGLNYPLETFVESLSNKGISDIIKVLVLREGQSAPLLSAHVNMPGSEGLAAA
```

Table T2:

Template	Seq Identity	Oligo-state	QSQE	Found by	Method	Resolution	Seq Similarity	Coverage	Description
4v0n.2.B	39.07	monomer		HHblits	X-ray	3.13Å	0.39	0.66	BARDET-BIEDL SYNDROME 1 PROTEIN
4v0m.1.B	39.07	monomer		HHblits	X-ray	3.45Å	0.39	0.66	BARDET-BIEDL SYNDROME 1 PROTEIN
4v0n.2.B	40.26	monomer		BLAST	X-ray	3.13Å	0.39	0.64	BARDET-BIEDL SYNDROME 1 PROTEIN
4v0m.1.B	40.26	monomer		BLAST	X-ray	3.45Å	0.39	0.64	BARDET-BIEDL SYNDROME 1 PROTEIN
5wyj.20.A	14.70	monomer		HHblits	EM	NA	0.28	0.47	U3 small nucleolar RNA-associated protein 21
5wyk.1.V	14.70	monomer		HHblits	EM	NA	0.28	0.47	U3 small nucleolar RNA-associated protein 21
5jpq.1.I	14.70	monomer		HHblits	EM	NA	0.28	0.47	U3 small nucleolar RNA-associated protein 21
5wlc.25.A	14.70	monomer		HHblits	EM	NA	0.28	0.47	Utp21
5tzs.1.1	13.06	monomer		HHblits	EM	NA	0.28	0.41	Utp21
6f38.1.c	14.95	monomer		HHblits	EM	NA	0.27	0.33	Cytoplasmic dynein 1 intermediate chain 2
6f38.1.b	14.95	monomer		HHblits	EM	NA	0.27	0.33	Cytoplasmic dynein 1 intermediate chain 2
6f38.1.4	14.95	monomer		HHblits	EM	NA	0.27	0.33	Cytoplasmic dynein 1 intermediate chain 2
6f38.1.3	14.95	monomer		HHblits	EM	NA	0.27	0.33	Cytoplasmic dynein 1 intermediate chain 2
6f1t.1.c	14.95	monomer		HHblits	EM	NA	0.27	0.33	Cytoplasmic dynein 1 intermediate chain 2
6f1t.1.b	14.95	monomer		HHblits	EM	NA	0.27	0.33	Cytoplasmic dynein 1 intermediate chain 2
6f1t.1.3	14.95	monomer		HHblits	EM	NA	0.27	0.33	Cytoplasmic dynein 1 intermediate chain 2
6f1t.1.4	14.95	monomer		HHblits	EM	NA	0.27	0.33	Cytoplasmic dynein 1 intermediate chain 2
6f38.1.b	10.61	monomer		HHblits	EM	NA	0.26	0.33	Cytoplasmic dynein 1 intermediate chain 2
5cvn.1.A	12.89	monomer		HHblits	X-ray	3.36Å	0.26	0.33	WD repeat-containing protein 48
5cvl.1.A	12.89	monomer		HHblits	X-ray	3.00Å	0.26	0.33	WD repeat-containing protein 48
4a0b.2.A	11.40	monomer		HHblits	X-ray	3.80Å	0.27	0.33	DNA DAMAGE-BINDING PROTEIN 1
4a0b.1.A	11.40	monomer		HHblits	X-ray	3.80Å	0.27	0.33	DNA DAMAGE-BINDING PROTEIN 1
3i7l.1.A	11.40	monomer		HHblits	X-ray	2.80Å	0.27	0.33	DNA damage-binding protein 1
3i7k.1.A	11.40	monomer		HHblits	X-ray	2.80Å	0.27	0.33	DNA damage-binding protein 1

3i7p.1.A	11.40	monomer		HHblits	X-ray	3.00Å	0.27	0.33	DNA damage-binding protein 1
6f38.1.c	10.61	monomer		HHblits	EM	NA	0.26	0.33	Cytoplasmic dynein 1 intermediate chain 2
6f38.1.4	10.61	monomer		HHblits	EM	NA	0.26	0.33	Cytoplasmic dynein 1 intermediate chain 2
6f38.1.3	10.61	monomer		HHblits	EM	NA	0.26	0.33	Cytoplasmic dynein 1 intermediate chain 2
6f1t.1.c	10.61	monomer		HHblits	EM	NA	0.26	0.33	Cytoplasmic dynein 1 intermediate chain 2
6f1t.1.b	10.61	monomer		HHblits	EM	NA	0.26	0.33	Cytoplasmic dynein 1 intermediate chain 2
6f1t.1.3	10.61	monomer		HHblits	EM	NA	0.26	0.33	Cytoplasmic dynein 1 intermediate chain 2
6f1t.1.4	10.61	monomer		HHblits	EM	NA	0.26	0.33	Cytoplasmic dynein 1 intermediate chain 2
5xwr.1.A	11.79	homo-dimer		HHblits	X-ray	2.69Å	0.25	0.33	Histone-binding protein RBBP4
5cyk.1.A	12.37	monomer		HHblits	X-ray	3.00Å	0.26	0.33	Ribosome biogenesis protein YTM1
4a09.1.A	11.40	monomer		HHblits	X-ray	3.10Å	0.27	0.33	DNA DAMAGE-BINDING PROTEIN 1
4a08.1.A	11.40	monomer		HHblits	X-ray	3.00Å	0.27	0.33	DNA DAMAGE-BINDING PROTEIN 1
5k1c.1.B	12.82	monomer		HHblits	X-ray	3.00Å	0.26	0.33	WD repeat-containing protein 48
5fqd.1.A	11.92	monomer		HHblits	X-ray	2.45Å	0.27	0.33	DNA DAMAGE-BINDING PROTEIN 1
5y1u.1.A	11.79	monomer		HHblits	X-ray	2.14Å	0.25	0.33	Histone-binding protein RBBP4
5y1u.2.A	11.79	monomer		HHblits	X-ray	2.14Å	0.25	0.33	Histone-binding protein RBBP4
3ei4.3.A	11.40	monomer		HHblits	X-ray	3.30Å	0.27	0.33	DNA damage-binding protein 1
3ei4.1.A	11.40	monomer		HHblits	X-ray	3.30Å	0.27	0.33	DNA damage-binding protein 1
6bnb.1.A	11.92	monomer		HHblits	X-ray	6.34Å	0.27	0.33	DNA damage-binding protein 1
6bn8.1.A	11.92	monomer		HHblits	X-ray	3.99Å	0.27	0.33	DNA damage-binding protein 1,DNA damage-binding protein 1
6bw3.1.A	11.79	monomer		HHblits	X-ray	2.20Å	0.25	0.33	Histone-binding protein RBBP4
4a0l.1.A	11.40	monomer		HHblits	X-ray	7.40Å	0.27	0.33	DNA DAMAGE-BINDING PROTEIN 1
5cvo.1.A	9.64	monomer		HHblits	X-ray	3.88Å	0.25	0.33	WD repeat-containing protein 48
5cvo.2.A	9.64	monomer		HHblits	X-ray	3.88Å	0.25	0.33	WD repeat-containing protein 48
5cxb.1.A	12.37	monomer		HHblits	X-ray	2.10Å	0.26	0.33	Ribosome biogenesis protein YTM1
6bly.1.B	8.02	monomer		HHblits	EM	NA	0.24	0.40	pre-mRNA 3' end processing protein WDR33

The table above shows the top 50 filtered templates. A further 732 templates were found which were considered to be less suitable for modelling than the filtered list.
3hxj.1.B, 3vl1.1.A, 3hxj.1.A, 4a0b.2.A, 5cvl.1.A, 5hy7.1.A, 5es4.2.A, 5cvo.2.A, 3fm0.1.A, 2ynp.1.A, 3dxm.1.C, 4tqo.1.A, 5yje.1.A, 5yje.1.B, 5yje.1.C, 5ukl.1.B, 3q54.1.A, 4e54.1.B, 4e54.1.A, 5naf.1.A, 2h13.1.A, 4tz4.1.A, 3sn6.1.B, 1ri6.1.A, 6bw3.1.A, 6c23.1.D, 5tzs.1.e, 6c23.1.F, 5wak.1.A, 6fbs.1.A, 6fbs.1.B, 1r5m.1.A, 4gq1.1.A, 1xip.1.A, 4ui9.1.Q, 1p22.1.A, 5fsb.1.A, 2oaj.1.A, 2yms.1.D, 2h6k.1.A, 5gvb.1.A, 2yms.1.C, 2yms.1.A, 5cyk.1.A, 3hfq.1.A, 5em2.2.B, 2xyi.1.A, 5tzs.1.1, 3v4v.1.A, 1tye.1.A, 5gm6.1.F, 1aof.1.A, 1aof.1.B, 5k19.2.A, 3w15.1.A, 5ffo.1.A, 3bws.1.A, 5fqd.1.A, 5naf.3.A, 5h13.1.A, 3k72.1.A, 5vyc.4.I, 5v1d.2.A, 5v1d.2.B, 4c8h.1.A, 4o5t.1.A, 4a0l.1.A, 4jsn.1.B, 4a7k.1.A, 1jmz.1.B, 1nex.2.B, 4aez.2.A, 5opt.1.A, 1gp2.1.B, 5wsg.1.U, 2vdu.1.A, 4d6v.1.A, 3jbt.1.A, 5cxc.1.A, 6gdg.1.B, 4aah.1.A, 4jxm.1.A, 6em3.1.E, 2i3s.1.A, 4cvc.1.A, 3s2k.1.B, 3s2k.1.A, 5es4.3.A, 6bcx.1.C, 6f3a.1.3, 3j7p.78.A, 5neu.3.E, 3sfz.1.A, 3j6x.75.A, 3s8z.1.A, 2ce9.2.B, 5jcs.1.3, 4nsx.1.A, 6g5i.1.6, 5wyk.1.U, 4a2m.2.A, 4yvd.1.A, 5wyk.1.R, 5tdh.1.B, 3jzn.1.A, 5wg6.1.B, 5lj5.1.d, 5t2a.48.A, 5igq.1.A, 1a0r.1.A, 5m1j.14.A, 4v5z.1.A, 5mqf.1.F, 5mqf.1.D, 5mqf.1.E, 4xmm.1.C, 5jut.45.A, 3shf.1.A, 4fhm.1.A, 3j81.1.5, 4pxw.1.A, 5h1k.1.A, 4v6w.2.A, 4v0m.1.B, 5fks.1.A, 5wyj.20.A, 3mbr.1.A, 5ndv.73.A, 4a2l.1.B, 5sv7.1.A, 4wjv.1.A, 3jap.1.i, 5sv7.1.B, 5sv7.1.C, 5a31.1.R, 5k1a.2.B, 5u5h.1.A, 6bn8.1.A, 3ei3.1.A, 4c8h.1.C, 5wlc.15.A, 4j87.1.A, 5ttw.2.A, 4neh.1.A, 4mae.1.A, 5h19.1.A, 4a0l.2.A, 5sv7.1.D, 3odt.1.A, 3dsm.1.A, 4v8m.8.A, 5afu.1.C, 2d0v.1.A, 5gmk.1.0, 6em5.1.5, 3s8v.2.A, 2z2n.1.A, 2c4d.1.A, 5wlc.27.A, 5m11.1.A, 2b5l.1.A, 5ods.2.A, 5h64.1.B, 5h64.1.C, 5fkq.1.A, 2yba.1.A, 2ovp.1.B, 2w18.1.A, 5tf2.1.A, 5xjc.1.W, 2l14.1.A, 5xjc.1.T, 2b5n.2.A, 2vdo.1.A, 4fa4.1.D, 2iaa.1.A, 1flg.1.A, 5xjc.1.E, 5ic7.1.A, 5ogs.1.A, 4cc9.1.A, 4x3e.1.A, 2be1.1.A, 4o02.1.A, 1mg2.1.A, 5gmk.1.J, 3hxj.2.B, 1w6s.1.A, 5gmk.1.X, 4z7o.1.A, 2b5n.4.A, 6ek0.64.A, 4wk0.1.A, 6fq3.1.A, 5zya.1.D, 6b3x.1.A, 2j57.1.C, 5vfc.1.A, 5ffg.1.A, 4wju.1.A, 5jus.45.A, 6az1.1.6, 5wlc.25.A, 2hes.1.A, 4y5r.1.C, 4wjs.1.A, 3ije.1.A, 2yms.1.B, 3j77.45.A, 4zlr.1.A, 4cag.1.A, 5gap.1.F, 4imm.2.A, 3u4y.1.A, 5nuv.1.A, 5wyj.19.A, 3j2t.1.A, 5cyk.1.B, 4yd8.1.A, 5hqg.1.A, 5v4b.1.B, 2xzh.1.A, 1pi6.1.A, 1c9l.1.A, 5xm3.1.A, 5n4a.1.A, 5l8w.1.B, 6em5.1.h, 1b9y.1.A, 4zb4.1.A, 3i2n.1.A, 5ayw.1.B, 2kkj.1.A, 5m89.2.A, 5wbk.1.A, 4v7f.1.j, 6cmo.1.C, 5guw.3.A, 4yzy.1.A, 3jcm.1.B, 3v7d.1.B, 4l9o.2.A, 2bcj.1.B, 3i7k.1.A, 5a2q.1.8, 6b20.1.A, 3prw.1.A, 6en4.1.A, 4o9d.1.A, 6d9j.78.A, 4hdj.1.A, 5kc2.1.B, 4a08.1.A, 4a08.1.B, 3ah8.1.B, 3fhc.1.A, 5ods.4.A, 5c2w.1.E, 3nok.1.A, 4lg8.1.A, 5a1u.1.S, 5a1u.1.T, 2xu7.1.A, 5flx.1.7, 2faw.1.A, 2xzg.1.A, 5juu.45.A, 1hzu.1.A, 1kbh.1.B, 4g55.1.A, 2zuy.1.A, 4cy2.1.A, 3wj9.1.A, 4v92.1.8, 5lks.64.A, 3k6s.2.A, 5k0y.1.8, 4ycz.1.A, 1hzv.1.A, 3mxx.1.A, 2j04.1.B, 5sui.1.A, 3jb9.1.L, 3ow8.1.A, 6gqv.75.A, 3jb9.1.K, 6bly.1.A, 6bly.1.B, 1vyh.1.C, 4yhc.2.A, 4ozu.1.A, 3c75.1.A, 5v3o.1.A, 2xl2.1.A, 5m5r.1.A, 6fec.1.e, 5fxy.2.A, 2bbk.1.A, 3jb9.1.S, 3mks.1.D, 3v9f.2.A, 4bts.27.A, 5wyj.17.A, 4v7e.7.A, 2o9k.1.A, 4xfv.1.A, 3dm0.1.A, 5y1u.1.A, 4up4.1.A, 4e5z.1.A, 3jan.80.A, 4e5z.1.B, 4v0n.2.B, 5it9.1.6, 5n1a.1.A, 5ukm.1.B, 2z2p.1.A, 2zux.1.A, 5mq0.1.I, 5u69.1.A, 4a0b.1.B, 2ynn.1.A, 6avr.1.A, 3qqz.1.A, 5wbi.1.A, 3iiy.1.A, 3bg0.1.A, 5oql.1.3, 5k1c.1.C, 5k1c.1.B, 3bg0.1.H, 3frx.1.A, 5igo.1.A, 5nnz.2.A, 4cy1.1.A, 4tqj.1.A, 5juy.1.B, 3va6.1.A, 5oql.1.X, 5d0o.1.B, 5juy.1.G, 5juy.1.D, 5juy.1.E, 6avu.1.A, 1h4i.1.A, 4a11.1.B, 2mta.1.A, 6exn.1.J, 4a11.1.A, 3ei4.3.A, 5oql.1.O, 5oql.1.L, 3n0d.1.A, 1xhm.1.A, 5oql.1.A, 5oql.1.F, 5oql.1.D, 5hyn.2.B, 6exn.1.a, 5juo.45.A, 1l0q.3.A, 3rfh.1.A, 6emk.1.D, 6emk.1.B, 5ov3.1.A,

5ov3.1.B, 4v7h.1.Q, 4v5o.1.0, 5wbu.1.B, 4bl0.2.A, 6fpt.1.A, 5ams.1.A, 5mzh.1.A, 3i7p.1.A, 3fcs.1.A, 5wg4.1.B, 6gqb.75.A, 3ei4.1.B, 1q7f.2.A, 3ei4.1.A, 5k0y.1.P, 4nen.1.A, 4mmz.1.A, 5m2n.1.A, 5h1j.1.A, 5f30.1.A, 4j73.1.A, 2pbi.2.B, 4z8l.1.A, 2b5n.1.A, 5cxb.1.B, 5cxb.1.A, 4c8s.1.A, 2co0.1.A, 5vlj.1.B, 5vlj.1.C, 6b3j.1.D, 3v9f.4.A, 5fvm.1.C, 6f9n.1.A, 6f9n.1.B, 5a5u.1.B, 4xf2.1.C, 5lcw.1.Q, 5lcw.1.R, 3vgz.1.A, 2p4o.1.A, 4bzj.1.D, 4bzj.1.B, 6fay.1.A, 1jju.1.B, 2dso.1.A, 3i7l.1.A, 6g16.4.A, 1l0q.1.A, 5nxq.1.A, 3va6.2.A, 5cvn.1.A, 2ymu.1.A, 3gd1.3.A, 4yhc.1.A, 4o9d.2.A, 5lyb.33.A, 5cxc.1.B, 5wve.1.K, 4fhl.1.A, 6g5h.1.8, 5vh9.1.B, 4zoz.1.A, 4exv.1.A, 5nem.1.E, 2ovr.1.B, 4gq2.1.B, 3j80.1.7, 4i79.1.A, 5es4.4.A, 5zcs.1.C, 4imm.1.A, 1erj.1.A, 1mda.1.A, 4a09.1.A, 2z2o.1.A, 6avq.1.A, 3uvo.1.A, 4czy.1.A, 3dwl.1.B, 1c9i.1.A, 4irz.1.A, 4av8.1.A, 4zov.1.A, 2gnq.1.A, 3acp.1.A, 1aoq.1.A, 5tga.33.A, 5g04.1.Q, 5wxe.1.A, 2aq5.1.A, 3v4v.2.A, 3hxj.2.A, 5wjc.1.A, 4o5s.1.A, 5wyk.1.V, 2hz6.1.A, 3e0c.1.A, 3jrp.1.A, 2v91.1.A, 2hye.1.A, 4j0x.1.A, 5fa5.1.B, 4ci8.1.A, 5k1a.1.B, 2xbg.1.A, 5nrl.1.W, 1dy7.1.A, 4x60.1.B, 2g99.1.A, 5nrl.1.O, 1e2r.1.B, 5aja.1.A, 5cvo.1.A, 4aez.1.A, 4xei.1.C, 3uzs.1.B, 6bnb.1.A, 3j78.45.A, 3vl1.2.A, 1e2r.1.A, 5mps.1.U, 4zox.1.A, 5v1d.1.C, 5v1d.1.A, 6byn.1.A, 5lj3.1.L, 3vi3.2.A, 2ojh.1.A, 3dr2.1.A, 6eoj.1.C, 2z2o.3.A, 3vu4.1.A, 6f3a.1.2, 4xga.1.A, 2ghs.1.A, 5hy7.2.A, 3rrm.1.C, 4a0a.1.B, 3ott.1.A, 3iiw.1.A, 2i3s.2.A, 5vai.1.D, 3mkq.1.E, 3vu4.2.A, 4a0b.1.A, 4gqb.1.B, 4a0l.1.B, 4zb4.2.A, 6dde.1.B, 5wlc.17.A, 4h5i.1.A, 5t2c.73.A, 6bcu.1.B, 4mh1.1.A, 4gm9.2.A, 4mh1.1.B, 2b5m.1.A, 4owr.1.A, 1gjq.1.A, 5o9z.1.L, 5mwj.1.A, 3nol.1.A, 3s8v.1.A, 5ods.3.A, 5o9z.1.F, 5mb4.1.A, 4wk4.1.A, 3nig.1.A, 3li5.1.A, 5ods.1.A, 5wyj.18.A, 4ggd.1.A, 5lj5.1.M, 5xyi.1.6, 4wju.2.A, 5mc6.15.A, 3bg0.1.D, 1k8k.1.C, 5xwr.1.A, 4g1m.1.A, 3n0e.1.A, 5tee.1.A, 3ei2.1.A, 3ei2.1.B, 5ukk.1.B, 4o45.1.A, 5vtb.1.A, 4gnb.1.A, 4j0w.1.A, 5jk7.2.A, 3jct.1.n, 5wg6.2.B, 4g56.1.B, 4q14.1.A, 3no2.1.A, 4cy3.1.A, 5lyb.108.A, 5jul.1.A, 5wlc.28.A, 5wlc.19.A, 5sxm.1.A, 5jk7.1.B, 5a9q.1.G, 5a9q.1.A, 5a9q.1.C, 6g16.1.A, 6bk8.1.P, 5wlc.26.A, 5l8e.1.A, 4cak.1.A, 2b5l.2.A, 4n14.1.A, 1gxr.1.B, 1gxr.1.A, 3mkq.1.A, 3ott.1.B, 3mkq.1.C, 3fcu.1.A, 6bk8.1.H, 4v6i.1.A, 1g72.1.A, 3ewe.1.A, 5grs.1.A, 5m23.1.A, 3j6y.75.A, 4a7j.1.A, 1kv9.1.A, 5hxb.1.B, 4kzz.1.6, 6d90.78.A, 4uuy.1.A, 4g1e.1.A, 2oit.1.A, 1bpo.1.C, 1bpo.1.B, 1bpo.1.A, 5c2v.1.B, 5sum.1.A, 3tc9.1.A, 4i0o.1.A, 3jam.1.7, 3jaq.1.i, 1m1x.1.A, 5nzu.1.C, 6cb1.1.a, 4psw.1.B, 1pev.1.A, 5y1u.2.A, 4v7r.20.A, 2g9a.1.A, 5nzu.1.A, 4d0k.1.A, 4lg9.1.A, 1yiq.1.A, 5wlc.24.A, 5dfz.1.C, 2yno.1.A, 4czv.1.A, 5obm.152.A, 5wlc.22.A, 5gxh.1.A, 5h3s.1.A, 5wlc.20.A, 3v64.1.A, 5ndv.147.A, 3vi3.1.A, 3v64.1.D, 2cnx.1.A, 5es4.1.A, 3fmo.1.A, 4wjk.1.A, 3hx6.1.A, 4v16.1.A, 1h4j.1.A, 5wyj.16.A, 2ias.1.A, 4pk1.1.A, 4mmx.1.A, 1tbg.1.E, 4xyh.1.A, 1tbg.1.A, 4u1e.1.A, 4ci1.1.A, 3lrv.1.A, 5m89.1.A, 3q7o.1.A, 3cfs.1.A, 5i2t.1.A, 1u8c.1.A, 4gga.1.A, 2yh3.1.A, 3cik.1.B, 4bh6.1.A, 6g18.1.L, 1lrw.1.C, 2qxv.1.A, 1lrw.1.A, 5ner.1.E, 3p1l.1.A, 5jpq.1.Y, 4j79.1.A, 5lzz.77.A, 2i3t.1.A, 3k6s.5.A, 5gva.1.A, 5jpq.1.I, 5nnz.1.A, 3zwl.1.A, 4um8.1.A, 3rfg.1.A, 3c9c.1.A, 4um9.1.A, 3emh.1.A, 4z7q.1.A, 3q7m.1.A, 6cvz.1.A, 3jro.1.A, 1kb0.1.A, 1yfq.1.A, 5ij7.1.B, 5ljo.1.A, 5igo.2.A, 3rfh.1.B, 5ife.1.D, 4d5l.1.7, 3sjl.1.D, 3gre.1.A, 4ggc.1.A, 5ex7.1.A, 2b5n.3.A, 6gq1.75.A, 2pbi.1.B, 3jai.77.A, 6fec.1.n, 4yzs.1.A, 3wj9.2.A, 4yzs.1.B, 1gq1.1.A, 4aow.1.A, 4v3p.1.A, 5wai.1.A, 5em2.1.B, 4zov.2.A, 5em2.1.A, 3mmy.1.A, 5ltd.1.A, 4a0k.1.C, 4l9o.1.A, 4gm3.1.A, 4a0k.1.D, 1got.1.B, 2c52.1.A, 2h9l.1.A, 6fai.1.E, 1utc.2.A, 2iwa.1.A, 3v9f.3.A, 1q7f.1.A, 5uz7.1.B, 3e5z.1.A, 5kdo.1.B, 2co0.2.A, 1u4c.1.A, 3v9f.1.A, 4ci8.2.A

SWISS-MODEL Homology Modelling Report

Model Building Report

This document lists the results for the homology modelling project "BBS2_HUMAN Q9BXC9 Bardet-Biedl syndrome 2 protein" submitted to SWISS-MODEL workspace on July 23, 2018, 3:46 p.m..The submitted primary amino acid sequence is given in Table T1.

If you use any results in your research, please cite the relevant publications:

- Waterhouse, A., Bertoni, M., Bienert, S., Studer, G., Tauriello, G., Gumienny, R., Heer, F.T., de Beer, T.A.P., Rempfer, C., Bordoli, L., Lepore, R., Schwede, T. SWISS-MODEL: homology modelling of protein structures and complexes. Nucleic Acids Res. 46(W1), W296-W303 (2018). doi
- Guex, N., Peitsch, M.C., Schwede, T. Automated comparative protein structure modeling with SWISS-MODEL and Swiss-PdbViewer: A historical perspective. Electrophoresis 30, S162-S173 (2009). doi
- Bienert, S., Waterhouse, A., de Beer, T.A.P., Tauriello, G., Studer, G., Bordoli, L., Schwede, T. The SWISS-MODEL Repository - new features and functionality. Nucleic Acids Res. 45, D313-D319 (2017). doi
- Benkert, P., Biasini, M., Schwede, T. Toward the estimation of the absolute quality of individual protein structure models. Bioinformatics 27, 343-350 (2011). doi
- Bertoni, M., Kiefer, F., Biasini, M., Bordoli, L., Schwede, T. Modeling protein quaternary structure of homo- and hetero-oligomers beyond binary interactions by homology. Scientific Reports 7 (2017). doi

Results

The SWISS-MODEL template library (SMTL version 2018-07-12, PDB release 2018-07-06) was searched with BLAST (Camacho et al.) and HHBlits (Remmert et al.) for evolutionary related structures matching the target sequence in Table T1. For details on the template search, see Materials and Methods. Overall 1530 templates were found (Table T2).

Models

No models have been built for this project.

Materials and Methods

Template Search

Template search with BLAST and HHBlits has been performed against the SWISS-MODEL template library (SMTL, last update: 2018-07-12, last included PDB release: 2018-07-06).

The target sequence was searched with BLAST against the primary amino acid sequence contained in the SMTL.

An initial HHblits profile has been built using the procedure outlined in (Remmert et al.), followed by 1 iteration of HHblits against NR20. The obtained profile has then be searched against all profiles of the SMTL. A total of 1574 templates were found.

Template Selection

For each identified template, the template's quality has been predicted from features of the target-template alignment. The templates with the highest quality have then been selected for model building.

Model Building

Models are built based on the target-template alignment using ProMod3. Coordinates which are conserved between the target and the template are copied from the template to the model. Insertions and deletions are remodelled using a fragment library. Side chains are then rebuilt. Finally, the geometry of the resulting model is regularized by using a force field. In case loop modelling with ProMod3 fails, an alternative model is built with PROMOD-II (Guex et al.).

Model Quality Estimation

The global and per-residue model quality has been assessed using the QMEAN scoring function (Benkert et al.) . For improved performance, weights of the individual QMEAN terms have been trained specifically for SWISS-MODEL.

Ligand Modelling

Ligands present in the template structure are transferred by homology to the model when the following criteria are met: (a) The ligands are annotated as biologically relevant in the template library, (b) the ligand is in contact with the model, (c) the ligand is not clashing with the protein, (d) the residues in contact with the ligand are conserved between the target and the template. If any of these four criteria is not satisfied, a certain ligand will not be included in the model. The model summary includes information on why and which ligand has not been included.

Oligomeric State Conservation

The quaternary structure annotation of the template is used to model the target sequence in its oligomeric form. The method (Bertoni et al.) is based on a supervised machine learning algorithm, Support Vector Machines (SVM), which combines interface conservation, structural clustering, and other template features to provide a quaternary structure quality estimate (QSQE). The QSQE score is a number between 0 and 1, reflecting the expected accuracy of the interchain contacts for a model built based a given alignment and template. Higher numbers indicate higher reliability. This complements the GMQE score which estimates the accuracy of the tertiary structure of the resulting model.

References

- **BLAST**
  Camacho, C., Coulouris, G., Avagyan, V., Ma, N., Papadopoulos, J., Bealer, K., Madden, T.L. BLAST+: architecture and applications. BMC Bioinformatics 10, 421-430 (2009). doi
- **HHblits**
  Remmert, M., Biegert, A., Hauser, A., Söding, J. HHblits: lightning-fast iterative protein sequence searching by HMM-HMM alignment. Nat Methods 9, 173-175 (2012). doi

Table T1:

Primary amino acid sequence for which templates were searched and models were built.

```
MLLPVFTLKLRHKISPRMVAIGRYDGTHPCLAAATQTGKVFIHNPHTRNQHVSASRVFQSPLESDVSLLNINQAVSCLTAGVLNPELGYDALLVGTQTNL
LAYDVYNNSDLFYREVADGANAIVLGTLGDISSPLAIIGGNCALQGFNHEGSDLFWTVTGDNVNSLALCDFDGDGKKELLVGSEDFDIRVFKEDEIVAEM
TETEIVTSLCPMYGSRFGYALSNGTVGVYDKTSRYWRIKSKNHAMSIHAFDLNSDGVNELITGWSNGKVDARSDRTGEVIFKDNFSSAIAGVVEGDYRMD
GHIQLICCSVDGEIRGYLPGTAEMRGNLMDTSAEQDLIRELSQKKQNLLLELRNYEENAKAELASPLNEADGHRGIIPANTRLHTTLSVSLGNETQTAHT
ELRISTSNDTIIRAVLIFAEGIFTGESHVVHPSIHNLSSSICIPIVPPKDVPVDLHLKAFVGYRSSTQFHVFESTRQLPRFSMYALTSLDPASEPISYVN
FTIAERAQRVVVWLGQNFLLPEDTHIQNAPFQVCFTSLRNGGHLHIKIKLSGEITINTDDIDLAGDIIQSMASFFAIEDLQVEADFPVYFEELRKVLVKV
DEYHSVHQKLSADMADHSNLIRSLLVGAEDARLMRDMKTMKSRYMELYDLNRDLLNGYKIRCNNHTELLGNLKAVNQAIQRAGRLRVGKPKNQVITACRD
AIRSNNINTLFKIMRVGTASS
```

Table T2:

Template	Seq Identity	Oligo-state	QSQE	Found by	Method	Resolution	Seq Similarity	Coverage	Description
5tee.1.A	18.28	monomer		HHblits	X-ray	1.65Å	0.28	0.39	Gem-associated protein 5
5igq.1.A	13.95	monomer		HHblits	X-ray	3.90Å	0.28	0.41	E3 ubiquitin-protein ligase RFWD2
5gxh.1.A	18.35	monomer		HHblits	X-ray	1.80Å	0.28	0.39	Gem-associated protein 5
5cvl.1.A	12.28	monomer		HHblits	X-ray	3.00Å	0.26	0.40	WD repeat-containing protein 48
5cvn.1.A	12.28	monomer		HHblits	X-ray	3.36Å	0.26	0.40	WD repeat-containing protein 48
5hqg.1.A	13.52	monomer		HHblits	X-ray	2.00Å	0.27	0.39	E3 ubiquitin-protein ligase RFWD2
4zn4.1.A	14.14	monomer		HHblits	X-ray	1.94Å	0.27	0.40	sqt1
5sxm.1.A	13.83	monomer		HHblits	X-ray	2.00Å	0.27	0.39	WD repeat-containing protein 5
5k1c.1.B	12.68	monomer		HHblits	X-ray	3.00Å	0.27	0.39	WD repeat-containing protein 48
5it9.1.6	13.38	monomer		HHblits	EM	3.80Å	0.27	0.39	Ribosomal protein RACK1
5cvo.1.A	12.32	monomer		HHblits	X-ray	3.88Å	0.26	0.39	WD repeat-containing protein 48
5l8e.1.A	12.32	monomer		HHblits	X-ray	2.30Å	0.27	0.39	WD repeat-containing protein 48
5l8w.1.B	12.32	monomer		HHblits	X-ray	2.79Å	0.27	0.39	WD repeat-containing protein 48
3j77.45.A	12.80	monomer		HHblits	EM	NA	0.26	0.40	Guanine nucleotide-binding protein sub-unit beta-like protein
3jbt.1.A	13.17	monomer		HHblits	EM	NA	0.28	0.39	Apoptotic protease-activating factor 1
5jus.45.A	12.80	monomer		HHblits	EM	NA	0.26	0.40	RACK1 (yeast Asc1)
5mc6.15.A	12.80	monomer		HHblits	EM	NA	0.26	0.40	Guanine nucleotide-binding protein sub-unit beta-like protein
4v6i.1.A	12.80	monomer		HHblits	EM	NA	0.26	0.40	40S ribosomal protein RACK1 (RACK1)
3j78.45.A	12.80	monomer		HHblits	EM	NA	0.26	0.40	Guanine nucleotide-binding protein sub-unit beta-like protein
3j6y.75.A	12.80	monomer		HHblits	EM	NA	0.26	0.40	Guanine nucleotide-binding protein sub-unit beta-like protein
3j6x.75.A	12.80	monomer		HHblits	EM	NA	0.26	0.40	Guanine nucleotide-binding protein sub-unit beta-like protein
5wve.1.K	13.57	monomer		HHblits	EM	NA	0.28	0.39	Apoptotic protease-activating factor 1
5k1a.1.B	12.37	monomer		HHblits	X-ray	2.30Å	0.27	0.39	WD repeat-containing protein 48
5k1a.2.B	12.37	monomer		HHblits	X-ray	2.30Å	0.27	0.39	WD repeat-containing protein 48
5u69.1.A	12.11	monomer		HHblits	X-ray	1.28Å	0.26	0.40	Polycomb protein EED
6byn.1.A	13.78	monomer		HHblits	X-ray	2.69Å	0.27	0.39	WD repeat-containing protein 5
3j2t.1.A	13.57	monomer		HHblits	EM	NA	0.28	0.39	Apoptotic protease-activating factor 1
4v92.1.8	13.07	monomer		HHblits	EM	3.70Å	0.27	0.39	RACK1

3shf.1.A	16.01	monomer		HHblits	X-ray	3.55Å	0.29	0.39	Apoptotic peptidase activating factor 1
5wlc.13.A	11.15	monomer		HHblits	EM	NA	0.25	0.40	Utp17
5juy.1.E	13.57	monomer		HHblits	EM	NA	0.28	0.39	Apoptotic protease-activating factor 1
5juy.1.D	13.57	monomer		HHblits	EM	NA	0.28	0.39	Apoptotic protease-activating factor 1
5juy.1.G	13.57	monomer		HHblits	EM	NA	0.28	0.39	Apoptotic protease-activating factor 1
5juy.1.B	13.57	monomer		HHblits	EM	NA	0.28	0.39	Apoptotic protease-activating factor 1
1pi6.1.A	14.13	monomer		HHblits	X-ray	2.50Å	0.27	0.39	Actin interacting protein 1
5wyj.18.A	11.99	monomer		HHblits	EM	NA	0.26	0.40	U3 small nucleolar RNA-associated protein 13
6b3x.1.A	13.12	monomer		HHblits	X-ray	2.30Å	0.27	0.39	Cleavage stimulation factor subunit 1
4gq2.1.B	11.95	monomer		HHblits	X-ray	2.40Å	0.25	0.41	Nup37
1s4u.1.A	14.18	monomer		HHblits	X-ray	2.10Å	0.27	0.39	Antiviral protein SKI8
3sfz.1.A	15.66	monomer		HHblits	X-ray	3.00Å	0.29	0.39	Apoptotic peptidase activating factor 1
4gq1.1.A	11.95	monomer		HHblits	X-ray	2.40Å	0.25	0.41	Nup37
5wlc.13.A	10.84	monomer		HHblits	EM	NA	0.26	0.40	Utp17
4zoy.1.A	14.24	monomer		HHblits	X-ray	1.50Å	0.27	0.40	Sqt1
2h9l.1.A	13.12	monomer		HHblits	X-ray	1.75Å	0.27	0.39	WD-repeat protein 5
3frx.1.A	12.80	monomer		HHblits	X-ray	2.13Å	0.26	0.40	Guanine nucleotide-binding protein subunit beta-like protein
2g99.1.A	14.18	monomer		HHblits	X-ray	1.90Å	0.27	0.39	WD-repeat protein 5
4a7j.1.A	13.12	monomer		HHblits	X-ray	1.90Å	0.27	0.39	WD REPEAT-CONTAINING PROTEIN 5
3uvo.1.A	13.43	monomer		HHblits	X-ray	2.20Å	0.27	0.39	WD repeat-containing protein 5
1erj.1.A	13.12	monomer		HHblits	X-ray	2.30Å	0.27	0.39	TRANSCRIPTIONAL REPRESSOR TUP1
4cy3.1.A	13.83	monomer		HHblits	X-ray	1.40Å	0.27	0.39	PROTEIN WILL DIE SLOWLY

The table above shows the top 50 filtered templates. A further 787 templates were found which were considered to be less suitable for modelling than the filtered list.
3fgb.1.A, 3hxj.1.B, 3vl1.1.A, 2vdu.1.A, 5i5m.1.A, 4a0b.2.A, 5cvl.1.A, 4czv.1.A, 5hy7.2.A, 5cvo.2.A, 3fm0.1.A, 2ynp.1.A, 3dxm.1.C, 4tqo.1.A, 5yje.1.A, 5yje.1.B, 5yje.1.C, 5ukl.1.B, 3q54.1.A, 4e54.1.B, 4e54.1.A, 5naf.1.A, 5wg4.1.B, 4tz4.1.A, 3sn6.1.B, 3hxj.1.A, 1ri6.1.A, 6bw3.1.A, 6c23.1.D, 5tzs.1.e, 5h1k.1.A, 5wak.1.A, 6fbs.1.B, 2iao.1.A, 1r5m.1.A, 4o9x.1.A, 4gq1.1.A, 1xip.1.A, 4ui9.1.Q, 1p22.1.A, 4ui9.1.I, 5vfc.1.A, 2h6k.1.A, 2yms.1.B, 2yms.1.A, 5cyk.1.A, 3hfq.1.A, 5cyk.1.B, 2xyi.1.A, 5tzs.1.1, 2pm9.1.A, 3v4v.1.A, 1tye.1.A, 3f3g.1.E, 5gm6.1.F, 4jio.2.A, 1aof.1.A, 1aof.1.B, 2iax.1.A, 5lks.64.A, 6en4.1.A, 3w15.1.A, 5ffo.1.A, 3bws.1.A, 2yvc.3.A, 5naf.3.A, 5h13.1.A, 3k72.1.A, 5vyc.4.I, 2c4d.1.A, 5v1d.2.B, 4c8h.1.A, 5v1d.2.A, 4jsn.1.B, 4a7k.1.A, 1jmz.1.B, 2x6p.1.A, 1nex.2.B, 4aez.2.A, 5opt.1.A, 1gp2.1.B, 4nox.1.A, 5wsg.1.U, 4a0l.1.A, 4d6v.1.A, 3jbt.1.A, 5cxc.1.A, 5k0m.1.A, 2yvc.1.A, 6gdg.1.B, 1jof.1.A, 4jxm.1.A, 6em3.1.E, 2i3s.1.A, 4cvc.1.A, 5v3o.1.A, 5es4.3.A, 6bcx.1.C, 6f3a.1.3, 3j7p.78.A, 5neu.3.E, 3sfz.1.A, 3vu4.2.A, 2ce9.2.B, 5jcs.1.3, 4nsx.1.A, 6g5i.1.6, 1isn.1.A, 5wyk.1.U, 4a2m.2.A, 5ukk.1.B, 5wyk.1.R, 5tdh.1.B, 3jzn.1.A, 5wg6.1.B, 5lj5.1.d, 5kc2.1.B, 5igq.1.A, 1a0r.1.A, 5m1j.14.A, 4v5z.1.A, 5mqf.1.F, 5mqf.1.D, 5mqf.1.E, 4xmm.1.C, 5kis.1.A, 5jut.45.A, 3shf.1.A, 4fhm.1.A, 3j81.1.5, 4pxw.1.A, 6c23.1.F, 4v6w.2.A, 4v0m.1.B, 3ewe.1.A, 1vlk.1.A, 3mbr.1.A, 5ndv.73.A, 4a2l.1.B, 5sv7.1.A, 4wjv.1.A, 3jap.1.i, 5sv7.1.B, 5sv7.1.C, 5a31.1.R, 5k1a.2.B, 5yfp.1.C, 5k1h.1.A, 5u5h.1.A, 3ei3.1.A, 4c8h.1.C, 5wlc.15.A, 4j87.1.A, 5bpw.1.A, 5wyk.1.V, 4neh.1.A, 4x51.1.A, 4mae.1.A, 5h19.1.A, 4a0l.2.A, 4zri.1.A, 5sv7.1.D, 5e6u.1.A, 3odt.1.A, 3dsm.1.A, 4v8m.8.A, 5afu.1.C, 4r40.1.A, 2d0v.1.A, 5gmk.1.0, 3li4.1.A, 6em5.1.5, 5wlc.27.A, 5m11.1.A, 4xyh.1.A, 5h64.1.B, 5h64.1.C, 6em5.1.h, 2ovp.1.B, 2w18.1.A, 5tf2.1.A, 5xjc.1.W, 2b5n.2.A, 4bzj.1.B, 3fhc.1.A, 1flg.1.A, 5xjc.1.E, 5ic7.1.A, 4cc9.1.A, 4x3e.1.A, 4o02.1.A, 4zoy.1.A, 5gmk.1.J, 5kkl.1.A, 1w6s.1.A, 5gmk.1.X, 4z7o.1.A, 2b5n.4.A, 6ek0.64.A, 4wk0.1.A, 6fq3.1.A, 5zya.1.D, 6b3x.1.A, 2oaj.1.A, 5ffg.1.A, 2ivz.1.A, 3uvo.1.A, 4wju.1.A, 5jus.45.A, 6az1.1.6, 5wlc.25.A, 5wuk.1.A, 2hes.1.A, 1s4u.1.A, 4wjs.1.A, 3hlh.1.A, 3j77.45.A, 4zlr.1.A, 2b5l.1.A, 4cag.1.A, 5gap.1.F, 4imm.2.A, 3u4y.1.A, 5nuv.1.A, 5wyj.19.A, 3j2t.1.A, 5em2.2.B, 4yd8.1.A, 5hqg.1.A, 5v4b.1.B, 1pi6.1.A, 1y6m.1.A, 1sq9.1.A, 5bjs.1.A, 5xm3.1.A, 5n4a.1.A, 6f0t.1.A, 5l8w.1.B, 5j9q.2.D, 2yba.1.A, 3f3p.2.B, 1b9y.1.A, 4zb4.1.A, 3i2n.1.A, 5ayw.1.B, 5m89.2.A, 5wbk.1.A, 4v7f.1.j, 6cmo.1.C, 5guw.3.A, 1lrw.1.C, 4yzy.1.A, 3jcm.1.B, 3v7d.1.B, 4l9o.2.A, 2bcj.1.B, 3j78.45.A, 3i7k.1.A, 2iat.1.A, 5a2q.1.8, 4ggd.1.A, 3prw.1.A, 6cb1.1.a, 4o9d.1.A, 5lj5.1.M, 4hdj.1.A, 5t2a.48.A, 4a08.1.A, 4a08.1.B, 4pwz.1.A, 4yhc.1.A, 3ah8.1.B, 5c2w.1.E, 4lg8.1.A, 5a1u.1.T, 2xu7.1.A, 5flx.1.7, 5juu.45.A, 1hzu.1.A, 3j80.1.7, 3mzk.1.A, 4um9.1.A, 1c5k.1.A, 2zuy.1.A, 4cy2.1.A, 3wj9.1.A, 4v92.1.8, 5k19.2.A, 3k6s.2.A, 5k0y.1.8, 4ycz.1.A, 1hzv.1.A, 3mxx.1.A, 3jan.80.A, 3jb9.1.L, 2ynn.1.A, 6gqv.75.A, 4buj.1.D, 4cy1.1.A, 6bly.1.B, 5gva.1.A, 1vyh.1.C, 4yhc.2.A, 4ozu.1.A, 6fec.1.n, 2xl2.1.A, 6fec.1.e, 5fxy.2.A, 3jb9.1.S, 3mks.1.D, 4ug3.1.B, 3v9f.2.A, 4bts.27.A, 5wyj.17.A, 4v7e.7.A, 2iap.1.A, 2o9k.1.A, 1k8v.1.A, 4xfv.1.A, 3dm0.1.A, 5y1u.1.A, 4up4.1.A, 4e5z.1.A, 5sui.1.A, 4e5z.1.B, 4v0n.2.B, 5it9.1.6, 5n1a.1.A, 5ukm.1.B, 2z2p.1.A, 4buj.1.C, 5hy7.1.A, 3vl1.2.A, 5u69.1.A, 3iiw.1.A, 3ow8.1.A, 1ilk.1.A, 6avr.1.A, 3li3.1.A, 3bg0.1.D, 3jb9.1.K, 3bg0.1.A, 5oql.1.3, 5k1c.1.C, 5k1c.1.B, 3bg0.1.H, 3frx.1.A, 5igo.1.A, 5nnz.2.A, 5j9t.3.B, 4tqj.1.A, 5juy.1.B, 3va6.1.A, 5d0o.1.B, 5juy.1.G, 5juy.1.D, 5juy.1.E, 6avu.1.A, 1h4i.1.A, 4a11.1.B, 6exn.1.J, 4a11.1.A, 5oql.1.N, 5oql.1.O, 5oql.1.L, 3n0d.1.A, 1xhm.1.A, 5oql.1.A, 5oql.1.F, 5oql.1.D, 5hyn.2.B, 6exn.1.a, 5juo.45.A, 1l0q.3.A, 3rfh.1.A, 2gnq.1.A, 6emk.1.B, 5ov3.1.A, 5ov3.1.B, 4v7h.1.Q, 4v5o.1.0, 5wbu.1.B, 5em2.1.A, 1jju.1.B, 5ams.1.A, 5mzh.1.A, 3i7p.1.A, 3fcs.1.A, 2h13.1.A, 6gqb.75.A, 3ei4.1.B, 1q7f.2.A, 3ei4.1.A, 5k0y.1.P, 4nen.1.A, 4mmz.1.A, 5m2n.1.A, 5h1j.1.A, 5f30.1.A, 4j73.1.A, 2pbi.2.B, 4z8l.1.A, 2b5n.1.A, 5cxb.1.B, 5cxb.1.A, 3jpx.1.A, 4c8s.1.A, 2co0.1.A, 4x51.1.B, 5vlj.1.B, 5vlj.1.C, 6b3j.1.D, 3v9f.4.A, 5fvm.1.C, 6f9n.1.B, 5a5u.1.B, 4u7a.1.A, 4xf2.1.C, 5lcw.1.Q, 5lcw.1.R, 3vgz.1.A, 2yvc.2.A, 4bzj.1.D, 4bzj.1.C, 5mc6.37.A, 4bzj.1.A, 4ug3.1.A, 3x23.1.A, 3i7l.1.A, 6g16.4.A, 1l0q.1.A, 2iaw.1.A, 5lcw.1.I, 2zpy.1.A, 3fb2.1.A, 5nxq.1.A, 3va6.2.A, 5cvn.1.A, 2ymu.1.A, 2i0s.1.C, 5lyb.33.A, 5cxc.1.B, 4jio.1.A, 5j9t.2.B, 5g05.1.I, 2agl.1.C, 2kc2.1.A, 5wve.1.K, 4fhl.1.A, 6g5h.1.8, 5vh9.1.B, 4zoz.1.A, 4exv.1.A, 5nem.1.E, 2ovr.1.B, 4gq2.1.B, 4bl0.2.A, 4i79.1.A, 5es4.4.A, 5zcs.1.C, 1erj.1.A, 4a09.1.A, 2ojy.1.C, 6avq.1.A, 4o9d.2.A, 4czy.1.A, 4bzk.1.D, 3dwl.1.B, 2x6p.1.B, 4irz.1.A, 2iar.1.A, 4av8.1.A, 4zov.1.A, 5tee.1.A, 4aah.1.A, 4xmn.1.A, 2ecf.1.A, 4uer.1.b, 3acp.1.A, 1aoq.1.A, 5tga.33.A, 5g04.1.Q, 2aq5.1.A, 3v4v.2.A, 3ije.1.A, 3hxj.2.A, 5wjc.1.A, 3hxj.2.B, 5g04.1.I, 2hz6.1.A, 3e0c.1.A, 3jrp.1.A, 2hye.1.A, 4j0x.1.A, 5fa5.1.B, 5wp3.1.A, 4ci8.1.A, 5k1a.1.B, 5nrl.1.W, 1dy7.1.A, 4x60.1.B, 2g99.1.A, 5nrl.1.O, 2vdo.1.A, 1e2r.1.B, 5aja.1.A, 2gvu.1.A, 5cvo.1.A, 4aez.1.A, 4xei.1.C, 3uzs.1.B, 2zux.1.A, 3ei4.3.A, 2gvx.1.A, 5mq0.1.I, 1e2r.1.A, 5mps.1.U, 4zox.1.A, 5v1d.1.C, 5v1d.1.A, 5es4.2.A, 6byn.1.A, 5lj3.1.L, 3vi3.2.A, 2ojh.1.A, 6eoj.1.A, 3dr2.1.A, 6eoj.1.C, 3vu4.1.A, 6f3a.1.2, 4xga.1.A, 2ghs.1.A, 4a0a.1.A, 3rrm.1.C, 4a0a.1.B, 3ott.1.A, 4a0b.1.B, 2i3s.2.A, 5vai.1.D, 3mkq.1.E, 3j6x.75.A, 4a0b.1.A, 4gqb.1.B, 4a0l.1.B, 2d11.3.A, 4zb4.2.A, 6dde.1.B,

5wlc.17.A, 4g1a.1.A, 4h5i.1.A, 5t2c.73.A, 6emk.1.D, 6bcu.1.B, 4mh1.1.A, 4gm9.2.A, 4mh1.1.B, 2b5m.1.A, 4owr.1.A, 1gjq.1.A, 5o9z.1.L, 5mwj.1.A, 5o9z.1.F, 5mb4.1.A, 4wk4.1.A, 3nig.1.A, 3li5.1.A, 2qlx.1.A, 5wyj.18.A, 4yzs.1.A, 5m5g.1.A, 6b20.1.A, 6d9j.78.A, 5bpt.1.A, 5xyi.1.6, 4wju.2.A, 5mc6.15.A, 5wbi.1.A, 1k8k.1.C, 5xwr.1.A, 4g1m.1.A, 3n0e.1.A, 2j04.1.B, 3ei2.1.A, 3ei2.1.B, 4yvd.1.A, 4o45.1.A, 4qrj.1.A, 5vtb.1.A, 4j0w.1.A, 3wa0.1.A, 5jk7.2.A, 3jct.1.n, 5wg6.2.B, 3fb2.2.A, 4g56.1.B, 3no2.1.A, 4cy3.1.A, 5lyb.108.A, 5jul.1.A, 5wlc.28.A, 2d11.1.A, 6f1t.1.b, 6f1t.1.c, 5wlc.19.A, 5sxm.1.A, 5jk7.1.B, 5a9q.1.G, 5a9q.1.A, 6f1t.1.4, 5a9q.1.C, 6g16.1.A, 3scy.1.A, 6bk8.1.P, 2iiu.1.A, 5wlc.26.A, 5l8e.1.A, 4cak.1.A, 2b5l.2.A, 4n14.1.A, 1gxr.1.B, 1gxr.1.A, 4v3p.1.A, 3mkq.1.A, 3ott.1.B, 3mkq.1.C, 3fcu.1.A, 6bk8.1.H, 4v6i.1.A, 1g72.1.A, 5kdo.1.B, 5grs.1.A, 5m23.1.A, 3j6y.75.A, 4a7j.1.A, 1kv9.1.A, 4r40.2.A, 5hxb.1.B, 4kzz.1.6, 6d90.78.A, 6f1t.1.3, 4g1e.1.A, 5i5i.1.A, 2oit.1.A, 5c2v.1.B, 5sum.1.A, 3jam.1.7, 3hli.1.A, 1y6n.1.A, 3jaq.1.i, 1m1x.1.A, 5nzu.1.C, 4psw.1.B, 1pev.1.A, 5y1u.2.A, 4v7r.20.A, 2g9a.1.A, 2iau.1.A, 4d0k.1.A, 4lg9.1.A, 1yiq.1.A, 5wlc.24.A, 3dw8.1.B, 4a0p.1.A, 3g4e.1.A, 5dfz.1.C, 2yno.1.A, 5obm.152.A, 5wlc.22.A, 6f38.1.3, 6f38.1.4, 3byc.1.A, 5gxh.1.A, 5h3s.1.A, 5wlc.20.A, 5ndv.147.A, 3vi3.1.A, 2cnx.1.A, 5es4.1.A, 2x6p.1.C, 3fmo.1.A, 4wjk.1.A, 3i1c.1.A, 3g4h.1.B, 3g4h.1.A, 4v16.1.A, 5e6s.2.A, 1h4j.1.A, 6f38.1.b, 6f38.1.c, 5wyj.16.A, 2ias.1.A, 4pk1.1.A, 4mmx.1.A, 1tbg.1.E, 5ttw.2.A, 4zn4.1.A, 1tbg.1.A, 4u1e.1.A, 4ci1.1.A, 3lrv.1.A, 5m89.1.A, 3q7o.1.A, 3cfs.1.A, 5i2t.1.A, 1u8c.1.A, 5oql.1.M, 4gga.1.A, 2yh3.1.A, 3cik.1.B, 4bh6.1.A, 6g18.1.L, 4u1f.1.A, 2qxv.1.A, 1lrw.1.A, 5ner.1.E, 3p1l.1.A, 5jpq.1.Y, 3ra3.1.B, 4j79.1.A, 5lzz.77.A, 2i3t.1.A, 3k6s.5.A, 5wyj.20.A, 5jpq.1.I, 5nnz.1.A, 3zwl.1.A, 4um8.1.A, 3rfg.1.A, 2iaq.1.A, 4igl.1.A, 3c9c.1.A, 2pm7.1.D, 3emh.1.A, 4z7q.1.A, 3q7m.1.A, 6cvz.1.A, 3jro.1.A, 1kb0.1.A, 1yfq.1.A, 5j9t.1.B, 5ij7.1.B, 5ljo.1.A, 5igo.2.A, 3rfh.1.B, 5ife.1.D, 4d5l.1.7, 3gre.1.A, 4ggc.1.A, 5ex7.1.A, 2b5n.3.A, 3iiy.1.A, 6gq1.75.A, 2pbi.1.B, 3jai.77.A, 3f3f.1.A, 3wj9.2.A, 4yzs.1.B, 1gq1.1.A, 4aow.1.A, 2i0r.1.C, 5wai.1.A, 6fpt.1.A, 5em2.1.B, 4zov.2.A, 5mc6.36.A, 2pm6.1.B, 4imm.1.A, 3mmy.1.A, 5ltd.1.A, 4a0k.1.C, 4gm3.1.A, 4a0k.1.D, 1got.1.B, 4ug3.2.A, 4ug3.2.B, 2h9l.1.A, 6fai.1.E, 3ra3.2.A, 3v9f.3.A, 1q7f.1.A, 5uz7.1.B, 3e5z.1.A, 4l9o.1.A, 2co0.2.A, 1u4c.1.A, 3v9f.1.A, 4ci8.2.A

SWISS-MODEL Homology Modelling Report

Model Building Report

This document lists the results for the homology modelling project "BBS4_HUMAN Q96RK4 Bardet-Biedl syndrome 4 protein" submitted to SWISS-MODEL workspace on July 23, 2018, 3:52 p.m..The submitted primary amino acid sequence is given in Table T1.

If you use any results in your research, please cite the relevant publications:

- Waterhouse, A., Bertoni, M., Bienert, S., Studer, G., Tauriello, G., Gumienny, R., Heer, F.T., de Beer, T.A.P., Rempfer, C., Bordoli, L., Lepore, R., Schwede, T. SWISS-MODEL: homology modelling of protein structures and complexes. Nucleic Acids Res. 46(W1), W296-W303 (2018). doi
- Guex, N., Peitsch, M.C., Schwede, T. Automated comparative protein structure modeling with SWISS-MODEL and Swiss-PdbViewer: A historical perspective. Electrophoresis 30, S162-S173 (2009). doi
- Bienert, S., Waterhouse, A., de Beer, T.A.P., Tauriello, G., Studer, G., Bordoli, L., Schwede, T. The SWISS-MODEL Repository - new features and functionality. Nucleic Acids Res. 45, D313-D319 (2017). doi
- Benkert, P., Biasini, M., Schwede, T. Toward the estimation of the absolute quality of individual protein structure models. Bioinformatics 27, 343-350 (2011). doi
- Bertoni, M., Kiefer, F., Biasini, M., Bordoli, L., Schwede, T. Modeling protein quaternary structure of homo- and hetero-oligomers beyond binary interactions by homology. Scientific Reports 7 (2017). doi

Results

The SWISS-MODEL template library (SMTL version 2018-07-12, PDB release 2018-07-06) was searched with BLAST (Camacho et al.) and HHBlits (Remmert et al.) for evolutionary related structures matching the target sequence in Table T1. For details on the template search, see Materials and Methods. Overall 2059 templates were found (Table T2).

Models

No models have been built for this project.

Materials and Methods

Template Search

Template search with BLAST and HHBlits has been performed against the SWISS-MODEL template library (SMTL, last update: 2018-07-12, last included PDB release: 2018-07-06).

The target sequence was searched with BLAST against the primary amino acid sequence contained in the SMTL. A total of 19 templates were found.

An initial HHblits profile has been built using the procedure outlined in (Remmert et al.), followed by 1 iteration of HHblits against NR20. The obtained profile has then be searched against all profiles of the SMTL. A total of 2046 templates were found.

Template Selection

For each identified template, the template's quality has been predicted from features of the target-template alignment. The templates with the highest quality have then been selected for model building.

Model Building

Models are built based on the target-template alignment using ProMod3. Coordinates which are conserved between the target and the template are copied from the template to the model. Insertions and deletions are remodelled using a fragment library. Side chains are then rebuilt. Finally, the geometry of the resulting model is regularized by using a force field. In case loop modelling with ProMod3 fails, an alternative model is built with PROMOD-II (Guex et al.).

Model Quality Estimation

The global and per-residue model quality has been assessed using the QMEAN scoring function (Benkert et al.) . For improved performance, weights of the individual QMEAN terms have been trained specifically for SWISS-MODEL.

Ligand Modelling

Ligands present in the template structure are transferred by homology to the model when the following criteria are met: (a) The ligands are annotated as biologically relevant in the template library, (b) the ligand is in contact with the model, (c) the ligand is not clashing with the protein, (d) the residues in contact with the ligand are conserved between the target and the template. If any of these four criteria is not satisfied, a certain ligand will not be included in the model. The model summary includes information on why and which ligand has not been included.

Oligomeric State Conservation

The quaternary structure annotation of the template is used to model the target sequence in its oligomeric form. The method (Bertoni et al.) is based on a supervised machine learning algorithm, Support Vector Machines (SVM), which combines interface conservation, structural clustering, and other template features to provide a quaternary structure quality estimate (QSQE). The QSQE score is a number between 0 and 1, reflecting the expected accuracy of the interchain contacts for a model built based a given alignment and template. Higher numbers indicate higher reliability. This complements the GMQE score which estimates the accuracy of the tertiary structure of the resulting model.

References

- **BLAST**
  Camacho, C., Coulouris, G., Avagyan, V., Ma, N., Papadopoulos, J., Bealer, K., Madden, T.L. BLAST+: architecture and applications. BMC Bioinformatics 10, 421-430 (2009). doi
- **HHblits**
  Remmert, M., Biegert, A., Hauser, A., Söding, J. HHblits: lightning-fast iterative protein sequence searching by HMM-HMM alignment. Nat Methods 9, 173-175 (2012). doi

Table T1:

Primary amino acid sequence for which templates were searched and models were built.

```
MAEERVATRTQFPVSTESQKPRQKKAPEFPILEKQNWLIHLHYIRKDYEACKAVIKEQLQETQGLCEYAIYVQALIFRLEGNIQESLELFQTCAVLSPQS
ADNLKQVARSLFLLGKHKAAIEVYNEAAKLNQKDWEISHNLGVCYIYLKQFNKAQDQLHNALNLNRHDLTYIMLGKIHLLEGDLDKAIEVYKKAVEFSPE
NTELLTTLGLLYLQLGIYQKAFEHLGNALTYDPTNYKAILAAGSMMQTHGDFDVALTKYRVVACAVPESPPLWNNIGMCFFGKKKYVAAISCLKRANYLA
PFDWKILYNLGLVHLTMQQYASAFHFLSAAINFQPKMGELYMLLAVALTNLEDIENAKRAYAEAVHLDKCNPLVNLNYAVLLYNQGEKKNALAQYQEMEK
KVSLLKDNSSLEFDSEMVEMAQKLGAALQVGEALVWTKPVKDPKSKHQTTSTSKPASFQQPLGSNQALGQAMSSAAAYRTLPSGAGGTSQFTKPPSLPLE
PEPAVESSPTETSEQIREK
```

Table T2:

Template	Seq Identity	Oligo-state	QSQE	Found by	Method	Resolution	Seq Similarity	Coverage	Description
5nnp.1.A	19.23	monomer		HHblits	X-ray	2.60Å	0.29	0.70	N-terminal acetyltransferase-like protein
5nnp.2.A	19.23	monomer		HHblits	X-ray	2.60Å	0.29	0.70	N-terminal acetyltransferase-like protein
5nnr.1.A	19.23	monomer		HHblits	X-ray	3.10Å	0.29	0.70	N-terminal acetyltransferase-like protein
5mc6.35.A	13.37	monomer		HHblits	EM	NA	0.27	0.75	Superkiller protein 3
6c9m.2.A	18.73	monomer		HHblits	X-ray	2.80Å	0.29	0.70	N-alpha-acetyltransferase 15, NatA auxiliary subunit
6c9m.1.A	18.73	monomer		HHblits	X-ray	2.80Å	0.29	0.70	N-alpha-acetyltransferase 15, NatA auxiliary subunit
6c95.1.A	18.73	monomer		HHblits	X-ray	3.15Å	0.29	0.70	N-alpha-acetyltransferase 15, NatA auxiliary subunit
4buj.1.B	13.37	monomer		HHblits	X-ray	3.70Å	0.27	0.75	SUPERKILLER PROTEIN 3
4buj.2.B	13.37	monomer		HHblits	X-ray	3.70Å	0.27	0.75	SUPERKILLER PROTEIN 3
4ui9.1.J	16.49	monomer		HHblits	EM	3.60Å	0.28	0.75	CELL DIVISION CYCLE PROTEIN 16 HOMOLOG
5a31.1.J	16.58	monomer		HHblits	EM	4.30Å	0.28	0.74	ANAPHASE-PROMOTING COMPLEX SUB-UNIT 6
5dse.2.A	18.31	monomer		HHblits	X-ray	2.90Å	0.28	0.71	Tetratricopeptide repeat protein 7B
4ui9.1.C	15.41	homo-dimer	0.26	HHblits	EM	3.60Å	0.28	0.71	CELL DIVISION CYCLE PROTEIN 23 HOMOLOG
5dse.1.A	18.31	monomer		HHblits	X-ray	2.90Å	0.28	0.71	Tetratricopeptide repeat protein 7B
4ui9.1.P	15.41	homo-dimer	0.26	HHblits	EM	3.60Å	0.28	0.71	CELL DIVISION CYCLE PROTEIN 23 HOMOLOG
5a31.1.P	15.85	homo-dimer	0.22	HHblits	EM	4.30Å	0.28	0.71	CELL DIVISION CYCLE PROTEIN 23 HOMOLOG
5a31.1.C	15.85	homo-dimer	0.22	HHblits	EM	4.30Å	0.28	0.71	CELL DIVISION CYCLE PROTEIN 23 HOMOLOG
6bq1.1.B	18.31	monomer		HHblits	EM	NA	0.28	0.71	Tetratricopeptide repeat protein 7B
5g04.1.P	15.85	homo-dimer	0.24	HHblits	EM	4.00Å	0.28	0.71	CELL DIVISION CYCLE PROTEIN 23 HOMOLOG

5g04.1.C	15.85	homo-dimer	0.24	HHblits	EM	4.00Å	0.28	0.71	CELL DIVISION CYCLE PROTEIN 23 HOMOLOG
5g05.1.C	15.85	homo-dimer	0.24	HHblits	EM	3.50Å	0.28	0.71	CELL DIVISION CYCLE PROTEIN 23 HOMOLOG
5lcw.1.C	15.85	homo-dimer	0.24	HHblits	EM	4.00Å	0.28	0.71	Cell division cycle protein 23 homolog
5mc6.35.A	14.21	monomer		HHblits	EM	NA	0.27	0.71	Superkiller protein 3
5g04.1.C	15.18	homo-dimer	0.26	HHblits	EM	4.00Å	0.27	0.71	CELL DIVISION CYCLE PROTEIN 23 HOMOLOG
5g05.1.C	15.18	homo-dimer	0.24	HHblits	EM	3.50Å	0.27	0.71	CELL DIVISION CYCLE PROTEIN 23 HOMOLOG
5lcw.1.C	15.18	homo-dimer	0.23	HHblits	EM	4.00Å	0.27	0.71	Cell division cycle protein 23 homolog
5nnp.2.A	13.28	monomer		HHblits	X-ray	2.60Å	0.27	0.71	N-terminal acetyltransferase-like protein
5nnp.1.A	13.28	monomer		HHblits	X-ray	2.60Å	0.27	0.71	N-terminal acetyltransferase-like protein
5g04.1.P	15.18	homo-dimer	0.25	HHblits	EM	4.00Å	0.27	0.71	CELL DIVISION CYCLE PROTEIN 23 HOMOLOG
2gw1.1.A	17.40	homo-dimer	0.08	HHblits	X-ray	3.00Å	0.28	0.70	Mitochondrial precursor proteins import receptor
2gw1.1.B	17.40	homo-dimer	0.08	HHblits	X-ray	3.00Å	0.28	0.70	Mitochondrial precursor proteins import receptor
5a31.1.C	15.14	homo-dimer	0.24	HHblits	EM	4.30Å	0.27	0.71	CELL DIVISION CYCLE PROTEIN 23 HOMOLOG
4ui9.1.K	16.85	monomer		HHblits	EM	3.60Å	0.28	0.71	CELL DIVISION CYCLE PROTEIN 16 HOMOLOG
5g04.1.J	16.58	homo-dimer	0.08	HHblits	EM	4.00Å	0.28	0.71	CELL DIVISION CYCLE PROTEIN 16 HOMOLOG
5nnr.1.A	13.32	monomer		HHblits	X-ray	3.10Å	0.27	0.71	N-terminal acetyltransferase-like protein
5a31.1.P	15.14	homo-dimer	0.24	HHblits	EM	4.30Å	0.27	0.71	CELL DIVISION CYCLE PROTEIN 23 HOMOLOG
5g05.1.K	16.58	homo-dimer	0.05	HHblits	EM	3.50Å	0.28	0.71	CELL DIVISION CYCLE PROTEIN 16 HOMOLOG
5g04.1.K	16.58	homo-dimer	0.08	HHblits	EM	4.00Å	0.28	0.71	CELL DIVISION CYCLE PROTEIN 16 HOMOLOG
4uzy.1.A	14.44	monomer		HHblits	X-ray	2.48Å	0.27	0.71	FLAGELLAR ASSOCIATED PROTEIN
4uzy.1.A	14.79	monomer		HHblits	X-ray	2.48Å	0.28	0.70	FLAGELLAR ASSOCIATED PROTEIN
6eou.1.A	21.76	monomer		HHblits	X-ray	1.75Å	0.29	0.70	UDP-N-acetylglucosamine--peptide N-acetylglucosaminyltransferase 110 kDa subunit
4rg6.1.B	14.67	homo-dimer	0.19	HHblits	X-ray	3.30Å	0.27	0.71	Cell division cycle protein 27 homolog
4rg6.1.A	14.67	homo-dimer	0.19	HHblits	X-ray	3.30Å	0.27	0.71	Cell division cycle protein 27 homolog
5aio.1.A	14.92	monomer		HHblits	X-ray	3.15Å	0.28	0.70	TRANSCRIPTION FACTOR TAU 131 KDA SUBUNIT
4rg6.1.B	16.53	monomer		HHblits	X-ray	3.30Å	0.28	0.71	Cell division cycle protein 27 homolog
4rg6.1.A	16.53	monomer		HHblits	X-ray	3.30Å	0.28	0.71	Cell division cycle protein 27 homolog
1w3b.1.A	21.43	homo-dimer		HHblits	X-ray	2.85Å	0.29	0.73	UDP-N-ACETYLGLUCOSAMINE--PEPTIDE N-ACETYLGLUCOSAMINYLTRANSFERASE 110
3fp3.1.A	16.90	monomer		HHblits	X-ray	1.98Å	0.28	0.70	TPR repeat-containing protein YHR117W
3fp2.1.A	16.90	monomer		HHblits	X-ray	1.98Å	0.28	0.70	TPR repeat-containing protein YHR117W
1w3b.1.B	21.43	homo-dimer		HHblits	X-ray	2.85Å	0.29	0.73	UDP-N-ACETYLGLUCOSAMINE--PEPTIDE N-ACETYLGLUCOSAMINYLTRANSFERASE 110

The table above shows the top 50 filtered templates. A further 1,025 templates were found which were considered to be less suitable for modelling than the filtered list.

5gm6.1.4, 3ru0.1.A, 5lyn.1.A, 5gm6.1.2, 2c2l.1.A, 1fpp.1.B, 4p29.1.A, 4a1s.1.A, 5efr.1.A, 5gjr.56.A, 1a17.1.A, 5a31.1.V, 3gw4.1.A, 1ya0.1.A, 3ax3.1.A, 4bt9.1.B, 1x81.1.A, 2ifu.2.A, 3r9a.1.D, 4di3.1.D, 5gjr.54.A, 5vgz.1.G, 3r9a.1.B, 1tnu.1.A, 5vgz.1.J, 5vgz.1.H, 5vgz.1.M, 1qqe.1.A, 6bq1.1.B, 4u0u.1.A, 4mbq.2.A, 5gjr.12.A, 5en7.2.A, 5m32.1.b, 4eba.1.A, 4d10.1.C, 2n8w.1.A, 5oql.1.E, 2if4.1.A, 5o2n.1.A, 4ui9.1.P, 4n5c.8.A, 4ui9.1.V, 4ui9.1.W, 4ui9.1.J, 4ui9.1.K, 4ui9.1.H, 3oxf.1.A, 4ui9.1.O, 3lku.1.A, 6c6k.1.A, 4ui9.1.C, 5oj8.1.A, 5w65.1.Q, 4ui9.1.F, 4n5c.6.A, 4e85.1.A, 2yhe.1.A, 3q15.1.A, 3ieg.2.A, 3ulq.1.A, 1ihg.1.A, 5iwb.1.B, 4rib.1.A, 2fo7.1.A, 5jzz.1.A, 2y4u.1.A, 2q7f.1.A, 3ash.1.A, 4osr.2.A, 6c9m.2.A, 4r8a.1.A, 1hh8.1.A, 4cr4.1.U, 4cr4.1.V, 4cr4.1.W, 5lfm.1.A, 4yvq.1.B, 3pz2.1.A, 4nur.1.A, 4cr4.1.X, 3kd7.1.A, 4leu.1.A, 5dse.1.A, 2bug.1.A, 2v1s.1.A, 6eou.1.A, 5xw7.3.A, 6fuz.1.A, 1nl4.1.A, 5xw7.5.A, 3hxe.1.A, 4jsn.1.A, 4yv6.2.B, 5izw.1.A, 4d10.1.A, 5bw8.1.C, 4pjq.1.A, 5wsg.1.R, 3mv3.1.B, 3lya.1.A, 5wsg.1.T, 5a5b.1.Z, 2yhc.1.A, 5a5b.1.X, 5g05.1.K, 4rid.2.A, 2v1s.3.A, 4i1a.1.A, 5a5b.1.W, 5g05.1.F, 5mpd.1.K, 3euv.1.A, 5mpd.1.I, 5mpd.1.H, 4ady.1.A, 4ga2.1.A, 4av7.1.A, 1ft1.1.A, 5mpe.1.K, 5mpd.1.G, 6bcx.1.A, 3qou.1.A, 2yq8.1.A, 4cr4.1.6, 4m59.1.B, 1hxi.1.A, 4m59.1.A, 3cvl.1.A, 1n9a.1.A, 5nbt.1.B, 2v1s.5.A, 5vgz.1.K, 6frk.1.o, 3c72.1.A, 3kae.1.A, 2r2l.1.A, 5fjy.1.B, 5fjy.1.A, 3bee.1.A, 5l0y.6.A, 4yv6.2.A, 4oe1.1.A, 5wvk.1.d, 1o1r.1.A, 5wvk.1.a, 5wvk.1.b, 5wvk.1.c, 1fch.1.A, 5mqf.1.O, 4bzj.1.C, 4gyo.1.A, 5xw7.1.A, 5a5t.1.C, 5ow5.2.B, 4lct.1.A, 4lct.1.B, 4i9c.1.A, 5ft9.2.A, 6epf.1.T, 5jjx.1.A, 3ma5.3.A, 5w4m.1.A, 4xmm.1.E, 4fhm.1.B, 3jcp.1.Z, 3jcp.1.Y, 3jcp.1.X, 5y7g.1.A, 6epf.1.V, 5wrv.1.B, 4y6w.1.A, 1om2.1.A, 2lsu.1.A, 1wm5.1.A, 3jck.1.D, 5np1.1.A, 5y7g.3.A, 5a31.1.O, 3jcp.1.1, 3jcp.1.0, 5ohu.1.A, 5a31.1.J, 5wrw.1.B, 5l4k.1.F, 5l4k.1.I, 5a31.1.F, 3jcp.1.8, 5c1d.1.A, 2c0l.1.A, 1iip.1.A, 2v1s.2.A, 5wvk.1.8, 5wvk.1.9, 5wrw.3.A, 5a31.1.W, 2j9q.1.B, 2j9q.1.A, 3nf1.1.A, 3zfw.1.A, 2avp.1.A, 6au8.1.A, 5mpe.2.L, 3c3r.1.A, 5mpe.2.H, 5mpe.2.E, 5diz.2.A, 5mpe.2.F, 6fv0.1.A, 3rjv.1.A, 5n5y.1.R, 5b26.1.A, 5b26.1.B, 4yg8.1.B, 4lct.2.B, 4m57.1.A, 4oe1.1.B, 5a6c.1.A, 3q4a.1.A, 4boc.1.A, 4i17.1.A, 2awi.1.A, 5a7d.4.B, 5a7d.4.A, 2fi7.1.A, 2zir.1.A, 2fi7.1.B, 2v5f.1.A, 3ma5.1.A, 5l0y.2.A, 5by9.1.B, 5njx.1.A, 5t0h.1.V, 5t0h.1.W, 5t0h.1.U, 4um2.1.A, 4q66.2.C, 1hz4.1.A, 5k18.1.A, 5mpq.1.A, 4bwr.1.A, 4d0p.1.A, 5a7d.2.A, 5h64.1.A, 2cg3.1.B, 5a7d.2.B, 1elr.1.A, 5gjr.9.A, 5o29.1.A, 5t0h.1.0, 5vat.2.A, 5ln3.1.W, 2xev.1.A, 4fsc.2.B, 4j8d.1.A, 5arf.1.A, 5n60.1.R, 5xjc.1.J, 5xjc.1.I, 2bed.1.A, 4pjr.1.A, 5mpc.1.f, 5en8.1.B, 5w5h.2.E, 5o7x.4.C, 4cgv.2.A, 4bta.1.B, 3zhe.1.B, 3ly9.1.A, 3as5.1.A, 6b85.1.A, 5xw7.2.A, 3si5.2.A, 3q5m.1.A, 4osw.2.A, 2mr3.1.A, 5c9s.1.A, 2aw6.1.A, 5gmk.1.R, 5xw7.4.A, 5gmk.1.W, 4cgq.1.A, 2ooe.1.A, 4abn.2.A, 3rkv.1.A, 5lvz.1.B, 5t0h.1.Y, 3cv0.1.A, 5m72.1.A, 3rib.1.A, 6erp.2.D, 4zlh.1.B, 4zlh.1.A, 2gw1.1.A, 2gw1.1.B, 2axu.3.B, 4eqf.1.A, 5wlc.21.A, 6fc4.1.A, 4kvm.1.A, 3fwv.2.A, 5i9g.1.A, 3urz.1.A, 5w4n.1.A, 5vat.1.A, 5gap.1.G, 4d18.1.C, 3vty.4.A, 5hq8.1.A, 5ojf.1.A, 3cvn.1.A, 5wft.1.A, 1dce.1.A, 3e4b.2.A, 3tgo.1.A, 5o1j.1.A, 5oa1.1.T, 5aem.1.A, 5o09.1.C, 5orm.1.A, 1sly.1.A, 5ow5.1.B, 5vhs.1.H, 4j0u.1.A, 2axu.1.C, 3ro3.1.A, 2axu.1.A, 5n4a.1.A, 5fzs.1.A, 4wsl.1.A, 3ly7.1.A, 3jck.1.B, 5omp.1.A, 5lyp.1.A, 5dbk.1.B, 5dbk.1.A, 5o01.2.A, 5mpc.1.k, 4cr2.1.Z, 6fbt.1.A, 4cr2.1.Y, 3qky.1.A, 5ayw.1.D, 4ymr.1.A, 4ymr.1.B, 4cr2.1.V, 4cr2.1.W, 4cr2.1.U, 2pqr.2.A, 1kt1.1.A, 5w5y.1.Q, 4bt9.1.A, 5kjk.1.A, 3jcm.1.D, 5jj7.1.A, 2ff4.2.A, 5jj7.1.B, 4gpk.2.B, 4gpk.2.C, 4d10.1.D, 4gpk.2.A, 4d10.1.B, 4cgw.1.A, 4gpk.2.D, 3e4b.4.A, 2xcb.2.A, 1pc2.1.A, 5jj6.1.A, 5jj6.1.B, 3edt.1.A, 1qbq.1.A, 3edt.1.B, 1p5q.1.B, 1mzc.1.A, 2rpa.1.A, 5ajl.1.B, 2vsy.1.A, 5en7.2.C, 1klx.1.A, 4ja9.1.A, 2wpv.1.A, 2r5s.1.A, 2crb.1.A, 5ods.4.A, 4uqy.1.A, 3ax2.3.A, 2xev.3.A, 4ryk.1.A, 5mpb.1.k, 5a1u.1.S, 5a1u.1.T, 3u64.2.H, 3lca.1.A, 5mpc.1.h, 5mpc.1.i, 5kcn.1.A, 5ctq.2.B, 5mpc.1.d, 5mpc.1.e, 3asg.1.A, 5mpc.1.g, 4cr2.1.6, 4mal.1.A, 2xpi.1.C, 2xpi.1.A, 5ccl.1.A, 5jjt.1.A, 3zn3.1.A, 2y4t.1.A, 3asf.2.A, 2grm.1.A, 3j96.1.J, 3j96.1.H, 5wwm.1.A, 4hou.2.A, 2kc7.1.A, 3j96.1.G, 2vgx.1.B, 3ax5.2.A, 1e96.1.B, 1p5q.1.A, 4hnx.1.A, 1p5q.1.C, 5v3h.1.A, 5a1y.1.U, 5en8.1.A, 5wyj.33.A, 4o6f.1.A, 4wne.1.A, 6c9m.1.A, 4i9e.1.B, 4i9e.1.A, 3cvq.1.A, 4yv6.1.A, 3jb9.1.4, 4d18.1.D, 2q7f.2.A, 4d18.1.B, 3gz1.1.A, 3jb9.1.3, 6epe.1.Z, 4buj.1.B, 4rec.1.A, 5vhf.1.H, 4gcn.2.A, 4wnd.1.A, 4yde.1.A, 4ry3.1.A, 4cr4.1.Y, 4a1g.1.A, 4cr4.1.Z, 3ax2.1.A, 4reb.1.C, 3si5.1.A, 5bt1.1.A, 6epe.1.U, 4kbq.2.A, 6epe.1.T, 1wy6.1.A, 3ax3.3.A, 5ctr.2.A, 4bta.1.A, 5yz0.1.A, 5yz0.1.B, 3sf4.1.A, 2xgm.2.A, 4g23.1.A, 5udl.1.A, 2y4t.3.A, 6fec.1.G, 2oew.1.A, 5mzu.1.A, 5ctq.1.B, 5vbg.1.A, 5vhf.1.J, 4wn4.2.A, 4bt8.1.B, 4bt8.1.A, 5a5t.1.G, 4h7y.3.A, 3upv.1.A, 3asd.1.A, 5y7q.1.A, 5gjr.57.A, 3ly8.1.A, 3lpz.1.A, 4ady.2.A, 5lfl.1.A, 5l4k.1.H, 2lni.1.A, 5mpd.1.M, 4eba.2.A, 5an3.1.A, 2vko.1.A, 5t0i.1.Y, 5t0i.1.X, 5udj.1.A, 5t0i.1.V, 5t0i.1.U, 5hrz.1.A, 4y49.1.A, 2kcv.1.A, 5jno.1.B, 4hny.2.A, 6epc.1.T, 6epc.1.W, 6epc.1.V, 6epc.1.X, 3j9m.81.A, 6epc.1.Z, 5hi7.1.A, 5nzu.1.C, 5nzu.1.A, 2v1t.1.A, 5d0o.1.D, 4u0s.1.A, 5wql.1.A, 4f3v.1.A, 3ax3.4.A, 5i9d.1.A, 3q15.2.A, 6exn.1.R, 6exn.1.S, 2xgs.1.A, 3lvh.1.B, 3lvh.1.A, 2awi.3.C, 5k04.1.A, 4ehm.1.A, 5ccm.1.A, 6emk.1.C, 6emk.1.A, 3fp2.1.A, 5wbu.1.A, 3ax3.2.A, 4xgl.1.A, 6cbx.2.A, 4fhn.2.B, 2v1s.6.A, 5m32.1.a, 4n5c.5.A, 5m32.1.c, 4wsn.6.B, 6f5d.1.J, 5ekq.1.B, 4wsn.6.D, 3uux.1.A, 4gco.1.A, 6f5d.1.L, 4g1t.1.A, 4hot.1.A, 4g1t.1.B, 4n5c.3.A, 4wsn.2.B, 4i1a.2.A, 4reb.1.D, 4wsn.2.A, 5hgv.1.A, 5tqb.1.B, 4wsn.2.D, 4l9p.1.A, 2ifu.1.A, 5ln3.1.0, 5w4n.1.B, 4n5c.1.A, 6fcq.1.A, 6epf.1.U, 2wqh.1.A, 6epf.1.W, 4gyw.1.A, 6epf.1.X, 5fvm.1.A, 1ft2.1.A, 2ho1.1.B, 2ho1.1.A, 5ln3.1.X, 3as8.1.A, 5mgx.1.A, 5fsh.1.A, 4nrh.1.B, 5ola.2.C, 5ln3.1.V, 4bzj.1.A, 1ltx.1.A, 5m32.1.8, 5m32.1.9, 4a1g.3.A, 4ga0.1.A, 2f0y.1.A, 4ynw.1.A, 5lcw.1.O, 2fbn.1.A, 5en6.1.A, 5cqs.2.A, 3qdn.2.A, 4i2w.1.A, 5ic8.3.A, 5ex0.1.A, 4yvo.1.A, 4j8e.1.A, 5lwv.1.A, 4in3.1.D, 1qsa.1.A, 5mps.1.R, 2v1s.4.A, 5ic8.1.A, 3kd7.2.A, 5flc.1.F, 5np0.1.A, 5ln3.1.Z, 5bt1.1.B, 2kcl.1.A, 4yv9.2.A, 4hoq.1.A, 4yv6.1.B, 5jzz.2.A, 5fzr.1.A, 5lcw.1.S, 3esk.1.A, 5a5b.1.Y, 6c6k.1.C, 1ya0.2.A, 3ma5.4.A, 2ifu.3.A, 4jsp.1.A, 3qww.1.A, 3ffl.2.B, 4gq2.1.A, 1fch.2.A, 1b89.1.A, 5g05.1.O, 3j9m.72.A, 5zcs.1.B, 5y7g.2.A, 3ffl.1.A, 4wjw.1.B, 3gw4.1.B, 5a01.1.A, 3c3q.1.A, 5y5a.1.A, 4me2.1.A, 4wsn.2.C, 5iww.1.D, 3ffl.1.B, 4ria.1.A, 3nyj.1.A, 4n5c.7.A, 3ieg.1.A, 4osr.1.A, 3dra.1.A, 4r89.1.A, 5g04.1.U, 5g04.1.T, 5mpd.1.J, 5lb7.1.B, 6epf.1.Z, 2pl2.1.A, 3tg5.1.A, 5ctq.1.A, 2c2l.2.A, 2mhk.1.A, 6fec.1.C, 5g04.1.F, 5mpe.1.J, 5g04.1.H, 5g04.1.K, 5g04.1.J, 2nc9.1.A, 2pzi.2.A, 5g04.1.O, 5xi8.1.A, 3oxg.1.A, 1na3.1.A, 4axh.1.A, 5wlc.41.A, 5nrl.1.Q, 4wsn.4.D, 5ln3.1.Y, 3ro2.1.A, 4pjq.2.A, 5hop.1.A, 3gz1.1.B, 5ft9.1.A, 4xmn.1.D, 4j8f.1.A, 5mpd.1.F, 2cpt.1.A, 5djs.1.A, 4cgu.1.A, 3jco.1.X, 2kat.1.A, 5n5z.1.R, 5a7d.3.A, 5a7d.3.B, 4h7x.1.A, 4jhr.1.A, 6erp.1.D, 3jco.1.Z, 4gcn.1.A, 1qz2.1.C, 1qz2.1.B, 1qz2.1.A, 5en7.1.C, 5ola.1.C, 5ulm.1.A, 5lj3.1.U, 5lj3.1.T, 5wcg.1.A, 4w9r.1.A, 5jpz.1.B, 3mkq.1.B, 4osw.1.A, 4n5c.2.A, 4uqz.1.A, 3mkq.1.E, 3spa.1.A, 5a7d.1.B, 6ez8.1.B, 4ric.1.A, 5a7d.1.A, 5uz5.1.D, 5uz5.1.E, 5jpz.1.A, 2c0m.1.A, 2vyi.1.A, 5fsh.1.B, 3mkq.1.F, 2xcc.1.A, 2xcc.1.B, 5l0y.7.A, 5b26.2.B, 6epd.1.Z, 2hr2.1.A, 5x6o.1.A, 6cbx.1.A, 5wql.2.A, 5wvi.1.c, 6bcu.1.A, 5l0y.5.B, 5l0y.5.A, 5jz6.1.A, 4lct.2.A, 4aif.2.A, 2vsy.2.A, 5wvi.1.U, 5wvi.1.N, 5wvi.1.O, 5wvi.1.L, 3mv2.1.B, 3jd5.1.3, 5wvi.1.K, 5ods.3.A, 5o9z.1.G, 2cfu.1.A, 4fhn.1.B, 3e37.1.A, 3s7f.1.A, 5wvi.1.V, 5ods.1.A, 3q75.1.A, 5jkp.1.A, 5mqf.1.M, 3jd5.1.U, 6epd.1.X, 4wuy.1.A, 5en6.2.A, 5lj5.1.U, 3mzk.1.B, 5lj5.1.V, 5dse.2.A, 5ftp.1.A, 5ftp.1.B, 4pwx.1.C, 5mpe.1.H, 5nps.1.A, 3as5.2.A, 5jjo.1.A, 3gz2.1.A, 5diz.1.A, 4g2v.1.A, 2vq2.1.A, 5cqs.1.A, 5t0i.1.W, 2vsn.1.A, 5by9.1.A, 3qdn.1.A, 3qwp.1.A, 2axu.2.C, 1zu2.1.A, 2vko.1.B, 4rea.1.A, 3n71.1.A, 3u3w.1.B, 3vty.1.A, 4zey.1.A, 5a9q.1.T, 3fwv.1.A, 4hnw.1.A, 5l0y.3.A, 3pz4.1.A, 5jhe.1.A, 5l0y.1.B, 5l0y.1.A, 1tkn.1.A, 3hym.1.B, 5a9q.1.B, 5n61.1.R, 6bk8.1.V, 6bk8.1.W, 5t0c.35.A, 1nzn.1.A, 1kt0.1.A, 3jco.1.0, 5wvk.1.k, 3jco.1.1, 4j8e.2.A, 5ods.2.A, 3jco.1.Y, 3e4b.1.A, 4b94.1.A, 3mkq.1.A, 6epc.1.U, 3mkq.1.C, 3jco.1.W, 5a9q.1.a, 3mkq.1.D, 5jqy.1.A, 4nq0.1.A, 5bwk.1.D, 5v7v.1.A, 2ond.1.A, 4y6c.1.A, 4n2s.1.A, 3zpj.1.A, 4ja7.1.A, 3jco.1.8, 3ax2.4.A, 3o48.1.A, 4cgv.1.A, 4abn.1.A, 6fpn.1.A, 3as4.1.A, 4q66.1.D, 3q7f.1.A, 1w3b.1.B, 4n2q.1.A, 1w3b.1.A, 2uy1.1.A, 2uy1.1.B, 5a9q.1.2, 5orq.1.A, 5lvv.1.A, 5y81.1.A, 5a6c.2.A, 2pzi.1.A, 3pdn.1.A, 3uq3.1.A, 3ax5.1.A, 1y8m.1.A, 3sf4.2.A, 4r7s.1.A, 4aif.1.A, 3asf.1.A, 2axz.1.A, 2wvi.1.A, 3j8b.1.C, 2qfc.1.A, 4ynd.1.A, 5d0q.1.C, 3vtx.2.A, 5ojs.1.A, 5l0w.1.A, 2l6j.1.A, 5che.1.E, 5che.1.F, 4apo.1.A, 4n3c.1.A, 4uqx.1.A, 3sz7.1.A, 1dce.2.A, 2axv.1.A, 5oej.1.A, 1tjc.1.A, 5i9f.1.A, 3vty.3.A, 3gz2.1.B, 5aio.1.A, 5o01.1.A, 3wxx.1.A, 2pqn.1.A, 5w4m.1.B, 2vko.2.A, 5jjw.1.A, 3oxl.1.A, 3k9i.1.A, 1zbp.1.A, 1d8d.1.A, 5t0g.1.Y, 5t0g.1.X, 2n8i.1.A, 1xnf.1.A, 5npr.1.A, 1wao.1.A, 3asg.2.A, 5t0g.1.V, 3jck.1.C, 4mal.2.A, 1elw.1.A, 1wao.3.A, 5t0j.1.V, 4xpd.1.A, 3jck.1.F, 3jbz.1.A, 4gpk.1.D, 5ctq.2.A, 4e6h.1.A, 4gpk.1.A, 4gpk.1.C, 4gpk.1.B, 6epd.1.V, 6epd.1.W, 6epd.1.T, 6epd.1.U, 3j98.1.I, 3j98.1.H, 2vko.2.B, 6epe.1.X, 6epe.1.W, 6epe.1.V, 3j97.1.H, 4gpk.3.D, 4gpk.3.C, 4gpk.3.B, 4gpk.3.A, 4buj.2.B, 3ceq.1.A, 5t0j.1.1, 3ceq.1.B, 4ay5.1.A, 5vhi.1.H, 1ouv.1.A, 3j8b.1.G, 2vkj.1.B, 4kvo.1.A, 2xev.2.A, 4xnh.1.A, 3pz1.1.A, 4kbq.1.A, 5t0g.1.0, 4xi0.1.A, 4cr2.1.X, 5fzr.1.B, 5mps.1.Q, 3mkr.1.B, 5gjr.53.A,

3mkr.1.A, 4wn4.1.A, 4cr3.1.Z, 5ljo.1.C, 3jck.1.A, 4hny.1.A, 3bee.2.A, 4hou.1.A, 2vgy.1.A, 4axh.1.B, 4ri9.1.A, 4cr3.1.6, 2vgx.1.A, 4n5c.4.A, 3lvg.1.A, 4ynv.1.A, 3lvg.1.C, 3lvg.1.B, 5fzq.1.C, 5fzq.1.B, 5fzq.1.A, 6c95.1.A, 4a1g.4.A, 2ff4.1.A, 4ozs.1.A, 5wrw.1.A, 5cqr.1.A, 5l4k.1.G, 1na0.1.A, 5a31.1.H, 4ga1.1.A, 4ri8.1.A, 4u04.1.A, 2kck.1.A, 5i9h.1.A, 2dba.1.A, 3fp3.1.A, 3txn.1.A, 2v1t.2.A, 5waq.1.A, 5w5i.1.A, 5l4k.1.J, 3e4b.3.A, 1iyg.1.A, 5o24.1.A, 4btb.1.A, 4wng.1.A, 5l4k.1.L, 4rea.1.B, 6f5d.1.K, 2lsv.1.A, 4rid.1.A, 5mpb.1.e, 5mpb.1.d, 5mpb.1.g, 5mpb.1.f, 3sfx.1.A, 5ctr.1.A, 2vkj.1.A, 3u4t.1.A, 3ks2.1.A, 4cr3.1.Y, 5gjq.1.9, 5mpb.1.i, 5mpb.1.h, 4a1g.2.A, 2e2e.1.A, 5ic8.4.A, 4am9.1.A, 5ex3.1.A

SWISS-MODEL Homology Modelling Report

Model Building Report

This document lists the results for the homology modelling project "BBS5_HUMAN Q8N3I7 Bardet-Biedl syndrome 5 protein" submitted to SWISS-MODEL workspace on July 23, 2018, 3:56 p.m..The submitted primary amino acid sequence is given in Table T1.

If you use any results in your research, please cite the relevant publications:

- Waterhouse, A., Bertoni, M., Bienert, S., Studer, G., Tauriello, G., Gumienny, R., Heer, F.T., de Beer, T.A.P., Rempfer, C., Bordoli, L., Lepore, R., Schwede, T. SWISS-MODEL: homology modelling of protein structures and complexes. Nucleic Acids Res. 46(W1), W296-W303 (2018). doi
- Guex, N., Peitsch, M.C., Schwede, T. Automated comparative protein structure modeling with SWISS-MODEL and Swiss-PdbViewer: A historical perspective. Electrophoresis 30, S162-S173 (2009). doi
- Bienert, S., Waterhouse, A., de Beer, T.A.P., Tauriello, G., Studer, G., Bordoli, L., Schwede, T. The SWISS-MODEL Repository - new features and functionality. Nucleic Acids Res. 45, D313-D319 (2017). doi
- Benkert, P., Biasini, M., Schwede, T. Toward the estimation of the absolute quality of individual protein structure models. Bioinformatics 27, 343-350 (2011). doi
- Bertoni, M., Kiefer, F., Biasini, M., Bordoli, L., Schwede, T. Modeling protein quaternary structure of homo- and hetero-oligomers beyond binary interactions by homology. Scientific Reports 7 (2017). doi

Results

The SWISS-MODEL template library (SMTL version 2018-07-12, PDB release 2018-07-06) was searched with BLAST (Camacho et al.) and HHBlits (Remmert et al.) for evolutionary related structures matching the target sequence in Table T1. For details on the template search, see Materials and Methods. Overall 38 templates were found (Table T2).

Models

No models have been built for this project.

Materials and Methods

Template Search

Template search with BLAST and HHBlits has been performed against the SWISS-MODEL template library (SMTL, last update: 2018-07-12, last included PDB release: 2018-07-06).

The target sequence was searched with BLAST against the primary amino acid sequence contained in the SMTL.

An initial HHblits profile has been built using the procedure outlined in (Remmert et al.), followed by 1 iteration of HHblits against NR20. The obtained profile has then be searched against all profiles of the SMTL. A total of 40 templates were found.

Template Selection

For each identified template, the template's quality has been predicted from features of the target-template alignment. The templates with the highest quality have then been selected for model building.

Model Building

Models are built based on the target-template alignment using ProMod3. Coordinates which are conserved between the target and the template are copied from the template to the model. Insertions and deletions are remodelled using a fragment library. Side chains are then rebuilt. Finally, the geometry of the resulting model is regularized by using a force field. In case loop modelling with ProMod3 fails, an alternative model is built with PROMOD-II (Guex et al.).

Model Quality Estimation

The global and per-residue model quality has been assessed using the QMEAN scoring function (Benkert et al.) . For improved performance, weights of the individual QMEAN terms have been trained specifically for SWISS-MODEL.

Ligand Modelling

Ligands present in the template structure are transferred by homology to the model when the following criteria are met: (a) The ligands are annotated as biologically relevant in the template library, (b) the ligand is in contact with the model, (c) the ligand is not clashing with the protein, (d) the residues in contact with the ligand are conserved between the target and the template. If any of these four criteria is not satisfied, a certain ligand will not be included in the model. The model summary includes information on why and which ligand has not been included.

Oligomeric State Conservation

The quaternary structure annotation of the template is used to model the target sequence in its oligomeric form. The method (Bertoni et al.) is based on a supervised machine learning algorithm, Support Vector Machines (SVM), which combines interface conservation, structural clustering, and other template features to provide a quaternary structure quality estimate (QSQE). The QSQE score is a number between 0 and 1, reflecting the expected accuracy of the interchain contacts for a model built based a given alignment and template. Higher numbers indicate higher reliability. This complements the GMQE score which estimates the accuracy of the tertiary structure of the resulting model.

References

- **BLAST**
  Camacho, C., Coulouris, G., Avagyan, V., Ma, N., Papadopoulos, J., Bealer, K., Madden, T.L. BLAST+: architecture and applications. BMC Bioinformatics 10, 421-430 (2009). doi
- **HHblits**
  Remmert, M., Biegert, A., Hauser, A., Söding, J. HHblits: lightning-fast iterative protein sequence searching by HMM-HMM alignment. Nat Methods 9, 173-175 (2012). doi

Table T1:

Primary amino acid sequence for which templates were searched and models were built.

```
MSVLDALWEDRDVRFDLSAQQMKTRPGEVLIDCLDSIEDTKGNNGDRGRLLVTNLRILWHSLALSRVNVSVGYNCILNITTRTANSKLRGQTEALYILTK
CNSTRFEFIFTNLVPGSPRLFTSVMAVHRAYETSKMYRDFKLRSALIQNKQLRLLPQEHVYDKINGVWNLSSDQGNLGTFFITNVRIVWHANMNDSFNVS
IPYLQIRSIKIRDSKFGLALVIESSQQSGGYVLGFKIDPVEKLQESVKEINSLHKVYSASPIFGVDYEMEEKPQPLEALTVEQIQDDVEIDSDGHTDAFV
AYFADGNKQQDREPVFSEELGLAIEKLKDGFTLQGLWEVMS
```

Table T2:

Template	Seq Identity	Oligo-state	QSQE	Found by	Method	Resolution	Seq Similarity	Coverage	Description
2cay.1.A	15.70	homo-tetramer		HHblits	X-ray	1.90Å	0.28	0.35	VACUOLAR PROTEIN SORTING PROTEIN 36
1zsq.1.A	16.50	monomer		HHblits	X-ray	1.82Å	0.28	0.30	Myotubularin-related protein 2
2cay.1.A	11.11	homo-tetramer		HHblits	X-ray	1.90Å	0.25	0.32	VACUOLAR PROTEIN SORTING PROTEIN 36
1m7r.1.A	16.83	monomer		HHblits	X-ray	2.60Å	0.28	0.30	Myotubularin-related Protein-2
1m7r.1.B	16.83	monomer		HHblits	X-ray	2.60Å	0.28	0.30	Myotubularin-related Protein-2
1lw3.1.A	16.83	monomer		HHblits	X-ray	2.30Å	0.28	0.30	Myotubularin-related protein 2
5gnh.1.A	17.00	monomer		HHblits	X-ray	2.60Å	0.28	0.29	Myotubularin-related protein 2
1zsq.1.A	22.47	monomer		HHblits	X-ray	1.82Å	0.31	0.26	Myotubularin-related protein 2
1m7r.1.A	22.99	monomer		HHblits	X-ray	2.60Å	0.30	0.26	Myotubularin-related Protein-2
1m7r.1.B	22.99	monomer		HHblits	X-ray	2.60Å	0.30	0.26	Myotubularin-related Protein-2
1lw3.1.A	22.99	monomer		HHblits	X-ray	2.30Å	0.30	0.26	Myotubularin-related protein 2
4f7u.1.F	17.02	monomer		HHblits	X-ray	1.90Å	0.29	0.28	Methylosome subunit pICln
2hth.1.B	21.69	monomer		HHblits	X-ray	2.70Å	0.30	0.24	Vacuolar protein sorting protein 36
5c16.1.A	15.00	monomer		HHblits	X-ray	2.07Å	0.29	0.29	Myotubularin-related protein 1
5gnh.1.A	22.99	monomer		HHblits	X-ray	2.60Å	0.30	0.26	Myotubularin-related protein 2
5xv8.1.B	25.32	monomer		HHblits	NMR	NA	0.32	0.23	General transcription factor IIH subunit 1
2rvb.1.B	25.32	monomer		HHblits	NMR	NA	0.32	0.23	General transcription factor IIH subunit 1
5gow.1.B	25.32	monomer		HHblits	NMR	NA	0.32	0.23	General transcription factor IIH subunit 1
2yf0.1.A	14.29	homo-dimer		HHblits	X-ray	2.65Å	0.27	0.23	MYOTUBULARIN-RELATED PROTEIN 6
2yf0.1.A	16.67	homo-dimer		HHblits	X-ray	2.65Å	0.28	0.23	MYOTUBULARIN-RELATED PROTEIN 6
5c16.1.A	15.91	monomer		HHblits	X-ray	2.07Å	0.28	0.26	Myotubularin-related protein 1
2rnr.1.B	21.05	monomer		HHblits	NMR	NA	0.29	0.22	TFIIH basal transcription factor complex p62 subunit
2ruk.1.B	21.05	monomer		HHblits	NMR	NA	0.29	0.22	General transcription factor IIH subunit 1
4v98.1.G	15.94	monomer		HHblits	X-ray	3.10Å	0.28	0.20	Icln
1pfj.1.A	25.32	monomer		HHblits	NMR	NA	0.32	0.23	TFIIH basal transcription factor complex p62 subunit
1pfj.1.A	21.05	monomer		HHblits	NMR	NA	0.29	0.22	TFIIH basal transcription factor complex p62 subunit
									General transcription factor IIH sub-

5gow.1.B	21.05	monomer		HHblits	NMR	NA	0.29	0.22	unit 1
2rvb.1.B	21.05	monomer		HHblits	NMR	NA	0.29	0.22	General transcription factor IIH subunit 1
5xv8.1.B	21.05	monomer		HHblits	NMR	NA	0.29	0.22	General transcription factor IIH subunit 1
2rnr.1.B	25.32	monomer		HHblits	NMR	NA	0.32	0.23	TFIIH basal transcription factor complex p62 subunit
2ruk.1.B	25.32	monomer		HHblits	NMR	NA	0.32	0.23	General transcription factor IIH subunit 1
4v98.1.G	14.93	monomer		HHblits	X-ray	3.10Å	0.29	0.20	Icln
1zyi.1.A	22.58	monomer		HHblits	NMR	NA	0.30	0.18	Methylosome subunit pICln
4f7u.1.F	16.18	monomer		HHblits	X-ray	1.90Å	0.30	0.20	Methylosome subunit pICln
2hth.1.B	20.00	monomer		HHblits	X-ray	2.70Å	0.30	0.18	Vacuolar protein sorting protein 36
1zyi.1.A	21.31	monomer		HHblits	NMR	NA	0.30	0.18	Methylosome subunit pICln
2dx5.1.A	23.81	monomer		HHblits	X-ray	3.35Å	0.32	0.18	Vacuolar protein sorting protein 36
2dx5.1.A	18.64	monomer		HHblits	X-ray	3.35Å	0.30	0.17	Vacuolar protein sorting protein 36

BIOZENTRUM
University of Basel
The Center for Molecular Life Sciences

SWISS-MODEL Homology Modelling Report

Model Building Report

This document lists the results for the homology modelling project "BBS7_HUMAN Q8IWZ6 Bardet-Biedl syndrome 7 protein" submitted to SWISS-MODEL workspace on July 23, 2018, 3:58 p.m..The submitted primary amino acid sequence is given in Table T1.

If you use any results in your research, please cite the relevant publications:

- Waterhouse, A., Bertoni, M., Bienert, S., Studer, G., Tauriello, G., Gumienny, R., Heer, F.T., de Beer, T.A.P., Rempfer, C., Bordoli, L., Lepore, R., Schwede, T. SWISS-MODEL: homology modelling of protein structures and complexes. Nucleic Acids Res. 46(W1), W296-W303 (2018). doi
- Guex, N., Peitsch, M.C., Schwede, T. Automated comparative protein structure modeling with SWISS-MODEL and Swiss-PdbViewer: A historical perspective. Electrophoresis 30, S162-S173 (2009). doi
- Bienert, S., Waterhouse, A., de Beer, T.A.P., Tauriello, G., Studer, G., Bordoli, L., Schwede, T. The SWISS-MODEL Repository - new features and functionality. Nucleic Acids Res. 45, D313-D319 (2017). doi
- Benkert, P., Biasini, M., Schwede, T. Toward the estimation of the absolute quality of individual protein structure models. Bioinformatics 27, 343-350 (2011). doi
- Bertoni, M., Kiefer, F., Biasini, M., Bordoli, L., Schwede, T. Modeling protein quaternary structure of homo- and hetero-oligomers beyond binary interactions by homology. Scientific Reports 7 (2017). doi

Results

The SWISS-MODEL template library (SMTL version 2018-07-12, PDB release 2018-07-06) was searched with BLAST (Camacho et al.) and HHBlits (Remmert et al.) for evolutionary related structures matching the target sequence in Table T1. For details on the template search, see Materials and Methods. Overall 1731 templates were found (Table T2).

Models

The following models were built (see Materials and Methods "Model Building"):

Model #01	File	Built with	Oligo-State	Ligands	GMQE	QMEAN
	PDB	ProMod3 Version 1.1.0.	monomer	None	0.18	-5.91

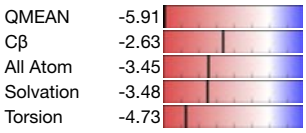

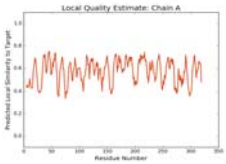

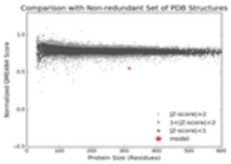

Template	Seq Identity	Oligo-state	Found by	Method	Resolution	Seq Similarity	Range	Coverage	Description
5wlc.19.A	10.96	monomer	HHblits	EM	NA	0.26	5 - 319	0.41	Utp4

The template contained no ligands.

```
Target    MDLILNRMDYLQVGVTSQKTMKLIPASR----HRATQKVVIGDHDGVVMCFGMKKGEAAA-VFKTLPGPKIARLELGGVI
5wlc.19.A ----VHRCRFVDFTPATITSLAFSHKSNINKLTPSDLRLAIGRSNGNIEIWNPRNNWFQEMVIEGGKDRSIEGLCWS-NV

Target    NTPQEKIFIAAAS-EIRGFTKR-GKQFLSFETNLTESIKAMHIS--GSDLFLS-ASYIYNHYC-D-CKDQH-----YYLS
5wlc.19.A NGESLRLFSIGGSTVVTEWDLATGLPLRNYD-CNSGVIWSISINDSQDKLSVGCDNGTVVLIDISGGPGVLEHDTILMRQ

Target    GDKINDVICLPVERLSRITPVLACQDRVLRVLQG-------SDVMYAVE------VPGPPTVLALHNGNGGDSGEDLLFG
5wlc.19.A EARVLTLAWKK---DD--FVIGGCSDGRIRIWSAQKNDENMGRLLHTMKVDKAKKESTLVWSVIYLPR-----TDQIASG

Target    TSDGKLALIQITTSKPVRKWEIQNEKKRGGILCIDSFDIVGDGVKDLLVGRDDGMVEVYSFDNAN------EPV-LRFDQ
5wlc.19.A DSTGSIKFWDFQFA--TLNQSFKAHD--ADVLCLTT---DTDNN-YVFSAGVDRKIFQFSQ-NTNKSQKNNRWVNSSNRL

Target    MLSESVTSIQGGCVGKDSYDEIVVSTYSGWVTGLTTEPIHKESGPGEELKINQEMQNKISSLRNELEHLQYKVLQERENY
5wlc.19.A LHGNDIRAICAY--QSKGADFLVSGGVEKTLVINSL----------------------------------------------

Target    QQSSQSSKAKSAVPSFGINDKFTLNKDDASYSLILEVQTAIDNVLIQSDVPIDLLLDVDKNSAVVSFSSCDSESNDNFLLA
5wlc.19.A ----------------------------------------------------------------------------------

Target    TYRCQADTTRLELKIRSIEGQYGTLQAYVTPRIQPKTCQVRQYHIKPLSLHQRTHFIDHDRPMNTLTLTGQFSFAEVHSW
```

```
5wlc.19.A ----------------------------------------------------------------------------

Target    VVFCLPEVPEKPPAGECVTFYFQNTFLDTQLESTYRKGEGVFKSDNISTISILKDVLSKEATKRKINLNISYEINEVSVK
5wlc.19.A ----------------------------------------------------------------------------

Target    HTLKLIHPKLEYQLLLAKKVQLIDALKELQIHEGNTNFLIPEYHCILEEADHLQEEYKKQPAHLERLYGMITDLFIDKFK
5wlc.19.A ----------------------------------------------------------------------------

Target    FKGTNVKTKVPLLLEILDSYDQNALISFFDAA
5wlc.19.A --------------------------------
```

Model #02	File	Built with	Oligo-State	Ligands	GMQE	QMEAN
	PDB	ProMod3 Version 1.1.0.	monomer	None	0.17	-5.59

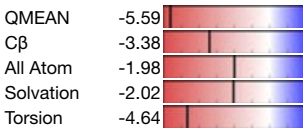

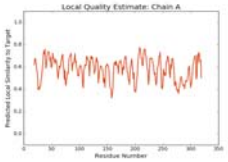

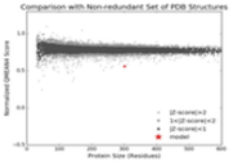

Template	Seq Identity	Oligo-state	Found by	Method	Resolution	Seq Similarity	Range	Coverage	Description
5gxh.1.A	12.32	monomer	HHblits	X-ray	1.80Å	0.25	19 - 319	0.40	Gem-associated protein 5

Ligand	Added to Model	Description
A	✕ - Binding site not conserved.	RNA (5'-R(*A*AP*UP*UP*UP*UP*UP*G)-3')
GOL	✕ - Not biologically relevant.	GLYCEROL
GOL	✕ - Not biologically relevant.	GLYCEROL
UNX	✕ - Not biologically relevant.	UNKNOWN ATOM OR ION
UNX	✕ - Not biologically relevant.	UNKNOWN ATOM OR ION
UNX	✕ - Not biologically relevant.	UNKNOWN ATOM OR ION

```
Target    MDLILNRMDYLQVGVTSQKTMKLIPASRHRATQKVVIGDHDGVVMCFGMKKGEAAAVFKTLPGPKIARLELGGVINTPQE
5gxh.1.A  ------------------SGFTFSHH-PG-QYNLCATSSDDGTVKIWDVETKTVVTEHALH-QHTISTLHWS-PR--VKD

Target    KIFIAAA-SEIRGFTKRGKQFLSFETNLTESIKAMHISG---SDLFLS-ASYIYNHYC-D-CKDQHYYLS--GDKINDVI
5gxh.1.A  LIVSGDEKGVVFCYWFNRNDSQHLF-IEPRTIFCLTCSPHHEDLVAIGYKDGIVVIIDISKKGEVIHRLRGHDDEIHSIA

Target    CLPVERL----------------------------SRITPVLACQDRVLRVLQG--SDVMYAVEV---------------
5gxh.1.A  WCPLPGEDCLSINQEETSEEAEITNGNAVAQAPVTKGCYLATGSKDQTIRIWSCSRGRGVMILKLPFLKRRGGGIDPTVK

Target    ------------------------------------------------------PGPPTVLALHNGNGGDSGEDLLFGTSDGK
5gxh.1.A  ERLWLTLHWPSNQPTQLVSSCFGGELLQWDLTQSWRRKYTLFSASSEGQNHSRIVFNLCPLQ--TEDDKQLLLSTSMDRD

Target    LALIQITTSKPVRKWEIQNEKKRGGILCIDSFDIVGDGVKDLLVGRDDGMVEVYSFDNANEPVLRFDQMLSESVTSIQGG
5gxh.1.A  VKCWDIATL--ECSWTLPSLG--GFAYSLAF---SSVDIGSLAIGVGDGMIRVWNT-LSIKNNYDVKNFWQGVKSKVTAL

Target    CVGKDSYDEIVVSTYSGWVTGLTTEPIHKESGPGEELKINQEMQNKISSLRNELEHLQYKVLQERENYQQSSQSSKAKSA
5gxh.1.A  CWHPTKEGCLAFGTDDGKVGLYDT----------------------------------------------------------

Target    VPSFGINDKFTLNKDDASYSLILEVQTAIDNVLIQSDVPIDLLDVDKNSAVVSFSSCDSESNDNFLLATYRCQADTTRLE
5gxh.1.A  ----------------------------------------------------------------------------

Target    LKIRSIEGQYGTLQAYVTPRIQPKTCQVRQYHIKPLSLHQRTHFIDHDRPMNTLTLTGQFSFAEVHSWVVFCLPEVPEKP
5gxh.1.A  ----------------------------------------------------------------------------

Target    PAGECVTFYFQNTFLDTQLESTYRKGEGVFKSDNISTISILKDVLSKEATKRKINLNISYEINEVSVKHTLKLIHPKLEY
5gxh.1.A  ----------------------------------------------------------------------------

Target    QLLLAKKVQLIDALKELQIHEGNTNFLIPEYHCILEEADHLQEEYKKQPAHLERLYGMITDLFIDKFKFKGTNVKTKVPL
5gxh.1.A  ----------------------------------------------------------------------------

Target    LLEILDSYDQNALISFFDAA
```

```
5gxh.1.A  --------------------
```

Model #03	File	Built with	Oligo-State	Ligands	GMQE	QMEAN
	PDB	ProMod3 Version 1.1.0.	monomer	None	0.16	-6.25

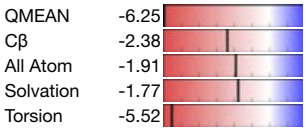

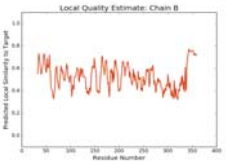

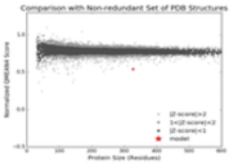

Template	Seq Identity	Oligo-state	Found by	Method	Resolution	Seq Similarity	Range	Coverage	Description
5a5u.1.B	7.12	monomer	HHblits	EM	9.00Å	0.24	33 - 359	0.41	EUKARYOTIC TRANSLATION INITIATION FACTOR 3 SUBUNIT B

The template contained no ligands.

```
Target    MDLILNRMDYLQVGVTSQKTMKLIPASRHRATQKVVIGD-------HDGVVMCFGMKKGEAAAVFKTLPGPKIARLELGG
5a5u.1.B  --------------------------------RYLVTFSPLMDTQDDPQAIIIWDILTGHKKRGFHCESSAHWPIFKWS-

Target    VINTPQEKIFIAAASEIRGFTKRGKQFLSFETNLTESIKAMHIS--GSDLFLSA------SYIYNHYC------------
5a5u.1.B  ---HDGKFFARMTLDTLSIYETPSMGLLDKKSLKISGIKDFSWSPGGNIIAFWVPEDKDIPARVTLMQLPSRQEIRVRNL

Target    ------------DCK-------------------DQHYYLS-----------GDKINDVICLPVERLSRITPVLACQDR-
5a5u.1.B  FNVVDCKLHWQKNGDYLCVKVDRTPKGTQGVVTNFEIFRMREKQVPVDVVEMKETIIAFAW---EPNG-SKFAVLHGEAP

Target    --VLRVLQGSD--VMYAV--EVPGPPTVLALHNGNGGDSGEDLLFGT---SDGKLALIQITTSKPVRKWEIQNEKKRGGI
5a5u.1.B  RISVSFYHVKSNGKIELSKMFDKQQANTIFWSPQ-----GQFVVLAGLRSMNGALAFVDTSDCT---VMNIAEH---YMA

Target    LCIDSFDIVGDGVKDLLVGRD------DGMVEVYSFDNANEPVLRFDQMLSESVTSIQGGCVGKDSYDEIVVSTYSGWVT
5a5u.1.B  SDV---EWDPTGR-YVVTSVSWWSHKVDNAYWLWTFQ--GR--LLQKNNK-DRFCQL---LWRPRP-PTLLSQEQIKQIK

Target    GLTTEPIHKESGPG--EELKINQEMQNKISSLRNELEHLQYKVLQERENYQQSSQSSKAKSAVPSFGINDKFTLNKDDAS
5a5u.1.B  KDLKKYSKIFEQKDRLSQSKASKELVERRRAMMEDFRKYGKAAQEL---------------------------------

Target    YSLILEVQTAIDNVLIQSDVPIDLLDVDKNSAVVSFSSCDSESNDNFLLATYRCQADTTRLELKIRSIEGQYGTLQAYVT
5a5u.1.B  --------------------------------------------------------------------------------

Target    PRIQPKTCQVRQYHIKPLSLHQRTHFIDHDRPMNTLTLTGQFSFAEVHSWVVFCLPEVPEKPPAGECVTFYFQNTFLDTQ
5a5u.1.B  --------------------------------------------------------------------------------

Target    LESTYRKGEGVFKSDNISTISILKDVLSKEATKRKINLNISYEINEVSVKHTLKLIHPKLEYQLLLAKKVQLIDALKELQ
5a5u.1.B  --------------------------------------------------------------------------------

Target    IHEGNTNFLIPEYHCILEEADHLQEEYKKQPAHLERLYGMITDLFIDKFKFKGTNVKTKVPLLLEILDSYDQNALISFFD
5a5u.1.B  --------------------------------------------------------------------------------

Target    AA
5a5u.1.B  --
```

Model #04	File	Built with	Oligo-State	Ligands	GMQE	QMEAN
	PDB	ProMod3 Version 1.1.0.	monomer	None	0.14	-5.98

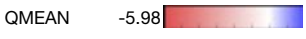

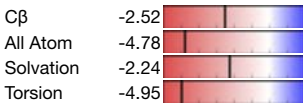

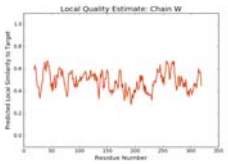

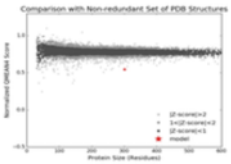

Template	Seq Identity	Oligo-state	Found by	Method	Resolution	Seq Similarity	Range	Coverage	Description
5nrl.1.W	9.47	monomer	HHblits	EM	NA	0.25	19 - 319	0.40	Pre-mRNA-splicing factor RSE1

Ligand	Added to Model	Description
GTP	× - Binding site not conserved.	GUANOSINE-5'-TRIPHOSPHATE
ZN	× - Binding site not conserved.	ZINC ION
ZN	× - Binding site not conserved.	ZINC ION
ZN	× - Binding site not conserved.	ZINC ION
ZN	× - Binding site not conserved.	ZINC ION
ZN	× - Binding site not conserved.	ZINC ION
ZN	× - Binding site not conserved.	ZINC ION
ZN	× - Binding site not conserved.	ZINC ION

```
Target    MDLILNRMDYLQVGVTSQKTMKLIPASRHRATQKVVIGDHDGVVMCFGMK--KG-EAAAVFK-TLPGPKIARLELGGVIN
5nrl.1.W  ------------------SKVAIVQ--DTQHADLLAIADNEGMIKIMSLKDQKEDFLTVISLQLVS-EKISDMIMV-RDS

Target    T-PQEKIFIAAASEIRGFTKR----GKQFLSFETNL-TESIKAMHI---------------------------------
5nrl.1.W  SIGQLNLHVGLENGVYMKFHIGDVDGSFTDIKRRFLGLKPVSLSYLREISVSLNNEEEEEEEEDDDDEKEEEEINSSGAK

Target    SGSDLFLSASYIYNHYC-DCKDQHYYLSGDKINDVICLPVERLSRI-TPVLAC-QDRVLRVLQGSDVM--------YAVE
5nrl.1.W  WMSCVVCHSSSTWVSYTWKNVWTIRQLKDQNMLSCS--KFVNADVAINGVCSISSSGRLNIGRVSNFPTLDNWFHVHESS

Target    VPGPPTVLALHNGNG----------------GDSGEDLL-----------FGT---SDGK-LAL-IQIT-TSKPVRKWEI
5nrl.1.W  V-NKQENGGGDESNEEEEDEMEEEMEMLQISTFRPRTILSFPNNPKSILFIDNHSGKKQCRISLQIDGECLKFGSSDHLY

Target    QNEKKRGGILCIDSFDIVGDGVKDLLVGRDDGMVEVYSFDNA-----NEPVLRFDQMLSESVTSIQGGCVGKDSYDEIVV
5nrl.1.W  KILDD-IDCVSAAIIDFTR-QADHLIICAGDKRLLTYKILVNKDKLSFDIELLHQTEIISPIHAMLKF----KN---FLL

Target    STYSGWVTGLTTEPIHKESGPGEELKINQEMQNKISSLRNELEHLQYKVLQERENYQQSSQSSKAKSAVPSFGINDKFTL
5nrl.1.W  TAMGSTIVLYGL-------------------------------------------------------------------

Target    NKDDASYSLILEVQTAIDNVLIQSDVPIDLLDVDKNSAVVSFSSCDSESNDNFLLATYRCQADTTRLELKIRSIEGQYGT
5nrl.1.W  -------------------------------------------------------------------------------

Target    LQAYVTPRIQPKTCQVRQYHIKPLSLHQRTHFIDHDRPMNTLTLTGQFSFAEVHSWVVFCLPEVPEKPPAGECVTFYFQN
5nrl.1.W  -------------------------------------------------------------------------------

Target    TFLDTQLESTYRKGEGVFKSDNISTISILKDVLSKEATKRKINLNISYEINEVSVKHTLKLIHPKLEYQLLLAKKVQLID
5nrl.1.W  -------------------------------------------------------------------------------

Target    ALKELQIHEGNTNFLIPEYHCILEEADHLQEEYKKQPAHLERLYGMITDLFIDKFKFKGTNVKTKVPLLLEILDSYDQNA
5nrl.1.W  -------------------------------------------------------------------------------

Target    LISFFDAA
5nrl.1.W  --------
```

Materials and Methods

Template Search

Template search with BLAST and HHBlits has been performed against the SWISS-MODEL template library (SMTL, last update: 2018-07-12, last included PDB release: 2018-07-06).

The target sequence was searched with BLAST against the primary amino acid sequence contained in the SMTL.

An initial HHblits profile has been built using the procedure outlined in (Remmert et al.), followed by 1 iteration of HHblits against

NR20. The obtained profile has then be searched against all profiles of the SMTL. A total of 1773 templates were found.

Template Selection

For each identified template, the template's quality has been predicted from features of the target-template alignment. The templates with the highest quality have then been selected for model building.

Model Building

Models are built based on the target-template alignment using ProMod3. Coordinates which are conserved between the target and the template are copied from the template to the model. Insertions and deletions are remodelled using a fragment library. Side chains are then rebuilt. Finally, the geometry of the resulting model is regularized by using a force field. In case loop modelling with ProMod3 fails, an alternative model is built with PROMOD-II (Guex et al.).

Model Quality Estimation

The global and per-residue model quality has been assessed using the QMEAN scoring function (Benkert et al.) . For improved performance, weights of the individual QMEAN terms have been trained specifically for SWISS-MODEL.

Ligand Modelling

Ligands present in the template structure are transferred by homology to the model when the following criteria are met: (a) The ligands are annotated as biologically relevant in the template library, (b) the ligand is in contact with the model, (c) the ligand is not clashing with the protein, (d) the residues in contact with the ligand are conserved between the target and the template. If any of these four criteria is not satisfied, a certain ligand will not be included in the model. The model summary includes information on why and which ligand has not been included.

Oligomeric State Conservation

The quaternary structure annotation of the template is used to model the target sequence in its oligomeric form. The method (Bertoni et al.) is based on a supervised machine learning algorithm, Support Vector Machines (SVM), which combines interface conservation, structural clustering, and other template features to provide a quaternary structure quality estimate (QSQE). The QSQE score is a number between 0 and 1, reflecting the expected accuracy of the interchain contacts for a model built based a given alignment and template. Higher numbers indicate higher reliability. This complements the GMQE score which estimates the accuracy of the tertiary structure of the resulting model.

References

- **BLAST**
  Camacho, C., Coulouris, G., Avagyan, V., Ma, N., Papadopoulos, J., Bealer, K., Madden, T.L. BLAST+: architecture and applications. BMC Bioinformatics 10, 421-430 (2009). doi
- **HHblits**
  Remmert, M., Biegert, A., Hauser, A., Söding, J. HHblits: lightning-fast iterative protein sequence searching by HMM-HMM alignment. Nat Methods 9, 173-175 (2012). doi

Table T1:

Primary amino acid sequence for which templates were searched and models were built.

```
MDLILNRMDYLQVGVTSQKTMKLIPASRHRATQKVVIGDHDGVVMCFGMKKGEAAAVFKTLPGPKIARLELGGVINTPQEKIFIAAASEIRGFTKRGKQF
LSFETNLTESIKAMHISGSDLFLSASYIYNHYCDCKDQHYYLSGDKINDVICLPVERLSRITPVLACQDRVLRVLQGSDVMYAVEVPGPPTVLALHNGNG
GDSGEDLLFGTSDGKLALIQITTSKPVRKWEIQNEKKRGGILCIDSFDIVGDGVKDLLVGRDDGMVEVYSFDNANEPVLRFDQMLSESVTSIQGGCVGKD
SYDEIVVSTYSGWVTGLTTEPIHKESGPGEELKINQEMQNKISSLRNELEHLQYKVLQERENYQQSSQSSKAKSAVPSFGINDKFTLNKDDASYSLILEV
QTAIDNVLIQSDVPIDLLDVDKNSAVVSFSSCDSESNDNFLLATYRCQADTTRLELKIRSIEGQYGTLQAYVTPRIQPKTCQVRQYHIKPLSLHQRTHFI
DHDRPMNTLTLTGQFSFAEVHSWVVFCLPEVPEKPPAGECVTFYFQNTFLDTQLESTYRKGEGVFKSDNISTISILKDVLSKEATKRKINLNISYEINEV
SVKHTLKLIHPKLEYQLLLAKKVQLIDALKELQIHEGNTNFLIPEYHCILEEADHLQEEYKKQPAHLERLYGMITDLFIDKFKFKGTNVKTKVPLLLEIL
DSYDQNALISFFDAA
```

Table T2:

Template	Seq Identity	Oligo-state	QSQE	Found by	Method	Resolution	Seq Similarity	Coverage	Description
5wlc.19.A	10.96	monomer		HHblits	EM	NA	0.26	0.41	Utp4
4nsx.1.A	14.13	monomer		HHblits	X-ray	2.10Å	0.27	0.39	U3 small nucleolar RNA-associated protein 21
5wlc.24.A	12.77	monomer		HHblits	EM	NA	0.25	0.39	Utp18
5wlc.25.A	14.08	monomer		HHblits	EM	NA	0.27	0.39	Utp21
5jpq.1.I	14.08	monomer		HHblits	EM	NA	0.27	0.39	U3 small nucleolar RNA-associated protein 21
5wyk.1.V	14.08	monomer		HHblits	EM	NA	0.27	0.39	U3 small nucleolar RNA-associated protein 21

5wyj.20.A	14.08	monomer		HHblits	EM	NA	0.27	0.39	U3 small nucleolar RNA-associated protein 21
5gxh.1.A	12.32	monomer		HHblits	X-ray	1.80Å	0.25	0.40	Gem-associated protein 5
4yd8.1.A	13.97	monomer		HHblits	X-ray	1.80Å	0.27	0.44	Protein PTHB1
4zn4.1.A	14.80	monomer		HHblits	X-ray	1.94Å	0.26	0.39	sqt1
3i2n.1.A	11.50	monomer		HHblits	X-ray	1.95Å	0.27	0.40	WD repeat-containing protein 92
5wlc.22.A	13.83	monomer		HHblits	EM	NA	0.26	0.39	Utp12
5wbi.1.A	11.79	monomer		HHblits	X-ray	3.00Å	0.26	0.39	Regulatory-associated protein of TOR 1
5wbk.1.A	11.79	monomer		HHblits	X-ray	3.11Å	0.26	0.39	Regulatory-associated protein of TOR 1
5h1j.1.A	12.81	monomer		HHblits	X-ray	2.00Å	0.26	0.39	Gem-associated protein 5
5tzs.1.1	14.08	monomer		HHblits	EM	NA	0.27	0.39	Utp21
5n1a.1.A	11.79	monomer		HHblits	X-ray	2.15Å	0.26	0.39	utp4
5wyk.1.U	12.77	monomer		HHblits	EM	NA	0.25	0.39	U3 small nucleolar RNA-associated protein 18
5wyj.19.A	12.77	monomer		HHblits	EM	NA	0.25	0.39	U3 small nucleolar RNA-associated protein 18
5tee.1.A	12.63	monomer		HHblits	X-ray	1.65Å	0.26	0.40	Gem-associated protein 5
5wlc.15.A	12.77	monomer		HHblits	EM	NA	0.27	0.38	Utp15
4zn4.1.A	14.13	monomer		HHblits	X-ray	1.94Å	0.26	0.39	sqt1
5h1k.1.A	12.81	monomer		HHblits	X-ray	1.90Å	0.26	0.39	Gem-associated protein 5
5tzs.1.e	11.89	monomer		HHblits	EM	NA	0.27	0.40	Ribosomal RNA-processing protein 9
5jpq.1.Y	11.89	monomer		HHblits	EM	NA	0.27	0.40	rrp9
5nzu.1.C	12.87	monomer		HHblits	EM	NA	0.28	0.38	Coatomer subunit beta'
5a1u.1.T	12.87	monomer		HHblits	EM	13.00Å	0.28	0.38	COATOMER SUBUNIT BETA'
5wyj.18.A	10.18	monomer		HHblits	EM	NA	0.24	0.40	U3 small nucleolar RNA-associated protein 13
5m2n.1.A	11.15	monomer		HHblits	X-ray	2.81Å	0.25	0.40	Elongator complex protein 2
5wjc.1.A	11.35	monomer		HHblits	X-ray	2.30Å	0.26	0.39	Kinetochore protein Mis16
4zoy.1.A	14.80	monomer		HHblits	X-ray	1.50Å	0.26	0.39	Sqt1
4xyh.1.A	11.70	monomer		HHblits	X-ray	2.30Å	0.26	0.39	Kinetochore protein Mis16
5a5u.1.B	7.12	monomer		HHblits	EM	9.00Å	0.24	0.41	EUKARYOTIC TRANSLATION INITIATION FACTOR 3 SUBUNIT B
4e54.1.B	11.87	monomer		HHblits	X-ray	2.85Å	0.26	0.39	DNA damage-binding protein 2
3mmy.1.A	12.68	monomer		HHblits	X-ray	1.65Å	0.27	0.39	mRNA export factor
5wbu.1.B	12.27	monomer		HHblits	X-ray	3.42Å	0.26	0.39	Target of rapamycin complex subunit LST8
4psw.1.B	11.74	monomer		HHblits	X-ray	2.10Å	0.26	0.39	Histone acetyltransferase type B subunit 2
5h64.1.C	12.27	monomer		HHblits	EM	NA	0.26	0.39	Target of rapamycin complex subunit LST8
6bcu.1.B	12.27	monomer		HHblit	EM	3.43Å	0.26	0.39	Target of rapamycin complex subunit

				s					LST8
5zcs.1.C	12.27	monomer		HHblits	EM	NA	0.26	0.39	Target of rapamycin complex subunit LST8
4l9o.1.A	10.18	monomer		HHblits	X-ray	1.60Å	0.25	0.40	Sec16,Protein transport protein SEC13
4l9o.2.A	10.18	monomer		HHblits	X-ray	1.60Å	0.25	0.40	Sec16,Protein transport protein SEC13
4zoz.1.A	13.62	monomer		HHblits	X-ray	1.70Å	0.26	0.39	Sqt1
5nrl.1.W	9.47	monomer		HHblits	EM	NA	0.25	0.40	Pre-mRNA-splicing factor RSE1
5gm6.1.F	9.47	monomer		HHblits	EM	3.50Å	0.25	0.40	Pre-mRNA-splicing factor RSE1
5oql.1.D	11.83	monomer		HHblits	EM	NA	0.26	0.39	Utp4
4uer.1.b	10.07	monomer		HHblits	EM	6.47Å	0.25	0.42	EIF3B
4nox.1.A	8.03	monomer		HHblits	X-ray	2.72Å	0.24	0.42	Eukaryotic translation initiation factor 3 subunit B
4jsn.1.B	12.27	monomer		HHblits	X-ray	3.20Å	0.26	0.39	Target of rapamycin complex subunit LST8
6fec.1.n	7.12	monomer		HHblits	EM	6.30Å	0.24	0.41	Eukaryotic translation initiation factor 3 subunit B

The table above shows the top 50 filtered templates. A further 988 templates were found which were considered to be less suitable for modelling than the filtered list.
3fgb.1.A, 3hxj.1.B, 3vl1.1.A, 3hxj.1.A, 4a0b.2.A, 5cvl.1.A, 4czv.1.A, 5hy7.2.A, 5cvo.2.A, 3fm0.1.A, 2ynp.1.A, 3dxm.1.C, 1zim.1.A, 4tqo.1.A, 5ukl.1.B, 3q54.1.A, 4e54.1.B, 4e54.1.A, 5m11.1.A, 5naf.1.A, 5wg4.1.B, 4tz4.1.A, 3sn6.1.B, 3p8m.1.C, 1ri6.1.A, 3p8m.1.D, 6bw3.1.A, 6c23.1.D, 3j81.1.5, 5h1k.1.A, 5wak.1.A, 6fbs.1.A, 6fbs.1.B, 2iao.1.A, 2z5h.1.B, 1r5m.1.A, 4o9x.1.A, 4gq1.1.A, 1xip.1.A, 4ui9.1.Q, 1p22.1.A, 4ui9.1.I, 5vfc.1.A, 2h6k.1.A, 2yms.1.A, 5cyk.1.A, 3hfq.1.A, 5em2.2.B, 2xyi.1.A, 5tzs.1.1, 2pm9.1.A, 3v4v.1.A, 1tye.1.A, 3f3g.1.E, 4y5r.1.C, 2ipz.1.A, 3azd.1.B, 1aof.1.A, 1aof.1.B, 1zim.1.C, 2iax.1.A, 2ipz.1.C, 5lks.64.A, 4pko.1.1, 4pko.1.0, 3w15.1.A, 5ffo.1.A, 3bws.1.A, 5fqd.1.A, 5naf.3.A, 5h13.1.A, 4qzv.2.A, 2ccf.1.B, 5vyc.4.I, 5v1d.2.A, 5v1d.2.B, 4c8h.1.A, 4o5t.1.A, 1tmz.1.B, 1tmz.1.A, 4a0l.1.A, 4jsn.1.B, 4a7k.1.A, 2z5h.1.A, 1jmz.1.B, 4nj0.1.A, 1nex.2.B, 4aez.2.A, 5opt.1.A, 1gp2.1.B, 4nox.1.A, 2z5i.1.B, 5wsg.1.U, 2vdu.1.A, 4d6v.1.A, 3jbt.1.A, 4q9t.1.A, 5cxc.1.A, 5k0m.1.A, 2z5i.2.A, 6gdg.1.B, 1jof.1.A, 4jxm.1.A, 6em3.1.E, 2i3s.1.A, 4cvc.1.A, 5v3o.1.A, 5es4.3.A, 6bcx.1.C, 4pko.1.W, 4pko.1.V, 6f3a.1.3, 3j7p.78.A, 4pko.1.S, 5neu.3.E, 3sfz.1.A, 3j6x.75.A, 4pko.1.Y, 2ce9.2.B, 5jcs.1.3, 4nsx.1.A, 6g5i.1.6, 5wyk.1.U, 4a2m.2.A, 5wyk.1.V, 3k72.1.A, 3mtu.1.F, 5wyk.1.R, 5tdh.1.B, 1unx.1.A, 3jzn.1.A, 5wg6.1.B, 4o5s.1.A, 5wlc.17.A, 1zii.1.B, 4o02.1.A, 5lj5.1.d, 3azd.1.A, 5kc2.1.B, 5sum.1.A, 1a0r.1.A, 5m1j.14.A, 4v5z.1.A, 5mqf.1.F, 5mqf.1.D, 5mqf.1.E, 4xmm.1.C, 5kis.1.A, 1uo2.1.B, 5jut.45.A, 3shf.1.A, 1zik.1.A, 1zik.1.B, 4fhm.1.A, 5tzs.1.e, 4pxw.1.A, 1zil.1.A, 6c23.1.F, 4v6w.2.A, 3w8v.1.C, 3w8v.1.B, 3wvl.2.J, 3wvl.2.K, 3wvl.2.H, 5ndv.73.A, 4a2l.1.B, 3wvl.2.L, 3dsm.1.A, 4wjv.1.A, 3jap.1.i, 5sv7.1.B, 5sv7.1.C, 5a31.1.R, 5k1a.2.B, 4pko.1.P, 5j3j.1.A, 5k1h.1.A, 5u5h.1.A, 6bn8.1.A, 3ei3.1.A, 4c8h.1.C, 2ipz.1.B, 3ck4.3.C, 2ipz.1.D, 5iir.1.A, 2nrn.1.D, 6bcu.1.B, 2nrn.1.A, 4j87.1.A, 2nrn.1.B, 4neh.1.A, 2iau.1.A, 5h19.1.A, 4a0l.2.A, 1unx.1.B, 5sv7.1.D, 5e6u.1.A, 3odt.1.A, 5sv7.1.A, 4v8m.8.A, 5afu.1.C, 4r40.1.A, 2d0v.1.A, 5gmk.1.0, 3li4.1.A, 1swi.1.A, 6em5.1.5, 2c4d.1.A, 5wlc.27.A, 3ck4.1.D, 3hlh.1.A, 4xyh.1.A, 2cn3.1.A, 5h64.1.B, 5h64.1.C, 6em5.1.h, 2ovp.1.B, 2w18.1.A, 5tf2.1.A, 5xjc.1.W, 2c7d.1.T, 2oxk.1.A, 5xjc.1.T, 1w5k.1.B, 4bzj.1.B, 4fa4.1.D, 2iaa.1.A, 1flg.1.A, 5xjc.1.E, 5ic7.1.A, 4cc9.1.A, 4x3e.1.A, 2be1.1.A, 5mwj.1.A, 1mg2.1.A, 4zoy.1.A, 5gmk.1.J, 5opx.1.Y, 5kkl.1.A, 5opx.1.Z, 3crp.1.A, 1w6s.1.A, 3crp.1.B, 3crp.1.D, 1piq.1.A, 5gmk.1.X, 3ck4.3.B, 4z7o.1.A, 3ow8.1.A, 6ek0.64.A, 4pkn.1.M, 3k7z.1.A, 4wk0.1.A, 6fq3.1.A, 1ce9.1.B, 5zya.1.D, 3k7z.1.C, 6b3x.1.A, 2b1f.1.B, 1ce9.1.D, 2oaj.1.A, 5ffg.1.A, 5iiv.1.A, 4wju.1.A, 5jus.45.A, 6az1.1.6, 2cce.1.A, 5wlc.25.A, 5wuk.1.A, 2hes.1.A, 1uo0.1.A, 1uny.1.A, 1s4u.1.A, 4wjs.1.A, 3ije.1.A, 3j77.45.A, 2b5l.1.A, 2iav.1.A, 4cag.1.A, 5gap.1.F, 4imm.2.A, 3u4y.1.A, 5nuv.1.A, 5wyj.19.A, 1w5h.1.A, 3j2t.1.A, 5cyk.1.B, 4yd8.1.A, 5hqg.1.A, 5v4b.1.B, 1pi6.1.A, 1w5k.2.A, 5kb1.1.A, 2wuk.2.A, 1sq9.1.A, 5bjs.1.A, 1unt.1.A, 2zta.1.B, 5xm3.1.A, 5n4a.1.A, 5l8w.1.B, 2yba.1.A, 3f3p.2.B, 1b9y.1.A, 4dmd.1.B, 2c7d.1.P, 4zb4.1.A, 3i2n.1.A, 2c7d.1.S, 5ayw.1.B, 2c7d.1.R, 3gjp.1.A, 5m89.2.A, 3gjp.1.B, 2c7d.1.U, 5wbk.1.A, 4v7f.1.j, 4gm3.1.A, 5guw.3.A, 1lrw.1.C, 4yzy.1.A, 3jcm.1.B, 3v7d.1.B, 4l9o.2.A, 2bcj.1.B, 3i7k.1.A, 2iat.1.A, 1ij0.1.B, 5a2q.1.8, 6b20.1.A, 3prw.1.A, 6en4.1.A, 1swi.1.C, 1swi.1.B, 4o9d.1.A, 5lj5.1.M, 4nj0.1.B, 1w5j.1.A, 1w5j.1.B, 1rb5.1.C, 1aon.1.O, 4hdj.1.A, 5t2a.48.A, 4a08.1.A, 4a08.1.B, 4pwz.1.A, 3ah8.1.B, 3fhc.1.A, 1kd9.2.B, 4lg8.1.A, 5a1u.1.S, 5a1u.1.T, 2xu7.1.A, 5flx.1.7, 1ij0.1.A, 1ij0.1.C, 1zij.1.B, 5juu.45.A, 1hzu.1.A, 1rb5.1.B, 1rb5.1.A, 3mzk.1.A, 4um9.1.A, 2zuy.1.A, 2wuk.2.B, 4cy2.1.A, 3wj9.1.A, 4v92.1.8, 4pko.1.O, 5k19.2.A, 2z5h.2.A, 2z5h.2.B, 3k6s.2.A, 5k0y.1.8, 4ycz.1.A, 1hzv.1.A, 2c7d.1.O, 3mxx.1.A, 2j04.1.B, 3jan.80.A, 3jb9.1.L, 2ynn.1.A, 6gqv.75.A, 3jb9.1.K, 4cy1.1.A, 6bly.1.B, 1vyh.1.C, 4yhc.2.A, 4ozu.1.A, 6fec.1.n, 2xl2.1.A, 6fec.1.e, 5fxy.2.A, 2bbk.1.A, 3jb9.1.S, 3v9f.4.A, 3ck4.2.A, 3v9f.2.A, 4bts.27.A, 5wyj.17.A, 4v7e.7.A, 3ck4.2.D, 2iap.1.A, 2o9k.1.A, 4xfv.1.A, 3dm0.1.A, 5y1u.1.A, 4up4.1.A, 4e5z.1.A, 3uvo.1.A, 4e5z.1.B, 4v0n.2.B, 3crp.1.C, 5it9.1.6, 5gm6.1.F, 2g99.1.A, 5cvo.1.A, 4buj.1.C, 5hy7.1.A, 3vl1.2.A, 5u69.1.A, 3crp.2.A, 3iiw.1.A, 1rb6.1.A, 1rb6.1.B, 4a0b.1.A, 2cce.1.B, 6avr.1.A, 3li3.1.A, 5sui.1.A, 4buj.1.D, 4o45.1.A, 2hy6.1.B, 5oql.1.3, 5k1c.1.C, 5k1c.1.B, 4pkn.1.N, 2hy6.1.G, 1rb4.1.B, 3bg0.1.H, 3frx.1.A, 5igo.1.A, 4q9t.2.A, 5nnz.2.A, 6bly.1.A, 4tqj.1.A, 5juy.1.B, 3va6.1.A, 5nzu.1.A, 5d0o.1.B, 5juy.1.G, 5juy.1.D, 5juy.1.E, 6avu.1.A, 1h4i.1.A, 4a11.1.B, 2mta.1.A, 6exn.1.J, 4a11.1.A, 3ei4.3.A, 5oql.1.N, 5oql.1.O, 5oql.1.L, 5oql.1.M, 1xhm.1.A, 5oql.1.A, 5oql.1.F, 5oql.1.D, 5hyn.2.B, 6exn.1.a, 5juo.45.A, 1w5l.1.B, 1l0q.3.A, 3rfh.1.A, 6emk.1.D, 6emk.1.B, 5ov3.1.A, 5ov3.1.B, 4v7h.1.Q, 4v5o.1.0, 5em2.1.B, 4bl0.2.A, 1jju.1.B, 5ams.1.A, 5wbi.1.A, 5mzh.1.A, 3i7p.1.A, 2c7c.1.T, 2c7c.1.U, 2c7c.1.R, 3fcs.1.A, 2h13.1.A, 2c7c.1.Q, 6gqb.75.A, 3ei4.1.B, 3ei4.1.A, 5k0y.1.P, 4nen.1.A, 4mmz.1.A, 5m2n.1.A, 2c7c.1.O, 5h1j.1.A, 2wq3.1.A, 2ccn.1.B, 2ccn.1.A, 2c7d.1.Q, 4j73.1.A, 2pbi.2.B, 2z5i.2.B, 1kdd.2.A, 4z8l.1.A, 5cxb.1.B, 5cxb.1.A, 3jpx.1.A, 4c8s.1.A, 1ce9.1.C, 2co0.1.A, 1uo1.1.B, 5vlj.1.B, 5vlj.1.C, 6b3j.1.D, 3mks.1.D, 5fvm.1.C, 6f9n.1.A, 6f9n.1.B, 5a5u.1.B, 4u7a.1.A, 4xf2.1.C, 5lcw.1.Q, 5lcw.1.R, 1unz.1.B, 3vgz.1.A, 3zq0.1.Q, 4bzj.1.D, 4bzj.1.C, 5mc6.37.A, 4bzj.1.A, 3zq0.1.P, 3i7l.1.A, 3k7z.1.B, 6g16.4.A, 1l0q.1.A, 2iaw.1.A, 5lcw.1.I, 5ukk.1.B, 5nxq.1.A, 2g8s.1.A, 1u2u.1.A, 3va6.2.A, 5cvn.1.A, 5kb0.1.A, 2zta.1.A, 2ahp.1.B, 2ymu.1.A, 2ahp.1.A, 6fb3.1.A, 4yhc.1.A, 4pkn.1.1, 2hy6.1.A, 5a9q.1.H, 5lyb.33.A, 5cxc.1.B, 5g05.1.I, 4pkn.1.L, 5wve.1.K, 4fhl.1.A, 6g5h.1.8, 5vh9.1.B, 4zoz.1.A, 4exv.1.A, 1uny.1.B, 5nem.1.E, 2ovr.1.B, 4gq2.1.B, 2x6p.1.C, 3j80.1.7, 4i79.1.A, 5es4.4.A, 1zil.1.B, 5zcs.1.C, 4imm.1.A, 1erj.1.A, 4a09.1.A, 3rfh.1.B, 6avq.1.A, 4pkn.1.0, 4o9d.2.A, 4czy.1.A, 1uo0.1.B, 4bzk.1.D, 3dwl.1.B, 4pkn.1.J, 4pkn.1.K, 4pkn.1.H, 4pkn.1.I, 4irz.1.A, 2iar.1.A, 4av8.1.A, 4zov.1.A,

4pkn.1.Z, 4pkn.1.X, 4pkn.1.Y, 4pkn.1.V, 4xmn.1.A, 1ij1.1.C, 4uer.1.b, 3acp.1.A, 1aoq.1.A, 5tga.33.A, 5g04.1.Q, 2g9j.1.B, 2aq5.1.A, 3v4v.2.A, 2g9j.1.D, 3hxj.2.A, 5wjc.1.A, 3hxj.2.B, 5g04.1.I, 2hz6.1.A, 3e0c.1.A, 3jrp.1.A, 2hye.1.A, 4j0x.1.A, 5fa5.1.B, 5wp3.1.A, 4ci8.1.A, 5k1a.1.B, 1gcl.1.D, 5nrl.1.W, 1dy7.1.A, 1got.1.B, 4x60.1.B, 1w5l.1.A, 5n1a.1.A, 5nrl.1.O, 2vdo.1.A, 4pkn.1.W, 1e2r.1.B, 5aja.1.A, 2gvu.1.A, 5ukm.1.B, 4aez.1.A, 4xei.1.C, 3uzs.1.B, 2zux.1.A, 6bnb.1.A, 3j78.45.A, 3wvl.1.M, 3wvl.1.L, 2gvx.1.A, 3wvl.1.I, 3wvl.1.H, 3wvl.1.K, 5mq0.1.I, 1e2r.1.A, 5mps.1.U, 4zox.1.A, 5v1d.1.C, 5v1d.1.A, 5es4.2.A, 6byn.1.A, 5lj3.1.L, 3vi3.2.A, 2ojh.1.A, 6eoj.1.A, 5j0k.1.B, 6eoj.1.C, 1ihq.1.B, 4pko.1.U, 1ihq.1.A, 3vu4.1.A, 6f3a.1.2, 4xga.1.A, 4a0a.1.A, 3rrm.1.C, 4a0a.1.B, 3ott.1.A, 4pko.1.R, 4a0b.1.B, 2i3s.2.A, 6cb1.1.a, 3mkq.1.E, 3vu4.2.A, 2ccf.1.A, 1rb6.1.C, 4gqb.1.B, 4a0l.1.B, 3w8v.1.A, 3u0s.1.A, 4zb4.2.A, 6dde.1.B, 3ewe.1.A, 4g1a.1.A, 5l8s.1.A, 4h5i.1.A, 5t2c.73.A, 2b1f.1.C, 5wlc.15.A, 4mh1.1.A, 4gm9.2.A, 4mh1.1.B, 2b5m.1.A, 4pko.1.X, 4owr.1.A, 1gjq.1.A, 5o9z.1.L, 5wlc.13.A, 5o9z.1.F, 5mb4.1.A, 4wk4.1.A, 3nig.1.A, 3zq0.1.R, 3li5.1.A, 3wvl.1.J, 1w5j.2.A, 2c7c.1.S, 5wyj.18.A, 4yzs.1.A, 5m5g.1.A, 4ggd.1.A, 6d9j.78.A, 5bpt.1.A, 5xyi.1.6, 4wju.2.A, 1zij.1.A, 5mc6.15.A, 1zij.1.C, 3bg0.1.D, 1k8k.1.C, 5xwr.1.A, 4g1m.1.A, 2c7c.1.P, 1unz.1.A, 1gcl.1.A, 3n0e.1.A, 5tee.1.A, 3ei2.1.A, 3ei2.1.B, 4yvd.1.A, 2x6p.1.A, 3bg0.1.A, 4qrj.1.A, 5vtb.1.A, 3wvl.1.N, 4j0w.1.A, 3mtu.1.E, 5jk7.2.A, 3jct.1.n, 5wg6.2.B, 2hy6.1.C, 4g56.1.B, 4v0m.1.B, 4aow.1.A, 5lyb.108.A, 5jul.1.A, 5wlc.28.A, 3zq0.1.U, 3zq0.1.T, 1uo1.1.A, 6f1t.1.b, 6f1t.1.c, 3zq0.1.S, 5wlc.19.A, 3zq0.1.O, 5sxm.1.A, 5jk7.1.B, 5a9q.1.G, 5a9q.1.A, 6d90.78.A, 5a9q.1.C, 6g16.1.A, 3scy.1.A, 6bk8.1.P, 1unt.1.B, 5wlc.26.A, 5l8e.1.A, 4cak.1.A, 2b5l.2.A, 4n14.1.A, 2oxj.1.C, 1gxr.1.B, 1gxr.1.A, 3mkq.1.A, 3ott.1.B, 3mkq.1.C, 3fcu.1.A, 6bk8.1.H, 4v6i.1.A, 1g72.1.A, 5kdo.1.B, 4pko.1.T, 1zii.1.A, 5iew.1.A, 1ce9.1.A, 4owi.1.B, 5grs.1.A, 5m23.1.A, 3j6y.75.A, 4a7j.1.A, 1kv9.1.A, 4r40.2.A, 5hxb.1.B, 4kzz.1.6, 6f1t.1.4, 2oxj.1.B, 6f1t.1.3, 1zim.1.B, 2oxj.1.A, 4g1e.1.A, 2oit.1.A, 1kd9.1.B, 5igq.1.A, 1w5i.1.B, 1w5i.1.A, 3jam.1.7, 3hli.1.A, 1kd9.3.A, 4dzn.1.A, 3jaq.1.i, 4dzn.1.C, 1m1x.1.A, 5nzu.1.C, 4psw.1.B, 1pev.1.A, 5y1u.2.A, 4v7r.20.A, 5wyj.20.A, 2g9a.1.A, 5oql.1.X, 4d0k.1.A, 4lg9.1.A, 1yiq.1.A, 1rb4.1.A, 5wlc.24.A, 3dw8.1.B, 4owi.1.A, 5dfz.1.C, 2yno.1.A, 5obm.152.A, 5wlc.22.A, 2k8x.1.A, 2k8x.1.B, 6f38.1.3, 6f38.1.4, 3byc.1.A, 1gcl.1.B, 5vai.1.D, 5gxh.1.A, 5h3s.1.A, 5wlc.20.A, 3no2.1.A, 5ndv.147.A, 3vi3.1.A, 2cnx.1.A, 5es4.1.A, 1ij1.1.A, 1ij1.1.B, 3fmo.1.A, 1zta.1.A, 4wjk.1.A, 3hx6.1.A, 3i1c.1.A, 1gcl.1.C, 4v16.1.A, 2b22.1.A, 5e6s.2.A, 1h4j.1.A, 6f38.1.b, 6f38.1.c, 3ck4.3.A, 5wyj.16.A, 2ias.1.A, 4pk1.1.A, 4mmx.1.A, 1tbg.1.E, 5ttw.2.A, 1w5k.1.A, 3ck4.1.C, 1tbg.1.A, 4u1e.1.A, 4ci1.1.A, 4dzn.1.B, 3lrv.1.A, 5m89.1.A, 3q7o.1.A, 3cfs.1.A, 5i2t.1.A, 1u8c.1.A, 3n0d.1.A, 4gga.1.A, 2yh3.1.A, 3cik.1.B, 4bh6.1.A, 6g18.1.L, 4u1f.1.A, 2qxv.1.A, 1lrw.1.A, 2wuk.1.A, 5ner.1.E, 2wuk.1.B, 3p1l.1.A, 5jpq.1.Y, 3ra3.1.B, 4j79.1.A, 4dmd.1.A, 4qzv.1.A, 5lzz.77.A, 2i3t.1.A, 3k6s.5.A, 5gva.1.A, 5jpq.1.I, 5nnz.1.A, 3zwl.1.A, 4um8.1.A, 3rfg.1.A, 2iaq.1.A, 4igl.1.A, 3c9c.1.A, 2pm7.1.D, 3emh.1.A, 1ce0.1.B, 4z7q.1.A, 3q7m.1.A, 3ck4.1.B, 1ce0.1.C, 6cvz.1.A, 3jro.1.A, 1ce0.1.A, 1rb4.1.C, 1kb0.1.A, 1yfq.1.A, 5ij7.1.B, 2l5g.1.B, 5ljo.1.A, 5igo.2.A, 2gnq.1.A, 5ife.1.D, 4d5l.1.7, 1uo2.1.A, 3gjp.1.C, 2b1f.1.D, 3sjl.1.D, 3gre.1.A, 4ggc.1.A, 5ex7.1.A, 3iiy.1.A, 6gq1.75.A, 2pbi.1.B, 3jai.77.A, 3f3f.1.A, 3wj9.2.A, 4yzs.1.B, 1gq1.1.A, 2x6p.1.B, 4cy3.1.A, 3ck4.1.A, 4v3p.1.A, 5wai.1.A, 6fpt.1.A, 5wbu.1.B, 4zov.2.A, 5j0k.1.A, 5mc6.36.A, 3wvl.2.I, 2pm6.1.B, 3wvl.2.N, 5em2.1.A, 3mmy.1.A, 5ltd.1.A, 4a0k.1.C, 6cmo.1.C, 2z5i.1.A, 4a0k.1.D, 2j57.1.C, 3wvl.2.M, 2h9l.1.A, 6fai.1.E, 3ra3.2.A, 3v9f.3.A, 5uz7.1.B, 3e5z.1.A, 1w5g.1.A, 4l9o.1.A, 3m48.1.A, 2co0.2.A, 1u4c.1.A, 3v9f.1.A, 4ci8.2.A

SWISS-MODEL Homology Modelling Report

Model Building Report

This document lists the results for the homology modelling project "TTC8_HUMAN Q8TAM2 Tetratricopeptide repeat protein 8" submitted to SWISS-MODEL workspace on July 23, 2018, 4 p.m..The submitted primary amino acid sequence is given in Table T1.

If you use any results in your research, please cite the relevant publications:

- Waterhouse, A., Bertoni, M., Bienert, S., Studer, G., Tauriello, G., Gumienny, R., Heer, F.T., de Beer, T.A.P., Rempfer, C., Bordoli, L., Lepore, R., Schwede, T. SWISS-MODEL: homology modelling of protein structures and complexes. Nucleic Acids Res. 46(W1), W296-W303 (2018). doi
- Guex, N., Peitsch, M.C., Schwede, T. Automated comparative protein structure modeling with SWISS-MODEL and Swiss-PdbViewer: A historical perspective. Electrophoresis 30, S162-S173 (2009). doi
- Bienert, S., Waterhouse, A., de Beer, T.A.P., Tauriello, G., Studer, G., Bordoli, L., Schwede, T. The SWISS-MODEL Repository - new features and functionality. Nucleic Acids Res. 45, D313-D319 (2017). doi
- Benkert, P., Biasini, M., Schwede, T. Toward the estimation of the absolute quality of individual protein structure models. Bioinformatics 27, 343-350 (2011). doi
- Bertoni, M., Kiefer, F., Biasini, M., Bordoli, L., Schwede, T. Modeling protein quaternary structure of homo- and hetero-oligomers beyond binary interactions by homology. Scientific Reports 7 (2017). doi

Results

The SWISS-MODEL template library (SMTL version 2018-07-12, PDB release 2018-07-06) was searched with BLAST (Camacho et al.) and HHBlits (Remmert et al.) for evolutionary related structures matching the target sequence in Table T1. For details on the template search, see Materials and Methods. Overall 2040 templates were found (Table T2).

Models

No models have been built for this project.

Materials and Methods

Template Search

Template search with BLAST and HHBlits has been performed against the SWISS-MODEL template library (SMTL, last update: 2018-07-12, last included PDB release: 2018-07-06).

The target sequence was searched with BLAST against the primary amino acid sequence contained in the SMTL. A total of 1 template was found.

An initial HHblits profile has been built using the procedure outlined in (Remmert et al.), followed by 1 iteration of HHblits against NR20. The obtained profile has then be searched against all profiles of the SMTL. A total of 2043 templates were found.

Template Selection

For each identified template, the template's quality has been predicted from features of the target-template alignment. The templates with the highest quality have then been selected for model building.

Model Building

Models are built based on the target-template alignment using ProMod3. Coordinates which are conserved between the target and the template are copied from the template to the model. Insertions and deletions are remodelled using a fragment library. Side chains are then rebuilt. Finally, the geometry of the resulting model is regularized by using a force field. In case loop modelling with ProMod3 fails, an alternative model is built with PROMOD-II (Guex et al.).

Model Quality Estimation

The global and per-residue model quality has been assessed using the QMEAN scoring function (Benkert et al.) . For improved performance, weights of the individual QMEAN terms have been trained specifically for SWISS-MODEL.

Ligand Modelling

Ligands present in the template structure are transferred by homology to the model when the following criteria are met: (a) The ligands are annotated as biologically relevant in the template library, (b) the ligand is in contact with the model, (c) the ligand is not clashing with the protein, (d) the residues in contact with the ligand are conserved between the target and the template. If any of these four criteria is not satisfied, a certain ligand will not be included in the model. The model summary includes information on why and which ligand has not been included.

Oligomeric State Conservation

The quaternary structure annotation of the template is used to model the target sequence in its oligomeric form. The method (Bertoni et al.) is based on a supervised machine learning algorithm, Support Vector Machines (SVM), which combines interface conservation, structural clustering, and other template features to provide a quaternary structure quality estimate (QSQE). The QSQE score is a number between 0 and 1, reflecting the expected accuracy of the interchain contacts for a model built based a given alignment and template. Higher numbers indicate higher reliability. This complements the GMQE score which estimates the accuracy of the tertiary structure of the resulting model.

References

- **BLAST**
  Camacho, C., Coulouris, G., Avagyan, V., Ma, N., Papadopoulos, J., Bealer, K., Madden, T.L. BLAST+: architecture and applications. BMC Bioinformatics 10, 421-430 (2009). doi
- **HHblits**
  Remmert, M., Biegert, A., Hauser, A., Söding, J. HHblits: lightning-fast iterative protein sequence searching by HMM-HMM alignment. Nat Methods 9, 173-175 (2012). doi

Table T1:

Primary amino acid sequence for which templates were searched and models were built.

```
MSSEMEPLLLAWSYFRRRKFQLCADLCTQMLEKSPYDQEPDPELPVHQAAWILKARALTEMVYIDEIDVDQEGIAEMMLDENAIAQVPRPGTSLKLPGTN
QTGGPSQAVRPITQAGRPITGFLRPSTQSGRPGTMEQAIRTPRTAYTARPITSSSGRFVRLGTASMLTSPDGPFINLSRLNLTKYSQKPKLAKALFEYIF
HHENDVKTIHLEDVVLHLGIYPFLLRNKNHIEKNALDLAALSTEHSQYKDWWWKVQIGKCYYRLGMYREAEKQFKSALKQQEMVDTFLYLAKVYVSLDQP
VTALNLFKQGLDKFPGEVTLLCGIARIYEEMNNMSSAAEYYKEVLKQDNTHVEAIACIGSNHFYSDQPEIALRFYRRLLQMGIYNGQLFNNLGLCCFYAQ
QYDMTLTSFERALSLAENEEEAADVWYNLGHVAVGIGDTNLAHQCFRLALVNNNNHAEAYNNLAVLEMRKGHVEQARALLQTASSLAPHMYEPHFNFATI
SDKIGDLQRSYVAAQKSEAAFPDHVDTQHLIKQLRQHFAML
```

Table T2:

Template	Seq Identity	Oligo-state	QSQE	Found by	Method	Resolution	Seq Similarity	Coverage	Description
6eou.1.A	20.42	monomer		HHblits	X-ray	1.75Å	0.30	0.62	UDP-N-acetylglucosamine--peptide N-acetylglucosaminyltransferase 110 kDa subunit
6exn.1.R	6.97	monomer		HHblits	EM	NA	0.24	0.82	Pre-mRNA-splicing factor CLF1
5mc6.35.A	16.77	monomer		HHblits	EM	NA	0.27	0.62	Superkiller protein 3
4buj.2.B	16.77	monomer		HHblits	X-ray	3.70Å	0.27	0.62	SUPERKILLER PROTEIN 3
4buj.1.B	16.77	monomer		HHblits	X-ray	3.70Å	0.27	0.62	SUPERKILLER PROTEIN 3
4ui9.1.F	15.34	homo-dimer	0.06	HHblits	EM	3.60Å	0.29	0.58	CELL DIVISION CYCLE PROTEIN 27 HOMOLOG
5a31.1.F	15.43	homo-dimer	0.06	HHblits	EM	4.30Å	0.29	0.57	ANAPHASE-PROMOTING COMPLEX SUBUNIT 3
5g04.1.F	15.65	homo-dimer	0.04	HHblits	EM	4.00Å	0.29	0.58	CELL DIVISION CYCLE PROTEIN 27 HOMOLOG
4ui9.1.H	15.34	homo-dimer	0.05	HHblits	EM	3.60Å	0.29	0.58	CELL DIVISION CYCLE PROTEIN 27 HOMOLOG
5a31.1.H	15.43	homo-dimer	0.05	HHblits	EM	4.30Å	0.29	0.57	ANAPHASE-PROMOTING COMPLEX SUBUNIT 3
6eou.1.A	17.33	monomer		HHblits	X-ray	1.75Å	0.29	0.55	UDP-N-acetylglucosamine--peptide N-acetylglucosaminyltransferase 110 kDa subunit
4kvm.1.A	15.55	monomer		HHblits	X-ray	2.60Å	0.26	0.61	N-terminal acetyltransferase A complex subunit nat1
4ui9.1.C	17.55	monomer		HHblits	EM	3.60Å	0.27	0.56	CELL DIVISION CYCLE PROTEIN 23 HOMOLOG
4xnh.1.A	13.11	monomer		HHblits	X-ray	2.10Å	0.25	0.61	N-terminal acetyltransferase A complex subunit NAT1
4xpd.1.A	13.11	monomer		HHblits	X-ray	2.81Å	0.25	0.61	N-terminal acetyltransferase A complex subunit NAT1
5g05.1.C	17.55	monomer		HHblits	EM	3.50Å	0.27	0.56	CELL DIVISION CYCLE PROTEIN 23 HOMOLOG
5lcw.1.C	17.55	monomer		HHblits	EM	4.00Å	0.27	0.56	Cell division cycle protein 23 homolog
5g04.1.C	17.55	monomer		HHblits	EM	4.00Å	0.27	0.56	CELL DIVISION CYCLE PROTEIN 23 HOMOLOG

4kvo.1.A	15.64	monomer		HHblits	X-ray	3.15Å	0.26	0.60	N-terminal acetyltransferase A complex subunit nat1
5mqf.1.O	10.84	monomer		HHblits	EM	NA	0.26	0.61	Crooked neck-like protein 1
5g04.1.H	15.65	homo-dimer	0.03	HHblits	EM	4.00Å	0.29	0.58	CELL DIVISION CYCLE PROTEIN 27 HOMOLOG
5a31.1.C	17.55	monomer		HHblits	EM	4.30Å	0.27	0.56	CELL DIVISION CYCLE PROTEIN 23 HOMOLOG
4y49.1.A	13.11	monomer		HHblits	X-ray	3.95Å	0.25	0.61	N-terminal acetyltransferase A complex subunit NAT1
4hnx.1.A	13.11	monomer		HHblits	X-ray	2.34Å	0.25	0.61	N-terminal acetyltransferase A complex subunit NAT1
5aem.1.A	14.15	monomer		HHblits	X-ray	3.40Å	0.27	0.59	TRANSCRIPTION FACTOR TAU 131 KDA SUBUNIT
4hnw.1.A	13.11	monomer		HHblits	X-ray	2.80Å	0.25	0.61	N-terminal acetyltransferase A complex subunit NAT1
6bq1.1.B	13.62	monomer		HHblits	EM	NA	0.27	0.56	Tetratricopeptide repeat protein 7B
5aio.1.A	14.47	monomer		HHblits	X-ray	3.15Å	0.27	0.59	TRANSCRIPTION FACTOR TAU 131 KDA SUBUNIT
4ui9.1.P	17.55	monomer		HHblits	EM	3.60Å	0.27	0.56	CELL DIVISION CYCLE PROTEIN 23 HOMOLOG
5g04.1.P	17.55	monomer		HHblits	EM	4.00Å	0.27	0.56	CELL DIVISION CYCLE PROTEIN 23 HOMOLOG
5g05.1.F	15.65	homo-dimer	0.05	HHblits	EM	3.50Å	0.29	0.58	CELL DIVISION CYCLE PROTEIN 27 HOMOLOG
4rg6.1.A	15.75	monomer		HHblits	X-ray	3.30Å	0.29	0.54	Cell division cycle protein 27 homolog
5aem.1.A	12.29	monomer		HHblits	X-ray	3.40Å	0.27	0.56	TRANSCRIPTION FACTOR TAU 131 KDA SUBUNIT
4hny.2.A	13.11	monomer		HHblits	X-ray	2.25Å	0.25	0.61	N-terminal acetyltransferase A complex subunit NAT1
4hny.1.A	13.11	monomer		HHblits	X-ray	2.25Å	0.25	0.61	N-terminal acetyltransferase A complex subunit NAT1
5aio.1.A	12.29	monomer		HHblits	X-ray	3.15Å	0.27	0.56	TRANSCRIPTION FACTOR TAU 131 KDA SUBUNIT
5a31.1.P	17.55	monomer		HHblits	EM	4.30Å	0.27	0.56	CELL DIVISION CYCLE PROTEIN 23 HOMOLOG
5xjc.1.J	10.84	monomer		HHblits	EM	3.60Å	0.26	0.61	Crooked neck-like protein 1
4hot.1.A	13.71	monomer		HHblits	X-ray	2.50Å	0.27	0.55	Interferon-induced protein with tetratricopeptide repeats 5
4hoq.1.A	13.71	monomer		HHblits	X-ray	2.07Å	0.27	0.55	Interferon-induced protein with tetratricopeptide repeats 5
4j0u.1.A	13.71	monomer		HHblits	X-ray	1.97Å	0.27	0.55	Interferon-induced protein with tetratricopeptide repeats 5
3e4b.1.A	13.03	monomer		HHblits	X-ray	2.50Å	0.25	0.57	AlgK
3e4b.3.A	13.03	monomer		HHblits	X-ray	2.50Å	0.25	0.57	AlgK
3e4b.2.A	13.03	monomer		HHblits	X-ray	2.50Å	0.25	0.57	AlgK
1w3b.1.A	20.72	homo-dimer		HHblits	X-ray	2.85Å	0.30	0.62	UDP-N-ACETYLGLUCOSAMINE--PEPTIDE N-ACETYLGLUCOSAMINYLTRANSFERASE 110
3e4b.4.A	13.03	monomer		HHblits	X-ray	2.50Å	0.25	0.57	AlgK
1w3b.1.B	20.72	homo-dimer		HHblits	X-ray	2.85Å	0.30	0.62	UDP-N-ACETYLGLUCOSAMINE--PEPTIDE N-ACETYLGLUCOSAMINYLTRANSFERASE 110
1w3b.1.A	17.33	homo-dimer		HHblits	X-ray	2.85Å	0.29	0.55	UDP-N-ACETYLGLUCOSAMINE--PEPTIDE N-ACETYLGLUCOSAMINYLTRANSFERASE 110
1w3b.1.B	17.33	homo-dimer		HHblits	X-ray	2.85Å	0.29	0.55	UDP-N-ACETYLGLUCOSAMINE--PEPTIDE N-ACETYLGLUCOSAMINYLTRANSFERASE 110

6frk.1.o	11.40	monomer		HHblits	EM	NA	0.25	0.79	Signal recognition particle subunit SRP72,Signal recognition particle subunit SRP72,Signal recognition particle subunit SRP72

The table above shows the top 50 filtered templates. A further 1,020 templates were found which were considered to be less suitable for modelling than the filtered list.

5gm6.1.4, 3ru0.1.A, 5lyn.1.A, 5gm6.1.2, 2c2l.1.A, 1fpp.1.B, 5ulm.1.A, 4a1s.1.A, 5efr.1.A, 5gjr.56.A, 1a17.1.A, 5a31.1.V, 3gw4.1.A, 1ya0.1.A, 3ax3.1.A, 4bt9.1.B, 1x81.1.A, 2ifu.2.A, 3r9a.1.D, 4di3.1.D, 5gjr.54.A, 5vgz.1.G, 3r9a.1.B, 1tnu.1.A, 5vgz.1.J, 4aif.2.A, 5vgz.1.M, 1qqe.1.A, 6bq1.1.B, 4u0u.1.A, 4mbq.2.A, 5gjr.12.A, 2avp.1.A, 5m32.1.b, 4eba.1.A, 4d10.1.C, 2n8w.1.A, 2if4.1.A, 5o2n.1.A, 4ui9.1.P, 4n5c.8.A, 4ui9.1.V, 4ui9.1.W, 5w5h.2.E, 4ui9.1.K, 4ui9.1.H, 5gjr.18.A, 4ui9.1.O, 5che.1.E, 6c6k.1.A, 4ui9.1.C, 5oj8.1.A, 5w65.1.Q, 4ui9.1.F, 4n5c.6.A, 4e85.1.A, 3q15.1.A, 3ieg.2.A, 3ulq.1.A, 1ihg.1.A, 5iwb.1.B, 4rib.1.A, 5vhr.1.H, 5jzz.1.A, 2y4u.1.A, 2q7f.1.A, 3ash.1.A, 6c9m.2.A, 5hb2.1.A, 4r8a.1.A, 2v1t.1.A, 1hh8.1.A, 4cr4.1.U, 4cr4.1.V, 4cr4.1.W, 5lfm.1.A, 4yvq.1.B, 4o6f.1.A, 4cr4.1.X, 3kd7.1.A, 4leu.1.A, 5dse.1.A, 2bug.1.A, 2v1s.1.A, 5xw7.3.A, 6fuz.1.A, 1nl4.1.A, 5xw7.5.A, 3hxe.1.A, 4jsn.1.A, 4yv6.2.B, 5izw.1.A, 5bw8.1.C, 4pjq.1.A, 5wsg.1.R, 3mv3.1.B, 3lya.1.A, 5wsg.1.T, 5a5b.1.Z, 2yhc.1.A, 5a5b.1.X, 5g05.1.K, 4rid.2.A, 2v1s.3.A, 4i1a.1.A, 5g05.1.C, 5a5b.1.W, 5g05.1.F, 5mpd.1.K, 3euv.1.A, 5mpd.1.I, 5mpd.1.H, 4ady.1.A, 4ga2.1.A, 1ft1.1.A, 5mpe.1.K, 5mpd.1.G, 6bcx.1.A, 3qou.1.A, 2yq8.1.A, 4cr4.1.6, 4m59.1.B, 1hxi.1.A, 4m59.1.A, 3cvl.1.A, 1n9a.1.A, 2v1s.5.A, 5vgz.1.K, 6frk.1.o, 3c72.1.A, 3vty.3.A, 2r2l.1.A, 5fjy.1.B, 5fjy.1.A, 5vgz.1.H, 5l0y.6.A, 4yv6.2.A, 4m57.1.A, 5wvk.1.d, 1o1r.1.A, 5wvk.1.a, 5wvk.1.b, 5wvk.1.c, 1fch.1.A, 5mqf.1.O, 4bzj.1.C, 4gyo.1.A, 5xw7.1.A, 5a5t.1.C, 4lct.1.A, 4lct.1.B, 4i9c.1.A, 5ft9.2.A, 6fcq.1.A, 5jjx.1.A, 3ma5.3.A, 5w4m.1.A, 4xmm.1.E, 4fhm.1.B, 3jcp.1.Z, 3jcp.1.Y, 3jcp.1.X, 5y7g.1.A, 2wqh.1.A, 5wrv.1.B, 4y6w.1.A, 1om2.1.A, 2lsu.1.A, 1wm5.1.A, 3jck.1.D, 5np1.1.A, 5y7g.3.A, 5a31.1.O, 5nnr.1.A, 3jcp.1.1, 3jcp.1.0, 5l4k.1.E, 5a31.1.J, 5wrw.1.B, 5l4k.1.F, 5l4k.1.I, 5a31.1.F, 3jcp.1.8, 5a31.1.C, 2c0l.1.A, 1iip.1.A, 2v1s.2.A, 5wvk.1.8, 5wvk.1.9, 5wrw.3.A, 5a31.1.W, 2j9q.1.B, 2j9q.1.A, 3nf1.1.A, 3zfw.1.A, 5a31.1.P, 6au8.1.A, 5mpe.2.L, 3c3r.1.A, 5mpe.2.H, 5mpe.2.E, 5diz.2.A, 5mpe.2.F, 6fv0.1.A, 3rjv.1.A, 5n5y.1.R, 5b26.1.A, 5b26.1.B, 4yg8.1.B, 4lct.2.B, 4oe1.1.A, 4oe1.1.B, 5a6c.1.A, 3k6b.1.A, 3q4a.1.A, 4boc.1.A, 4i17.1.A, 2awi.1.A, 5a7d.4.B, 5a7d.4.A, 2fi7.1.A, 2zir.1.A, 2fi7.1.B, 2v5f.1.A, 3ma5.1.A, 5l0y.2.A, 5njx.1.A, 5gjr.9.A, 5t0h.1.W, 5t0h.1.U, 4um2.1.A, 4q66.2.C, 1hz4.1.A, 5k18.1.A, 5mpq.1.A, 4bwr.1.A, 5a7d.2.A, 3e4b.2.A, 5a7d.2.B, 1elr.1.A, 5t0h.1.V, 5o29.1.A, 5t0h.1.0, 5vat.2.A, 5cqr.1.A, 2xev.1.A, 4fsc.2.B, 4j8d.1.A, 5arf.1.A, 5n60.1.R, 5xjc.1.J, 5xjc.1.I, 2bed.1.A, 4pjr.1.A, 5mpc.1.f, 5kcn.1.A, 4ui9.1.J, 5o7x.4.C, 4cgv.2.A, 4bta.1.B, 3ly9.1.A, 3as5.1.A, 6b85.1.A, 5xw7.2.A, 3si5.2.A, 3si5.1.A, 3q5m.1.A, 4mal.1.A, 5c9s.1.A, 2aw6.1.A, 5gmk.1.R, 5xw7.4.A, 5gmk.1.W, 4cgq.1.A, 2ooe.1.A, 4abn.2.A, 3rkv.1.A, 5t0h.1.Y, 3cv0.1.A, 5m72.1.A, 3rib.1.A, 6erp.2.D, 4zlh.1.B, 4zlh.1.A, 2gw1.1.A, 2gw1.1.B, 2axu.3.B, 4eqf.1.A, 5wlc.21.A, 6fc4.1.A, 4kvm.1.A, 3fwv.2.A, 5i9g.1.A, 3urz.1.A, 5w4n.1.A, 5vat.1.A, 5gap.1.G, 4d18.1.C, 3lvh.1.A, 3vty.4.A, 5hq8.1.A, 3asf.2.A, 3cvn.1.A, 5wft.1.A, 1dce.1.A, 5mpc.1.h, 5h64.1.A, 3tgo.1.A, 5o1j.1.A, 5oa1.1.T, 5o09.1.C, 5orm.1.A, 1sly.1.A, 5vhs.1.H, 4j0u.1.A, 2axu.1.C, 3ro3.1.A, 2axu.1.A, 5n4a.1.A, 5fzs.1.A, 4wsl.1.A, 3ly7.1.A, 3jck.1.B, 5omp.1.A, 5lyp.1.A, 5dbk.1.B, 5dbk.1.A, 5o01.2.A, 5mpc.1.k, 4cr2.1.Z, 4cr2.1.X, 4cr2.1.Y, 3qky.1.A, 2fo7.1.A, 5ayw.1.D, 4ymr.1.A, 4ymr.1.B, 4cr2.1.V, 4cr2.1.W, 4cr2.1.U, 2pqr.2.A, 1kt1.1.A, 5w5y.1.Q, 4bt9.1.A, 5kjk.1.A, 3jcm.1.D, 5jj7.1.A, 2ff4.2.A, 5jj7.1.B, 4gpk.2.B, 4gpk.2.C, 4d10.1.D, 4gpk.2.A, 4d10.1.B, 4cgw.1.A, 4gpk.2.D, 3e4b.4.A, 4h7y.3.A, 1pc2.1.A, 6cfc.1.A, 5jj6.1.A, 5jj6.1.B, 3edt.1.A, 1qbq.1.A, 3edt.1.B, 1p5q.1.B, 1mzc.1.A, 2vsy.1.A, 3bee.1.A, 1klx.1.A, 4ja9.1.A, 2wpv.1.A, 2r5s.1.A, 5ods.4.A, 4uqy.1.A, 3ax2.3.A, 2xev.3.A, 4ryk.1.A, 5a1u.1.S, 5a1u.1.T, 3u64.2.H, 3lca.1.A, 5a7d.3.B, 5ods.2.A, 5mpc.1.i, 5ctq.2.B, 5mpc.1.d, 5mpc.1.e, 3asg.1.A, 5mpc.1.g, 4cr2.1.6, 2mr3.1.A, 2xpi.1.C, 2xpi.1.A, 5ccl.1.A, 5jjt.1.A, 3zn3.1.A, 2y4t.1.A, 5ojf.1.A, 3j96.1.J, 3j96.1.H, 5wwm.1.A, 4hou.2.A, 4n2q.1.A, 2kc7.1.A, 3j96.1.G, 2vgx.1.B, 3ax5.2.A, 1e96.1.B, 1p5q.1.A, 4hnx.1.A, 1p5q.1.C, 5v3h.1.A, 5a1y.1.U, 4d0p.1.A, 5wyj.33.A, 4wne.1.A, 6c9m.1.A, 4i9e.1.B, 5vhm.1.H, 4i9e.1.A, 3cvq.1.A, 4yv6.1.A, 3jb9.1.4, 4d18.1.D, 2q7f.2.A, 4d18.1.B, 3gz1.1.A, 3jb9.1.3, 3j98.1.H, 4buj.1.B, 4rec.1.A, 5vhf.1.H, 4gcn.2.A, 4wnd.1.A, 4yde.1.A, 4ry3.1.A, 4cr4.1.Y, 4a1g.1.A, 5t0c.44.A, 4cr4.1.Z, 5vhj.1.H, 4reb.1.C, 5vhf.1.S, 6cf9.1.A, 5bt1.1.A, 6epe.1.U, 4kbq.2.A, 4gpk.3.D, 1wy6.1.A, 3ax3.3.A, 6epe.1.S, 4bta.1.A, 4hoq.1.A, 5yz0.1.B, 3sf4.1.A, 2xgm.2.A, 4gpk.3.A, 5udl.1.A, 2y4t.3.A, 5mgx.1.A, 2oew.1.A, 3pz2.1.A, 5ctq.1.B, 5vbg.1.A, 5vhf.1.J, 4wn4.2.A, 4bt8.1.B, 4bt8.1.A, 5a5t.1.G, 5ohu.1.A, 3upv.1.A, 3asd.1.A, 5y7q.1.A, 5gjr.57.A, 3ly8.1.A, 5t0j.1.1, 4ady.2.A, 5lfl.1.A, 2lni.1.A, 5mpd.1.M, 4eba.2.A, 5an3.1.A, 2vko.1.A, 5t0i.1.Y, 5t0i.1.X, 5udj.1.A, 5t0i.1.V, 5t0i.1.U, 5hrz.1.A, 4y49.1.A, 2kcv.1.A, 6epc.1.S, 5jno.1.B, 4hny.2.A, 6epc.1.T, 6epc.1.W, 6epc.1.V, 6epc.1.X, 3j9m.81.A, 6epc.1.Z, 5juf.1.A, 5hi7.1.A, 5nzu.1.C, 5nzu.1.A, 5nnp.1.A, 5d0o.1.D, 4u0s.1.A, 5wql.1.A, 4f3v.1.A, 3ax3.4.A, 5vhi.1.H, 5i9d.1.A, 3q15.2.A, 6exn.1.R, 6exn.1.S, 2xgs.1.A, 3lvh.1.B, 5oql.1.E, 2awi.3.C, 5k04.1.A, 4ehm.1.A, 5ccm.1.A, 6emk.1.C, 5ctr.2.A, 3fp2.1.A, 5wbu.1.A, 3ax3.2.A, 4xgl.1.A, 4uzy.1.A, 5fd4.1.A, 6cbx.2.A, 4fhn.2.B, 3ax2.1.A, 2v1s.6.A, 5m32.1.a, 4n5c.5.A, 5m32.1.c, 4wsn.6.B, 6f5d.1.J, 5ekq.1.B, 4wsn.6.D, 3uux.1.A, 4gco.1.A, 6f5d.1.L, 4g1t.1.A, 4hot.1.A, 4g1t.1.B, 4n5c.3.A, 4wsn.2.B, 5zcs.1.B, 4reb.1.D, 4wsn.2.A, 5hgv.1.A, 5tqb.1.B, 4wsn.2.D, 4l9p.1.A, 2ifu.1.A, 5ln3.1.0, 5w4n.1.B, 4n5c.1.A, 6epf.1.T, 6epf.1.U, 6epf.1.V, 6epf.1.W, 6epf.1.S, 4gyw.1.A, 6epf.1.X, 5fvm.1.A, 1ft2.1.A, 2ho1.1.B, 2ho1.1.A, 5ln3.1.X, 3as8.1.A, 5mzu.1.A, 5fsh.1.A, 4nrh.1.B, 5ola.2.C, 5ln3.1.V, 4bzj.1.A, 1ltx.1.A, 5m32.1.8, 5m32.1.9, 4a1g.3.A, 4ga0.1.A, 2f0y.1.A, 5lcw.1.C, 4ynw.1.A, 5ln3.1.A, 5lcw.1.O, 2fbn.1.A, 5mc6.35.A, 5cqs.2.A, 3qdn.2.A, 4i2w.1.A, 5ic8.3.A, 5ex0.1.A, 4yvo.1.A, 4j8e.1.A, 5lwv.1.A, 4in3.1.D, 1qsa.1.A, 3lpz.1.A, 2v1s.4.A, 5ic8.1.A, 3kd7.2.A, 5flc.1.F, 5np0.1.A, 5ln3.1.Z, 2grm.1.A, 2kcl.1.A, 4y6c.1.A, 4yv6.1.B, 5jzz.2.A, 5fzr.1.A, 3esk.1.A, 5a5b.1.Y, 6c6k.1.C, 1ya0.2.A, 3ma5.4.A, 2ifu.3.A, 4jsp.1.A, 3qww.1.A, 3oxg.1.A, 5y7g.2.A, 4gq2.1.A, 1fch.2.A, 1b89.1.A, 5g05.1.O, 3j9m.72.A, 4i1a.2.A, 6cf8.1.A, 3ffl.1.A, 4wjw.1.B, 3gw4.1.B, 5a01.1.A, 4rg6.1.A, 4rg6.1.B, 4me2.1.A, 4wsn.2.C, 5iww.1.D, 3ffl.1.B, 4ria.1.A, 1iyg.1.A, 3c3q.1.A, 4n5c.7.A, 3ieg.1.A, 6fec.1.G, 5g04.1.P, 3dra.1.A, 4r89.1.A, 5g04.1.U, 5g04.1.T, 5mpd.1.J, 6epf.1.Z, 2pl2.1.A, 3tg5.1.A, 5ctq.1.A, 2c2l.2.A, 5g04.1.C, 2mhk.1.A, 6fec.1.C, 5g04.1.F, 5mpe.1.J, 5g04.1.H, 5g04.1.K, 5g04.1.J, 2nc9.1.A, 2pzi.2.A, 5g04.1.O, 5xi8.1.A, 1na3.1.A, 5wlc.41.A, 5nrl.1.Q, 5ln3.1.W, 4wsn.4.D, 5ln3.1.Y, 3ro2.1.A, 4pjq.2.A, 3gz1.1.B, 5ft9.1.A, 4xmn.1.D, 4j8f.1.A, 5mpd.1.F, 5djs.1.A, 4cgu.1.A, 2kat.1.A, 5n5z.1.R, 5a7d.3.A, 5mps.1.R, 4h7x.1.A, 4jhr.1.A, 6erp.1.D, 3jco.1.Z, 4gcn.1.A, 1qz2.1.C, 1qz2.1.B, 1qz2.1.A, 2v1t.2.A, 4p29.1.A, 5lj3.1.U, 5lj3.1.T, 5wcg.1.A, 4w9r.1.A, 3lvg.1.A, 4ynv.1.A, 4uqz.1.A, 3mkq.1.E, 3spa.1.A, 5a7d.1.B, 6ez8.1.B, 4ric.1.A, 5a7d.1.A, 5uz5.1.D, 5uz5.1.E, 5jpz.1.A, 2c0m.1.A, 2vyi.1.A, 5fsh.1.B, 2xcc.1.A, 2xcc.1.B, 5l0y.7.A, 5b26.2.B, 6epd.1.Z, 2hr2.1.A, 5x6o.1.A, 6cbx.1.A, 5wql.2.A, 5wvi.1.c, 6bcu.1.A, 5l0y.5.B, 5l0y.5.A, 5jz6.1.A, 4lct.2.A, 5y5a.1.A, 2vsy.2.A, 5wvi.1.U, 5wvi.1.N, 5wvi.1.O, 5wvi.1.L, 3mv2.1.B, 3jd5.1.3, 5wvi.1.K, 5ods.3.A, 5o9z.1.G, 4fhn.1.B, 3e37.1.A, 3zhe.1.B, 5wvi.1.V, 5ods.1.A, 3q75.1.A, 5jkp.1.A, 5mqf.1.M, 3jd5.1.U, 6epd.1.X, 4wuy.1.A, 5lj5.1.U, 5lj5.1.V, 5dse.2.A, 5ftp.1.A, 5ftp.1.B, 5mpe.1.H, 5nps.1.A, 3as5.2.A, 5jjo.1.A, 3gz2.1.A, 5diz.1.A, 5c1d.1.A, 4g2v.1.A, 2vq2.1.A, 5cqs.1.A, 5t0i.1.W, 2vsn.1.A, 3qdn.1.A, 3qwp.1.A, 2axu.2.C, 1zu2.1.A, 2vko.1.B, 4rea.1.A, 3n71.1.A, 3u3w.1.B, 3vty.1.A, 5mpb.1.k, 5a9q.1.T, 3fwv.1.A, 4zey.1.A, 4hnw.1.A, 5l0y.3.A, 3pz4.1.A, 5jhe.1.A, 5l0y.1.B, 5l0y.1.A, 3hym.1.B, 5a9q.1.B, 5n61.1.R, 6bk8.1.V, 6bk8.1.W, 5t0c.35.A, 1nzn.1.A, 1kt0.1.A, 3jco.1.0, 5wvk.1.k, 3jco.1.1, 4j8e.2.A, 3jco.1.X, 3jco.1.Y, 3e4b.1.A, 4b94.1.A, 3mkq.1.A, 6epc.1.U, 3mkq.1.C, 3jco.1.W, 5a9q.1.a, 5jqy.1.A, 4nq0.1.A, 5bwk.1.D, 5v7v.1.A, 2ond.1.A, 3s7f.1.A, 4n2s.1.A, 3zpj.1.A, 4pwx.1.C, 3jco.1.8, 6epe.1.Z, 3ax2.4.A, 3o48.1.A, 4cgv.1.A, 4abn.1.A, 6fpn.1.A, 3as4.1.A, 4q66.1.D, 3q7f.1.A, 4yv9.2.A, 1y8m.1.A, 2uy1.1.A, 2uy1.1.B, 5a9q.1.2, 5orq.1.A, 5lvv.1.A, 5y81.1.A, 5a6c.2.A, 2pzi.1.A, 3pdn.1.A, 3uq3.1.A, 3ax5.1.A, 3j8b.1.G, 3sf4.2.A, 4r7s.1.A, 4aif.1.A, 3asf.1.A, 2axz.1.A, 3j8b.1.C, 2qfc.1.A, 4ynd.1.A, 5d0q.1.C, 3vtx.2.A, 5ojs.1.A, 5l0w.1.A, 2l6j.1.A, 5ola.1.C, 5che.1.F, 4apo.1.A, 5hb3.2.A, 4n3c.1.A, 4uqx.1.A, 3sz7.1.A, 1dce.2.A, 2axv.1.A, 5oej.1.A, 1tjc.1.A, 5i9f.1.A, 3kae.1.A, 3gz2.1.B, 5o01.1.A, 2xcb.2.A, 2pqn.1.A, 5w4m.1.B, 2vko.2.A, 5jjw.1.A, 3ffl.2.B, 3oxl.1.A, 3k9i.1.A, 1zbp.1.A, 1d8d.1.A, 5t0g.1.Y, 5t0g.1.X, 2n8i.1.A, 1xnf.1.A,

5npr.1.A, 1wao.1.A, 3asg.2.A, 5t0g.1.V, 3jck.1.C, 4mal.2.A, 1elw.1.A, 1wao.3.A, 5t0j.1.V, 4xpd.1.A, 3jck.1.F, 3jbz.1.A, 4gpk.1.D, 5ctq.2.A, 4e6h.1.A, 4gpk.1.A, 4gpk.1.C, 4gpk.1.B, 6epd.1.V, 6epd.1.W, 6epd.1.T, 6epd.1.U, 3j98.1.I, 6epd.1.S, 2vko.2.B, 6epe.1.X, 6epe.1.W, 6epe.1.V, 3j97.1.H, 6epe.1.T, 4gpk.3.C, 4gpk.3.B, 4g23.1.A, 4buj.2.B, 3oxf.1.A, 3ceq.1.A, 3lku.1.A, 3ceq.1.B, 5bt1.1.B, 5hb3.1.A, 4ay5.1.A, 4d10.1.A, 5jub.1.A, 1ouv.1.A, 5jub.1.B, 5vhi.1.S, 2vkj.1.B, 4kvo.1.A, 2xev.2.A, 4xnh.1.A, 5ctr.1.A, 4kbq.1.A, 5t0g.1.0, 4xi0.1.A, 5t0g.1.5, 4ja7.1.A, 5fzr.1.B, 5mps.1.Q, 5gjr.53.A, 3mkr.1.A, 4wn4.1.A, 6fbt.1.A, 3ks2.1.A, 5ljo.1.C, 3jck.1.A, 4hny.1.A, 3bee.2.A, 4hou.1.A, 2vgy.1.A, 4ri9.1.A, 4cr3.1.6, 2vgx.1.A, 4n5c.4.A, 5jpz.1.B, 4n5c.2.A, 3lvg.1.C, 3lvg.1.B, 5fzq.1.C, 5fzq.1.B, 5fzq.1.A, 6c95.1.A, 4a1g.4.A, 2ff4.1.A, 6emk.1.A, 4ozs.1.A, 5wrw.1.A, 5l4k.1.G, 1na0.1.A, 5yz0.1.A, 5a31.1.H, 4ga1.1.A, 4ri8.1.A, 4u04.1.A, 2kck.1.A, 5i9h.1.A, 5l4k.1.H, 3fp3.1.A, 3txn.1.A, 5nnp.2.A, 5waq.1.A, 5w5i.1.A, 5l4k.1.J, 3e4b.3.A, 5vhq.1.H, 5o24.1.A, 4btb.1.A, 4wng.1.A, 5l4k.1.L, 4rea.1.B, 3wxx.1.A, 6f5d.1.K, 2lsv.1.A, 4rid.1.A, 5mpb.1.e, 5mpb.1.d, 5mpb.1.g, 5mpb.1.f, 3sfx.1.A, 3pz1.1.A, 2vkj.1.A, 3u4t.1.A, 4cr3.1.Z, 4cr3.1.Y, 5gjq.1.9, 5mpb.1.i, 5mpb.1.h, 4a1g.2.A, 2e2e.1.A, 5ic8.4.A, 4am9.1.A, 5ex3.1.A, 2dba.1.A

SWISS-MODEL Homology Modelling Report

Model Building Report

This document lists the results for the homology modelling project "PTHB1_HUMAN Q3SYG4 Protein PTHB1" submitted to SWISS-MODEL workspace on July 23, 2018, 4:01 p.m..The submitted primary amino acid sequence is given in Table T1.

If you use any results in your research, please cite the relevant publications:

- Waterhouse, A., Bertoni, M., Bienert, S., Studer, G., Tauriello, G., Gumienny, R., Heer, F.T., de Beer, T.A.P., Rempfer, C., Bordoli, L., Lepore, R., Schwede, T. SWISS-MODEL: homology modelling of protein structures and complexes. Nucleic Acids Res. 46(W1), W296-W303 (2018). doi
- Guex, N., Peitsch, M.C., Schwede, T. Automated comparative protein structure modeling with SWISS-MODEL and Swiss-PdbViewer: A historical perspective. Electrophoresis 30, S162-S173 (2009). doi
- Bienert, S., Waterhouse, A., de Beer, T.A.P., Tauriello, G., Studer, G., Bordoli, L., Schwede, T. The SWISS-MODEL Repository - new features and functionality. Nucleic Acids Res. 45, D313-D319 (2017). doi
- Benkert, P., Biasini, M., Schwede, T. Toward the estimation of the absolute quality of individual protein structure models. Bioinformatics 27, 343-350 (2011). doi
- Bertoni, M., Kiefer, F., Biasini, M., Bordoli, L., Schwede, T. Modeling protein quaternary structure of homo- and hetero-oligomers beyond binary interactions by homology. Scientific Reports 7 (2017). doi

Results

The SWISS-MODEL template library (SMTL version 2018-07-12, PDB release 2018-07-06) was searched with BLAST (Camacho et al.) and HHBlits (Remmert et al.) for evolutionary related structures matching the target sequence in Table T1. For details on the template search, see Materials and Methods. Overall 1094 templates were found (Table T2).

Models

No models have been built for this project.

Materials and Methods

Template Search

Template search with BLAST and HHBlits has been performed against the SWISS-MODEL template library (SMTL, last update: 2018-07-12, last included PDB release: 2018-07-06).

The target sequence was searched with BLAST against the primary amino acid sequence contained in the SMTL. A total of 1 template was found.

An initial HHblits profile has been built using the procedure outlined in (Remmert et al.), followed by 1 iteration of HHblits against NR20. The obtained profile has then be searched against all profiles of the SMTL. A total of 1135 templates were found.

Template Selection

For each identified template, the template's quality has been predicted from features of the target-template alignment. The templates with the highest quality have then been selected for model building.

Model Building

Models are built based on the target-template alignment using ProMod3. Coordinates which are conserved between the target and the template are copied from the template to the model. Insertions and deletions are remodelled using a fragment library. Side chains are then rebuilt. Finally, the geometry of the resulting model is regularized by using a force field. In case loop modelling with ProMod3 fails, an alternative model is built with PROMOD-II (Guex et al.).

Model Quality Estimation

The global and per-residue model quality has been assessed using the QMEAN scoring function (Benkert et al.) . For improved performance, weights of the individual QMEAN terms have been trained specifically for SWISS-MODEL.

Ligand Modelling

Ligands present in the template structure are transferred by homology to the model when the following criteria are met: (a) The ligands are annotated as biologically relevant in the template library, (b) the ligand is in contact with the model, (c) the ligand is not clashing with the protein, (d) the residues in contact with the ligand are conserved between the target and the template. If any of these four criteria is not satisfied, a certain ligand will not be included in the model. The model summary includes information on why and which ligand has not been included.

Oligomeric State Conservation

The quaternary structure annotation of the template is used to model the target sequence in its oligomeric form. The method (Bertoni et al.) is based on a supervised machine learning algorithm, Support Vector Machines (SVM), which combines interface conservation, structural clustering, and other template features to provide a quaternary structure quality estimate (QSQE). The QSQE score is a number between 0 and 1, reflecting the expected accuracy of the interchain contacts for a model built based a given alignment and template. Higher numbers indicate higher reliability. This complements the GMQE score which estimates the accuracy of the tertiary structure of the resulting model.

References

- **BLAST**
  Camacho, C., Coulouris, G., Avagyan, V., Ma, N., Papadopoulos, J., Bealer, K., Madden, T.L. BLAST+: architecture and applications. BMC Bioinformatics 10, 421-430 (2009). doi
- **HHblits**
  Remmert, M., Biegert, A., Hauser, A., Söding, J. HHblits: lightning-fast iterative protein sequence searching by HMM-HMM alignment. Nat Methods 9, 173-175 (2012). doi

Table T1:

Primary amino acid sequence for which templates were searched and models were built.

```
MSLFKARDWWSTILGDKEEFDQGCLCLANVDNSGNGQDKIIVGSFMGYLRIFSPHPAKTGDGAQAEDLLLEVDLRDPVLQVEVGKFVSGTEMLHLAVLHS
RKLCVYSVSGTLGNVEHGNQCQMKLMYEHNLQRTACNMTYGSFGGVKGRDLICIQSMDGMLMVFEQESYAFGRFLPGFLLPGPLAYSSRTDSFLTVSSCQ
QVESYKYQVLAFATDADKRQETEQQKLGSGKRLVVDWTLNIGEQALDICIVSFNQSASSVFVLGERNFFCLKDNGQIRFMKKLDWSPSCFLPYCSVSEGT
INTLIGNHNNMLHIYQDVTLKWATQLPHIPVAVRVGCLHDLKGVIVTLSDDGHLQCSYLGTDPSLFQAPNVQSRELNYDELDVEMKELQKIIKDVNKSQG
VWPMTEREDDLNVSVVVSPNFDSVSQATDVEVGTDLVPSVTVKVTLQNRVILQKAKLSVYVQPPLELTCDQFTFEFMTPDLTRTVSFSVYLKRSYTPSEL
EGNAVVSYSRPTDRNPDGIPRVIQCKFRLPLKLICLPGQPSKTASHKITIDTNKSPVSLLSLFPGFASQSDDDQVNVMGFHFLGGARITVLASKTSQRYR
IQSEQFEDLWLITNELILRLQEYFEKQGVKDFACSFSGSIPLQEYFELIDHHFELRINGEKLEELLSERAVQFRAIQRRLLARFKDKTPAPLQHLDTLLD
GTYKQVIALADAVEENQGNLFQSFTRLKSATHLVILLIALWQKLSADQVAILEAAFLPLQEDTQELGWEETVDAAISHLLKTCLSKSSKEQALNLNSQLN
IPKDTSQLKKHITLLCDRLSKGGRLCLSTDAAAPQTMVMPGGCTTIPESDLEERSVEQDSTELFTNHRHLTAETPRPEVSPLQGVSE
```

Table T2:

Template	Seq Identity	Oligo-state	QSQE	Found by	Method	Resolution	Seq Similarity	Coverage	Description
4yd8.1.A	100.00	monomer		BLAST	X-ray	1.80Å	0.61	0.46	Protein PTHB1
4yd8.1.A	100.00	monomer		HHblits	X-ray	1.80Å	0.61	0.46	Protein PTHB1
5l8e.1.A	12.00	monomer		HHblits	X-ray	2.30Å	0.26	0.34	WD repeat-containing protein 48
5xwr.1.A	9.84	homo-dimer		HHblits	X-ray	2.69Å	0.26	0.34	Histone-binding protein RBBP4
5l8w.1.B	12.00	monomer		HHblits	X-ray	2.79Å	0.26	0.34	WD repeat-containing protein 48
5mqf.1.D	12.92	monomer		HHblits	EM	NA	0.26	0.31	Pleiotropic regulator 1
5fa5.1.B	12.05	monomer		HHblits	X-ray	2.34Å	0.25	0.35	Methylosome protein 50
5cvl.1.A	12.19	monomer		HHblits	X-ray	3.00Å	0.26	0.31	WD repeat-containing protein 48
5wlc.20.A	12.04	monomer		HHblits	EM	NA	0.26	0.34	Utp1
5cvn.1.A	12.19	monomer		HHblits	X-ray	3.36Å	0.26	0.31	WD repeat-containing protein 48
4pk1.1.A	13.26	monomer		HHblits	X-ray	3.10Å	0.28	0.31	Chimera protein of Outer membrane protein assembly factors BamA and BamB
5wyk.1.R	12.04	monomer		HHblits	EM	NA	0.26	0.34	Periodic tryptophan protein 2
5wyj.16.A	12.04	monomer		HHblits	EM	NA	0.26	0.34	Periodic tryptophan protein 2
6exn.1.J	12.32	monomer		HHblits	EM	NA	0.25	0.31	Pre-mRNA-splicing factor PRP46
5wve.1.K	12.23	monomer		HHblits	EM	NA	0.26	0.31	Apoptotic protease-activating factor 1
5cyk.1.A	13.24	monomer		HHblits	X-ray	3.00Å	0.26	0.31	Ribosome biogenesis protein YTM1
5juy.1.E	12.23	monomer		HHblits	EM	NA	0.26	0.31	Apoptotic protease-activating factor 1
5juy.1.D	12.23	monomer		HHblits	EM	NA	0.26	0.31	Apoptotic protease-activating factor 1
				HHblit					

5juy.1.B	12.23	monomer		s	EM	NA	0.26	0.31	Apoptotic protease-activating factor 1
5juy.1.G	12.23	monomer		HHblits	EM	NA	0.26	0.31	Apoptotic protease-activating factor 1
5gmk.1.J	12.27	monomer		HHblits	EM	3.40Å	0.25	0.31	Pre-mRNA-splicing factor PRP46
5mq0.1.I	12.27	monomer		HHblits	EM	NA	0.25	0.31	Pre-mRNA-splicing factor PRP46
6bk8.1.H	12.27	monomer		HHblits	EM	NA	0.25	0.31	Pre-mRNA-splicing factor PRP46
3jbt.1.A	12.23	monomer		HHblits	EM	NA	0.26	0.31	Apoptotic protease-activating factor 1
5i2t.1.A	9.82	monomer		HHblits	X-ray	2.54Å	0.25	0.32	Periodic tryptophan protein 2
4gga.1.A	14.13	monomer		HHblits	X-ray	2.04Å	0.26	0.30	Cell division cycle protein 20 homolog
3acp.1.A	10.60	monomer		HHblits	X-ray	2.00Å	0.25	0.32	WD repeat-containing protein YGL004C
3vl1.1.A	10.56	monomer		HHblits	X-ray	1.60Å	0.25	0.32	26S proteasome regulatory subunit RPN14
3vl1.2.A	10.56	monomer		HHblits	X-ray	1.60Å	0.25	0.32	26S proteasome regulatory subunit RPN14
5lj3.1.L	12.32	monomer		HHblits	EM	3.80Å	0.25	0.31	PRP46
6f1t.1.4	9.64	monomer		HHblits	EM	NA	0.25	0.32	Cytoplasmic dynein 1 intermediate chain 2
6f1t.1.3	9.64	monomer		HHblits	EM	NA	0.25	0.32	Cytoplasmic dynein 1 intermediate chain 2
6f1t.1.b	9.64	monomer		HHblits	EM	NA	0.25	0.32	Cytoplasmic dynein 1 intermediate chain 2
6f1t.1.c	9.64	monomer		HHblits	EM	NA	0.25	0.32	Cytoplasmic dynein 1 intermediate chain 2
6f38.1.3	9.64	monomer		HHblits	EM	NA	0.25	0.32	Cytoplasmic dynein 1 intermediate chain 2
6f38.1.4	9.64	monomer		HHblits	EM	NA	0.25	0.32	Cytoplasmic dynein 1 intermediate chain 2
6f38.1.b	9.64	monomer		HHblits	EM	NA	0.25	0.32	Cytoplasmic dynein 1 intermediate chain 2
6f38.1.c	9.64	monomer		HHblits	EM	NA	0.25	0.32	Cytoplasmic dynein 1 intermediate chain 2
4ggd.1.A	13.33	monomer		HHblits	X-ray	2.44Å	0.26	0.30	Cell division cycle protein 20 homolog
5lj5.1.M	12.27	monomer		HHblits	EM	3.80Å	0.25	0.31	Pre-mRNA-splicing factor PRP46
5wlc.20.A	9.96	monomer		HHblits	EM	NA	0.25	0.32	Utp1
5wyj.16.A	9.96	monomer		HHblits	EM	NA	0.25	0.32	Periodic tryptophan protein 2
3j2t.1.A	12.54	monomer		HHblits	EM	NA	0.26	0.31	Apoptotic protease-activating factor 1
5wyk.1.R	9.96	monomer		HHblits	EM	NA	0.25	0.32	Periodic tryptophan protein 2
3mkq.1.A	12.18	homo-trimer		HHblits	X-ray	2.50Å	0.26	0.31	Coatomer beta'-subunit
3mkq.1.C	12.18	homo-trimer		HHblits	X-ray	2.50Å	0.26	0.31	Coatomer beta'-subunit
3mkq.1.E	12.18	homo-trimer		HHblits	X-ray	2.50Å	0.26	0.31	Coatomer beta'-subunit
4gqb.1.B	11.58	monomer		HHblits	X-ray	2.06Å	0.25	0.35	Methylosome protein 50
5i2t.1.A	12.08	monomer		HHblits	X-ray	2.54Å	0.26	0.34	Periodic tryptophan protein 2
4x60.1.B	11.73	monomer		HHblits	X-ray	2.35Å	0.24	0.35	Methylosome protein 50

The table above shows the top 50 filtered templates. A further 611 templates were found which were considered to be less suitable for

modelling than the filtered list.
3vl1.1.A, 5cvl.1.A, 5hy7.1.A, 5cvo.2.A, 3fm0.1.A, 2ynp.1.A, 3dxm.1.C, 4tqo.1.A, 5yje.1.A, 5yje.1.B, 5yje.1.C, 5ukl.1.B, 4nox.1.A, 4i0u.2.B, 4e54.1.B, 4i0u.2.A, 5naf.1.A, 2h13.1.A, 4i0u.2.D, 4i0u.2.E, 3sn6.1.B, 1xhm.1.A, 6c23.1.D, 5tzs.1.e, 6c23.1.F, 5wak.1.A, 6fbs.1.B, 1r5m.1.A, 4gq1.1.A, 5chx.1.A, 4jo7.1.D, 5chx.1.B, 2bbj.1.A, 4jo7.1.C, 4eeb.1.A, 4ui9.1.Q, 1p22.1.A, 3t98.1.B, 5vfc.1.A, 4czv.1.A, 5cyk.1.A, 5cyk.1.B, 2xyi.1.A, 5tzs.1.1, 2pm9.1.A, 3f3g.1.E, 5gm6.1.F, 5k19.2.A, 3w15.1.A, 3bws.1.A, 5naf.3.A, 5j1g.1.A, 5h13.1.A, 5vyc.4.I, 5v1d.2.A, 5v1d.2.B, 4jsn.1.B, 4jo9.1.B, 1nex.2.B, 1w6s.1.A, 5opt.1.A, 6g16.4.A, 3q54.1.A, 5wsg.1.U, 4d6v.1.A, 3jbt.1.A, 5cxc.1.A, 5k0m.1.A, 4i0u.2.C, 6gdg.1.B, 4aah.1.A, 4jxm.1.A, 2i3s.1.A, 4cvc.1.A, 6bcx.1.C, 4q9v.1.A, 6f3a.1.3, 3j7p.78.A, 6cb1.1.a, 3vu4.2.A, 4jo7.2.C, 2ce9.2.B, 5jcs.1.3, 4nsx.1.A, 6g5i.1.6, 5wyk.1.U, 4yvd.1.A, 2iub.1.C, 2iub.1.A, 5tdh.1.B, 5n9y.1.B, 3jzn.1.A, 5wg6.1.B, 5n9y.1.C, 5lj5.1.d, 5ayh.1.A, 5igq.1.A, 1a0r.1.A, 5m1j.14.A, 4v5z.1.A, 5mqf.1.F, 5mqf.1.D, 5mqf.1.E, 4xmm.1.C, 5n9y.1.D, 5jut.45.A, 3shf.1.A, 4fhm.1.A, 3j81.1.5, 4ev6.1.D, 4v6w.2.A, 3ewe.1.A, 3jcf.1.E, 5ndv.73.A, 4ev6.1.A, 1kj1.1.B, 4wjv.1.A, 3jap.1.i, 5sv7.1.B, 5afu.1.C, 5a31.1.R, 5k1a.2.B, 3wuq.1.A, 5u5h.1.A, 3jch.1.C, 3jch.1.B, 3jch.1.A, 3jch.1.D, 5wlc.15.A, 4j87.1.A, 4mae.1.A, 5h19.1.A, 5sv7.1.D, 4ev6.1.E, 3odt.1.A, 5sv7.1.A, 4v8m.8.A, 5sv7.1.C, 5gmk.1.0, 6em5.1.5, 5wlc.27.A, 5ttw.2.A, 4jq5.2.B, 1pi6.1.A, 5h64.1.C, 2yba.1.A, 2ovp.1.B, 2w18.1.A, 5tf2.1.A, 5xjc.1.W, 5xjc.1.T, 3na7.1.A, 4bzj.1.B, 1flg.1.A, 5xjc.1.E, 5ic7.1.A, 4cc9.1.A, 4x3e.1.A, 5mwj.1.A, 4zoy.1.A, 5gmk.1.J, 5kkl.1.A, 5gmk.1.X, 6ek0.64.A, 6b3x.1.A, 4wju.1.A, 5jus.45.A, 4jq5.1.C, 5wlc.25.A, 5wuk.1.A, 1kb0.1.A, 2h6k.1.A, 1s4u.1.A, 4wjs.1.A, 4q9v.1.B, 3j77.45.A, 5gap.1.F, 4imm.2.A, 5nuv.1.A, 5wyj.19.A, 3j2t.1.A, 5em2.2.B, 4yd8.1.A, 5hqg.1.A, 5v4b.1.B, 2mtl.1.A, 5h64.1.B, 4l6y.1.B, 4l6y.1.A, 1sq9.1.A, 5bjs.1.A, 5xm3.1.A, 5n4a.1.A, 5l8w.1.B, 6em5.1.h, 3f3p.2.B, 1b9y.1.A, 3i2n.1.A, 5ayw.1.B, 5wbk.1.A, 4v7f.1.j, 6g18.1.L, 5cws.2.D, 3hh0.1.D, 4yzy.1.A, 3jcm.1.B, 3v7d.1.B, 3hh0.1.B, 3hh0.1.C, 2bcj.1.B, 5nug.1.A, 4ev6.1.B, 5a2q.1.8, 6b20.1.A, 3prw.1.A, 6en4.1.A, 4o9d.1.A, 5lj5.1.M, 4jo7.2.A, 4ev6.1.C, 4hdj.1.A, 5kc2.1.B, 4a08.1.B, 3ah8.1.B, 4lg8.1.A, 5a1u.1.S, 4uxv.1.A, 5a1u.1.T, 2xu7.1.A, 5flx.1.7, 5juu.45.A, 3j80.1.7, 1k8k.1.C, 4cy2.1.A, 4v92.1.8, 5lks.64.A, 3hh0.1.A, 5k0y.1.8, 4ycz.1.A, 3mxx.1.A, 2j04.1.B, 3jan.80.A, 4buj.1.C, 2ynn.1.A, 6gqv.75.A, 3jb9.1.K, 4cy1.1.A, 6bly.1.B, 1vyh.1.C, 4ozu.1.A, 2xl2.1.A, 6fec.1.e, 5fxy.2.A, 3jb9.1.S, 3mks.1.D, 4jq5.1.A, 4bts.27.A, 5wyj.17.A, 2o9k.1.A, 4xfv.1.A, 3dm0.1.A, 5y1u.1.A, 4jq5.3.A, 3a6m.1.A, 3uvo.1.A, 4e5z.1.B, 4v0n.2.B, 5it9.1.6, 2g99.1.A, 5ukm.1.B, 3jb9.1.L, 3vl1.2.A, 5u69.1.A, 4a0b.1.B, 3ow8.1.A, 5aps.1.A, 5wbi.1.A, 4buj.1.D, 4o45.1.A, 5oql.1.3, 5k1c.1.C, 5k1c.1.B, 3bg0.1.H, 3frx.1.A, 5igo.1.A, 5nnz.2.A, 5juy.1.B, 5nzu.1.A, 5d0o.1.B, 5juy.1.G, 5juy.1.D, 5juy.1.E, 4a11.1.B, 6exn.1.J, 5oql.1.N, 5oql.1.O, 3q7o.1.A, 3n0d.1.A, 6bw3.1.A, 5oql.1.A, 5oql.1.F, 5oql.1.D, 5hyn.2.B, 6exn.1.a, 5juo.45.A, 1l0q.3.A, 3rfh.1.A, 3rfh.1.B, 5ov3.1.A, 5ov3.1.B, 4v7h.1.Q, 4v5o.1.0, 5em2.1.B, 5em2.1.A, 5ams.1.A, 5ijn.1.G, 5mzh.1.A, 3no2.1.A, 5wg4.1.B, 5m89.2.A, 3ei4.1.B, 4eeb.1.B, 5k0y.1.P, 5m2n.1.A, 4ky3.2.A, 4j73.1.A, 2pbi.2.B, 2osz.1.D, 2osz.1.C, 5cxb.1.A, 3jpx.1.A, 2co0.1.A, 5vlj.1.B, 5vlj.1.C, 6b3j.1.D, 5fvm.1.C, 6f9n.1.B, 4u7a.1.A, 4xf2.1.C, 5lcw.1.Q, 5lcw.1.R, 4bzj.1.D, 4bzj.1.C, 5mc6.37.A, 4bzj.1.A, 3iiy.1.A, 4jq5.1.B, 1gp2.1.B, 1l0q.1.A, 5ukk.1.B, 5cvn.1.A, 2ymu.1.A, 5mg8.2.B, 5a9q.1.H, 5lyb.33.A, 3a6m.1.B, 5wve.1.K, 4fhl.1.A, 6g5h.1.8, 5vh9.1.B, 4i0u.1.E, 4i0u.1.D, 4i0u.1.A, 4i0u.1.C, 4i0u.1.B, 2ovr.1.B, 4gq2.1.B, 4bl0.2.A, 4i79.1.A, 5zcs.1.C, 2hn2.1.C, 5a9q.1.C, 4o9d.2.A, 4czy.1.A, 4bzk.1.D, 3dwl.1.B, 4zov.1.A, 4mp2.1.A, 4xmn.1.A, 4uer.1.b, 3acp.1.A, 5tga.33.A, 5g04.1.Q, 2aq5.1.A, 5wjc.1.A, 2hz6.1.A, 3jrp.1.A, 4j0x.1.A, 5fa5.1.B, 5wp3.1.A, 4ci8.1.A, 5k1a.1.B, 5nrl.1.W, 1bwu.1.D, 4x60.1.B, 5n1a.1.A, 5nrl.1.O, 5j6a.1.A, 5aja.1.A, 5cvo.1.A, 4xei.1.C, 3uzs.1.B, 3j78.45.A, 5mq0.1.I, 5mps.1.U, 4zox.1.A, 5v1d.1.C, 5v1d.1.A, 5y05.1.A, 6byn.1.A, 5lj3.1.L, 6eoj.1.C, 3vu4.1.A, 6f3a.1.2, 4xga.1.A, 5hy7.2.A, 4a0a.1.B, 3iiw.1.A, 2i3s.2.A, 3sfz.1.A, 6bk8.1.H, 3j6x.75.A, 4gqb.1.B, 4a0l.1.B, 6dde.1.B, 5wlc.17.A, 5n9y.1.A, 4h5i.1.A, 5n9y.1.E, 5t2c.73.A, 6bcu.1.B, 4mh1.1.A, 4gm9.2.A, 4mh1.1.B, 4owr.1.A, 5o9z.1.L, 5wlc.13.A, 5o9z.1.F, 5wyj.18.A, 3f3f.1.A, 5m5g.1.A, 4ggd.1.A, 6d9j.78.A, 5xyi.1.6, 4wju.2.A, 5mc6.15.A, 3bg0.1.D, 3mzk.1.A, 5xwr.1.A, 3n0e.1.A, 5tee.1.A, 3ei2.1.B, 5wyk.1.V, 5cw9.1.A, 3bg0.1.A, 4j0w.1.A, 3jct.1.n, 5wg6.2.B, 4g56.1.B, 4v0m.1.B, 4eed.1.C, 4aow.1.A, 5lyb.108.A, 5jul.1.A, 5wlc.28.A, 6f1t.1.b, 6f1t.1.c, 5wlc.19.A, 5sxm.1.A, 5jk7.1.B, 5a9q.1.G, 5a9q.1.A, 6d90.78.A, 1erj.1.A, 6g16.1.A, 6bk8.1.P, 5wlc.26.A, 5l8e.1.A, 1gxr.1.B, 1gxr.1.A, 3mkq.1.A, 3mkq.1.C, 3mkq.1.E, 4v6i.1.A, 1g72.1.A, 5kdo.1.B, 4h3o.1.A, 5jtg.1.B, 5grs.1.A, 5m23.1.A, 3j6y.75.A, 4a7j.1.A, 1kv9.1.A, 4kzz.1.6, 6gqb.75.A, 6f1t.1.4, 6f1t.1.3, 5sum.1.A, 3jam.1.7, 3jaq.1.i, 1bwu.1.A, 5nzu.1.C, 4psw.1.B, 1pev.1.A, 5y1u.2.A, 4v7r.20.A, 5wyj.20.A, 5jtg.1.A, 2g9a.1.A, 5oql.1.X, 4d0k.1.A, 5wlc.24.A, 3dw8.1.B, 5dfz.1.C, 2yno.1.A, 5obm.152.A, 5wlc.22.A, 2z5h.1.D, 6f38.1.3, 6f38.1.4, 5vai.1.D, 5gxh.1.A, 5h3s.1.A, 5ndv.147.A, 2cnx.1.A, 3jcg.1.D, 3jcg.1.E, 6f38.1.b, 6f38.1.c, 3jcg.1.A, 3jcg.1.B, 3jcg.1.C, 4pk1.1.A, 1tbg.1.E, 4xyh.1.A, 4zn4.1.A, 4jq5.2.C, 1tbg.1.A, 4u1e.1.A, 3lrv.1.A, 5m89.1.A, 5oql.1.L, 3cfs.1.A, 5oql.1.M, 4gga.1.A, 2yh3.1.A, 3cik.1.B, 4bh6.1.A, 5vtb.1.A, 1lrw.1.C, 2qxv.1.A, 1lrw.1.A, 4kyz.1.A, 3p1l.1.A, 5jpq.1.Y, 4j79.1.A, 5lzz.77.A, 5jtg.1.C, 2i3t.1.A, 5gva.1.A, 5jpq.1.I, 5nnz.1.A, 3zwl.1.A, 5cws.1.D, 3rfg.1.A, 3c9c.1.A, 2pm7.1.D, 3emh.1.A, 3q7m.1.A, 5jtg.1.D, 6cvz.1.A, 3jro.1.A, 1yfq.1.A, 5ij7.1.B, 5ljo.1.A, 5igo.2.A, 2gnq.1.A, 4d5l.1.7, 5sui.1.A, 5mg8.1.B, 3gre.1.A, 4ky3.3.A, 4rh7.1.A, 4l3i.1.A, 6gq1.75.A, 2pbi.1.B, 4l3i.1.B, 3jai.77.A, 4ky3.1.A, 4yzs.1.A, 4yzs.1.B, 4cy3.1.A, 5wai.1.A, 5wbu.1.B, 4zov.2.A, 5mc6.36.A, 2pm6.1.B, 4imm.1.A, 3mmy.1.A, 6cmo.1.C, 4a0k.1.D, 1got.1.B, 2h9l.1.A, 6fai.1.E, 4jq5.2.A, 1kj1.1.A, 5uz7.1.B, 4gm3.1.A, 2co0.2.A, 1u4c.1.A, 4ci8.2.A